

**EVALUATION OF MULTIPLE CORROSION PROTECTION
SYSTEMS AND CORROSION INHIBITORS FOR REINFORCED
CONCRETE BRIDGE DECKS**

By

Lihua Xing

David Darwin

JoAnn Browning

A Report on Research Sponsored by

FEDERAL HIGHWAY ADMINISTRATION
Contract No. DTFH61-03-C-00131

KANSAS DEPARTMENT OF TRANSPORTATION
Contract Nos. C1131 and C1281

Structural Engineering and Engineering Materials
SM Report No. 99

THE UNIVERSITY OF KANSAS CENTER FOR RESEARCH, INC.
LAWRENCE, KANSAS

May 2010

ABSTRACT

The corrosion performance of different corrosion protection systems is evaluated using the mortar-wrapped rapid macrocell test, bench-scale tests (the Southern Exposure, cracked beam, and ASTM G109 tests), and field tests. The systems include conventional steel with three different corrosion inhibitors (DCI-S, Hycrete, and Rheocrete), epoxy-coated reinforcement with three different corrosion inhibitors and ECR with a primer coating containing microencapsulated calcium nitrite, multiple-coated reinforcement with a zinc layer underlying an epoxy coating, ECR with zinc chromate pretreatment before application of the epoxy coating to improve adhesion between the epoxy and the underlying steel, ECR with improved adhesion epoxy coatings, and pickled 2205 duplex stainless steel. Conventional steel in concretes with two different water-cement ratios (0.45 and 0.35) is also tested. Of these systems, specimens containing conventional steel or conventional epoxy-coated steel serve as controls. The critical chloride thresholds of conventional steel in concrete with different corrosion inhibitors and zinc-coated reinforcement are determined. The results of the tests are used in an economic analysis of bridge decks containing different corrosion protection systems over a design life of 75 years.

The results indicate that a reduced water-cement ratio improves the corrosion resistance of conventional steel in uncracked concrete compared to the same steel in concrete with a higher water-cement ratio. The use of a corrosion inhibitor improves the corrosion resistance of conventional steel in both cracked and uncracked concrete and delays the onset of corrosion in uncracked concrete, but provides only a very limited improvement in the corrosion resistance of epoxy-coated reinforcement due to the high corrosion resistance provided by the epoxy coating itself. Based on results in

the field tests, the epoxy-coated bars with a primer containing microencapsulated calcium nitrite show no improvement in the corrosion resistance compared to conventional epoxy-coated reinforcement.

Increased adhesion between the epoxy coating and reinforcing steel provides no improvement in the corrosion resistance of epoxy-coated reinforcement. The corrosion losses for multiple-coated reinforcement are comparable with those of conventional epoxy-coated reinforcement in the field tests in uncracked and cracked concrete. Corrosion potential measurements show that the zinc is corroded preferentially, providing protection for the underlying steel. Pickled 2205 stainless steel demonstrates excellent corrosion resistance, and no corrosion activity is observed for the pickled 2205 stainless steel in bridge decks, or in the SE, CB, or field test specimens after four years.

ECR, ECR with increased adhesion, and pickled 2205 stainless steel are the most cost-effective corrosion protection systems based on the economic analyses of a 216-mm (8.5-in.) thick bridge deck over a 75-year design life.

Key Words: chloride, concrete, corrosion, corrosion inhibitor, epoxy coatings, multiple corrosion protection systems, threshold, zinc-coated steel

ACKNOWLEDGEMENTS

This report is based on a thesis submitted by Lihua Xing in partial fulfillment of the requirements of the Ph.D. degree. Major funding and material support for this research was provided by the United States Department of Transportation Federal Highway Administration under Contract No. DTFH61-03-C-00131, with technical oversight by Yash Paul Virmani, and the Kansas Department of Transportation under Contract Nos. C1131 and C1281, with technical oversight by Dan Scherschligt and Don Whisler. Additional support for this project was provided by the Concrete Steel Reinforcing Institute, DuPont Powder Coatings, 3M Corporation, Valspar Corporation, Degussa Construction Chemicals (now BASF Construction Chemicals), W. R. Grace & Co., Broadview Technologies, Inc. (now Hycrete Technologies), Western Coating, Inc., and LRM Industries.

TABLE OF CONTENTS

ABSTRACT	ii
ACKNOWLEDGEMENTS	iv
LIST OF TABLES	x
LIST OF FIGURES	xiv
CHAPTER 1 – INTRODUCTION	1
1.1 GENERAL INFORMATION	1
1.2 CORROSION MECHANISM OF REINFORCING STEEL IN CONCRETE.....	3
1.2.1 Chloride-Induced Corrosion	6
1.2.2 Carbonation	8
1.3 CHLORIDE CONCENTRATION AND CRITICAL THRESHOLD....	10
1.4 CORROSION MONITORING TECHNIQUES	13
1.4.1 Corrosion Potential	14
1.4.2 Corrosion Rate	16
1.4.3 Linear Polarization Resistance	18
1.4.4 Electrochemical Impedance Spectroscopy	20
1.4.5 Electrochemical Noise	21
1.5 CORROSION TESTS	23
1.5.1 Rapid Macrocell Test	23
1.5.2 Bench-Scale Tests	25
1.5.3 Field Test	26
1.6 CORROSION PROTECTION SYSTEMS	27
1.6.1 Epoxy-Coated Reinforcement	28
1.6.2 Zinc-Coated Reinforcement	32
1.6.3 Stainless Steel	34
1.6.4 Corrosion Inhibitors	36
1.6.5 Low Permeability Concrete	42

1.7	OBJECTIVE AND SCOPE	43
CHAPTER 2 – EXPERIMENTAL WORK		45
2.1	CORROSION PROTECTION SYSTEMS	45
2.2	RAPID MACROCELL TEST	48
2.2.1	Test Materials and Apparatus	49
2.2.2	Specimen Preparation	52
2.2.3	Test Setup.....	56
2.2.4	Test Procedure	58
2.2.5	Test Program	58
2.3	BENCH-SCALE TESTS	58
2.3.1	Testing Materials and Apparatus	59
2.3.2	Specimen Preparation	62
2.3.3	Test Setup.....	66
2.3.4	Test Procedure	67
2.3.5	Test Program	69
2.4	FIELD TEST	71
2.4.1	Testing Materials and Apparatus	71
2.4.2	Specimen Preparation	73
2.4.3	Test Setup.....	80
2.4.4	Test Procedure	82
2.4.5	Test Program	84
2.5	KDOT BRIDGE PROJECTS	85
2.5.1	Bridge Information	85
2.5.2	Bridge Test Setup.....	87
2.5.3	Bridge Potential Mapping	90
2.5.4	Field Test Specimens	91
2.5.5	Bench-Scale Specimens	97
2.6	LINEAR POLARIZATION RESISTANCE TEST	98

2.7	CRITICAL CHLORIDE THRESHOLD TEST	101
2.7.1	Test Procedure	102
2.7.2	Test Program.....	106
CHAPTER 3 – RESULTS AND EVALUATION		107
3.1	RAPID MACROCELL TEST	112
3.2	BENCH-SCALE TESTS	133
3.2.1	Conventional Steel and Epoxy-coated Reinforcement	135
3.2.2	Conventional Steel with Corrosion Inhibitors	142
3.2.2.1	Southern Exposure Test	143
3.2.2.2	Cracked Beam Test	147
3.2.3	Conventional, ECR, and Multiple-Coated Bars Evaluated Using the ASTM G109 Test.....	153
3.3	FIELD TEST	164
3.3.1	Conventional Steel and ECR	166
3.3.1.1	Field Specimens without Cracks	166
3.3.1.2	Field Specimens with Cracks	174
3.3.2	ECR with Corrosion Inhibitors	181
3.3.2.1	Field Specimens without Cracks	182
3.3.2.2	Field Specimens with Cracks	190
3.3.3	Multiple-Coated Reinforcement	199
3.3.3.1	Field Test Specimens without Cracks	199
3.3.3.2	Field Test Specimens with Cracks	204
3.3.4	ECR with Increased Adhesion.....	210
3.3.4.1	Field Specimens without Cracks	210
3.3.4.2	Field Specimens with Cracks	216
3.3.5	Visual Inspection	223
3.3.6	Summary	226
3.4	KDOT BRIDGE PROJECTS	228

3.4.1	Bench-scale Tests	228
3.4.2	Field Test	237
3.4.2.1	Doniphan County Bridge	238
3.4.2.2	Mission Creek Bridge	243
3.4.3	Bridge Corrosion Potential Mapping.....	251
3.4.3.1	Doniphan County Bridge	251
3.4.3.2	Mission Creek Bridge	254
3.4.4	Summary	257
3.5	LINEAR POLARIZATION RESISTANCE TEST.....	258
3.5.1	Microcell Corrosion	260
3.5.2	Microcell Corrosion versus Macrocell Corrosion	274
3.6	CRITICAL CHLORIDE THRESHOLD TEST	278
3.6.1	Conventional Steel with Corrosion Inhibitors	279
3.6.2	Zinc-Coated Reinforcing Steel	288
CHAPTER 4 – SUMMARY OF RESULTS AND ECONOMIC ANALYSIS		306
4.1	SUMMARY OF TEST RESULTS	306
4.1.1	Conventional Steel and Epoxy-Coated Reinforcement	307
4.1.2	Corrosion Inhibitors and Low Water-Cement Ratios	309
4.1.3	Multiple-Coated Reinforcement	311
4.1.4	Epoxy-Coated Reinforcement with Increased Adhesion.....	312
4.1.5	KDOT Bridge Projects	313
4.2	COMPARISON OF TEST METHODS	314
4.2.1	Southern Exposure Test versus Rapid Macrocell Test	317
4.2.2	Cracked Beam Test versus Rapid Macrocell Test	319
4.2.3	Cracked Beam Test versus Southern Exposure Test	319
4.2.4	Summary	322
4.3	LIFE EXPECTANCY AND COST EFFECTIVENESS.....	323
4.3.1	Life Expectancy	324

4.3.2 Cost Effectiveness	335
CHAPTER 5 – ECONOMIC ANALYSIS	345
5.1 SUMMARY	345
5.2 CONCLUSION	347
5.3 RECOMMENDATIONS	351
REFERENCES	353
APPENDIX A	367
APPENDIX B	422
APPENDIX C	435
APPENDIX D	443

LIST OF TABLES

Table 1.1 – Corrosion conditions based on half-cell potential readings	15
Table 2.1 – Chemical compositions of 2205p stainless steel and conventional steel.....	47
Table 2.2 – Mechanical properties of 2205p stainless steel and conventional steel.....	47
Table 2.3 – Mortar mixture proportions for rapid macrocell specimens	55
Table 2.4 – Rapid macrocell test programs.....	59
Table 2.5 – Concrete mixture proportions for bench-scale tests.....	60
Table 2.6 – Test program for Southern Exposure tests	69
Table 2.7 – Test program for cracked beam tests	70
Table 2.8 – Test program for ASTM G 09 tests.....	70
Table 2.9 – Concrete mixture proportions for field tests	72
Table 2.10 – Concrete batches for field tests	79
Table 2.11 – Concrete properties for field tests	80
Table 2.12 – Concrete compressive strength for field tests	80
Table 2.13 – KDOT salt usage history.....	81
Table 2.14 – Test program for field tests	84
Table 2.15 – Bridge configurations.....	86
Table 2.16 – Test bar in Doniphan County Bridge	88
Table 2.17 – Test bar in Mission Creek Bridge	88
Table 2.18 – Concrete mixture proportions for Doniphan County Bridge and Mission Creek Bridge	89

Table 2.19 – Concrete properties for Doniphan County Bridge	90
Table 2.20 – Concrete properties for Mission Creek Bridge	90
Table 2.21 – Concrete properties for field test specimens of Doniphan County Bridge and Mission Creek Bridge.....	95
Table 2.22 – Test program for the field tests for the Doniphan County Bridge and Mission Creek Bridge.....	97
Table 2.23 – Test program for the bench-scale tests for the Doniphan County Bridge and Mission Creek Bridge.....	98
Table 2.24 – Parameter difference for LPR tests	100
Table 2.25 – Test program for LPR tests	102
Table 2.26 – Concrete properties for chloride threshold tests.....	103
Table 2.27 – Test program for chloride threshold beam tests.....	106
Table 3.1 – Factors for converting corrosion rates and losses based on total and to those based on exposed area	108
Table 3.2 – Corrosion losses at 15 weeks for conventional steel with different inhibitors in rapid macrocell test.....	113
Table 3.3 – Corrosion losses at 42 weeks for control and inhibitor specimens in the Southern Exposure test based on total and exposed area	140
Table 3.4 – Corrosion losses at 42 weeks for conventional steel with different inhibitors in the cracked beam test.....	149
Table 3.5 – Corrosion losses at 209 weeks for specimens in the ASTM G109 test based on total and exposed area	158
Table 3.6 – Corrosion losses for conventional steel and ECR in the field test, without cracks	170
Table 3.7 – Corrosion losses for conventional steel and ECR in the field test, with simulated cracks.....	176
Table 3.8 – Corrosion losses for ECR with a primer containing calcium nitrite and ECR with corrosion inhibitors in the field test, without cracks.....	186

Table 3.9 – Corrosion losses for ECR with a primer containing calcium nitrite and ECR with corrosion inhibitors in the field test, with simulated cracks.....	194
Table 3.10 – Corrosion losses for multiple-coated bars in the field test, without cracks.....	202
Table 3.11 – Corrosion losses for multiple-coated bars in the field test, with simulated cracks.....	207
Table 3.12 – Corrosion losses for ECR with increased adhesion in the field test, without cracks.....	214
Table 3.13 – Corrosion losses for ECR with increased adhesion in the field test, with simulated cracks.....	220
Table 3.14 – Corrosion losses at 203 weeks for pickled 2205 stainless steel in bench-scale tests for the DCB and MCB.....	230
Table 3.15 – Corrosion losses at 215 weeks for conventional steel, pickled 2205 stainless steel, and ECR in field test for the Doniphan County Bridge.....	240
Table 3.16 – Corrosion losses at 189 weeks for conventional steel, pickled 2205 stainless steel, and ECR in field test for the Mission Creek Bridge.....	247
Table 3.17 – Guideline for interpretation of corrosion current densities in LPR test.....	259
Table 3.18 – Total corrosion losses at 40 weeks from linear polarization resistance method for the Southern Exposure and cracked beam test.....	265
Table 3.19 – Total corrosion losses from linear polarization resistance method for the ASTM G109 test.....	269
Table 3.20 – Microcell corrosion rates from linear polarization resistance method for specimens without cracks in the field test.....	272
Table 3.21 – Microcell corrosion rates from linear polarization resistance method for specimens with simulated cracks in the field test.....	273
Table 3.22 – Microcell and macrocell corrosion losses at 40 weeks for specimens in the Southern Exposure and cracked beam test.....	275
Table 3.23 – Critical chloride thresholds for conventional steel with DCI inhibitor in initiation beam test.....	280

Table 3.24 – Critical chloride thresholds for conventional steel with Hycrete inhibitor in initiation beam test	282
Table 3.25 – Critical chloride thresholds for conventional steel with Rheocrete inhibitor in initiation beam test.....	283
Table 3.26 – Critical chloride thresholds for conventional steel with no inhibitors in modified Southern Exposure and initiation beam test	285
Table 3.27 – Critical chloride thresholds for zinc-coated steel in initiation beam test.....	292
Table 3.28 – Critical chloride thresholds for MMFX microcomposite steel in modified Southern Exposure and initiation beam test	294
Table 3.29 – Comparison of the average critical chloride thresholds	304
Table 4.1 – Average corrosion rates for specimens in the rapid macrocell test (at 15 weeks) and the bench-scale tests (at 42 weeks)	316
Table 4.2 – Average corrosion losses for specimens in the rapid macrocell test (at 15 weeks) and the bench-scale tests (at 42 weeks)	316
Table 4.3 – Coefficients of determination R^2 between results using different test methods for conventional steel in mortar or concrete without and with different inhibitors	323
Table 4.4 – Time to corrosion initiation for bridge decks with different corrosion protection systems.....	327
Table 4.5 – Time to first repair for bridge decks containing different corrosion protection systems.....	329
Table 4.6 – In-place cost for different construction items in new bridge decks.....	338
Table 4.7a – Economic analysis for bridge decks containing different corrosion protection systems, monolithic decks	341
Table 4.7b – Economic analysis for bridge decks containing different corrosion protection systems, silica fume overlay decks.....	342

LIST OF FIGURES

Figure 1.1 – Mechanism of interaction between carbonation and chloride penetration	9
Figure 2.1 – Mortar-wrapped specimen.....	53
Figure 2.2 – Mold for mortar-wrapped specimens	53
Figure 2.3 – Rapid Macrocell test with mortar-wrapped specimens	57
Figure 2.4 – Southern Exposure test specimen	63
Figure 2.5 – Cracked Beam test specimen.....	63
Figure 2.6 – ASTM G109 test specimen.....	64
Figure 2.7 – Field test specimens.....	74
Figure 2.8 – Shim holder for field specimens.....	77
Figure 2.9 – Potential test points for field specimens.....	83
Figure 2.10 – Test bar locations and potential test points on Doniphan County Bridge.....	88
Figure 2.11 – Test bar locations and potential test points on Mission Creek Bridge.....	89
Figure 2.12 – Field test specimens for Doniphan County Bridge.....	93
Figure 2.13 – Field test specimens for Mission Creek Bridge.....	94
Figure 2.14 – Potential test points for field test specimens for Doniphan County Bridge	96
Figure 2.15 – Potential test points for field test specimens for Mission Creek Bridge	96
Figure 2.16 – Input window for LPR test	99
Figure 2.17 – Beam specimen end view	104

Figure 2.18 – Side view showing sampling locations.....	104
Figure 3.1a – Macrocell Test. Average corrosion rates for specimens with conventional steel and different inhibitors, $w/c = 0.45$	115
Figure 3.1b – Macrocell Test. Average corrosion losses for specimens with conventional steel and different inhibitors, $w/c = 0.45$	116
Figure 3.2a – Macrocell Test. Average anode corrosion potentials with respect to a saturated calomel electrode for specimens with conventional steel and different inhibitors, $w/c = 0.45$	116
Figure 3.2b – Macrocell Test. Average cathode corrosion potentials with respect to a saturated calomel electrode for specimens with conventional steel and different inhibitors, $w/c = 0.45$	117
Figure 3.3a – Macrocell Test. Average corrosion rates for specimens with conventional steel and different inhibitors, $w/c = 0.35$	118
Figure 3.3b – Macrocell Test. Average corrosion losses for specimens with conventional steel and different inhibitors, $w/c = 0.35$	119
Figure 3.4a – Macrocell Test. Average anode corrosion potentials with respect to a saturated calomel electrode for specimens with conventional steel and different inhibitors, $w/c = 0.35$	119
Figure 3.4b – Macrocell Test. Average cathode corrosion potentials with respect to a saturated calomel electrode for specimens with conventional steel and different inhibitors, $w/c = 0.35$	120
Figure 3.5a – Macrocell Test. Average corrosion rates for specimens with conventional steel and different water-cement ratios, no inhibitors	121
Figure 3.5b – Macrocell Test. Average corrosion losses for specimens with conventional steel and different water-cement ratios, no inhibitors	121
Figure 3.6a – Macrocell Test. Average anode corrosion potentials with respect to a saturated calomel electrode for specimens with conventional steel and different water-cement ratios, no inhibitors.....	122
Figure 3.6b – Macrocell Test. Average cathode corrosion potentials with respect to a saturated calomel electrode for specimens with conventional steel and different water-cement ratios, no inhibitors.....	122

Figure 3.7a – Macrocell Test. Average corrosion rates for specimens with conventional steel and different water-cement ratios, DCI inhibitor.....	124
Figure 3.7b – Macrocell Test. Average corrosion losses for specimens with conventional steel and different water-cement ratios, DCI inhibitor.....	124
Figure 3.8a – Macrocell Test. Average anode corrosion potentials with respect to a saturated calomel electrode for specimens with conventional steel and different water-cement ratios, DCI inhibitor	125
Figure 3.8b – Macrocell Test. Average cathode corrosion potentials with respect to a saturated calomel electrode for specimens with conventional steel and different water-cement ratios, DCI inhibitor	125
Figure 3.9a – Macrocell Test. Average corrosion rates for specimens with conventional steel and different water-cement ratios, Hycrete inhibitor.....	126
Figure 3.9b – Macrocell Test. Average corrosion losses for specimens with conventional steel and different water-cement ratios, Hycrete inhibitor.....	126
Figure 3.10a – Macrocell Test. Average anode corrosion potentials with respect to a saturated calomel electrode for specimens with conventional steel and different water-cement ratios, Hycrete inhibitor.....	127
Figure 3.10b – Macrocell Test. Average cathode corrosion potentials with respect to a saturated calomel electrode for specimens with conventional steel and different water-cement ratios, Hycrete inhibitor.....	127
Figure 3.11a – Macrocell Test. Average corrosion rates for specimens with conventional steel and different water-cement ratios, Rheocrete inhibitor	128
Figure 3.11b – Macrocell Test. Average corrosion losses for specimens with conventional steel and different water-cement ratios, Rheocrete inhibitor	129
Figure 3.12a – Macrocell Test. Average anode corrosion potentials with respect to a saturated calomel electrode for specimens with conventional steel and different water-cement ratios, Rheocrete inhibitor.....	129
Figure 3.12b – Macrocell Test. Average cathode corrosion potentials with respect to a saturated calomel electrode for specimens with conventional steel and different water-cement ratios, Rheocrete inhibitor.....	130
Figure 3.13 – Macrocell Test. Anode specimen (M-Conv.-NO45-1) with	

conventional steel showing stains on cracked mortar surface at week 15.....	131
Figure 3.14 – Macrocell Test. Anode specimen (M-Conv.-NO45-2) with conventional steel showing spalled mortar cover at week 15.....	131
Figure 3.15 – Macrocell Test. Conventional steel from anode specimen (M-Conv.-HY45-1) showing severe corrosion products at week 15	132
Figure 3.16 – Macrocell Test. Conventional steel from anode specimen (M-Conv.-RH35-6) showing slightly corrosion products at week 25.....	132
Figure 3.17 – Macrocell Test. Conventional steel from cathode specimen (M-Conv.-DCI45-3) showing no corrosion products at week 15	132
Figure 3.18a – Southern Exposure Test. Average corrosion rates for specimens with conventional steel and ECR (ECR with four holes through the epoxy).....	136
Figure 3.18b – Southern Exposure Test. Average corrosion rates for specimens with conventional steel and ECR (ECR with four holes through the epoxy). (Different scale)	136
Figure 3.19 – Southern Exposure Test. Average corrosion rates for specimens with ECR. * Based on exposed area (ECR with four holes through the epoxy).....	137
Figure 3.20a – Southern Exposure Test. Average corrosion losses for specimens with conventional steel and ECR (ECR with four holes through the epoxy).....	137
Figure 3.20b – Southern Exposure Test. Average corrosion losses for specimens with conventional steel and ECR (ECR with four holes through the epoxy). (Different scale)	138
Figure 3.21 – Southern Exposure Test. Average corrosion losses for specimens with ECR. * Based on exposed area (ECR with four holes through the epoxy).....	138
Figure 3.22a – Southern Exposure Test. Average top mat corrosion potentials with respect to a copper-copper sulfate electrode for specimens with conventional steel and ECR (ECR with four holes through the epoxy).....	140
Figure 3.22b – Southern Exposure Test. Average bottom mat corrosion potentials with respect to a copper-copper sulfate electrode for specimens	

with conventional steel and ECR (ECR with four holes through the epoxy) 141

Figure 3.23 – Southern Exposure Test. Average mat-to-mat resistances for specimens with conventional steel and ECR (ECR with four holes through the epoxy)..... 142

Figure 3.24 – Southern Exposure Test. Average corrosion rates for specimens with conventional steel and different inhibitors 144

Figure 3.25 – Southern Exposure Test. Average corrosion losses for specimens with conventional steel and different inhibitors 144

Figure 3.26a – Southern Exposure Test. Average top mat corrosion potentials with respect to a copper-copper sulfate electrode for specimens with conventional steel and different inhibitors..... 146

Figure 3.26b – Southern Exposure Test. Average bottom mat corrosion potentials with respect to a copper-copper sulfate electrode for specimens with conventional steel and different inhibitors..... 146

Figure 3.27 – Southern Exposure Test. Average mat-to-mat resistances for specimens with conventional steel and different inhibitors 147

Figure 3.28 – Cracked Beam Test. Average corrosion rates for specimens with conventional steel and different inhibitors..... 148

Figure 3.29 – Cracked Beam Test. Average corrosion losses for specimens with conventional steel and different inhibitors..... 149

Figure 3.30a – Cracked Beam Test. Average top mat corrosion potentials with respect to a copper-copper sulfate electrode for specimens with conventional steel and different inhibitors..... 151

Figure 3.30b – Cracked Beam Test. Average bottom mat corrosion potentials with respect to a copper-copper sulfate electrode for specimens with conventional steel and different inhibitors..... 151

Figure 3.31 – Cracked Beam Test. Average mat-to-mat resistances for specimens with conventional steel and different inhibitors 152

Figure 3.32a – ASTM G109 Test. Average corrosion rates for specimens with conventional steel, ECR, and multiple-coated bars (four and ten holes through the epoxy) 154

Figure 3.32b – ASTM G109 Test. Average corrosion rates for specimens with conventional steel, ECR, and multiple-coated bars (four and ten holes through the epoxy). (Different scale)..... 154

Figure 3.33 – ASTM G109 Test. Average corrosion rates for specimens with ECR and multiple-coated bars. * Based on exposed area (four and ten holes through the epoxy)..... 155

Figure 3.34a – ASTM G109 Test. Average corrosion losses for specimens with conventional steel, ECR, and multiple-coated bars (four and ten holes through the epoxy) 156

Figure 3.34b – ASTM G109 Test. Average corrosion losses for specimens with conventional steel, ECR, and multiple-coated bars (four and ten holes through the epoxy). (Different scale)..... 156

Figure 3.35 – ASTM G109 Test. Average corrosion losses for specimens with ECR and multiple-coated bars. * Based on exposed area (four and ten holes through the epoxy)..... 157

Figure 3.36a – ASTM G109 Test. Average top mat corrosion potentials with respect to a copper-copper sulfate electrode for specimens with conventional steel, ECR, and multiple-coated bars (four and ten holes through the epoxy) 160

Figure 3.36b – ASTM G109 Test. Average bottom mat corrosion potentials with respect to a copper-copper sulfate electrode for specimens with conventional steel, ECR, and multiple-coated bars (four and ten holes through the epoxy) 160

Figure 3.37 – ASTM G109 Test. Average mat-to-mat resistances for specimens with conventional steel, ECR, and multiple-coated bars (four and ten holes through the epoxy)..... 161

Figure 3.38 – ASTM G109 Test. Specimen with conventional steel (G-N4-Conv.-3) showing a crack on the top surface at week 174 162

Figure 3.39 – ASTM G109 Test. Specimen with conventional steel (G-N4-Conv.-6) showing cracks and stains on the side at week 174..... 163

Figure 3.40 – ASTM G109 Test. Conventional steel (G-N4-Conv.-1) showing severe corrosion on both top (top) and bottom (bottom) mats of steel at week 174..... 163

Figure 3.41 – ASTM G109 Test. Conventional steel from bottom mat of the specimen (G-N4-Conv.-6) showing severe corrosion at week 174	164
Figure 3.42a – Field Test. Average corrosion rates for specimens with conventional steel and ECR, without cracks (ECR with 16 holes through the epoxy).....	167
Figure 3.42b – Field Test. Average corrosion rates for specimens with conventional steel and ECR, without cracks (ECR with 16 holes through the epoxy). (Different scale).....	168
Figure 3.43 –Field Test. Average corrosion rates for specimens with ECR, without cracks. * Based on exposed area (ECR with 16 holes through the epoxy).....	168
Figure 3.44a – Field Test. Average corrosion losses for specimens with conventional steel and ECR, without cracks (ECR with 16 holes through the epoxy).....	169
Figure 3.44b – Field Test. Average corrosion losses for specimens with conventional steel and ECR, without cracks (ECR with 16 holes through the epoxy). (Different scale).....	169
Figure 3.45 – Field Test. Average corrosion losses for specimens with ECR, without cracks. * Based on exposed area (ECR with 16 holes through the epoxy).....	170
Figure 3.46a – Field Test. Average top mat corrosion potentials with respect to a copper-copper sulfate electrode for specimens with conventional steel and ECR, without cracks (ECR with 16 holes through the epoxy)	172
Figure 3.46b – Field Test. Average bottom mat corrosion potentials with respect to a copper-copper sulfate electrode for specimens with conventional steel and ECR, without cracks (ECR with 16 holes through the epoxy)	172
Figure 3.47a – Field Test. Average mat-to-mat resistances for specimens with conventional steel and ECR, without cracks (ECR with 16 holes through the epoxy)	173
Figure 3.47b – Field Test. Average mat-to-mat resistances for specimens with conventional steel and ECR, without cracks (ECR with 16 holes through the epoxy). (Different scale).....	173
Figure 3.48a – Field Test. Average corrosion rates for specimens with	

conventional steel and ECR, with cracks (ECR with 16 holes through the epoxy).....	174
Figure 3.48b – Field Test. Average corrosion rates for specimens with conventional steel and ECR, with cracks (ECR with 16 holes through the epoxy). (Different scale).....	175
Figure 3.49 –Field Test. Average corrosion rates for specimens with ECR, with cracks. * Based on exposed area (ECR with 16 holes through the epoxy).....	175
Figure 3.50a – Field Test. Average corrosion losses for specimens with conventional steel and ECR, with cracks (ECR with 16 holes through the epoxy).....	177
Figure 3.50b – Field Test. Average corrosion losses for specimens with conventional steel and ECR, with cracks (ECR with 16 holes through the epoxy). (Different scale).....	177
Figure 3.51 – Field Test. Average corrosion losses for specimens with conventional steel and ECR, with cracks. * Based on exposed area (ECR with 16 holes through the epoxy).....	178
Figure 3.52a – Field Test. Average top mat corrosion potentials with respect to a copper-copper sulfate electrode for specimens with conventional steel and ECR, with cracks (ECR with 16 holes through the epoxy).....	178
Figure 3.52b – Field Test. Average bottom mat corrosion potentials with respect to a copper-copper sulfate electrode for specimens with conventional steel and ECR, with cracks (ECR with 16 holes through the epoxy).....	179
Figure 3.53a – Field Test. Average mat-to-mat resistances for specimens with conventional steel and ECR, with cracks (ECR with 16 holes through the epoxy).....	180
Figure 3.53b – Field Test. Average mat-to-mat resistances for specimens with conventional steel and ECR, with cracks (ECR with 16 holes through the epoxy). (Different scale).....	180
Figure 3.54a – Field Test. Average corrosion rates for specimens with ECR, ECR with a primer containing calcium nitrite, and ECR with corrosion inhibitors in concrete, without cracks, specimen No. 1. (ECR with 16 holes through the epoxy).....	182
Figure 3.54b – Field Test. Average corrosion rates for specimens with ECR,	

ECR with a primer containing calcium nitrite, and ECR with corrosion inhibitors in concrete, without cracks, specimen No. 2 and 3. (ECR with 16 holes through the epoxy)..... 183

Figure 3.55a – Field Test. Average corrosion rates for specimens with ECR, ECR with a primer containing calcium nitrite, and ECR with corrosion inhibitors in concrete, without cracks, specimen No. 1. * Based on exposed area (ECR with 16 holes through the epoxy)..... 183

Figure 3.55b – Field Test. Average corrosion rates for specimens with ECR, ECR with a primer containing calcium nitrite, and ECR with corrosion inhibitors in concrete, without cracks, specimen No. 2 and 3. * Based on exposed area (ECR with 16 holes through the epoxy)..... 184

Figure 3.56 – Field Test. Average corrosion losses for specimens with ECR, ECR with a primer containing calcium nitrite, and ECR with corrosion inhibitors in concrete, without cracks (ECR with 16 holes through the epoxy) 185

Figure 3.57 – Field Test. Average corrosion losses for specimens with ECR, ECR with a primer containing calcium nitrite, and ECR with corrosion inhibitors in concrete, without cracks. * Based on exposed area (ECR with 16 holes through the epoxy)..... 186

Figure 3.58a – Field Test. Average top mat corrosion potentials with respect to a copper-copper sulfate electrode for specimens with ECR, ECR with a primer containing calcium nitrite, and ECR with corrosion inhibitors in concrete, without cracks, specimen No. 1. (ECR with 16 holes through the epoxy)..... 187

Figure 3.58b – Field Test. Average top mat corrosion potentials with respect to a copper-copper sulfate electrode for specimens with ECR, ECR with a primer containing calcium nitrite, and ECR with corrosion inhibitors in concrete, without cracks, specimen No. 2 and 3. (ECR with 16 holes through the epoxy) 187

Figure 3.58c – Field Test. Average bottom mat corrosion potentials with respect to a copper-copper sulfate electrode for specimens with ECR, ECR with a primer containing calcium nitrite, and ECR with corrosion inhibitors in concrete, without cracks, specimen No. 1. (ECR with 16 holes through the epoxy)..... 188

Figure 3.58d – Field Test. Average bottom mat corrosion potentials with respect to a copper-copper sulfate electrode for specimens with ECR, ECR with a primer containing calcium nitrite, and ECR with corrosion inhibitors

in concrete, without cracks, specimen No. 2 and 3. (ECR with 16 holes through the epoxy) 188

Figure 3.59 – Field Test. Average mat-to-mat resistances for specimens with ECR, ECR with a primer containing calcium nitrite, and ECR with corrosion inhibitors in concrete, without cracks (ECR with 16 holes through the epoxy)..... 189

Figure 3.60a – Field Test. Average corrosion rates for specimens with ECR, ECR with a primer containing calcium nitrite, and ECR with corrosion inhibitors in concrete, with cracks, specimen No. 1. (ECR with 16 holes through the epoxy) 190

Figure 3.60b – Field Test. Average corrosion rates for specimens with ECR, ECR with a primer containing calcium nitrite, and ECR with corrosion inhibitors in concrete, with cracks, specimen No. 2 and 3. (ECR with 16 holes through the epoxy)..... 191

Figure 3.61a – Field Test. Average corrosion rates for specimens with ECR, ECR with a primer containing calcium nitrite, and ECR with corrosion inhibitors in concrete, with cracks, specimen No. 1. * Based on exposed area (ECR with 16 holes through the epoxy) 191

Figure 3.61b – Field Test. Average corrosion rates for specimens with ECR, ECR with a primer containing calcium nitrite, and ECR with corrosion inhibitors in concrete, with cracks, specimen No. 2 and 3. * Based on exposed area (ECR with 16 holes through the epoxy)..... 192

Figure 3.62 – Field Test. Average corrosion losses for specimens with ECR, ECR with a primer containing calcium nitrite, and ECR with corrosion inhibitors in concrete, with cracks (ECR with 16 holes through the epoxy) 193

Figure 3.63 – Field Test. Average corrosion losses for specimens with ECR, ECR with a primer containing calcium nitrite, and ECR with corrosion inhibitors in concrete, with cracks. * Based on exposed area (ECR with 16 holes through the epoxy)..... 193

Figure 3.64a – Field Test. Average top mat corrosion potentials with respect to a copper-copper sulfate electrode for specimens with ECR, ECR with a primer containing calcium nitrite, and ECR with corrosion inhibitors in concrete, with cracks, specimen No. 1. (ECR with 16 holes through the epoxy)..... 195

Figure 3.64b – Field Test. Average top mat corrosion potentials with

respect to a copper-copper sulfate electrode for specimens with ECR, ECR with a primer containing calcium nitrite, and ECR with corrosion inhibitors in concrete, with cracks, specimen No. 2 and 3. (ECR with 16 holes through the epoxy).....	196
Figure 3.64c – Field Test. Average bottom mat corrosion potentials with respect to a copper-copper sulfate electrode for specimens with ECR, ECR with a primer containing calcium nitrite, and ECR with corrosion inhibitors in concrete, with cracks, specimen No. 1. (ECR with 16 holes through the epoxy).....	196
Figure 3.64d – Field Test. Average bottom mat corrosion potentials with respect to a copper-copper sulfate electrode for specimens with ECR, ECR with a primer containing calcium nitrite, and ECR with corrosion inhibitors in concrete, with cracks, specimen No. 2 and 3. (ECR with 16 holes through the epoxy).....	197
Figure 3.65 – Field Test. Average mat-to-mat resistances for specimens with ECR, ECR with a primer containing calcium nitrite, and ECR with corrosion inhibitors in concrete, with cracks (ECR with 16 holes through the epoxy).....	197
Figure 3.66 – Field Test. Average corrosion rates for specimens with ECR and multiple-coated bars, without cracks (ECR with 16 holes through the coating).....	200
Figure 3.67 – Field Test. Average corrosion rates for specimens with ECR and multiple-coated bars, without cracks. * Based on exposed area (ECR with 16 holes through the coating).....	200
Figure 3.68 – Field Test. Average corrosion losses for specimens with ECR and multiple-coated bars, without cracks (ECR with 16 holes through the coating).....	201
Figure 3.69 – Field Test. Average corrosion losses for specimens with ECR and multiple-coated bars, without cracks. * Based on exposed area (ECR with 16 holes through the coating).....	201
Figure 3.70a – Field Test. Average top mat corrosion potentials with respect to a copper-copper sulfate electrode for specimens with ECR and multiple-coated bars, without cracks (ECR with 16 holes through the coating).....	203
Figure 3.70b – Field Test. Average bottom mat corrosion potentials with respect to a copper-copper sulfate electrode for specimens with ECR and	

multiple-coated bars, without cracks (ECR with 16 holes through the coating).....	203
Figure 3.71 – Field Test. Average mat-to-mat resistances for specimens with ECR and multiple-coated bars, without cracks (ECR with 16 holes through the coating)	204
Figure 3.72 – Field Test. Average corrosion rates for specimens with ECR and multiple-coated bars, with cracks (ECR with 16 holes through the coating).....	205
Figure 3.73 – Field Test. Average corrosion rates for specimens with ECR and multiple-coated bars, with cracks. * Based on exposed area (ECR with 16 holes through the coating).....	205
Figure 3.74 – Field Test. Average corrosion losses for specimens with ECR and multiple-coated bars, with cracks (ECR with 16 holes through the coating).....	206
Figure 3.75 – Field Test. Average corrosion losses for specimens with ECR and multiple-coated bars, with cracks. * Based on exposed area (ECR with 16 holes through the coating).....	207
Figure 3.76a – Field Test. Average top mat corrosion potentials with respect to a copper-copper sulfate electrode for specimens with ECR and multiple-coated bars, with cracks (ECR with 16 holes through the coating)	208
Figure 3.76b – Field Test. Average bottom mat corrosion potentials with respect to a copper-copper sulfate electrode for specimens with ECR and multiple-coated bars, with cracks (ECR with 16 holes through the coating)	209
Figure 3.77 – Field Test. Average mat-to-mat resistances for specimens with ECR and multiple-coated bars, with cracks (ECR with 16 holes through the coating).....	209
Figure 3.78 – Field Test. Average corrosion rates for specimens with ECR and ECR with increased adhesion, without cracks (ECR with 16 holes through the epoxy)	211
Figure 3.79 – Field Test. Average corrosion rates for specimens with ECR and ECR with increased adhesion, without cracks. * Based on exposed area (ECR with 16 holes through the epoxy)	211
Figure 3.80 – Field Test. Average corrosion losses for specimens with ECR and ECR with increased adhesion, without cracks (ECR with 16 holes	

through the epoxy)	213
Figure 3.81 – Field Test. Average corrosion losses for specimens with ECR and ECR with increased adhesion, without cracks. * Based on exposed area (ECR with 16 holes through the epoxy)	213
Figure 3.82a – Field Test. Average top mat corrosion potentials with respect to a copper-copper sulfate electrode for specimens with ECR and ECR with increased adhesion, without cracks (ECR with 16 holes through the epoxy).....	215
Figure 3.82b – Field Test. Average bottom mat corrosion potentials with respect to a copper-copper sulfate electrode for specimens with ECR and ECR with increased adhesion, without cracks (ECR with 16 holes through the epoxy).....	215
Figure 3.83 – Field Test. Average mat-to-mat resistances for specimens with ECR and ECR with increased adhesion, without cracks (ECR with 16 holes through the epoxy).....	216
Figure 3.84 – Field Test. Average corrosion rates for specimens with ECR and ECR with increased adhesion, with cracks (ECR with 16 holes through the epoxy).....	217
Figure 3.85 – Field Test. Average corrosion rates for specimens with ECR and ECR with increased adhesion, with cracks. * Based on exposed area (ECR with 16 holes through the epoxy)	217
Figure 3.86 – Field Test. Average corrosion losses for specimens with ECR and ECR with increased adhesion, with cracks (ECR with 16 holes through the epoxy).....	219
Figure 3.87 – Field Test. Average corrosion losses for specimens with ECR and ECR with increased adhesion, with cracks. * Based on exposed area (ECR with 16 holes through the epoxy)	219
Figure 3.88a – Field Test. Average top mat corrosion potentials with respect to a copper-copper sulfate electrode for specimens with ECR and ECR with increased adhesion, with cracks (ECR with 16 holes through the epoxy).....	221
Figure 3.88b – Field Test. Average bottom mat corrosion potentials with respect to a copper-copper sulfate electrode for specimens with ECR and ECR with increased adhesion, with cracks (ECR with 16 holes through the	

epoxy).....	221
Figure 3.89 – Field Test. Average mat-to-mat resistances for specimens with ECR and ECR with increased adhesion, with cracks (ECR with 16 holes through the epoxy).....	222
Figure 3.90 – Field test specimen Conv. (1) at week 205, showing cracking, spalling, and heavy staining on portions of the surface	224
Figure 3.91 – Field test specimen ECR(DCI) (1) with simulated cracks at week 179, showing light staining on the surface	224
Figure 3.92 – Field test specimen ECR(Hycrete) (2) with simulated cracks at week 169, showing scaling on the surface	225
Figure 3.93 – Field test specimen ECR (1) at week 205, showing no cracking or staining of the surface	225
Figure 3.94 – Southern Exposure Test. Average corrosion rates for specimens with pickled 2205 stainless steel for the DCB and MCB.....	229
Figure 3.95 – Southern Exposure Test. Southern Exposure Test. Average corrosion losses for specimens with pickled 2205 stainless steel for the DCB and MCB.....	230
Figure 3.96a – Southern Exposure Test. Average top mat corrosion potentials with respect to a copper-copper sulfate electrode for specimens with pickled 2205 stainless steel for the DCB and MCB	231
Figure 3.96b – Southern Exposure Test. Average bottom mat corrosion potentials with respect to a copper-copper sulfate electrode for specimens with pickled 2205 stainless steel for the DCB and MCB	232
Figure 3.97 – Southern Exposure Test. Average mat-to-mat resistances for specimens with pickled 2205 stainless steel for the DCB and MCB.....	232
Figure 3.98 – Cracked Beam Test. Average corrosion rates for specimens with pickled 2205 stainless steel for the DCB and MCB	234
Figure 3.99 – Cracked Beam Test. Average corrosion losses for specimens with pickled 2205 stainless steel for the DCB and MCB	234
Figure 3.100a – Cracked Beam Test. Average top mat corrosion potentials with respect to a copper-copper sulfate electrode for specimens with pickled	

2205 stainless steel for the DCB and MCB	235
Figure 3.100b – Cracked Beam Test. Average bottom mat corrosion potentials with respect to a copper-copper sulfate electrode for specimens with pickled 2205 stainless steel for the DCB and MCB	236
Figure 3.101 – Cracked Beam Test. Average mat-to-mat resistances for specimens with pickled 2205 stainless steel for the DCB and MCB.....	237
Figure 3.102a – Field Test. Average corrosion rates for specimens with conventional steel, pickled 2205 stainless steel, and ECR for the Doniphan County Bridge.....	239
Figure 3.102b – Field Test. Average corrosion rates for specimens with conventional steel, pickled 2205 stainless steel, and ECR for the Doniphan County Bridge. (Different scale).....	239
Figure 3.103a – Field Test. Average corrosion losses for specimens with conventional steel, pickled 2205 stainless steel, and ECR for the Doniphan County Bridge.....	241
Figure 3.103b – Field Test. Average corrosion losses for specimens with conventional steel, pickled 2205 stainless steel, and ECR for the Doniphan County Bridge. (Different scale).....	241
Figure 3.104a – Field Test. Average top mat corrosion potentials with respect to a copper-copper sulfate electrode for specimens with conventional steel, pickled 2205 stainless steel, and ECR for the Doniphan County Bridge	242
Figure 3.104b – Field Test. Average bottom mat corrosion potentials with respect to a copper-copper sulfate electrode for specimens with conventional steel, pickled 2205 stainless steel, and ECR for the Doniphan County Bridge	242
Figure 3.105a – Field Test. Average mat-to-mat resistances for specimens with conventional steel, pickled 2205 stainless steel, and ECR for the Doniphan County Bridge	244
Figure 3.105b – Field Test. Average mat-to-mat resistances for specimens with conventional steel, pickled 2205 stainless steel, and ECR for the Doniphan County Bridge. (Different scale).....	244
Figure 3.106a – Field Test. Average corrosion rates for specimens with conventional steel, pickled 2205 stainless steel, and ECR for the Mission Creek Bridge	245

Figure 3.106b – Field Test. Average corrosion rates for specimens with conventional steel, pickled 2205 stainless steel, and ECR for the Mission Creek Bridge. (Different scale).....	245
Figure 3.107a – Field Test. Average corrosion losses for specimens with conventional steel, pickled 2205 stainless steel, and ECR for the Mission Creek Bridge	246
Figure 3.107b – Field Test. Average corrosion losses for specimens with conventional steel, pickled 2205 stainless steel, and ECR for the Mission Creek Bridge. (Different scale).....	247
Figure 3.108a – Field Test. Average top mat corrosion potentials with respect to a copper-copper sulfate electrode for specimens with conventional steel, pickled 2205 stainless steel, and ECR for the Mission Creek Bridge	249
Figure 3.108b – Field Test. Average bottom mat corrosion potentials with respect to a copper-copper sulfate electrode for specimens with conventional steel, pickled 2205 stainless steel, and ECR for the Mission Creek Bridge	249
Figure 3.109a – Field Test. Average mat-to-mat resistances for specimens with conventional steel, pickled 2205 stainless steel, and ECR for the Mission Creek Bridge	250
Figure 3.109b – Field Test. Average mat-to-mat resistances for specimens with conventional steel, pickled 2205 stainless steel, and ECR for the Mission Creek Bridge. (Different scale).....	250
Figure 3.110 – Corrosion potential map for the Doniphan County Bridge (1 st survey, September 17, 2004)	252
Figure 3.111 – Corrosion potential map for the Doniphan County Bridge (5 th survey, October 9, 2006)	253
Figure 3.112 – Corrosion potential map for the Doniphan County Bridge (8 th survey, April 11, 2008).....	254
Figure 3.113 – Corrosion potential map for the Mission Creek Bridge (1 st survey, September 1, 2004)	255
Figure 3.114 – Corrosion potential map for the Mission Creek Bridge (5 th survey, October 16, 2006).....	255
Figure 3.115 – Corrosion potential map for the Mission Creek Bridge (8 th	

survey, April 7, 2008)	256
Figure 3.116 – Reinforcing bar cages at the east abutment for the Mission Creek Bridge, showing mild steel form ties used in the bridge decks	257
Figure 3.117a – Microcell corrosion rates from LPR method for specimens with conventional steel and ECR in the Southern Exposure test (ECR have four holes through the epoxy)	261
Figure 3.117b – Microcell corrosion rates from LPR method for specimens with conventional steel and ECR in the Southern Exposure test (ECR have four holes through the epoxy). (Different scale).....	261
Figure 3.118a – Microcell corrosion losses from LPR method for the top mats in specimens with conventional steel and ECR in the Southern Exposure test (ECR with four holes through the epoxy)	262
Figure 3.118b – Microcell corrosion losses from LPR method for the top mats in specimens with conventional steel and ECR in the Southern Exposure test (ECR with four holes through the epoxy). (Different scale).....	262
Figure 3.119 – Microcell corrosion rates from LPR method for specimens with conventional steel and different inhibitors in the Southern Exposure test.....	263
Figure 3.120 – Microcell corrosion losses from LPR method for the top mats in specimens with conventional steel and different inhibitors in the Southern Exposure test	264
Figure 3.121 – Microcell corrosion rates from LPR method for specimens with conventional steel and different inhibitors in the cracked beam test.....	266
Figure 3.122 – Microcell corrosion losses from LPR method for the top mats in specimens with conventional steel and different inhibitors in the cracked beam test.....	266
Figure 3.123a – Microcell corrosion rates from LPR method for specimens with conventional steel, ECR, and multiple-coated bars in the ASTM G109 test (ECR have four and ten holes through the epoxy)	268
Figure 3.123b – Microcell corrosion rates from LPR method for specimens with conventional steel, ECR, and multiple-coated bars in the ASTM G109 test (ECR have four and ten holes through the epoxy). (Different scale).....	268

Figure 3.124a – Microcell corrosion losses from LPR method for the top mats in specimens with conventional steel, ECR, and multiple-coated bars in the ASTM G109 test (ECR have four and ten holes through the epoxy).	270
Figure 3.124b – Microcell corrosion losses from LPR method for the top mats in specimens with conventional steel, ECR, and multiple-coated bars in the ASTM G109 test (ECR have four and ten holes through the epoxy). (Different scale)	270
Figure 3.125 – Southern Exposure Test. Microcell versus macrocell corrosion losses for specimens with conventional steel and ECR with different inhibitors, results based on total area for conventional steel and exposed area for ECR, with average values for specimens with four and ten holes.....	277
Figure 3.126 – Cracked Beam Test. Microcell versus macrocell corrosion losses for specimens with conventional steel and ECR with different inhibitors, results based on total area for conventional steel and exposed area for ECR, with average values for specimens with four and ten holes	277
Figure 3.127 – Comparison of the ranges of chloride sample values at corrosion initiation for conventional steel without inhibitors and with DCI, Hycrete, and Rheocrete inhibitor	287
Figure 3.128 – Initiation Beam Test. Conventional steel in the top mat (B-N4-Hycrete-45N-3) showing slight corrosion	287
Figure 3.129 – Initiation Beam Test. Conventional steel in the top mat (B-N4-Rheocrete-45N-4) showing severe corrosion	287
Figure 3.130 – Initiation Beam Test. Conventional steel in the bottom mat (B-N4-Rheocrete-45N-2) showing slight corrosion	288
Figure 3.131 – Corrosion rates for specimens with zinc-coated reinforcing steel in initiation beam test	289
Figure 3.132a – Top bar corrosion potential with respect to a copper-copper sulfate electrode for specimens with zinc-coated reinforcing steel in initiation beam test.....	289
Figure 3.132b – Bottom bar corrosion potential with respect to a copper-copper sulfate electrode for specimens with zinc-coated reinforcing steel in initiation beam test.....	290

Figure 3.133 – Mat-to-mat resistance for specimens with zinc-coated reinforcing steel in initiation beam test.....	290
Figure 3.134 – Comparison of the ranges of chloride sample values at corrosion initiation for zinc-coated (Zinc), conventional (Conv.), and MMFX reinforcement.....	295
Figure 3.135 – Initiation Beam Test. (a) Top bar (top) and bottom bars (bottom) for specimens with zinc-coated reinforcement after autopsy (B-Zn-45N-8). (b) Corrosion product on top bar, showing large white crystalline corrosion products.....	297
Figure 3.136 – Initiation Beam Test. (a) Top bar (top) and bottom bars (bottom) for specimens with zinc-coated reinforcement after autopsy (B-Zn-45N-3). (b) Corrosion product on top bar showing exposure of underlying steel.....	298
Figure 3.137 – Initiation Beam Test. Zinc-coated reinforcement after autopsy (B-Zn-45N-11) showing corrosion on top bar (top) and bottom bars (bottom).....	298
Figure 3.138 – Initiation Beam Test. Zinc-coated reinforcement after autopsy (B-Zn-45N-4) showing corrosion on the bottom bar exposing underlying steel.....	299
Figure 3.139 – Typical corrosion at initiation on conventional steel.....	299
Figure 3.140 – Initiation Beam Test. Specimen with zinc-coated reinforcement after autopsy (B-Zn-45N-10) showing visible interior staining of the concrete.....	300
Figure 3.141 – Initiation Beam Test. Specimen with zinc-coated reinforcement after autopsy (B-Zn-45N-2) showing increased porosity of concrete below the bar relative to the concrete above the bar. (a) Above and (b) Below the bar	301
Figure 3.142 – Initiation Beam Test. Specimen with zinc-coated reinforcement after autopsy (B-Zn-45N-2, another bar) showing increased porosity of concrete below the bar relative to the concrete above the bar. (a) Above and (b) Below the bar	302
Figure 3.143 – Initiation Beam Test. Specimen with conventional reinforcement after autopsy showing increased porosity of concrete below the bar relative to the concrete above the bar. (a) Above and (b) Below the	

bar.....	303
Figure 4.1 – (a) Comparison of average corrosion rates and (b) corrosion losses for the Southern Exposure test (at 42 weeks) versus the rapid macrocell test with mortar-wrapped specimens with a w/c of 0.35 (at 15 weeks).....	318
Figure 4.2 – (a) Comparison of average corrosion rates and (b) corrosion losses for the cracked beam test (at 42 weeks) versus the rapid macrocell test with mortar-wrapped specimens with a w/c of 0.35 (at 15 weeks).....	320
Figure 4.3 – (a) Comparison of average corrosion rates and (b) corrosion losses for the cracked beam test (at 42 weeks) versus the Southern Exposure test (at 42 weeks)	321
Figure 4.4 – Chloride content taken at cracks interpolated at a depth of 76.2 mm (3 in.) versus placement age for bridges with an AADT greater than 7500.....	326
Figure A.1 – Macrocell Test. (a) Corrosion rates and (b) total corrosion losses for specimens with conventional steel and no inhibitors, $w/c=0.45$	367
Figure A.2 – Macrocell Test. (a) Anode corrosion potentials and (b) cathode corrosion potentials with respect to a saturated calomel electrode for specimens with conventional steel and no inhibitors, $w/c=0.45$	367
Figure A.3 – Macrocell Test. (a) Corrosion rates and (b) total corrosion losses for specimens with conventional steel and DCI inhibitor, $w/c=0.45$	368
Figure A.4 – Macrocell Test. (a) Anode corrosion potentials and (b) cathode corrosion potentials with respect to a saturated calomel electrode for specimens with conventional steel and DCI inhibitor, $w/c=0.45$	368
Figure A.5 – Macrocell Test. (a) Corrosion rates and (b) total corrosion losses for specimens with conventional steel and Hycrete inhibitor, $w/c=0.45$	369
Figure A.6 – Macrocell Test. (a) Anode corrosion potentials and (b) cathode corrosion potentials with respect to a saturated calomel electrode for specimens with conventional steel and Hycrete inhibitor, $w/c=0.45$	369
Figure A.7 – Macrocell Test. (a) Corrosion rates and (b) total corrosion losses for specimens with conventional steel and Rheocrete inhibitor, $w/c=0.45$	370

Figure A.8 – Macrocell Test. (a) Anode corrosion potentials and (b) cathode corrosion potentials with respect to a saturated calomel electrode for specimens with conventional steel and Rheocrete inhibitor, $w/c=0.45$	370
Figure A.9 – Macrocell Test. (a) Corrosion rates and (b) total corrosion losses for specimens with conventional steel and no inhibitors, $w/c=0.35$	371
Figure A.10 – Macrocell Test. (a) Anode corrosion potentials and (b) cathode corrosion potentials with respect to a saturated calomel electrode for specimens with conventional steel and no inhibitors, $w/c=0.35$	371
Figure A.11 – Macrocell Test. (a) Corrosion rates and (b) total corrosion losses for specimens with conventional steel and DCI inhibitor, $w/c=0.35$	372
Figure A.12 – Macrocell Test. (a) Anode corrosion potentials and (b) cathode corrosion potentials with respect to a saturated calomel electrode for specimens with conventional steel and DCI inhibitor, $w/c=0.35$	372
Figure A.13 – Macrocell Test. (a) Corrosion rates and (b) total corrosion losses for specimens with conventional steel and Hycrete inhibitor, $w/c=0.35$	373
Figure A.14 – Macrocell Test. (a) Anode corrosion potentials and (b) cathode corrosion potentials with respect to a saturated calomel electrode for specimens with conventional steel and Hycrete inhibitor, $w/c=0.35$	373
Figure A.15 – Macrocell Test. (a) Corrosion rates and (b) total corrosion losses for specimens with conventional steel and Rheocrete inhibitor, $w/c=0.35$	374
Figure A.16 – Macrocell Test. (a) Anode corrosion potentials and (b) cathode corrosion potentials with respect to a saturated calomel electrode for specimens with conventional steel and Rheocrete inhibitor, $w/c=0.35$	374
Figure A.17 – Southern Exposure Test. (a) Corrosion rates and (b) total corrosion losses for specimens with conventional steel (controls).....	375
Figure A.18 – Southern Exposure Test. (a) Top mat corrosion potentials and (b) bottom mat corrosion potentials with respect to a copper-copper sulfate electrode for specimens with conventional steel (controls).....	375
Figure A.19 – Southern Exposure Test. (a) Corrosion rates and (b) total corrosion losses for specimens with ECR (four holes).....	376

Figure A.20 – Southern Exposure Test. (a) Top mat corrosion potentials and (b) bottom mat corrosion potentials with respect to a copper-copper sulfate electrode for specimens with ECR (four holes).....	376
Figure A.21 – Southern Exposure Test. (a) Corrosion rates and (b) total corrosion losses for specimens with conventional steel and no inhibitor.....	377
Figure A.22 – Southern Exposure Test. (a) Top mat corrosion potentials and (b) bottom mat corrosion potentials with respect to a copper-copper sulfate electrode for specimens with conventional steel and no inhibitor.....	377
Figure A.23 – Cracked Beam Test. (a) Corrosion rates and (b) total corrosion losses for specimens with conventional steel and no inhibitor.....	378
Figure A.24 – Cracked Beam Test. (a) Top mat corrosion potentials and (b) bottom mat corrosion potentials with respect to a copper-copper sulfate electrode for specimens with conventional steel and no inhibitor.....	378
Figure A.25 – Southern Exposure Test. (a) Corrosion rates and (b) total corrosion losses for specimens with conventional steel and DCI inhibitor.....	379
Figure A.26 – Southern Exposure Test. (a) Top mat corrosion potentials and (b) bottom mat corrosion potentials with respect to a copper-copper sulfate electrode for specimens with conventional steel and DCI inhibitor.....	379
Figure A.27 – Cracked Beam Test. (a) Corrosion rates and (b) total corrosion losses for specimens with conventional steel and DCI inhibitor.....	380
Figure A.28 – Cracked Beam Test. (a) Top mat corrosion potentials and (b) bottom mat corrosion potentials with respect to a copper-copper sulfate electrode for specimens with conventional steel and DCI inhibitor.....	380
Figure A.29 – Southern Exposure Test. (a) Corrosion rates and (b) total corrosion losses for specimens with conventional steel and Hycrete inhibitor.....	381
Figure A.30 – Southern Exposure Test. (a) Top mat corrosion potentials and (b) bottom mat corrosion potentials with respect to a copper-copper sulfate electrode for specimens with conventional steel and Hycrete inhibitor.....	381
Figure A.31 – Cracked Beam Test. (a) Corrosion rates and (b) total corrosion losses for specimens with conventional steel and Hycrete inhibitor.....	382
Figure A.32 – Cracked Beam Test. (a) Top mat corrosion potentials and (b) bottom mat corrosion potentials with respect to a copper-copper sulfate	

electrode for specimens with conventional steel and Hycrete inhibitor	382
Figure A.33 – Southern Exposure Test. (a) Corrosion rates and (b) total corrosion losses for specimens with conventional steel and Rheocrete inhibitor.....	383
Figure A.34 – Southern Exposure Test. (a) Top mat corrosion potentials and (b) bottom mat corrosion potentials with respect to a copper-copper sulfate electrode for specimens with conventional steel and Rheocrete inhibitor.....	383
Figure A.35 – Cracked Beam Test. (a) Corrosion rates and (b) total corrosion losses for specimens with conventional steel and Rheocrete inhibitor.....	384
Figure A.36 – Cracked Beam Test. (a) Top mat corrosion potentials and (b) bottom mat corrosion potentials with respect to a copper-copper sulfate electrode for specimens with conventional steel and Rheocrete inhibitor.....	384
Figure A.37 – ASTM G109 Test. (a) Corrosion rates and (b) total corrosion losses for specimens with conventional steel.....	385
Figure A.38 – ASTM G109 Test. (a) Top mat corrosion potentials and (b) bottom mat corrosion potentials with respect to a copper-copper sulfate electrode for specimens with conventional steel	385
Figure A.39 – ASTM G109 Test. (a) Corrosion rates and (b) total corrosion losses for specimens with ECR (four holes).....	386
Figure A.40 – ASTM G109 Test. (a) Top mat corrosion potentials and (b) bottom mat corrosion potentials with respect to a copper-copper sulfate electrode for specimens with ECR (four holes).....	386
Figure A.41 – ASTM G109 Test. (a) Corrosion rates and (b) total corrosion losses for specimens with ECR (ten holes).....	387
Figure A.42 – ASTM G109 Test. (a) Top mat corrosion potentials and (b) bottom mat corrosion potentials with respect to a copper-copper sulfate electrode for specimens with ECR (ten holes).....	387
Figure A.43 – ASTM G109 Test. (a) Corrosion rates and (b) total corrosion losses for specimens with multiple-coated bars (four holes, only epoxy penetrated)	388
Figure A.44 – ASTM G109 Test. (a) Top mat corrosion potentials and (b)	

bottom mat corrosion potentials with respect to a copper-copper sulfate electrode for specimens with multiple-coated bars (four holes, only epoxy penetrated)	388
Figure A.45 – ASTM G109 Test. (a) Corrosion rates and (b) total corrosion losses for specimens with multiple-coated bars (four holes, both layers penetrated)	389
Figure A.46 – ASTM G109 Test. (a) Top mat corrosion potentials and (b) bottom mat corrosion potentials with respect to a copper-copper sulfate electrode for specimens with multiple-coated bars (four holes, both layers penetrated).....	389
Figure A.47 – ASTM G109 Test. (a) Corrosion rates and (b) total corrosion losses for specimens with multiple-coated bars (ten holes, only epoxy penetrated)	390
Figure A.48 – ASTM G109 Test. (a) Top mat corrosion potentials and (b) bottom mat corrosion potentials with respect to a copper-copper sulfate electrode for specimens with multiple-coated bars (ten holes, only epoxy penetrated).....	390
Figure A.49 – ASTM G109 Test. (a) Corrosion rates and (b) total corrosion losses for specimens with multiple-coated bars (ten holes, both layers penetrated).....	391
Figure A.50 – ASTM G109 Test. (a) Top mat corrosion potentials and (b) bottom mat corrosion potentials with respect to a copper-copper sulfate electrode for specimens with multiple-coated bars (ten holes, both layers penetrated).....	391
Figure A.51 – Field Test. (a) Corrosion rates and (b) total corrosion losses for specimens with conventional steel, without crack.	392
Figure A.52 – Field Test. (a) Top mat corrosion potentials and (b) bottom mat corrosion potentials with respect to a copper-copper sulfate electrode for specimens with conventional steel, without cracks.....	392
Figure A.53 – Field Test. (a) Corrosion rates and (b) total corrosion losses for specimens with conventional steel, with cracks.....	393
Figure A.54 – Field Test. (a) Top mat corrosion potentials and (b) bottom mat corrosion potentials with respect to a copper-copper sulfate electrode for specimens with conventional steel, with cracks.....	393

Figure A.55 – Field Test. (a) Corrosion rates and (b) total corrosion losses for specimens with ECR, without cracks.....	394
Figure A.56 – Field Test. (a) Top mat corrosion potentials and (b) bottom mat corrosion potentials with respect to a copper-copper sulfate electrode for specimens with ECR, without cracks.....	394
Figure A.57 – Field Test. (a) Corrosion rates and (b) total corrosion losses for specimens with ECR, with cracks.....	395
Figure A.58 – Field Test. (a) Top mat corrosion potentials and (b) bottom mat corrosion potentials with respect to a copper-copper sulfate electrode for specimens with ECR, with cracks.....	395
Figure A.59 – Field Test. (a) Corrosion rates and (b) total corrosion losses for specimens with ECR with a primer containing calcium nitrite, without cracks.....	396
Figure A.60 – Field Test. (a) Top mat corrosion potentials and (b) bottom mat corrosion potentials with respect to a copper-copper sulfate electrode for specimens with ECR with a primer containing calcium nitrite, without cracks.....	396
Figure A.61 – Field Test. (a) Corrosion rates and (b) total corrosion losses for specimens with ECR with a primer containing calcium nitrite, with cracks.....	397
Figure A.62 – Field Test. (a) Top mat corrosion potentials and (b) bottom mat corrosion potentials with respect to a copper-copper sulfate electrode for specimens with ECR with a primer containing calcium nitrite, with cracks.....	397
Figure A.63 – Field Test. (a) Corrosion rates and (b) total corrosion losses for specimens with ECR and DCI inhibitor in concrete, without cracks.....	398
Figure A.64 – Field Test. (a) Top mat corrosion potentials and (b) bottom mat corrosion potentials with respect to a copper-copper sulfate electrode for specimens with ECR and DCI inhibitor in concrete, without cracks.....	398
Figure A.65 – Field Test. (a) Corrosion rates and (b) total corrosion losses for specimens with ECR and DCI inhibitor in concrete, with cracks.....	399
Figure A.66 – Field Test. (a) Top mat corrosion potentials and (b) bottom mat corrosion potentials with respect to a copper-copper sulfate electrode	

for specimens with ECR and DCI inhibitor in concrete, with cracks	399
Figure A.67 – Field Test. (a) Corrosion rates and (b) total corrosion losses for specimens with ECR and Rheocrete inhibitor in concrete, without cracks	400
Figure A.68 – Field Test. (a) Top mat corrosion potentials and (b) bottom mat corrosion potentials with respect to a copper-copper sulfate electrode for specimens with ECR and Rheocrete inhibitor in concrete, without cracks	400
Figure A.69 – Field Test. (a) Corrosion rates and (b) total corrosion losses for specimens with ECR and Rheocrete inhibitor in concrete, with cracks.....	401
Figure A.70 – Field Test. (a) Top mat corrosion potentials and (b) bottom mat corrosion potentials with respect to a copper-copper sulfate electrode for specimens with ECR and Rheocrete inhibitor in concrete, with cracks.....	401
Figure A.71 – Field Test. (a) Corrosion rates and (b) total corrosion losses for specimens with ECR and Hycrete inhibitor in concrete, without cracks	402
Figure A.72 – Field Test. (a) Top mat corrosion potentials and (b) bottom mat corrosion potentials with respect to a copper-copper sulfate electrode for specimens with ECR and Hycrete inhibitor in concrete, without cracks	402
Figure A.73 – Field Test. (a) Corrosion rates and (b) total corrosion losses for specimens with ECR and Hycrete inhibitor in concrete, with cracks	403
Figure A.74 – Field Test. (a) Top mat corrosion potentials and (b) bottom mat corrosion potentials with respect to a copper-copper sulfate electrode for specimens with ECR and Hycrete inhibitor in concrete, with cracks	403
Figure A.75 – Field Test. (a) Corrosion rates and (b) total corrosion losses for specimens with multiple-coated bars, without cracks	404
Figure A.76 – Field Test. (a) Top mat corrosion potentials and (b) bottom mat corrosion potentials with respect to a copper-copper sulfate electrode for specimens with multiple-coated bars, without cracks	404
Figure A.77 – Field Test. (a) Corrosion rates and (b) total corrosion losses for specimens with multiple-coated bars, with cracks	405
Figure A.78 – Field Test. (a) Top mat corrosion potentials and (b) bottom mat corrosion potentials with respect to a copper-copper sulfate electrode for specimens with multiple-coated bars, with cracks	405

Figure A.79 – Field Test. (a) Corrosion rates and (b) total corrosion losses for specimens with ECR with increased adhesion Valspar coating, without cracks..... 406

Figure A.80 – Field Test. (a) Top mat corrosion potentials and (b) bottom mat corrosion potentials with respect to a copper-copper sulfate electrode for specimens with ECR with increased adhesion Valspar coating, without cracks..... 406

Figure A.81 – Field Test. (a) Corrosion rates and (b) total corrosion losses for specimens with ECR with increased adhesion Valspar coating, with cracks..... 407

Figure A.82 – Field Test. (a) Top mat corrosion potentials and (b) bottom mat corrosion potentials with respect to a copper-copper sulfate electrode for specimens with ECR with increased adhesion Valspar coating, with cracks..... 407

Figure A.83 – Field Test. (a) Corrosion rates and (b) total corrosion losses for specimens with ECR with increased adhesion DuPont coating, without cracks..... 408

Figure A.84 – Field Test. (a) Top mat corrosion potentials and (b) bottom mat corrosion potentials with respect to a copper-copper sulfate electrode for specimens with ECR with increased adhesion DuPont coating, without cracks..... 408

Figure A.85 – Field Test. (a) Corrosion rates and (b) total corrosion losses for specimens with ECR with increased adhesion DuPont coating, with cracks..... 409

Figure A.86 – Field Test. (a) Top mat corrosion potentials and (b) bottom mat corrosion potentials with respect to a copper-copper sulfate electrode for specimens with ECR with increased adhesion DuPont coating, with cracks..... 409

Figure A.87 – Field Test. (a) Corrosion rates and (b) total corrosion losses for specimens with ECR with zinc chromate pretreatment, without cracks 410

Figure A.88 – Field Test. (a) Top mat corrosion potentials and (b) bottom mat corrosion potentials with respect to a copper-copper sulfate electrode for specimens with ECR with zinc chromate pretreatment, without cracks 410

Figure A.89 – Field Test. (a) Corrosion rates and (b) total corrosion losses

for specimens with ECR with zinc chromate pretreatment, with cracks	411
Figure A.90 – Field Test. (a) Top mat corrosion potentials and (b) bottom mat corrosion potentials with respect to a copper-copper sulfate electrode for specimens with ECR with zinc chromate pretreatment, with cracks	411
Figure A.91 – Southern Exposure Test. (a) Corrosion rates and (b) total corrosion losses for specimens with pickled 2205 stainless steel for the Doniphan County Bridge	412
Figure A.92 – Southern Exposure Test. (a) Top mat corrosion potentials and (b) bottom mat corrosion potentials with respect to a copper-copper sulfate electrode for specimens with pickled 2205 stainless steel for the Doniphan County Bridge	412
Figure A.93 – Cracked Beam Test. (a) Corrosion rates and (b) total corrosion losses for specimens with pickled 2205 stainless steel for the Doniphan County Bridge	413
Figure A.94 – Cracked Beam Test. (a) Top mat corrosion potentials and (b) bottom mat corrosion potentials with respect to a copper-copper sulfate electrode for specimens with pickled 2205 stainless steel for the Doniphan County Bridge	413
Figure A.95 – Southern Exposure Test. (a) Corrosion rates and (b) total corrosion losses for specimens with pickled 2205 stainless steel for the Mission Creek Bridge	414
Figure A.96 – Southern Exposure Test. (a) Top mat corrosion potentials and (b) bottom mat corrosion potentials with respect to a copper-copper sulfate electrode for specimens with pickled 2205 stainless steel for the Mission Creek Bridge	414
Figure A.97 – Cracked Beam Test. (a) Corrosion rates and (b) total corrosion losses for specimens with pickled 2205 stainless steel for the Mission Creek Bridge	415
Figure A.98 – Cracked Beam Test. (a) Top mat corrosion potentials and (b) bottom mat corrosion potentials with respect to a copper-copper sulfate electrode for specimens with pickled 2205 stainless steel for the Mission Creek Bridge	415
Figure A.99 – Field Test. (a) Corrosion rates and (b) total corrosion losses for specimens with conventional steel for the Doniphan County Bridge	

(without cracks) 416

Figure A.100 – Field Test. (a) Top mat corrosion potentials and (b) bottom mat corrosion potentials with respect to a copper-copper sulfate electrode for specimens with conventional steel for the Doniphan County Bridge (without cracks) 416

Figure A.101 – Field Test. (a) Corrosion rates and (b) total corrosion losses for specimens with pickled 2205 stainless steel for the Doniphan County Bridge (without cracks)..... 417

Figure A.102 – Field Test. (a) Top mat corrosion potentials and (b) bottom mat corrosion potentials with respect to a copper-copper sulfate electrode for specimens with pickled 2205 stainless steel for the Doniphan County Bridge (without cracks)..... 417

Figure A.103 – Field Test. (a) Corrosion rates and (b) total corrosion losses for specimens with ECR for the Doniphan County Bridge (without cracks) 418

Figure A.104 – Field Test. (a) Top mat corrosion potentials and (b) bottom mat corrosion potentials with respect to a copper-copper sulfate electrode for specimens with ECR for the Doniphan County Bridge (without cracks) 418

Figure A.105 – Field Test. (a) Corrosion rates and (b) total corrosion losses for specimens with conventional steel for the Mission Creek Bridge (No. 2 with cracks)..... 419

Figure A.106 – Field Test. (a) Top mat corrosion potentials and (b) bottom mat corrosion potentials with respect to a copper-copper sulfate electrode for specimens with conventional steel for the Mission Creek Bridge (No. 2 with cracks)..... 419

Figure A.107 – Field Test. (a) Corrosion rates and (b) total corrosion losses for specimens with pickled 2205 stainless steel for the Mission Creek Bridge (No. 2 with cracks)..... 420

Figure A.108 – Field Test. (a) Top mat corrosion potentials and (b) bottom mat corrosion potentials with respect to a copper-copper sulfate electrode for specimens with pickled 2205 stainless steel for the Mission Creek Bridge (No. 2 with cracks)..... 420

Figure A.109 – Field Test. (a) Corrosion rates and (b) total corrosion losses for specimens with ECR for the Mission Creek Bridge (No. 2 with cracks)..... 421

Figure A.110 – Field Test. (a) Top mat corrosion potentials and (b) bottom mat corrosion potentials with respect to a copper-copper sulfate electrode for specimens with ECR for the Mission Creek Bridge (No. 2 with cracks)..... 421

Figure B.1 – Southern Exposure Test. Mat-to-mat resistances for specimens with conventional steel (controls)..... 422

Figure B.2 – Southern Exposure Test. Mat-to-mat resistances for specimens with ECR (ECR with four holes)..... 422

Figure B.3 – Southern Exposure Test. Mat-to-mat resistances for specimens with conventional steel and no inhibitors 423

Figure B.4 – Cracked Beam Test. Mat-to-mat resistances for specimens with conventional steel and no inhibitors 423

Figure B.5 – Southern Exposure Test. Mat-to-mat resistances for specimens with conventional steel and DCI inhibitor 423

Figure B.6 – Cracked Beam Test. Mat-to-mat resistances for specimens with conventional steel and DCI inhibitor 423

Figure B.7 – Southern Exposure Test. Mat-to-mat resistances for specimens with conventional steel and Hycrete inhibitor 424

Figure B.8 – Cracked Beam Test. Mat-to-mat resistances for specimens with conventional steel and Hycrete inhibitor 424

Figure B.9 – Southern Exposure Test. Mat-to-mat resistances for specimens with conventional steel and Rheocrete inhibitor..... 424

Figure B.10 – Cracked Beam Test. Mat-to-mat resistances for specimens with conventional steel and Rheocrete inhibitor..... 424

Figure B.11 – ASTM G109 Test. Mat-to-mat resistances for specimens with conventional steel..... 425

Figure B.12 – ASTM G109 Test. Mat-to-mat resistances for specimens with ECR (four holes)..... 425

Figure B.13 – ASTM G109 Test. Mat-to-mat resistances for specimens with ECR (ten holes)..... 425

Figure B.14 – ASTM G109 Test. Mat-to-mat resistances for specimens with

multiple-coated bars (four holes, only epoxy penetrated)	426
Figure B.15 – ASTM G109 Test. Mat-to-mat resistances for specimens with multiple-coated bars (four holes, both layers penetrated).....	426
Figure B.16 – ASTM G109 Test. Mat-to-mat resistances for specimens with multiple-coated bars (ten holes, only epoxy penetrated)	426
Figure B.17 – ASTM G109 Test. Mat-to-mat resistances for specimens with multiple-coated bars (ten holes, both layers penetrated)	426
Figure B.18 – Field Test. Mat-to-mat resistances for specimens with conventional steel, without cracks	427
Figure B.19 – Field Test. Mat-to-mat resistances for specimens with conventional steel, with cracks	427
Figure B.20 – Field Test. Mat-to-mat resistances for specimens with ECR, without cracks	427
Figure B.21 – Field Test. Mat-to-mat resistances for specimens with ECR, with cracks.	427
Figure B.22 – Field Test. Mat-to-mat resistances for specimens with ECR with a primer containing calcium nitrite, without cracks	428
Figure B.23 – Field Test. Mat-to-mat resistances for specimens with ECR with a primer containing calcium nitrite, with cracks.....	428
Figure B.24 – Field Test. Mat-to-mat resistances for specimens with ECR and DCI inhibitor, without cracks.....	428
Figure B.25 – Field Test. Mat-to-mat resistances for specimens with ECR and DCI inhibitor, with cracks.....	428
Figure B.26 – Field Test. Mat-to-mat resistances for specimens with ECR and Rheocrete inhibitor, without cracks	429
Figure B.27 – Field Test. Mat-to-mat resistances for specimens with ECR and Rheocrete inhibitor, with cracks	429
Figure B.28 – Field Test. Mat-to-mat resistances for specimens with ECR and Hycrete inhibitor, without cracks	429

Figure B.29 – Field Test. Mat-to-mat resistances for specimens with ECR and Hycrete inhibitor, with cracks 429

Figure B.30 – Field Test. Mat-to-mat resistances for specimens with multiple-coated bars, without cracks 430

Figure B.31 – Field Test. Mat-to-mat resistances for specimens with multiple-coated bars, with cracks 430

Figure B.32 – Field Test. Mat-to-mat resistances for specimens with ECR with increased adhesion Valspar coating, without cracks 430

Figure B.33 – Field Test. Mat-to-mat resistances for specimens with ECR with increased adhesion Valspar coating, with cracks..... 430

Figure B.34 – Field Test. Mat-to-mat resistances for specimens with ECR with increased adhesion DuPont coating, without cracks..... 431

Figure B.35 – Field Test. Mat-to-mat resistances for specimens with ECR with increased adhesion DuPont coating, with cracks..... 431

Figure B.36 – Field Test. Mat-to-mat resistances for specimens with ECR with zinc chromate pretreatment, without cracks 431

Figure B.37 – Field Test. Mat-to-mat resistances for specimens with ECR with zinc chromate pretreatment, without cracks 431

Figure B.38 – Southern Exposure Test. Mat-to-mat resistances for specimens with pickled 2205 stainless steel for the Doniphan County Bridge 432

Figure B.39 – Cracked Beam Test. Mat-to-mat resistances for specimens with pickled 2205 stainless steel for the Doniphan County Bridge..... 432

Figure B.40 – Southern Exposure Test. Mat-to-mat resistances for specimens with pickled 2205 stainless steel for the Mission Creek Bridge 432

Figure B.41 – Cracked Beam Test. Mat-to-mat resistances for specimens with pickled 2205 stainless steel for the Mission Creek Bridge..... 432

Figure B.42 – Field Test. Mat-to-mat resistances for specimens with conventional steel for the Doniphan County Bridge..... 433

Figure B.43 – Field Test. Mat-to-mat resistances for specimens with pickled 2205 stainless steel for the Doniphan County Bridge..... 433

Figure B.44 – Field Test. Mat-to-mat resistances for specimens with ECR for the Doniphan County Bridge..... 433

Figure B.45 – Field Test. Mat-to-mat resistances for specimens with conventional steel for the Mission Creek Bridge..... 434

Figure B.46 – Field Test. Mat-to-mat resistances for specimens with pickled 2205 stainless steel for the Mission Creek Bridge..... 434

Figure B.47 – Field Test. Mat-to-mat resistances for specimens with ECR for the Mission Creek Bridge..... 434

Figure C.1 – Corrosion potential map for the Doniphan County Bridge (1st survey on September 17, 2004) 435

Figure C.2 – Corrosion potential map for the Doniphan County Bridge (2nd survey on April 26, 2005) 435

Figure C.3 – Corrosion potential map for the Doniphan County Bridge (3rd survey on October 14, 2005)..... 436

Figure C.4 – Corrosion potential map for the Doniphan County Bridge (4th survey on June 13, 2006) 436

Figure C.5 – Corrosion potential map for the Doniphan County Bridge (5th survey on October 9, 2006)..... 437

Figure C.6 – Corrosion Potential Mapping for the Doniphan County Bridge (6th survey on May 11, 2007)..... 437

Figure C.7 – Corrosion potential map for the Doniphan County Bridge (7th survey on October 12, 2007)..... 438

Figure C.8 – Corrosion potential map for the Doniphan County Bridge (8th survey on April 11, 2008) 438

Figure C.9 – Corrosion potential map for the Mission Creek Bridge (1st survey on September 1, 2004) 439

Figure C.10 – Corrosion potential map for the Mission Creek Bridge (2nd survey on April 1, 2005) 439

Figure C.11 – Corrosion potential map for the Mission Creek Bridge (3rd survey on September 27, 2005) 440

Figure C.12 – Corrosion potential map for the Mission Creek Bridge (4th survey on June 19, 2006) 440

Figure C.13 – Corrosion potential map for the Mission Creek Bridge (5th survey on October 16, 2006)..... 441

Figure C.14 – Corrosion potential map for the Mission Creek Bridge (6th survey on May 17, 2007) 441

Figure C.15 – Corrosion potential map for the Mission Creek Bridge (7th survey on October 10, 2007)..... 442

Figure C.16 – Corrosion potential map for the Mission Creek Bridge (8th survey on April 7, 2008) 442

Figure D.1 – LPR Test. (a) Corrosion rates, (b) total corrosion losses, and (c) corrosion potentials with respect to a copper-copper sulfate electrode for Southern Exposure specimens with conventional steel (controls)..... 443

Figure D.2 – LPR Test. (a) Corrosion rates, (b) total corrosion losses, and (c) corrosion potentials with respect to a copper-copper sulfate electrode for Southern Exposure specimens with ECR (four holes)..... 444

Figure D.3 – LPR Test. (a) Corrosion rates, (b) total corrosion losses, and (c) corrosion potentials with respect to a copper-copper sulfate electrode for Southern Exposure specimens with conventional steel and no inhibitor..... 445

Figure D.4 – LPR Test. (a) Corrosion rates, (b) total corrosion losses, and (c) corrosion potentials with respect to a copper-copper sulfate electrode for cracked beam specimens with conventional steel and no inhibitor 446

Figure D.5 – LPR Test. (a) Corrosion rates, (b) total corrosion losses, and (c) corrosion potentials with respect to a copper-copper sulfate electrode for Southern Exposure specimens with conventional steel and DCI inhibitor..... 447

Figure D.6 – LPR Test. (a) Corrosion rates, (b) total corrosion losses, and (c) corrosion potentials with respect to a copper-copper sulfate electrode for cracked beam specimens with conventional steel and DCI inhibitor 448

Figure D.7 – LPR Test. (a) Corrosion rates, (b) total corrosion losses, and (c) corrosion potentials with respect to a copper-copper sulfate electrode for Southern Exposure specimens with conventional steel and Hycrete inhibitor 449

Figure D.8 – LPR Test. (a) Corrosion rates, (b) total corrosion losses, and (c) corrosion potentials with respect to a copper-copper sulfate electrode for

cracked beam specimens with conventional steel and Hycrete inhibitor 450

Figure D.9 – LPR Test. (a) Corrosion rates, (b) total corrosion losses, and (c) corrosion potentials with respect to a copper-copper sulfate electrode for Southern Exposure specimens with conventional steel and Rheocrete inhibitor..... 451

Figure D.10 – LPR Test. (a) Corrosion rates, (b) total corrosion losses, and (c) corrosion potentials with respect to a copper-copper sulfate electrode for cracked beam specimens with conventional steel and Rheocrete inhibitor 452

Figure D.11 – LPR Test. (a) Corrosion rates, (b) total corrosion losses, and (c) corrosion potentials with respect to a copper-copper sulfate electrode for ASTM G109 specimens with conventional steel..... 453

Figure D.12 – LPR Test. (a) Corrosion rates, (b) total corrosion losses, and (c) corrosion potentials with respect to a copper-copper sulfate electrode for ASTM G109 specimens with ECR (four holes) 454

Figure D.13 – LPR Test. (a) Corrosion rates, (b) total corrosion losses, and (c) corrosion potentials with respect to a copper-copper sulfate electrode for ASTM G109 specimens with ECR (ten holes) 455

Figure D.14 – LPR Test. (a) Corrosion rates, (b) total corrosion losses, and (c) corrosion potentials with respect to a copper-copper sulfate electrode for ASTM G109 specimens with multiple-coated bars (four holes, only epoxy penetrated)..... 456

Figure D.15 – LPR Test. (a) Corrosion rates, (b) total corrosion losses, and (c) corrosion potentials with respect to a copper-copper sulfate electrode for ASTM G109 specimens with multiple-coated bars (four holes, both layers penetrated) 457

Figure D.16 – LPR Test. (a) Corrosion rates, (b) total corrosion losses, and (c) corrosion potentials with respect to a copper-copper sulfate electrode for ASTM G109 specimens with multiple-coated bars (ten holes, only epoxy penetrated) 458

Figure D.17 – LPR Test. (a) Corrosion rates, (b) total corrosion losses, and (c) corrosion potentials with respect to a copper-copper sulfate electrode for ASTM G109 specimens with multiple-coated bars (ten holes, both layers penetrated) 459

CHAPTER 1

INTRODUCTION

1.1 GENERAL INFORMATION

Concrete is the number-one man-made material. In 2006, there were about seven billion cubic meters of concrete produced. More than 55,000 miles of freeways and highways in America are made of concrete (Minerals website 2008). As a material, concrete is strong in compression and weak in tension. As a result, reinforcing steel must be added to provide tensile strength. Under certain conditions, however, reinforcing steel can corrode in concrete. In 2006, according to the U.S. Department of Transportation (DOT), one of every eight bridges in the nation was structurally deficient. More than \$65 billion could be invested immediately in a cost-effective way, by all levels of government, to replace or otherwise address existing bridge deficiencies (USDOT 2007).

The consequences of steel corrosion include the reduction of the steel cross section, possible loss of steel ductility, and reduced concrete-steel bond strength (Andrade and Alonso 2001). All of these can result in serviceability problems or even lead to structural failure. For prestressed concrete structures, this is especially true because prestressing steel is more susceptible than normal reinforcing steel to stress corrosion and hydrogen embrittlement in aggressive environments.

Corrosion of reinforcing steel in concrete bridge decks is typically caused by chloride contamination of the concrete. The main source of chlorides in bridge decks is deicing chemicals. During the winter months, many highway agencies use large quantities of salt-based deicing chemicals, the most common of which is sodium chloride. Due to its low price and efficiency in melting ice or snow, a large amount of

salt is used during wintertime. The lowest temperature at which sodium chloride melts ice is $-21.12\text{ }^{\circ}\text{C}$ ($-6.02\text{ }^{\circ}\text{F}$). More than 40% of dry salt produced in the United States is used for highway deicing (Minerals website 2008). Over the past half-century, more than a half-trillion tons of salt have been applied to keep North American highways safe from ice and snow during winter. The United States uses 13.6 to 18 million metric tons of deicing salt per year, while Canada uses 3.6 to 4.5 million metric tons (Salt Institute website 2008).

A variety of deicing salts are used; in addition to sodium chloride (NaCl), these include magnesium chloride (MgCl_2), calcium chloride (CaCl_2), potassium acetate ($\text{K O}_2\text{CCH}_3$), and calcium magnesium acetate (CMA). MgCl_2 and CaCl_2 are used individually or as part of mixtures when lower temperatures are anticipated. Because of the corrosive nature of sodium chloride, several states (e.g., Montana and Michigan) have decreased the quantity of NaCl and are in favor of MgCl_2 . The American Trucking Association Foundation, however, has reported a direct correlation between increased MgCl_2 use and a significant road concrete deterioration. This conclusion was also supported by Cody et al. (1996), who found that MgCl_2 could cause severe deterioration to concrete and was the most destructive deicing chemical, followed by CaCl_2 . Among the deicing chemicals, CMA does not cause corrosion of steel embedded in concrete (Callahan 1989, Martinez et al. 1990, Schwensen, Darwin, and Locke 1995, Ge et al. 2004), but Lee et al. (2000) and Ge et al. (2004) have observed that CMA aggressively attacks concrete. Lee et al. (2000) also found that magnesium acetate [$\text{Mg}(\text{O}_2\text{CCH}_3)_2$] produced similar damage to that caused by CMA and that NaCl was the least deleterious to concrete.

Many researchers use either weight percentage or the molar concentration of a deicer in solution (number of moles of solute dissolved in one liter of solution) to

interpret salt-induced corrosion (Cody et al. 1996, Lee et al. 2000). Actually, both cations (positive ions) and anions (negative ions) affect ice melting; therefore, using the total number of ions in solution is more reasonable when interpreting deicer capacities. Darwin et al. (2007) used the total number of ions in a given quantity of water, instead of the weight percentage or molar concentration in their research. After studying concrete properties at different levels of deicer exposure, they concluded that CaCl_2 , MgCl_2 , and CMA will cause significantly more damage to concrete than NaCl .

Salt influences corrosion in several ways. First, salt is hygroscopic, which increases the moisture content of the concrete. Second, salt increases the electrical conductivity of concrete and speeds up the corrosion process. Third, chloride ions can penetrate the protective passive film on the steel surface. The effect of chlorides on corrosion of reinforcing steel will be discussed in greater detail in Section 1.2.

Many corrosion protection systems have been developed with goal of extending the service life of reinforced concrete in bridge decks. These include the use of increased concrete cover, lower permeability concrete, corrosion inhibitors, surface sealers, alternative concrete reinforcement, including metallic or alloyed steel, galvanized reinforcing steel, epoxy-coated reinforcement (ECR), and a combination of these systems. Cathodic protection and electrochemical extraction of chlorides are also used. The corrosion protection systems used in this study are detailed in Section 1.6.

1.2 CORROSION MECHANISMS OF REINFORCING STEEL IN CONCRETE

Corrosion of steel is a spontaneous electrochemical process that involves both anodic and cathodic reactions. For corrosion to occur, four elements must be present

– an anode, a cathode, an electrolyte, and an electron path. The anode is the site that gives up electrons, where metal is lost, and corrosion products are deposited. The cathode is the site that consumes electrons, where the electrons react with oxygen (O_2) and water to form hydroxyl ions (OH^-). The electrolyte is a medium capable of conducting electric current through ion transport. In concrete, the electrolyte is present within concrete pore solution. The electron path is provided by metal within the concrete, connecting the anode and the cathode to complete a closed circuit. The reinforcing bars themselves or steel tie wires and chairs can function as part of the electron path.

At the anode, iron is oxidized to ferrous ions, releasing two electrons. This process is called the half-cell oxidation or anodic reaction.



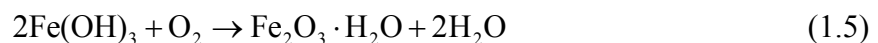
The electrons released by the iron travel to the cathode where they combine with water and oxygen to form hydroxyl ions. This reaction is called the half-cell reduction or cathodic reaction.



The hydroxyl ions migrate through the electrolyte to the anode where they react with the ferrous ions to produce ferrous hydroxide.



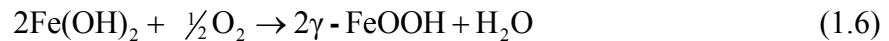
Ferrous hydroxide, in turn, reacts with oxygen and water to form ferric hydroxide $Fe(OH)_3$ and ferric oxide (Fe_2O_3), which is commonly known as rust.



The iron oxides occupy as much as six times the volume of the original iron atoms (Mehta and Monteiro 2006). When the oxidization reaction takes place on the

steel surface in concrete, rust forms, expands and eventually causes the concrete to crack, which not only weakens the structure, but also accelerates the corrosion process, because more oxygen, moisture, and chlorides from the atmosphere can now reach the steel.

Although steel's natural tendency is to corrode, the highly alkaline concrete pore solution (pH value of 13 to 13.6) provides reinforcing steel with corrosion protection. In an alkaline environment, ferrous hydroxide [Eq. (1.3)] is oxidized into γ -ferric oxyhydroxide (γ -FeOOH) rather than ferric hydroxide (Mindess, Young, and Darwin 2003).



γ -FeOOH forms a tightly adhering protective barrier on the steel surface. This passive layer limits access of moisture and oxygen to the underlying steel and limits the solubility of the ferrous ions, preventing corrosion. The process is called passivation. When the pH of the concrete pore solution drops below 11.5, which can occur due to carbonation, the protective film on the steel surface becomes unstable (Verbeck 1975).

For steel in concrete, the passive corrosion rate is typically just 0.1 $\mu\text{m}/\text{year}$. The ingress of aggressive species, however, can cause a breakdown of the passive film. A uniform corrosion loss of about 25 μm (0.001 in., 1 mil) on a reinforcing bar can cause concrete to crack (Pfeifer 2000). For localized corrosion in a small region, however, the quantity of corrosion products needed to crack concrete depends on anodic length and member dimensions, including concrete clear cover and reinforcing bar diameter. Thus, depending on the exposed area, a thickness loss of 30 to 270 μm (1.2 and 10.7 mils) of the reinforcing bar maybe needed to cause concrete to crack (Torres-Acosta and Sagües 2004).

In concrete bridge decks, it is generally believed that macrocell corrosion between the top and bottom mats of reinforcing steel is the primary cause of early age bridge deck deterioration and that microcell corrosion (anode and cathode located on adjacent parts of the same metal) is of less importance (Virmani 1990). Chloride ions from deicing salts placed on top of a bridge deck make the top mat of reinforcing steel more negative than the bottom mat. The resulting galvanic cell drives electrons from the top mat bars (anode) to the bottom (cathode) causing macrocell corrosion. The electron path is usually provided by tie wire, bar chairs, truss bars, expansion dams, and/or scuppers (Virmani, Clear, and Pasko 1983).

Because of the inherent corrosion protection provided by concrete, reinforcing steel does not corrode in the majority of concrete structures. Concrete cover provides a physical barrier to oxygen, moisture and chlorides and limits the corrosion of reinforcing steel in harsh environments. The two most common causes of deterioration of concrete are the ingress of chloride ions and neutralization of the concrete pore solution by atmospheric carbonation, discussed in the next two sections.

1.2.1 Chloride-Induced Corrosion

Exposure of reinforced concrete to chloride ions is the primary cause of premature corrosion of steel reinforcement. Sources of chlorides include deicing salts, concrete admixtures, contaminated aggregates and/or mixing water, as well as airborne salts and salt in ground water.

When chlorides appear in the solution around steel, the chloride ions react with iron ions in the passive film on the steel surface to form an iron-chloride complex.



The iron-chloride complex subsequently hydrolyzes with water to form ferrous hydroxide and chloride.



In the reactions in Eqs. (1.7) and (1.8), no chloride is consumed, making the chloride available again to combine with iron ions. The consumption of OH^- in Eq. (1.8) lowers the pH of the surrounding concrete pore solution. The precipitated hydroxide on the steel surface can increase the space adjacent to the steel and allow more water or moisture to access the reinforcement. At the same time, with the lower pH of the concrete pore solution, less chloride is needed to initiate corrosion.

Another reason for chloride-induced corrosion is the electrical potential difference caused by differences in chloride ion concentration (Kelestemur and Yildiz 2006). The concentration of chloride ions is not uniform in reinforced concrete. For example, the surface of bridge decks has a higher concentration than the bottom of bridge decks. The potential difference caused by uneven distribution of chloride ions helps to drive the corrosion process. For contaminated concrete, when delaminated or spalled concrete is patched with new chloride-free concrete, strong macrocells are set up near the interface. Due to the large chloride concentration difference within a very short distance between the anode and cathode, the corrosion of concrete reinforcement can be accelerated. Impurities in the steel, such as carbon and other metals in the reinforcement, can also cause corrosion.

Although chlorides are directly responsible for the initiation of corrosion, they appear to play only an indirect role in the rate of corrosion after initiation. The primary rate-controlling factors are the availability of oxygen, the electrical resistivity, the relative humidity of the concrete, the pH of the pore solution, and the temperature.

1.2.2 Carbonation

When CO₂ from air or water enters concrete through the pores, first alkalis and then calcium hydroxide are converted to carbonates; this process is called carbonation. The alkalinity of concrete drops during the carbonation process because the hydroxyl ions in the pore solution are consumed.

The carbonation process depends on the porosity and relative humidity of the concrete. The optimal relative humidity for carbonation is 25-75%. Below 25%, the degree of carbonation is considered insignificant. Above 75%, moisture in the pores restricts CO₂ penetration. Carbonation-induced corrosion often occurs in regions that are exposed to rainfall, shaded from sunlight, and have low concrete cover over the reinforcing steel.

Compared to chloride-induced corrosion, carbonation is generally a slow process. In high-quality concrete, it has been estimated that carbonation will proceed at a rate of no more than 1.0 mm (0.04 in.) per year. The carbonation rate is significantly increased in concrete with a high water-cement ratio, low cement content, short curing period, low strength, and highly permeable or porous paste. In a well-cured concrete with a low *w/c* ratio, carbonation is generally limited to a depth about 25 mm (1 in.) (Mindess et al. 2003). By decreasing the pH of concrete, carbonation also lowers the concentration of chloride ions needed to promote corrosion. In new concrete with a pH of 13 to 13.6, about 7,000 to 8,000 ppm (parts-per-million) of chlorides in total are required to initiate steel corrosion. When the pH of the concrete drops below 11.5, the passivity of steel in concrete will be lost and corrosion will occur without the presence of chloride if oxygen and moisture are available to the reinforcing steel.

Carbonation also changes concrete properties, such as increasing the concrete weight, strength, and surface hardness, and causing cracking due to the lower volume of the carbonated materials.

The corrosion protection provided by the high alkalinity of the surrounding concrete may be diminished by either carbonation or chloride attack. Corrosion-induced deterioration of reinforced concrete is rarely caused by a single component. In most cases in reinforced concrete bridge decks, chloride penetration and carbonation interact together to accelerate the corrosion process. The interaction between chlorides and carbonation can be described using Figure 1.1 (Yoon 2007). Carbonation lowers the pH of the concrete pore solution, decreases the chloride binding capability (chloride ions can react with tricalcium aluminate within the cement to form calcium chloroaluminate), and makes more free chlorides available in concrete to promote corrosion. At the same time, carbonation can be accelerated through the microcracks in concrete that form due to stresses in the concrete caused by the higher volume of the corrosion products.

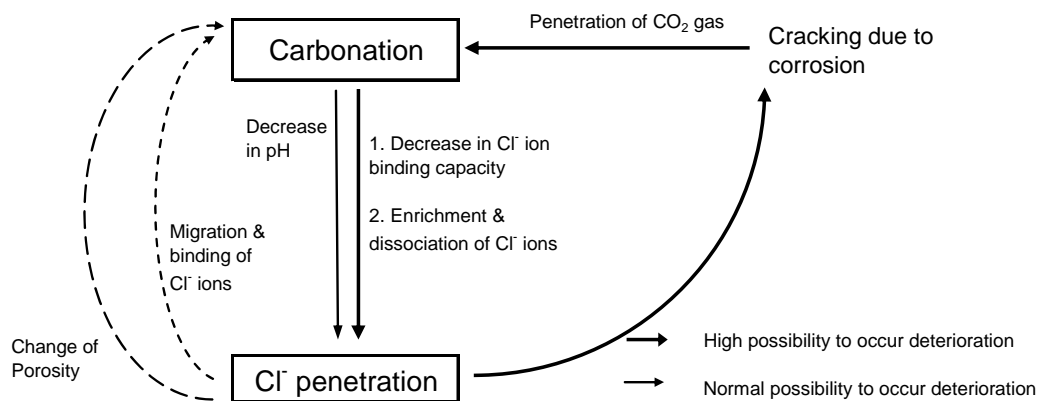


Figure 1.1 – Mechanism of interaction between carbonation and chloride penetration (after Yoon 2007)

1.3 CHLORIDE CONCENTRATION AND CRITICAL THRESHOLD

Chloride (Cl^-) concentration and concrete pH play very important roles in the corrosion process (Vinod 1988, Kayyali, and Haque 1995, Moreno et al. 2004). The concentration of chloride ions required to break down the passive film on the reinforcing steel surface and trigger corrosion is defined as the critical chloride threshold (Daigle, Lounis, and Cusson 2004).

There are no universal standards for determining the onset of corrosion. Various methods have been used in practice, including those based on macrocell corrosion rate (Schiessl 1992), microcell corrosion rate (Goni and Andrade 1990, Alonso et al. 2000, Trejo 2002), mass loss (Thomas 1996), corrosion potential (Hausmann 1967, Gouda 1970, Oh, Jang, and Shin 2003), and a combination of these methods (Trépanier, Hope, and Hansson 2001). Most often, a rise in the positive macrocell current along with rapid negative shifts of corrosion potential is used for corrosion onset indication (Clemeña 2003).

Many studies have been conducted to determine the critical chloride threshold. In 1962, Lewis reported, that the minimum concentration of chloride to initiate corrosion was 0.15% soluble chloride by weight of cement. According to research conducted by the Federal Highway Administration (FHWA), the lowest chloride concentration in concrete needed to initiate corrosion is 0.033% total chloride (free and bound chloride in concrete, acid-soluble) by weight of concrete (Berman 1974, Clear 1976).

The value of the critical chloride threshold varies widely for different concretes (Funahashi 1990). Several factors can contribute to the variation of the chloride threshold, such as the pH value of the concrete pore solution, the availability of oxygen and moisture, and the presence of voids at the steel/concrete interface

(Bertolini et al. 2004). In higher pH environments, more chlorides are required to initiate corrosion. As a result, several researchers have proposed expressing the chloride threshold by using the chloride/hydroxyl ion (Cl^-/OH^-) ratio (Hausmann 1967, Gouda 1970, Diamond 1986, Goni and Andrade 1990). However, chloride thresholds expressed as Cl^-/OH^- can vary from 0.22 to 40, which provides no advantage compared to the total chloride content (Glass and Buenfeld 1997). Furthermore, measuring the OH^- concentration in mortar or concrete presents significant difficulties. Expressing the chloride content in concrete in terms of mass percentage of cement or weight per volume is more convenient. The chloride threshold for conventional steels in typical reinforced structures ranges from 0.6 to 0.9 kg/m^3 (1.0 to 1.5 lb/yd^3) (Mehta and Monteiro 2006).

Not all of the chlorides present in concrete or mortar will contribute to the corrosion process. The total chloride content consists of the water-soluble chloride ions dissolved in the pore solution and other chloride ions bound to the cement or aggregate components. Tricalcium aluminate (C_3A) within the cement can react with chloride ions to form calcium chloroaluminate ($3\text{CaO}\cdot\text{Al}_2\text{O}_3\cdot\text{CaCl}_2\cdot 10\text{H}_2\text{O}$), also known as Friedel's salt. This process is called chloride binding. Among free and bound chlorides in concrete, usually, free chloride is the only chloride to react with the passive layer on reinforcement and promote corrosion. This provides the theoretical base for the chloride threshold level. However, when the pH of the pore solution drops below 12, the bound chlorides can be released into the surrounding environment and pose a potential threat to the reinforcement (Bertolini et al. 2004, Mehta and Monteiro 2006).

For water-soluble chloride ("free" chloride) measurement, the concrete sample is boiled in water to dissolve all of the non-bound chlorides. After filtration, the

chloride content is measured by titration using a chloride sensitive electrode. The accuracy of this method is a function of the particle size of the prepared sample and the amount of water, temperature, time and agitation allowed (Arya and Newman 1990). Because sampling is required, destruction of the concrete is inevitable, at least on a small scale.

A nondestructive method of monitoring Cl^- concentrations and pH values at the steel/concrete interface was introduced by Du et al. (2006). Two electrodes, a modified Ag/AgCl electrode serving as the Cl^- concentration sensor and an Ir/IrO₂ electrode, serving as the pH sensor, were combined into a multiplex sensor, which was embedded in concrete close to the steel/concrete interface to provide an in situ long-term measurement of Cl^- and pH. With the change in Cl^- concentrations and pH values at the steel/concrete interface, the corrosion potential and corrosion rate were observed to change accordingly.

In uncracked concrete, chloride penetration is a complex process involving diffusion and capillary suction. It is highly affected by the surface boundary conditions. For uncracked concrete, the penetration rate of chloride ions is closely related to the concrete pore properties and the environment temperature, and can be described by Fick's Second Law.

$$\frac{\partial C(x,t)}{\partial t} = D_c \frac{\partial^2 C(x,t)}{\partial x^2} \quad (1.9)$$

where

$C(x,t)$ = chloride concentration at depth x and time t ;

D_c = diffusion coefficient.

Based on bridge surveys on northeastern Kansas, Lindquist et al. (2006) found that the chloride content in uncracked concrete could be modeled using Fick's Second

Law. At a depth of 76 mm (3.0 in.) in bridge decks with ages of 12 years or less, the concrete remained below the corrosion threshold for conventional reinforcing steel (0.6 kg/m^3 , 1.0 lb/yd^3). In cracked concrete, however, the chloride content was significantly higher. The chloride content at cracks increased linearly with age, decreased with depth, and exceeded 0.6 kg/m^3 (1.0 lb/yd^3) at a depth of 76 mm (3.0 in.) in the majority of the decks by the end of the second year.

1.4 CORROSION MONITORING TECHNIQUES

The economic cost of corrosion is enormous, and sometimes corrosion-induced failure represents a threat to human life and safety. Corrosion is usually a slow process that can be detected before a structural failure occurs and corrosion monitoring is becoming increasingly important for scheduling maintenance and for structural life prediction purposes. Corrosion monitoring is used to ensure that structures remain safe and fully operational. It provides information for timely and cost-effective intervention to prevent unacceptable damage and to allow structures to extend service life. Corrosion monitoring also helps to develop durability models and related predictive techniques to enhance the understanding of macrocell corrosion environments. The earlier corrosion in reinforced concrete is detected, the lower the cost for maintenance. Therefore, it is important to have appropriate detection techniques to evaluate the corrosion in reinforced concrete structures.

Corrosion monitoring of reinforcing steel presents many challenges. Direct inspection or on-site continuous monitoring without damaging the structure is very difficult. Concrete is a complex composite material; its structure and properties change with time as it is exposed to the environment. Corrosion is commonly localized, and typically manifests itself over many years. Furthermore, concrete is

highly variable due to the different mixtures that are used.

Several methods are used to monitor steel corrosion in concrete in the lab. These include corrosion potential, corrosion rate, linear polarization resistance (LPR), electrical impedance spectroscopy, electrochemical noise (EN), and galvanostatic pulse transient (GPT) measurements. Some, but not all of these are also used in the field. The most common detection techniques are described next.

1.4.1 Corrosion Potential (CP)

Corrosion potential is associated with electrochemical free-energy change at equilibrium, which can be used to evaluate the oxidation tendency of the reinforcement. The potential difference between reinforcement and the surrounding environment is the driving force of the corrosion. As steel becomes more prone to corrosion, its electrochemical potential becomes more negative with respect to the surrounding environment. Although a corrosion potential measurement does not give an indication the rate of corrosion, it does indicate the tendency for corrosion to occur, and, thus, represents a useful tool. In a combination of other techniques, it can be used to detect and evaluate the corrosion performance of reinforced concrete structures.

The corrosion potential of reinforcing steel can be measured with respect to a reference electrode using a high-impedance voltmeter. The standard hydrogen electrode (SHE) is the reference electrode, used to establish the zero point on the electrochemical scale. It is, however, not convenient for use in most laboratory or field applications, and as a result, other reference electrodes are used. The most commonly used reference electrodes for studying the corrosion of reinforcing steel are the saturated calomel electrode (SCE) and the copper-copper sulfate electrode

(CSE). The SCE is widely used in the laboratory, while CSE is used in both the lab and the field. The half-cell potentials of the SCE and CSE differ by 0.241 V and 0.316 V, respectively, from half-cell potentials measured with the SHE.

Corrosion potential measurements are widely accepted as a steel corrosion detection method for reinforcing steel (Escalante 1990, Naish, Harker, and Carney 1990, ASTM C876 1999). The standard test method for electrical half-cell potential of uncoated reinforcing steel in concrete is described in ASTM C876. Interpretations of the potential readings are shown in Table 1.1.

Table 1.1 - Corrosion conditions based on half-cell potential readings (ASTM C876 1999)

Half-cell Potential Reading (V)		Corrosion Condition
SCE	CSE	
> -0.200	> -0.125	Low (>90% chance of not corroding)
-0.200 to -0.350	-0.125 to -0.275	Intermediate corrosion activity
< -0.350	< -0.275	High (>90% chance of corroding)

In practice, when interpreting half-cell potential data, a number of factors, such as concrete resistance, carbonation, oxygen, chloride concentration and other effects, have to be considered. Gu and Beaudoin (1998) discussed these factors and their effects on the potential readings. They concluded that only corrosion conditions related to carbonation, chloride ingress, and the use of anodic corrosion inhibitors can be evaluated using ASTM C876.

Steel in concrete structures immersed in water or buried in the earth often have very negative potentials due to restricted oxygen access. In the transition region of the structure (splash zone or just above ground), negative potentials result due to galvanic coupling with immersed reinforcement. Oxygen concentrations at the interface of the steel reinforcement can affect half-cell potential readings. Decreasing the oxygen

concentration at the surface causes a more negative reading. In dense concrete with a low oxygen concentration, the potential reading is also more negative; in this case, the reading is not related to corrosion of the reinforcement and, therefore, does not represent a high probability of corrosion (Gu and Beaudoin 1998).

Potential readings are also affected by high concrete resistance. For accurate potential measurements, a high resistance voltmeter and a reduction in concrete resistance, obtained by wetting the concrete surface, should be used. Weather, humidity, and the presence of ions in the pore solution also affect the electrical resistivity of concrete. Differences in resistivity may cause variations in corrosion potential of ± 50 mV. Potential measurement is not a useful technique for epoxy-coated reinforcement in field applications due to the high electrical resistance of the coating, but it has been used successfully in the lab (Gu and Beaudoin 1998).

1.4.2 Corrosion Rate

To evaluate corrosion protection systems and predict the remaining service life of reinforced concrete structures, a measure of the corrosion rate is needed. Corrosion rate depends on the electron flow at the reacting interface of a metal in a corrosive environment. Historically, corrosion rate has been expressed as a current density, typically in $\mu\text{A}/\text{cm}^2$. Often, however, it is more meaningful to express the rate in terms of the thickness loss per unit time, commonly in $\mu\text{m}/\text{year}$. The relationship between these two is described by Faraday's Law (So and Millard 2007).

$$R_{corr} = k \frac{ia}{nF\rho} \quad (1.10)$$

where

R_{corr} = corrosion rate, in terms of thickness loss per unit time, $\mu\text{m}/\text{year}$,

$$R_{corr} = 11.59 i \text{ for iron and } R_{corr} = 14.96 i \text{ for zinc};$$

i = corrosion current density, $\mu\text{A}/\text{cm}^2$;

k = conversion factor, $3.15 \times 10^4 \text{ amp} \cdot \mu\text{m} \cdot \text{sec} / \mu\text{A} \cdot \text{cm} \cdot \text{year}$;

a = atomic weight, 55.8 g/mol for iron and 65.4 for zinc;

n = number of equivalents exchanged, $n = 2$ for both iron and zinc;

F = Faraday's constant, 96,500 Coulombs/mole;

ρ = density of the metal, g/cm^3 , 7.87 for iron and 7.13 for zinc.

In structures, reinforcing bars are usually connected electrically by steel tie wires or bar chairs, and the measurement of the macrocell corrosion rate is often infeasible. In the laboratory, however, tests can be designed to specifically measure corrosion rate. To do this, specimens are constructed with the regions of steel that serve as the anode and as the cathode electrically connected across a resistor. The voltage drop across the resistor can be measured using a voltmeter, and the corrosion rate can be calculated according to Ohm's Law.

$$i = \frac{V}{RA} \quad (1.11)$$

where

V = voltage drop across the resistor, mV;

R = resistance of the resistor, $\text{k}\Omega$;

A = surface area of the anode, cm^2 .

The corrosion rate only captures the instantaneous oxidation status of the steel. To evaluate long-term corrosion effects, corrosion loss is introduced. After taking corrosion rate readings at specific time intervals over a period, estimated total material loss can be calculated by numerically integrating the corrosion rates over

time. Since the corrosion rate fluctuates over time, corrosion loss often provides a better measure of corrosion performance.

Because macrocell corrosion measurements only capture the portion of the total corrosion caused by electrons flowing through the resistor, they do not capture the microcell corrosion occurring on the same steel. Microcell corrosion, however, can be measured using linear polarization resistance (LPR), electrochemical impedance spectroscopy (EIS), and electrochemical noise (EN) techniques.

1.4.3 Linear Polarization Resistance (LPR)

The linear polarization resistance (LPR) test provides a rapid non-destructive measurement of corrosion rate, which is based on the observation that the corrosion potential-current polarization curve is linear in the vicinity of the equilibrium potential E_{oc} (usually $\pm 10\text{mV}$ of the equilibrium potential). To perform the test, the metal is perturbed by a small amount from its equilibrium potential. The potential change ΔE is related to the change in current density Δi . There are two ways of perturbing the system: one is by changing potential by a fixed amount ΔE , then monitoring the decay of the current density Δi ; the other is by changing the current density, then measuring the change of the potential ΔE . The slope of the curve $\Delta E/\Delta i$, which is called the polarization resistance (R_p), is defined as (Jones 1996)

$$R_p = \left(\frac{\Delta E}{\Delta i} \right)_{\Delta E \rightarrow 0} \quad (1.12)$$

The linear polarization resistance is related to the instantaneous corrosion rate (expressed as corrosion current density) through the Stern-Geary equation.

$$i = \frac{B}{R_p} \quad (1.13)$$

$$B = \frac{(\beta_a \beta_c)}{2.3(\beta_a + \beta_c)} \quad (1.14)$$

where

i = corrosion current density, $\mu\text{A}/\text{cm}^2$;

R_p = polarization resistance, $\text{k}\Omega/\text{cm}^2$;

B = Stern-Gary constant;

β_a = anodic Tafel constant, mV/decade ;

β_c = cathodic Tafel constant, mV/decade ;

The Stern-Geary constant B may vary from 13 to 52 mV depending on the different metal/electrolyte system (Stern and Weisert 1958). For reinforcing steel in concrete, values of B have been reported to range from 26 mV to 52 mV depending on whether the steel is corroding or non-corroding (Broomfield 1997). Usually, a value of 120 mV/decade for both the anodic and cathodic Tafel coefficients, resulting in a value of 26 mV for the constant B , is suggested for reinforcing steel in concrete (Lambert, Page, and Vassie 1991, McDonald, Pfeifer, and Sherman 1998).

LPR measurements are most commonly performed using a potentiostat, which is composed of a working electrode (the corroding reinforcing steel), a counter-electrode (a platinum rod), and a reference electrode (such as SCE or CSE).

In the LPR test, accurately measuring the surface area on the steel is very important. In some cases, especially in the field, this is difficult due to a lack of clarity of the region of steel undergoing measurement (Feliu et al. 1988, Feliu, Gonzalez, and Andrade 1994). Flis, Pickering, and Osseo-Asare (1998) pointed out that the polarization area can be affected by various parameters, including the thickness, temperature, and humidity of the concrete. Andrade and Alonso (2001) suggested that several measurements to be taken over a long period to minimize weather effects. A guard ring has been used to better control the surface area of the

steel being evaluated and, thus, improve the accuracy of the test (Gowers, Millard, and Bungey 1997).

1.4.4 Electrochemical Impedance Spectroscopy (EIS)

Electrochemical impedance spectroscopy (EIS), also called AC impedance spectroscopy, is used as a non-destructive technique to characterize corrosion of reinforcing steel in concrete. Impedance is a measure of the ability of a circuit to resist the flow of electrical circuit. Electrochemical impedance is usually measured by applying a small AC excitation to the steel embedded in concrete and measuring the current through the steel. In the most EIS test, AC current and AC potential are measured as the frequency of the excitation is varied over a very wide range (Gamry 1999). The relationship between the voltage and the current is used to evaluate the corrosion rate of the steel under coatings and for quality assurance of coatings. EIS has been successfully applied to the study of corrosion systems for thirty years and been proven to be a powerful and accurate method for measuring corrosion rates (Hope, Page, and Ip 1986, Qiao and Ou 2007). To access the polarization resistance, which is proportional to the corrosion rate at the monitored interface, EIS's results have to be interpreted using a model of the interface, which takes the form of an equivalent electronic circuit.

A number of papers have been published on EIS theory and its application to corrosion measurements (MacDonald and McKubre 1981, Turgoose and Cottis 1991, MacDonald 2006). An advantage of EIS over other techniques is the possibility of using very small amplitude signals without significantly disturbing the corrosion properties. An alternating voltage of from 5 to 10 mV is applied to the specimen over a range of frequencies of 0.001 Hz to 100,000 Hz (Husain et al. 2004). In some cases,

selected frequencies can be used to reduce the time required for corrosion monitoring. EIS can give detailed information about the mechanisms and kinetics of the electrochemical process during corrosion. More importantly, the solution resistance in low conductivity environments can be separated from the actual polarization resistance, so that EIS techniques are much more effective than LPR techniques when evaluating coated or inhibited materials.

The major limitation of EIS is that the analysis process is relatively complex compared to LPR and other technologies. Also, data interpretation is often ambiguous and difficult because of the need for a theoretical equivalent circuit for analysis.

1.4.5 Electrochemical Noise (EN)

The electrochemical noise (EN) concept was first proposed in 1968 by Iverson. He noticed that “corroding metals produce bursts of metal ions from various point anodes” and detected transient fluctuations in electrical charge in an experiment. EN refers to naturally occurring fluctuations in corrosion potential and corrosion current, generated spontaneously by the corrosion process, which are caused by the transport of electroactive species (anion, cation, and electrons) and various alterations in the metal/electrolyte interface (Mariaca et al. 1997).

The general approach of EN technique is to measure current transients of two identical electrodes shorted together using a zero resistance ammeter and the potential transients between the pair and a reference electrode or a third identical electrode (Frankel 2008). Roberge, Beaudoin, and Sastri (1989) described the measurement of electrochemical noise and its relationship to localized corrosion. However, based on observations of crevice corrosion of stainless steel, Simoes and Ferreira (1987) concluded that there was no directly consistent correlation between noise transients

and physical phenomena. Searson and Dawson (1988) proposed the existence of a relation between the standard deviation of the potential noise fluctuations and the corrosion rate in 1988.

Mariaca et al. (1997) studied the corrosion rate of carbon steels embedded in a $30 \times 100 \times 160$ mm ($1.18 \times 3.94 \times 6.30$ in.) mortar beam specimen using the EN technique and found that EN was effective in estimating the corrosion rate for steel embedded in concrete. Legat, Leban, and Bajt (2004) used the EN technique on concrete specimens that contained reinforcing steel and were subjected to wetting and drying cycles. The results showed that EN could indicate the current level of corrosion activity of steel in concrete, especially transitions from the passive state to active corrosion. Smulko, Darowicki, and Zieliński (2006) studied corrosion rate changes using a three-electrode system that consisted of two working electrodes made of carbon steel and embedded in concrete and a silver reference electrode using EN techniques. The test results indicated that EN techniques could recognize the rate shifts in the corrosion process.

One of the most important advantages of the EN method is that its application does not involve artificial disturbance of the system. Therefore, it has a much higher sensitivity than other more traditional techniques (Song and Saraswathy 2007). The EN technique can capture corrosion dynamics in concrete; therefore, it could be used for assessing the onset of localized corrosion and to characterize different corrosion types, such as pitting and crevice corrosion, uniform corrosion, and stress-corrosion cracking (Legat et al 2004). There are other advantages of EN, such as a shorter measurement time, simple implementation, and simple evaluation of test results and the corrosion tendency at the material surface.

1.5 CORROSION TESTS

A variety of tests have been developed to investigate corrosion performance of the reinforcement in concrete. The current study uses one rapid macrocell test, three bench-scale tests, and one field test. The rapid macrocell test gives results in a relatively short time, usually 15 to 25 weeks. The bench-scale and field tests simulate conditions of reinforcement in concrete bridge decks and are used to evaluate the long-term performance of reinforcement. The bench-scale tests are performed in the laboratory environment, while the field test exposes the specimens to the weather, as occurs for bridge decks. A brief discussion of the development of the methods is provided in this section; the details of these methods are given in Chapter 2.

1.5.1 Rapid Macrocell Test

Yonezawa, Ashworth, and Procter (1988) used mortar specimens to study the effects of the concrete pore solution composition and chlorides on the corrosion of the reinforcing steel in concrete. Two different configurations were used in their tests. One configuration consisted of a 140-mm (5.51-in.) long \times 8-mm (0.31-in.) diameter mild steel electrode embedded in a 22-mm (0.87-in.) mortar cube; the other consisted of the same mild steel embedded in a 100-mm (3.94-in.) long \times 40-mm (1.57-in.) diameter cylinder. In 1990, the configurations were modified and first used in the rapid macrocell test by Martinez et al. (1990) at the University of Kansas. In their study, “lollipop” specimens (named for the shape) were used to determine the effects of three deicing chemicals, NaCl, CaCl₂, and CMA, on the corrosion of reinforcing steel. The specimen consisted of a 127-mm (5-in.) long, No.13 (No.4) reinforcing bar, symmetrically embedded 76 mm (3 in.) into a 100-mm (3.94-in.) long \times 30-mm (1.18-in.) diameter mortar cylinder. The cylindrical mortar specimen provided

uniform cover and was easy to fabricate. An epoxy band at the steel-mortar interface was used to prevent crevice corrosion. A 100,000-ohm resistor was used between the anode and cathode. Because of the very low corrosion current, Martinez et al. (1990) concluded that a much lower resistance should be used in future macrocell tests.

The rapid macrocell test has been updated since its first use. Schwensen, Darwin, and Locke (1995), Senecal, Darwin, and Locke (1995) and Smith, Darwin, and Locke (1995) used the rapid macrocell test to evaluate the corrosion properties of different reinforcing steels under the NCHRP-IDEA program, and several modifications were made to improve the test. A 10-ohm resistor was used instead of a 100,000-ohm resistor to obtain greater and more stable macrocell corrosion current. A No. 16 (No. 5) bar was used instead of the No. 13 (No. 4) bar to reduce the mortar cover thickness, and thereby shorten the time to corrosion initiation. Compressed air, scrubbed to remove CO₂, was bubbled into the solution around the cathode to provide an oxygen source. Open circuit corrosion potentials were adopted in the measurement. Two times as many specimens were used for the cathode as for the anode to ensure that the cathodic reaction was not limiting the corrosion rate.

The configuration of the rapid macrocell continued to be modified in subsequent studies (Darwin et al. 1999, Kahrs, Darwin, and Locke 2001, Ge et al. 2004, Balma et al. 2005, Gong et al. 2006). The “lollipop” specimen was replaced by the “mortar-wrapped” specimen (the bar is totally embedded in the mortar) to minimize the potential for corrosion of the exposed steel, caused by the high humidity of the surrounding air. Bare bar specimens were also used in the macrocell test. The container lid was lowered to just above the solution. In the current study, the specimen mold was redesigned by Guo et al. (2006) to improve the casting operation.

1.5.2 Bench-scale Tests

The bench-scale tests include the Southern Exposure (SE), cracked beam (CB), and ASTM G109 tests. The SE test simulates conditions of reinforcement in uncracked bridge decks, while the CB test simulates conditions at a crack directly above and parallel to the reinforcement, the most common crack condition on bridge decks. The SE and CB specimens undergo 96-week ponding and drying cycles with a 15% salt solution on the top surface to simulate a harsh environment. According to Perenchio (1992), the SE and CB tests generally simulate 15 to 20 years of exposure for marine structures and 30 to 40 years of exposure for bridges within a 48-week period. The ASTM G109 test evaluates reinforcement under a relatively less severe exposure regime using a 3% salt solution.

The Southern Exposure test is named after the ponding and drying procedure used in the test, which simulates alternate wetting and drying conditions in a warm climate. The SE test was first developed as an accelerated corrosion method by Pfeifer and Scali (1981). They evaluated different concrete sealers for bridge decks using small concrete slabs, which consisted one mat of steel, and were subjected to a weekly ponding and drying cycle use a 15% salt solution. The specimens were exposed to a constant temperature of 38°C (100°F) in a chamber. Tournay and Berke (1993) used a version of the CB test in a study of corrosion inhibitors. A crack, perpendicular to and directly above the reinforcing steel, was made using flexural loading. The crack was shimmed to a constant width of 0.25 mm (0.01 in.) for salt exposure during the test. The SE and CB tests were modified in subsequent research (Pfeifer, Landgren, and Zoob 1987, French, Leon, and Lorentz 1992, Senecal et al. 1995, McDonald et al. 1998). A second layer of steel was added and the two mats were electrically connected across a 10-ohm resistor. The sides of the concrete slabs

were coated with epoxy to ensure that the salt remained within the concrete. A concrete dam was cast monolithically with the specimen to help pond the salt, and the test period was extended to 96 weeks.

The ASTM G109 test was first developed to evaluate the performance of corrosion inhibiting chemical admixtures. The test has also been used to evaluate the corrosion performance of different types of reinforcing steel (Trejo 2002, Balma et al. 2005). The SE, CB, and G109 tests were used in the evaluation of different corrosion protection systems (Balma et al. 2005, Gong et al. 2006, Guo et al. 2006). Corrosion rate and corrosion potential measurements were used to compare corrosion performance.

1.5.3 Field Test

Field tests are designed to evaluate the long-term performance of reinforcement in bridge decks under realistic exposure conditions. Specimens are usually large-scale and exposed to the outdoor weather conditions.

Virmani et al. (1983) used field tests to evaluate the corrosion resistance of conventional and epoxy-coated steel. Reinforced concrete slabs with dimensions of 610×1524×152 mm (24×60×6 in.) were stored outdoors and continuously ponded with a 3% salt solution. Corrosion rates were used to evaluate different corrosion protection systems. In a field test performed by Gaidis and Rosenberg (1987), corrosion potentials were measured on a grid pattern and corrosion rates measured at different points were weighted according to the potential values. The effectiveness of calcium nitrite as a corrosion inhibitor in bridge decks was evaluated based on the weighted corrosion rates. Liu and Weyers (1998) conducted a field test to determine the factors that control the time to corrosion cracking in reinforced concrete structures

using 1180×1180×216 mm (46.5×46.5×8.5 in.) concrete slabs exposed to the weather. They concluded that the time to corrosion cracking decreased as the corrosion rate and the size of the reinforcing steel increased and as the cover depth decreased. They proposed a corrosion cracking model based on their observations.

1.6. CORROSION PROTECTION SYSTEMS

Although the high alkalinity of concrete provides excellent protection for embedded steel, concrete is permeable, and even good-quality concrete can be penetrated by chloride ions, water, carbon dioxide, and other chemicals. Once the passive film on the reinforcement is broken down by chlorides or carbonation, corrosion begins. To help prevent corrosion of reinforcement and to lengthen the service life of reinforced concrete structures, a variety of corrosion protection systems have been developed. The types of systems can be divided into four categories:

- Alternative reinforcement, such as epoxy-coated and multiple-coated steel, galvanized steel, stainless steel, and other corrosion resistant alloys.
- Corrosion inhibitors, such as organic and inorganic.
- Barrier methods, such as the use of low permeability concrete, low water/cement ratio mix designs, the use of mineral admixtures such as silica fume, fly ash, and blast furnace slag, overlays, waterproof membranes.
- Electrochemical protection, such as cathodic protection and chloride extraction.

Typically, the service life of a structure (the time to first repair) can be divided into two time periods, the *corrosion initiation period* and the *corrosion propagation period*. The corrosion initiation period is the time it takes for chloride ions to penetrate the concrete cover and reach the chloride threshold at the level of the steel

and trigger corrosion. The corrosion propagation period is the time after corrosion initiation until first repair is required or the structure has reached the end of its service life. Corrosion protection systems function by lengthening one or both periods. This section will focus on the corrosion protection systems used in this study.

1.6.1 Epoxy-Coated Reinforcement (ECR)

Epoxy-coated reinforcement (ECR) was first used in the Schuylkill River Bridge near Philadelphia in 1973. By 1977, it had become the standard corrosion protection system in 17 U.S. states (Manning 1996), and by 1987, the consumption of the epoxy-coated steel had reached 18,000 tons. Currently, ECR is the most used corrosion protection method for concrete bridges in the United States. ASTM A775 and ASTM 944 provide the standard specifications for ECR.

Many studies have been undertaken to assess the effectiveness of ECR in preventing corrosion. Some studies have shown that ECR provides a positive means of preventing salt-induced reinforcement corrosion (Kilareski 1977), while others have cast doubt on the ability of ECR to provide long-term protection.

Kobayashi and Takewaka (1984) found that the corrosion protection provided by epoxy with a coating thickness of approx 0.2 μm (0.008 mils) was better than that provided by galvanized steel. Higgins (1987) reported that ECR was impervious to chlorides and also totally resistant to the alkine conditions within the concrete. Rasheeduzzafar et al. (1992) studied the corrosion behavior of bare mild, galvanized, epoxy-coated, and stainless clad steel at 2.4, 4.8, and 19.2 kg/m^3 (4, 8 and 32 lb/yd^3) chloride levels over a 7-year period. The results showed that bare mild steel exhibited moderate corrosion and cracking at a chloride level of 2.4 kg/m^3 (4 lb/yd^3) and severe corrosion accompanied by heavy cracking of concrete at chloride contents of 4.8 and

19.2 kg/m³ (8 and 32 lb/yd³). The use of galvanized steel delayed corrosion failure by only a short period of time compared to bare mild steel. In contrast, ECR performed exceedingly well at chloride levels of 2.4 and 4.8 kg/m³ (4 and 8 lb/yd³) and exhibited significant corrosion only at a chloride level of 19.2 kg/m³ (32 lb/yd³), accompanied by a breakdown of the coating and cracking of the concrete. The results indicated that epoxy coatings have a finite tolerance limit for the chlorides. In a field test for the Indiana bridge decks, Hasan, Ramirez, and Cleary (1995) examined core samples of six bridge decks that were reinforced with ECR and exposed to chloride from deicers. No signs of rusting, debonding, or under film corrosion were found in the cores. They concluded that the combination of adequate concrete cover and epoxy coating could provide a good corrosion protection system in Indiana.

Weyers and Cady (1987) studied the corrosion-protection performance of ECR in three 17-year old bridge decks in Virginia. They observed that the epoxy coating would disbond at a faster rate when exposed to high humidity and high chloride contents and concluded that for 95% of the bridge decks in Virginia, the epoxy coating would debond from the steel before the chloride arrived and, therefore, provide no additional service life.

In 1986, five to seven years after reconstruction using ECR, the Florida Keys Bridges showed signs of premature corrosion of the epoxy-coated bars, especially in the portions of the substructure located in the splash zone, which are subjected to wetting and drying, and high water and air temperatures. Bridge surveys revealed a dramatic reduction in adhesion bond between the epoxy coating and the underlying metal (Sagues 1994). It was found that the reduction in bond was independent of the chloride level at the reinforcement and that bond reduction was observed even in chloride-free concrete. This observation was further confirmed in laboratory tests. In

1992, the Florida Department of Transportation discontinued the use of ECR in all construction (Manning 1996).

The Oregon Department of Transportation removed two concrete test beams reinforced with ECR after a number of years of exposure in the tidal zone in Yaquina Bay in Newport, Oregon. The beams were removed in 1989 and 1998 after, respectively, nine and eighteen years of exposure. Both beams suffered significant corrosion and adhesion loss between the epoxy and the steel. It was, therefore, recommended that ECR not be used for long-term protection against corrosion in coastal bridges in Oregon (Griffith and Laylor 1999).

The negative results from the Florida Keys bridges and the tests in Yaquina Bay resulted in the initiation of an investigation of the long-term performance of epoxy coating systems. After comparing ECR to bare steel in bridge decks, Brown, Weyers, and Sprinkel (2006) concluded that the service life of ECR was only about 5 years longer than that of bare steel. Weyers et al. (1998) investigated the piles in three marine structures and the decks on three bridges in Virginia. They concluded that the loss of adhesion between the epoxy coating and the steel surface could occur in 6 years in marine structures and in 15 years in bridge decks, regardless of the type of epoxy used to coat the steel. Smith and Virmani (2000) studied ECR on a total of 92 bridge decks, two bridge barrier walls, and one noise barrier reinforced with ECR in service for three to twenty years. They concluded that (1) there was more corrosion activity on ECR segments where the deck was cracked, (2) reduction in adhesion and softening occurred as a result of prolonged exposure to a moist environment, (3) ECR had superior performance in decks with both top and bottom mats reinforced with ECR compared to decks with only top mat reinforced with ECR, and (4) and in spite of this, ECR performed well in resisting corrosion and avoiding corrosion-induced

concrete deterioration.

Epoxy coating is a barrier system intended to protect steel from corrosion by preventing access of chlorides, oxygen, and moisture to the surface of the steel. The high electrical resistance of epoxy coating also serves to electrically insulate the steel to minimize the flow of corrosion current. The ability of an epoxy coating to prevent corrosion is closely related to its surface defects (holidays) and its adhesion to the underlying steel. ECR needs extra care to prevent coating damage during shipment and placement. Once the coating surface is broken, the protection it offers to the underlying steel is reduced. It takes longer for ECR in bridge decks to disbond compared to ECR in piles in marine environments, where seawater can penetrate the epoxy through imperfections (holidays) and migrate along the steel causing a loss in bond. Once the coating has disbonded, crevice corrosion (localized corrosion of the steel in the narrow openings between steel and epoxy coating) can occur.

Recently, after examining a major, five-year old highway bridge near Montreal, Canada, Cusson et al. (2008) found that ECR provides very good resistance to corrosion during the first year. With time, the probability of corrosion increases, due to the defects in the epoxy coating.

Overall, there has been and continues to be controversy about the effectiveness of ECR. Options range from the conclusion that ECR provide satisfactory corrosion protection performance, significantly extending the structure service life, to the conclusion that because of coating disbondment, ECR is not more effective than conventional steel reinforcement.

1.6.2 Zinc-Coated Reinforcement

Zinc-coated reinforcement has been used for many years, but with inconsistent results. Steel is coated with zinc, which provides protection in two ways: (1) It acts as a barrier and (2) provides cathodic protection to the underlying steel. As a barrier, the zinc layer prevents access of oxygen and moisture to the underlying steel. When there are breaks in the coating, the zinc provides cathodic protection by serving as a sacrificial anode, which corrodes first to protect the exposed steel (Jones 1996). The half-cell electrical potential of zinc (-0.763 V versus standard hydrogen electrode SHE) is lower than that of steel (-0.440 V versus SHE), so once corrosion occurs, the zinc layer reacts first. When the surrounding environment is homogeneous, the steel starts to corrode only after all of the zinc has been lost. The time during which protection is provided depends on the availability of zinc on the steel surface. In reality, differences in chloride, oxygen, and moisture create potential differences around galvanized reinforcement and the underlying steel can corrode even before the entire zinc layer has been lost.

Zinc-coated steel has been used in concrete since the early 1940s. Among the procedures for applying zinc coating, hot-dipping is most commonly used for reinforcing steel. The coating is applied by immersing the steel in a molten bath of zinc at a temperature of 460 °C (860 °F). A metallurgical bond forms between the steel and the zinc coating.

Hofsoy and Gukild (1969) reported that the zinc coating on hot-dip galvanized reinforcement retarded corrosion in concrete. They also showed that the bond strength between galvanized steel and concrete was stronger than that obtained with ungalvanized steel. Corderoy, Ford, and Herzog (1977) concluded that the corrosion-resistance improvement exhibited by hot-dip galvanized and zinc-rich coated

reinforcement was approximately equal to a 50% increase in concrete cover. After studying the corrosion performance of the galvanized steel, Treadaway, Brown, and Cox (1980) found that galvanized steel can delay concrete cracking compared to uncoated mild steel. However, Hill, Spellman, and Stratfull (1976) reported that concrete specimens reinforced with galvanized steel and bare mild steel exhibited corrosion initiation at the same time when exposed to saturated NaCl solution.

Although there have been different conclusions about the level of corrosion protection provided by zinc coatings, it is generally agreed that the nature of the protection is as follows: The zinc metal layer on the steel surface reacts with water or the alkaline concrete pore solution to form zinc hydroxide and hydrogen gas. Upon decomposition, zinc hydroxide forms zinc oxide and water.



Zinc oxide further reacts with calcium ions to form calcium hydroxyzincate. For $\text{pH} < 13.3$, calcium hydroxyzincate forms a stable coating consisting of small crystal that passivates the zinc. When the pH is above 13.3, the corrosion products consist of large crystals, which do not provide corrosion protection (Andrade and Macias 1988, Bentur et. al. 1997). ZnO occupies 50% more space than zinc, in contrast to Fe_2O_3 which occupies 100% or more of the volume (Hime and Machin 1993).

To improve the corrosion resistance of zinc-coated reinforcement, the steel is often immersed in an aqueous solution containing potassium chromate ($\text{K}_2\text{Cr}_2\text{O}_7$), followed by water rinsing. This treatment helps to form a protective layer, containing chromium oxide and zinc chromate, on the steel surface. The standard procedure of the hot-dipped zinc-coated reinforcing steel is specified in ASTM A767. Since

hexavalent chromium salts can cause serious health problems for workers and the environment, research on hexavalent chromium free surface treatments has been initiated. Two hexavalent chromium free passivation treatments of galvanized bars for reinforced concrete were obtained by immersing the reinforcement in a trivalent chromium based solution and in a cobalt and titanium salt solution. The specimens with treated reinforcing steel were subjected to wetting and drying cycles in a 3% NaCl solution for one year. The corrosion potential, corrosion rate, and a visual inspection of the galvanized bars indicated that the corrosion performance of the two hexavalent chromium free passivation treatments are comparable or better than that obtained using the conventional chromating treatment, independent of the type of cement used (Bellezze, Coppola, and Fratesi 2000).

There have been cases in which galvanized bars have performed in a superior manner (McCrum and Arnold 1993), and other cases, in which they have not (Manning et al. 1982, Pianca and Schell 2005). A number of studies have shown that zinc-coated steel has a higher chloride threshold in concrete than steel (Tonini and Dean 1976, Yeomans 1994, Bautista, and Gonzalez 1996).

1.6.3 Stainless Steel

Stainless steel is defined as an iron-carbon alloy with a minimum of 12% chromium content. The high chromium content can result in the formation of a passive film of a mixed iron-chromium oxide on the steel surface (Nurnberger 1996). ASTM A955 (2007) specifies that a minimum of 16% chromium content must be used for stainless steel reinforcement used in concrete. Stainless steel resists corrosion and staining and has low maintenance, which makes it an ideal material for corrosion-resistant applications. Although stainless steel reinforcement has been used since the

1930s, due to the cost of the alloy, an overwhelming majority of concrete reinforcement is still carbon steel.

Among stainless steel reinforcing bars, austenitic and duplex alloys have generally received the most attention. The most commonly used stainless steels in concrete are 304, 316, and 316LN, which are austenitic steels with 18-20% chromium and 8-10% nickel and more recently 2205 Duplex (ferritic/austenitic) stainless steel, which contains 22% chromium and 5% nickel, due to both its excellent corrosion resistance and its high strength (Smith and Tullman 1999). Like iron, chromium also forms an oxide film (Cr_2O_3) with oxygen. Even when scratched, the Cr_2O_3 film can quickly reform, keeping the steel passive. Besides chromium, typical alloying elements in stainless steel are molybdenum, nickel, and nitrogen. Nickel is used to improve the formability and ductility of stainless steel. Increasing the level of alloying elements (chromium, nickel, and molybdenum) increases the corrosion resistance of steel.

Due to alloy microstructure, surface finishing, and presence of welding scale, stainless steel can undergo corrosion if the chloride content in concrete resulting from seawater or de-icing salts is high enough. Stainless steel, however, has a much higher chloride threshold than normal carbon steel. The Progreso Bridge in the Yucatan, Mexico was built between 1937 and 1941 using stainless steel reinforcement. The bridge has not required maintenance to date. A parallel bridge, built with carbon steel in the 1960s, was beyond repair and closed in 1982 (Stainless Steel 2008).

The barrier to using stainless steel reinforcement is its high initial cost. However, the high initial cost is more than compensated by its long service life and low cost associated with the loss of the facility during maintenance and repair, especially when used in the more vulnerable part of structures, such as in bridge decks or marine environments.

Balma et al. (2005) studied 2101 and 2205 duplex stainless steel. They found that both steels had much better corrosion resistance than conventional reinforcing steel, with the average corrosion losses ranging from 0.3% to 1.8% of that exhibited by conventional reinforcing steel; 2205 steel performed better than 2101 steel. Guo et al. (2006) examined the performance of pickled 2205 stainless steel in two bridges in Kansas. Their results showed that there was no corrosion activity observed on the bridge decks and that the pickled 2205 stainless steel reinforcement exhibited excellent corrosion performance. The performance of stainless steel reinforcement in these two bridges has continued to be monitored, and the results of those observations will be presented in Chapter 3.

Stainless steel clad carbon steel has also been used as reinforcement. Gong et al. (2006) and Darwin et al. (2007) reported on the performance of 316LN stainless steel clad (SMI-316 SCTM) reinforcement. They concluded that the stainless steel clad reinforcement has very good corrosion resistance when the cladding is intact. They also found that the corrosion rate of SMI-316 SCTM stainless steel was less than 0.4% of that for conventional reinforcement and concluded that bridge decks reinforced with SMI-316 SCTM would not require repair due to corrosion-induced concrete cracking during a 75-year service life.

1.6.4 Corrosion Inhibitors

For best corrosion performance, a protection system should limit corrosion initiation throughout the duration of a structure's service life. Corrosion inhibitors, thus, represent an alternative protection method. In use for over 100 years, chemical inhibitors have been extensively used in many fields, such as the oil and gas industry.

The use of an inhibitor in reinforced concrete structures is an extension of this concept (Berke, Pfeifer, and Weil 1988).

According to ISO 8044 (1989), a corrosion inhibitor for steel in concrete is defined as “a chemical substance that decreases the corrosion rate when present in the corrosion system at a suitable concentration, without significant reaction with the components of the environment.” Inhibitors can prevent corrosion in several ways (Hansson, Mammoliti, and Hope 1998, Soylev and Richardson 2008):

- by forming a passive film on the surface of reinforcement prior to the ingress of chlorides;
- by buffering the pH at the corrosion site;
- by competitive surface adsorption processes between inhibitor and chloride ions;
- by competitive migration of inhibitor and chloride ions to the corrosion site;
- scavenging oxygen dissolved in the concrete pore solution; and
- blocking the ingress of oxygen.

Corrosion inhibitors can be divided into three categories, anodic inhibitors, cathodic inhibitors, and mixed inhibitors, based on the chemical mechanisms by which they affect the corrosion process. They can also be categorized as inorganic and organic inhibitors based on their compositions. Organic inhibitors can be further classified into two categories, inhibitors that are added to fresh concrete as an admixture, and migrating corrosion inhibitors (MCI) that are applied on the hardened concrete surface (Jamil et al. 2004, Soylev and Richardson 2008).

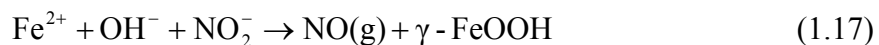
An anodic inhibitor can promote the stabilization of the natural passivating layer on steel, thereby delaying corrosion initiation and controlling the rate of

corrosion. Cathodic inhibitors form insoluble precipitates on the metal surface. Oxygen, thus, cannot pick up electrons to be reduced to OH^- on the cathodic surface and the rate of corrosion at the anodic site decreases correspondingly. Mixed corrosion inhibitors act at both the anodic and cathodic sites by forming a corrosion-resistant film that adheres to the metal surface; the corrosion rate, therefore, is reduced without a significant change in the corrosion potentials (Soylev and Richardson 2008). This section focuses on the corrosion inhibitors used in this study.

- Calcium nitrite

Calcium nitrite $[\text{Ca}(\text{NO}_2)_2]$ was the first anodic inhibitor used on a large scale for reinforcing steel. Compared to other anodic inhibitors, calcium nitrite not only gives better corrosion resistance, but also, because it is an accelerator, increases the 28-day strength for concrete with water-cement ratios below 0.5 (Gaidis 2004). However, on the negative side, its ability to act as an accelerator is not always needed; this can be controlled by using minor amounts of retarder to give set times as long as or longer than obtained for concrete without an accelerator, with due attention paid to timing of admixture addition. Many commercial accelerators are based on calcium nitrite, the first being Darex Corrosion Inhibitor DCI from W. R. Grace, available since 1978. DCI-S, which contains a concrete set retarder, is also available (Pyc et al. 1999).

When calcium nitrite is added to concrete, the ferrous ion can be oxidized by the nitrite ion to form a protective $\gamma\text{-FeOOH}$ film on the steel surface.



Nitrite ions must be present in sufficient quantity and come in immediate contact, by diffusion, with the reinforcement to provide protection. The nitrite ions aid in the formation of this stable passive layer even in the presence of chloride ions

(Gu et al. 1997). This reaction is much more rapid than the transport of ferrous ions (Fe^{2+}) via chloride ion complex formation, discussed previously in Section 1.2. If the chloride concentration level is relative high, however, the chlorides ion can still serve to initiate corrosion. As a result, the chloride-to-nitrite ratio determines the level of nitrite required for protection of reinforcing bars.

A portion of nitric oxide (NO) gas [Eq. (1.17)] will be lost and a portion may be trapped in the concrete. When oxygen is available, the very reactive NO can combine with oxygen to form nitrogen dioxide (NO_2) [Eq. (1.18)]. NO_2 , also a gas, can react with OH^- to form nitrate (NO_3^-) and nitrite (NO_2^-) ions [Eq. (1.19)] (Gaidis 2004). Over time, the loss of NO and the formation of nitrate, results in a reduction in the quantity of nitrite available to inhibit corrosion.



According to Gaidis and Rosenberg (1987), the addition of 2% calcium nitrite based on the weight of portland cement can increase the chloride threshold to 8.14 kg/m^3 (13.7 lb/yd^3) at a $\text{Cl}^-/\text{NO}_2^-$ weight ratio of 1.611. Based on an accelerated corrosion study that included 1,200 samples, 15 mix designs, and three dosage rates of calcium nitrite, Berke et al. (1988) concluded that calcium nitrite can significantly delay corrosion initiation and reduce the corrosion rate of reinforcing steel. Their test results show that the more calcium nitrite used, the greater the protective benefits provided. When the dosage rate of calcium nitrite increases from 10 to 30 L/m^3 (2 to 6 gal/yd³) of a 30% solution, the chloride threshold increases from 3.56 to 9.50 kg/m^3 (6 to 16 lb/yd³).

- Rheocrete 222+

Rheocrete 222+ is a mixed type of organic inhibitor, functioning on both the anodic and cathodic reactions. The admixture is manufactured by BASF Construction Chemicals. It contains amines and esters. It is an improved formulation based on the original formulation marketed as Rheocrete 222. The amines help to form the film on the steel surface; the esters reduce the concrete permeability by hydrolysis of the esters to form a calcium salt of a fatty acid with hydrophobic properties (Gartner and Gaidis 1989). Tests have revealed that Rheocrete has little effect on slump and setting time; but its use in concrete may require increasing the amount of air-entraining agent (AEA) and extending the mixing time to achieve a given air content (Nmai, Stephens, and Bobrowski 1992). Concrete compressive strength is reduced marginally, but Rheocrete has no effects on concrete-steel bond strength or freeze-thaw resistance.

Three corrosion inhibitors, DCI (calcium nitrite), Rheocrete 222 (amines and esters), and Armatec 2000 (alcohol and amine), were evaluated by Pyc et al. (1999). The corrosion inhibitor DCI provided the best performance, while both Rheocrete 222 and Armatec 2000 appeared to provide little or no corrosion inhibition. In addition, rapid concrete chloride permeability tests indicated that there was no significant difference either in the rate of chloride ingress or in the diffusion coefficients for concretes with and without corrosion inhibitors. Ge et al. (2004) studied the inhibitor effects using the Southern Exposure and cracked beam tests and found that Rheocrete and DCI-S greatly improved the corrosion performance of conventional steel in uncracked concrete but not in cracked concrete.

- Hycrete DSS

Hycrete DSS is a relatively new corrosion inhibitor, originally developed by Broadview Technologies and now marketed by Hycrete Technologies. Hycrete is

referred as an alkali metal and ammonium salt of alkenyl-substituted succinic acid; DSS stands for disodium tetrapropenyl succinate. Hycrete provides protection to steel by reducing the concrete permeability. Hycrete is a foaming agent; a defoaming agent is typically needed to achieve the target air content. Allyn and Frantz (2001a, 2001b) studied corrosion inhibitors using lollipop and slab specimens. Test results indicated that Hycrete could prevent corrosion initiation in intact concrete and prevent or significantly reduce corrosion in cracked concrete.

Based on a study of different inhibitors in slab specimens over 108 weeks, Civjan et al. (2005) found that Hycrete was very effective in preventing corrosion. Civjan et al. observed that calcium nitrite, as a single admixture, had excellent performance in corrosion protection in uncracked concrete, but not in cracked concrete, while Hycrete DSS provided protection for reinforcing steel from corrosion in both uncracked and cracked concrete, even if the cracks extended to the level of the reinforcing steel. Results from chloride content analyses, obtained from non-cracked specimens with a water-cement ratio of 0.40 at a depth of 25-38 mm (1-1.5 in.) after the tests, indicated that Hycrete at a dosage of $\frac{1}{2}\%$ of the cement content by weight could reduce water-soluble chloride content to 0.05% of the concrete by weight compared to 0.46% of control specimens without any inhibitor.

Civjan et al. proposed optimum dosages for the three corrosion inhibitors discussed here based on a balance of many factors, such as corrosion performance, strength reduction, and economy consideration, etc. (Civjan et al. 2003, Civjan and Crellin 2006):

(1) Calcium nitrite: 15 to 25 L/m³ (3 to 5 gal/yd³) with a water-cement ratio less than 0.50;

(2) Rheocrete 222: 5 L/m³ (1 gal/yd³) with a *w/c* of 0.50; and

(3) Hycrete: $\frac{1}{4}$ to $\frac{1}{2}$ % by weight of cementitious materials.

1.6.5 Low Permeability Concrete

The durability of reinforced concrete structures is affected by the transport of aggressive substances, such as chlorides, oxygen, and moisture, through its pore system, which can potentially cause deterioration. Therefore, an important indicator of the long-term durability of reinforced concrete is its permeability. Low permeability significantly slows down the ingress of aggressive species, such as chloride ions and carbon dioxide, thus providing protection to the reinforcement. Low permeability concrete can be achieved by using low water-cement ratios (w/c) and adding mineral admixtures to the concrete mix. A maximum w/c ratio of 0.40 is recommended in ACI 318R-08 for reinforced concrete structures exposed to chloride environments.

Zemajtis, Weyers, and Sprinkel (1999) studied low permeability concrete containing the mineral admixture, fly ash, slag cement, and silica fume with and without DCI-S inhibitor. A water-reducing admixture (WRDA-19) and an air entraining agent (Daravair-M) were used in all the concrete specimens. Zemajtis et al. found that concrete with low permeability, especially concrete with silica fume and DCI-S, significantly improved the corrosion performance of reinforcing steel. Ge et al. (2004) studied the effect of w/c ratio (0.35, 0.45 or 0.50) on the corrosion rate and corrosion potentials of conventional steel using bench-scale tests. The results showed that the specimens with a lower w/c ratio exhibited lower corrosion rates and less negative potentials in uncracked specimens, while corrosion performance was independent of the w/c ratio in cracked concrete. Two w/c ratios and three corrosion inhibitors were used in a FHWA study to evaluate the corrosion performance of

eleven systems combining epoxy-coated reinforcement with other corrosion protection systems using Southern Exposure and cracked beam tests (Darwin et al. 2007). Test results indicated that the reduced water-cement ratio and corrosion inhibitors improved the corrosion performance for both conventional and epoxy-coated reinforcement in uncracked concrete but not in cracked concrete.

1.7 OBJECTIVE AND SCOPE

The objectives of this study are to evaluate the corrosion performance of (1) three corrosion inhibitors: DCI-S, Rheocrete 222+, and Hycrete DSS; (2) multiple corrosion protection strategies in conjunction with the use of epoxy-coated reinforcement; and (3) 2205 pickled stainless steel in Kansas bridge decks. The following corrosion protection systems for concrete reinforcing steel are included in this study:

- Conventional reinforcing steel with or without one of the three corrosion inhibitors, DCI-S, Rheocrete 222+, or Hycrete DSS.
- Conventional epoxy-coated reinforcement (ECR) with or without one of three corrosion inhibitors, DCI-S, Rheocrete 222+, or Hycrete DSS, or ECR with a primer coating containing microencapsulated calcium nitrite [$\text{Ca}(\text{NO}_2)_2$].
- Multiple-coated reinforcement with a zinc layer (nominal thickness of 0.05 mm or 2 mils, composition of 98% zinc and 2% aluminum) underlying DuPont 8-2739 epoxy coating (flex west blue).
- ECR pretreated with zinc chromate of the steel to improve adhesion between the epoxy and the steel, ECR with improved adhesion epoxies developed by DuPont and Valspar.
- Pickled 2205 duplex stainless steel.

- Zinc-coated (galvanized) reinforcement without chromate treatment.

Unless otherwise specified, the epoxy coating used on ECR bars is 3M™ Scotchkote™ 413 Fusion Bonded Epoxy.

The corrosion protection systems are evaluated using rapid macrocell, bench-scale (ASTM G109, Southern Exposure, and cracked beam), and field test specimens. The 2205 pickled stainless steel is monitored using periodic potential mapping in the reinforced bridges. The test techniques are described in detail in Chapter 2.

Chapter 3 covers the test results and analysis.

Chapter 4 compares the corrosion protection systems based on their life-cycle cost effectiveness.

Chapter 5 presents the conclusions based on the results and analysis in this report and gives recommendations for the future work.

CHAPTER 2

EXPERIMENTAL WORK

This chapter describes the experimental work performed in this study. The rapid macrocell test, bench-scale tests, and field test are used to evaluate the corrosion protection systems. The corrosion rate, mat-to-mat resistance, corrosion potentials, and linear polarization resistance are recorded. Two bridges reinforced with pickled 2205 stainless steel are also included in this study. Corrosion potentials are measured twice each year on the bridges. This study also involves the determination of the critical chloride threshold of conventional and galvanized steel using bench scale tests. Specimen fabrication, test procedures, apparatus, and materials involved in the tests are described in this chapter.

2.1 CORROSION PROTECTION SYSTEMS

The reinforcing steels, corrosion inhibitors, water-cement ratios evaluated in the study are described in this section.

Reinforcing Steels

No. 16 (No. 5) deformed reinforcing bars are used for all tests.

Conv. – Conventional steel; meets the requirements of ASTM A615.

ECR – Conventional epoxy-coated reinforcement; meets the requirements of ASTM A775.

ECR(Chromate) – Epoxy-coated reinforcement pretreated with zinc chromate to improve the adhesion between the epoxy and the steel.

ECR(DuPont) – Epoxy-coated reinforcement with increased adhesion to reinforcing steel produced by DuPont.

ECR(Valspar) – Epoxy-coated reinforcement with increased adhesion to reinforcing steel produced by Valspar.

ECR(primer/Ca(NO₂)₂) – Epoxy-coated reinforcement with a primer coating containing microencapsulated calcium nitrite.

MC – Multiple-coated reinforcement with a zinc layer underlying epoxy coating produced by DuPont. The zinc layer contains 98% zinc and 2% aluminum and has a nominal thickness of approximately 0.05 mm (2 mils). The epoxy is DuPont 8-2739 epoxy (flex west blue).

2205p – Pickled 2205 duplex stainless steel used as deck reinforcement in two bridges. The designation, 2205, indicates that steel contains approximately 22% chromium and 5% nickel by weight.

Zn – Galvanized reinforcement; meets the requirements of ASTM A767, with the exception that it is not treated with a chromate salt after galvanizing.

The epoxy coating used for the conventional ECR, ECR(Chromate), and ECR(Primer/Ca(NO₂)₂) reinforcement is 3M™ Scotchkote™ 413 Fusion Bonded Epoxy.

Corrosion Inhibitors

DCI – Darex Corrosion Inhibitor (DCI-S) manufactured by W. R. Grace; calcium nitrate plus a retarder.

Rheocrete – Rheocrete 222+ manufactured by BASF Construction Chemicals, aqueous mixture of amines and esters.

Hycrete – Hycrete DSS manufactured by Hycrete Technologies, containing organic alkenyl dicarboxylic acid salts and additives.

Water-cement ratios

Water-cement ratios 0.35 and 0.45 are used in the rapid macrocell and bench-

scale test specimens.

The chemical compositions and the mechanical properties of pickled 2205 stainless steel and conventional steel, as provided by manufacturers, are presented in Tables 2.1 and 2.2.

Table 2.1 – Chemical compositions of 2205p stainless steel and conventional steel

Steel ^a	Bar No.	Heat No.	C	Mn	Si	P	S	CR	Ni	Mo	Cu	N	B
DCB-2205p	16 (5)	150694	0.02	1.72	0.41	0.021	0.001	21.53	4.85	2.60	0.19	0.16	-
DCB-2205p	13 (4)	150692	0.02	1.80	0.47	0.023	0.004	21.30	4.67	2.65	0.22	0.16	-
MCB-2205p	16 (5)	150876	0.02	1.75	0.47	0.024	0.003	21.55	4.75	2.59	0.26	0.16	0.0025
MCB-2205p	13 (4)	150863	0.02	1.73	0.42	0.027	0.003	21.54	4.72	2.59	0.22	0.18	0.0027
Conv.	16 (5)	231159	0.43	0.95	0.21	0.014	0.046	0.200	0.17	0.038	0.49	-	0.0005

^a DCB-2205p = 2205 pickled stainless steel for the Doniphan County Bridge.

MCB-2205p = 2205 pickled stainless steel for the Mission Creek Bridge.

Conv. = conventional steel.

Table 2.2 – Mechanical properties of 2205p stainless steel and conventional steel

Steel ^a	Bar No.	Heat No.	Yield Strength		Tensile Strength		Elongation (%) in 203 mm (8 in.)
			(MPa)	(ksi)	(MPa)	(ksi)	
DCB-2205p	16 (5)	150694	632	91.5	1255	182.0	28.0
DCB-2205p	13 (4)	150692	655	95.0	848	123.0	25.0
MCB-2205p	16 (5)	150876	627	91.0	848	123.0	25.0
MCB-2205p	13 (4)	150863	717	104.0	883	128.0	25.0
Conv.	16 (5)	231159	442.7	64.2	713.6	103.5	15.0

^a DCB-2205p = 2205 pickled stainless steel for the Doniphan County Bridge.

MCB-2205p = 2205 pickled stainless steel for the Mission Creek Bridge.

Conv. = conventional steel.

In summary, the multiple corrosion protection systems evaluated under this study include:

- Conventional steel with or without one of three corrosion inhibitors, DCI-S, Rheocrete 222+, or Hycrete DSS.
- Conventional epoxy-coated reinforcement with or without one of the three corrosion inhibitors, DCI-S, Rheocrete 222+, or Hycrete DSS, or epoxy-coated

reinforcement with a primer coating containing microencapsulated calcium nitrite [$\text{Ca}(\text{NO}_2)_2$].

- Epoxy-coated reinforcement with the steel pretreated with zinc chromate to improve adhesion between the epoxy and the steel and epoxy-coated reinforcement with improved adhesion epoxies developed by DuPont and Valspar.
- Multiple-coated reinforcement.
- Pickled 2205 duplex stainless steel.
- Zinc-coated (galvanized) reinforcement without chromate treatment.

2.2 RAPID MACROCELL TEST

The rapid macrocell test is designed to accelerate the corrosion process so that the chloride ions can reach the reinforcement rapidly. The goal of the test is to obtain a realistic measure of the performance of corrosion protection systems in a short time, usually within 15-25 weeks, as a function of the type of reinforcement, water-cement ratio of the mortar, and the chloride concentration surrounding the specimen. The contact surface between the mortar and the bar simulates the contact between concrete and reinforcing bars in structures through the use of realistic water-cement and sand-cement ratios. In rapid macrocell tests, mortar-wrapped specimens are placed in simulated concrete pore solution with a 1.6-molal ion concentration of sodium chloride (NaCl) under this study.

The rapid macrocell test involves the determination of the corrosion rates and losses of the conventional steels in mortar with three different inhibitors, DCI-S, Rheocrete 222+, or Hycrete or in mortar without any inhibitors. The specimens are autopsied following the tests.

2.2.1 Testing Materials and Apparatus

The materials and apparatus used for the macrocell tests are detailed as below.

- 1) *Reinforcing steel* – No. 16 (No. 5) conventional bars that meet the requirements of ASTM A615. The bars are prepared according to the procedures described in Section 2.3.2
- 2) *Mortar* – The mortar mixture proportions are shown in Table 2.3 in Section 2.2.2. The properties of the materials are as follows: Type I/II portland cement meeting the requirements in ASTM C150, graded Ottawa sand meeting the requirements in ASTM C778, and deionized water. When a corrosion inhibitor is used, the mix water is adjusted to account for the water in the corrosion inhibitor.
- 3) *Mortar Fill* - Mortar fill has the same mixture proportions as the test specimens. It is placed in the solutions that surround the specimens to simulate the environment found in bulk concrete. The fill is cast on a 25-mm (1-in.) deep metal baking sheet, following the same mixing procedure used when casting the specimens, and is then broken into pieces about 40 mm (1.5 in.) on a side within 24 hours of casting and stored for use. No corrosion inhibitor is used in mortar fill.
- 4) *Pore Solution* – The simulated concrete pore solution is prepared based on the analysis by Fazammehr (1985), but without the chloride content. One liter of the concrete pore solution contains 974.8 g of deionized water, 18.81 g of KOH, and 17.87 g of NaOH. The pH of the simulated concrete pore solution is 13.4.
- 5) *Pore Solution Containing NaCl* – A 1.6 molal ion concentration of NaCl is used in this study. To prepare the solution, 45.6 g of NaCl is added to one liter of the simulated concrete pore solution.
- 6) *Container* – Each anode and cathode is held at a 3.0-L (0.8-gallon) plastic container with a lid. The container is 178 mm (7 in.) in diameter and 191 mm

(7.5 in.) in height.

- 7) *Salt Bridge* – A salt bridge provides an ionic path between two container solutions (anode and cathode). It consists of a flexible latex tube filled with a conductive gel. The gel is prepared following the procedures described by Steinbach and King (1950). 4.5 g (0.16 oz) of agar and 30 g (1.06 oz) of potassium chloride (KCl) are added into 100 g (3.53 oz) of deionized water in a pot and heated over a hotplate until it starts to congeal. The mixture is poured into a 0.6-m (2-ft) long latex tube and then two ends are tied together using a rubber band. The gel should be continuous to avoid air bubbles in the tubing and, therefore, provide an effective ionic path between anode and cathode. One batch can fill four tubes. The filled tubes are placed in boiling water with tied ends upwards for one hour and then allowed to cool to room temperature. The ends of the salt bridges, along with the rubber bands, are cut off before use.
- 8) *Air Scrubber* – An air scrubber is used to remove carbon dioxide from compressed air before it passes through the simulated pore solution at the cathode to ensure an adequate supply of oxygen for the cathodic reaction. The air scrubber is prepared following the procedure described by Balma et al. (2005). Two barbed fittings are installed on the top of a 19-liter (5-gallon) plastic container. Compressed air is directed through one fitting. One end of a 1.5-m (5-ft) long perforated plastic tube is connected to the other side of the barbed fitting from the interior of the container. The other end of the tube is sealed. Crushed rock is used to hold down the coiled end of the tube at the bottom of the container. The container is filled with 1M sodium hydroxide (NaOH) solution. The scrubbed air is distributed to the cathodic solutions for multiple specimens through the second barbed fitting to latex tubing and polypropylene T-shaped connectors. Screw

clamps on each branch of tubing are used to adjust the amount of the air entering the containers. The scrubber solution is checked periodically to insure an adequate level of solution. Deionized water and NaOH are added to maintain a pH value of 13.4.

- 9) *Epoxy* – Sewer Guard HBS 100 Epoxy Liner, from ChemRex, Inc.
- 10) *Agar* – Agar with high gel strength, manufactured by Sigma Chemical Co.
- 11) *KOH* – Used to make simulated concrete pore solution, from Fisher Scientific.
- 12) *NaOH* – Used to make simulated concrete pore solution and air scrubber, from Fisher Scientific.
- 13) *NaCl* – Used to make anodic solution, from Fisher Scientific.
- 14) *Voltmeter* – Keithley digital nanovoltmeter, Model 2182A. Used to measure the voltage drop across the 10-ohm resistor and the corrosion potential of the anode and cathode.
- 15) *Saturated Calomel Electrode (SCE)* – Fisher Scientific Accumet epoxy body calomel reference electrode, Catalog No. 13-620-258. Corrosion potentials in the rapid macrocell test are measured with respect to an SCE.
- 16) *Resistor* – A 10-ohm resistor with 5% tolerance based on manufacturer's specification (actual resistance is 10 ± 0.3 ohms for all resistors used in this study). Used to connect the anode and cathode for making corrosion current measurements.
- 17) *Mortar Mixer* – Hobart mixer, Model N-50. The mixer is used to mix the mortar needed to fabricate mortar-wrapped macrocell specimens. Complies with ASTM C305.
- 18) *Terminal Box* – The terminal box is assembled for convenience in making measurements. Anodes from the macrocell are connected to red binding posts and

cathodes to black posts. For each test assembly, red and black posts are paired with a switch in the middle. A 10-ohm resistor is connected in series between the switch and the red post. The circuit is closed and open as the switch is turned on and off.

- 19) *Wire* – 16-gage electrical copper wire is used to connect the anode and cathode to the terminal box.
- 20) *Bolts and Washers* – 10-24×38 mm (1½ in.) threaded bolts are used to hold the testing bars in place in the molds during casting. 10-24×13 mm (½ in.) stainless steel threaded bolts are used for final assembly, accommodated with the stainless steel washers.

2.2.2 Specimen Preparation

The mortar-wrapped specimen consists of a 127-mm (5-in.) long No. 16 (No. 5) reinforcing bar, which is embedded 127 mm (5 in.) in a 154-mm (6-in.) high mortar cylinder, as shown in Figure 2.1. The mortar cylinder is 30 mm (1.2 in.) in diameter, which provides a mortar cover thickness of 7 mm (0.28 in.) around the reinforcing bar.

Specimen fabrication proceeds as follows:

1) Reinforcing bar preparation

No. 16 (No. 5) conventional reinforcing steel is cut to a length of 127 mm (5 in.) and the sharp edges at the ends are smoothed with a grinder. One end of the bar is drilled and tapped 13 mm (0.5 in.) deep to accommodate a 10-24 stainless steel threaded bolt. Conventional bars are cleaned with acetone to remove dust and grease. Epoxy-coated bars, not evaluated using this test in this study, are cleaned with soap and warm water, and then left to air dry.

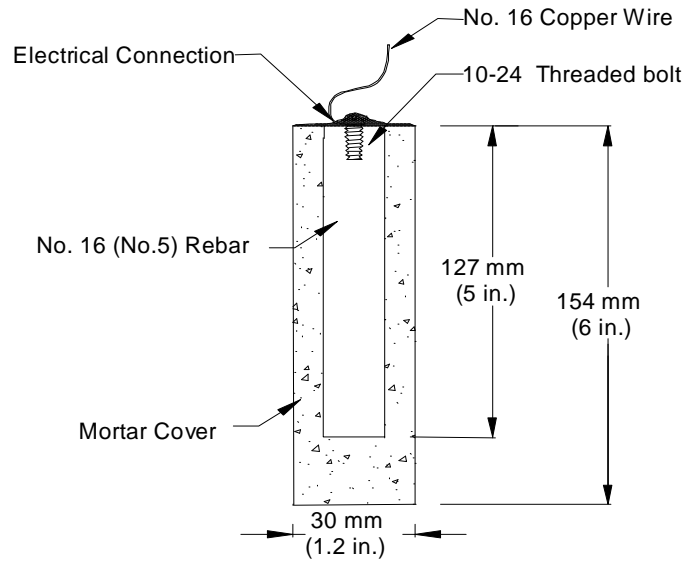


Figure 2.1 – Mortar-wrapped specimen

2) Mold assembly

The mold used for the mortar-wrapped specimens is made of polymerized vinyl chloride (PVC) pipe. The specimen mold and the mold holder consist of the following materials, as shown in Figure 2.2.

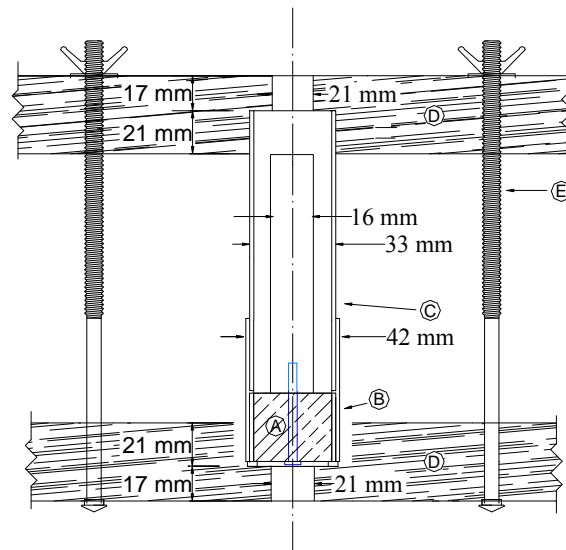


Figure 2.2 – Mold for mortar-wrapped specimens

A. One ASTM D2466 32-mm (1.25-in) long PVC pipe ending connector (part

No. 4449-010) filled with Sewer Guard epoxy, with a 4-mm ($\frac{1}{6}$ -in.) diameter hole at the center.

- B. One ASTM D2466 32 mm (1.25 in.) to 32 mm (1.25 in.) PVC fitting (part No. 429-010) with 42-mm (1.65-in.) external diameter, total length of 60 mm (2.375 in.).
- C. One ASTM D2241 SDR 21 25.4-mm (1-in.) PVC pipe with 30-mm (1.18-in.) internal diameter and 152 mm (6 in.) long. The pipe is sliced longitudinally to facilitate the removal of the specimen. To prevent the mortar from leaking, the slice is covered with masking tape during casting.
- D. Two pieces of 38 × 203 × 381 mm (1.5 × 8 × 15 in.) pressure treated lumber. Holes and recesses are bored into the flat surfaces to hold the specimen molds in position during casting.
- E. Six threaded rods, 6-mm (0.25-in.) diameter, 305-mm (12-in.) long, are inserted between the two pieces of lumber, three in each row.

The mold is assembled as follows (see Figure 2.2):

- a) The PVC pipe ending connector, **A**, is inserted in the machined end of the PVC fitting, **B**.
- b) A 38-mm (1.5-in.) long 10-24 threaded bolt is inserted into the hole centered in the ending connector. The tapped end of the reinforcing bar is then attached to the bolt.
- c) The longitudinal slice along the side of the PVC pipe, **C**, is covered using masking tape. The pipe is then inserted in the free end of the PVC fitting.
- d) The assembled mold is placed between the two pieces of lumber, **D**, in the holes and recesses, as provided. The threaded rods, **E**, are then inserted through the two pieces of lumber to hold the molds together.

3) Specimen Casting

The mortar mixture proportions are given in Table 2.3. The dosage rates are based on the dosage rates for bench-scale specimens by concrete volume (Guo et al. 2006) and are converted to the proportions by mortar volume. For the inhibitor Hycrete, the dosage rates by mortar volume used for the rapid macrocell specimens are the same as those used for the bench-scale specimens (for example, for a w/c of 0.45, the Hycrete dosage rate is 8 kg/m³ for concrete, which is 13.14 kg/m³ based on the volume of mortar in a cubic meter of concrete; for a w/c of 0.35, the dosage rate is 9.9 kg/m³ by concrete volume and 15.94 kg/m³ by mortar volume). For DCI and Rheocrete, the mix designs are adapted from Ge et al. (2004). Dosage rates by mortar volume used for the rapid macrocell specimens are 56% of the dosage rates used for the bench-scale specimens by Guo et al. (for the DCI and Rheocrete inhibitors, respectively, the dosage rates are 8.47 and 2.84 kg/m³ by concrete volume and 13.91 and 4.66 kg/m³ by mortar volume for a w/c of 0.45 and 8.79 and 2.95 kg/m³ by concrete volume and 14.15 and 4.75 kg/m³ by mortar volume for a w/c of 0.35).

Table 2.3 – Mortar mixture proportions for rapid macrocell specimens

Mixture ID ^a	w/c ^b	Water (g)	Cement (g)	Sand (g)	DCI-S (ml)	Hycrete (ml)	Rheocrete (ml)
M-NO45	0.45	400	889	1526	-	-	-
M-DCI45	0.45	389	889	1526	17.6	-	-
M-HY45	0.45	388	889	1526	-	16	-
M-RH45	0.45	396	889	1526	-	-	5.9
M-NO35	0.35	400	1143	1315	-	-	-
M-DCI35	0.35	389	1143	1315	17.9	-	-
M-HY35	0.35	385	1143	1315	-	20	-
M-RH35	0.35	396	1143	1315	-	-	6

^a M = Macrocell. NO = Conventional steel with no inhibitors mixed in the mortar.

DCI = Conventional steel with corrosion inhibitor DCI-S mixed in the mortar.

HY = Conventional steel with corrosion inhibitor Hycrete mixed in the mortar.

RH = Conventional steel with corrosion inhibitor Rheocrete mixed in the mortar.

45 = Water-cement ratio is 0.45. 35 = Water-cement ratio is 0.35.

^b Water in the inhibitor is included in the water-cement ratio.

The mixes have water-cement ratios of 0.35 or 0.45. Deionized water is used for the mixes. The mortar is made in accordance with ASTM C305. Specimens are cast in four equal layers and each layer is rodded 25 times with a 2-mm (0.08-in.) diameter, 305-mm (12-in.) long rod, followed by consolidation for 30 seconds on a vibrating table with an amplitude of 0.15 mm (0.006 in.) and a frequency of 60 Hz. The upper surface is finished using a wooden float.

4) Curing

The specimens are cured for 24 hours in the molds at a temperature of 21.1 to 24.5°C (70 to 76°F), and then removed from the molds and cured in saturated lime water at $22.8 \pm 1.7^\circ\text{C}$ ($73 \pm 3^\circ\text{F}$) for 13 days. After curing, the specimens are surface-dried with compressed air and then dried in a vacuum desiccator for one day.

5) Wiring

A 16-gage copper electrical wire is attached to the tapped end of each specimen with a 13-mm ($1/2$ -in.) long 10-24 stainless threaded bolt. The electrical connection is covered with two layers of Sewer Guard epoxy for the mortar-wrapped specimens to prevent crevice corrosion. Each layer is left to dry for about 4 hours before proceeding to the next step.

2.2.3 Test Setup

The rapid macrocell test is illustrated in Figure 2.3. It requires two containers and three specimens. Two specimens, which function as the cathode, are placed in a 3.0-L (0.8-gallon) plastic container with simulated concrete pore solution. The third specimen, which functions as the anode, is placed in another container containing the same pore solution with a 1.6-molal ion concentration of NaCl. Crushed mortar fill, made using the same mix as the specimens, is added to the containers to more closely

simulate the concrete environment. The solution is maintained at the depth of 102 mm (4 in.), which exposes 76 mm (3 in.) of the bar to the solution.

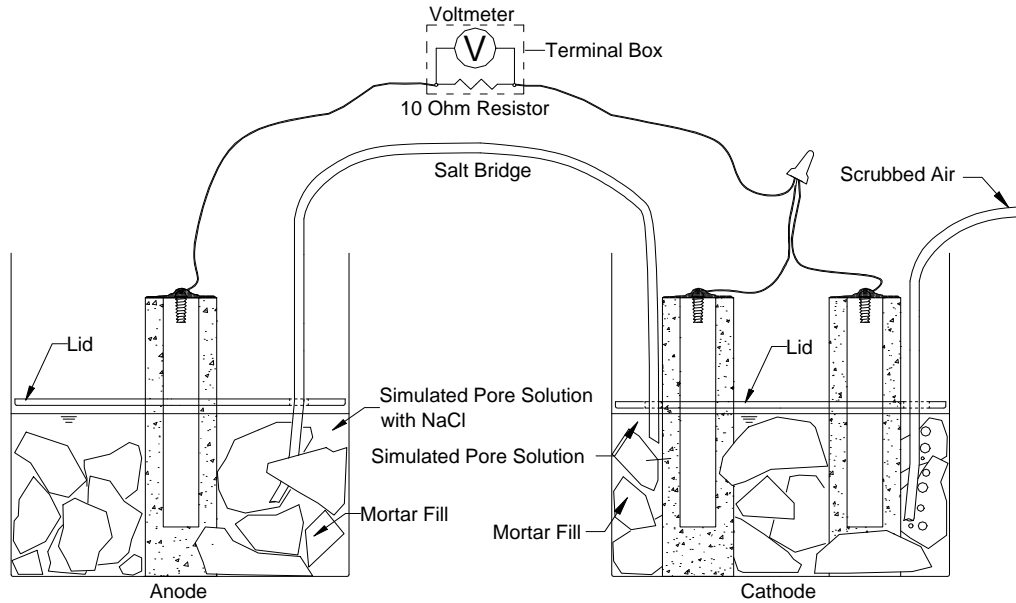


Figure 2.3 – Rapid macrocell test with mortar-wrapped specimens

The anode and cathode specimens are electrically connected across a 10-ohm resistor. A salt bridge connects the solutions in two containers to form an ionic path. The resistors are mounted between the binding posts in a terminal box to consolidate the wiring. Compressed air, scrubbed to remove carbon dioxide (CO_2), is bubbled into the cathode solution to ensure an adequate supply of oxygen for the cathodic reaction.

Plastic lids are placed in the two containers just above the surface of the solution to hold the specimen in place and to reduce the evaporation of the solutions. Holes are placed in the lids to introduce the test specimens, salt bridge, and tubing from the air scrubber. The solution level is checked regularly and maintained constant by adding deionized water. The solutions in both containers are replaced once every

five weeks to reduce the effects of carbonation and maintain the pH of the solution above 13.4.

2.2.4 Test Procedure

The voltage drop and open circuit corrosion potentials of the specimens are recorded daily for the first week and once every week thereafter. The voltage drop across the 10-ohm resistor is measured using a voltmeter and the circuit is then opened about two hours before measuring the corrosion potentials. Both anode and cathode corrosion potentials are measured with respect to a saturated calomel electrode (SCE). The test lasts for 25 weeks.

2.2.5 Test Program

Conventional steel with three different inhibitors, DCI-S, Rheocrete 222+, and Hycrete are tested in the study. Mortar-wrapped macrocells without an inhibitor are also tested for comparison. Water-cement ratios of 0.35 and 0.45 are used. Six macrocell tests are used for each protection system for a total of 48 tests. The test program is summarized in Table 2.4.

2.3 BENCH-SCALE TESTS

Three bench-scale tests, the Southern Exposure (SE), Cracked Beam (CB), and ASTM G109 tests are used in the study. Of these tests, the SE and the CB give useful data in a relatively short period of time using a 15% NaCl solution to pond the specimens; the ASTM G109 tests use a 3% NaCl solution and provide a much milder degree of exposure to the specimens.

Table 2.4 – Rapid macrocell test program

Test ID ^a	w/c	NaCl Concentration	Number of Tests
M-NO45	0.45	1.6 m	6
M-DCI45	0.45	1.6 m	6
M-HY45	0.45	1.6 m	6
M-RH45	0.45	1.6 m	6
M-NO35	0.35	1.6 m	6
M-DCI35	0.35	1.6 m	6
M-HY35	0.35	1.6 m	6
M-RH35	0.35	1.6 m	6

^a M = Macrocell. NO = Conventional steel with no inhibitors mixed in the mortar.
DCI = Conventional steel with corrosion inhibitor DCI-S mixed in the mortar.
HY = Conventional steel with corrosion inhibitor Hycrete mixed in the mortar.
RH= Conventional steel with corrosion inhibitor Rheocrete mixed in the mortar.
45 = Water-cement ratio is 0.45. 35 = Water-cement ratio is 0.35.
No. 16 (No. 5) conventional steel is used in all test specimens.

The SE and the CB tests are used to compare the corrosion performance of conventional steel in conjunction with three different corrosion inhibitors, DCI-S, Rheocrete 222+, and Hycrete. Specimens with conventional and epoxy-coated steel without inhibitors are also tested as controls. SE and CB specimens are also used to evaluate stainless steel cast with the same concrete mix as used for two bridges, and are used to compare corrosion performance in the lab and in the field. The bridge specimens are described in Section 2.5. The G109 tests are used to determine the corrosion rates and losses of the conventional steel, multiple-coated, and epoxy-coated steel in concrete without corrosion inhibitors.

No. 16 (No. 5) reinforcing bars are used to fabricate all test specimens. The corrosion rate and loss values are compared for the different specimens, which are autopsied following the tests.

2.3.1 Testing Materials and Apparatus

The materials and apparatus used in the bench-scale tests are listed below:

1) *Concrete* – The concrete contains $6 \pm 1\%$ entrained air and has a 76 ± 13 mm (3 ± 0.5 in.) slump. A water-cement (*w/c*) ratio of 0.45 is used for all systems. The concrete mixture proportions are shown in Table 2.5.

The properties of the materials are as follows:

- i) Type I/II portland cement;
- ii) *Coarse aggregate* – Crushed limestone from Fogle Quarry with maximum size of 19 mm ($\frac{3}{4}$ in.), bulk specific gravity (SSD) = 2.58, absorption (dry) = 2.27 %, unit weight = 1536 kg/m^3 (95.9 lb/ft^3);
- iii) *Fine aggregate* – Kansas River sand with bulk specific gravity (SSD) = 2.62, absorption (dry) = 0.78%, fineness modulus = 3.18;
- iv) *Air-entraining agent* – Daravair 1400 by W. R. Grace, Inc; and
- v) *Water* – Tap water and water in the corrosion inhibitors is included in the water-cement ratio.

Table 2.5 - Concrete mixture proportions for bench-scale tests

<i>w/c</i>	Cement	Water ^a	Coarse Aggregate	Fine Aggregate	Air-entraining Agent ^b	DCI-S	Hycrete	Rheocrete
	kg/m^3 (lb/yd^3)	kg/m^3 (lb/yd^3)	kg/m^3 (lb/yd^3)	kg/m^3 (lb/yd^3)	mL/m^3 (oz/yd^3)	L/m^3 (gal/yd^3)	kg/m^3 (lb/yd^3)	L/m^3 (gal/yd^3)
0.45	355 (598)	160 (270)	881 (1484)	852 (1436)	90 (2.33)	-	-	-
	355 (598)	147.4 (248.5)	881 (1484)	852 (1436)	140 (3.62)	15 (3.03)	-	-
	355 (598)	154 (259.6)	881 (1484)	852 (1436)	35 (0.90)	-	8 (13.5)	-
	355 (598)	155.7 (262.4)	881 (1484)	852 (1436)	300 (7.76)	-	-	5 (1.01)
Inhibitor dosage rate:								
Rheocrete 222+: 5 L/m^3 (1.01 gal/yd^3)								
DCI-S: 15 L/m^3 (3.03 gal/yd^3)								
Hycrete: 2.25% of cement content								

^a Water in the inhibitor is included in the water-cement ratio.

^b Daravair 1400 is used as Air - entraining agent

2) *Salt Solution* – 15% NaCl concentration by mass dissolved in deionized water for the SE and CB specimens, 3% NaCl concentration by mass dissolved in deionized

water for the ASTM G109 specimens.

- 3) *NaCl* – Used to make the salt solutions, from Fisher Scientific.
- 4) *Epoxy* – Sewer Guard HBS 100 Epoxy Liner, from ChemRex, Inc.
- 5) *Silicon Caulk* – The 100% silicon caulk by Macklenburg-Duncan.
- 6) *Voltmeter* – Keithley digital nanovoltmeter, Model 2182A. Used to measure the voltage drop across the resistor and the corrosion potential of the anode and cathode.
- 7) *Ohmmeter* – Agilent digital 1 kHz AC milliohmmeter, Model 4338B.
- 8) *Saturated Calomel Electrode (SCE)* – Fisher Scientific Accumet epoxy body calomel reference electrodes, Catalog No. 13-620-258.
- 9) *Resistor* – A 10-ohm resistor connects the top and bottom mat bars for the SE and CB specimens, and a 100-ohm resistor is used for the ASTM G109 specimens. Used to measure the corrosion current. The tolerance of these resistors is 5% based on the manufacturer's specification (an actual tolerance of 3% was measured for all resistors used in this study).
- 10) *Concrete Mixer* – Lancaster Counter Current Batch Mixer with a capacity of 0.06 m³ (2 ft³), manufactured by Lancaster Iron Works Inc. The mixer complies with ASTM C192.
- 11) *Terminal Box* – The terminal box is assembled for convenience in making measurements. Anodes from the top mat of specimens are connected to red binding posts and cathodes to black posts. For each test specimen, red and black posts are paired with a switch in the middle. A 10-ohm (for SE and CB) or 100-ohm (for G109) resistor is connected in series between the switch and the red post. The circuit is closed and open as the switch is turned on and off.
- 12) *Wire* – 16-gage electrical copper wire is used to connect the anode and cathode to the terminal box.

13) *Bolts and Washers* – 10-24×38 mm (1½ in.) threaded bolts are used to hold the testing bars in place in the molds during casting, while 10-24×13 mm (½ in.) stainless steel threaded bolts are used for final assembly, accommodated with the stainless steel washer.

14) *Shop Vacuum Cleaner* – Used to vacuum salt solution for bench-scale specimens between the ponding and drying cycles.

15) *Heating Tents* - The heating tents are used in the ponding-drying cycles. Tents are 1.2 m (3.5 ft) high, 1.33 (4 ft) wide and 2.67 m (8 ft) long. The tents are movable and can hold 12 SE and 12 CB specimens at one time. The structure is made of plywood and lumber and is covered with two layers of plastic sheeting. Three 250-watt heating lamps are evenly spaced along the roof. A thermostat with a temperature sensor is installed within the tent to maintain a temperature of $38 \pm 1.5^{\circ}\text{C}$ ($100 \pm 3^{\circ}\text{F}$).

2.3.2 Specimen Preparation

The SE test specimen, as shown in Figure 2.4, is a $305 \times 305 \times 178$ mm ($12 \times 12 \times 7$ in.) concrete slab consisting of two mats of reinforcing bars. Of these two mats, two 305-mm (12-in.) long No. 16 (No. 5) bars are placed in the top mat and four similar bars in the bottom mat with a clear concrete cover of 25.4 mm (1 in.) to the top and bottom bars. A concrete dam is cast monolithically on top of the specimen for ponding the 15% salt solution.

The CB test specimen (Figure 2.5) is used to model corrosion of reinforcing steel in which the steel is directly exposed to deicing salts due to the formation of a crack above and parallel to the bar. It is otherwise similar to SE test specimen, except half the width. The CB specimen has dimensions of $305 \times 152 \times 178$ mm ($12 \times 6 \times 7$ in.) with one bar on the top and two bars on the bottom. A 152-mm (6-in.) long, 25-

mm (1-in.) deep simulated crack is made in the concrete directly above and parallel to the top bar using a 0.3-mm (12-mil) stainless steel shim, simulating cracks that form in bridge decks.

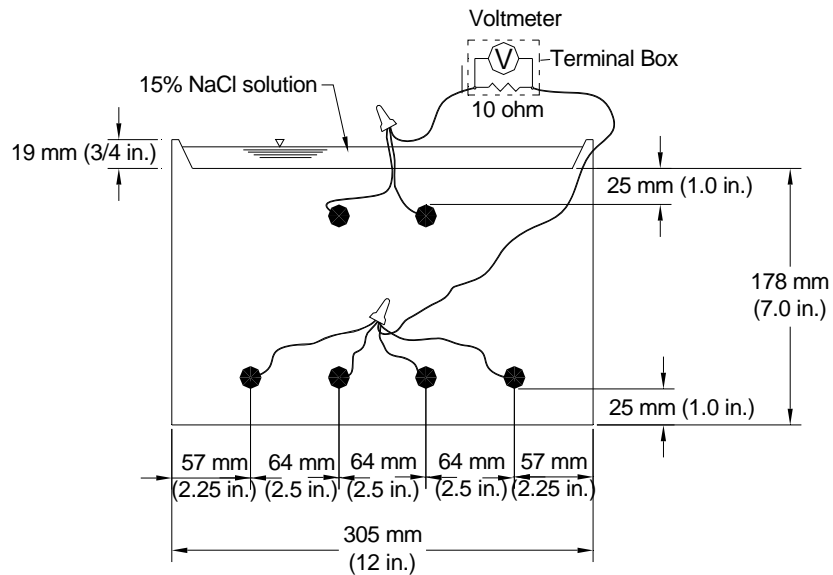


Figure 2.4 – Southern Exposure test specimen

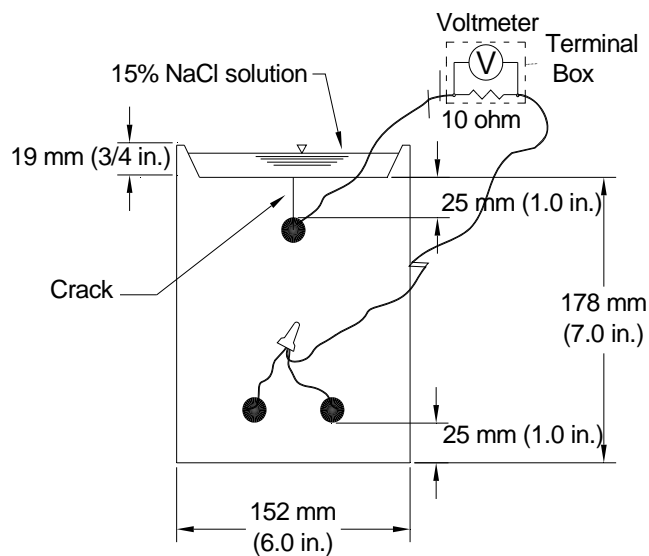


Figure 2.5 – Cracked Beam test specimen

The ASTM G109 test specimen (Figure 2.6) has dimensions of $279 \times 152 \times 114$ mm ($11 \times 6 \times 4.5$ in.). It also contains one top and two bottom bars with a clear concrete cover of 25 mm (1 in.) for the top and bottom bars. The two mats of steel are electrically connected across a 100-ohm resistor. A 150×75 mm (6×3 in.) Plexiglass dam is attached to the top surface of specimen using silicon caulk for ponding the 3% salt solution.

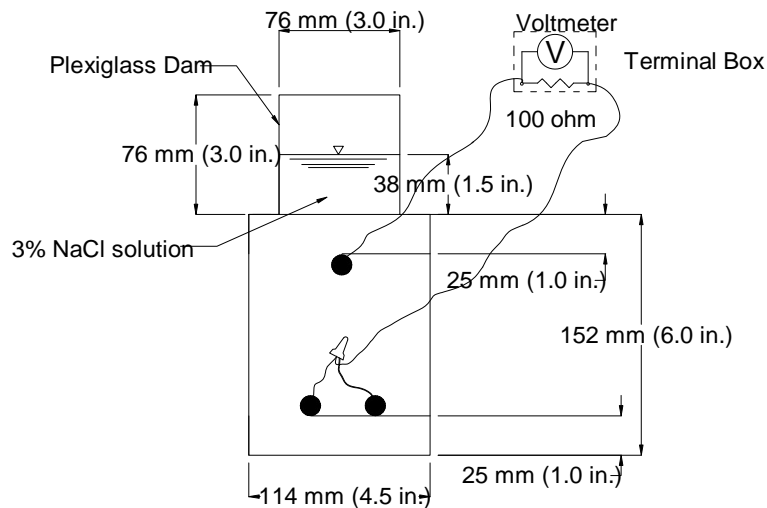


Figure 2.6 – ASTM G109 test specimen

The SE, CB, and ASTM G109 test specimens are fabricated as follows:

1) Reinforcing bar preparation

No. 16 (No. 5) reinforcing bars are cut to a length of 305 mm (12 in.) for the SE and CB test specimens and 279 mm (11 in.) for the G109 test specimens. Sharp edges at the ends of the bars are smoothed with a grinder. Both ends of the bars are drilled and tapped to a depth of 13 mm (0.5 in.) to accommodate a 10-24 stainless steel threaded bolt. Conventional and stainless steel bars are cleaned with acetone, while epoxy-coated bars are cleaned with soap and warm water, and left to air dry. To simulate the damage typically found at the construction site, the coating on the epoxy-

coated and multiple-coated bars is penetrated with four or ten 3.2-mm ($\frac{1}{8}$ -in.) diameter holes, representing 1% or 2% coating damage, respectively. The holes are drilled to a depth of 0.4 mm (16 mils) from the outer coating surface using a 3-mm ($\frac{1}{8}$ -in.) diameter four-flute drill bit mounted on a milling machine. Two or five holes are evenly distributed on each side of the bar along its length with four or ten holes in total for each bar. For some multiple-coated bars, holes are drilled to just damage the epoxy coating without exposing the underlying zinc. A soldering gun is set at a temperature of 205°C (493°F) and used to burn off the remaining epoxy around the hole and expose the underlying zinc. This temperature is above the melting point of the epoxy and below that of the zinc, 420°C (787°F), so that the zinc layer will not be damaged.

2) Mold assembly

The forms are made of 19-mm ($\frac{3}{4}$ -in.) thick plywood. Small holes are drilled in the two ends of the form to hold the reinforcing bars in position. The specimens are cast upside down. For SE and CB specimen forms, a rectangular piece of plywood with beveled edge is fixed to the inside bottom of the form to create a dam edge. For the CB specimens, a 152-mm (6-in.) long cut-through notch is made parallel to the length at the center of the beveled piece. Four side and bottom pieces are fastened together using bolts and clamps. All corners are sealed with masking tape and modeling clay both from inside to avoid leakage. The bars are bolted into the forms after mineral oil is applied as a bond breaker. For CB test specimens, a 0.3-mm (12-mil) thick stainless steel shim is inserted to the notch in the beveled bottom piece before bolting and placed in contact with top bar to simulate the concrete crack.

3) Specimen Casting

The mixture proportions are given in the Table 2.5. The corrosion inhibitor

dosage rates are based on the recommended dosage rates for the concrete. The concrete is made in accordance with ASTM C192. The specimen is cast in two equal layers and each layer is consolidated for 30 seconds on a vibrating table with an amplitude of 0.15 mm (0.006 in.) and a frequency of 60 Hz. The upper surface is finished with a wooden float. The SE and CB specimens are cast in an inverted position to monolithically create the dam on top of the specimen. The ASTM G109 test specimens are also cast upside down to obtain a smooth top surface to which the Plexiglass dams are attached.

4) Curing

The specimens are cured for 24 hours in the molds at room temperature and then removed from the molds. The stainless steel shims are taken out of the CB test specimens 8 to 12 hours after casting. The SE and CB test specimens are next cured for two days in a plastic bag filled with deionized water. They are then removed from the bags and cured in air for 25 days. After demolding, the G109 test specimens are placed in a curing room with a temperature of $23 \pm 2^{\circ}\text{C}$ ($73.4 \pm 3.6^{\circ}\text{F}$) and a relative humidity above 95% for 28 days. The specimens are then allowed to dry for two weeks at a relative humidity of 50% at room temperature.

2.3.3 Test Setup

The top surface of all specimens is lightly sanded. For G109 specimens, the Plexiglass dams are attached to the top center surface with superglue two days before testing. The corners where the Plexiglass meet are sealed with silicone to prevent leaking. A 16-gage copper electrical wire is attached to the tapped end of each steel bar with a 13-mm ($1/2$ -in.) long 10-24 stainless threaded bolt. The four sides of the specimens are covered with two layers of Sewer Guard epoxy to limit the salt

penetration through the sides of the specimen. Each layer of epoxy is left to dry for about 4 hours before proceeding to the next step.

The 16-gage copper wires from the top mat bars are connected to the red binding posts of a terminal box, while the wires from the bottom mat bars are connected to the paired black binding posts. A switch is connected to the red binding post through a 10-ohm resistor. The switches are turned on and off to close and open the electrical circuits.

2.3.4 Test Procedure

The SE and CB tests follow the same test procedure. The specimens are ponded with 600 ml (0.16 gal) of 15% NaCl solution for four days at room temperature. A plastic sheet is used to cover the specimens to reduce evaporation. On the fifth day, the voltage drop across the 10-ohm resistor is recorded for each specimen using a voltmeter. The circuit is then disconnected and the mat-to-mat resistance is measured using an ohmmeter. Two hours after disconnecting the circuit, the corrosion potentials of the top and bottom mat bars are measured with respect to a saturated calomel electrode (SCE). The circuits are then reconnected, and the ponded salt solution is removed using a shop vacuum. The specimens are placed under a heating tent for three days at a temperature of $38 \pm 1.5^{\circ}\text{C}$ ($100 \pm 3^{\circ}\text{F}$). This weekly ponding-drying cycle is repeated for 12 weeks. The specimens are then continuously ponded with the 15% NaCl solution for 12 weeks at room temperature. On the fifth day of each week, the voltage drop, mat-to-mat resistance, and corrosion potentials of the top and bottom mats are measured with respect to an SCE. This 24-week cycle is repeated three more times to complete 96 weeks of testing. During ponding periods, the solution level is checked regularly and maintained at a constant level by adding

deionized water. The SE specimens are drilled to obtain chloride samples at the time of corrosion initiation (the time that specimens start to show signs of corrosion, Section 2.7.1), the 48th week, and the end of testing life.

The ASTM G109 test uses a different salt solution and ponding-drying regime from the SE and CB tests. The specimens are ponded with 300 ml (0.08 gal) of 3% NaCl solution for two weeks at room temperature. At the end of each week, the voltage drop across the 100-ohm resistor is recorded using a voltmeter. The circuit is then disconnected and the mat-to-mat resistance is measured using an ohmmeter. Two hours after opening the circuit, the corrosion potentials of the top and bottom mats are measured with respect to an SCE. The circuits are then reconnected. After taking readings at the end of second week, the salt solution is removed with a shop vacuum. The specimens are then allowed to dry for two weeks at room temperature. Only the voltage drops and mat-to-mat resistances are measured weekly during this drying cycle. The 4-week ponding and drying cycle is repeated throughout the test period. The corrosion rates and losses for the ASTM G109 specimens are much lower than those for the corresponding SE and CB specimens due to the much less severe exposure condition provided by the ASTM G109 test. The test results for all of the specimens will be presented in Chapter 3.

The testing period for the SE and CB specimens is usually 96 weeks. For some specimens containing highly corrosion-resistant bars, such as stainless steel, the tests may be continued for longer periods. A testing period of 240 weeks is used for the ASTM G109 specimens in this study.

In addition to the voltage drop, mat-to-mat resistance, and open circuit corrosion potentials, which are measured weekly, linear polarization resistance tests are performed every four weeks throughout the testing period for selected bench-scale

specimens.

2.3.5 Test Program

The SE and CB tests are used to compare the performance of conventional steel with three different corrosion inhibitors, DCI-S, Rheocrete 222+, and Hycrete. Specimens with conventional steel and ECR are also tested as controls. Three SE and CB specimens are tested for each inhibitor and six SE specimens are tested for each control group, all with concrete with a water-cement ratio of 0.45. The test programs are summarized in Tables 2.6 and 2.7. SE and CB specimens containing stainless steel were cast with the same concrete mix as the two bridges used to monitor the corrosion rates and losses in the field, the Doniphan County and Mission Creek bridges. These are discussed separately in Section 2.5.

Table 2.6 – Test program for Southern Exposure tests

Test ID ^a	Number of Tests	LPR Test Specimen No.
Control		
SE-Conv.	6	4
SE-ECR	6	4
Corrosion Inhibitors		
SE-N5-NO	3	1
SE-N5-DCI	3	1
SE-N5-HY	3	1
SE-N5-RH	3	1

^a Conv. = conventional steel. ECR = conventional epoxy-coated reinforcement.

N5 = conventional steel with different heat.

NO = Conventional steel with no inhibitors mixed in the concrete.

DCI = Conventional steel with corrosion inhibitor DCI-S mixed in the concrete.

HY = Conventional steel with corrosion inhibitor Hycrete mixed in the concrete.

RH= Conventional steel with corrosion inhibitor Rheocrete 222+ mixed in the concrete.

Table 2.7 – Test program for cracked beam tests

Test ID ^a	Number of Tests	LPR Test Specimen No.
CB-N5-NO	3	1
CB-N5-DCI	3	1
CB-N5-HY	3	1
CB-N5-RH	3	1

^a N5 = conventional steel.

NO = Conventional steel with no inhibitors mixed in the concrete.

DCI = Conventional steel with corrosion inhibitor DCI-S mixed in the concrete.

HY = Conventional steel with corrosion inhibitor Hycrete mixed in the concrete.

RH= Conventional steel with corrosion inhibitor Rheocrete 222+ mixed in the concrete.

The G109 tests involve the determination of the corrosion rates and losses of the conventional, multiple-coated, and epoxy-coated steels in concrete without inhibitors. All specimens had a water-cement ratio of 0.45. The testing program is summarized in Table 2.8. Specimens are autopsied following the tests.

Table 2.8 – Test program for ASTM G109 tests

Steel Designation ^a	Number of Tests	LPR Test Specimen No.
Conv.	6	6
ECR	3	3
ECR-10h	6	6
MC(only epoxy penetrated)	3	3
MC(only epoxy penetrated)-10h	3	3
MC(both layers penetrated)	3	3
MC(both layers penetrated)-10h	3	3

^a Conv. = conventional steel. ECR= normal epoxy-coated steel.

MC(both layers penetrated) = multiple coated steel with both layers penetrated.

MC(only epoxy penetrated) = multiple coated steel with only epoxy layer penetrated.

10h = epoxy coated steel penetrated with ten 3 mm ($\frac{1}{8}$ in.) holes, otherwise 4 holes.

* Water/ cement ratio of 0.45 are used for all specimens.

Linear polarization resistance (LPR) tests are used to determine the microcell corrosion rate and loss for bench-scale test specimens. Tests are conducted on a single specimen for each system. The tested specimen is listed under “LPR Test Specimen No.” in Tables 2.6 through 2.8. The linear polarization resistance test is described in Section 2.6.

2.4 FIELD TEST

The field test is designed to obtain a measure of the performance of corrosion protection systems under realistic exposure conditions. Test specimens are placed outdoors at the Adams Campus of the University of Kansas. Some specimens have uncracked concrete and some specimens have simulated cracks directly above and parallel to selected reinforcing bars. Field tests involve the determination of corrosion rates and losses of different reinforcing steels, including epoxy-coated steel with increased adhesion coatings, steel in concrete with corrosion inhibitors, or a combination of these protection systems. A dam made of weatherstrip tape is attached to the top concrete surface to hold the salt solution, which is 10% rock salt solution that is ponded on the specimens every four weeks.

2.4.1 Testing Materials and Apparatus

The materials and apparatus used in the field test are described below:

- 1) *Concrete* – The concrete has a water-cement (w/c) ratio of 0.45, with $6 \pm 1\%$ entrained air and 76 ± 13 mm (3 ± 0.5 in.) slump. The concrete mixture proportions are shown in Table 2.9.

The properties of the materials are as follows:

- i) Type I/II portland cement;
- ii) *Coarse Aggregate* – Crushed limestone from Fogle Quarry with maximum size of 19 mm ($3/4$ in.), bulk specific gravity (SSD) = 2.58, absorption (dry) = 2.27 %, unit weight of 1536 kg/m^3 (95.9 lb/ft^3);
- iii) *Fine Aggregate* – Kansas River sand with bulk specific gravity (SSD) = 2.62, absorption (dry) = 0.78%, fineness modulus = 3.18;
- iv) *Air-entraining Agent* – Daravair 1400, from W. R. Grace, Inc.; and

- v) *Water* – Tap water and water in the corrosion inhibitors is included in the water-cement ratio.

Table 2.9 - Concrete mixture proportions for field tests

<i>w/c</i>	Cement	Water ^a	Coarse Aggregate	Fine Aggregate	Air-entraining Agent ^b	DCI-S	Hycrete	Rheocrete
	kg/m ³ (lb/yd ³)	mL/m ³ (oz/yd ³)	L/m ³ (gal/yd ³)	kg/m ³ (lb/yd ³)	L/m ³ (gal/yd ³)			
0.45	355 (598)	160 (270)	881 (1484)	852 (1436)	90 (2.33)	-	-	-
	355 (598)	147.4 (248.5)	881 (1484)	852 (1436)	140 (3.62)	15 (3.03)	-	-
	355 (598)	154 (259.6)	881 (1484)	852 (1436)	35 (0.90)	-	8 (13.5)	-
	355 (598)	155.7 (262.4)	881 (1484)	852 (1436)	300 (7.76)	-	-	5 (1.01)
Inhibitor dosage rate:								
Rheocrete 222+: 5 L/m ³ (1.01 gal/yd ³)								
DCI-S: 15 L/m ³ (3.03 gal/yd ³)								
Hycrete: 2.25% of cement content								

^a Water in the inhibitor is included in the water-cement ratio.

^b Daravair 1400 is used as Air - entraining agent

- 2) *Salt solution* – 10% rock salt solution is used for the field test specimen. The quantity is based on the salt usage by the Kansas Transportation Department (see Section 2.4.3). The rock salt is obtained from the KDOT Lawrence Maintenance Office.
- 3) *Epoxy* – 3M Scotchkote™ Brush Grade Rebar Patch Kit.
- 4) *Silicon Caulk* – GE MAX3500 siliconized acrylic caulk.
- 5) *Weatherstrip* – Marine & Automotive weatherstrip tape with a thickness of 9.5 mm (0.375 in.) and a width of 12.7 mm (0.5 in.), manufactured by MD Specialty.
- 6) *Heat Shrinkable Tube* – Polyvinyl Chloride (PVC) tubing from McMASTER-CARR, with an expanded inner diameter of 19 mm (³/₄ in.) and shrunk inner diameter of 9.5 mm (³/₈ in.).
- 7) *Voltmeter* – Agilent digital voltmeter, Model 34401A. Used to measure the voltage drop and corrosion potentials.

- 8) *Ohmmeter* – Agilent digital 1 kHz AC milliohmmeter, Model 4338B.
- 9) *Copper-Copper Sulfate Electrode (CSE)* – MC Miller Co. Electrode Model RE-5.
All corrosion potentials are measured with respect to a CSE.
- 10) *Resistor* – A 10-ohm resistor with 5% tolerance based on the manufacturer's specification (actual resistance is 10 ± 0.3 ohms for all resistors used in this study).
Used to connect the anode and cathode for making corrosion current measurements.
- 11) *Terminal Box* – The terminal box is assembled for convenience in making measurements. Anodes from the top mat of specimens are connected to red binding posts and cathodes to black posts. For each test specimen, several red and black posts are paired with switches between them; the number of pairs depends on the specific specimen. A 10-ohm resistor is connected in series between the switch and the red post. The circuit is closed and opened as the switch is turned on and off.
- 12) *Wire* – 14-gage electrical copper wire is used to connect the anode and cathode in the field test specimens.
- 13) *PVC Pipe* – PVC pipe with a length of 1370 mm (54 in.), an outside diameter of 25 mm (1 in.), and an inside diameter of 19 mm ($\frac{3}{4}$ in.).
- 14) *Form Braces* – Braces are made of two pieces of lumber with dimensions of $51 \times 102 \times 1524$ mm ($2 \times 4 \times 60$ in.) and two 1829-mm (6-ft) long all-threaded rods. They are assembled using bolts and washers to hold the form pieces in place.

2.4.2 Specimen Preparation

Each field test specimen consists of a $1219 \times 1219 \times 165$ mm ($48 \times 48 \times 6.5$ in.) concrete slab with two mats of No. 16 (No. 5) reinforcing bars. Both mats have seven

bars in both the longitudinal and transverse directions, with clear concrete covers of 25 mm (1 in.) from the top and bottom and 76 mm (3 in.) from the ends. Selected top and corresponding bottom bars are electrically connected across a 10-ohm resistor to form one test point. The specimen dimensions are shown in Figure 2.7.

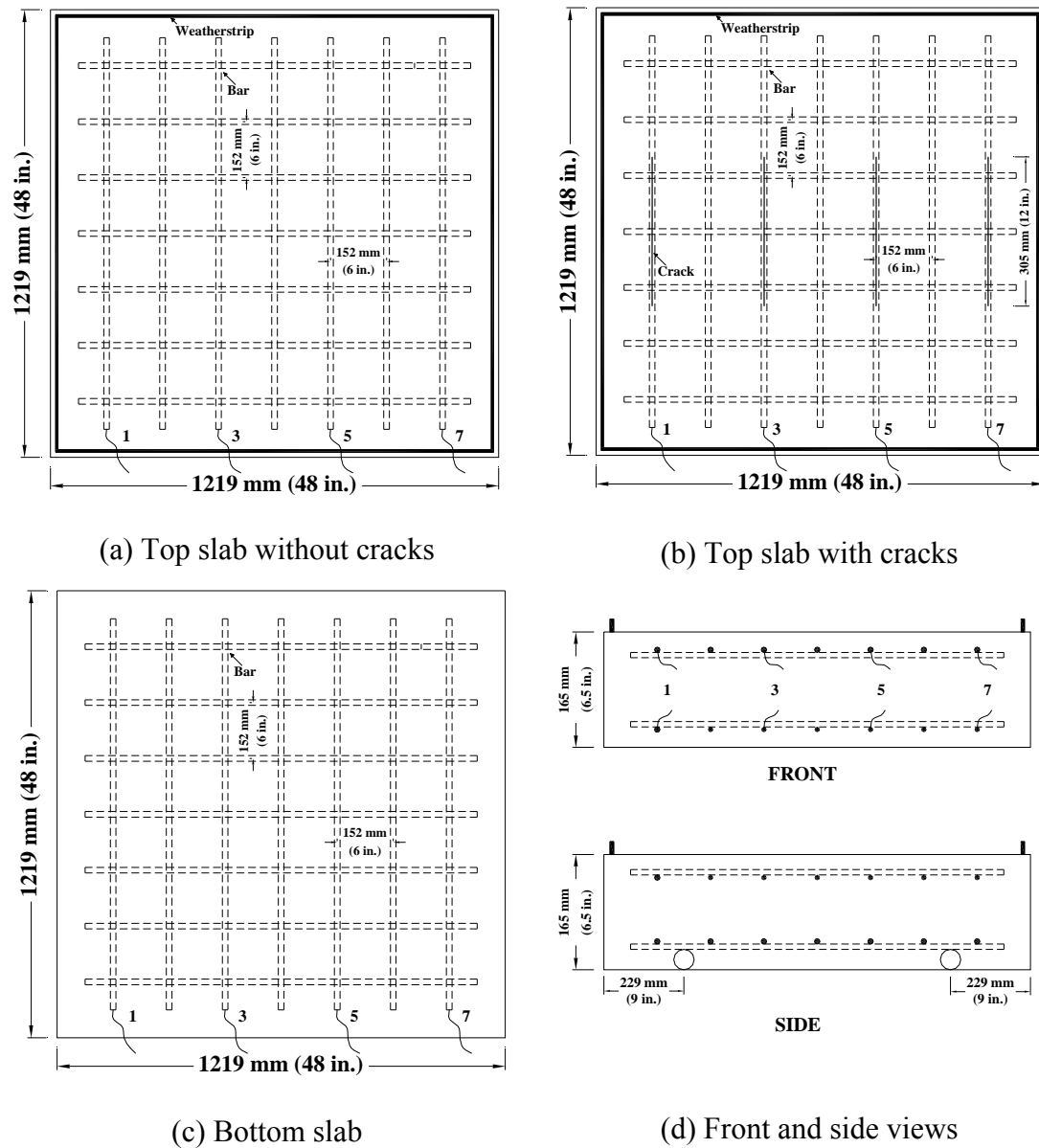


Figure 2.7 – Field test specimens

Field test specimens are fabricated as follows:

1) Reinforcing bar preparation

Reinforcing bars are cut to 1067 mm (42 in.) and the sharp edges at the ends are smoothed with a grinder. One end of the bar is drilled and tapped to a depth of 13 mm (0.5 in.) to accommodate a 10-24 stainless steel threaded bolt. Conventional and stainless steel bars are cleaned with acetone while epoxy-coated bars are cleaned with soap and warm water, and left to dry in the air.

To simulate the damage typically found on a construction site, the coatings on the epoxy-coated and multiple-coated bars are penetrated with sixteen 3.2-mm ($1/8$ -in.) diameter holes. The holes are drilled to a depth of 0.4 mm (16 mils) from the epoxy coating surface using a 3-mm ($1/8$ -in.) diameter four-flute drill bit mounted on a milling machine. Eight holes are evenly distributed on each side of the bar along the length, with sixteen holes in total for each bar, representing 0.24% damage of the coating surface. For multiple-coated bars, both the epoxy and zinc layers are penetrated.

A 914-mm (36-in.) long 14-gage electrical copper wire is connected to the tapped end of the test bars with a 10-mm ($3/8$ -in.) 10-24 stainless steel threaded bolt. The connection and all other exposed ends of epoxy-coated and multiple-coated bars are coated with 3M Rebar Patch epoxy. After the epoxy dries, a 76-mm (3-in.) long heat shrinkable tube is used to protect and direct the copper wire out of the specimen. The interface between the shrinkable tube and the tapped end is patched with epoxy.

As shown in Figure 2.7, bars numbered 1, 3, 5, and 7 are connected across 10-ohm resistors. In some early test specimens, only bars 3 and 5 were connected.

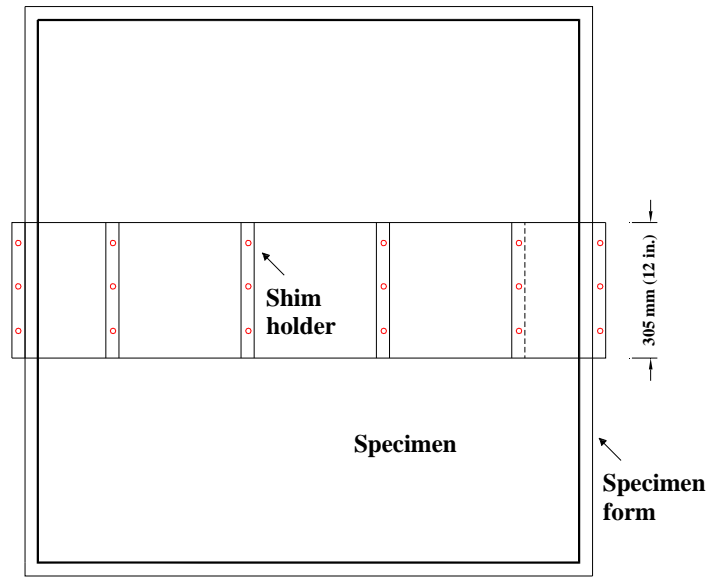
2) Form assembly

The forms used for the field test specimens are made of 19-mm ($3/4$ -in.) thick

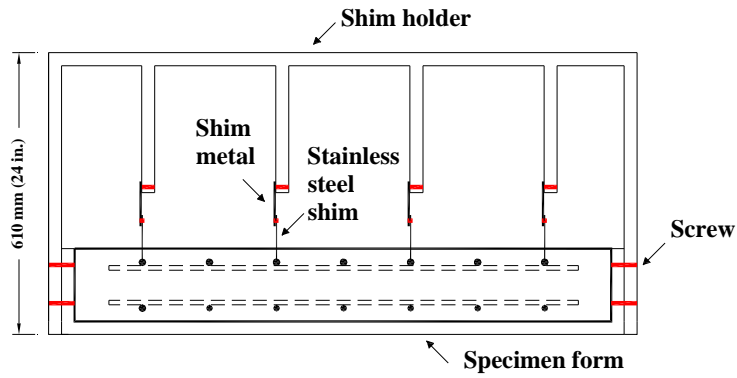
plywood and held in position with wood screws and clamps. All corners are sealed with modeling clay from the inside to avoid leakage. The inside of the form is coated with mineral oil after cleaning to remove dust. The front and back form pieces are predrilled; two 25-mm (1-in.) diameter holes are centered 229 mm (9 in.) away from the specimen sides. Two 1.37-m (4.5-ft) long PVC pipes are installed through holes that are perpendicular to the test bars. Two 1.83-m (6-ft) long No. 16 (No. 5) conventional bars are inserted into the PVC pipes to aid in lifting the specimens, as shown in Figure 2.7(d).

25-mm (1-in.) high plastic chairs are used to support bottom mat bars and 108-mm (4.25-in.) high plastic chairs are used to support top mat bars to provide 25-mm (1-in.) clear concrete covers. Plastic rather than metal chairs are used to avoid unplanned electrical connections between the top and bottom bars. The steel within each mat is connected using conventional tie wire for conventional steels and plastic-coated tie wire for epoxy-coated steels. The top and bottom mats are fixed in position by attaching them to the side of the forms using stainless steel tie wires.

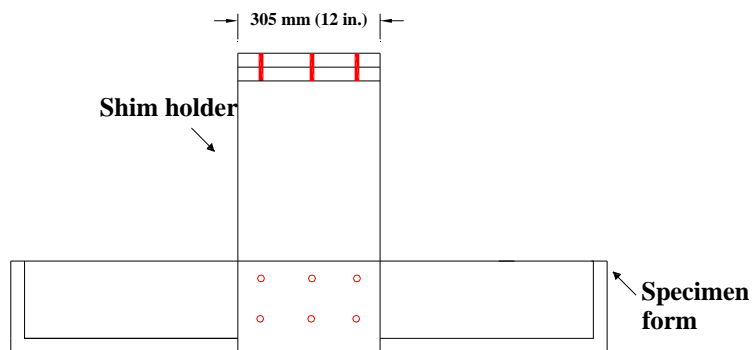
For specimens with simulated cracks from the top surface, 0.3-mm (12-mils) thick, 305-mm (12-in.) long stainless steel shims are placed directly above and parallel to the test bars. The crack length is designed based on the Kansas bridge deck crack surveys (Lindquist, Darwin, and Browning 2005). A shim holder is used to position stainless steel shims in place. It is made of plywood and structured as shown in Figure 2.8. The stainless steel shims are attached to the top of the shim holder and the holder is attached into the form using wood screws.



(a) Top view



(b) Front view



(c) Side view

Figure 2.8 – Shim holder for field specimens

3) Specimen Casting

Concrete is ordered from a local ready mix (Lawrence Ready Mix) plant. The mixture proportions are the same as the Bench-scale specimens and repeated in Table 2.9.

Concrete is consolidated during casting using an electric internal vibrator with a 33-mm ($1\frac{3}{8}$ -in.) diameter head. The upper surface is finished with a screed, followed by a bullfloat. For cracked specimens, a wooden float is used instead of the bullfloat. The stainless steel shims are removed from the concrete about 12 hours after casting.

During casting, concrete slump, temperature, unit weight, and air content are measured according to ASTM standards. Test cylinders are made for each batch and stored with the specimens, in a curing room, and in a curing tank containing saturated lime water. The cylinders are tested at 28 days to determine compressive strength. Concrete batch information and the properties of the plastic and hardened concrete are summarized in Tables 2.10 through 2.12.

4) Curing

The field specimens are cured in accordance with the *Kansas Standard Specifications for State Road and Bridge Construction* (1990). The specimens are covered with saturated burlap and plastic sheeting for seven days in the lab. After seven days, the specimens are demolded and moved outdoors and cured in air for three months.

Table 2.10 – Concrete batches for field tests

Batch No.	Steel Designation ^a	Number of Specimens	Total Number of Specimens
1	Conv.	2	6
	ECR	2	
	ECR(Valspar)	2	
2	ECR(DuPont)	2	6
	ECR(Chromate)	2	
	MC	2	
3	ECR(primer/Ca(NO ₂) ₂)	2	6
	Conv.	2	
	ECR	2	
4	ECR(Valspar)	2	6
	ECR(DuPont)	2	
	ECR(Chromate)	2	
5	MC	2	4
	ECR(primer/Ca(NO ₂) ₂)	2	
6	ECR(DCI)	4	4
7	ECR(DCI)	2	2
8	ECR(Rheocrete)	4	4
9	ECR(Hycrete)	4	4

^a Conv. = conventional steel. ECR = conventional epoxy-coated reinforcement. All epoxy-coated bars are penetrated with 16 surface holes.

MC = multiple coated bars. Multiple coated bars have both the zinc and epoxy layers penetrated.

ECR(Chromate) = ECR with the chromate pre-treatment.

ECR(DuPont) = ECR with high adhesion DuPont coating. ECR(Valspar) = ECR with high adhesion Valspar coating.

ECR(DCI) = ECR in concrete with DCI inhibitor. ECR(Hycrete) = ECR in concrete with Hycrete inhibitor.

ECR(Rheocrete) = ECR in concrete with Rheocrete inhibitor.

ECR(primer/Ca(NO₂)₂) = ECR with a primer containing calcium nitrite.

Table 2.11 – Concrete properties for field tests

Batch No.	w/c	Slump mm (in.)	Temp. °C (°F)	Unit Weight kg/m ³ (lb/ft ³)	Air content (%)	
					(Pressure)	(Volumetric)
1	0.39	100 (4)	19 (66)	2219 (138.4)	7.00	6.25
2	0.43	100 (4)	19 (67)	2319 (144.7)	6.20	5.00
3	0.41	50 (2)	28 (82)	2307 (143.9)	5.30	4.00
4	0.42	125 (5)	24 (75)	2296 (143.2)	7.80	5.75
5	0.44	110 (4.25)	23 (73)	2291 (142.9)	6.40	5.25
6	0.48	210 (8.25)	22 (72)	2255 (140.7)	11.00	7.25
7	0.40	25 (1) ^a	21 (70)	-	-	5.50
8	0.44	165 (6.5)	23 (73)	2295 (143.2)	7.00	5.50
9	0.41	185 (7.25)	16 (61)	2216 (138.2)	-	5.65

^a A slump of 150 mm (6 in.) slump was obtained at the Lawrence Ready Mix Plant before transporting concrete to the lab.

Table 2.12 – Concrete compressive strength for field tests

Batch No.	Average Concrete Compressive Strength ^a MPa (psi)		
	Curing Tank	Curing Room	With Specimens
1	-	28.4 (4110)	30.6 (4440)
2	-	35.7 (5180)	37.4 (5430)
3	-	34.4 (4990)	36.9 (5350)
4	-	32.5 (4710)	32.9 (4780)
5	32.8 (4760)	32.6 (4730)	33.2 (4810)
6	35.3 (5110)	30.9 (4480)	29.6 (4290)
7	36.8 (5340)	35.9 (5210)	-
8	29.1 (4220)	28.5 (4130)	28.1 (4080)
9	15.0 (2170)	13.5 (1960)	13.1 (1900)

^a Average of three cylinders.

2.4.3 Test Setup

Test specimens are moved to the Adams Campus of the University of Kansas seven days before testing. The specimens are spaced 914 mm (3 ft) apart and placed 203 mm (8 in.) above the ground using 203 × 203 × 406 mm (8 × 8 × 16 in.) concrete blocks.

A 9.5-mm ($\frac{3}{8}$ -in.) thick dam made of weatherstrip tape is attached to the top concrete surface, around the edges, and sealed with silicon caulk to prevent leakage. The specimens are ponded with 3.3 L (0.87 gal) 10% rock salt solution, which contains 0.30 kg (0.66 lb) of rock salt, every four weeks. On occasions, in the winter, rock salt alone is used.

The salt exposure program is based on Kansas salt usage history from 1998 to 2002, as shown in Table 2.13 (Guo et al. 2006). The average application rate is based on a total length of all driving lanes of 33,742 km (20,967 miles), with an average lane width of 3.7 m (12 ft). The yearly average salt application is 0.66 kg/m² (0.13 lb/ft²). Based on the average salt application rate, the yearly average salt usage for each field specimen, with a top surface area of 1.49 m² (16 ft²), would be 0.98 kg (2.15 lb).

Table 2.13 – KDOT salt usage history (adapted from Guo et al. 2006)

Fiscal Year	Rock Salt Total		Average Application Rate	
	Ton	Metric Ton	kg/m ²	lb/ft ²
1998	95,374	86,507	0.71	0.14
1999	70,840	64,254	0.52	0.11
2000	64,588	58,583	0.48	0.1
2001	137,392	124,619	1.02	0.21
2002	74,609	67,673	0.55	0.11
Average	88,561	80,327	0.66	0.13

The *KDOT Maintenance Manual* (2001) provides general guidelines for salt applications in snow season. According to Daniel (2004), bridge decks can receive four to five times the amount of salt of the adjacent pavement due to lower temperatures on bridge decks. Therefore, four times the application rate of the yearly average salt usage in Kansas is applied to the field test specimens, which is 2.64 kg/m² (0.52 lb/ft²), or 3.92 kg (8.32 lb) per specimen per year, which is normally 0.30 kg (0.66 lb) of rock salt every four weeks, as described above. Based on the fact that

the field test is a long-term performance test, the salt is applied at four-week intervals.

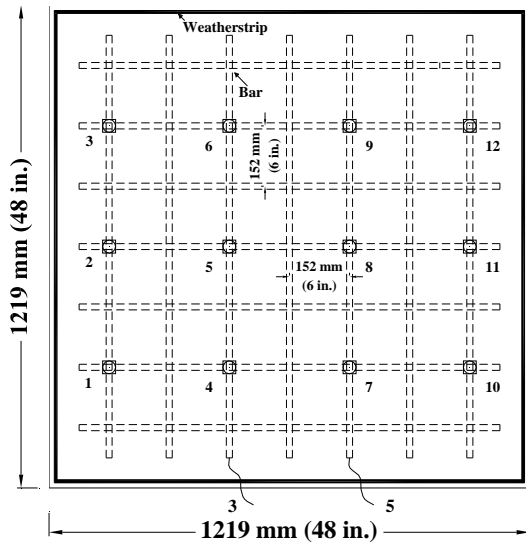
The 16-gage copper wires from the top mat bars are connected to the red binding posts, while the wires from the bottom mat bars are connected to the paired black binding posts. A switch is connected to the red binding post through a 10-ohm resistor. The switches are turned on and off to control the electrical circuits close and open. Binding posts of several specimens are centered together in a terminal box for testing convenience.

2.4.4 Test Procedure

The test specimens are ponded with 3.3 L (0.87 gal) of 10% rock salt solution on the first day. Two weeks later, the voltage drops across the 10-ohm resistors are measured using a voltmeter. The circuits are then opened and the mat-to-mat resistances are recorded using an ohmmeter. The corrosion potentials are measured about two hours after opening the circuits. Both anode and cathode corrosion potentials are measured with respect to a copper-copper sulfate electrode (CSE). The circuits are then closed after all the readings are taken. To achieve consistent measurements, specimens are watered before taking readings, usually about an hour before voltage drops.

The test cycle is repeated every four weeks. The specimens are ponded at the same time as readings are taken. After the specimens reach about 96 weeks, readings are taken every eight weeks, but the ponding cycle is maintained at four weeks.

Corrosion potentials are measured at fixed grid points on the top specimen surface, as illustrated in Figure 2.9. The number of potential test points is shown in Table 2.14.



(a) Conventional steel specimen

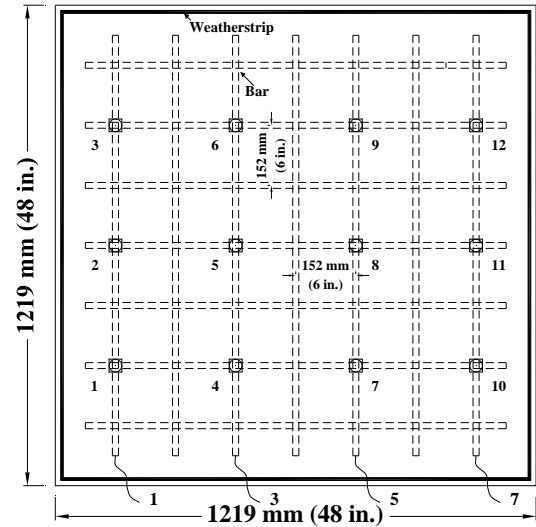
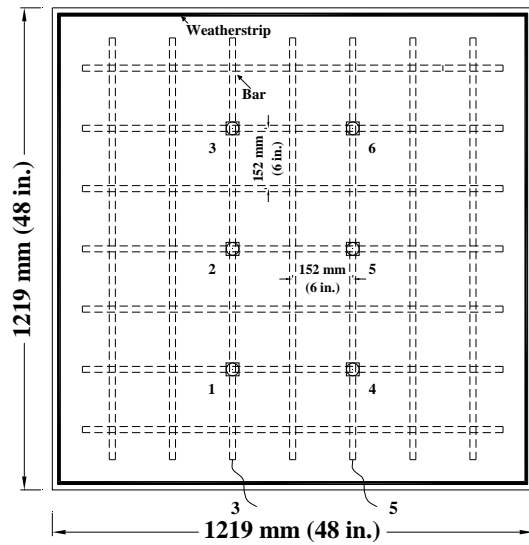
(b) Epoxy-coated bar specimen
with four test bars(c) Epoxy-coated bar specimen
with two test bars**Figure 2.9** – Potential test points for field specimens

Table 2.14 – Test program for field tests

Without Cracks			With Cracks		
Steel Designation ^a	Number of Tests ^b	Number of Potential Test Points	Steel Designation ^a	Number of Tests ^b	Number of Potential Test Points
Control					
Conv. (1)	2	12	Conv. (1)	2	12
Conv. (2)	2	12	Conv. (2)	2	12
ECR (1)	2	6	ECR (1)	2	6
ECR (2)	4	12	ECR (2)	4	12
Corrosion Inhibitors					
ECR(primer/Ca(NO ₂) ₂) (1)	4	12	ECR(primer/Ca(NO ₂) ₂) (1)	4	12
ECR(primer/Ca(NO ₂) ₂) (2)	4	12	ECR(primer/Ca(NO ₂) ₂) (2)	4	12
ECR(DCI) (1)	4	12	ECR(DCI) (1)	4	12
ECR(DCI) (2)	4	12	ECR(DCI) (2)	4	12
ECR(DCI) (3)	4	12	ECR(DCI) (3)	4	12
ECR(Rheocrete) (1)	4	12	ECR(Rheocrete) (1)	4	12
ECR(Rheocrete) (2)	4	12	ECR(Rheocrete) (2)	4	12
ECR(Hycrete) (1)	4	12	ECR(Hycrete) (1)	4	12
ECR(Hycrete) (2)	4	12	ECR(Hycrete) (2)	4	12
Multiple Coated Bars					
MC (1)	2	6	MC (1)	2	6
MC (2)	4	12	MC (2)	4	12
Increased Adhesion					
ECR(Valspar) (1)	2	6	ECR(Valspar) (1)	2	6
ECR(Valspar) (2)	4	12	ECR(Valspar) (2)	4	12
ECR(DuPont) (1)	2	6	ECR(DuPont) (1)	2	6
ECR(DuPont) (2)	4	12	ECR(DuPont) (2)	4	12
ECR(Chromate) (1)	2	6	ECR(Chromate) (1)	2	6
ECR(Chromate) (2)	4	12	ECR(Chromate) (2)	4	12

^a Conv. = conventional steel. ECR = conventional epoxy-coated reinforcement. All epoxy-coated bars are penetrated with 16 surface holes.

MC = multiple coated bars. Multiple coated bars have both the zinc and epoxy layers penetrated.

ECR(Chromate) = ECR with the chromate pre-treatment.

ECR(DuPont) = ECR with high adhesion DuPont coating. ECR(Valspar) = ECR with high adhesion Valspar coating.

ECR(DCI) = ECR in concrete with DCI inhibitor. ECR(Hycrete) = ECR in concrete with Hycrete inhibitor.

ECR(Rheocrete) = ECR in concrete with Rheocrete inhibitor.

ECR(primer/Ca(NO₂)₂) = ECR with a primer containing calcium nitrite.

^b This is the total number of tests in each field test specimen.

2.4.5 Test Program

Specimens reinforced with conventional black steel and conventional epoxy-coated steel function as control specimens. Four different corrosion inhibitors, three

increased adhesion epoxy coatings and multiple-coated bars are evaluated in this study. A total of 42 field specimens are tested. Four specimens are tested for each corrosion protection system, two without simulated cracks and two with cracks, with the exception of the DCI-S inhibitor specimens, which have three specimens each without and with simulated cracks. The test program is summarized in Table 2.14.

2.5 KDOT BRIDGE PROJECTS

To study the corrosion performance of stainless steel reinforcement on a bigger scale, two bridge decks in Kansas – the Doniphan County Bridge (DCB) and Mission Creek Bridge (MCB) – were constructed with pickled 2205 duplex stainless steel. The reinforcement contains about 22% chromium and 5% nickel and meets the requirements of ASTM A955, *Standard Specification for Deformed and Plain Stainless Steel Bars for Concrete Reinforcement*. In addition to the deck reinforcement, stainless steel test bars were installed in both bridge decks to aid in corrosion potential mapping. Bench-scale specimens with pickled 2205 stainless steel and field test specimens with conventional, epoxy-coated, and pickled 2205 stainless steel were also fabricated using the same concrete mix as used on the bridges. Measurements are taken regularly and used to evaluate the corrosion performance of the decks.

2.5.1 Bridge Information

The Doniphan County Bridge (Bridge No. 7-22-18.21(004)) is located on K-7 over the Wolf River in Northeast Kansas. It is a 75.8-m (249-ft) long, three-span continuous composite steel girder bridge. The bridge deck was cast on February 26, 2004 to replace the previous deck, which had deteriorated due to corrosion of the

reinforcing steel.

The Mission Creek Bridge (Bridge No. 4-89-4.58(281)) is located on K-4 over Mission Creek in Shawnee County, Kansas. It is a 27.45-m (90-ft) long, one-span composite steel girder bridge. The bridge deck was cast on August 25, 2004.

Both bridge decks are monolithic. The reinforcing bar spacings listed in Table 2.15 are those at the midspan region. Over the piers, the spacing of the top longitudinal reinforcement is reduced to one-half of the value shown in Table 2.15.

Table 2.15 – Bridge configurations

Bridge		DCB	MCB	
Bridge No.		7-22-18.21 (004)	4-89-4.58 (281)	
Bridge Deck Cast Date ^a		February 26, 2004	August 25, 2004	
Length m (ft)		75.8 (249)	27.45 (90)	
Deck Width m (ft)		8 (26)	11 (36)	
Number of Girders		5	6	
Type of Girder		Composite	Composite	
Number of Spans		3	1	
Abutment		Integral	Integral	
Deck Type		Monolithic	Monolithic	
Deck Depth mm (in.)		210 (8.3)	210 (8.3)	
Top Clear Cover mm (in.)		65 (2.6)	65 (2.6)	
Bottom Clear Cover mm (in.)		30 (1.2)	30 (1.2)	
Reinforcement ^b	Direction	Bar Size	Spacing ^d mm (in.)	
Top	Longitudinal	No.16 (No.5)	290 (11.4)	300 (11.8)
	Transverse	No.16 (No.5)	170 (6.7)	170 (6.7)
Bottom	Longitudinal	No.16 (No.5)	260 (10.2)	250 (9.8)
	Transverse	No.16/13 (No.5/4) ^c	170 (6.7)	170 (6.7)

^a Bridge deck replacement for DCB, and new construction for MCB.

^b Reinforcement in midspan region.

^c No.16 (No.5) and No.13 (No.4) bars are alternated.

^d Spacing in the midspan region. Over the piers, spacing of the top longitudinal reinforcement is reduced to half.

2.5.2 Bridge Test Setup

Stainless steel test bars are installed in both bridge decks. The test bars are prepared in a manner that is similar to that used for lab specimens. They are cut into the length specified in the Table 2.16 for the Doniphan County Bridge and Table 2.17 for the Mission Creek Bridge. One end of the test bar is drilled and tapped. A 14-gage electrical wire is attached to it using a 13-mm (0.5-in.) long 10-24 stainless steel threaded bolt for monitoring connections. The test bars are placed in the transverse direction and tied to transverse reinforcing bars using stainless steel tie wire. For testing convenience, the connecting electrical wires are directed out of the concrete deck from holes drilled in the bottom formwork, which are 1-m (3.28-ft) away from the east abutment, as shown in Figures 2.10 and 2.11. Foam sealant is used around the holes to prevent concrete from leaking and a polyvinyl chloride (PVC) pipe is used in the Mission Creek Bridge to protect the wire from the damage during the construction.

For identification purposes, bar locations and wire colors are also listed in the Tables 2.16 and 2.17 (adapted from Guo et al. 2006). Due to the fact that the length of the Doniphan County Bridge is about three times of that of the Mission Creek Bridge, two sets of the test bars are placed in the Doniphan County Bridge deck and only one set in the Mission Creek Bridge deck. Each set of test bars in the Doniphan County Bridge includes three top and two bottom bars, making five for each set and total of ten for the bridge. They are located on the north side of the bridge and 23.01 m (75.5 ft) and 11.51 (37.75 ft), respectively, away from the east abutment. The set in the Mission Creek Bridge includes three bars in both the top and bottom, making a total of six for the bridge. The center of test bars is located on the south side of the bridge and 3 m (9.84 ft) away from the east abutment. The locations are shown in Figures 2.10 and 2.11.

Table 2.16 – Test bars in Doniphan County Bridge

Position	Location	No.	Wire Color	Bar Length cm (ft)	Bar Location
Pier #2	Top	1	Blue	183 (6)	East
		2	Blue	183 (6)	Center
		3	Blue	183 (6)	West
	Bottom	4	Black	46 (1.5)	East
		5	White	46 (1.5)	West
Midspan	Top	6	Yellow	183 (6)	East
		7	Green	183 (6)	Center
		8	Black	183 (6)	West
	Bottom	9	White	46 (1.5)	East
		10	Black	46 (1.5)	West

Table 2.17 – Test bars in Mission Creek Bridge

Position	Location	No.	Wire Color	Bar Length cm (ft)	Bar Location
About 3 m (10 ft) away from the east abutment	Top	1	Black	91 (3)	West
		2	Black	91 (3)	Center
		3	Black	91 (3)	East
	Bottom	4	Yellow	91 (3)	West
		5	Yellow	91 (3)	Center
		6	Yellow	91 (3)	East

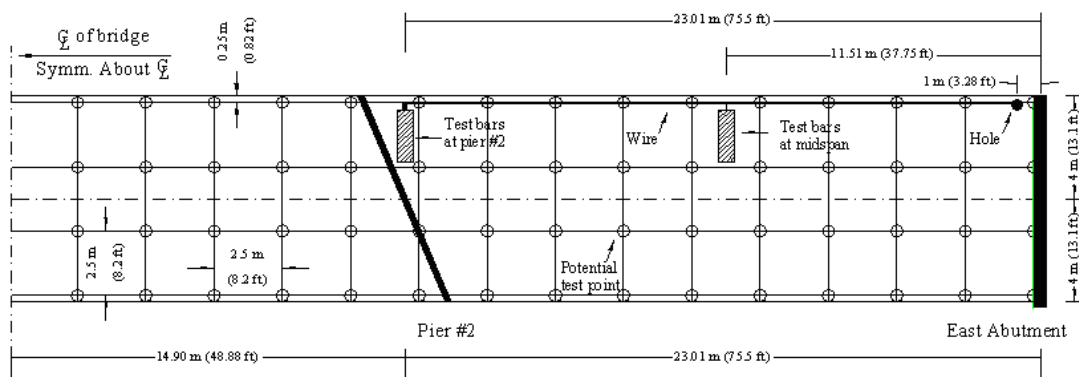


Figure 2.10 – Test bar locations and potential test points on Doniphan County Bridge

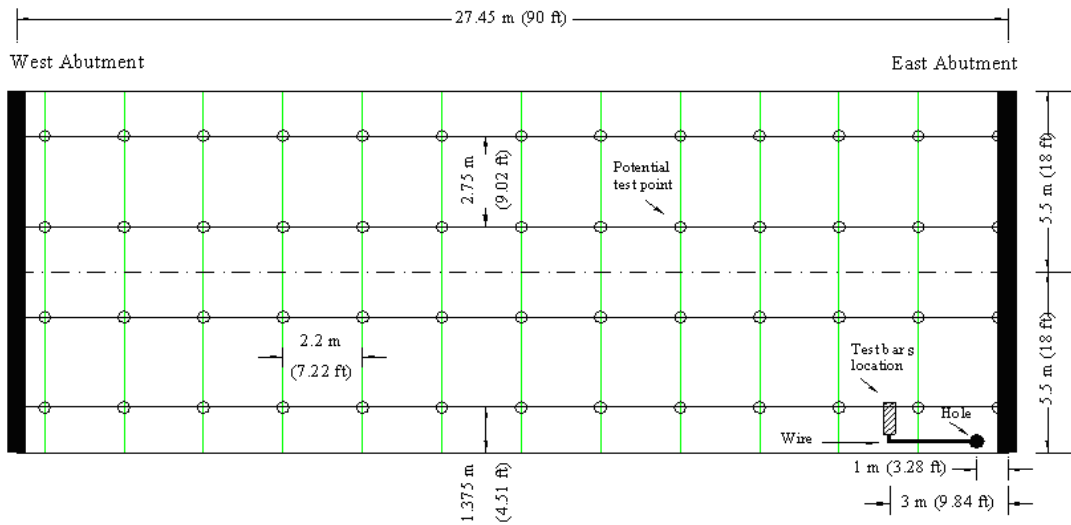


Figure 2.11 – Test bar locations and potential test points on Mission Creek Bridge

The concrete mixture proportions used for the Doniphan County Bridge and Mission Creek Bridge are listed in the Table 2.18 and the properties of the concrete for both bridges, provided by the Kansas Department of Transportation (KDOT), are summarized in Tables 2.19 and 2.20.

Table 2.18 – Concrete mixture proportions for Doniphan County Bridge and Mission Creek Bridge

Bridge		DCB	MCB
Water	kg/m ³ (lb/yd ³)	143 (241)	129 (217)
Cement	kg/m ³ (lb/yd ³)	357 (602)	357 (602)
CA	kg/m ³ (lb/yd ³)	883 (1487)	893 (1504)
FA	kg/m ³ (lb/yd ³)	883 (1487)	893 (1504)
AE	mL/m ³ (oz/yd ³)	290 (7.5)	154 (4)
Design <i>w/c</i>		0.40	0.36
Design Slump	mm (in.)	75 (2.95)	55 (2.25)
Design Air Content	(%)	6.5	6.5
Design Unit Weight	kg/m ³ (lb/ft ³)	2267 (141.37)	2272 (141.70)

Table 2.19 – Concrete properties for Doniphan County Bridge

Sample Location	Slump mm (in.)	Unit Weight kg/m ³ (lb/ft ³)	Air Content ^a (%)	Air Temp. °C (°F)	Conc. Temp. °C (°F)	Compressive Strength ^b MPa (psi)
Pump	90 (3.5)	2313 (144.26)	2.5	7 (45)	11 (52)	41.9 (6080)
Pump	100 (4.0)	2333 (145.28)	2	9 (49)	16 (60)	41.0 (5950)
Pump	90 (3.5)	2321 (144.74)	1	12 (53)	21 (70)	40.8 (5920)
Deck	90 (3.5)	2177 (135.78)	8	12 (53)	21 (70)	35.6 (5160)
Deck	75 (3.0)	2174 (135.59)	9	12 (53)	21 (70)	-
Deck	75 (3.0)	2200 (137.22)	6.5	12 (53)	21 (70)	-
Deck	75 (3.0)	2171 (135.41)	8	12 (53)	21 (70)	-
Deck	75 (3.0)	2170 (135.41)	8	12 (53)	21 (70)	-
Deck	75 (3.0)	2177 (135.78)	8	12 (53)	21 (70)	-

^a Pressure method was used to test concrete air content.

^b Average of three cylinders.

Table 2.20 – Concrete test results for Mission Creek Bridge

Sample Location	Slump mm (in.)	Unit Weight kg/m ³ (lb/ft ³)	Air Content ^a (%)	Air Temp. °C (°F)	Conc. Temp. °C (°F)	Compressive Strength ^b MPa (psi)
East Abutment	100 (4.0)	2269 (141.52)	6.1	27 (81)	31 (88)	-
West Abutment	90 (3.5)	2253 (140.52)	5.25	25 (77)	34 (92)	-
Bridge Deck	75 (3.0)	2304 (143.70)	4.25	28 (82)	32 (89)	42.7 (6190)
Bridge Deck	50 (2.0)	2293 (143.00)	5	25 (77)	33 ((91)	42.1 (6110)
Bridge Deck	65 (2.5)	2264 (141.19)	6	25 (77)	35 (94)	-
North Handrail	50 (2.0)	2294 (143.11)	5.5	25 (77)	30 (86)	-
South Handrail	145 (5.75)	2253 (140.52)	5	18 (64)	28 (82)	-

^a Pressure method was used to test concrete air content.

^b Average of three cylinders.

2.5.3 Bridge Potential Mapping

The resistance between the top and bottom test bars is measured with an ohmmeter. Zero resistance between the top and bottom bars is recorded, indicating that an electrical connection exists between the top and bottom bars. This connection can be provided by truss bars, tie wires, and scuppers. Therefore, corrosion potentials, rather than corrosion current, are used to monitor the long-term corrosion

performance of the 2205 stainless steel in both bridge decks.

Corrosion potentials are measured with respect to a copper-copper sulfate electrode (CSE) every six months on a fixed grid using a voltmeter. For the Doniphan County Bridge, measuring points are distributed on a 2.5×2.5 m (8.2×8.2 ft) grid across the full bridge length (not including the abutments), making 4 rows of 31 and a total of 124 potential measuring points. For the Mission Creek Bridge, the test points are distributed on a 2.75×2.2 m (9.0×7.2 ft) grid across the full bridge length (not including the abutments), making 4 rows of 13 and a total of 52 test points. The measurements are used to map the corrosion potential contours. The test points are shown in the Figures 2.10 and 2.11.

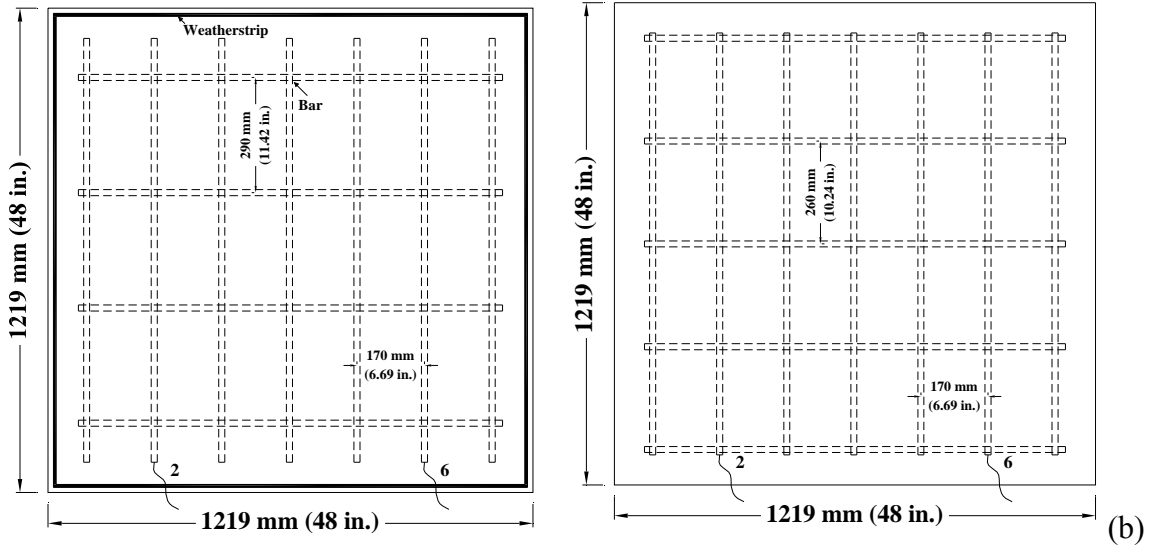
Corrosion potentials are measured as followings: The bridge deck is wet down using a water tank truck about one hour before testing. The test grid points are marked with crayon before measurement. For convenience in marking the deck, nylon string marked with the knots at the test point spacing is used together with a measuring tape. The positive probe of the voltmeter is connected to the test bars via the electrical connections and the negative probe is connected to a CSE through a large spool of wire. The end of the electrode is wrapped with a wet sponge to provide a better electrical connection. Traffic control is provided by KDOT during the bridge survey. Deck water spray and a generator used for the test equipment power are also provided by KDOT. The voltmeter and electrode used in the survey are the same as these used in the field tests.

2.5.4 Field Test Specimens

Field test specimens reinforced with 2205 stainless steel were cast for both Doniphan County Bridge and Mission Creek Bridge bridge. For comparison,

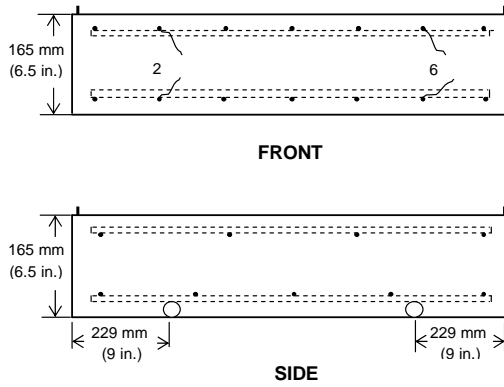
specimens reinforced with conventional steel and epoxy-coated steel were also made. The specimen configuration is similar to that used for the other field test specimens (Section 2.4). Each field test specimen consists of a $1219 \times 1219 \times 165$ mm ($48 \times 48 \times 6.5$ in.) concrete slab with two mats of No. 16 (No. 5) reinforcing bars. Clear concrete covers are 25 mm (1 in.) from the top and bottom and 76 mm (3 in.) from the side. Seven bars are used in the longitudinal direction for both mats, with four bars for the top mat and five for the bottom mat in the transverse direction. Selected longitudinal top and the corresponding bottom bars are electrically connected across a 10-ohm resistor. The specimen dimensions are shown in Figures 2.12 and 2.13.

For the Mission Creek Bridge, three specimens, one for each type of reinforcing steel, are fabricated with four 305-mm (12-in.) long simulated cracks parallel to and directly above the reinforcement. The epoxy-coated bars in the Mission Creek Bridge are drilled with sixteen 3-mm ($1/8$ -in.) diameter holes to simulate 0.24% of the coating damage typically found on construction sites. For the Doniphan County Bridge, all specimens are fabricated without simulated cracks and all of the epoxy-coated bars used in the test have no drilled holes on the coating. Stainless steel tie wire is used for stainless steel specimens and plastic-coated tie wire is used for epoxy-coated steel. All of the specimens contain plastic chairs to support both mats. The field test specimens were cast with trial-batch concrete for the bridges at the ready mix plant using the same mix design as used in the bridge decks. Haul time from the plant to the jobsite was used for the specimen concrete to simulate bridge construction, 55 minutes for the Doniphan County Bridge and 30 minutes for the Mission Creek Bridge. The Doniphan County Bridge specimens were cast at Builders Choice Concrete (St. Joseph, MO) on January 16, 2004 and the Mission Creek Bridge specimens were cast at Meier's Ready Mix, Inc. (Topeka, KS) on July 15, 2004.



(a) Top slab

Bottom slab



(c) Front and side views

Figure 2.12 – Field test specimens for Doniphan County Bridge

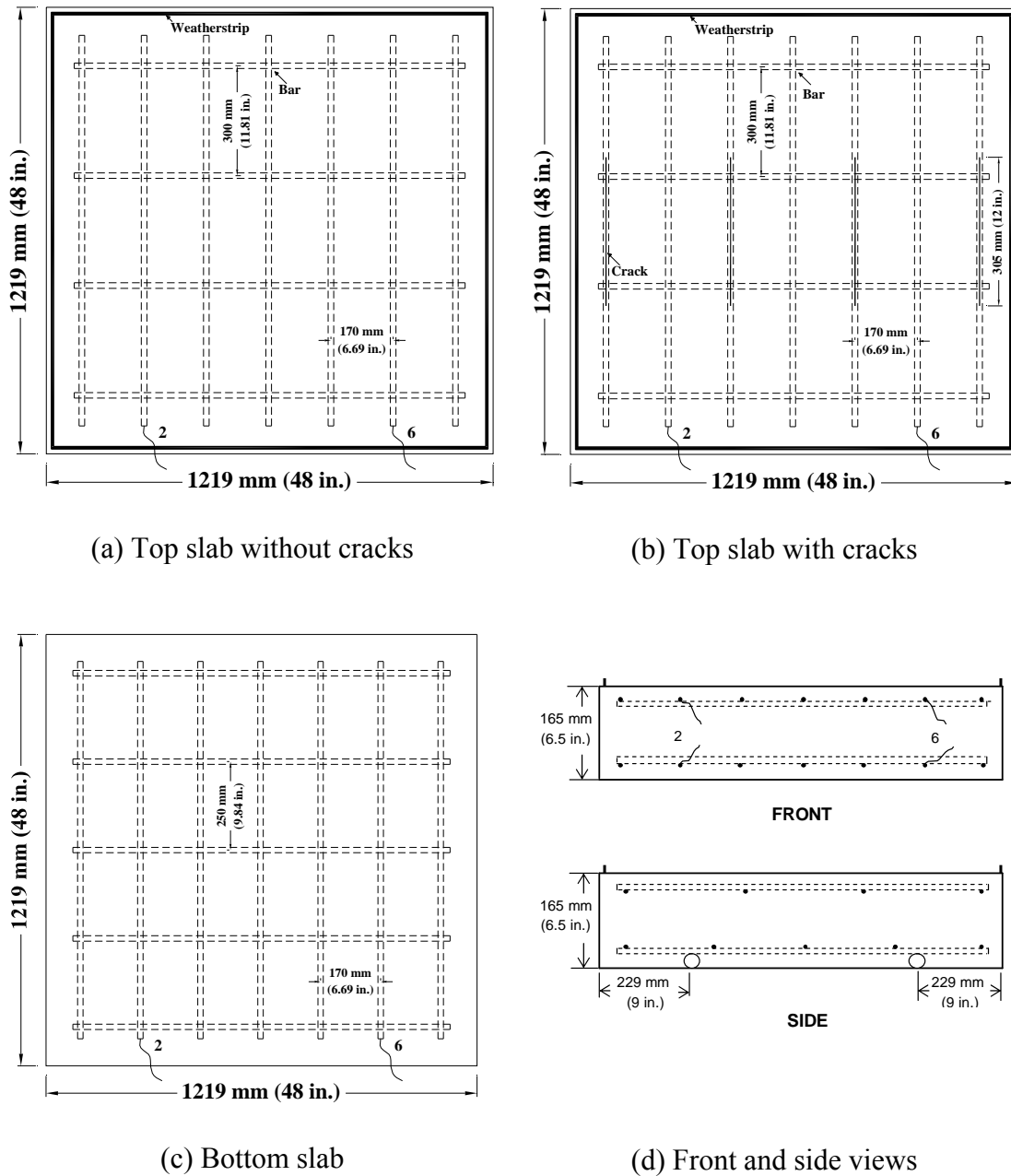


Figure 2.13 – Field test specimens for Mission Creek Bridge

The specimens were cured with wet burlap and plastic sheeting for seven days outdoors. Insulation blankets were used for the Doniphan County Bridge specimens due to the winter temperature. After seven days, the specimens were demolded and transported to the Adams Campus of the University of Kansas.

The concrete properties for field test specimens of both bridges are summarized in Table 2.21.

Table 2.21 – Concrete properties for field test specimens of Doniphan County Bridge and Mission Creek Bridge

Bridge	DCB	MCB
Specimen Cast Date ^a	January 16, 2004	July 15, 2004
Simulated Haul Time (min.) ^b	55	30
Slump mm (in.)	55 (2.25)	50 (2)
Air Content (%) ^c	5	5.25
Air Temp. °C (°F)	7 (45)	35 (95)
Concrete Temp. °C (°F)	20 (68)	27 (80)
Unit Weight kg/m ³ (lb/ft ³)	2292 (142.96)	2261 (141.04)
Concrete Compressive Strength MPa (psi) ^d		
Curing Room	32.8 (4750)	35.4 (5140)
With Field Specimens	28.9 (4190)	38.2 (5540)

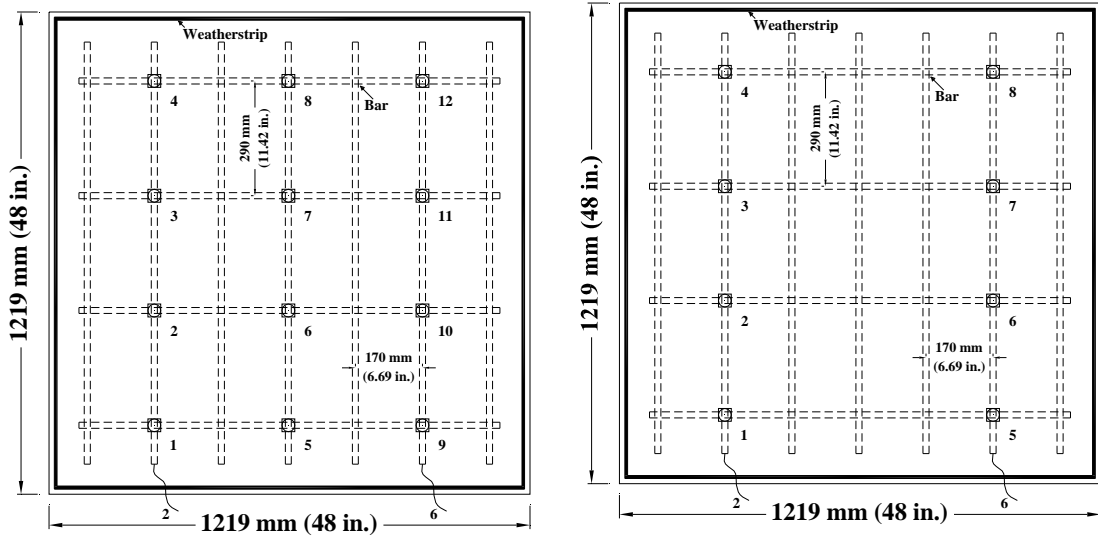
^a Bridge trial-batch concrete were used for field test specimens.

^b DCB specimens were cast at Builder Choice Concrete (St. Joseph, MO);
MCB specimens were cast at Meier's Ready Mix, Inc. (Topeka, KS).

^c Pressure method was used for DCB and Volumetric method was used for MCB.

^d Average of three cylinders.

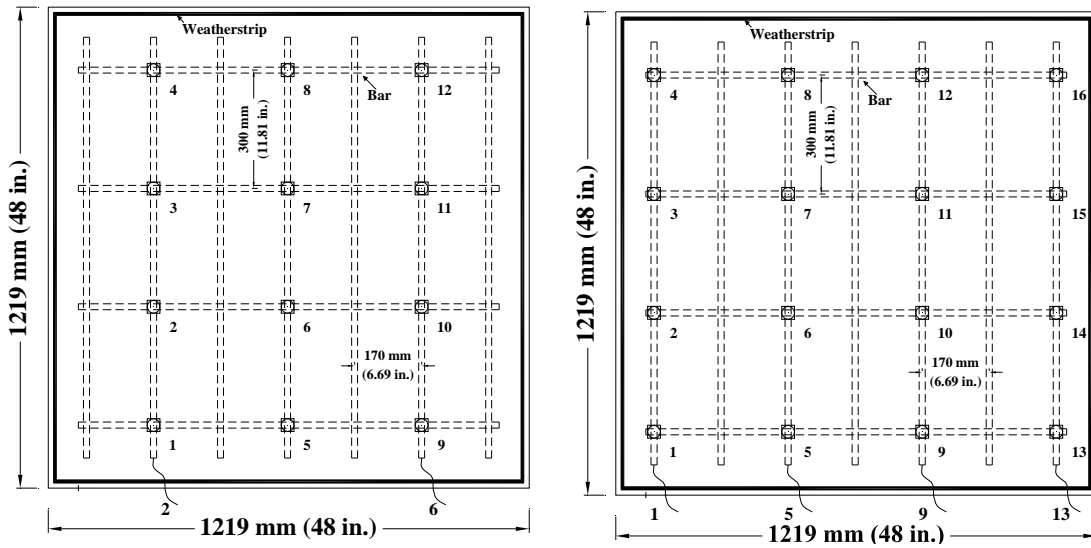
Due to the effect of temperature on the rate of strength development, the tested compressive strength of the Doniphan County Bridge is a little bit lower compared to the Mission Creek Bridge. The Doniphan County Bridge was cast in winter with an air temperature of 7°C (45°F), while the Mission Creek Bridge was cast in summer with an air temperature of 35°C (95°F). For cylinders stored with field specimens, the 28-day comprehensive strength of the Doniphan County Bridge was 28.9 MPa (4190 psi), compared to 38.2 MPa (5540 psi) of the Mission Creek Bridge. The concrete used for the Mission Creek Bridge set up so quickly that the cracked specimens had to be finished without the top surface receiving a final finish.



(a) Conventional and stainless steel

(b) Epoxy-coated reinforcement

Figure 2.14 – Potential test points for field test specimens for Doniphan County Bridge



(a) Conventional or stainless steel

(b) Epoxy-coated reinforcement

Figure 2.15 – Potential test points for field test specimens for Mission Creek Bridge

Table 2.22 – Test program for the field tests for the Doniphan County Bridge and Mission Creek Bridge

Bridge	Steel Designation ^a	Number of Test Bars	Potential Test Points	Notes
DCB	Conv. (1)	2	12	
	Conv. (2)	2	12	
	ECR (1)	2	8	
	ECR (2)	2	8	
	2205p (1)	2	12	
	2205p (2)	2	12	
MCB	Conv. (1)	2	12	
	Conv. (2)	2	12	with cracks
	ECR (1)	4	16	with 16 drilled holes
	ECR (2)	4	16	with cracks and 16 drilled holes
	2205p (1)	2	12	
	2205p (2)	2	12	with cracks

^a Conv. = conventional steel.

ECR = conventional epoxy-coated reinforcement.

2205p = 2205 pickled stainless steel used in the bridge decks.

The test procedure for the bridge field specimens is the same as used for the other field test specimens as described in Section 2.4.4. The corrosion potential test points are shown in Figures 2.14 and 2.15 and summarized in Table 2.22.

2.5.5 Bench-Scale Specimens

Bench-scale specimens reinforced with 2205 stainless steel were fabricated and tested in the lab to evaluate the corrosion performance of the stainless steel in the Doniphan County Bridge and the Mission Creek Bridge. The bench-scale test specimens were cast together with the field specimens using the bridge trial-batch concrete. An internal electric vibrator with a 19-mm (³/₄-in.) diameter head was used to consolidate the concrete instead of the vibrating table used in the lab. Otherwise, the specimen fabrication and testing procedures are the same as the other bench-scale specimens described in Section 2.3. The test programs of both bridges are

summarized in Table 2.23.

Table 2.23 – Test programs for bench-scale tests for the Doniphan County Bridge and the Mission Creek Bridge

Bridge	Steel	Number
	Designation ^a	of Test Specimens
Southern Exposure (SE) Test		
DCB	SE-2205p	6
MCB	SE-2205p	5
Cracked Beam (CB) Test		
DCB	CB-2205p	3
MCB	SE-2205p	6

^a 2205p = Pickled 2205 stainless steel used in the bridges decks.

2.6 LINEAR POLARIZATION RESISTANCE (LPR) TEST

Linear polarization resistance is a rapid, non-intrusive electrochemical technique for determining the instantaneous corrosion rate of metals. It is based on the observation that the potential-current of the metal is nearly linear in the vicinity of the equilibrium corrosion potential (usually ± 10 mV of the equilibrium potential). The slope of the linear region is referred to as the polarization resistance R_p and is inversely proportional to the corrosion current density, and thus the corrosion rate of the metal. The relationship can be described using the Stern-Geary equation [Eq. (1.13), Section 1.4.3].

A PCI4/750 Potentiostat and a DC105 data acquisition system from Gamry Instruments are used in this study. The potentiostat is used to perturb the equilibrium corrosion process and the DC105 is used to collect the data. Part of the DC105 software package, the polarization resistance data analysis macro POLRES, is used to analyze the data and calculate the corrosion current. The tests are performed on the bench-scale and field test specimens in this study.

Polarization Resistance

Default Save Restore OK Cancel

Estat * Pstat1

Test Identifier Polarization Resistan.

Output File SE-top.DTA

Notes...

Initial E (V) -0.02 vs Eoc

Final E (V) 0.02 vs Eoc

Scan Rate (mV/s) 0.125

Sample Period (s) 2

Sample Area (cm²) 304

Density (gm/cm³) 7.87

Equiv. Wt 27.92

Beta An. (V/Dec) 0.12

Beta Cat. (V/Dec) 0.12

Conditioning Off Time (s) 15 E (V) 0

Init. Delay Off Time (s) 300 Stab. (mV/s) 0.1

IR Comp On

Figure 2.16 – Input window for LPR test

Figure 2.16 shows the input window for the LPR test. It lists the parameters used in LPR test. *Initial and Final E* define the starting and ending points of the potential scan range during data acquisition. *Scan Rate* defines the speed of the potential sweep in mV/sec. *Sample Period* defines the data collecting spacing in seconds. *Sample Area* is the surface area of measured reinforcing steel in concrete in cm². *Density* defines the density of measured metal in g/cm³ and *Equiv. Wt* is the equivalent weight of metal (atomic weight of an element divided by its valence). *Beta An.* and *Beta Cat.* are the anodic and cathodic Tafel constants in V/Decade. *Conditioning* is used to insure the metal has a known initial surface condition and is set to Off during the test. *Conditioning Time* and *E* are the applied time and potential during the conditioning phase of the experiment. *Init. Delay* allows E_{oc} (open circuit

corrosion potential of the sample) to stabilize before the scan. *Time* and *Stab.* define the conditions to start the scan after the initial delay. *Init. Delay* is set to Off during the test since circuits are manually disconnected to stabilize the open circuit corrosion potential before the test to save running time. *IR Comp.* is set to On to let each applied potential be adjusted for the *IR* drop (potential change in the electrode/solution contact surface) caused by the solution resistance in an electrochemical cell.

The function icons at the top of the window control the parameters set in the window. *Default* sets all the parameters of this window to their default values. *Save* sets the parameters to their current defined values. *Restore* recovers the saved parameter values and uses them for repetitive tests.

The parameters listed in Figure 2.16 are modified according to the sample being evaluated. The areas and metal parameters used in the tests are summarized in the Table 2.24.

Table 2.24 – Parameter difference for LPR tests

Sample Area (cm ²)	SE	CB	G109
Top Mat	304	152	139
Bottom Mat	608	304	278
	Iron		Zinc
Density (gm/cm ³)	7.87		7.13
Equivalent Weight	27.92		32.68

The PCI4/750 Potentiostat is a three-electrode Potentiostat, using a working electrode, a reference electrode, and a counter electrode. The reinforcing steel in the test specimens serve as the working electrode. A saturated calomel electrode and a platinum strip are separately immersed in the 15% NaCl solution ponded on top of the specimen and serve as the reference and counter electrode, respectively. Readings are

taken every four weeks with the top and bottom mats disconnected.

The polarization resistance data are analyzed using the POLRES package. A graph is plotted when the data file is loaded. The potential region is set from -10 to $+10$ mV relative to equilibrium potential E_{oc} . With the input Tafel constants, the program performs the linear least squares fit over the selected region to calculate the polarization resistance. The corrosion current density and corrosion rate are then calculated using the Stern-Geary equation [Eq. (1.13), Section 1.4.3].

One specimen is tested for each of the corrosion protection systems. The test program is summarized in Table 2.25.

2.7 CRITICAL CHLORIDE THRESHOLD TEST

The tests used in this study involve the direct analysis of the chloride content in concrete beam specimens adjacent to reinforcing steel when corrosion starts. In this study, the chloride threshold associated with corrosion initiation for concrete with three different inhibitors, DCI-S, Rheocrete 222+, and Hycrete, is evaluated. The threshold for Class I galvanized bars that meet the requirements of ASTM A767 but lack chromate treatment is also evaluated. Test specimens are fabricated the same way as the cracked beam specimens (Section 2.3), the simulated crack is not placed in the specimen. No. 16 (No. 5) bars are used in all the tests. The chloride threshold results for the galvanized steel are compared with those of conventional reinforcing steel meeting the requirements of ASTM A615 and MMFX microcomposite steel meeting the requirements of ASTM A1035 (Ji et al. 2005). The specimens are autopsied following the tests for the presence of corrosion products on the bars. For the galvanized steel, evidence of increased porosity in the concrete around the non-chromated bars, possibly caused by excessive hydrogen evolution during initial

curing, is also investigated.

Table 2.25 - Test program for LPR tests

Specimen Type	Steel Designation ^a	LPR Test Specimen No.
G 109	Conv.	6
	ECR	3
	ECR-10h	6
	MC(only epoxy penetrated)	3
	MC(only epoxy penetrated)-10h	3
	MC(both layers penetrated)	3
	MC(both layers penetrated)-10h	3
SE & CB	Conv.	4
	ECR	4
	N5-NO	1
	N5-DCI	1
	N5-HY	1
	N5-RH	1
FT (without cracks & with cracks)	Conv.	1
	ECR	1
	ECR(primer/Ca(NO ₂) ₂)	1
	ECR(DCI)	1
	ECR(Rheocrete)	1
	ECR(Hycrete)	1
	MC(both layers penetrated)	1
	ECR(Valspar)	1
	ECR(DuPont)	1
ECR(Chromate)	1	

^a Conv. = conventional steel. ECR = conventional epoxy-coated reinforcement.

MC = multiple coated bars. N5 = conventional steel with different heat.

10h = epoxy-coated steel penetrated with ten 3 mm ($\frac{1}{8}$ in.) holes.

DCI = corrosion inhibitor DCI-S mixed in concrete.

HY = corrosion inhibitor Hycrete mixed in concrete.

RH = corrosion inhibitor Rheocrete 222+ mixed in concrete.

ECR(primer/Ca(NO₂)₂) = ECR with a primer containing calcium nitrite.

ECR(Valspar) = ECR with high adhesion Valspar coating.

ECR(DuPont) = ECR with high adhesion DuPont coating.

ECR(Chromate) = ECR with the chromate pretreatment.

2.7.1 Test Procedure

Test bar preparation and specimen fabrication are the same as used for the CB specimens (Section 2.3). Galvanized bars are cleaned with acetone without

wirebrushing to avoid coating damage. The zinc coating on the steel is checked for defects before the specimens are cast. The concrete mix and the materials are the same as used for the SE and CB specimens (Section 2.3.1). The properties of the concrete are summarized in Table 2.26. For specimens without inhibitors, the 28-day compressive strength was 35.8 MPa (5190 psi). Specimens with DCI, which can act as an accelerator, had the highest 28-day compressive strength of 40.0 MPa (5805 psi). Specimens with Hycrete had the lowest 28-day compressive strength of 14.2 MPa (2055 psi), followed by Rheocrete specimens with 30.4 MPa (4410 psi).

Figure 2.26 – Concrete properties for chloride threshold tests

Specimen Designation ^a	Slump mm (in.)	Air Content (%)	Compressive Strength ^b MPa (psi)	Standard Deviation MPa (psi)	COV
B-NO	2.25	5.25	35.8 (5190)	2.35 (341)	0.07
B-DCI	3.75	5	40.0 (5805)	3.65 (529)	0.09
B-RH	2	4	30.4 (4410)	4.45 (646)	0.15
B-HY	3.5	5.25	14.2 (2055)	1.93 (280)	0.14

^a NO = concrete with no inhibitors. DCI = concrete with inhibitor DCI-S.

RH = concrete with inhibitor Rheocrete. HY = concrete with inhibitor Hycrete.

^b Average of eight cylinders, cured in the mold for one day and then in a saturated lime tank for 27 days.

The same ponding and drying cycles are used for the beams as for the SE and CB specimens. The corrosion rate, mat-to-mat resistance, and top and bottom corrosion potentials are measured weekly during the test period.

The test is terminated once corrosion is initiated (criteria described later in this section). At this point, 20 samples, 10 from each side of the specimen, are obtained by drilling at the level of the top reinforcing bar. For each sample, drilled holes are positioned so that the top of the holes and the top surface of the reinforcing bar are at the same level, as shown in Figures 2.17 and 2.18. To do this, the actual level of the top reinforcing bar in each specimen is measured.

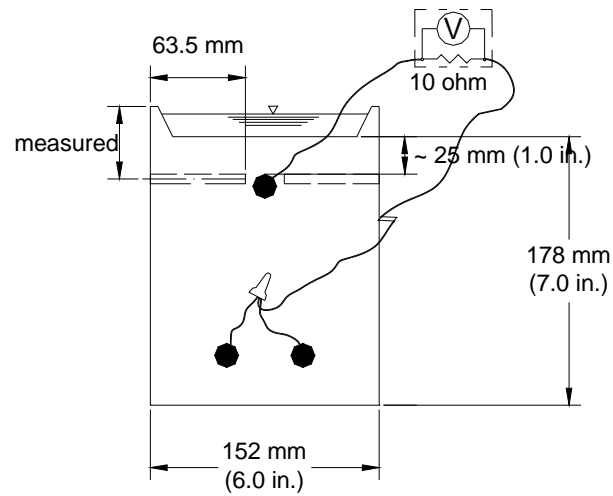


Figure 2.17 – Beam specimen end view

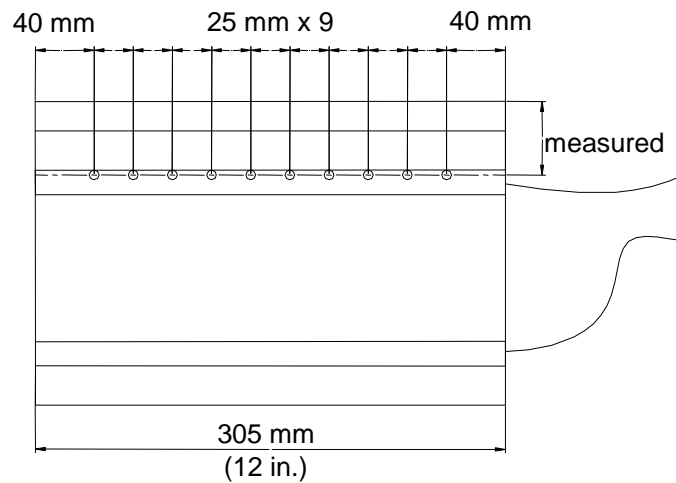


Figure 2.18 - Side view showing sampling locations

The sampling and testing procedures for chloride ion concentration are those adopted by Ji et al. (2005). Pulverized concrete samples are obtained by drilling 6.4 mm (0.25 in.) diameter holes into the specimen using a rotary impact-type drill. Prior to sampling, the drilled concrete surface is cleaned three times, first using soap and

water, then using tap water, and finally using deionized water. It is then dried using paper towels. Drilling positions are measured and marked. A 152-mm (6-in.) long, 6.4-mm (0.25-in.) diameter drill bit is mounted to a heavy-duty drill. The specimen is drilled perpendicular to the reinforcing steel (parallel to the top surface of the specimen). The sample obtained from the first 12.7 mm (0.5 in.) depth contains epoxy coating from the exterior of the specimen and is discarded. The drilling continues to a depth of 63.5 mm (2.5 in.) to obtain approximately four grams of powder. The pulverized concrete sample from each hole is collected using two pieces of copy paper and transferred to labeled zip-lock plastic bags. The drill bit is cleaned before and between each sample to avoid contamination. A shop vacuum, reserved for drilling, is used during the procedure.

The chloride content of concrete is obtained using the water-soluble chloride ion content procedure and the potentiometric titration test method described in AASHTO T260-97 (2001), *Standard Method of Test for Sampling and Testing for Chloride Ion in Concrete and Concrete Raw Materials*. The procedure involves using boiled distilled water to dissolve Cl^- contained in the powdered concrete sample and titrating Cl^- with a silver nitrate (AgNO_3) solution. Millivoltmeter readings are taken when titrating the sample solution using an Irion 961700 chloride ion selective electrode. The equivalence point of the titration is indicated by the largest difference in two consecutive millivoltmeter readings. The titration continues until the millivoltmeter readings are at least 40 mV past the approximate equivalence point. The details of the analysis procedure and calculations are outlined in Sections 5.1, 5.3, and 5.4.1 in AASHTO T 260-97. The chloride content, in percent of weight of concrete, is converted to lb/yd^3 of concrete by multiplying by the unit weight of concrete, taken as 3786 lb/yd^3 .

For conventional reinforcing steel, corrosion initiation is considered to occur when either the macrocorrosion rate [Eqs. (1.10) and (1.11), Section 1.4.2] first reaches a value greater than or equal to $0.3 \mu\text{m}/\text{year}$ or the corrosion potential of the top mat of steel first shifts to a value more negative than -0.350 V with respect to a copper-copper sulfate electrode (CSE), which is nominally equal to the value measured using a SCE minus 0.075 V . For zinc-coated steel, corrosion initiation is based on a corrosion rate of $0.3 \mu\text{m}/\text{year}$ [Eqs. (1.10) and (1.11), Section 1.4.2] or when a sharp change in corrosion potential is observed, with the former serving as the primary guide.

2.7.2 Test Program

The test program consists of six beam specimens for each inhibitor, six beam specimens for each heat of conventional steel, and twelve beam specimens for galvanized reinforcing bars. The test program is summarized in the Table 2.27.

Table 2.27 - Test program for chloride threshold beam tests

Test ID ^a	Number of Tests
B-N4-DCI	6
B-N4-HY	6
B-N4-RH	6
B-N5-NO	6
B-N5-HY	6
B-Zn	12

^a N4, N5 = Conventional steel with different heat.

DCI = Conventional steel with DCI-S mixed in the concrete.

HY = Conventional steel with Hycrete mixed in the concrete.

RH = Conventional steel with Rheocrete 222+ mixed in the concrete.

NO = Conventional steel with no inhibitors in the concrete.

Zn = Galvanized steel with zinc coating on the outside of the conventional steel, no inhibitors.

CHAPTER 3

RESULTS AND EVALUATION

This chapter presents the test results for one rapid macrocell test series, three bench-scale test series, one field test series, and one critical chloride threshold test series. Corrosion protection systems include conventional and epoxy-coated (ECR) steel with and without corrosion inhibitors, multiple-coated (MC) and zinc-coated (galvanized) reinforcing steel, and pickled 2205 stainless steel. The performance of pickled 2205 stainless steel in two KDOT bridges – the Doniphan County Bridge (DCB) and Mission Creek Bridge (MCB) – is also described.

The test results include corrosion rate, total corrosion loss, corrosion potentials of both the anode and cathode (top and bottom mats of steel for bench-scale and field test specimen), and mat-to-mat resistance. Because the corrosion rate only captures an instantaneous value of corrosion, the total corrosion loss based on the integration of corrosion rate over time is used to evaluate the long-term effects of corrosion. The corrosion potentials for all macrocell tests were measured with respect to a saturated calomel electrode (SCE), while those for bench-scale and field tests were measured with respect to a copper-copper sulfate electrode (CSE). As described in Chapter 1, SCE readings are about 0.075 mV more positive than CSE readings. For the critical chloride threshold tests, the results include water-soluble chloride content. For the two KDOT bridges reinforced with pickled 2205 stainless steel, corrosion potential maps from semi-annual surveys, along with the results of the accompanying bench-scale and field test specimens are reported. All specimens were checked periodically and autopsied upon completion of the tests to allow visual inspection of the corrosion products.

In this chapter, the test results are reported based on average values (the average of several specimens). In many cases, conventional and ECR results are evaluated as “controls” for comparison with the other corrosion protection systems. The results for individual specimens are presented in Appendix A (corrosion rate, total corrosion loss, and corrosion potentials) and Appendix B (mat-to-mat resistance).

For ECR and MC specimens, 4, 10, or 16 intentional holes were placed in the coating to simulate damage that may occur in practice. For MC specimens, the holes through the coating were made by penetrating either the epoxy layer only, or both the zinc and epoxy coatings. The corrosion rates and the total corrosion losses for those specimens are reported based on both the total area (the bar surface area submerged in the anode solution for macrocell tests and full surface area of top mat bars in bench-scale tests) and the exposed area (the area of the holes placed in the coatings). Table 3.1 lists the factors that are used to convert corrosion rates based on total area to those based on exposed area.

Table 3.1 - Factors for converting corrosion rates and losses based on total and to those based on exposed area

Test Method	Rapid	Bench-scale Tests			Field Test
	Macrocell Test	SE	CB	ASTM G109	
Number of Bars	1	2	1	1	1
Bar Length mm (in.)	64 (2.5) ^b	305 (12)	305 (12)	279 (11)	991 (39.0) ^c
Total Area mm ² (in. ²)	3.2x10 ³ (4.9)	3.0 x10 ⁴ (47.1)	1.5x10 ⁴ (23.6)	1.4x10 ⁴ (21.6)	4.9x10 ⁴ (76.6)
with 4 Holes	Exposed Area mm ² (in. ²)	63 (0.10)	32 (0.05)	32 (0.05)	
	Factor ^a	480	480	440	
with 10 Holes	Exposed Area mm ² (in. ²)	159 (0.25)	79 (0.12)	79 (0.12)	
	Factor ^a	192	192	176	
with 16 Holes	Exposed Area mm ² (in. ²)				127 (0.20)
	Factor ^a				390
^a Factors for converting values based on total area to those based on exposed area.					
^b The test bar is 127 mm (5 in.) long with 64 mm (2.5 in.) in solution					
^c The test bar is 1067 mm (42 in.) long with a 76-mm (3-in.) long heat shrinkable tube at the threaded end.					

The corrosion rates presented in this study are based on “filtered” data. The reason is that the voltage drops across the resistors in the tests listed in Table 3.1 were measured with a voltmeter with a resolution of 0.001 mV. Based on the observation that when the voltage drop readings are near zero, they fluctuate between -0.003 and 0.003 mV, and beyond this range the readings become much more stable, it was concluded that the readings between -0.003 and 0.003 mV can be attributed to noise rather than actual corrosion activity, and therefore, they were treated as zero for individual specimens.

All of the tests in this study are designed so that (1) the top mat (or reinforcement serving as the anode in the macrocell test) is exposed to chlorides and (2) the bottom mat (or reinforcement serving as the cathode in the macrocell test) has more reinforcement than the top mat (anode) to ensure that corrosion is not limited by the cathode. In most cases, the current flows* from the bottom mat to top, which is defined as “positive corrosion,” indicating that the top mat is acting as the anode. In some cases, the current flows in the opposite direction, from top to bottom, which is defined as “negative corrosion” in this study, indicating that the bottom mat is acting as the anode. In all corrosion rate plots, “negative corrosion” is indicated by negative values.

Due to the long-term nature of the tests in this study, only the results as of May 31, 2008 are reported.

Mortar-wrapped rapid macrocell specimens and conventional steel were used to evaluate the effect of three corrosion inhibitors, DCI-S, Hycrete, and Rheocrete 222+, and two water-cement ratios, 0.35 and 0.45, on corrosion performance. Six specimens were tested for each system. The test results indicate that the use of the lower water-

* By convention, electrical current “flows” in the opposite direction of the electrons.

cement ratio had a greater impact on corrosion performance than did the use of the corrosion inhibitors.

Corrosion protection systems incorporating corrosion inhibitors, ECR, and MC reinforcement were evaluated using bench-scale tests. Systems with corrosion inhibitors include conventional steel with the three corrosion inhibitors (DCI-S, Hycrete, and Rheocrete 222+). MC reinforcement was evaluated with only epoxy layer or both epoxy and zinc layers penetrated with holes. Two different exposure areas (four or ten holes) were used for both ECR and MC reinforcement. Three bench-scale tests, the Southern Exposure (SE), cracked beam (CB), and ASTM G109 tests were used in this study. Six specimens each with conventional steel and ECR served as controls for the SE test. Three specimens, each with conventional steel, without and with one of the three inhibitors were evaluated using SE and CB tests. Three types of reinforcement (conventional, ECR, and MC steel) were evaluated using the ASTM G109 test. Test results indicate that both ECR and MC significantly improve corrosion resistance of conventional steel. Corrosion inhibitors improve corrosion resistance of conventional steel in both uncracked and cracked concrete and delay the onset of corrosion in uncracked concrete.

Three corrosion inhibitors, MC reinforcement, and three types ECR with increased adhesion were evaluated using field test specimens. The systems with corrosion inhibitors include ECR cast in concrete with DCI, Hycrete, and Rheocrete and ECR with a primer containing microencapsulated calcium nitrite. The three types of ECR with increased adhesion include coating products by DuPont and Valspar and ECR with a zinc-chromate pretreatment. Specimens containing conventional steel and ECR served as control. In most cases, two specimens with and two specimens without simulated cracks were used for each system, except three specimens with and without

cracks were used for ECR with the inhibitor DCI. Two or four top bars were individually monitored in each specimen, as shown in Table 2.14. Results for the field test specimens indicate that ECR with corrosion inhibitors, MC reinforcement, and ECR with increased adhesion provide significantly improved corrosion resistance compared to conventional steel. The corrosion inhibitors provide no improvement in corrosion resistance for ECR. Increased adhesion between the epoxy and reinforcing steel provides no benefits in corrosion performance of ECR under the exposure conditions provided by the field test.

In the KDOT bridge projects, pickled 2205 stainless steel was evaluated, along with ECR and conventional steel. Bench-scale tests using specimens containing pickled 2205 stainless steel and field tests using specimens containing pickled 2205 stainless steel, ECR, and conventional steel, cast in concrete with the same mixture proportions and materials as placed in the corresponding bridge decks (the Doniphan County Bridge and the Mission Creek Bridge) and bridge potential mapping of decks containing the stainless steel were used. The test results demonstrate that stainless steel provides excellent corrosion performance.

In the critical chloride threshold tests, conventional steel with three corrosion inhibitors and zinc-coated (galvanized) reinforcement without chromate treatment were evaluated. Comparisons to a previous study of the conventional steel without inhibitors and MMFX microcomposite reinforcement were also included. Six specimens for conventional steel with each of the three corrosion inhibitors and twelve specimens with the zinc-coated steel were used in the test. The test results show that the average critical chloride threshold for the conventional steel with Hycrete is low compared to those of other systems. The zinc-coated reinforcement

has a higher average critical chloride threshold than those observed for conventional and MMFX steel.

The results for each test are presented in detail in the following sections in this Chapter.

3.1 RAPID MACROCELL TEST

This section summarizes the results of the rapid macrocell tests, including the results for corrosion rate, total corrosion loss, and anode and cathode corrosion potentials. Mortar-wrapped specimens were used to evaluate conventional steel in 1.6 molal ion concentration NaCl in simulated concrete pore solution. Three different inhibitors (DCI-S, Hycrete, and Rheocrete 222+) and two water-cement ratios ($w/c = 0.35$ and 0.45) were tested. Six specimens cast in two batches of concrete, three in each batch, were tested for each combination. Specimens with a w/c ratio of 0.45 were tested for a period of 15 weeks, while specimens with a w/c ratio of 0.35 were tested for 20 weeks for Batch 1 and 25 weeks for Batch 2. Specimens with a w/c ratio of 0.35 were tested for extended periods of time because they exhibited a longer time to corrosion initiation than the 0.45 w/c ratio specimens, as described in Section 2.4.1.

The test designations used in tables and figures are as follows:

M = Macrocell

NO = no inhibitor

DCI = DCI-S

HY = Hycrete

RH= Rheocrete 222+

45, 35 = water/cement ratio 0.45 and 0.35 , respectively.

Test results of individual specimens are presented in Figures A.1 to A.16 in Appendix A.

Corrosion losses for specimens are obtained by integrating the corrosion rates of the corresponding specimens over time. The total corrosion losses for conventional steel cast in mortar without and with corrosion inhibitors at week 15 are summarized in Table 3.2. For specimens with a w/c ratio of 0.45, the average total losses at week 15 ranged from 1.80 to 2.65 μm . For specimens with a w/c ratio of 0.35, the average total losses ranged from 0.25 to 0.53 μm . The average corrosion losses for the 0.45 w/c ratio specimens with inhibitor were slightly higher than those of specimens without an inhibitor, but there were not significant differences among the inhibitor specimens. The average corrosion losses of specimens with no inhibitor and

Table 3.2 – Corrosion losses at 15 weeks for conventional steel with different inhibitors in rapid macrocell test ^a

Steel Designation ^b	Specimen Corrosion Losses (μm)						Average	Standard Deviation
	1	2	3	4	5	6		
$w/c = 0.45$								
M-NO45	3.28	2.48	1.19	1.08	1.92	0.87	1.80	0.94
M-DCI45	5.11	2.31	2.90	0.79	0.67	4.12	2.65	1.78
M-HY45	4.19	5.25	3.01	β	0.41	1.98	2.47	2.08
M-RH45	2.70	2.55	2.32	0.93	2.56	3.46	2.42	0.83
$w/c = 0.35$								
M-NO35	1.38	0.12	0.12	0.59	0.01	0.13	0.39	0.52
M-DCI35	0.65	0.96	0.13	1.08	0.08	0.28	0.53	0.43
M-HY35	2.43	β	0.01	0.13	-0.05	β	0.42	0.99
M-RH35	0.81	0.16	0.04	-0.02	0.51	0.02	0.25	0.34

^a Test continued 25 weeks for specimens with $w/c = 0.35$.

^b M = Macrocell. NO = Conventional steel with no inhibitors mixed in the mortar.

DCI = Conventional steel with corrosion inhibitor DCI-S in the mortar.

HY = Conventional steel with corrosion inhibitor Hycrete in the mortar.

RH = Conventional steel with corrosion inhibitor Rheocrete in the mortar.

45 = water-cement ratio is 0.45. 35 = water-cement ratio is 0.35.

No. 16 (No. 5) conventional steel is used in all test specimens.

β = Corrosion loss (absolute value) less than 0.005 μm .

Rheocrete had relatively small standard deviations (0.94 and 0.83 μm , respectively), while the corrosion losses for specimens with Hycrete had the largest standard deviation (2.08 μm), with average values ranging from less than 0.005 to 5.25 μm . For specimens with a w/c ratio of 0.35, there was little variance among the average corrosion losses for the four types of specimens. Again, a larger standard deviation (0.99 μm) was observed for the Hycrete specimens, with values ranging from less than 0.005 to 2.43 μm , compared to other specimens with a w/c ratio of 0.35, which had corrosion loss standard deviations that ranged from 0.25 to 0.53 μm .

The average corrosion rates for specimens cast with different inhibitors and with a w/c ratio of 0.45 are presented in Figure 3.1a. As shown in the figure, the specimens without and with inhibitors had similar corrosion rates through week 11, after which, the specimens without inhibitors, which reached a maximum rate of approximately 11 $\mu\text{m}/\text{yr}$, gradually exhibited a lower corrosion rate than the other specimens, dropping to 3.89 $\mu\text{m}/\text{yr}$ at week 15. Figure 3.1b shows the corrosion losses obtained by integrating the area under the corrosion rate curves. As the result of their relatively low corrosion rates during the final four weeks of the tests, the specimens with no inhibitors exhibited the lowest corrosion loss at 15 weeks, 1.80 μm , while the corrosion losses of the other specimens were approximately 2.50 μm . Average anode and cathode corrosion potentials with respect to SCE are plotted in Figures 3.2a and 3.2b, respectively. The corrosion potentials of all anodes had dropped below -0.275 V by week 15. Values of -0.417 V or below with respect to the SCE, had been attained by 15 weeks, indicating a high probability of corrosion. The Hycrete specimens had a relatively less negative anode potential than other inhibitor specimens with the value of -0.417 V, while the Rheocrete specimens had the most negative average anode potential at week 15, with a value of -0.576 V. The

corrosion potentials of the cathodes were more stable than those of the anodes. All the specimens had the similar average cathode potentials, with values around -0.200 V at the beginning of the test and -0.250 V at week 15, indicating a low probability of corrosion. Hycrete had the lowest cathode potentials among all the specimens, with an average value of -0.243 V at week 15 with respect to a SCE.

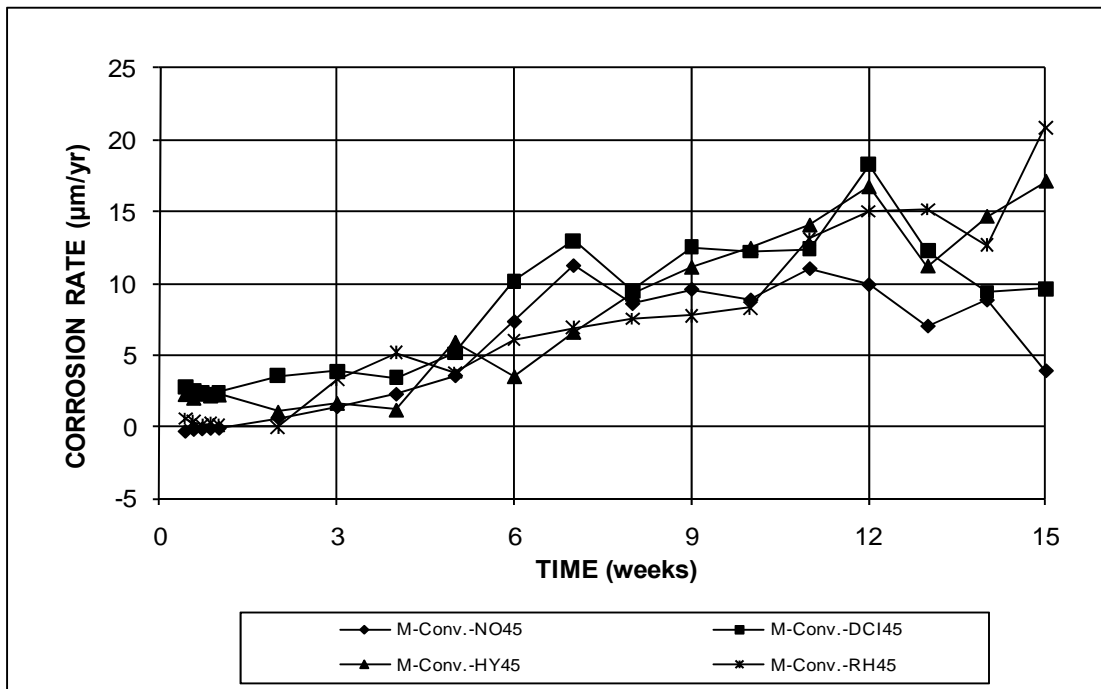


Figure 3.1a – Macrocell Test. Average corrosion rates for specimens with conventional steel and different inhibitors, $w/c = 0.45$.

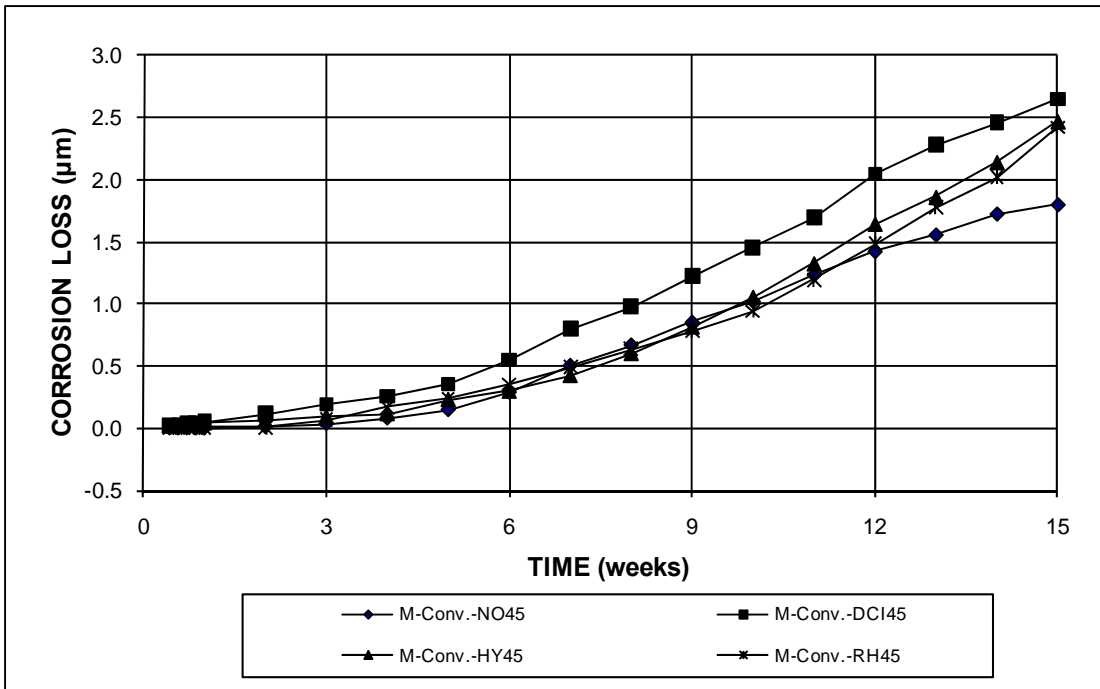


Figure 3.1b – Macrocell Test. Average corrosion losses for specimens with conventional steel and different inhibitors, $w/c = 0.45$.

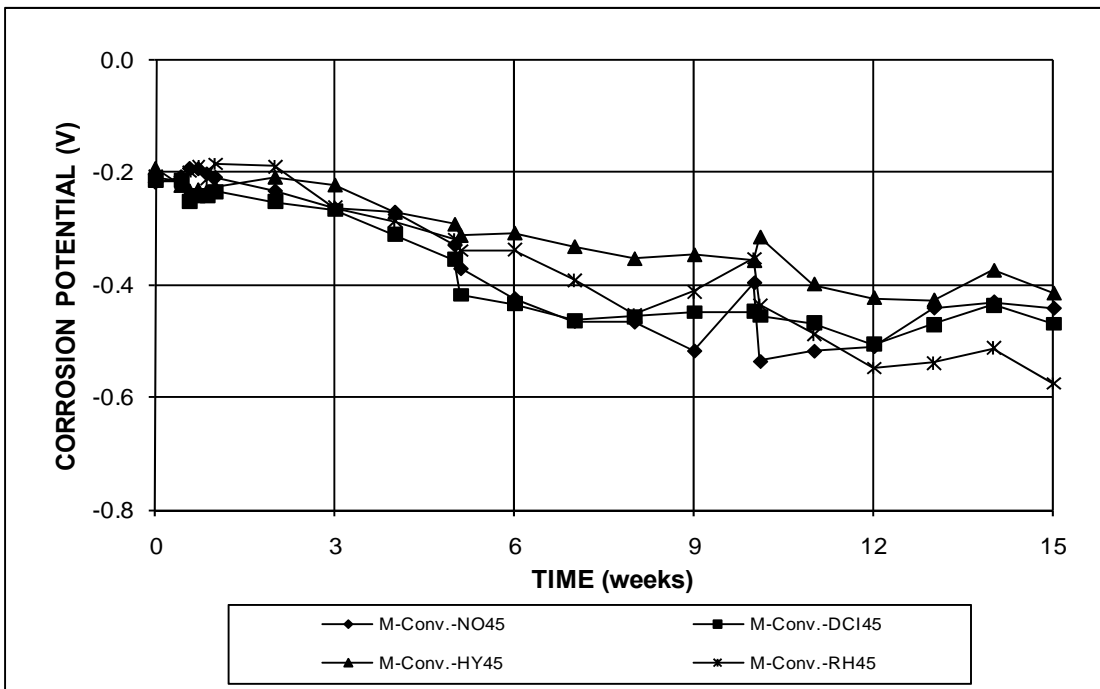


Figure 3.2a – Macrocell Test. Average anode corrosion potentials with respect to a saturated calomel electrode for specimens with conventional steel and different inhibitors, $w/c = 0.45$.

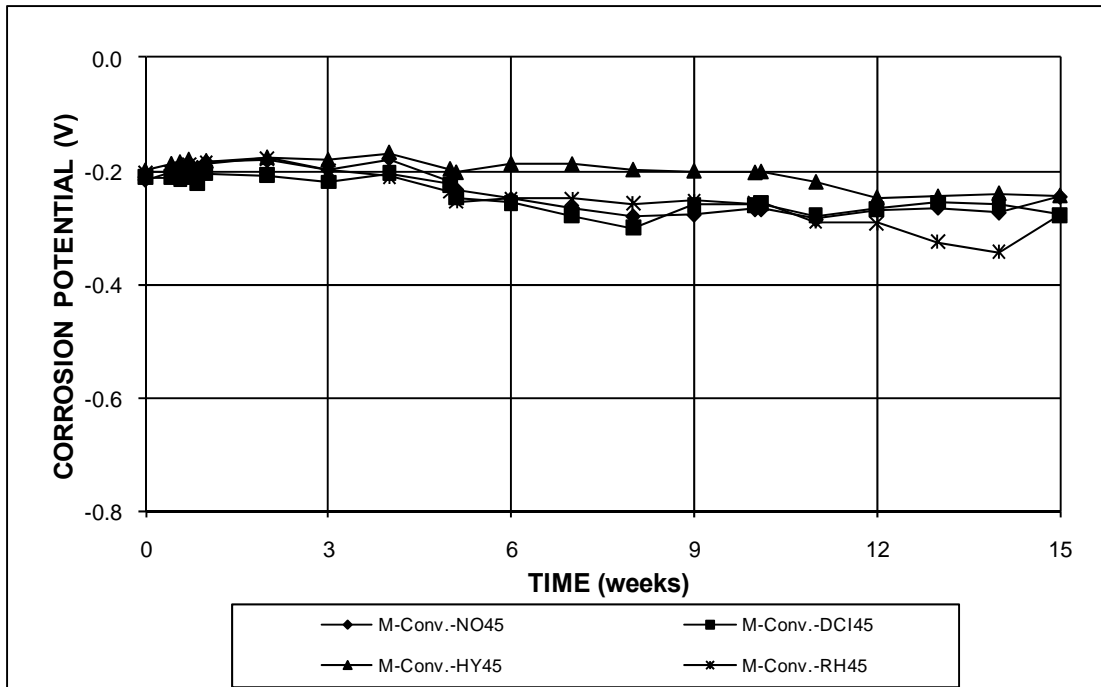


Figure 3.2b – Macrocell Test. Average cathode corrosion potentials with respect to a saturated calomel electrode for specimens with conventional steel and different inhibitors, $w/c = 0.45$.

Figures 3.3a through 3.4b compare the performance of inhibitors in mortar with a w/c of 0.35. The results are based on the average of six specimens up to week 20, and after that time, the values are based on the average of three specimens, except two specimens are used for Hycrete after week 20 due to aberrant readings for one specimen. As shown in Figure 3.3a, the Hycrete specimens had the highest average peak corrosion rate of $14.43 \mu\text{m}/\text{yr}$ with a negative anode corrosion potential of -0.581 V at week 24 (Figure 3.4a). The specimens without inhibitors (M-Conv.-NO35) exhibited average corrosion rates of approximately $10 \mu\text{m}/\text{yr}$ between weeks 16 and 20 and $8.34 \mu\text{m}/\text{yr}$ at week 23, which were higher than the other specimens at these points in time. As shown in Figure 3.3b, all specimens had similar average corrosion losses before week 15, and after that, the relative performance as represented by the total losses changed significantly. Specimens with no inhibitors

(M-Conv.-NO35) had the highest average corrosion loss, 1.86 μm , at week 25, and the Rheocrete specimens had the lowest average corrosion loss, 0.38 μm , at week 25. As shown in Figure 3.4a, the average anode corrosion potentials for most of specimens were more negative than -0.275 V after week 15 with respect to SCE, indicating a high probability of corrosion, except those of the RH specimens, which were close to -0.275 V. The average corrosion potentials of the anodes for the specimens with no inhibitors shifted to more negative values between weeks 14 and 22, agreeing with a noted increase in average corrosion rates. The anodes and cathodes of the RH specimens exhibited relatively less negative corrosion potentials than the other specimens throughout most of the test period.

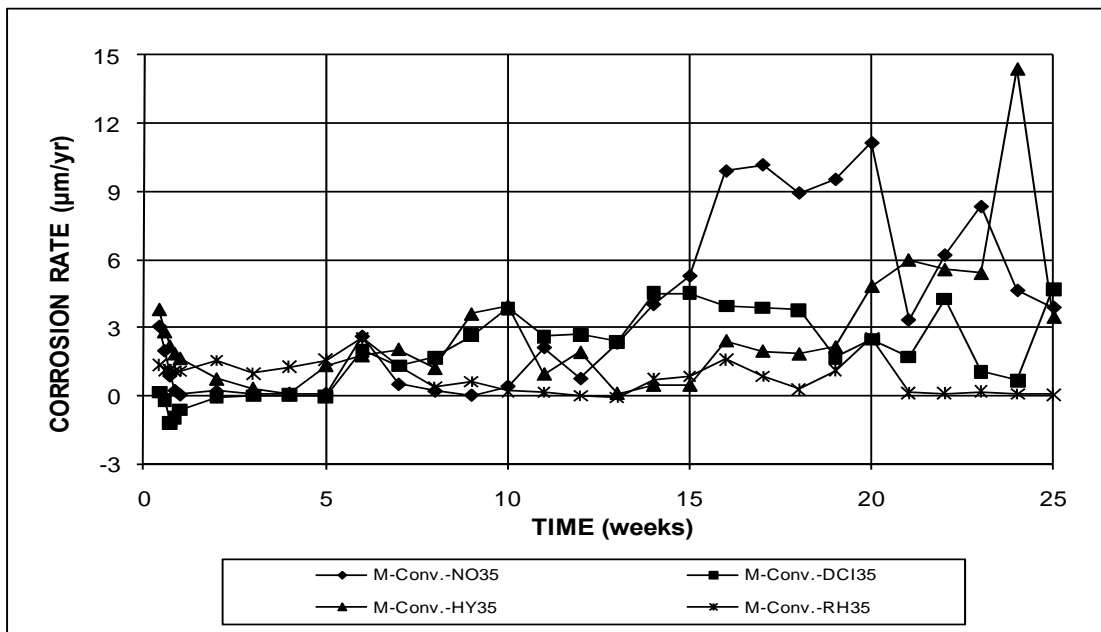


Figure 3.3a – Macrocell Test. Average corrosion rates for specimens with conventional steel and different inhibitors, $w/c = 0.35$. (Based on average of six specimens before week 20 and three specimens after, except two specimens are used for Hycrete after week 20)

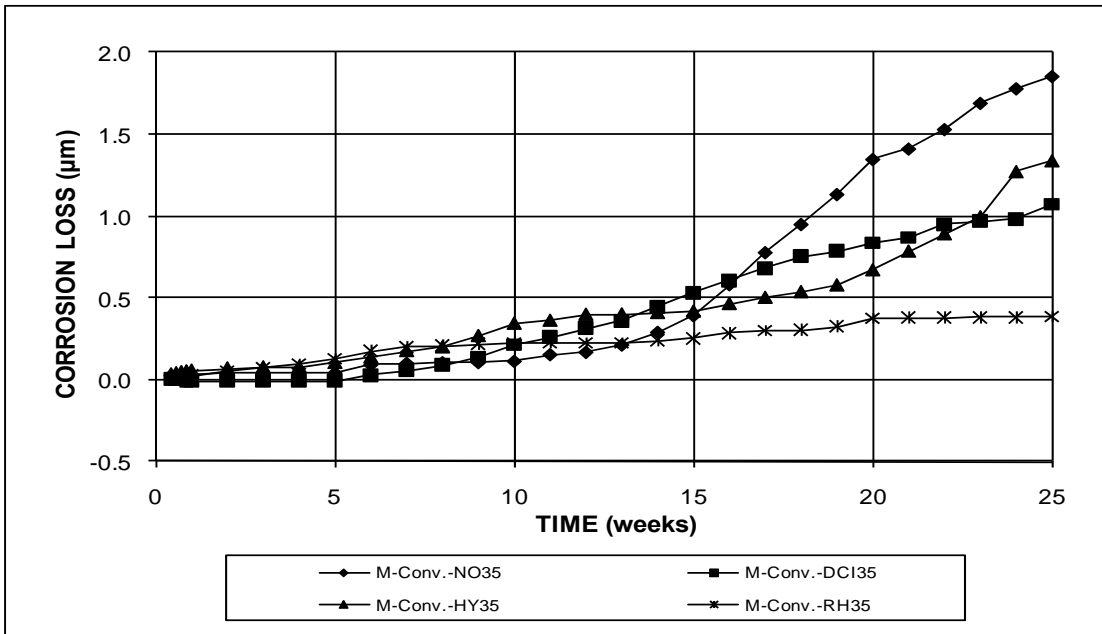


Figure 3.3b – Macrocell Test. Average corrosion losses for specimens with conventional steel and different inhibitors, $w/c = 0.35$. (Based on average of six specimens before week 20 and three specimens after, except two specimens are used for Hycrete after week 20)

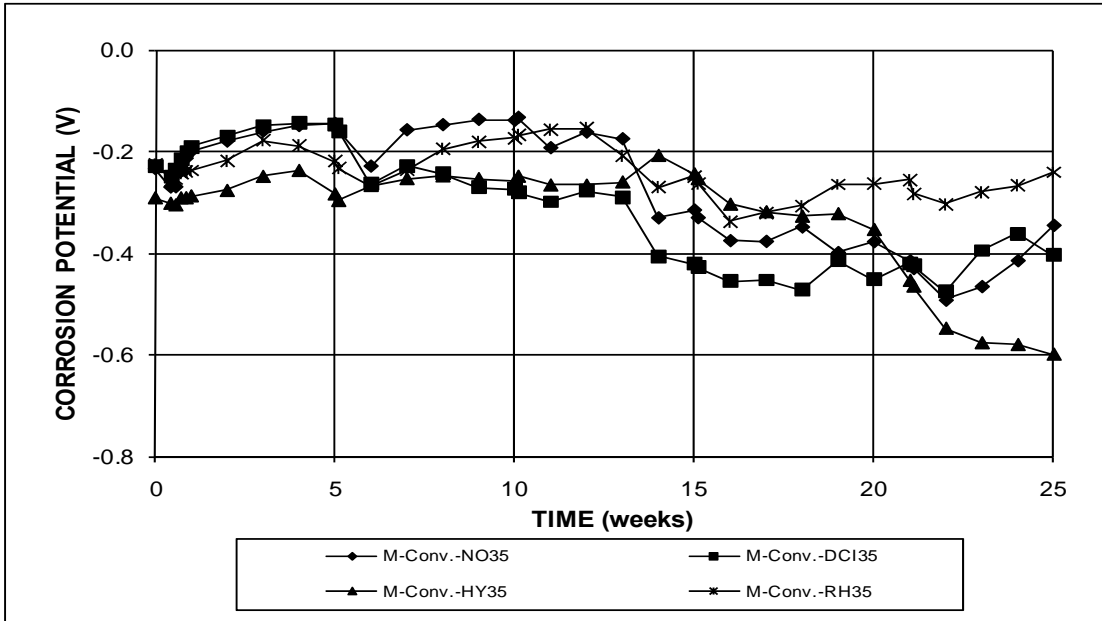


Figure 3.4a – Macrocell Test. Average anode corrosion potentials with respect to a saturated calomel electrode for specimens with conventional steel and different inhibitors, $w/c = 0.35$. (Based on average of six specimens before week 20 and three specimens after, except two specimens are used for Hycrete after week 20)

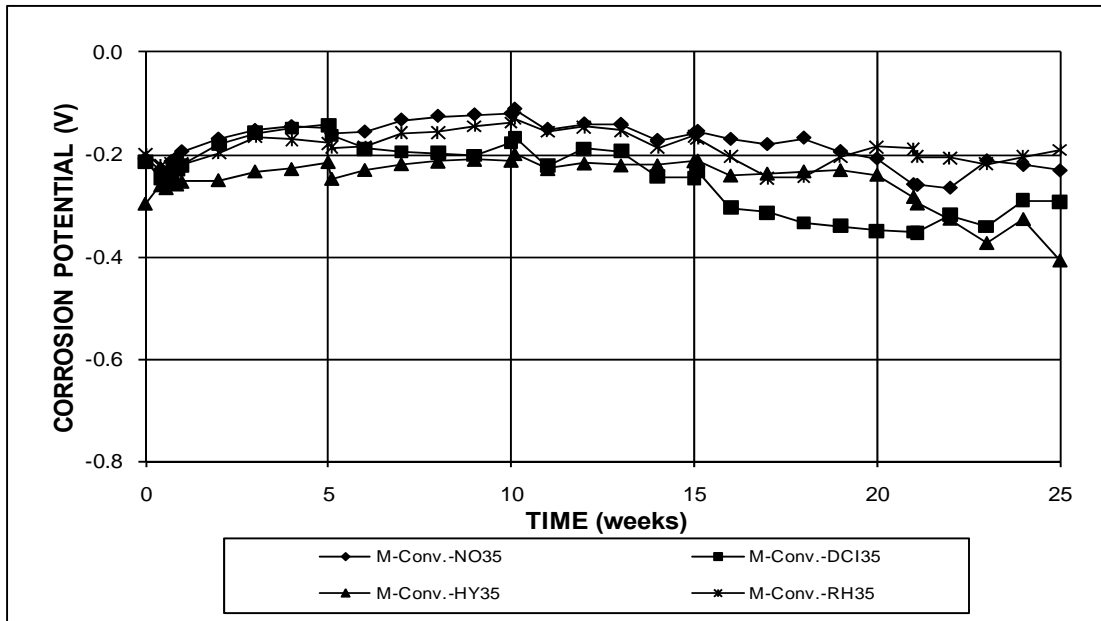


Figure 3.4b – Macrocell Test. Average cathode corrosion potentials with respect to a saturated calomel electrode for specimens with conventional steel and different inhibitors, $w/c = 0.35$. (Based on average of six specimens before week 20 and three specimens after, except two specimens are used for Hycrete after week 20)

The corrosion behavior for specimens with different water-cement ratios and no inhibitors is shown in Figures 3.5a through 3.6b. The specimens with a w/c ratio of 0.45 exhibited more corrosion activity, with higher average corrosion rates (Figure 3.5a) and average total losses (Figure 3.5b) and more negative average anode (Figure 3.6a) and cathode (Figure 3.6b) potentials than the specimens with a w/c ratio of 0.35 for the 15-week period. After week 13, the average anode corrosion potentials for specimens with a w/c ratio of 0.35 shifted to more negative values, but the low value, -0.492 V, remained above the low value, -0.537 V, for the w/c ratio 0.45 specimens. At week 15, the average corrosion loss for specimens with a w/c ratio of 0.45 was 1.80 μm , about 4.6 times the corrosion loss of specimens with a w/c ratio of 0.35, 0.39 μm . After week 15, the corrosion loss of specimens with a w/c ratio of 0.35 continually increased, reaching 1.86 μm at week 25.

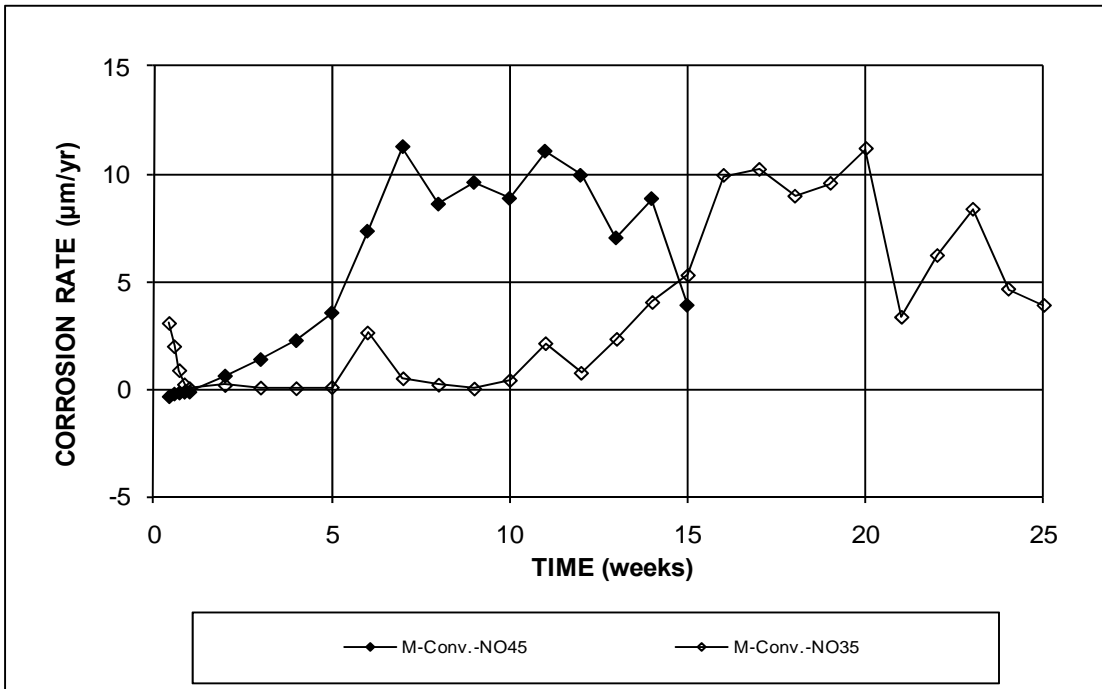


Figure 3.5a – Macrocell Test. Average corrosion rates for specimens with conventional steel and different water-cement ratios, no inhibitors.

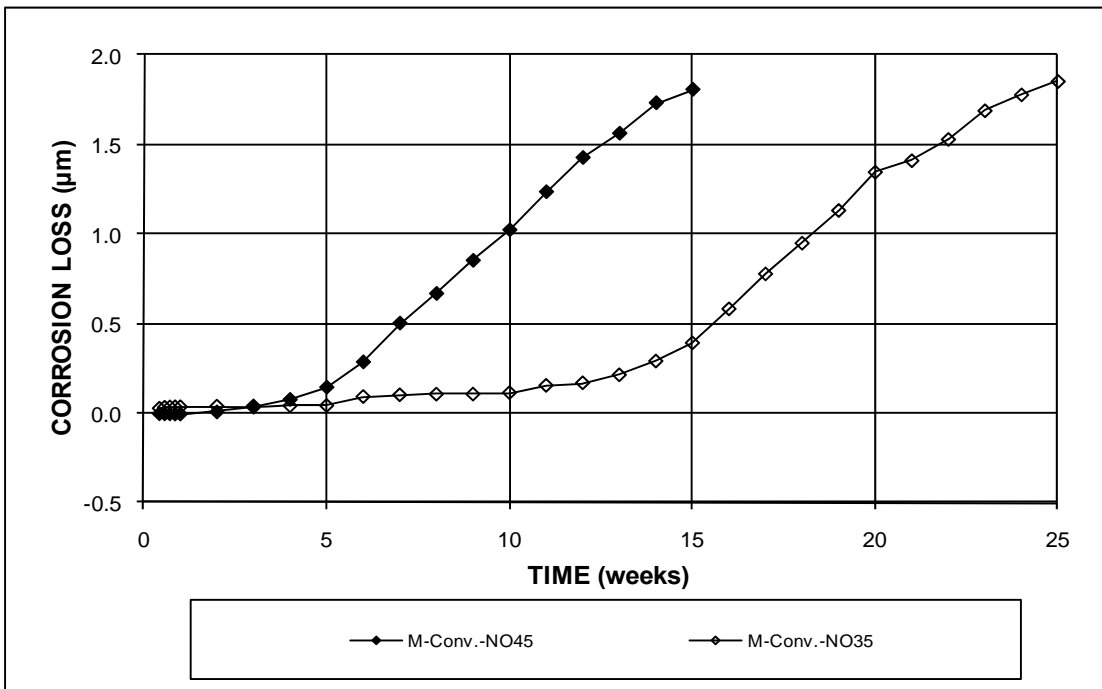


Figure 3.5b – Macrocell Test. Average corrosion losses for specimens with conventional steel and different water-cement ratios, no inhibitors.

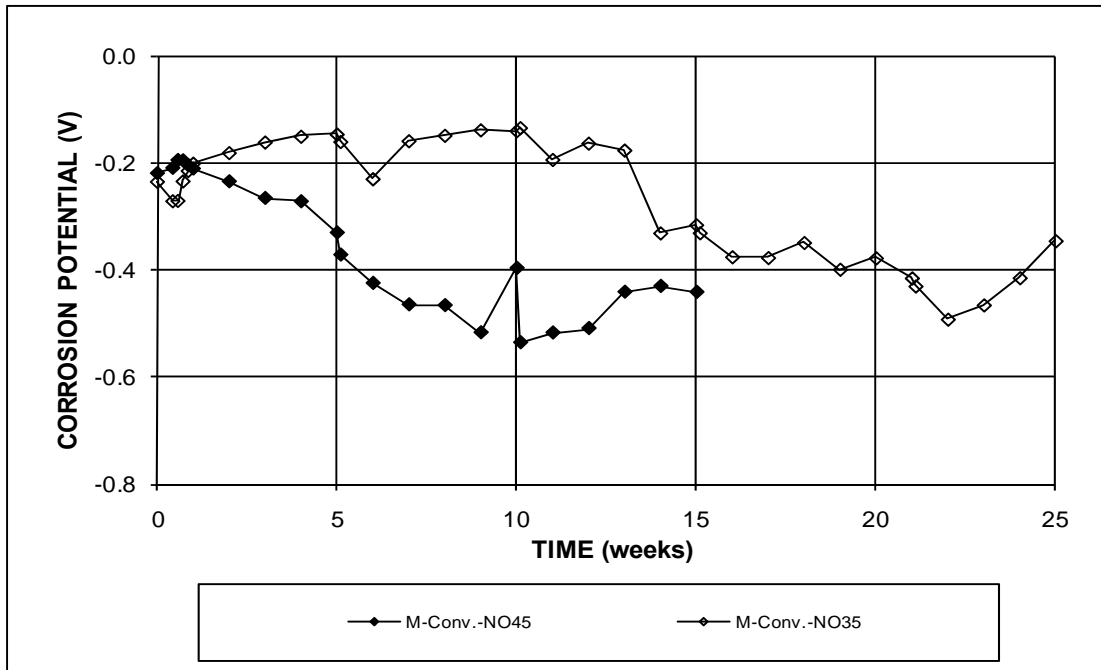


Figure 3.6a – Macrocell Test. Average anode corrosion potentials with respect to a saturated calomel electrode for specimens with conventional steel and different water-cement ratios, no inhibitors.

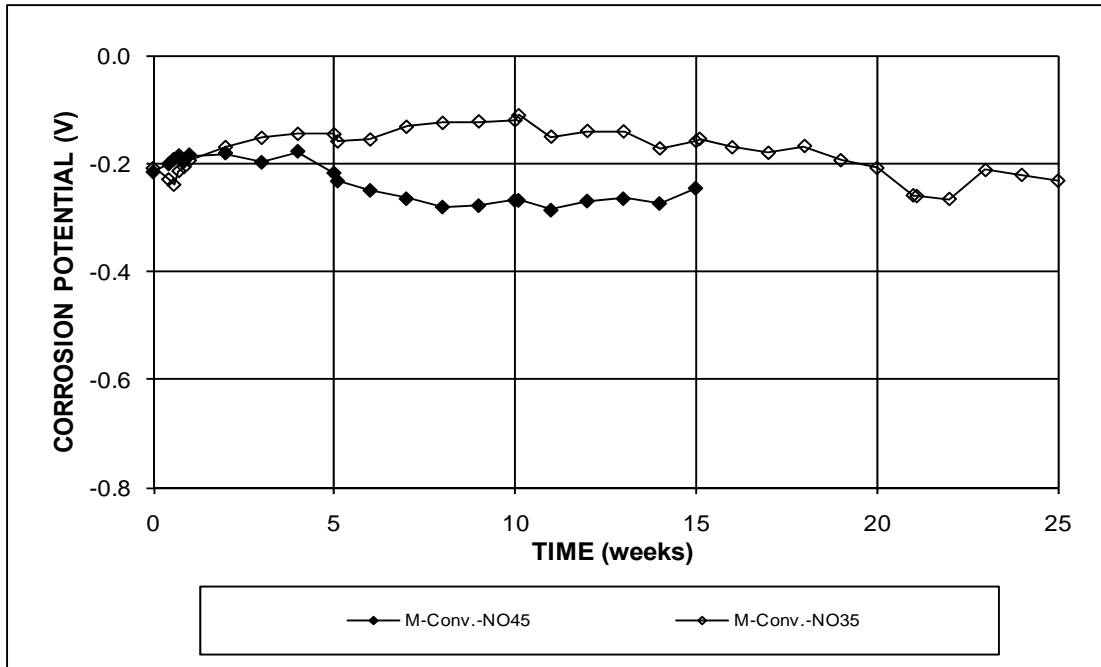


Figure 3.6b – Macrocell Test. Average cathode corrosion potentials with respect to a saturated calomel electrode for specimens with conventional steel and different water-cement ratios, no inhibitors.

The average corrosion rates, corrosion losses, and potential readings for the specimens with different water-cement ratios and corrosion inhibitors are plotted in Figures 3.7a through 3.12b. For specimens containing DCI, those with a w/c ratio of 0.45 had higher average corrosion rates (Figure 3.7a) and losses (Figure 3.7b) for the 15-week period than those with a w/c ratio of 0.35. At week 15, the average corrosion loss for specimens with a w/c ratio of 0.45 was 2.65 μm , about 5 times the corrosion loss of specimens with a w/c ratio of 0.35 (average loss of 0.53 μm). The average anode corrosion potentials (Figure 3.8a) for specimens with a w/c ratio of 0.35 were less negative than the corrosion potentials of specimens with a w/c ratio of 0.45 before week 15. After week 15, the average corrosion potentials for specimens with a w/c ratio of 0.35 remained at about -0.450 V. The average cathode potentials (Figure 3.8b) for specimens with a w/c ratio of 0.35 were less negative than those for specimens with a w/c ratio of 0.45 through week 15. After week 15, the average corrosion rates for specimens with a w/c ratio of 0.35 remained below 5 $\mu\text{m}/\text{yr}$, with an average corrosion loss of 1.07 μm at week 25. The anode corrosion potentials remained below -0.362 V through week 25.

For the specimens containing Hycrete, those with a w/c ratio of 0.45 had a large increase in corrosion activity after week 5, as demonstrated by higher corrosion rates (Figure 3.9a) and losses (Figure 3.9b) and more negative anode corrosion potentials (Figure 3.10a). At week 15, the average corrosion loss for specimens with a w/c ratio of 0.45 was 2.47 μm , about 6 times the average corrosion loss for specimens with a w/c ratio of 0.35 (average loss of 0.42 μm). The cathode potentials (Figure 3.10b) for specimens with the two water-cement ratios were approximately the same through week 15. After week 15, the average corrosion rates for specimens with a w/c ratio of 0.35 remained below 5.20 $\mu\text{m}/\text{yr}$, with an average corrosion loss of 1.64 μm at week

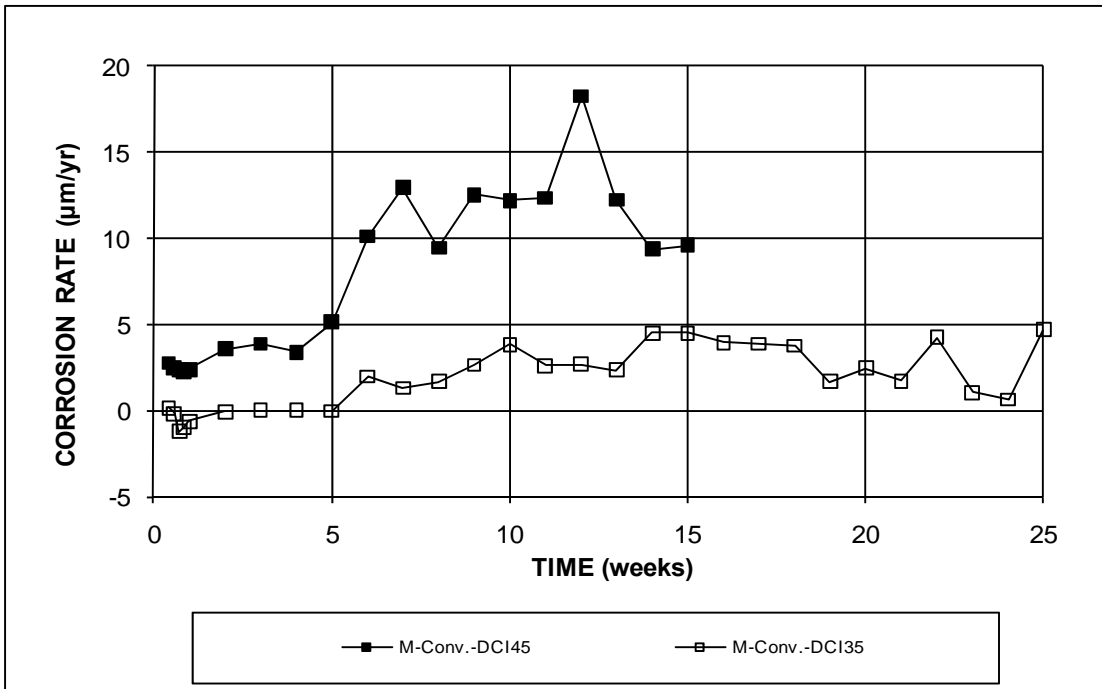


Figure 3.7a – Macrocell Test. Average corrosion rates for specimens with conventional steel and different water-cement ratios, DCI inhibitor.

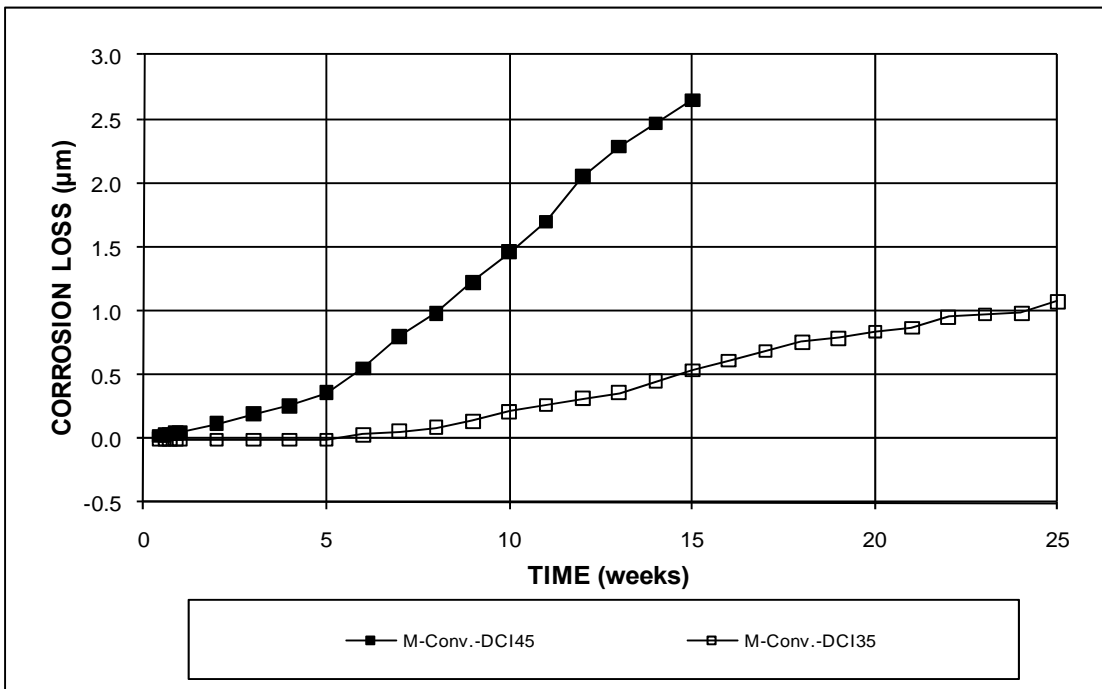


Figure 3.7b – Macrocell Test. Average corrosion losses for specimens with conventional steel and different water-cement ratios, DCI inhibitor.

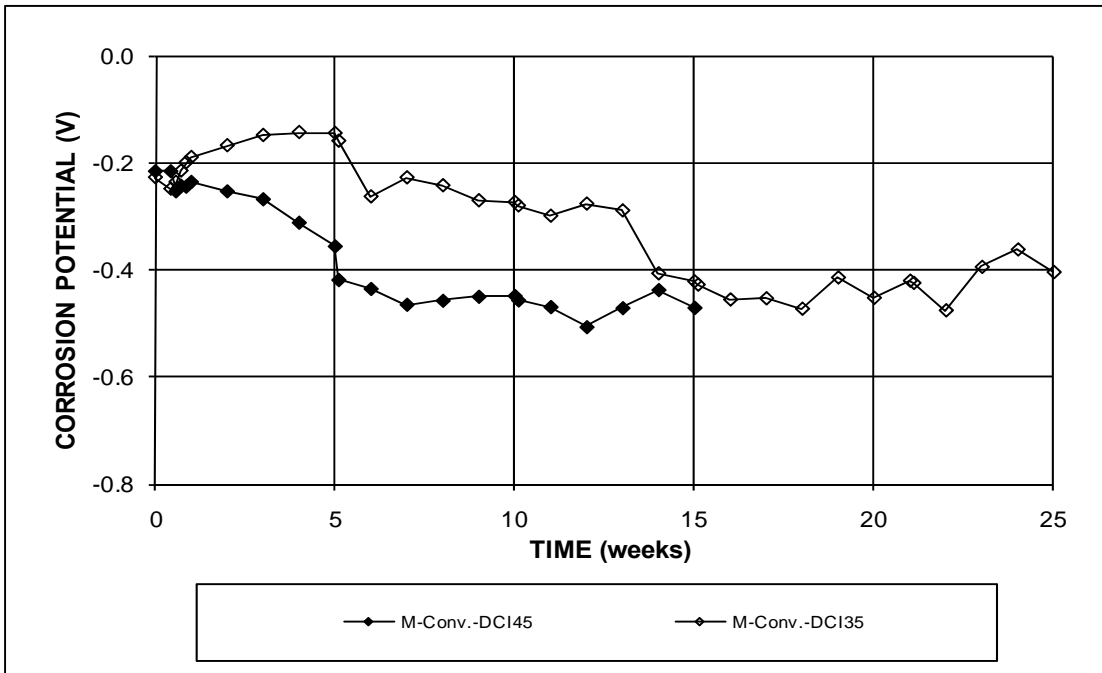


Figure 3.8a – Macrocell Test. Average anode corrosion potentials with respect to a saturated calomel electrode for specimens with conventional steel and different water-cement ratios, DCI inhibitor.

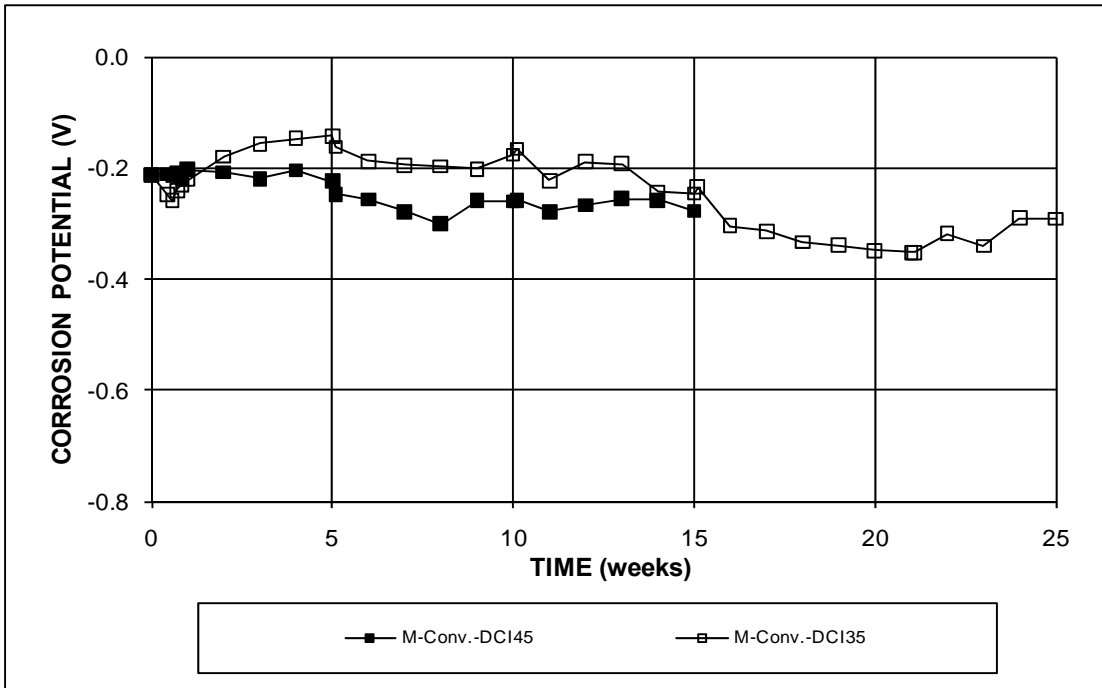


Figure 3.8b – Macrocell Test. Average cathode corrosion potentials with respect to a saturated calomel electrode for specimens with conventional steel and different water-cement ratios, DCI inhibitor.

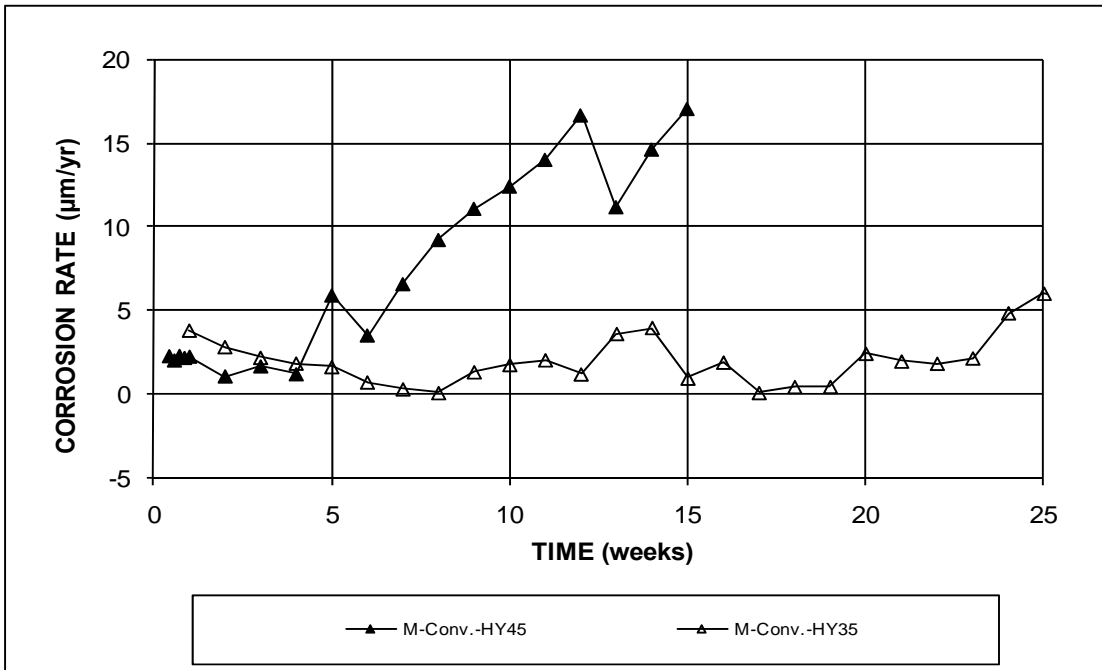


Figure 3.9a – Macrocell Test. Average corrosion rates for specimens with conventional steel and different water-cement ratios, Hycrete inhibitor.

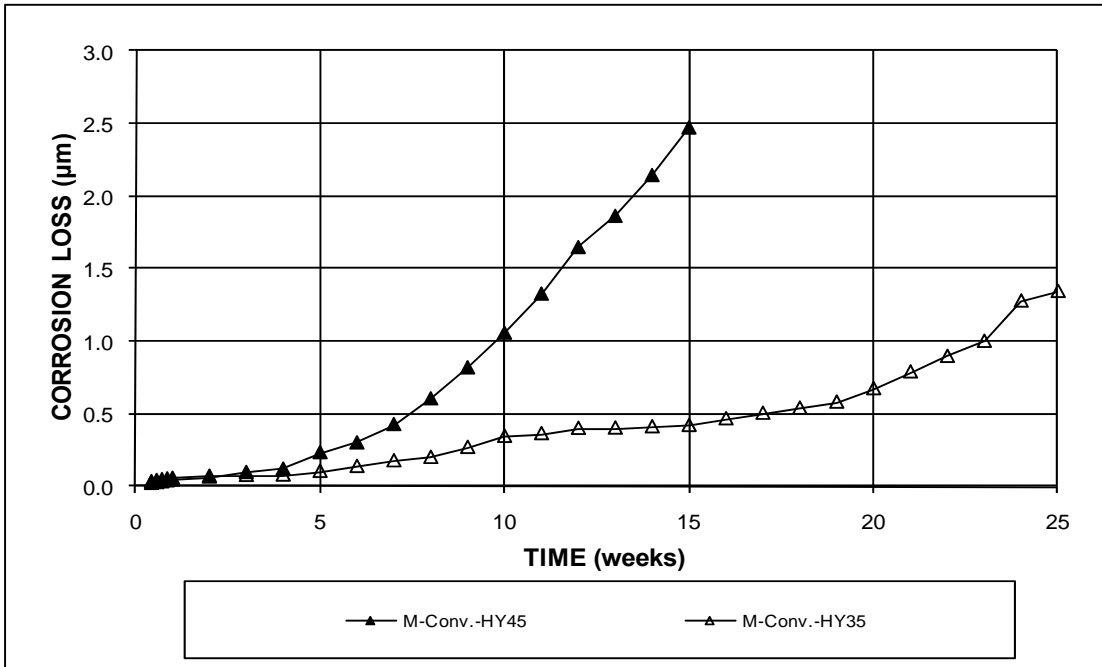


Figure 3.9b – Macrocell Test. Average corrosion losses for specimens with conventional steel and different water-cement ratios, Hycrete inhibitor.

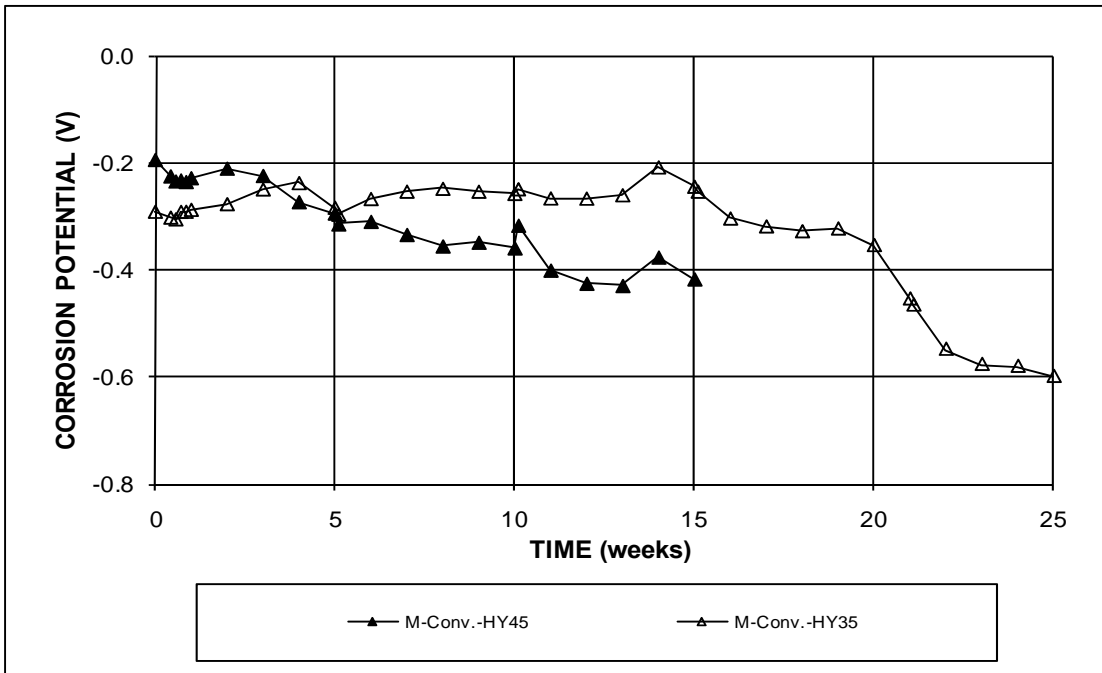


Figure 3.10a – Macrocell Test. Average anode corrosion potentials with respect to a saturated calomel electrode for specimens with conventional steel and different water-cement ratios, Hycrete inhibitor.

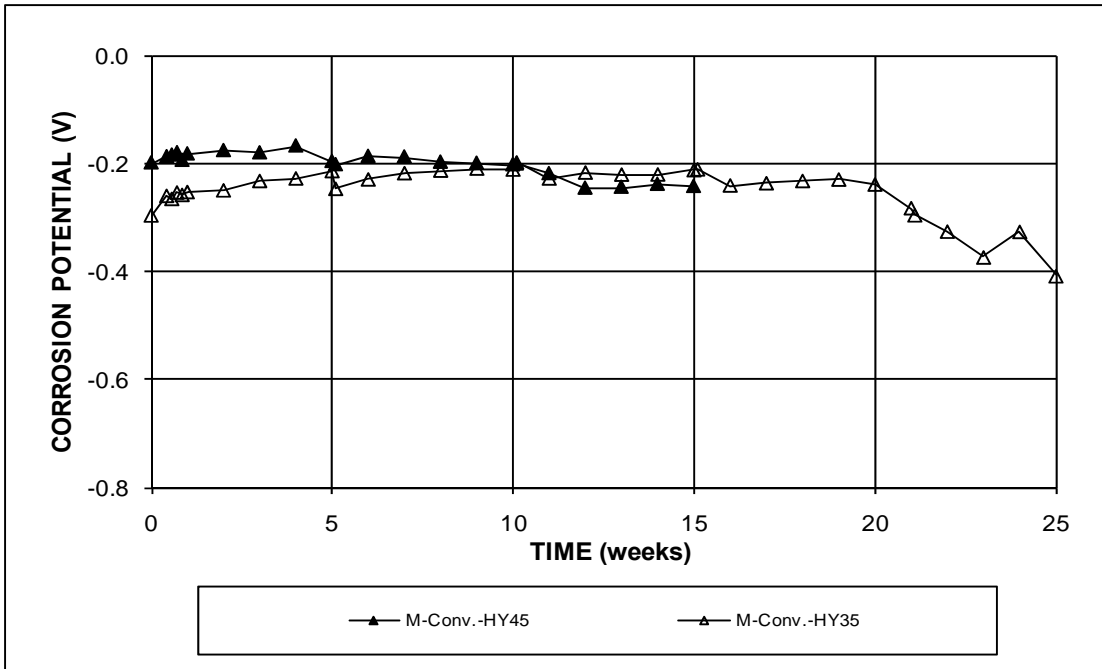


Figure 3.10b – Macrocell Test. Average cathode corrosion potentials with respect to a saturated calomel electrode for specimens with conventional steel and different water-cement ratios, Hycrete inhibitor.

25. The average corrosion potentials gradually decreased and reached to -0.600 V for anode and -0.408 V for cathode at week 25.

For the specimens containing Rheocrete, those with a w/c ratio of 0.45 had a large increase in corrosion activity after week 3 as demonstrated by higher corrosion rates (Figure 3.11a) and losses (Figure 3.11b) and more negative anode corrosion potentials (Figure 3.12a). At week 15, the average corrosion loss for specimens with a w/c ratio of 0.45 was $2.42 \mu\text{m}$, about 10 times the corrosion loss for specimens with a w/c ratio of 0.35 ($0.25 \mu\text{m}$). The cathode potentials (Figure 3.12b) for specimens with a w/c ratio of 0.45 were slightly more negative than those for specimens with a w/c ratio of 0.35 after week 2. After week 15, the average corrosion rates for specimens with a w/c ratio of 0.35 remained below $2.60 \mu\text{m/yr}$, with an average corrosion loss of $0.38 \mu\text{m}$ at week 25. The average corrosion potentials stabilized around -0.300 V for anode and -0.200 V for cathode through week 25.

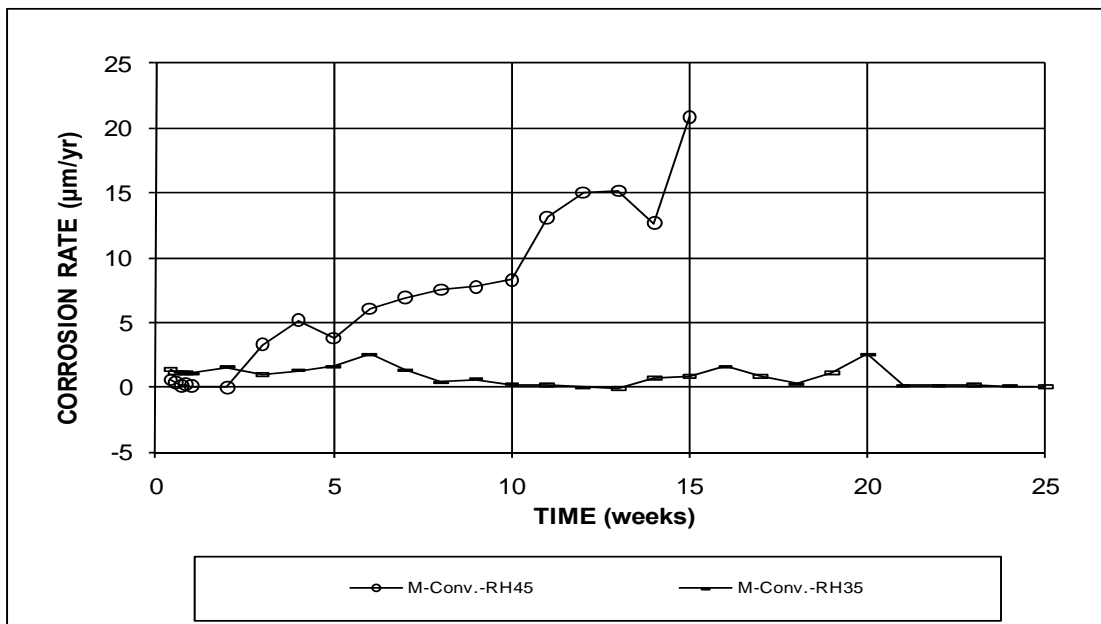


Figure 3.11a – Macrocell Test. Average corrosion rates for specimens with conventional steel and different water-cement ratios, Rheocrete inhibitor.

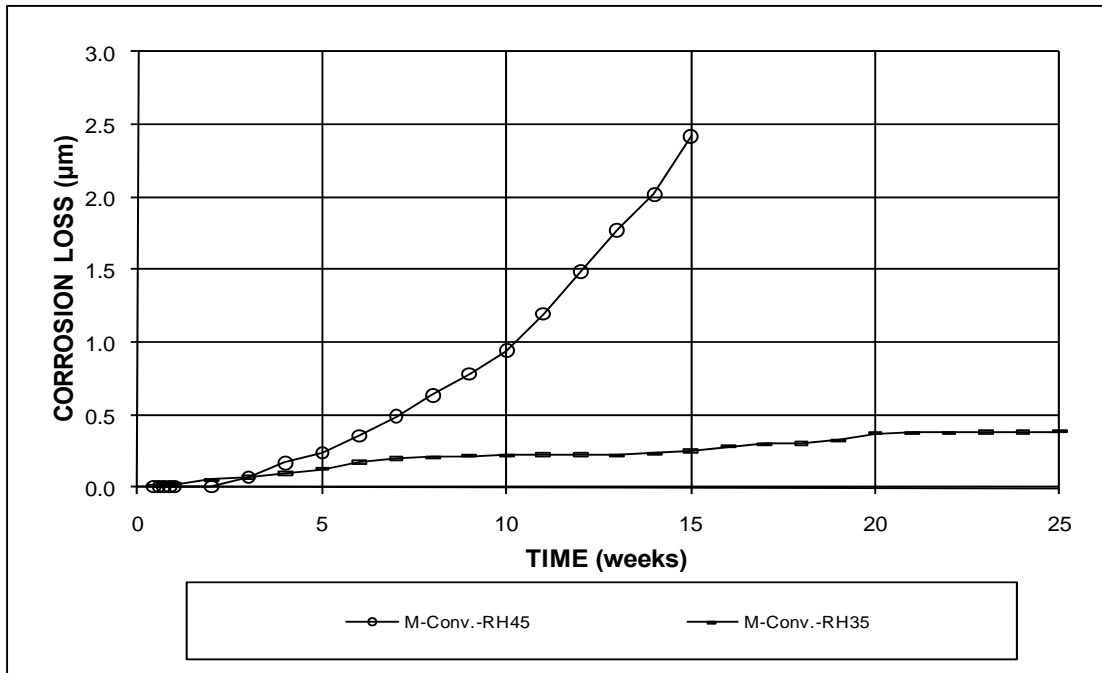


Figure 3.11b – Macrocell Test. Average corrosion losses for specimens with conventional steel and different water-cement ratios, Rheocrete inhibitor.

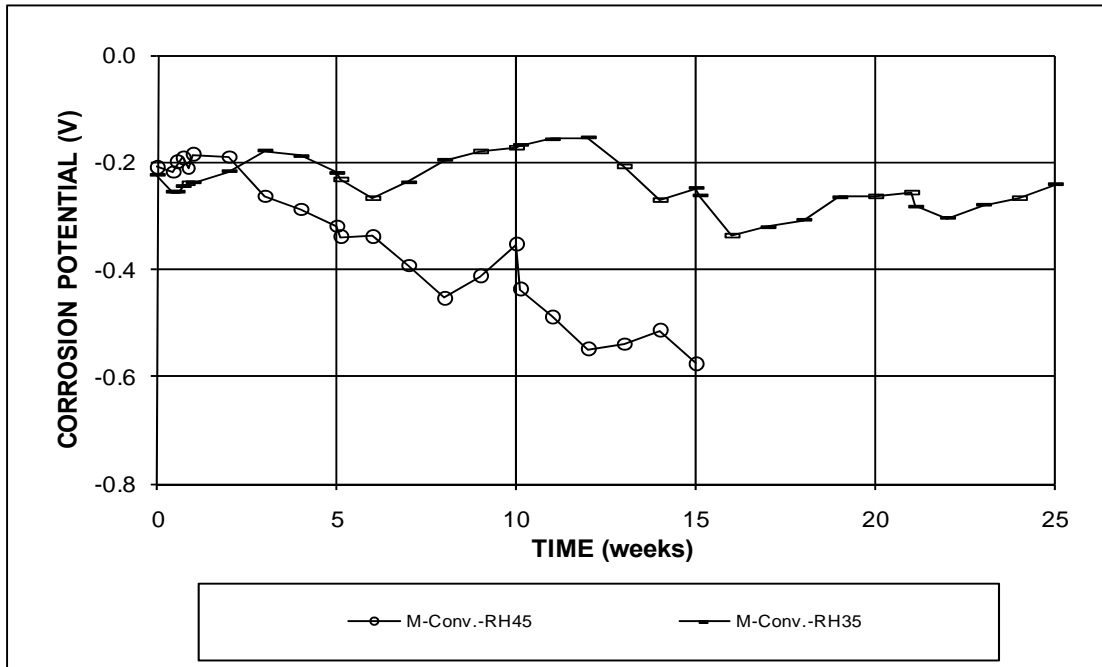


Figure 3.12a – Macrocell Test. Average anode corrosion potentials with respect to a saturated calomel electrode for specimens with conventional steel and different water-cement ratios, Rheocrete inhibitor.

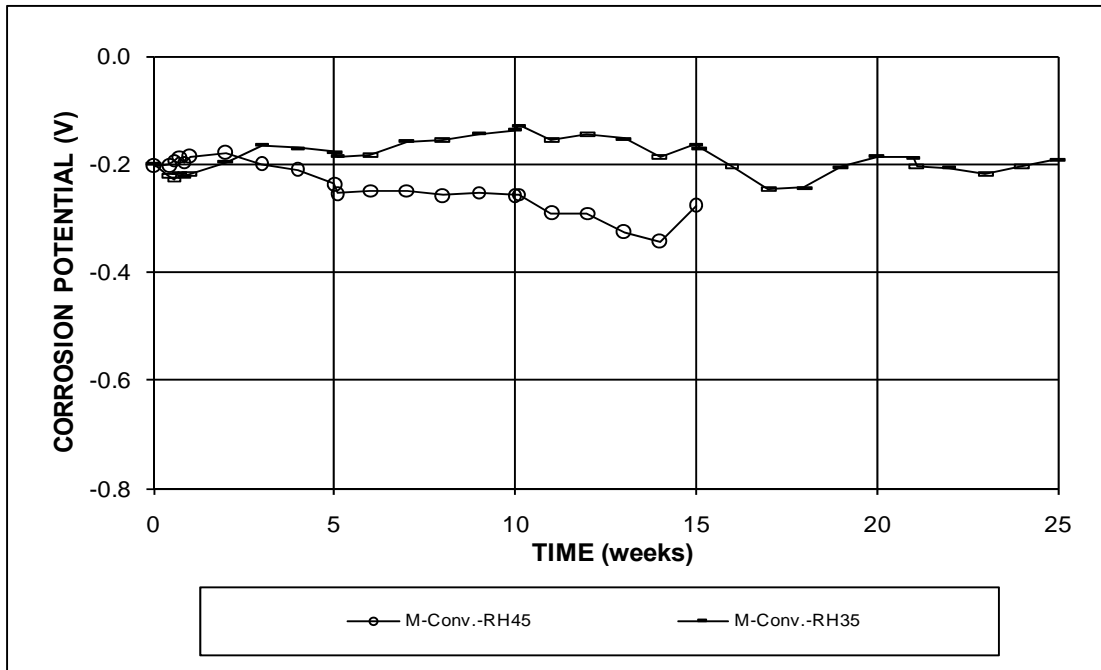


Figure 3.12b – Macrocell Test. Average cathode corrosion potentials with respect to a saturated calomel electrode for specimens with conventional steel and different water-cement ratios, Rheocrete inhibitor.

The specimens were inspected at the completion of the test. Many specimens had surface cracks in the mortar, including both anode and cathode specimens. Stains were found on some cracked anode specimens, as shown in Figure 3.13. Part of the mortar cover of the anode specimen M-Conv.-NO45-2 spalled off (Figure 3.14). No stains were observed on any of cathode specimens.

After visually inspecting the mortar for signs of corrosion stains, the mortar was removed and the conventional steel was visually inspected for corrosion products. Most anode specimens with a w/c of 0.45 exhibited severe corrosion with dark brown corrosion products on the bar surface (Figure 3.15), except one Hycrete bar showed minor light brown stains. For specimens with cracks through the mortar, the locations of corrosion products were not always directly underneath the cracks. Many anode specimens with a w/c of 0.35 had relatively small areas with corrosion products as compared to the areas noted for specimens with a w/c of 0.45 (Figure 3.16), while

others had corrosion areas comparable to those for specimens with a w/c of 0.45. No corrosion products were found on any of the cathode bars (Figure 3.17). The specimens with and without different inhibitors showed no difference on corrosion performance based on visual appearance in rapid macrocell test conducted in this study.



Figure 3.13 – Macrocell Test. Anode specimen (M-Conv.-NO45-1) with conventional steel showing stains on cracked mortar surface at week 15.



Figure 3.14 – Macrocell Test. Anode specimen (M-Conv.-NO45-2) with conventional steel showing spalled mortar cover at week 15.



Figure 3.15 – Macrocell Test. Conventional steel from anode specimen (M-Conv.-HY45-1) showing severe corrosion products at week 15.



Figure 3.16 – Macrocell Test. Conventional steel from anode specimen (M-Conv.-RH35-6) showing slightly corrosion products at week 25.



Figure 3.17 – Macrocell Test. Conventional steel from cathode specimen (M-Conv.-DCI45-3) showing no corrosion products at week 15.

In summary, for the macrocell tests, the water-cement ratio had a larger influence than the corrosion inhibitors on the corrosion behavior of the different corrosion protection systems. The lower water-cement ratio provided better corrosion protection. For the same water-cement ratio, all of the specimens with corrosion inhibitors performed in a similar manner. This is mainly because conventional steel has a high tendency to corrode under the severe exposure conditions provided by the

mortar-wrapped macrocell test and the small mortar cover thickness (7 mm or 0.288 in.), which allows the chloride ions easy access to the steel surface.

For the lower water-cement ratio (0.35), all inhibitor specimens had similar corrosion losses before week 15. After that, the corrosion losses for the Hycrete specimens increased gradually, exceeding those of DCI and Rheocrete specimens at week 25. The specimens with Rheocrete had the lowest average corrosion loss between weeks 15 and 25. As described in Section 1.6.4, different inhibitors provide protection to steel in different ways. DCI provides protection by reacting with iron to form a stable passive layer on the steel surface. Rheocrete reacts by forming a protective film on the steel surface and by reducing the concrete permeability, and Hycrete provides protection to steel by reducing the concrete permeability.

3.2 BENCH-SCALE TESTS

Three bench-scale tests, the Southern Exposure (SE), cracked beam (CB), and ASTM G109 tests were used in this study. Corrosion rate, total corrosion loss, corrosion potentials of both anode and cathode with respect to CSE, and mat-to-mat resistance are reported for the tests. Six SE specimens each for conventional steel and ECR served as controls. To test inhibitor effectiveness in protecting conventional steel, three SE and three CB specimens were used for each inhibitor (DCI-S, Hycrete, and Rheocrete 222+) along with three specimens without an inhibitor. The results for these SE and CB tests are reported as of week 42. Three types of reinforcement (conventional, ECR, and MC steel) were evaluated using the ASTM G109 test, with the results are reported as of week 209. Because the tests are still ongoing, the ages used for comparison are based on the shortest duration of any bench-scale test used in

the comparisons. Figures for some comparisons include the test results as they appeared on the cutoff date, May 31, 2008.

The average values for each variable are presented in Tables 3.3 through 3.5 and Figures 3.18a through 3.37b. The test results of individual specimens are presented in Figures A.17 to A.37 (corrosion rate, total loss and potentials) and Figures B.1 to B.20 (mat-to-mat resistance). The test designations used in tables and figures in this section are:

SE = Southern Exposure

CB = Cracked Beam

G = ASTM G109

NO = no inhibitor

DCI = DCI-S

HY = Hycrete

RH= Rheocrete 222+

Conv. = conventional steel

N5 = conventional steel from different heat

ECR = conventional epoxy-coated reinforcement

MC = multiple-coated reinforcement

4 (4h), 10 (10h) = Epoxy-coated or multiple-coated reinforcing steel with four or ten 3-mm ($\frac{1}{8}$ -in.) diameter holes through the coating. ECR bars have four holes through the coating unless otherwise indicated.

Unless otherwise indicated, corrosion rates and losses are based on the total surface area of the top mat of steel. Corrosion rates and losses based on the area exposed at the holes through the coating are marked with an asterisk (*) on the specimen designation in the tables and figures of this Section.

3.2.1 Conventional Steel and Epoxy-Coated Reinforcement

The average test results are shown in Figures 3.18 through 3.23, and the total corrosion losses are summarized in Table 3.3. The individual results for conventional steel and ECR are presented in Figures A.17 through A.20 and B.1 and B.2.

Figures 3.18 and 3.19 show the average corrosion rates for conventional steel and ECR based on total and exposed area, respectively. Conventional steel had much higher corrosion rates than ECR. During the first 42 weeks, the highest corrosion rate for conventional steel was $4.58 \mu\text{m/yr}$ at week 37, while the highest rate for ECR was $0.15 \mu\text{m/yr}$ at week 37 based on total area. The average corrosion rate for conventional steel remained approximately zero until week 20 (when it reached a value of $0.35 \mu\text{m/yr}$), and at that time began to gradually increase until it stabilized at approximately $4.00 \mu\text{m/yr}$ between weeks 36 and 47, increasing again to $5.50 \mu\text{m/yr}$ between weeks 50 and 67. The average corrosion rate of ECR showed slightly negative values from week 9 to 30 (except week 23), with the lowest values of -0.02 and $-8.24 \mu\text{m/yr}$ based on total and exposed area, respectively. As shown in Figure A.17a, four out of six specimens with ECR exhibited negative corrosion rates (Specimens No. 2, 3, 4 and 6) with the corresponding negative corrosion losses shown in Figure A.17b. Because the corrosion potentials of the top mats were very close to those of the bottom mats, specimens with ECR exhibited a very low corrosion rate (less than $0.3 \mu\text{m/yr}$ based on total area, as described in Section 2.7.1). The average corrosion rate for ECR specimens peaked at week 37 due to the active corrosion of specimen SE-ECR-1 during weeks 32 to 48.

The average corrosion losses for conventional steel and ECR are plotted in Figures 3.20 and 3.21. Conventional steel had much higher corrosion losses than ECR.

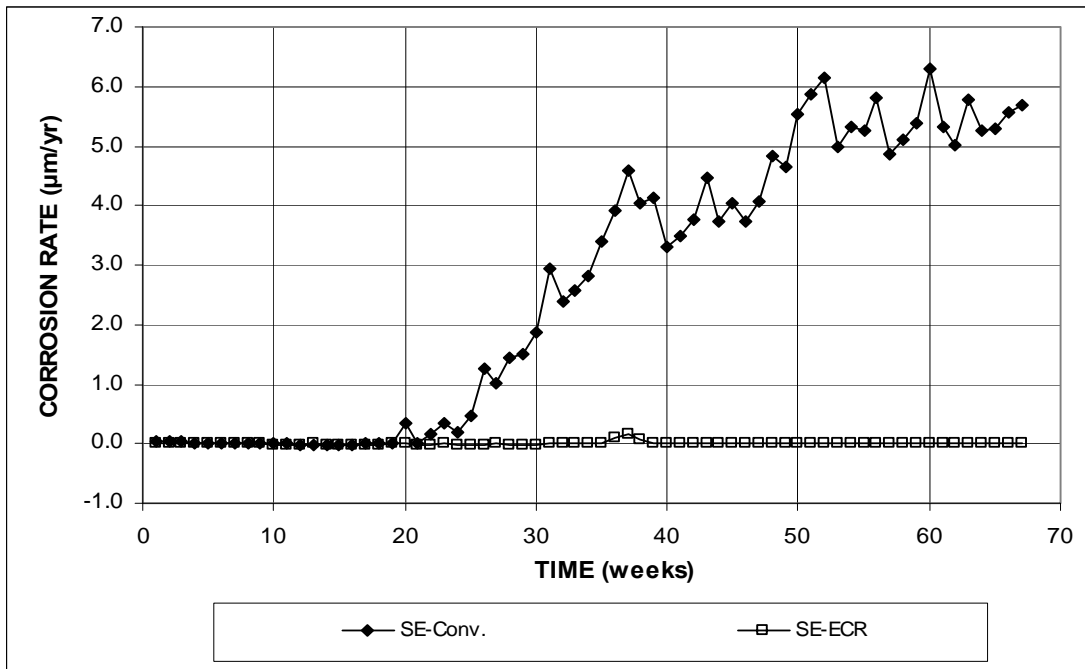


Figure 3.18a – Southern Exposure Test. Average corrosion rates for specimens with conventional steel and ECR (ECR with four holes through the epoxy).

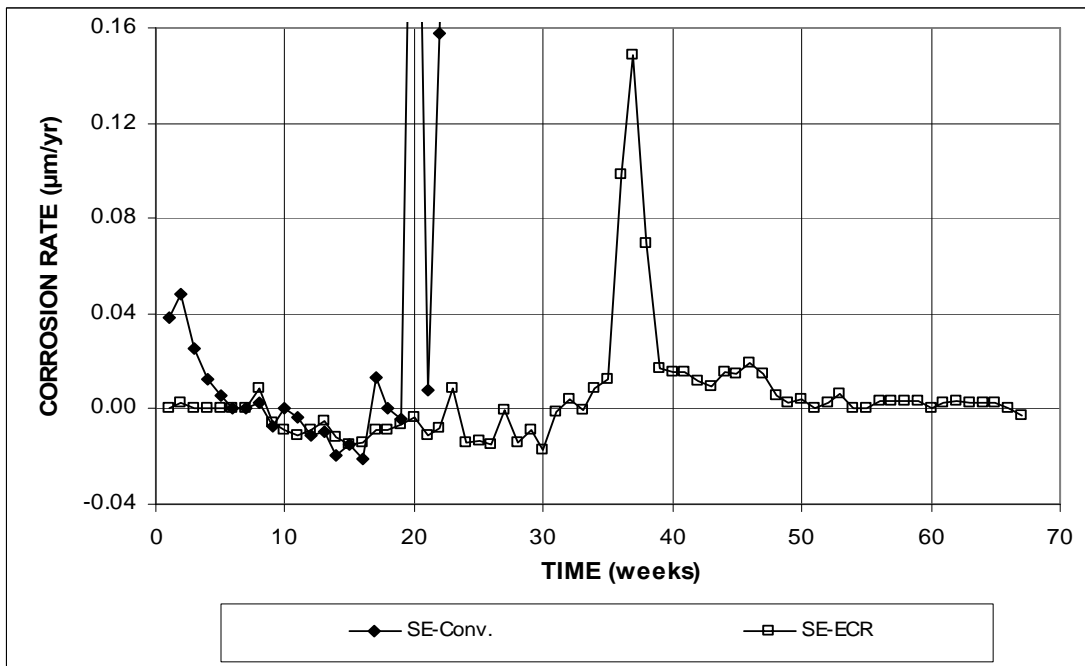


Figure 3.18b – Southern Exposure Test. Average corrosion rates for specimens with conventional steel and ECR (ECR with four holes through the epoxy). (Different scale)

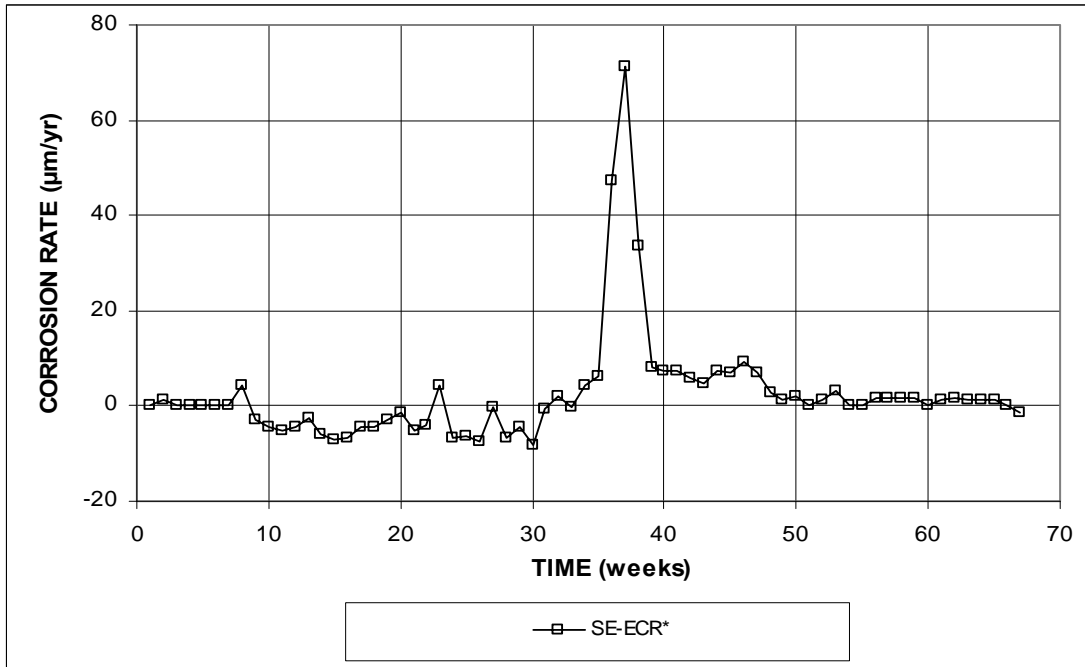


Figure 3.19 – Southern Exposure Test. Average corrosion rates for specimens with ECR. * Based on exposed area (ECR with four holes through the epoxy).

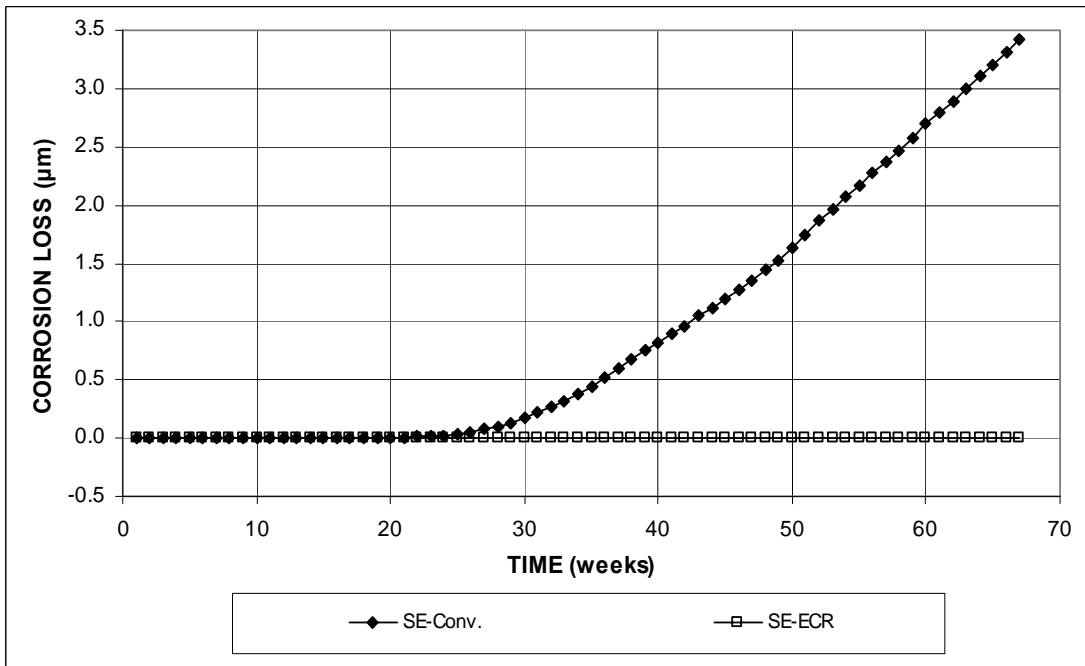


Figure 3.20a – Southern Exposure Test. Average corrosion losses for specimens with conventional steel and ECR (ECR with four holes through the epoxy).

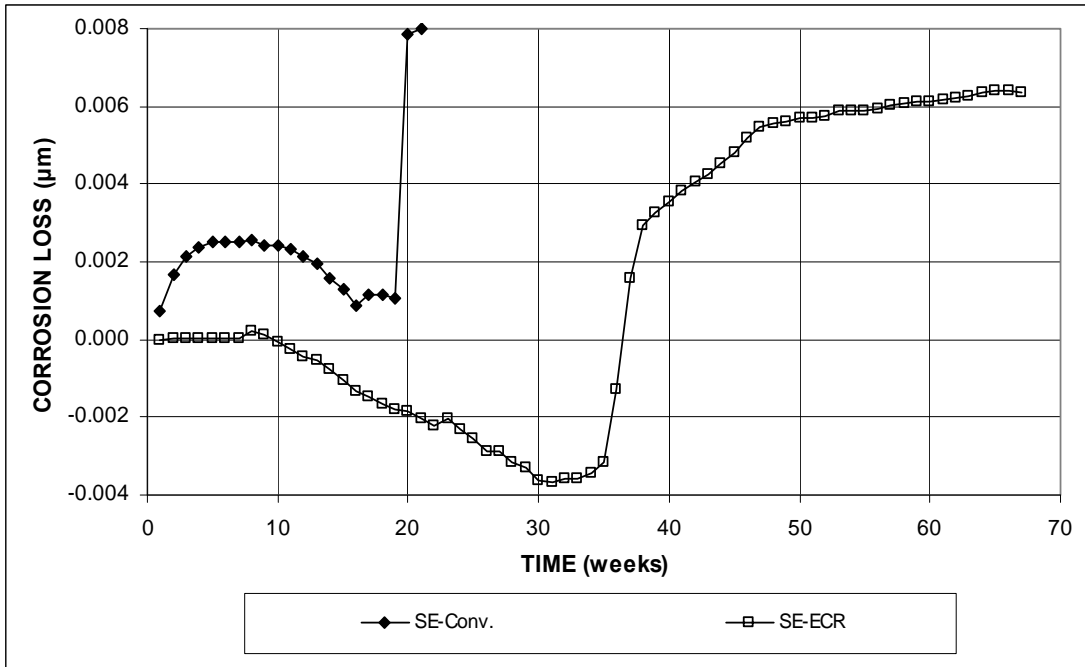


Figure 3.20b – Southern Exposure Test. Average corrosion losses for specimens with conventional steel and ECR (ECR with four holes through the epoxy). (Different scale)

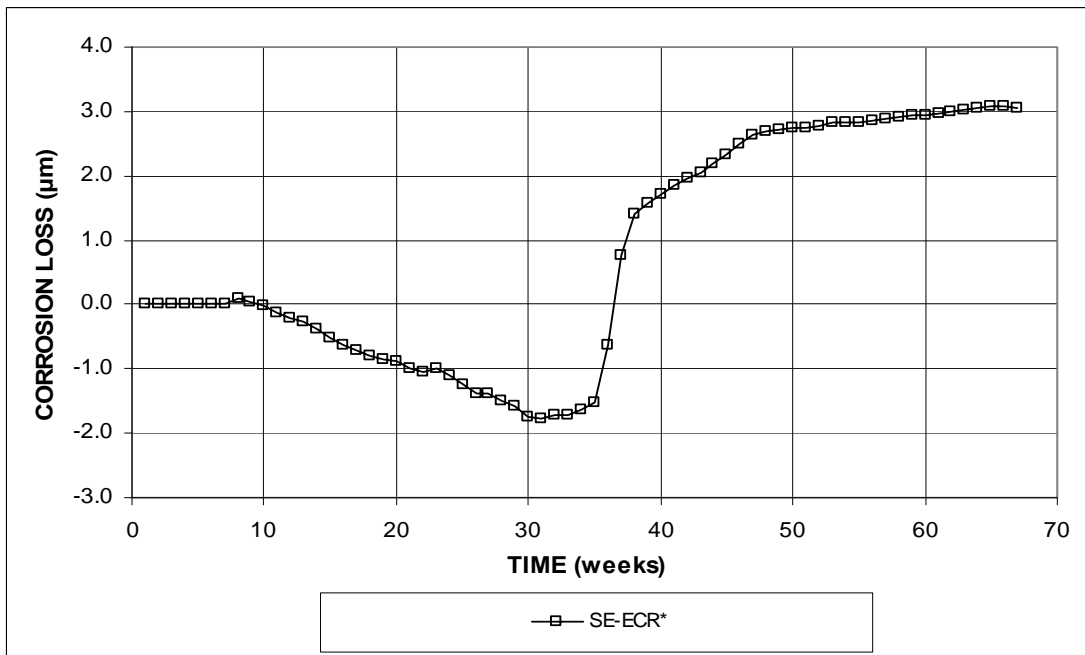


Figure 3.21 – Southern Exposure Test. Average corrosion losses for specimens with ECR. * Based on exposed area (ECR with four holes through the epoxy).

The losses for conventional steel increased steadily from approximately zero losses (0.001 μm) at week 19 to a value of 0.96 μm at week 42 and 3.42 μm by week 67. ECR changed from the most negative values of -0.004 and -1.72 μm between weeks 30 and 33 to the positive values of 0.004 and 1.95 μm at week 42, and reached to 0.006 and 3.04 μm by week 67, based on total and exposed area, respectively. Here, the negative corrosion losses are not really “negative corrosion.” The term is used to describe the case in which oxidation is greater on the bottom mat than on the top mat. As shown in Figure A.19b, the increase in the average corrosion loss was due to the corrosion activity of ECR specimen No. 1 between weeks 32 and 48. As shown in Table 3.3, at week 42, the average corrosion loss of the conventional steel specimen was 0.96 μm , while the corrosion loss of ECR specimen was less than 0.005 and 1.95 μm , based on total and exposed area, respectively. As described earlier, the average behavior of the ECR specimens was dominated by one specimen. ECR No. 1 specimen had a corrosion loss of 0.05 and 22.28 μm at week 42, compared to the other ECR specimens that had corrosion losses of less than 0.001 and 0.67 μm based on total and exposed area, respectively. The total corrosion losses for the ECR bars based on exposed area were similar to the total losses of the conventional steel bars. The scatter in the test results for ECR is higher than for conventional steel. This is because epoxy coating provides high corrosion resistance to the underlying steel and access of chlorides, oxygen, and moisture to the surface of the steel is limited to the holes in the coating.

Figure 3.22 shows the average corrosion potentials of the top and bottom mats of steel with respect to a copper-copper sulfate electrode. Conventional steel had more negative corrosion potentials than ECR for both the top and bottom mats. The top mat corrosion potential for conventional steel became more negative than -0.350 V

Table 3.3 – Corrosion losses at 42 weeks for control and inhibitor specimens in the Southern Exposure test based on total and exposed area

Steel Designation ^a	Specimen Corrosion Losses (µm)						Average	Standard Deviation
	1	2	3	4	5	6		
Based on Total Area								
Control								
Conv.	1.27	0.73	1.24	0.10	1.24	1.20	0.96	0.47
ECR	0.05	-0.01	-0.01	0.00	0.00	0.00	0.00	0.02
Corrosion Inhibitors								
N5	2.02	2.36	6.42				3.60	2.45
N5-DCI	1.37	2.23	1.86				1.82	0.43
N5-HY	0.02	0.45	0.68				0.38	0.34
N5-RH	0.42	0.01	1.34				0.59	0.68
Based on Exposed Area								
ECR*	22.28	-4.65	-4.08	-0.84	0.67	-1.65	1.95	10.15

^a Conv. = conventional steel.

ECR = conventional epoxy-coated reinforcement, with four 3-mm (1/8 in.) diameter holes through the coating.

N5 = conventional steel, different heat. DCI = concrete mixed with DCI inhibitor.

HY = concrete mixed with Hycrete inhibitor. RH = concrete mixed with Rhecrete inhibitor.

* Corrosion loss based on exposed area.

β Corrosion loss (absolute value) less than 0.005 µm

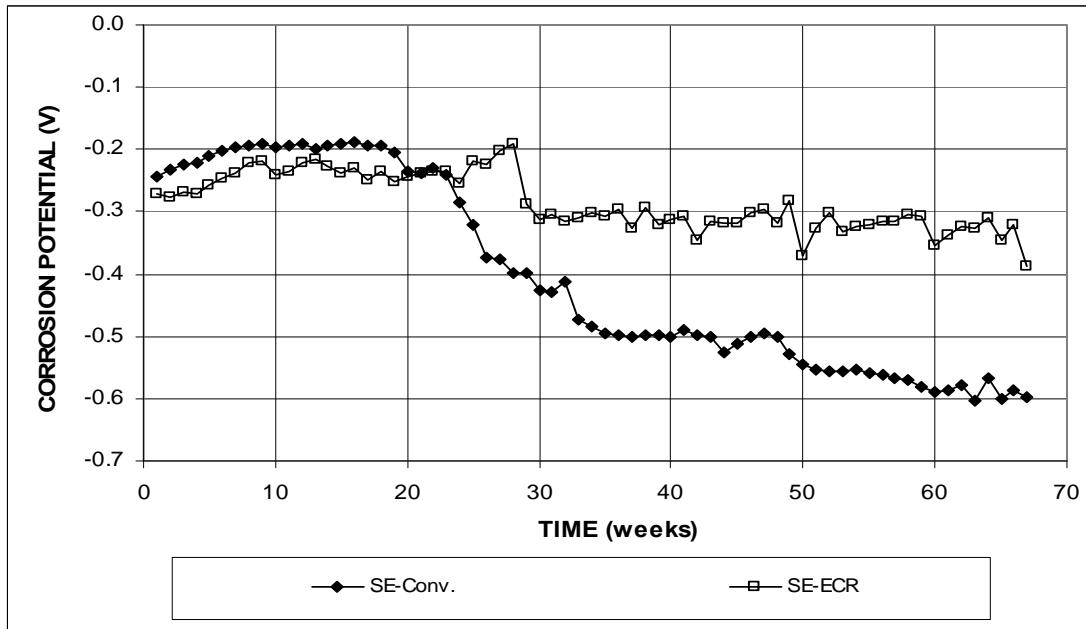


Figure 3.22a – Southern Exposure Test. Average top mat corrosion potentials with respect to a copper-copper sulfate electrode for specimens with conventional steel and ECR (ECR with four holes through the epoxy).

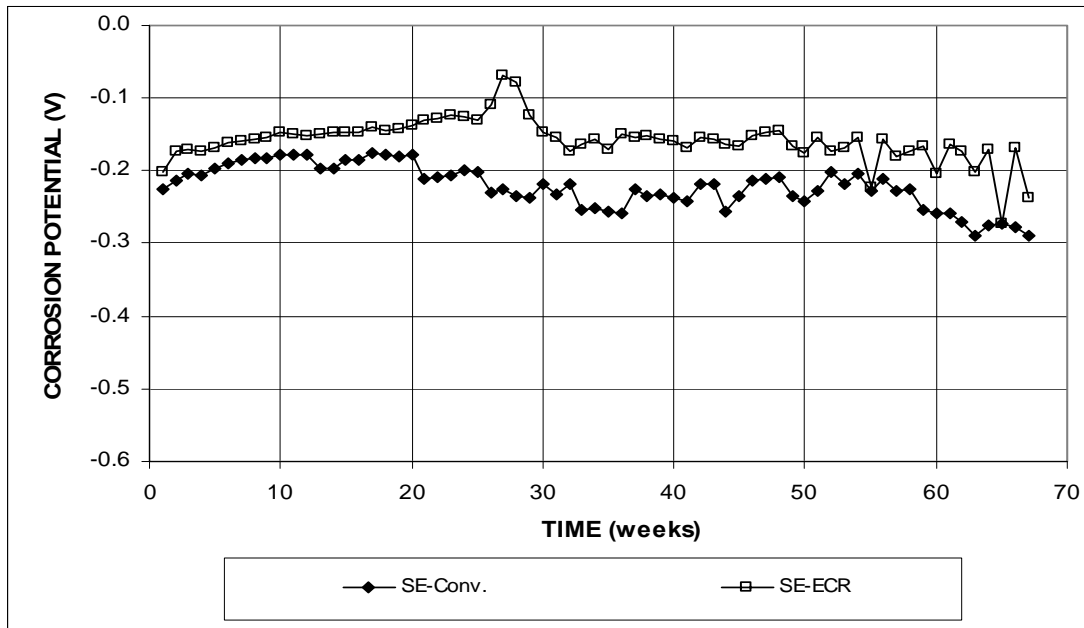


Figure 3.22b – Southern Exposure Test. Average bottom mat corrosion potentials with respect to a copper-copper sulfate electrode for specimens with conventional steel and ECR (ECR with four holes through the epoxy).

at week 26 with a value of -0.373 V, indicating a high possibility of active corrosion according to ASTM C876. The ECR specimens had average corrosion potentials for the top mat that were more positive than -0.350 V, except at weeks 50, 60, and 67. The bottom mat corrosion potentials for both conventional and ECR steel ranged from -0.100 V to -0.300 V, except for ECR at weeks 27 and 28. For both types of specimens, the corrosion potentials on the top mat of steel were more negative than the bottom mat potentials.

As shown in Figure 3.23, the average mat-to-mat resistance increased with time for specimens with both types of steel. Specimens with conventional steel had average mat-to-mat resistances below 400 ohms, while that of ECR increased from around 2,100 to 11,000 ohms, with a spike to 13,249 ohms at week 36 caused by specimens No. 1 and 4 (see Figure B.2). The high resistance of the ECR bars is caused

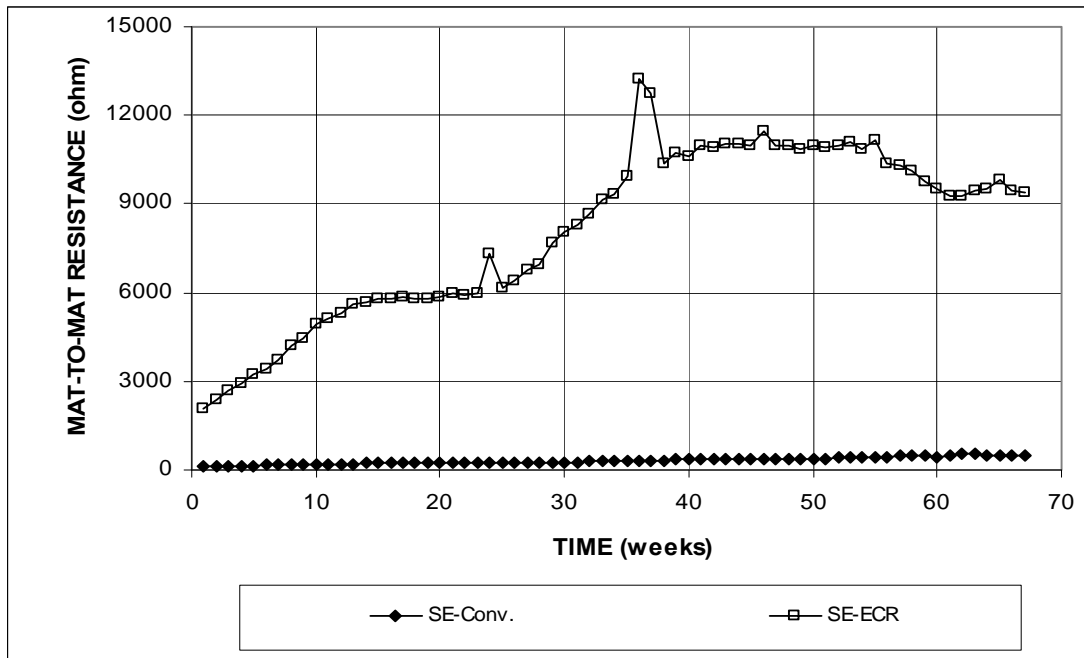


Figure 3.23 – Southern Exposure Test. Average mat-to-mat resistances for specimens with conventional steel and ECR (ECR with four holes through the epoxy).

by the high electrical resistance of the epoxy, which electrically insulates the steel from the surrounding environment and minimizes the corrosion current.

In summary, ECR had significantly improved corrosion resistance compared with conventional steel. The total corrosion losses for ECR bars based on exposed area were similar to the total losses on the uncoated bars.

3.2.2 Conventional Steel with Corrosion Inhibitors

The average test results for conventional steel cast in concrete containing different inhibitors are shown in Figures 3.24 through 3.31, and the total corrosion losses are shown in Tables 3.3 and 3.4. The individual results are presented in Appendixes A and B.

3.2.2.1 Southern Exposure Test

The average test results for the Southern Exposure specimens are shown in Figures 3.24 through 3.27, and the total corrosion losses are summarized in Table 3.3.

As shown in Figure 3.24, specimens without inhibitors had the highest average corrosion rates over the entire period starting from week 15 (except for week 34), followed by specimens with DCI (calcium nitrite). The average corrosion rate for specimens without inhibitors increased steadily from 0.20 $\mu\text{m}/\text{yr}$ at week 15 to 8.95 $\mu\text{m}/\text{yr}$ at week 27. After that, the corrosion rate stabilized at about 9.00 $\mu\text{m}/\text{yr}$ through week 45. The DCI specimens exhibited gradually increasing average corrosion rates between weeks 21 and 25, which then jumped sharply at week 33 to a value of 8.12 $\mu\text{m}/\text{yr}$, a value that was similar to the average corrosion rates of specimens without inhibitors between weeks 33 and 37. After that, the average corrosion rate of the DCI specimens decreased gradually. The specimens with increased corrosion rates also exhibited large drops in their corrosion potential at the anode, as shown in Figure 3.26a. The corrosion rate of Rheocrete specimens increased slightly from 1.04 $\mu\text{m}/\text{yr}$ after corrosion initiation at week 27 to 2.24 $\mu\text{m}/\text{yr}$ at week 45. The Hycrete inhibitor specimens had the lowest corrosion rates after week 30 with values around 1 $\mu\text{m}/\text{yr}$ compared to the other specimens.

As shown in Figure 3.25, the average corrosion losses for all inhibitor specimens increased progressively over time. Specimens without inhibitors had the highest average corrosion losses, followed by DCI specimens. The Hycrete specimens had the lowest average corrosion losses. As shown in Table 3.3, at week 42, the average corrosion loss of specimens without inhibitors was 3.60 μm , which was twice the average corrosion loss of the DCI specimens (1.82 μm), and 5 to 7.5 times the losses for the Rheocrete and Hycrete specimens (0.59 and 0.38 μm), respectively.

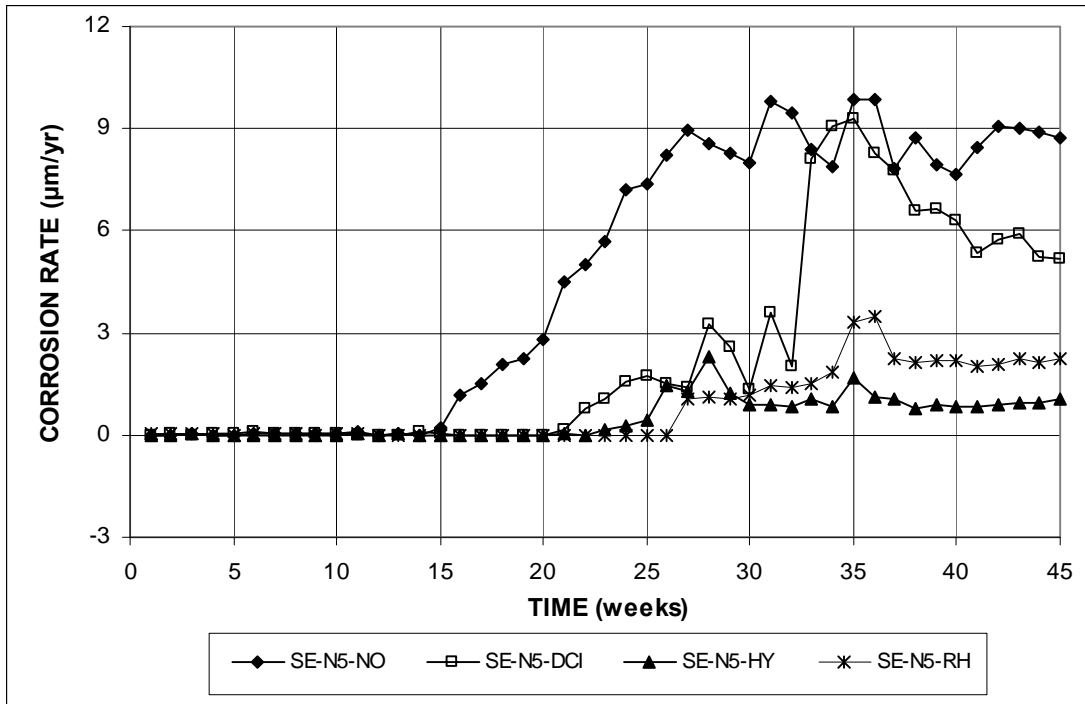


Figure 3.24 – Southern Exposure Test. Average corrosion rates for specimens with conventional steel and different inhibitors.

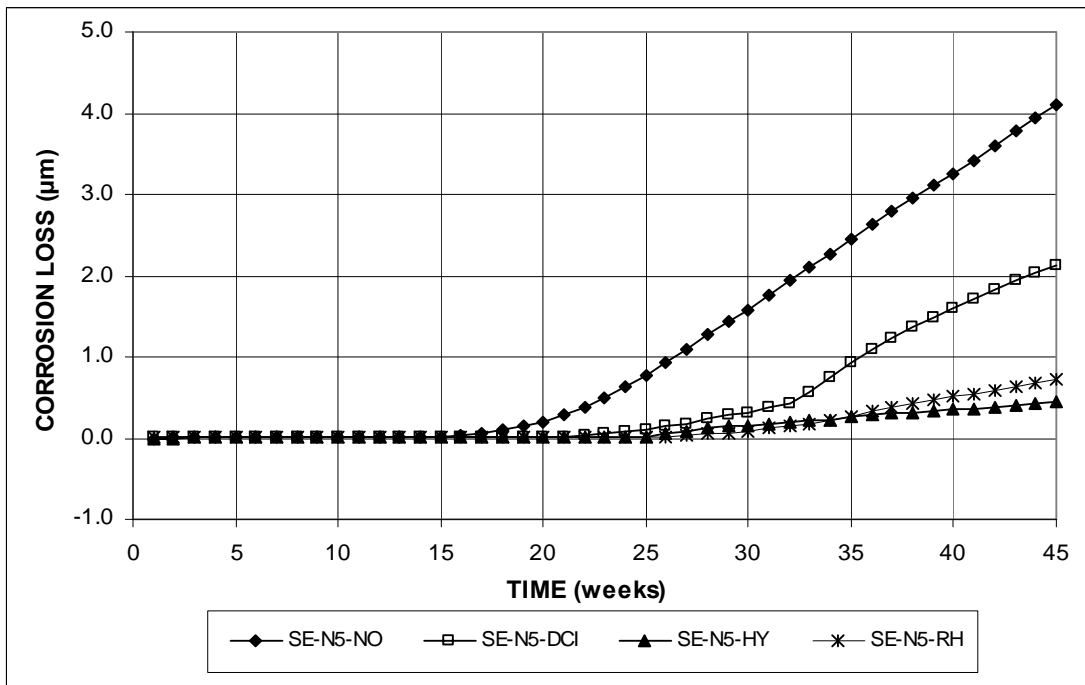


Figure 3.25 – Southern Exposure Test. Average corrosion losses for specimens with conventional steel and different inhibitors.

Specimen No. 3 without inhibitors had the highest corrosion loss, 6.42 μm ; while Hycrete No. 1 and Rheocrete No. 2 had very low corrosion losses, 0.02 and 0.01 μm , respectively. From the individual results presented in Figures A.29 and A.30 for Hycrete specimens and Figures A.33 and A.34 for Rheocrete specimens, the corrosion rates of specimens Hycrete No. 1 and Rheocrete No. 2 were approximately zero and the corrosion potentials of the top mat of the steel were more positive than -0.200 V through week 44, indicating a high probability of no corrosion activity for these two specimens.

The average corrosion potentials with respect to a CSE are presented in Figure 3.26. Rheocrete and Hycrete specimens had top bar corrosion potentials less negative than -0.350 V throughout the test, with the exception of the Hycrete specimens at week 34. The DCI specimens and specimens without inhibitors had top bar corrosion potentials more negative than -0.350 V after week 24, indicating a high probability of corrosion activity. The average corrosion potentials of the bottom mat bars for all of the specimens were similar in value, with values more positive than -0.230 V , except for Hycrete at week 34, with a value of -0.313 V . As shown in Figure A.32, the shift to more negative values of corrosion potential for top and bottom mat bars at week 34 for the Hycrete specimens was mainly influenced by the negative shift of a single specimen, No. 3.

As shown in Figure 3.27, the average mat-to-mat resistances increased from a range of 60 to 118 ohms at the beginning of the test to a range of 283 to 473 ohms at week 45, with the Hycrete specimens exhibiting the highest resistance throughout the test period. The increases occurred at a similar rate for all the specimens and were due to the formation of corrosion products on the steel surface and continued hydration within the concrete.

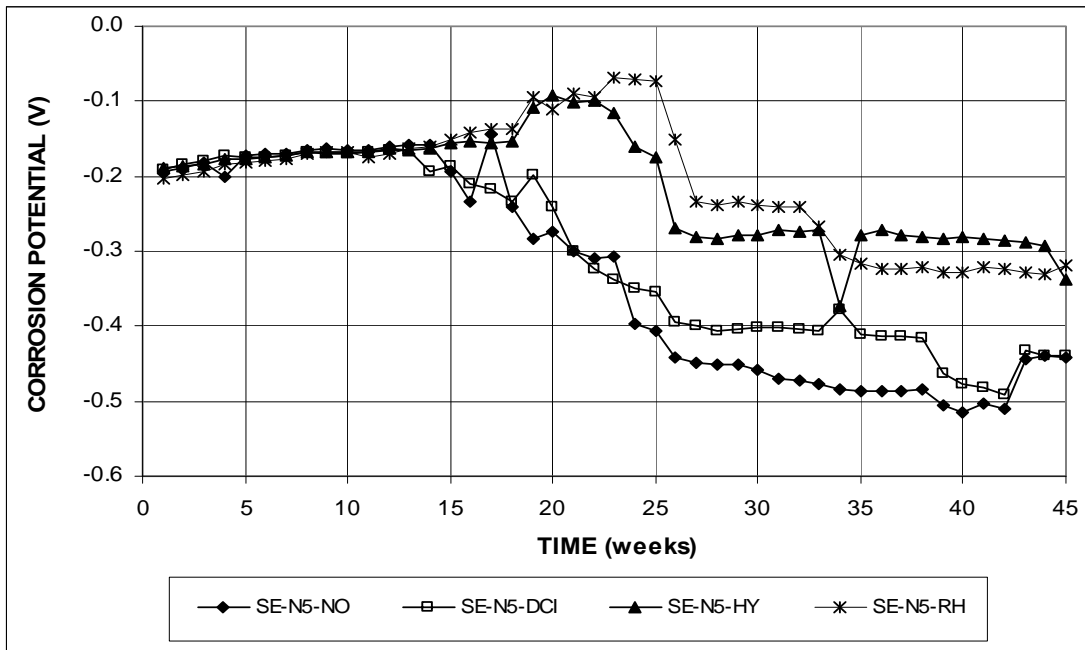


Figure 3.26a – Southern Exposure Test. Average top mat corrosion potentials with respect to a copper-copper sulfate electrode for specimens with conventional steel and different inhibitors.

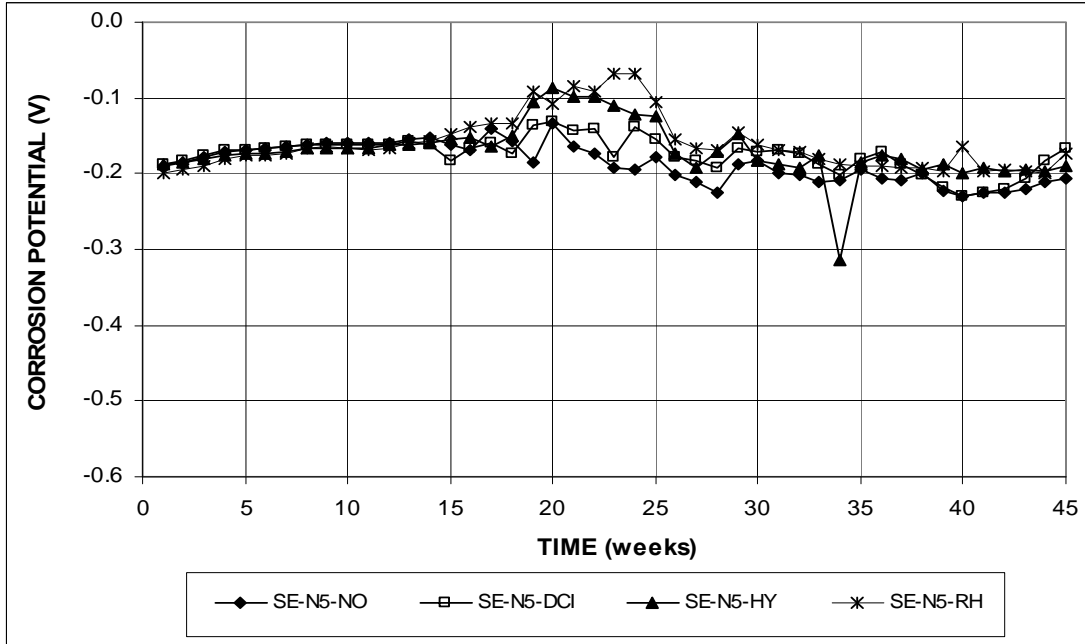


Figure 3.26b – Southern Exposure Test. Average bottom mat corrosion potentials with respect to a copper-copper sulfate electrode for specimens with conventional steel and different inhibitors.

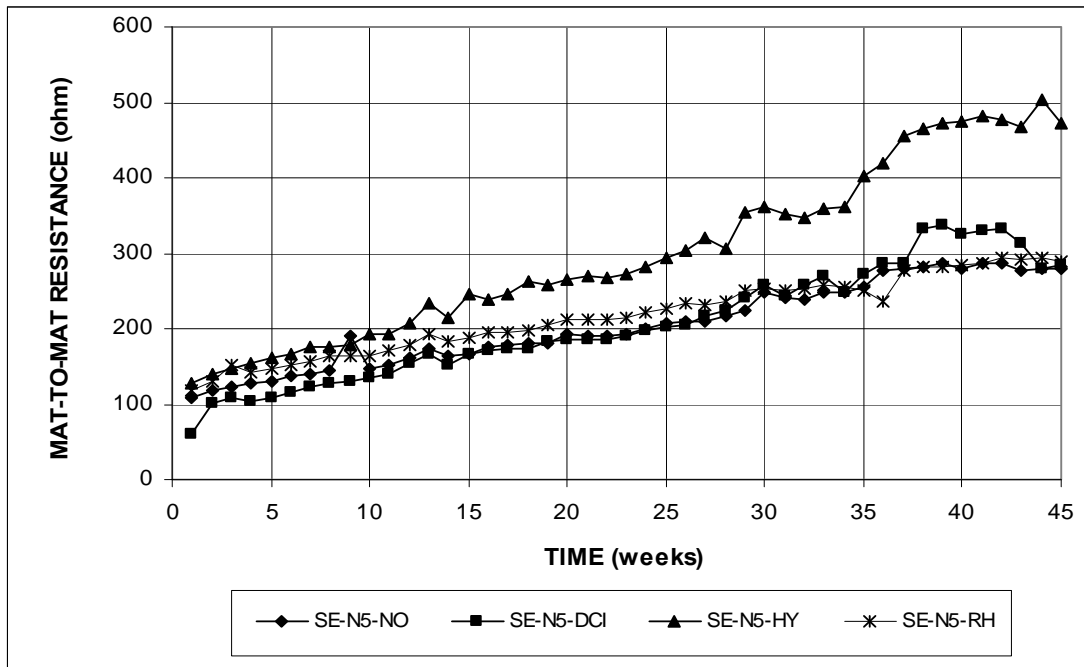


Figure 3.27 – Southern Exposure Test. Average mat-to-mat resistances for specimens with conventional steel and different inhibitors.

3.2.2.2 Cracked Beam Test

The average test results for the cracked beam test for conventional steel and corrosion inhibitors are presented in Figures 3.28 through 3.31. The total corrosion losses are summarized in Table 3.4.

As shown in Figure 3.28, specimens without inhibitors had the highest average corrosion rates at all times, followed by the DCI and Rheocrete specimens. The Hycrete specimens had the lowest average corrosion rates. The plots of average corrosion rate show similar trends for all of the specimens, first increasing to a peak value and then decreasing gradually. The decrease is caused by deposits of corrosion products on the surface of the top bar that limit access of moisture, oxygen, and chlorides, along with the continued hydration of the concrete, which limits access of moisture and oxygen to the bottom bars. The highest corrosion rate for the specimens

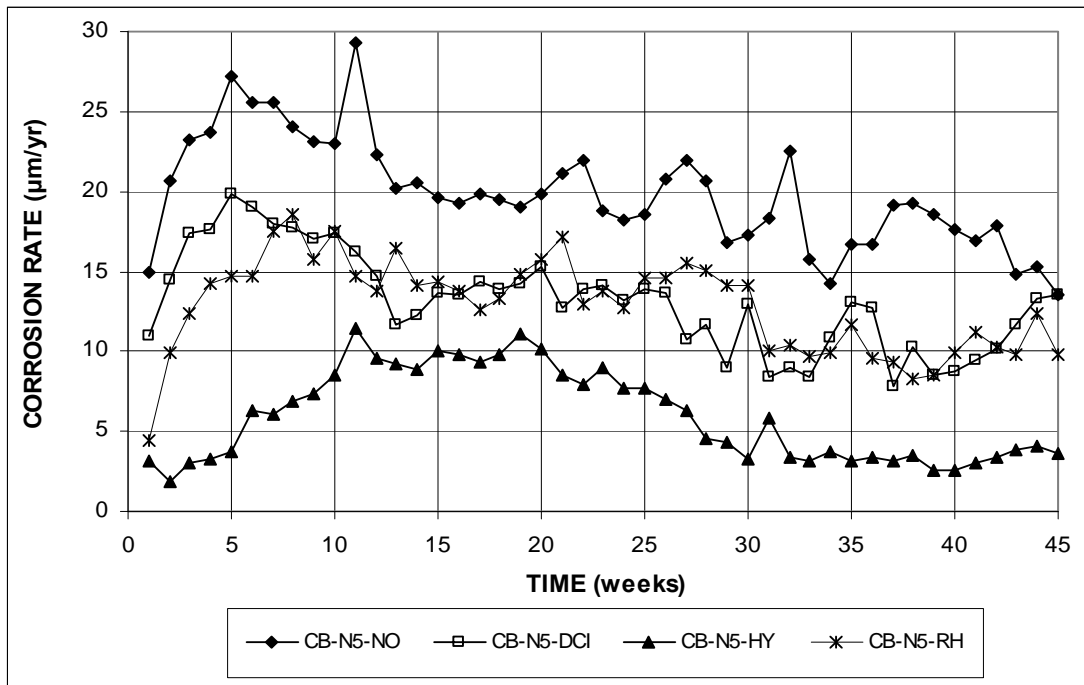


Figure 3.28 – Cracked Beam Test. Average corrosion rates for specimens with conventional steel and different inhibitors.

without inhibitors was $29.27 \mu\text{m/yr}$ at week 11, which was primarily caused by a jump in corrosion rate for specimen No. 1 at week 11. After reaching $27.17 \mu\text{m/yr}$ at week 5, the average corrosion rates of the specimens without inhibitors gradually decreased (with the exception of week 11) to a value of $17.85 \mu\text{m/yr}$ at week 42 and $13.50 \mu\text{m/yr}$ at week 45. The DCI and Rheocrete specimens reached their highest average corrosion rates of around $19 \mu\text{m/yr}$ at weeks 5 and 8; the rate then gradually decreased to around $10 \mu\text{m/yr}$ at week 42 and became 13.50 and $9.81 \mu\text{m/yr}$ at week 45, respectively, for the DCI and Rheocrete specimens. The Hycrete specimens had a relatively stable corrosion rate of approximately $10 \mu\text{m/yr}$ between weeks 11 and 20, which decreased to approximately $3 \mu\text{m/yr}$ after week 33.

The average corrosion losses are presented in Figure 3.29 and summarized in Table 3.4. The corrosion losses for all specimens increased progressively, with the

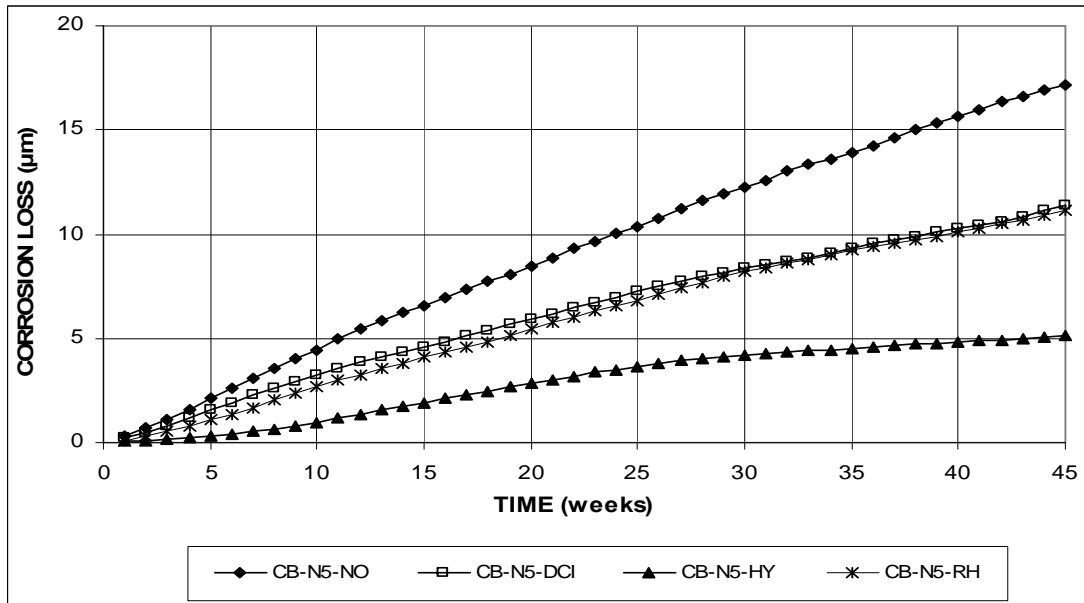


Figure 3.29 – Cracked Beam Test. Average corrosion losses for specimens with conventional steel and different inhibitors.

Table 3.4 – Corrosion losses at 42 weeks for conventional steel with different inhibitors in the cracked beam test

Steel Designation ^a	Specimen Corrosion Losses (µm)			Average	Standard Deviation
	1	2	3		
Corrosion Inhibitors					
N5	23.25	14.20	11.60	16.35	6.12
N5-DCI	9.91	11.80	10.18	10.63	1.02
N5-HY	4.68	4.20	5.92	4.93	0.89
N5-RH	12.48	9.19	9.86	10.51	1.74

^a N5 = conventional steel, 5th batch. DCI = concrete mixed with DCI inhibitor.

HY = concrete mixed with Hycrete inhibitor. RH = concrete mixed with Rheocrete inhibitor.

specimens without inhibitors exhibiting the highest average corrosion losses, followed by the DCI and Rheocrete specimens with nearly equal losses through week 45. The Hycrete specimens had the lowest average corrosion losses. As shown in Table 3.4, at week 42, the average corrosion loss for the specimens without inhibitors was 16.35 µm, which is 50% higher than the value for the DCI and Rheocrete specimens (10.63 and 10.51 µm, respectively), and more than three times higher than

that of the Hycrete specimens (4.93 μm). Specimen No. 1 without inhibitors had the highest corrosion loss of 23.25 μm , while the Hycrete specimens had the lowest corrosion losses, varying from 4.20 to 5.92 μm .

The average corrosion potentials of the top and bottom mats of steel with respect to a CSE are plotted in Figure 3.30. All specimens had top mat corrosion potentials between -0.350 and -0.600 V, with the exception of the Rheocrete specimens at the first week and the Hycrete specimens before week 5. For most of the test period, the Hycrete specimens exhibited the most negative corrosion potentials for the top mat steel, followed by the DCI, Rheocrete, and specimens without inhibitors. The top mat corrosion potentials were relatively stable from the beginning for all of the specimens, while the majority of the bottom mat corrosion potentials fluctuated between -0.160 and -0.300 V with several spikes in the negative direction below -0.350 V, especially for the specimens with Rheocrete and without inhibitors. Specimens without inhibitors had average bottom mat corrosion potentials of -0.376 and -0.386 V at week 37 and 42, respectively, and the Rheocrete specimens had a value of -0.358 V at week 26, indicating a high probability of corrosion occurring on the bottom mats of steel. From the individual results presented in Figure A.24 for specimens without inhibitors and Figure A.36 for the Rheocrete specimens, the bottom mat corrosion potentials for specimens No. 2 and 3 without inhibitors and Rheocrete No. 2 had values more negative than -0.350 V for many weeks, indicating that the chloride had reached the bottom mat of steel when aided by the direct path provided by the intentional crack.

Figure 3.31 shows the mat-to-mat resistances for the cracked beam specimens. The average mat-to-mat resistances increased with time, with a similar trend for all of

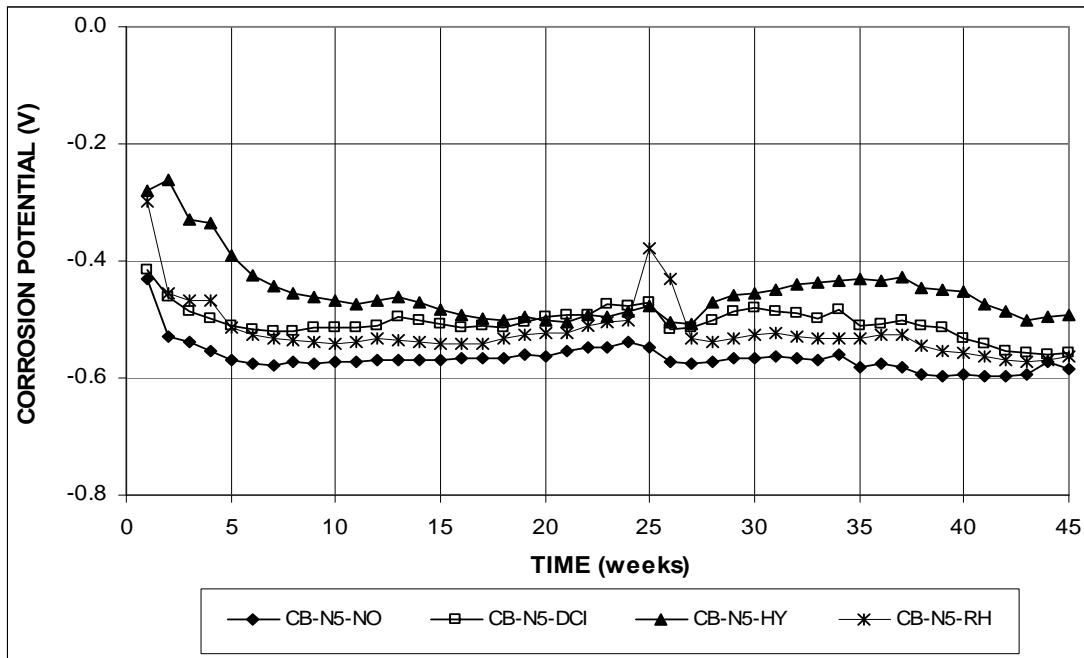


Figure 3.30a – Cracked Beam Test. Average top mat corrosion potentials with respect to a copper-copper sulfate electrode for specimens with conventional steel and different inhibitors.

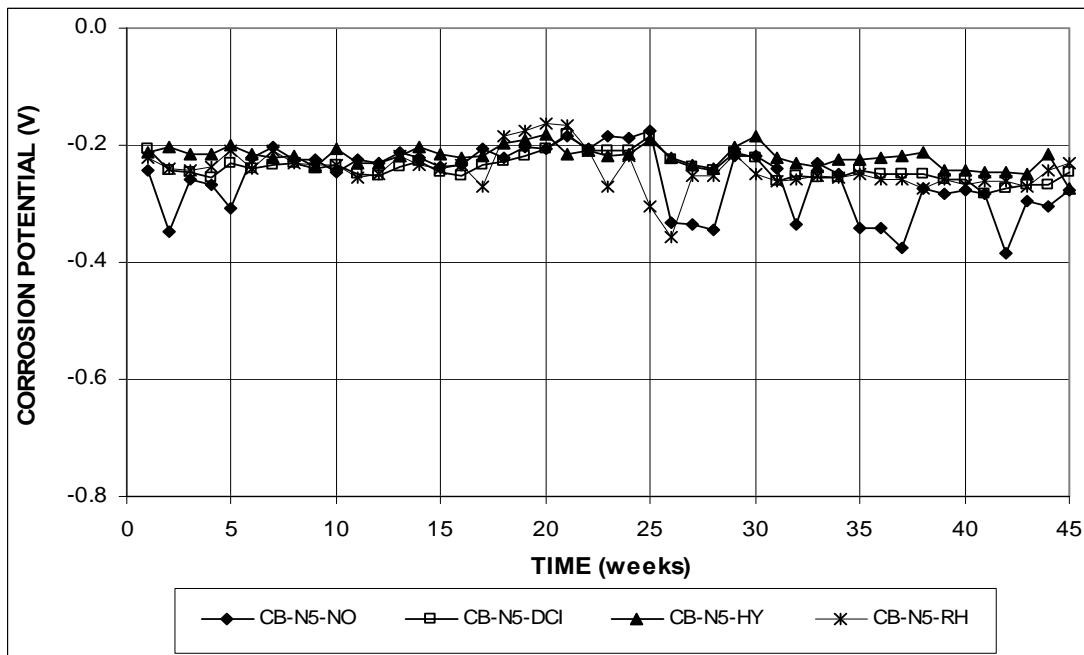


Figure 3.30b – Cracked Beam Test. Average bottom mat corrosion potentials with respect to a copper-copper sulfate electrode for specimens with conventional steel and different inhibitors.

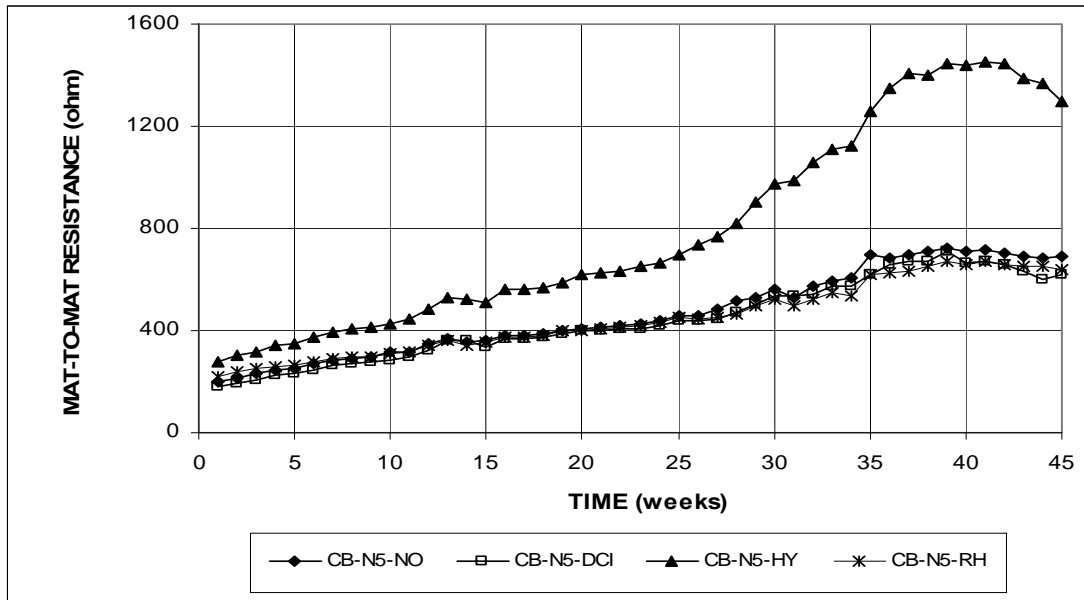


Figure 3.31 – Cracked Beam Test. Average mat-to-mat resistances for specimens with conventional steel and different inhibitors.

the specimens up to week 39, and then slowly decreased after week 41, which was primarily caused by corrosion products accumulating first on the steel surface to form a protective film and then breaking down later on in the aggressive environment. Specimens containing Hycrete had much higher resistances than the other specimens, ranging from 276 ohms at the beginning of the test to 1,446 ohms at week 42 and 1,297 ohms at week 45, while the other specimens had resistances ranging from 198 to 220 ohms at the beginning of the test to 670 to 719 ohms at week 41, and finally reaching a range of 621 to 691 ohms at week 45. The high resistance exhibited by the Hycrete specimens, for CB as well as SE specimens, likely played a key role in limiting the rate of corrosion.

In summary, corrosion inhibitors improved corrosion resistance of conventional steel in both uncracked and cracked concrete, and delayed the onset of corrosion in uncracked concrete. Hycrete performed better in preventing corrosion of the conventional steel than Rheocrete and DCI in both uncracked and cracked concrete,

due at least in part to its effect on the resistance of the concrete. Rheocrete performed better than DCI in uncracked concrete but not in cracked concrete.

3.2.3 Conventional, ECR, and Multiple-Coated Bars Evaluated Using the ASTM G109 Test

Three types of reinforcing steel, conventional, ECR, and multiple-coated reinforcing steel were evaluated using the ASTM G109 test. The average results for the test specimens are shown in Figures 3.32 through 3.37, and the total corrosion losses at week 209 are summarized in Table 3.5. The individual test results are presented in Figures A.37 through A.50 and B.11 and B.17. For conventional steel, five out of six specimens exhibited cracking of the concrete due to corrosion and the tests were discontinued at week 174. After week 174, the results for conventional steel are based solely on the remaining conventional steel specimen, No. 5. Some of mat-to-mat resistance readings could not be taken because the ohmmeter was malfunctioning during that period of the test.

Figures 3.32 and 3.33 show the average corrosion rates for ASTM G109 specimens. Conventional steel exhibited relatively high corrosion activity after it initiated corrosion at week 58. From week 99 to 123 and at week 174, the corrosion rates of the conventional steel specimens had negative values, indicating that bottom mat corrosion was occurring. From the individual results shown in Figures A.37a and A.38, the negative corrosion of the conventional steel was primarily influenced by specimens No. 5 and 6, with the corresponding bottom mat corrosion potentials showing more negative values than that of the top mat. After week 123, positive corrosion rates dominated the corrosion activity of the conventional steel with the highest corrosion rate of 7.16 $\mu\text{m}/\text{yr}$ at week 163. This average rate (approximately

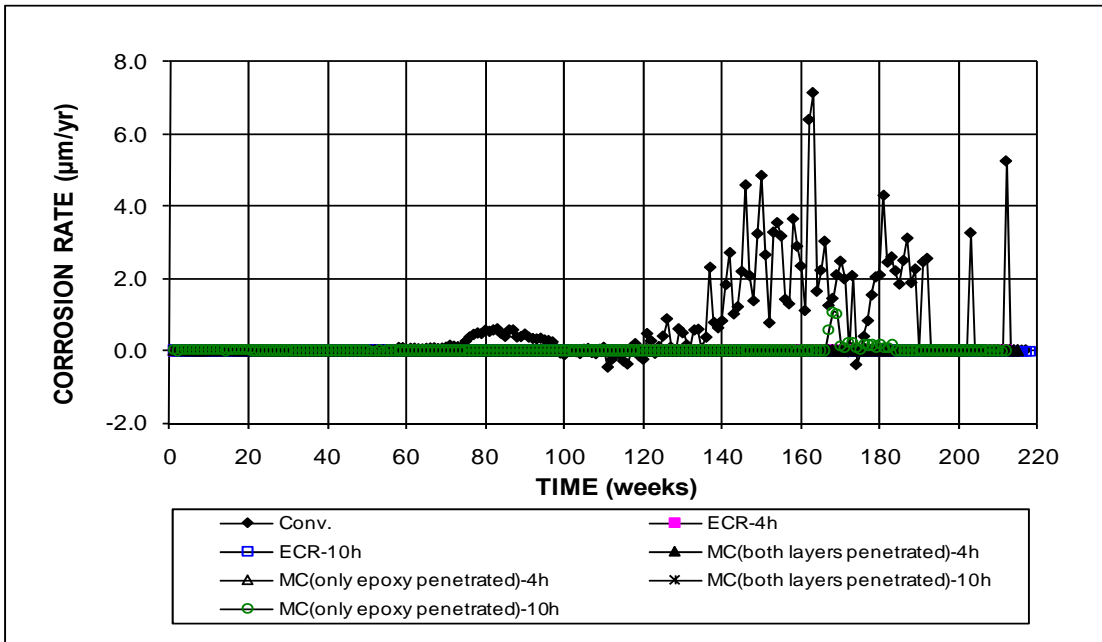


Figure 3.32a – ASTM G109 Test. Average corrosion rates for specimens with conventional steel, ECR, and multiple-coated bars (four and ten holes through the epoxy). (Data for Conv. is based on one specimen after week 174)

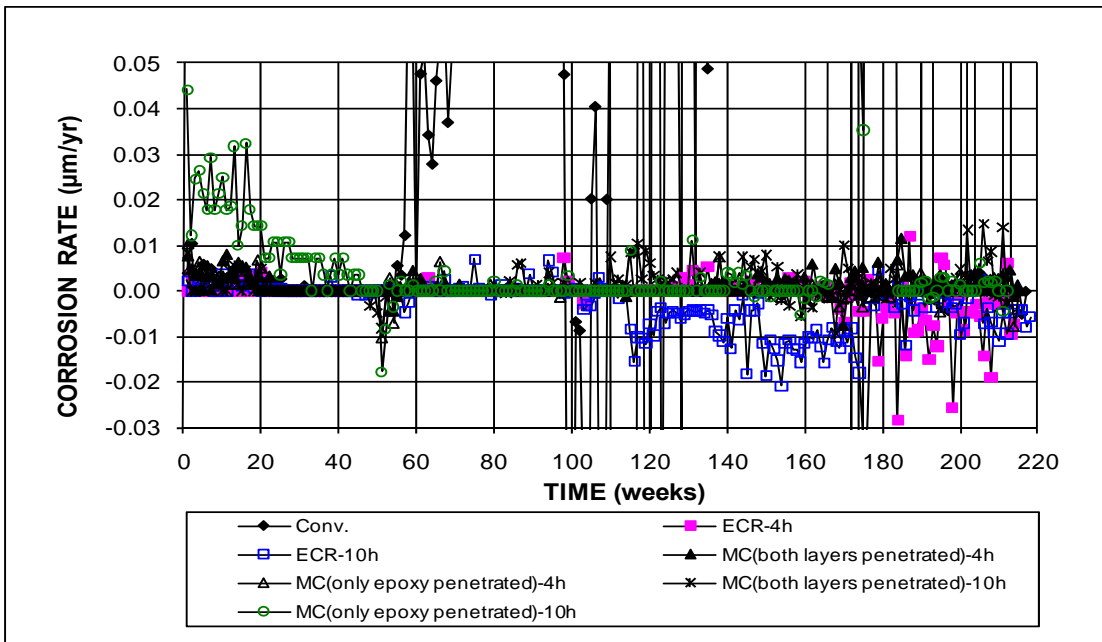


Figure 3.32b – ASTM G109 Test. Average corrosion rates for specimens with conventional steel, ECR, and multiple-coated bars (four and ten holes through the epoxy). (Data for Conv. is based on one specimen after week 174; different scale)

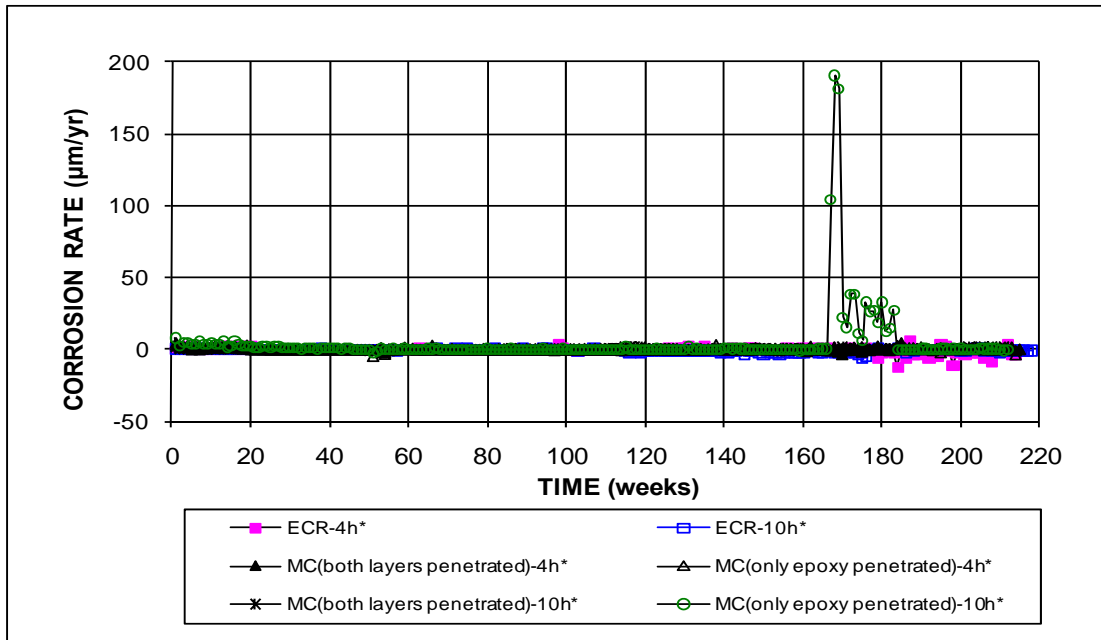


Figure 3.33 – ASTM G109 Test. Average corrosion rates for specimens with ECR and multiple-coated bars. * Based on exposed area (ECR with four and ten holes through the epoxy).

2.00 $\mu\text{m}/\text{yr}$) is much less than observed for the corresponding SE specimens (5.50 $\mu\text{m}/\text{yr}$) after week 50. This is mainly because that the exposure condition for G109 specimens is much less severe than obtained with SE specimens. The MC specimens with ten holes penetrating only the epoxy exhibited higher corrosion rates than the other MC and conventional ECR specimens before week 17 and between weeks 167 and 183, with the highest value of 1.08 and 190.51 $\mu\text{m}/\text{yr}$ at week 168 based on total and exposed area, respectively. As shown in Figure A.47, the high rate was mainly caused by the corrosion of specimen MC(only epoxy layer penetrated)-10h No. 3.

The average total corrosion losses for the ASTM G109 specimens are plotted in Figures 3.34 and 3.35 and summarized at week 209 in Table 3.5. The average corrosion losses of the conventional steel increased slowly before week 137 and relatively rapidly after that, reaching 2.76 μm at week 217. The corrosion losses of the MC specimens with ten holes penetrating only the epoxy showed higher corrosion

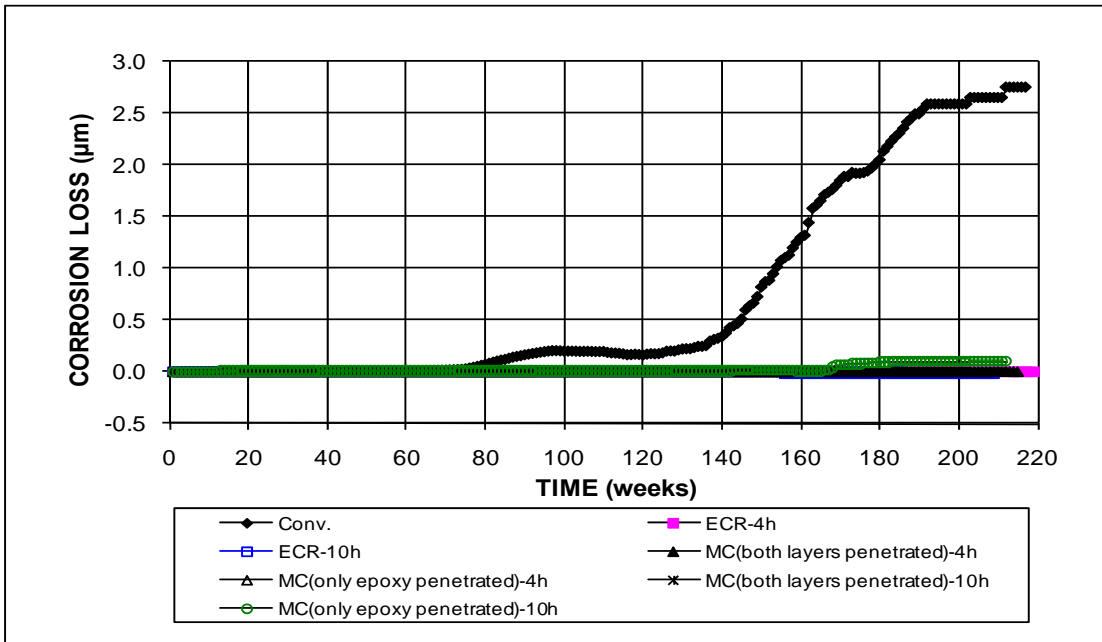


Figure 3.34a – ASTM G109 Test. Average corrosion losses for specimens with conventional steel, ECR, and multiple-coated bars (four and ten holes through the epoxy). (Data for Conv. is based on one specimen after week 174)

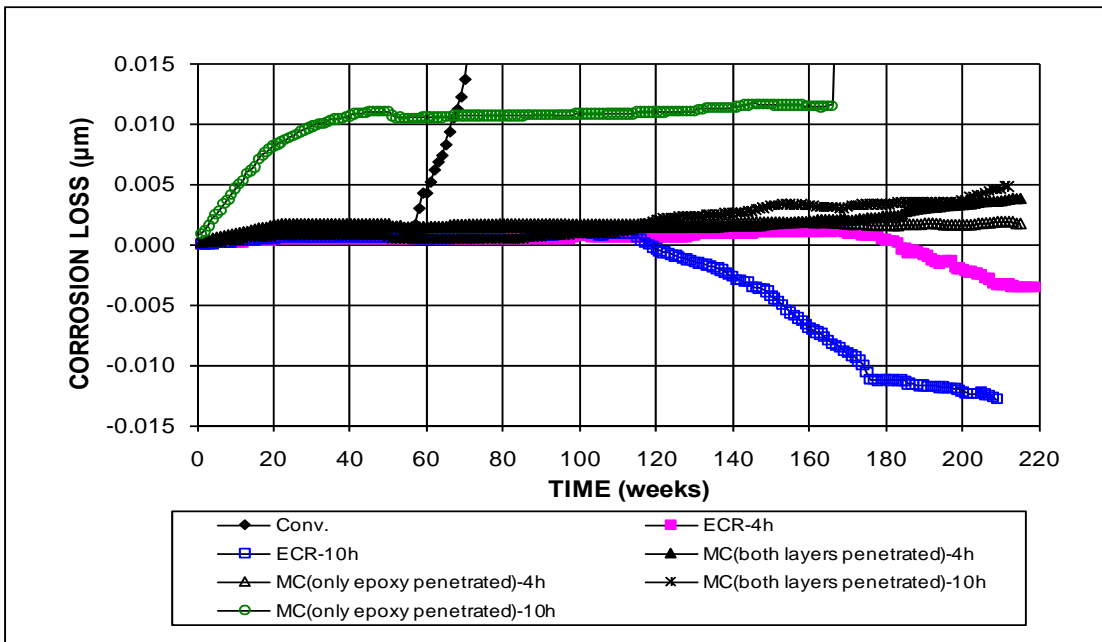


Figure 3.34b – ASTM G109 Test. Average corrosion losses for specimens with conventional steel, ECR, and multiple-coated bars (four and ten holes through the epoxy). (Data for Conv. is based on one specimen after week 174; different scale)

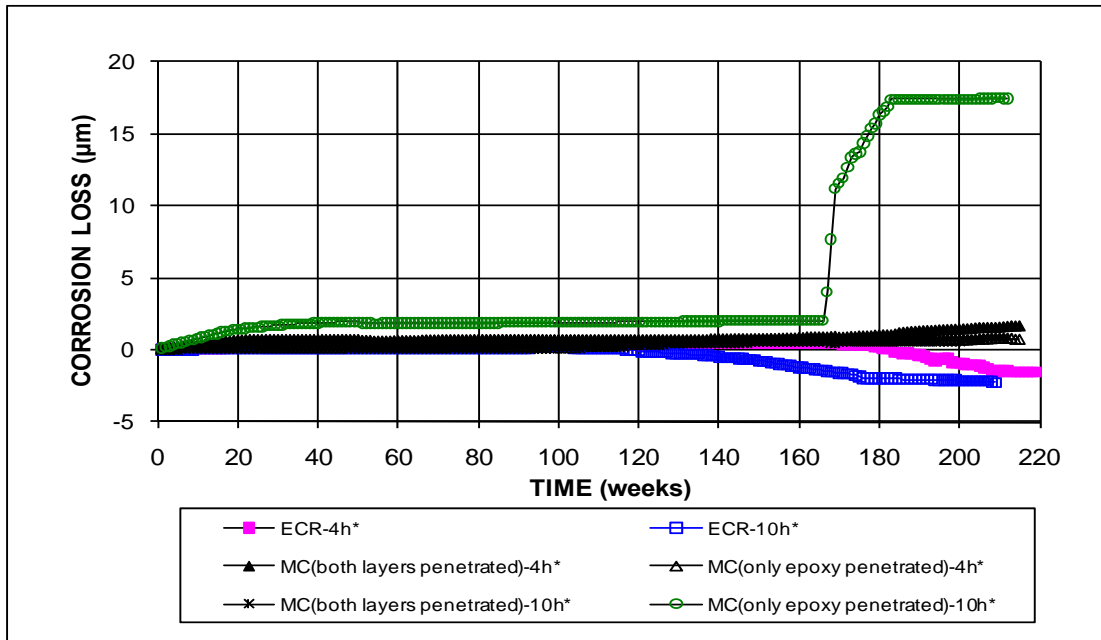


Figure 3.35 – ASTM G109 Test. Average corrosion losses for specimens with ECR and multiple-coated bars (four and ten holes). * Based on exposed area (ECR with four and ten holes through the epoxy).

losses than the other MC and conventional ECR specimens. The conventional ECR specimens showed increasing negative corrosion losses, indicating corrosion of the bottom mat of steel, with the ten-hole specimens exhibiting more negative corrosion losses than the four-hole specimens after week 115. Conventional steel had an average corrosion loss of 2.05 μm at week 209 (the final corrosion losses of the removed specimens were included in the average corrosion loss), which is 20 times more than that of the MC(only epoxy layer penetrated)-10h specimens based on total area. This average loss is much less than that observed for the SE conventional specimens, 3.42 μm at week 67. The conventional ECR specimens with four holes through the epoxy had a low negative corrosion loss, $-0.01 \mu\text{m}$; while the other MC and ECR specimens exhibited average corrosion losses of less than 0.005 μm based on total area. Based on the exposed area, the average corrosion loss of the MC(only epoxy layer penetrated)-10h specimens was 17.49 μm , which is 10 times more than

Table 3.5 – Corrosion losses at 209 weeks for specimens in the ASTM G109 test based on total and exposed area

Steel Designation ^a	Specimen Corrosion Losses (μm)						Average ^b	Standard Deviation
	1	2	3	4	5	6		
Based on Total Area								
Control								
Conv. ^c	4.27 ^c	3.32 ^c	3.86 ^c	3.67 ^c	-0.62	-2.22 ^c	2.05	-
ECR-4h	β	β	-0.01				β	β
ECR-10h	-0.07	-0.01	β	β	β	β	-0.01	0.03
Multiple Coated Bars								
MC(both layers penetrated)-4h	β	β	β				β	β
MC(both layers penetrated)-10h	β	β	0.01				β	β
MC(only epoxy penetrated)-4h	β	β	β				β	β
MC(only epoxy penetrated)-10h	β	β	0.29				0.10	0.17
Based on Expose Area								
Control								
ECR-4h*	0.47	-1.30	-3.53				-1.45	2.00
ECR-10h*	-12.09	-1.91	-0.20	0.07	-0.08	0.72	-2.25	4.76
Multiple Coated Bars								
MC(both layers penetrated)-4h*	2.19	0.54	1.92				1.55	0.88
MC(both layers penetrated)-10h*	0.81	0.67	0.94				0.81	0.14
MC(only epoxy penetrated)-4h*	0.60	0.63	1.19				0.80	0.33
MC(only epoxy penetrated)-10h*	0.36	0.20	51.90				17.49	29.80

^a Conv. = conventional steel. ECR = conventional epoxy-coated reinforcement. MC(both layers penetrated) = multiple coating bars with both layers penetrated. MC(only epoxy penetrated) = multiple coating bars with only epoxy penetrated. 4h, 10h = epoxy-coated reinforcement with 4 or 10 holes through the epoxy.

^b Based on top mat only.

^c Specimens 1, 2, 3, 4 and 6 exhibited cracking of concrete and were removed from testing on week 174. Corrosion losses for these specimens are presented as final values before testing was terminated.

* Corrosion loss based on exposed area.

β Corrosion loss (absolute value) less than 0.005 μm

1.55 μm for the MC(both layers penetrated)-4h specimens, and 20 times more than 0.81 and 0.80 μm for the MC(both layers penetrated)-10h and MC(only epoxy layer penetrated)-4h specimens, respectively. The conventional ECR had negative corrosion losses of -2.25 and -1.45 μm for specimens with ten and four holes, respectively. As explained earlier, the negative values here are not really “negative corrosion,” but rather, indicate greater oxidation in the bottom mat of steel than in the top mat.

Figure 3.36 shows the average corrosion potentials for all specimens. The top mat corrosion potentials of conventional steel shifted to values more negative than -0.350 V at week 78, which is consistent with the increase in the corresponding corrosion rates. The MC specimens with both layers penetrated exhibited similar corrosion potentials to those of the conventional steel specimens before week 80 (around -0.200 V) and slightly less negative values than those of the conventional steel specimens after that (above -0.400 V compared to below -0.400 V). Specimens with only the epoxy layer penetrated exhibited much more negative corrosion potentials (about -0.400 and -0.320 V, respectively) than those of the conventional steel specimens for both the top and bottom mats (-0.200 V) before week 80 and 100, respectively, and had similar corrosion potentials after that (about -0.400 V for the top mat and -0.320 V for the bottom mat). This is because zinc is more active and has a more negative corrosion potential than steel, as described in Section 1.3. The top mat corrosion potentials of the MC specimens with both layers penetrated shifted in the negative direction gradually with the mild salt exposure (3% NaCl concentration) and limited exposed area. The top mat corrosion potentials of the MC(only epoxy layer penetrated)-10h specimens shifted toward more negative values beginning at week 169 (-0.467 V), which is consistent with the corresponding sharp increase of the corrosion rates at week 167 (no corrosion potential readings were taken during the drying cycle between weeks 167 and 168). The conventional ECR specimens had stable top mat corrosion potentials more positive than -0.350 V at all times, while the bottom mat potentials exhibited slight shifts in the negative direction and were more negative than -0.350 V at weeks 173 and 176 for the ECR-4h specimens.

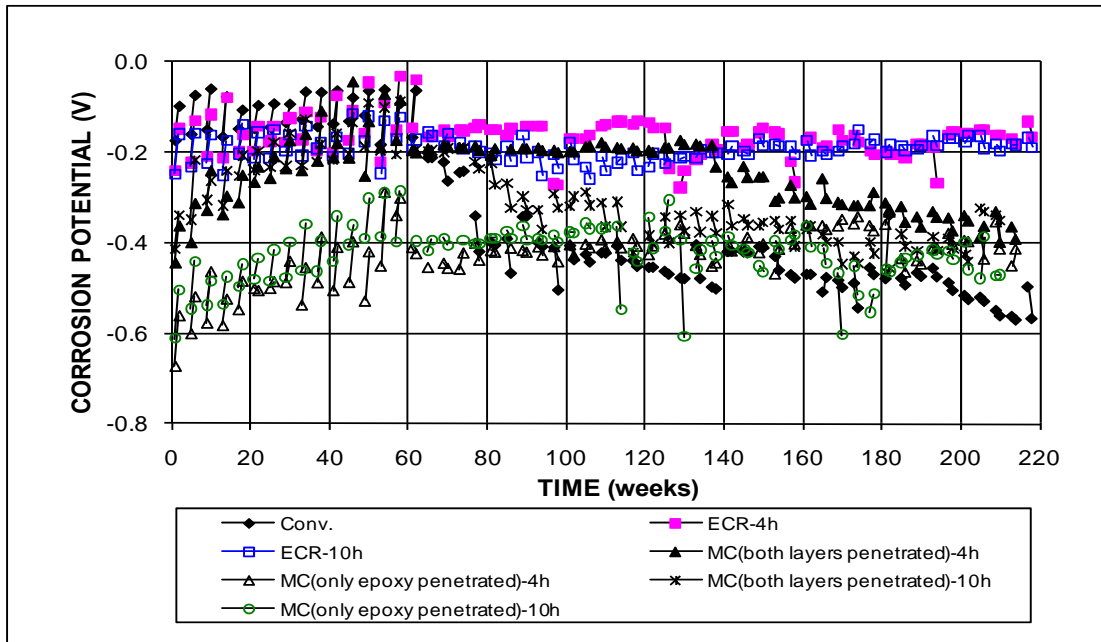


Figure 3.36a – ASTM G109 Test. Average top mat corrosion potentials with respect to a copper-copper sulfate electrode for specimens with conventional steel, ECR, and multiple-coated bars (four and ten holes through the epoxy).

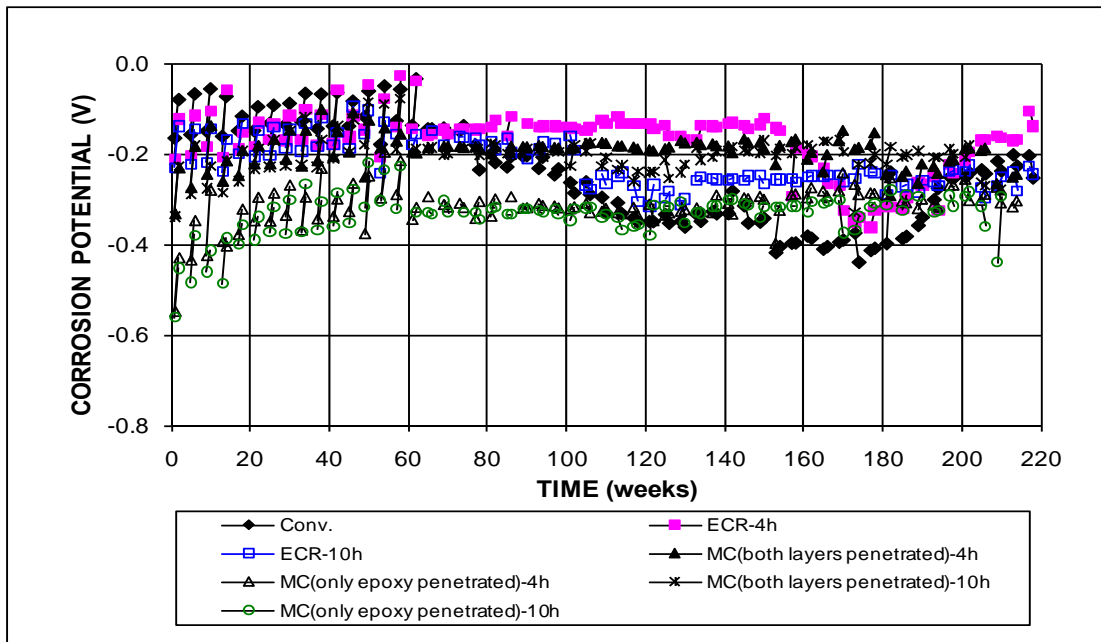


Figure 3.36b – ASTM G109 Test. Average bottom mat corrosion potentials with respect to a copper-copper sulfate electrode for specimens with conventional steel, ECR, and multiple-coated bars (four and ten holes through the epoxy).

The average mat-to-mat resistances increased progressively during the test until about week 100 and then became stable, as shown in Figure 3.37. The ohmmeter was out of service for a repair during weeks 67 to 81. The resistance readings of the ten-hole specimens decreased after ohmmeter was repaired, while others did not exhibit any changes. The specimens with conventional steel had the lowest mat-to-mat resistance (below 4,184 ohms). The MC and ECR specimens with four holes through the epoxy had the highest average resistances, from 23,000 to 33,000 ohms after week 180, while the MC and ECR with ten holes through the epoxy had resistances below 10,000 ohms before week 187, gradually increasing to 20,000 ohms at week 209. The epoxy coating provides the high electrical resistance. The resistance decreases as the exposed area increases with more holes through the coating.

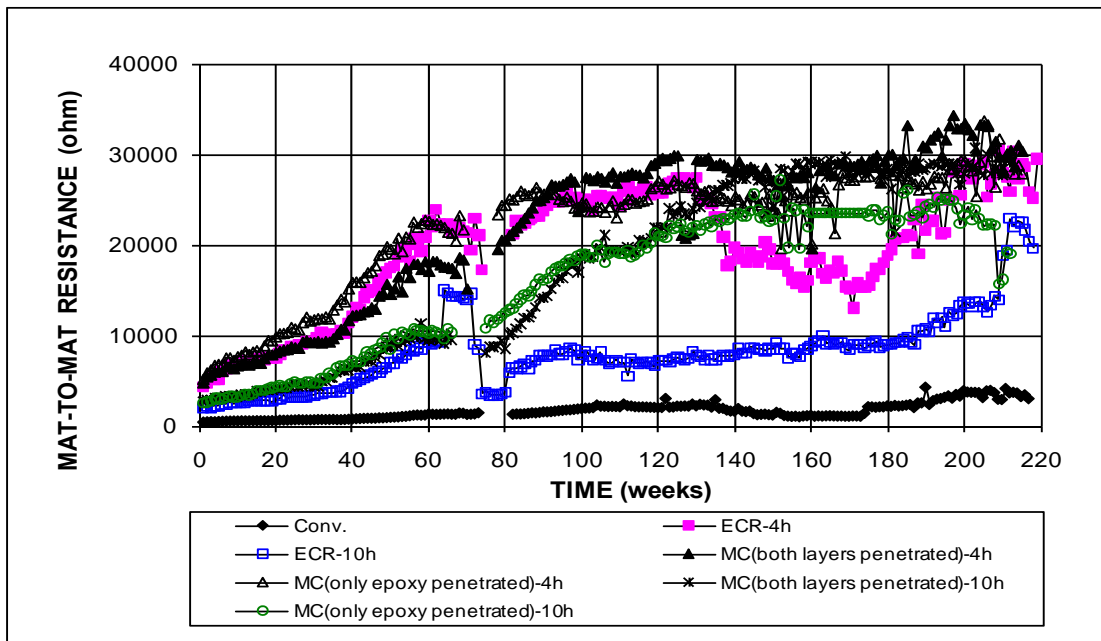


Figure 3.37 – ASTM G109 Test. Average mat-to-mat resistances for specimens with conventional steel, ECR, and multiple-coated bars (four and ten holes through the epoxy).

Visual inspection was performed on the five specimens with conventional steel that were removed from the test at week 174. Specimens No. 1, 2, 3 and 4 had positive corrosion losses at week 174 and exhibited cracks on the top and side surfaces (with the exception of specimen No. 4 on the side, as shown in Figure 3.38. Specimens No. 2 and 3 showed stains on the side cracks. Specimen No. 6 had a negative corrosion loss at week 174 and exhibited cracks along the bottom mat of steel. A corner of the concrete was almost detached from the specimen, and stains were visible on some cracks (Figure 3.39). The steel was inspected after the concrete was removed. Both top and bottom mats of steel had corrosion products on all of the specimens, as shown in Figure 3.40, except specimen No. 4, which had no corrosion products visible on the bottom. Many bars, including bottom bars, showed severe corrosion (Figure 3.41).



Figure 3.38 – ASTM G109 Test. Specimen with conventional steel (G-N4-Conv.-3) showing a crack on the top surface at week 174.

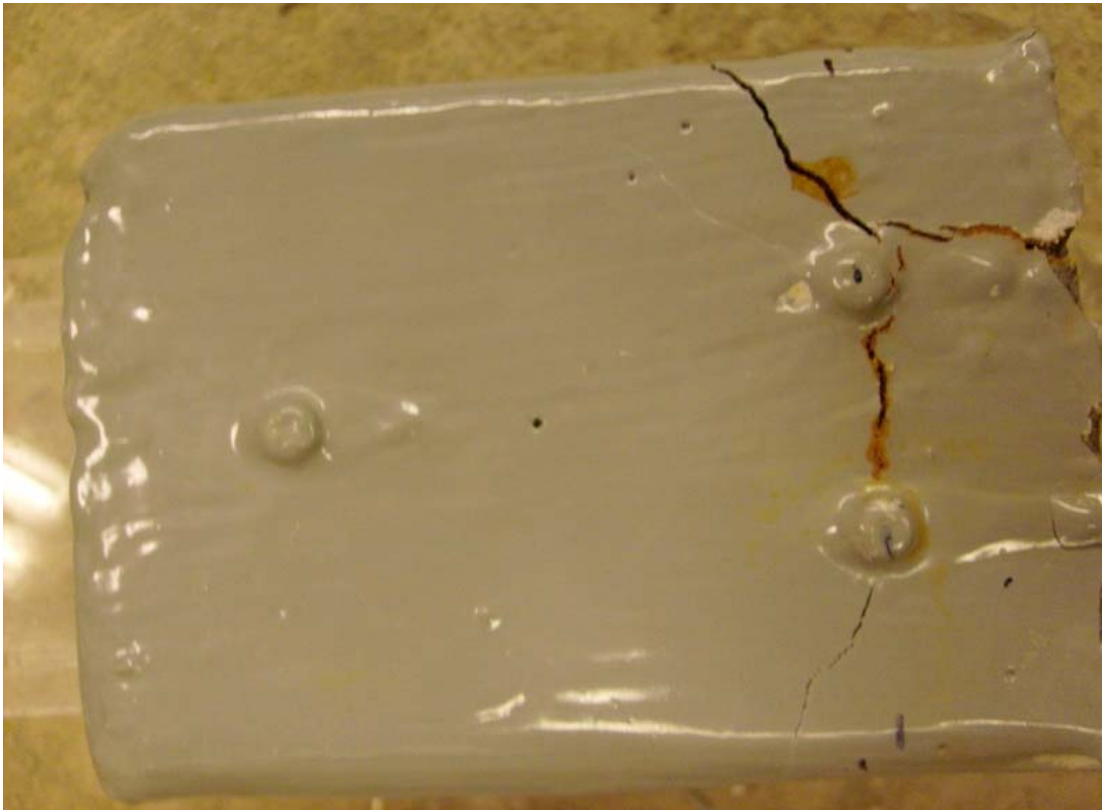


Figure 3.39 – ASTM G109 Test. Specimen with conventional steel (G-N4-Conv.-6) showing cracks and stains on the side at week 174.



Figure 3.40 – ASTM G109 Test. Conventional steel (G-N4-Conv.-1) showing severe corrosion on both top (top) and bottom (bottom) mats of steel at week 174.



Figure 3.41 – ASTM G109 Test. Conventional steel from bottom mat of the specimen (G-N4-Conv.-6) showing severe corrosion at week 174.

Overall, both ECR and MC exhibited significantly better corrosion performance than conventional reinforcement. Because of the high resistance of the epoxy coating and the mild exposure conditions inherent in the G109 test, specimens with ECR and MC exhibited very low corrosion losses compared to specimens with conventional steel, which had very high corrosion losses and developed cracks in the concrete for five out of six specimens. The corrosion losses of the ECR and MC specimens were comparable in ASTM G109 test.

3.3 FIELD TEST

The field test specimens evaluated in this study included specimens with and without simulated cracks. Specimens containing conventional steel and ECR served as control specimens. Three corrosion protection systems were evaluated, corrosion inhibitors, MC reinforcement, and ECR with increased adhesion. Systems with corrosion inhibitors included ECR cast in concrete with DCI, Hycrete, and Rheocrete, along with ECR with a primer containing microencapsulated calcium nitrite [primer/ $\text{Ca}(\text{NO}_2)_2$]. ECR with increased adhesion included coating products by DuPont and Valspar and ECR with a zinc-chromate pretreatment. In most cases, two specimens, each with and without cracks were tested for each system, except three specimens of each type were used for ECR with the inhibitor DCI. Two or four bars

were monitored separately in each specimen (see Table 2.14 in Section 2.4.5). The test designations used in the tables and figures in this section are as follows:

Conv. = conventional steel

ECR = conventional epoxy-coated reinforcement

ECR(primer/Ca(NO₂)₂) = ECR with a calcium nitrite primer

ECR(DCI) = ECR in concrete with DCI inhibitor

ECR(Rheocrete) = ECR in concrete with Rheocrete inhibitor

ECR(Hycrete) = ECR in concrete with Hycrete inhibitor

MC = multiple-coated reinforcement

ECR(Valspar) = high adhesion Valspar reinforcement

ECR(DuPont) = high adhesion DuPont reinforcement

ECR(Chromate) = ECR with the zinc chromate pretreatment.

The coating on all epoxy-coated bars was penetrated with 16 3-mm (¹/₈-in.) diameter holes, eight on each side. The MC bars had both the zinc and epoxy layers penetrated. The corrosion rates and losses are calculated based on the total surface area of the top mat of steel for conventional steel and the total surface area underneath the coating of one test bar for ECR and MC specimens unless otherwise indicated. As indicated in Table 3.1, the corrosion rates and losses based on exposed area (the area exposed by the holes) for ECR and MC specimens are 390 times those of the corresponding specimens based on total area. The corrosion rates and losses for specimens marked with an asterisk (*) are based on the exposed area. For example, ECR* (1)-2, represents conventional ECR specimen No. 1, test bar No. 2, and the reported values are based on exposed area.

Average results are based on two or four test bars for each specimen depending on the test setup (Table 2.14 in Section 2.4.5). Individual results for each test bar are

presented in Appendices A and B. The corrosion potentials are reported with respect to a copper-copper sulfate electrode. According to ASTM C876, the half cell potential of a copper-copper sulfate electrode with respect to a standard hydrogen electrode is -0.316 V at 22.2 °C (72 °F). The potential decreases by 0.0009 V/°C (0.0005 V/°F) as temperature goes up from 0 to 49 °C (32 to 120 °F). All of the recorded potential readings in the field have been corrected for the temperature effect and are equivalent to readings at 22.2 °C (72 °F). Because maintenance was required for several circuits, some mat-to-mat resistance readings were not recorded for several weeks.

Because the tests were initiated on different dates for each specimen and measurements were not taken on a weekly basis, the reported ages are based on the shortest duration of any of the field test specimens, 169 weeks, for comparisons. For the other specimens, the reported ages are chosen such that the differences on the exposure age among the specimens are small. Since the tests are still ongoing, figures for some specimens are plotted several weeks beyond that point corresponding to the cutoff date, May 31, 2008.

3.3.1 Conventional Steel and ECR

The test results for control specimens with conventional steel and ECR are presented in Figures 3.42 through 3.53, and the total corrosion losses are summarized in Tables 3.6 and 3.7.

3.3.1.1 Field Specimens without Cracks

The results for the field test specimens without cracks are plotted in Figures 3.42 through 3.47, and the average corrosion losses are summarized in Table 3.6.

As shown in Figure 3.42, the average corrosion rates began increasing in value at weeks 40 and 81 to peak values of 1.34 and 1.77 $\mu\text{m}/\text{yr}$ at weeks 153 and 205 for specimens Conv. (1) and (2), respectively. The ECR specimens had corrosion rates of less than 0.03 $\mu\text{m}/\text{yr}$ at all times based on total area. Based on exposed area, the highest average corrosion rates were around 10 $\mu\text{m}/\text{yr}$ for both ECR specimens (Figure 3.43).

Specimen Conv. (1) had the highest average corrosion loss, 1.27 μm at week 173, followed by specimen Conv. (2) with a value of 0.50 μm at week 169, as shown in Figure 3.44 and Table 3.6. Specimen ECR (2) exhibited negative corrosion losses after initiating corrosion at week 69, and began showing mild positive corrosion losses after week 145, as shown by the slope changes in Figures 3.44b and 3.45. The average corrosion losses for the ECR specimens were less than 0.02 μm based on total area; while based on exposed area, the average corrosion losses were 5.02 and -2.89 μm for specimens ECR (1) at week 173 and ECR (2) at week 169, respectively.

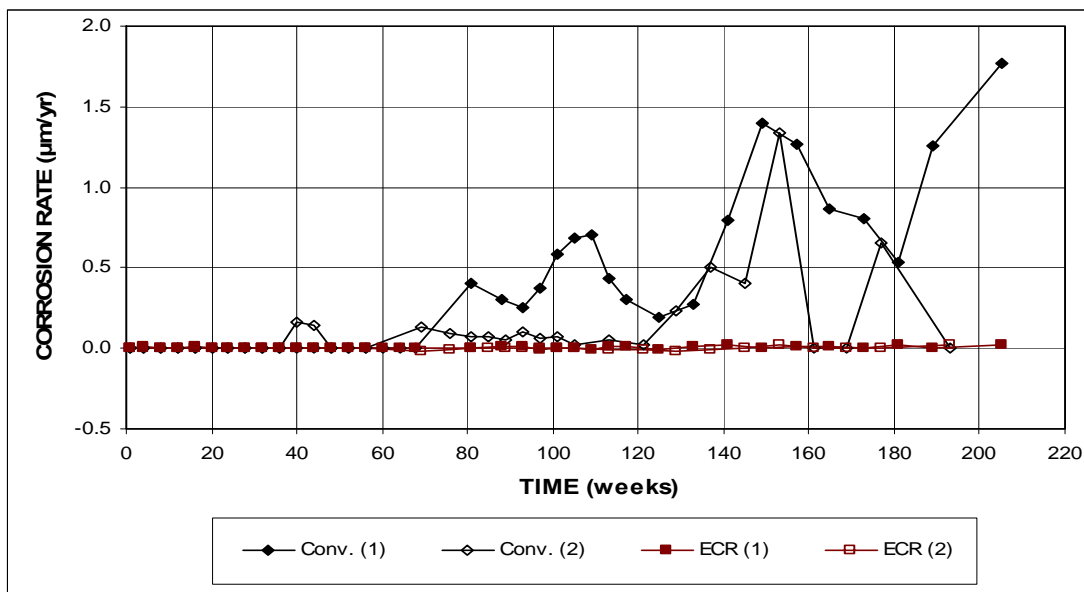


Figure 3.42a – Field Test. Average corrosion rates for specimens with conventional steel and ECR, without cracks (ECR with 16 holes through the epoxy).

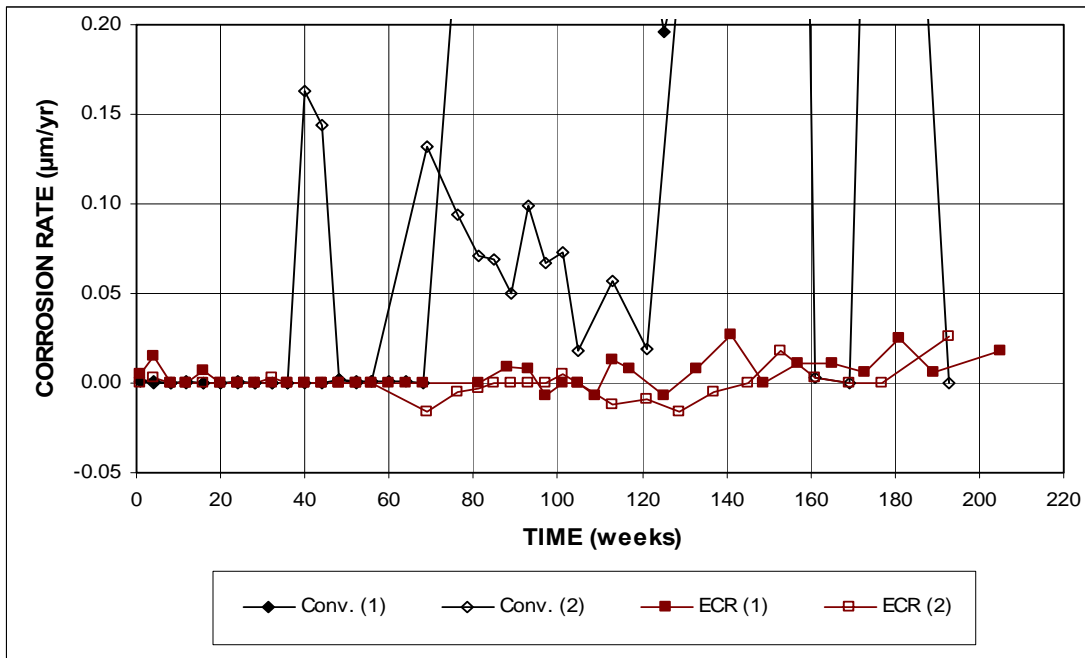


Figure 3.42b – Field Test. Average corrosion rates for specimens with conventional steel and ECR, without cracks (ECR with 16 holes through the epoxy)). (Different scale)

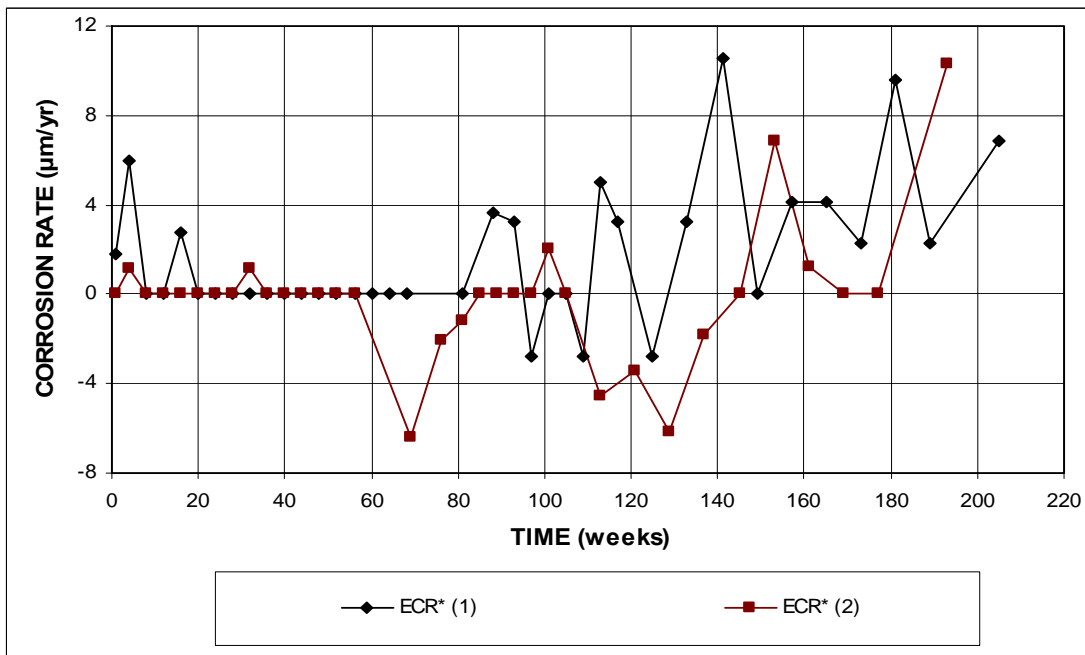


Figure 3.43 –Field Test. Average corrosion rates for specimens with ECR, without cracks. * Based on exposed area (ECR with 16 holes through the epoxy).

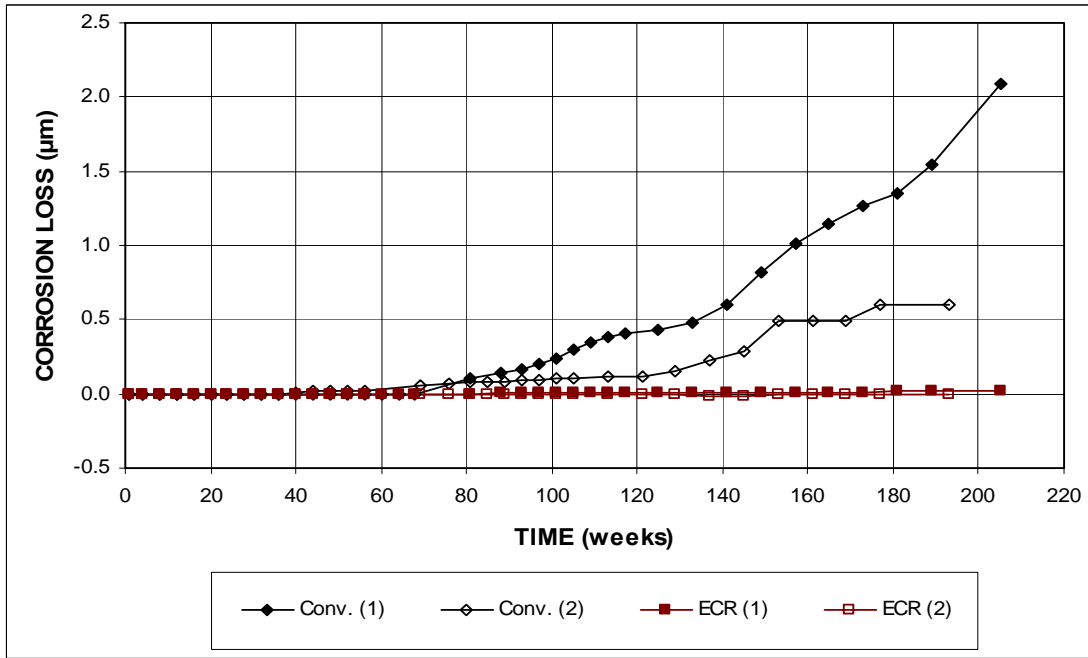


Figure 3.44a – Field Test. Average corrosion losses for specimens with conventional steel and ECR, without cracks (ECR with 16 holes through the epoxy).

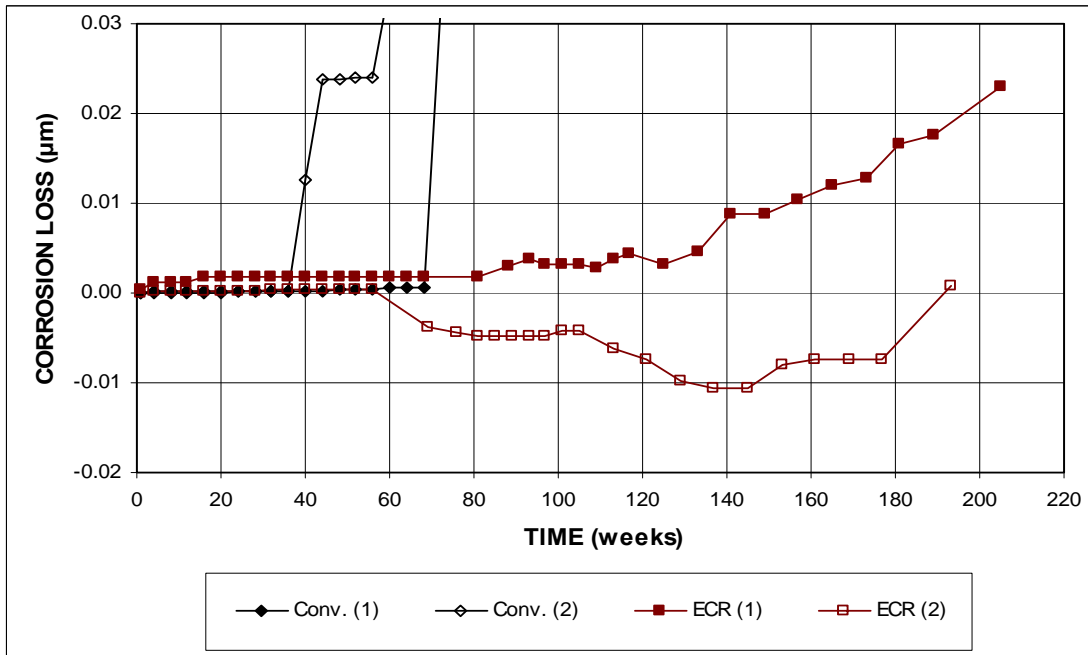


Figure 3.44b – Field Test. Average corrosion losses for specimens with conventional steel and ECR, without cracks (ECR with 16 holes through the epoxy). (Different scale)

Table 3.6 – Corrosion losses for conventional steel and ECR in the field test, without cracks

Control without Cracks							
Steel Designation ^a	Exposure time (weeks)	Test Bar Corrosion Losses (µm)				Average	Standard Deviation
		1	2	3	4		
Based on Total Area							
Conv. (1)	173	1.10	1.43			1.27	0.24
Conv. (2)	169	0.06	0.94			0.50	0.62
ECR (1)	173	β	0.02			0.01	0.01
ECR (2)	169	β	-0.01	-0.01	-0.01	-0.01	0.01
Based on Exposed Area							
ECR* (1)	173	1.22	8.82			5.02	5.38
ECR* (2)	169	1.76	-3.19	-5.57	-4.58	-2.89	3.25

^a Conv. = conventional steel. ECR = conventional epoxy-coated reinforcement. ECR has 16 3-mm (1/8-in.) diameter holes through the epoxy.

* Based on exposed area.

β Corrosion loss (absolute value) less than 0.005 µm.

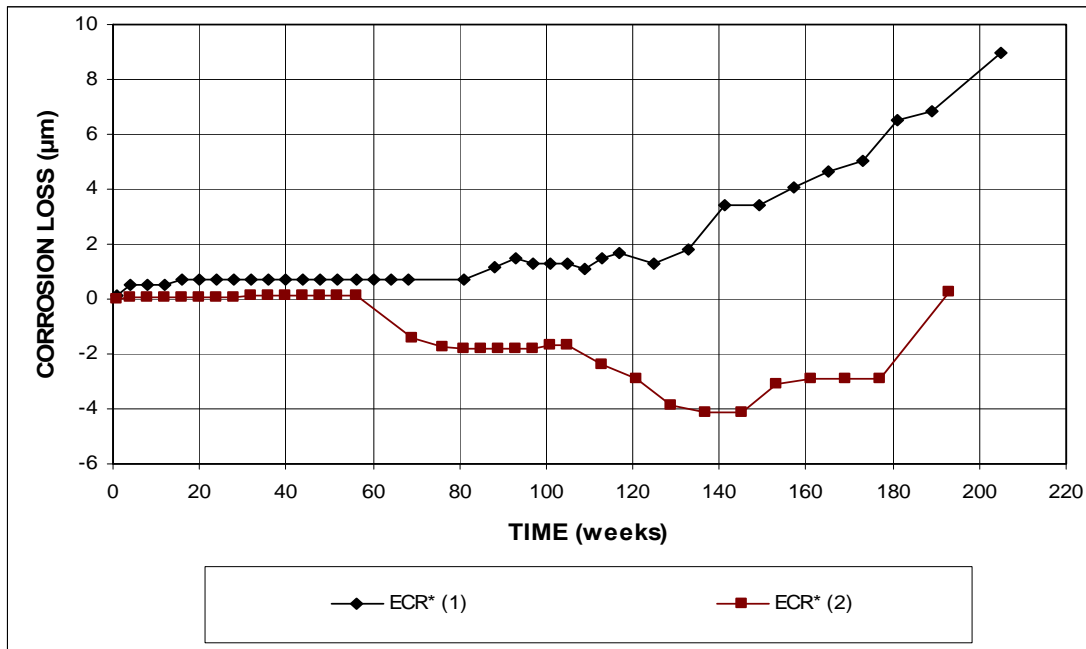


Figure 3.45 – Field Test. Average corrosion losses for specimens with ECR, without cracks. * Based on exposed area (ECR with 16 holes through the epoxy)

As shown in Figure 3.46, the corrosion potentials became more negative with time for both top and bottom mats. The potentials of the top bars for specimens with conventional steel fluctuated between -0.300 and -0.500 V after week 100, while those of the ECR specimens fluctuated between -0.100 and -0.355 V throughout the test. In both cases, a downward trend is observed. The potentials of bottom bars fluctuated as well, with most of the values above -0.350 V, except those of Conv. (2) at weeks 105, 137, and 193, and ECR (1) at week 189. The fluctuations in the readings for the field specimens are mainly caused by the outdoor exposure. As temperature and the concrete moisture content change, the rate of corrosion changes accordingly.

As shown in Figure 3.47, the mat-to-mat resistances for the specimens increased with time, with the exception of specimen, ECR (1), after week 81. All increases are not monotonic. The resistances of the ECR specimens increased from approximately 1,000 to 7,000 ohms, with a peak value of 21,941 at week 181 for specimen ECR (2), while the conventional steel specimens had resistance values below 130 ohms, except for Conv. (1), which had values as high as 1,207 ohms at week 181. The resistances of the ECR specimens are about five times more than those of the conventional steel due to high electrical resistance of their epoxy coating. Compared to the bench-scale specimens, the field specimens for both conventional steel and ECR had relatively lower mat-to-mat resistances. This is because the reinforcement in the field specimens had relatively larger areas in contact with concrete than in the bench-scale specimens, and therefore, more area was available for ion flow, which resulted in the lower resistance values.

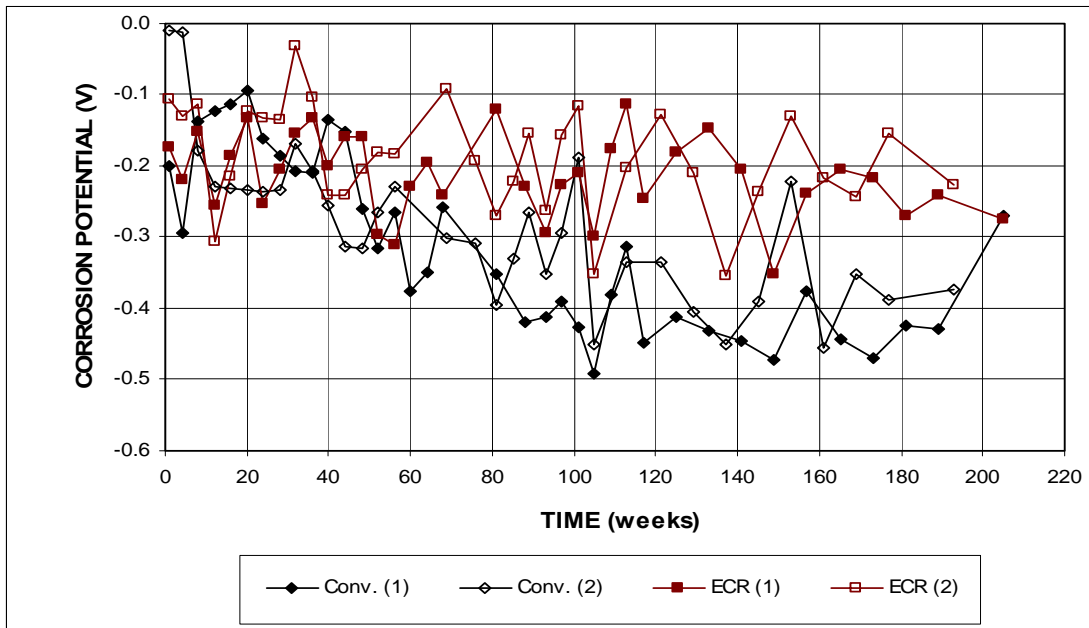


Figure 3.46a – Field Test. Average top mat corrosion potentials with respect to a copper-copper sulfate electrode for specimens with conventional steel and ECR, without cracks (ECR with 16 holes through the epoxy).

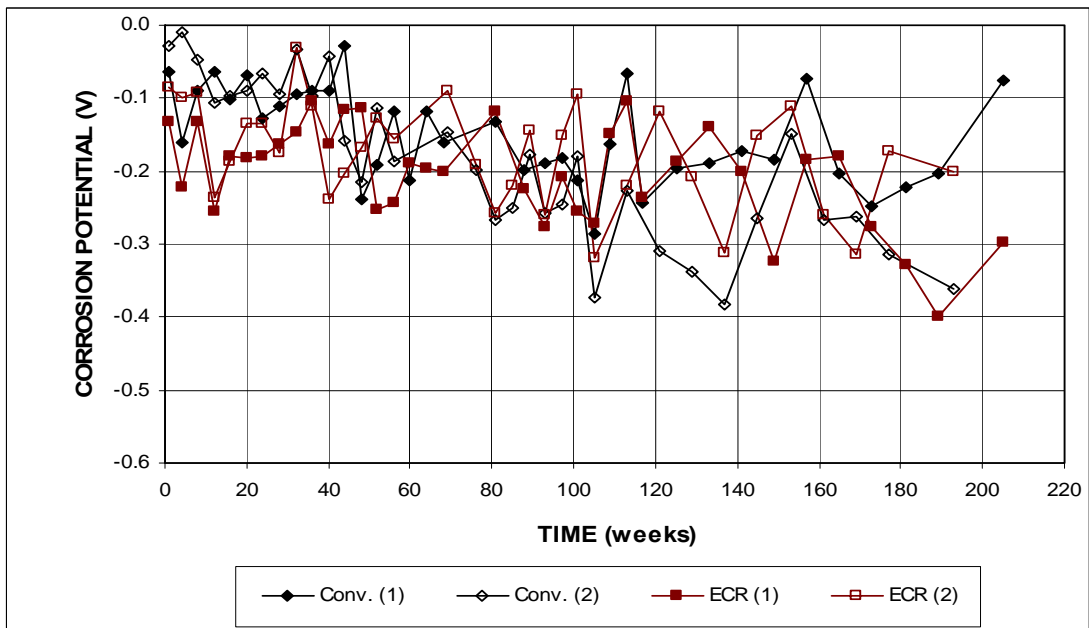


Figure 3.46b – Field Test. Average bottom mat corrosion potentials with respect to a copper-copper sulfate electrode for specimens with conventional steel and ECR, without cracks (ECR with 16 holes through the epoxy).

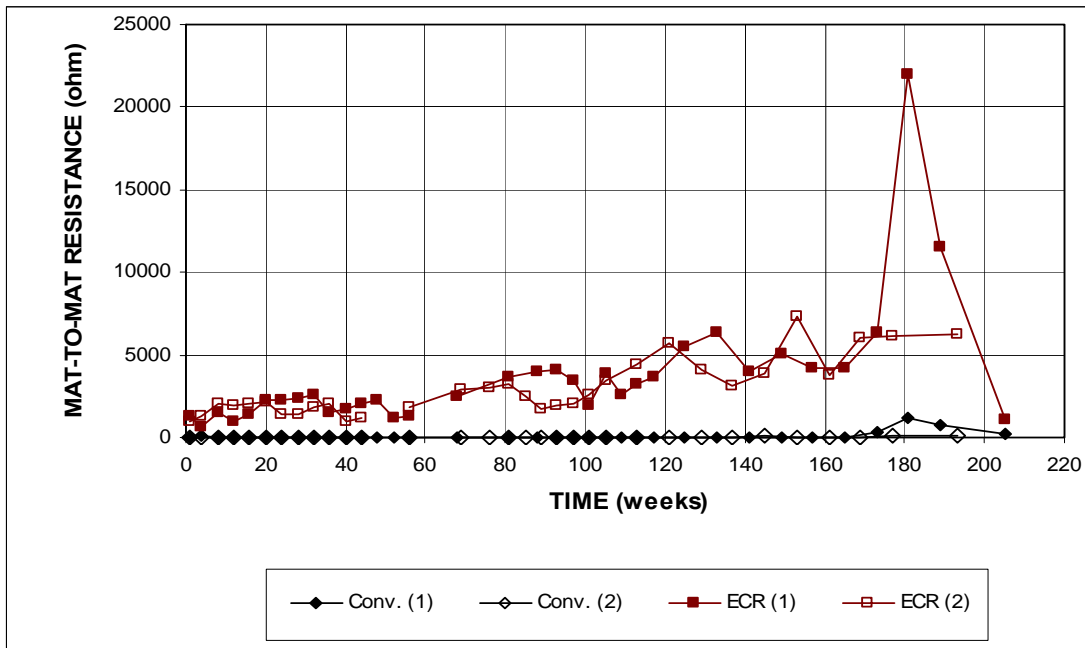


Figure 3.47a – Field Test. Average mat-to-mat resistances for specimens with conventional steel and ECR, without cracks (ECR with 16 holes through the epoxy).

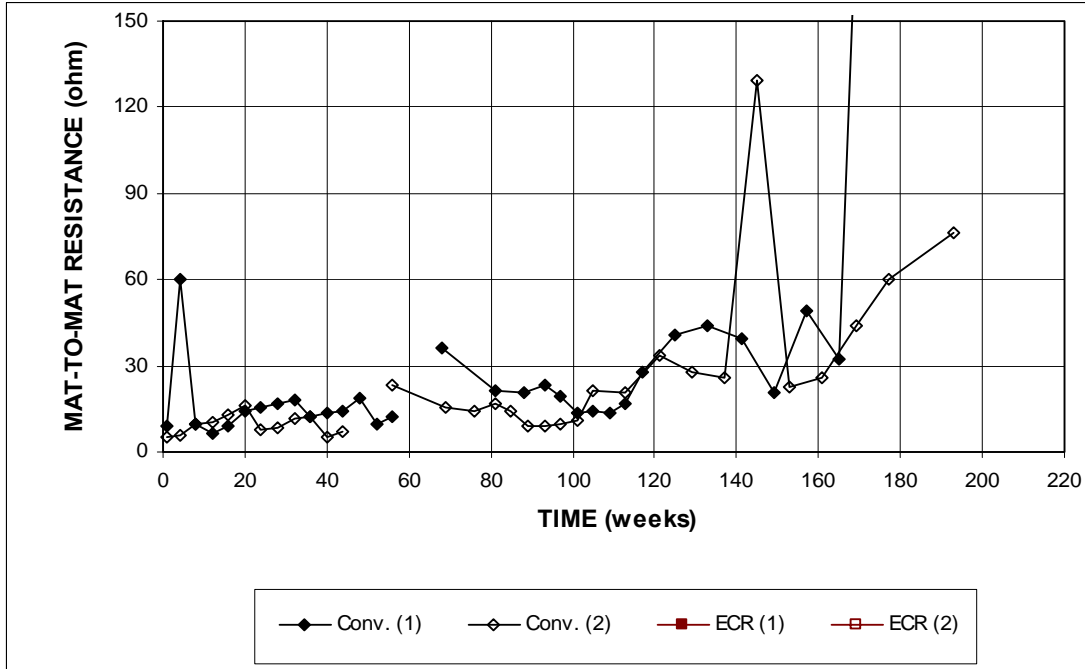


Figure 3.47b – Field Test. Average mat-to-mat resistances for specimens with conventional steel and ECR, without cracks (ECR with 16 holes through the epoxy). (Different scale)

3.3.1.2 Field Specimens with Cracks

The results for the conventional and ECR specimens with cracks are shown in Figures 3.48 through 3.53, and the average corrosion losses are summarized in Table 3.7.

Figures 3.48 and 3.49 show the average corrosion rates for the cracked specimens. The conventional steel specimens had much higher average corrosion rates than the ECR specimens, with high values of 1.97 and 1.83 $\mu\text{m}/\text{yr}$ at weeks 44 and 189 for specimens Conv. (2) and (1), respectively. The ECR specimens had corrosion rates less than 0.04 $\mu\text{m}/\text{yr}$ at all times based on total area. Based on exposed area, the highest corrosion rate was no more than 17.40 $\mu\text{m}/\text{yr}$ for either ECR specimen. The corrosion rates for the field test specimens exhibited more fluctuations than did the bench-scale specimens due to the changes in the concrete moisture content caused by the outdoor exposure.

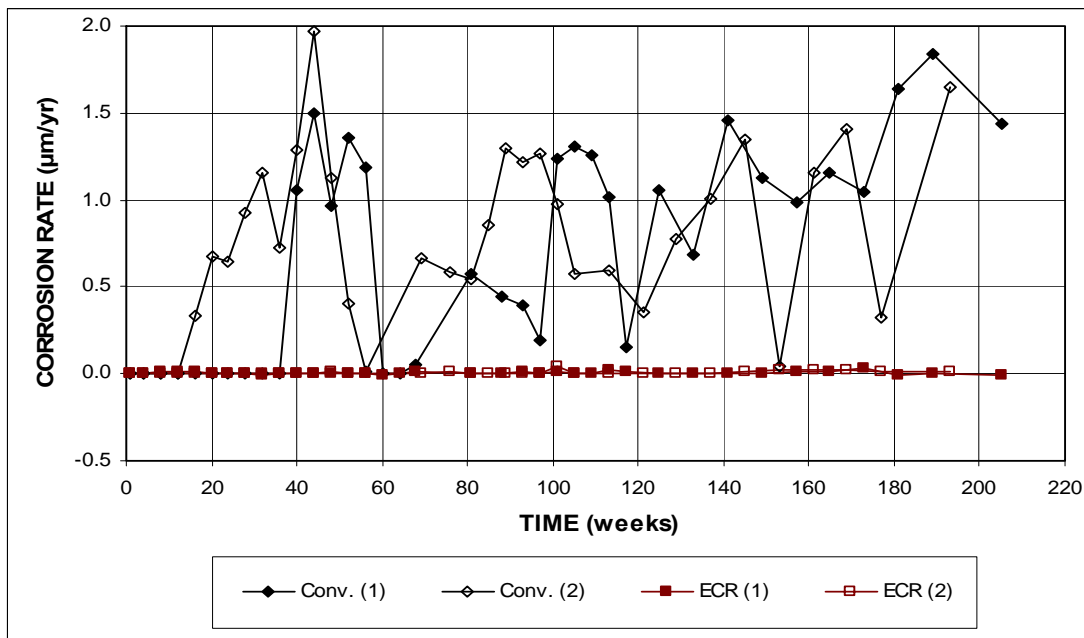


Figure 3.48a – Field Test. Average corrosion rates for specimens with conventional steel and ECR, with cracks (ECR with 16 holes through the epoxy).

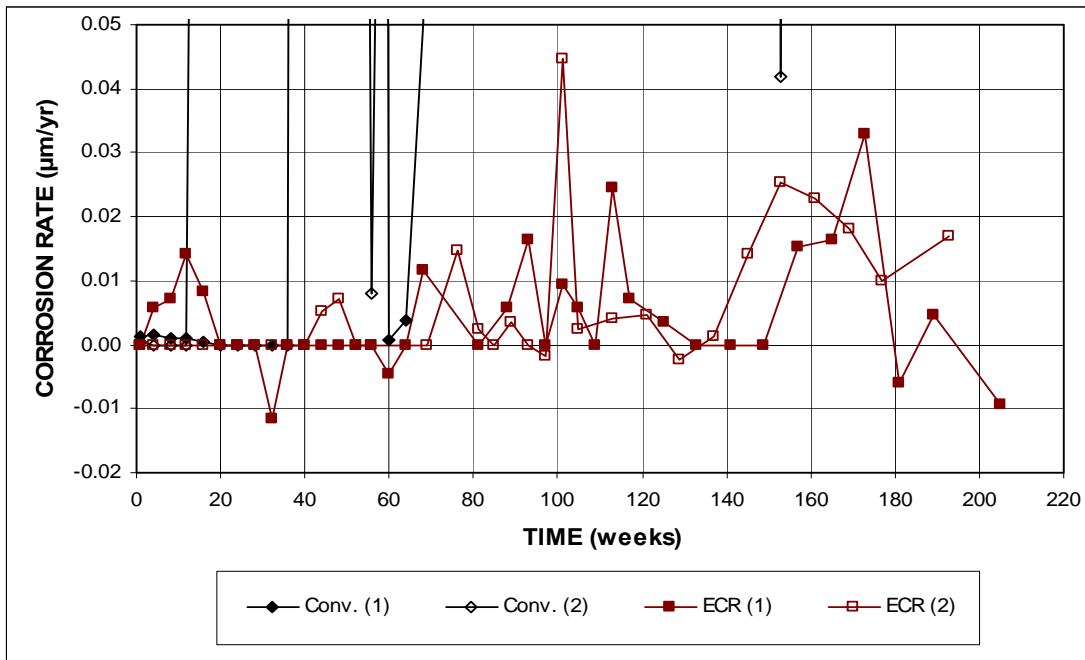


Figure 3.48b – Field Test. Average corrosion rates for specimens with conventional steel and ECR, with cracks (ECR with 16 holes through the epoxy). (Different scale)

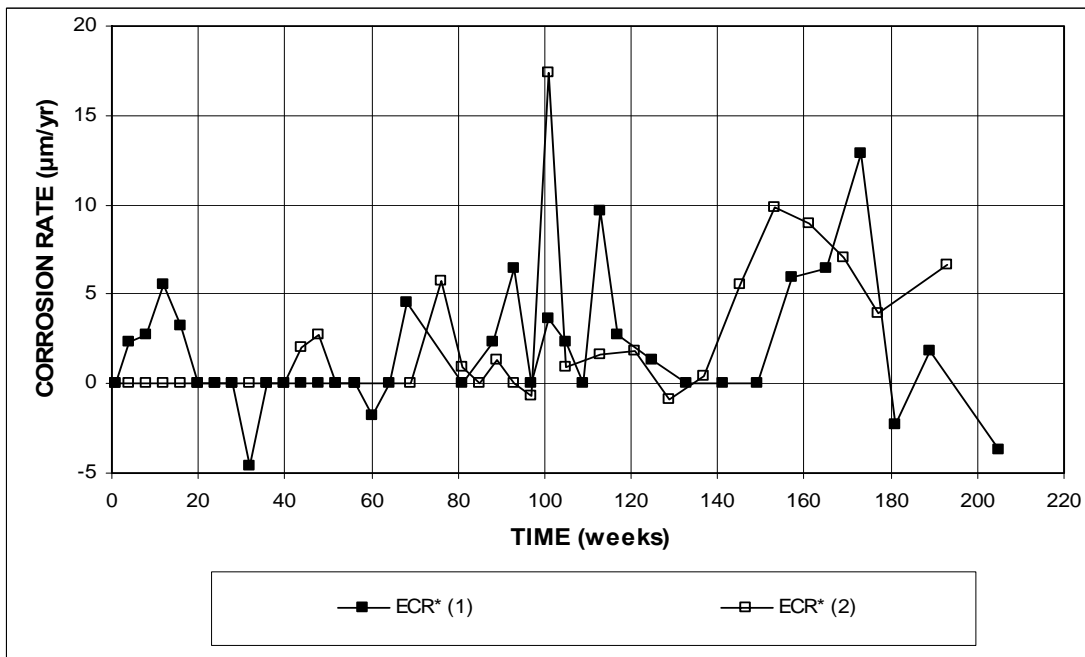


Figure 3.49 –Field Test. Average corrosion rates for specimens with ECR, with cracks. * Based on exposed area (ECR with 16 holes through the epoxy).

The average corrosion losses are plotted in Figures 3.50 and 3.51 and are summarized in Table 3.7. The average corrosion losses for specimens with conventional steel increased steadily with time and reached 2.26 μm for specimen Conv. (1) by week 173 and 2.51 μm for specimen Conv. (2) by week 169, respectively. These values are more than 100 times the corrosion losses of the ECR specimens, 0.02 μm for specimens ECR (1) and ECR (2) at weeks 173 and 169, respectively, based on total area. Based on exposed area, the corrosion losses were 7.29 μm for ECR (1) at week 173 and 7.97 μm for ECR (2) at week 169, respectively. The corrosion losses for the cracked specimens are higher than those of the specimens without cracks. As presented in Table 3.6, for the uncracked field specimens, the average corrosion losses were, respectively, 1.27 and 0.50 μm for specimens Conv. (1) and (2) and, respectively, 0.01 μm and negative for specimens ECR (1) and (2).

Table 3.7 – Corrosion losses for conventional steel and ECR in the field test, with simulated cracks

Control with Cracks							
Steel Designation ^a	Exposure time (weeks)	Test Bar Corrosion Losses (μm)				Average	Standard Deviation
		1	2	3	4		
Based on Total Area							
Conv. (1)	173	0.75	3.78			2.26	2.14
Conv. (2)	169	2.28	2.75			2.51	0.33
ECR (1)	173	0.01	0.03			0.02	0.01
ECR (2)	169	0.03	0.02	0.02	0.01	0.02	0.01
Based on Exposed Area							
ECR* (1)	173	3.75	10.83			7.29	5.01
ECR* (2)	169	10.21	7.73	8.95	5.00	7.97	2.23

^a Conv. = conventional steel. ECR = conventional epoxy-coated reinforcement.
ECR has 16 3-mm ($1/8$ -in.) diameter holes through the epoxy.

* Based on exposed area.

β Corrosion loss (absolute value) less than 0.005 μm .

As shown in Figure 3.52, the corrosion potentials shifted to more negative values with time for both the top and bottom mat bars for all specimens. The top mat bar potential readings fluctuated between -0.240 and -0.625 V after week 105, with

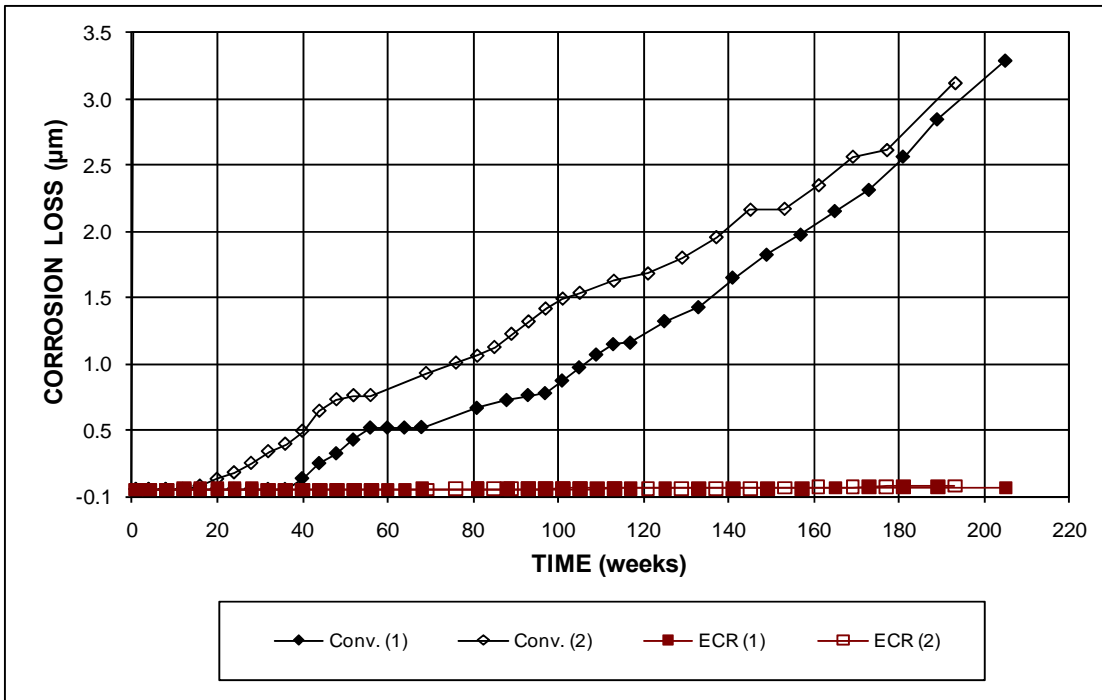


Figure 3.50a – Field Test. Average corrosion losses for specimens with conventional steel and ECR, with cracks (ECR with 16 holes through the epoxy).

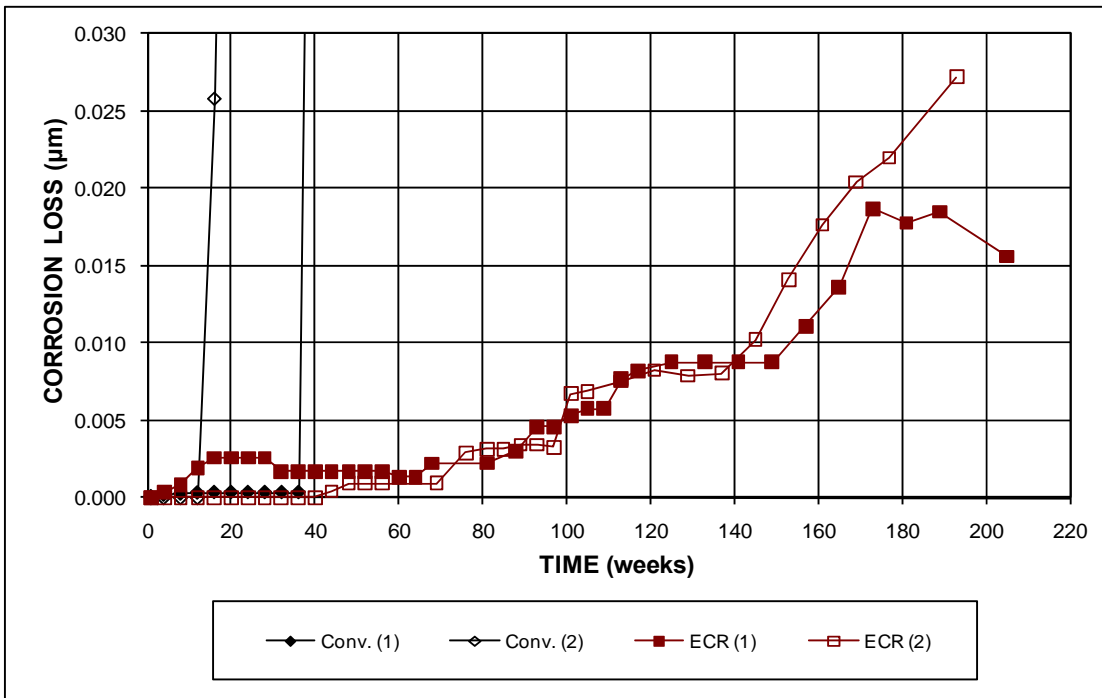


Figure 3.50b – Field Test. Average corrosion losses for specimens with conventional steel and ECR, with cracks (ECR with 16 holes through the epoxy). (Different scale)

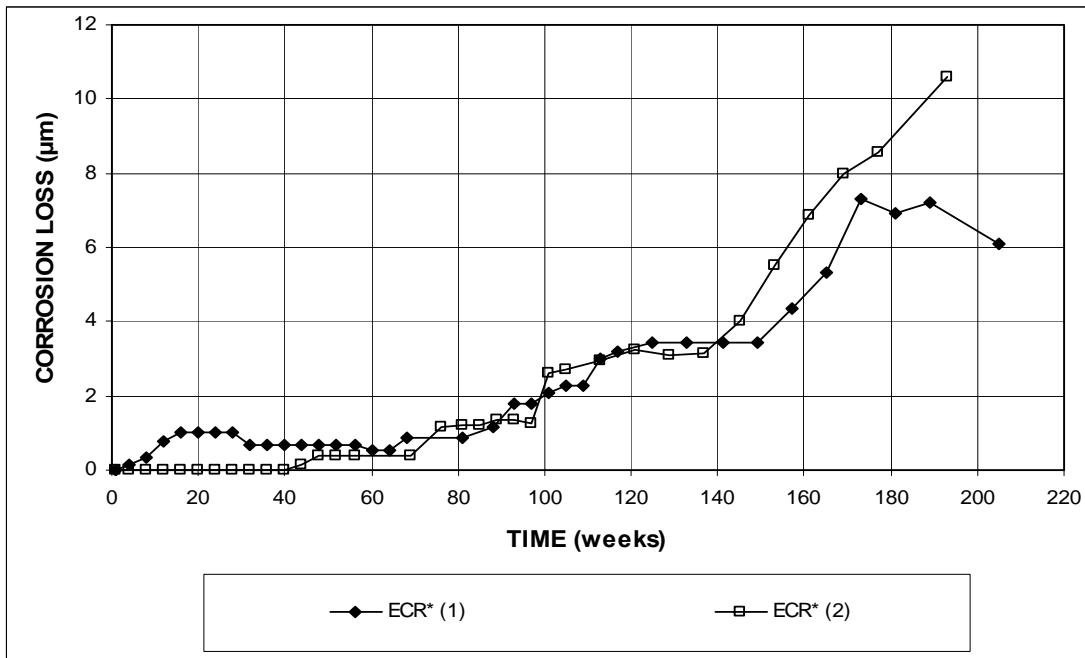


Figure 3.51 – Field Test. Average corrosion losses for specimens with ECR, with cracks. * Based on exposed area (ECR with 16 holes through the epoxy).

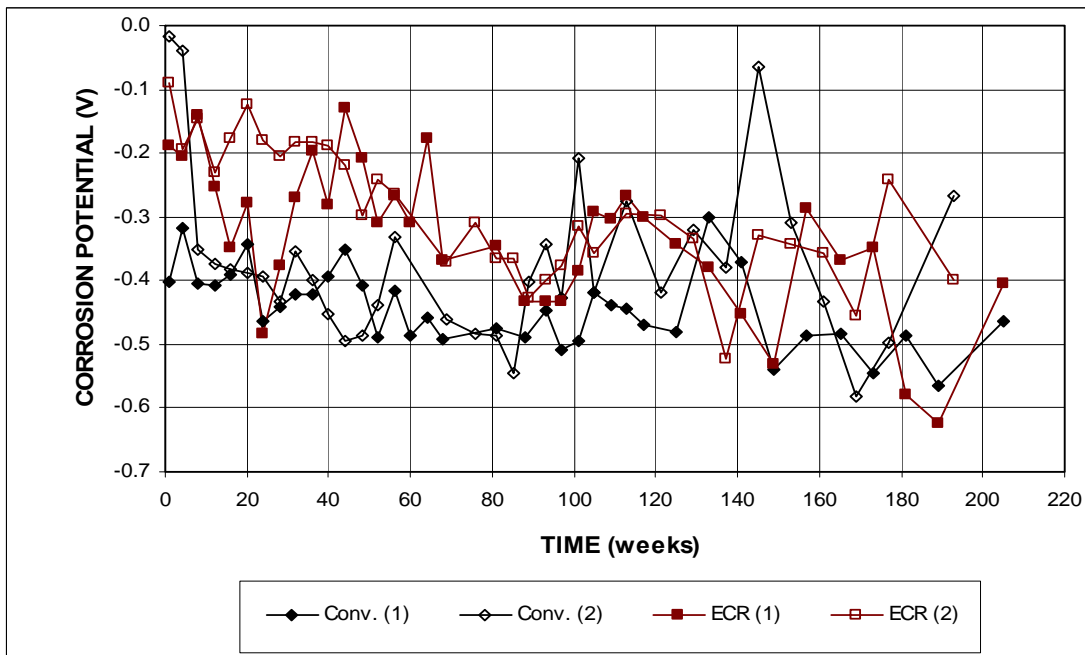


Figure 3.52a – Field Test. Average top mat corrosion potentials with respect to a copper-copper sulfate electrode for specimens with conventional steel and ECR, with cracks (ECR with 16 holes through the epoxy).

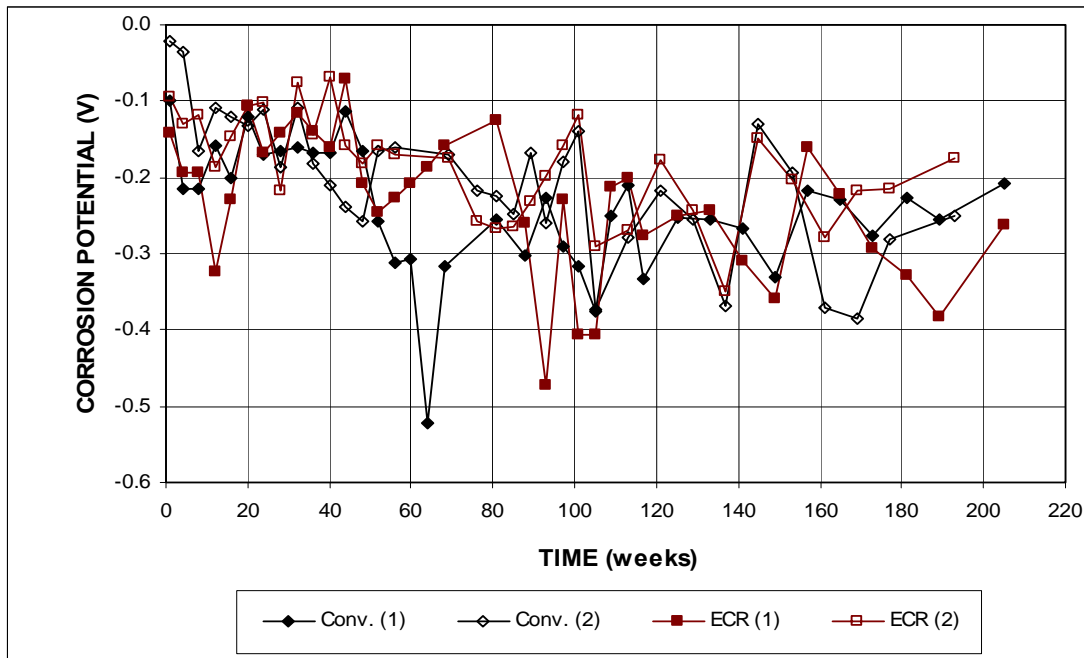


Figure 3.52b – Field Test. Average bottom mat corrosion potentials with respect to a copper-copper sulfate electrode for specimens with conventional steel and ECR, with cracks (ECR with 16 holes through the epoxy).

the exception of specimen Conv. (2) at week 145, which had a top mat bar potential of -0.065 V. The bottom mat potentials fluctuated between -0.068 and -0.325 V before week 109, with the exceptions of Conv. (1) at week 64 and ECR (1) at weeks of 93, and the values fluctuated between -0.130 and -0.400 V after that.

Figure 3.53 shows the mat-to-mat resistance plots for the conventional and ECR specimens with cracks. The mat-to-mat resistances of the ECR specimens increased gradually with time, with values below 1,500 ohms at the beginning of the test and above 6,000 ohms after week 160, except for ECR (1) at week 173, which had a mat-to-mat resistance of 5,490 ohms before again increasing above 6,000 ohms. The conventional steel specimens had values below 22 ohms before week 81, and after that time, the mat-to-mat resistances fluctuated, reaching a value of 7,444 ohms for Conv. (1) at week 105 before again decreasing to values below 3,300 ohms. The

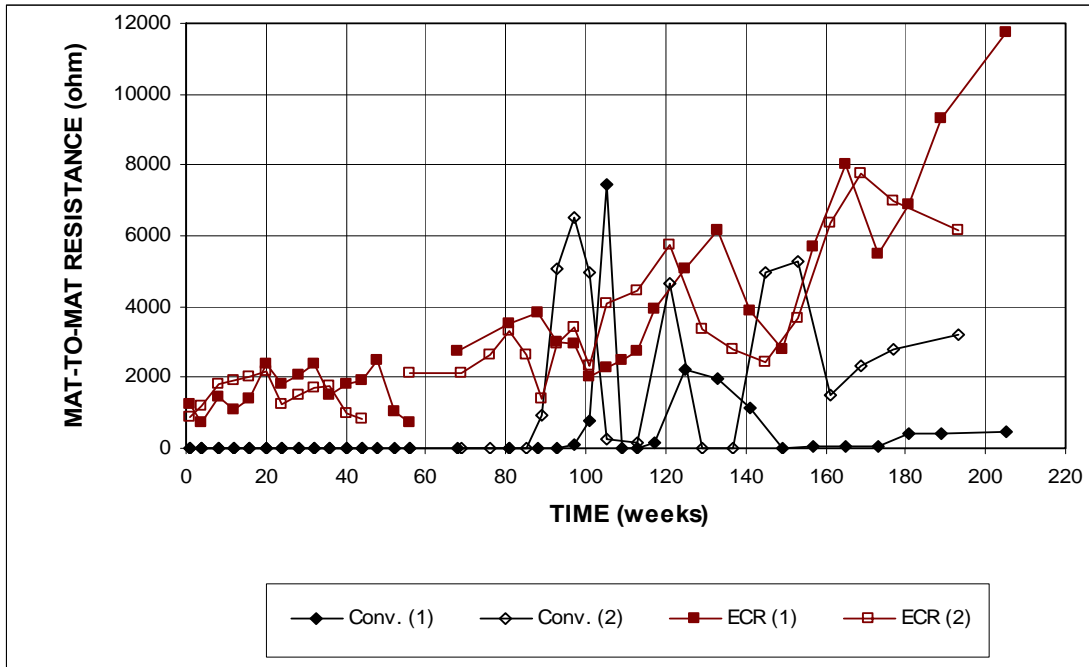


Figure 3.53a – Field Test. Average mat-to-mat resistances for specimens with conventional steel and ECR, with cracks (ECR with 16 holes through the epoxy).

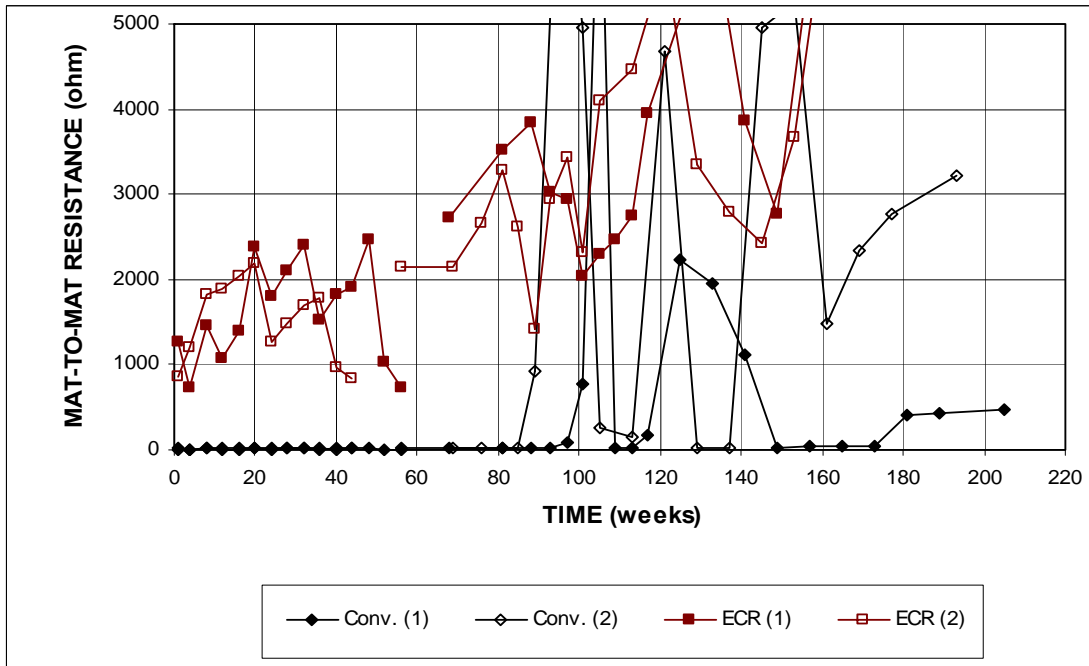


Figure 3.53b – Field Test. Average mat-to-mat resistances for specimens with conventional steel and ECR, with cracks (ECR with 16 holes through the epoxy). (Different scale)

mat-to-mat resistances of ECR specimens are much higher than those of the conventional steel specimens, due to high electrical resistance of the epoxy coating and the very limited exposed area at the holes on the epoxy.

In summary, conventional steel specimens exhibited more active corrosion than the ECR specimens. The average corrosion rate for conventional steel was approximately 60 times the average corrosion rate of ECR in both uncracked and cracked concrete. The corrosion losses of ECR based on exposed area were generally higher than those for uncoated steel. This behavior, however, does not necessarily mean that corrosion losses on damaged regions of ECR were higher than local metal losses due to corrosion on uncoated conventional steel reinforcement, because losses recorded for uncoated conventional steel represent values that are averaged over the full contact surface. In practice, corrosion losses on uncoated bars are not uniformly distributed over the bar surface but, rather, may be much greater in some area than others. In addition, the losses calculated for the coated bars may include losses that occur under the coating, not just on the exposed regions. The average corrosion rates and losses for cracked specimens were approximately twice those of the specimens without cracks for both conventional and ECR specimens.

3.3.2 ECR with Corrosion Inhibitors

This section includes the test results for specimens with ECR in concrete with a primer containing microencapsulated calcium nitrite and ECR in concrete with one of the three inhibitors, DCI, Hycrete, or Rheocrete. Average results as of May 31, 2008 are presented in Figures 3.54 through 3.65. The individual test results are included in Appendices A and B.

3.3.2.1 Field Specimens without Cracks

The average corrosion rates for specimens without simulated cracks are shown in Figures 3.54 and 3.55. All specimens had similar corrosion rates, with values less than 0.04 and 15.00 $\mu\text{m}/\text{yr}$ based on total and exposed area, respectively, except for two readings: ECR(primer/Ca(NO₂)₂) (1) had the highest corrosion rate of 0.05 and 18.32 $\mu\text{m}/\text{yr}$ at week 161, followed by ECR(Hycrete) (1) with corrosion rates of 0.04 and 15.80 $\mu\text{m}/\text{yr}$ at week 105 based on total and exposed area, respectively. Some specimens exhibited negative corrosion, especially ECR(Rheocrete) (1) and (2) and ECR(primer/Ca(NO₂)₂) (1) during the test period between weeks 40 and 140. ECR(Rheocrete) (1) had the most negative corrosion rate, -0.03 and $-12.36 \mu\text{m}/\text{yr}$ at week 89 based on total and exposed area, respectively. Again, the specimens exhibit far more fluctuations in corrosion rate than those do bench-scale specimens due to changes in the concrete moisture content caused by the outdoor exposure.

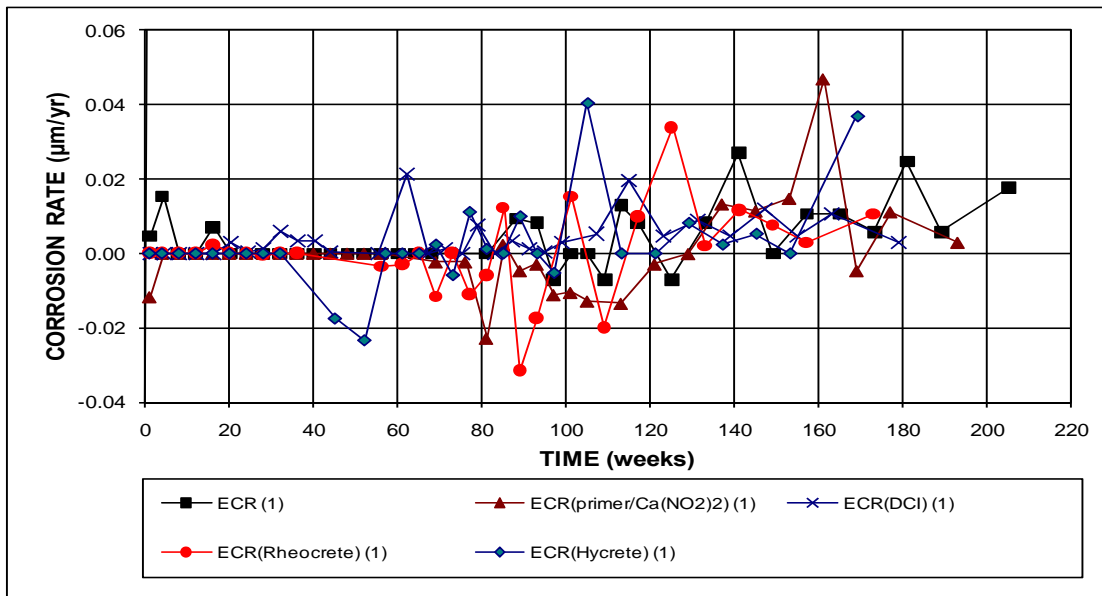


Figure 3.54a – Field Test. Average corrosion rates for specimens with ECR, ECR with a primer containing calcium nitrite, and ECR with corrosion inhibitors in concrete, without cracks, specimen No. 1. (ECR with 16 holes through the epoxy)

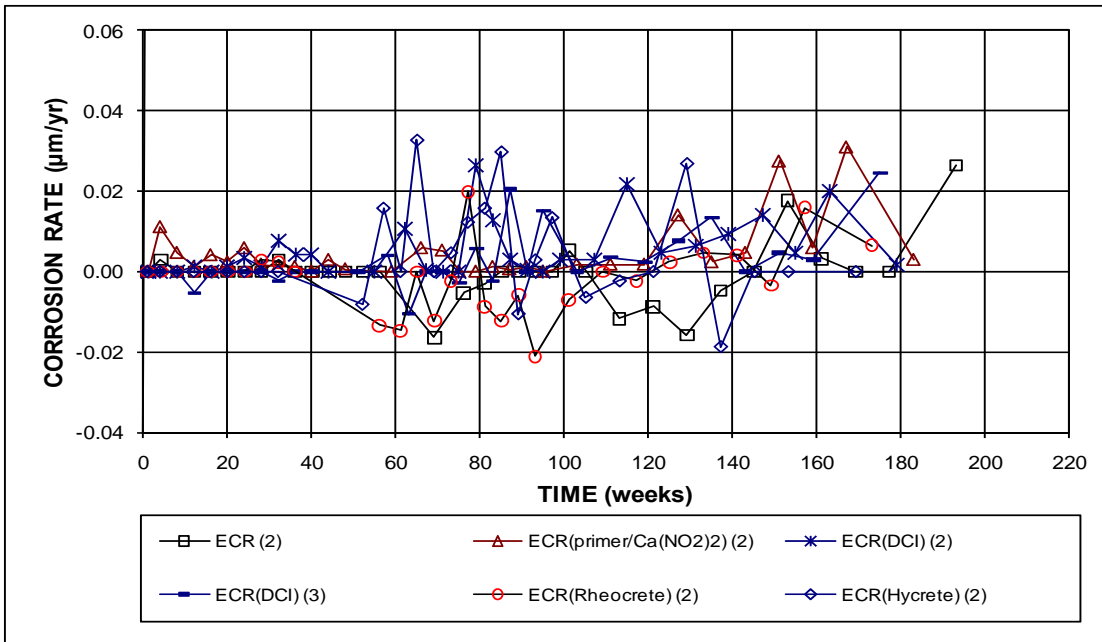


Figure 3.54b – Field Test. Average corrosion rates for specimens with ECR, ECR with a primer containing calcium nitrite, and ECR with corrosion inhibitors in concrete, without cracks, specimen No. 2 and 3. (ECR with 16 holes through the epoxy)

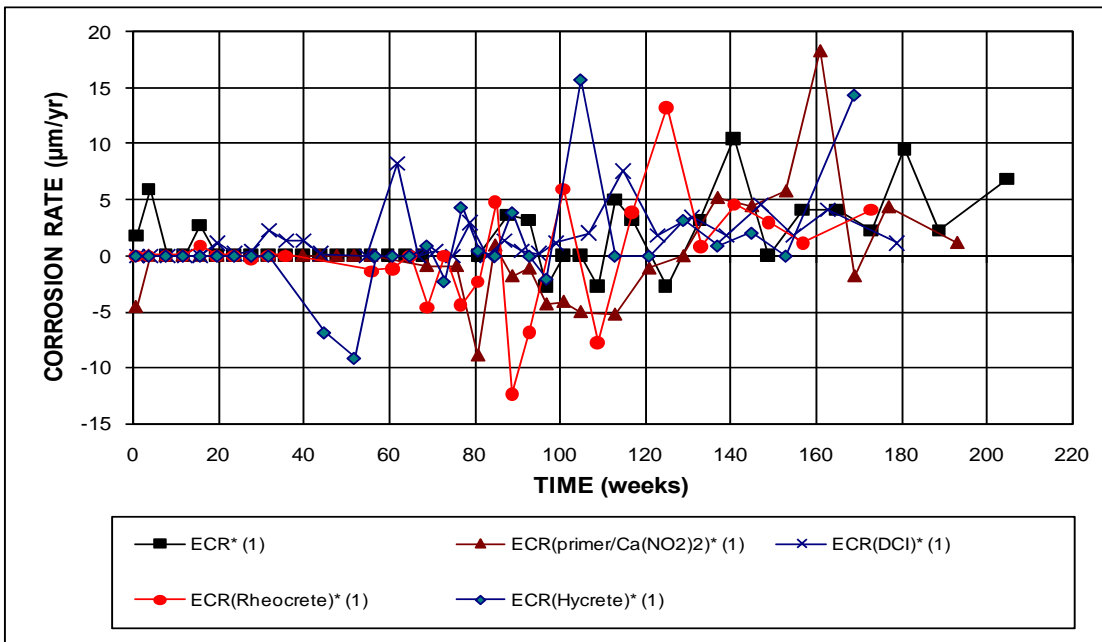


Figure 3.55a – Field Test. Average corrosion rates for specimens with ECR, ECR with a primer containing calcium nitrite, and ECR with corrosion inhibitors in concrete, without cracks, specimen No. 1. * Based on exposed area (ECR with 16 holes through the epoxy)

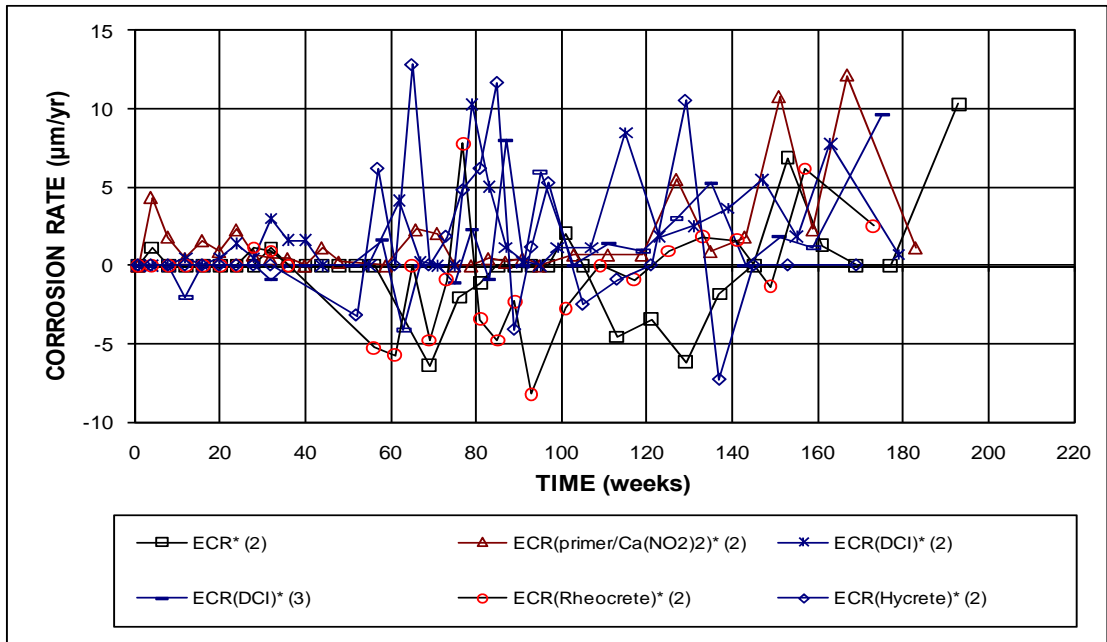


Figure 3.55b – Field Test. Average corrosion rates for specimens with ECR, ECR with a primer containing calcium nitrite, and ECR with corrosion inhibitors in concrete, without cracks, specimen No. 2 and 3.
 * Based on exposed area (ECR with 16 holes through the epoxy)

The average corrosion losses are shown in Figures 3.56 and 3.57 and are summarized in Table 3.8. ECR(DCI) (1) and (2) had higher corrosion losses than ECR (1) and (2) after week 60. The average corrosion losses for ECR(Rheocrete) (2) were consistently negative after initiation; while the average corrosion losses for ECR(Rheocrete) (1), ECR(primer/Ca(NO₂)₂) (1), and ECR(Hycrete) (1) shifted from negative to positive between weeks 120 and 160, and continued with values below ECR(1) and above ECR(2), except ECR(Hycrete) (1) at week 169, which had a corrosion loss slightly higher than ECR(1) (0.01 and 5.27 µm based on total and exposed area, respectively). As shown in Table 3.8, all of the specimens had average corrosion losses of no more than 0.02 for ages ranging from 163 to 175 weeks based on total area and 7.67 µm based on exposed area. ECR(DCI) (2) exhibited the highest corrosion loss of 7.67 µm based on exposed area at week 163, followed by

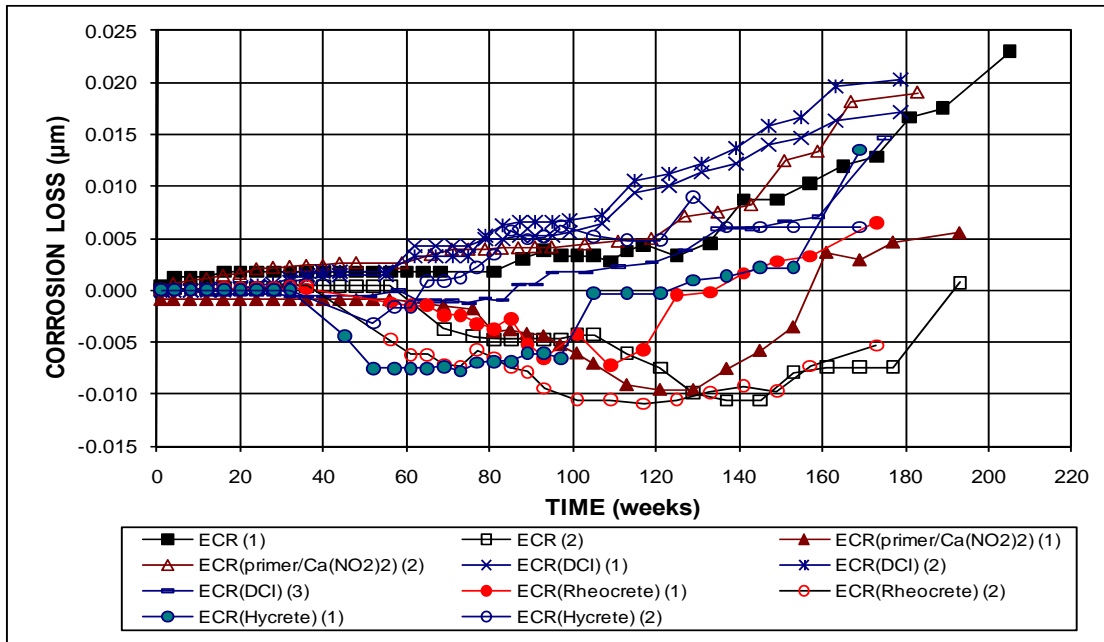


Figure 3.56 – Field Test. Average corrosion losses for specimens with ECR, ECR with a primer containing calcium nitrite, and ECR with corrosion inhibitors in concrete, without cracks (ECR with 16 holes through the epoxy).

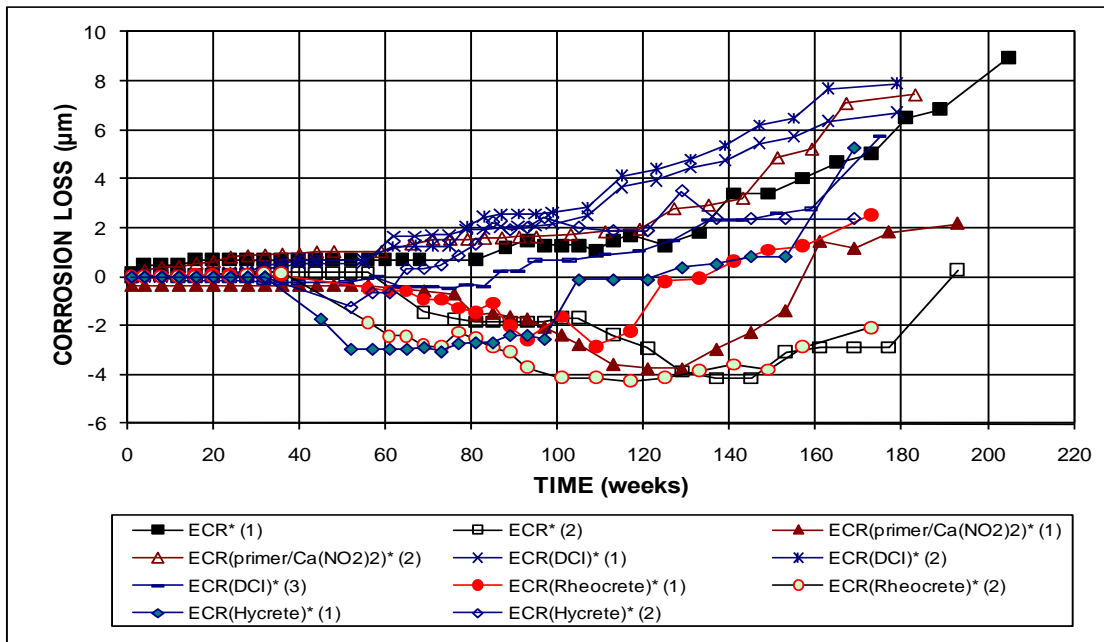


Figure 3.57 – Field Test. Average corrosion losses for specimens with ECR, ECR with a primer containing calcium nitrite, and ECR with corrosion inhibitors in concrete, without cracks. * Based on exposed area (ECR with 16 holes through the epoxy).

Table 3.8 – Corrosion losses for ECR with a primer containing calcium nitrite and ECR with corrosion inhibitors in the field test, without cracks

Corrosion Inhibitors without Cracks							
Steel Designation ^a	Exposure time (weeks)	Test Bar Corrosion Losses (μm)				Average	Standard Deviation
		1	2	3	4		
Based on Total Area							
ECR(primer/Ca(NO ₂) ₂) (1)	169	-0.01	0.01	0.03	-0.01	β	0.02
ECR(primer/Ca(NO ₂) ₂) (2)	167	0.04	0.01	0.01	0.01	0.02	0.01
ECR(DCI) (1)	163	0.01	0.02	0.02	0.02	0.02	β
ECR(DCI) (2)	163	0.03	0.03	0.02	0.01	0.02	0.01
ECR(DCI) (3)	175	0.01	0.03	β	0.02	0.01	0.01
ECR(Rheocrete) (1)	173	β	0.03	-0.01	β	0.01	0.02
ECR(Rheocrete) (2)	173	β	-0.02	-0.01	β	-0.01	0.01
ECR(Hycrete) (1)	169	β	β	0.02	0.03	0.01	0.01
ECR(Hycrete) (2)	169	0.01	β	β	0.01	0.01	β
Based on Exposed Area							
ECR(primer/Ca(NO ₂) ₂)* (1)	169	-3.80	4.21	9.97	-5.78	1.15	7.29
ECR(primer/Ca(NO ₂) ₂)* (2)	167	13.75	4.56	4.17	5.83	7.08	4.51
ECR(DCI)* (1)	163	4.14	7.77	7.57	5.95	6.36	1.69
ECR(DCI)* (2)	163	10.32	10.53	7.75	2.10	7.67	3.93
ECR(DCI)* (3)	175	3.80	10.44	1.46	7.17	5.72	3.92
ECR(Rheocrete)* (1)	173	0.26	11.84	-3.24	1.27	2.53	6.50
ECR(Rheocrete)* (2)	173	0.35	-7.91	-1.97	1.20	-2.08	4.11
ECR(Hycrete)* (1)	169	1.23	1.53	5.97	12.36	5.27	5.20
ECR(Hycrete)* (2)	169	2.54	1.06	1.50	4.40	2.37	1.49

^a ECR = conventional epoxy-coated reinforcement.

All ECRs have 16 3-mm (¹/₈-in.) diameter holes through the epoxy.

ECR(primer/Ca(NO₂)₂) = ECR with a primer containing calcium nitrite.

ECR(DCI) = conventional ECR with DCI inhibitor in concrete.

ECR(Rheocrete) = conventional ECR with Rheocrete inhibitor in concrete.

ECR(Hycrete) = conventional ECR with Hycrete inhibitor in concrete.

* Based on exposed area.

β Corrosion loss (absolute value) less than 0.005 μm .

ECR(primer/Ca(NO₂)₂) (2) with 7.08 μm at week 167 and ECR(DCI) (1) with 6.36 μm at week 163. Only specimen ECR(Rheocrete) (2), showed a negative average corrosion loss, -2.08 μm at week 173.

The average corrosion potentials with respect to a CSE are shown in Figure 3.58. Both the top and bottom mat corrosion potentials for all specimens slowly shifted in the negative direction with time. ECR(DCI) (1) and (3), ECR(Rheocrete) (2), and ECR(Hycrete) (1) and (2) exhibited top mat corrosion potentials that were

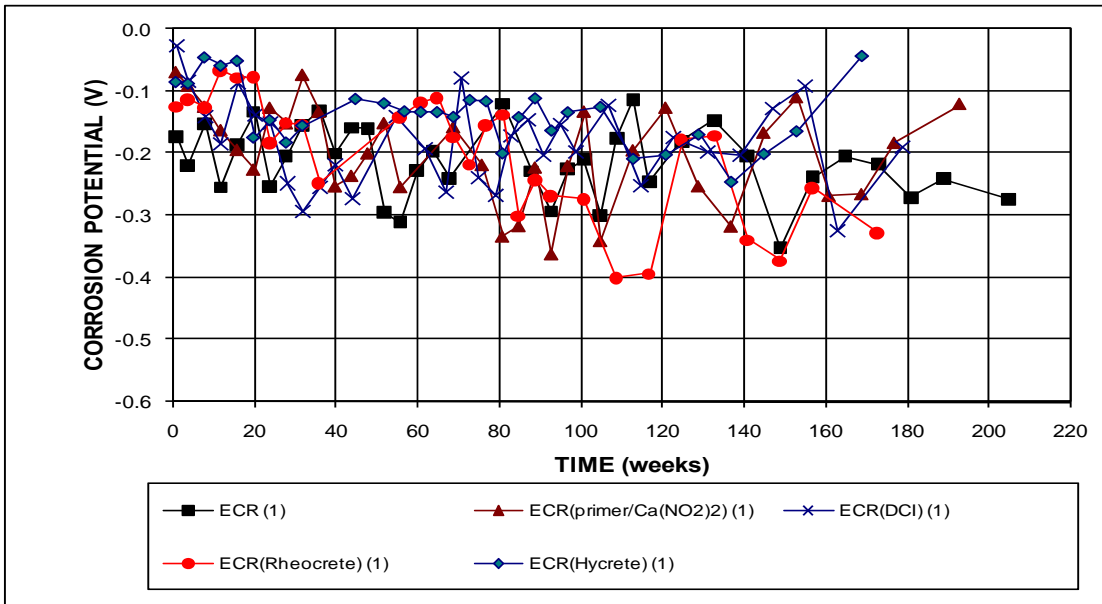


Figure 3.58a – Field Test. Average top mat corrosion potentials with respect to a copper-copper sulfate electrode for specimens with ECR, ECR with a primer containing calcium nitrite, and ECR with corrosion inhibitors in concrete, without cracks, specimen No. 1. (ECR with 16 holes through the epoxy)

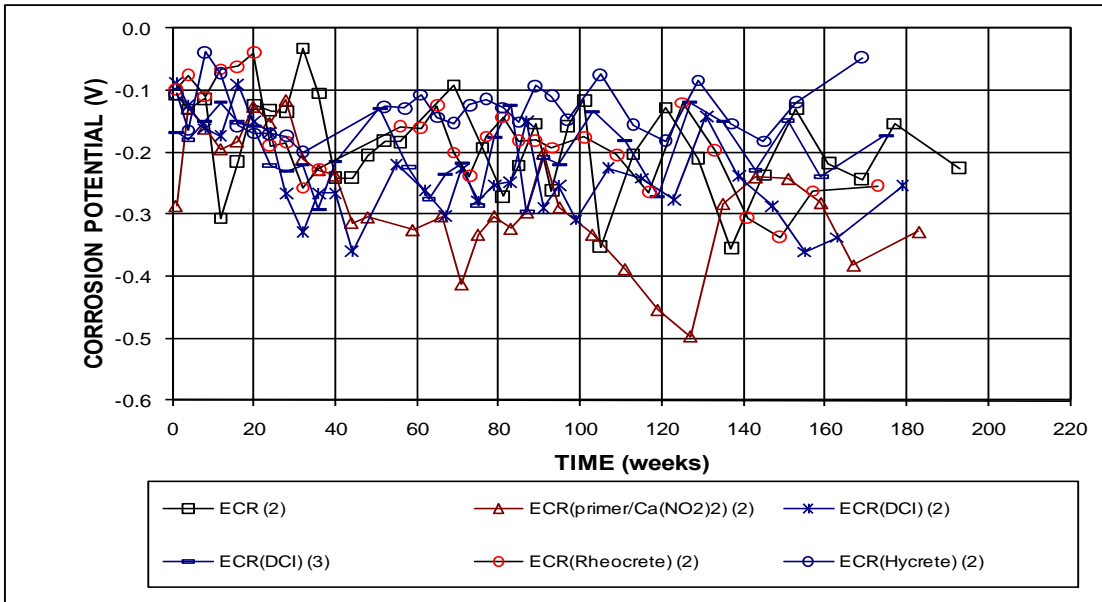


Figure 3.58b – Field Test. Average top mat corrosion potentials with respect to a copper-copper sulfate electrode for specimens with ECR, ECR with a primer containing calcium nitrite, and ECR with corrosion inhibitors in concrete, without cracks, specimen No. 2 and 3. (ECR with 16 holes through the epoxy)

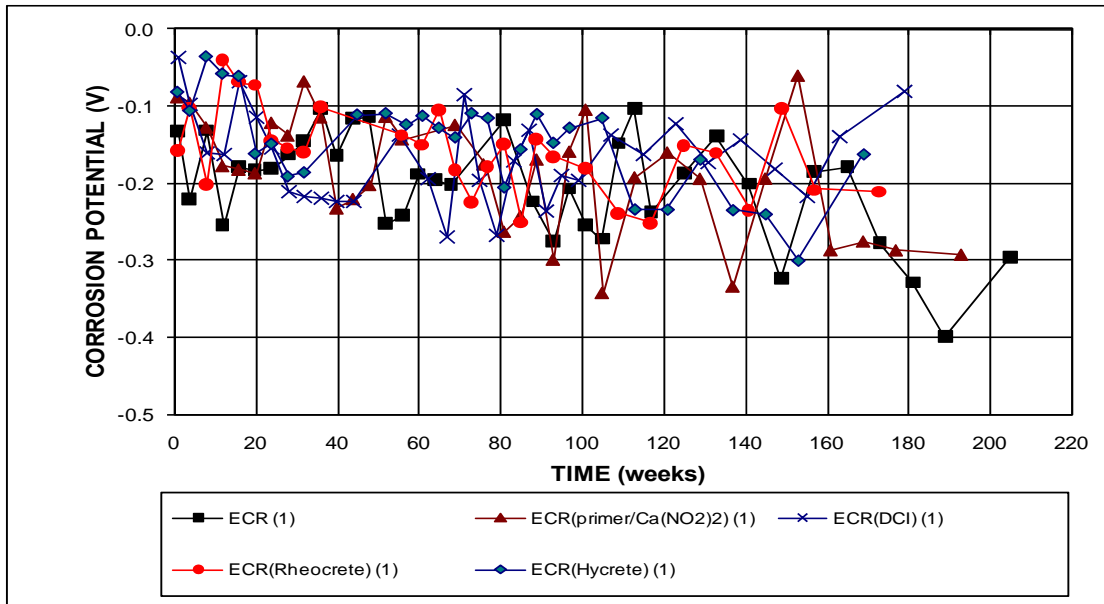


Figure 3.58c – Field Test. Average bottom mat corrosion potentials with respect to a copper-copper sulfate electrode for specimens with ECR, ECR with a primer containing calcium nitrite, and ECR with corrosion inhibitors in concrete, without cracks, specimen No. 1. (ECR with 16 holes through the epoxy)

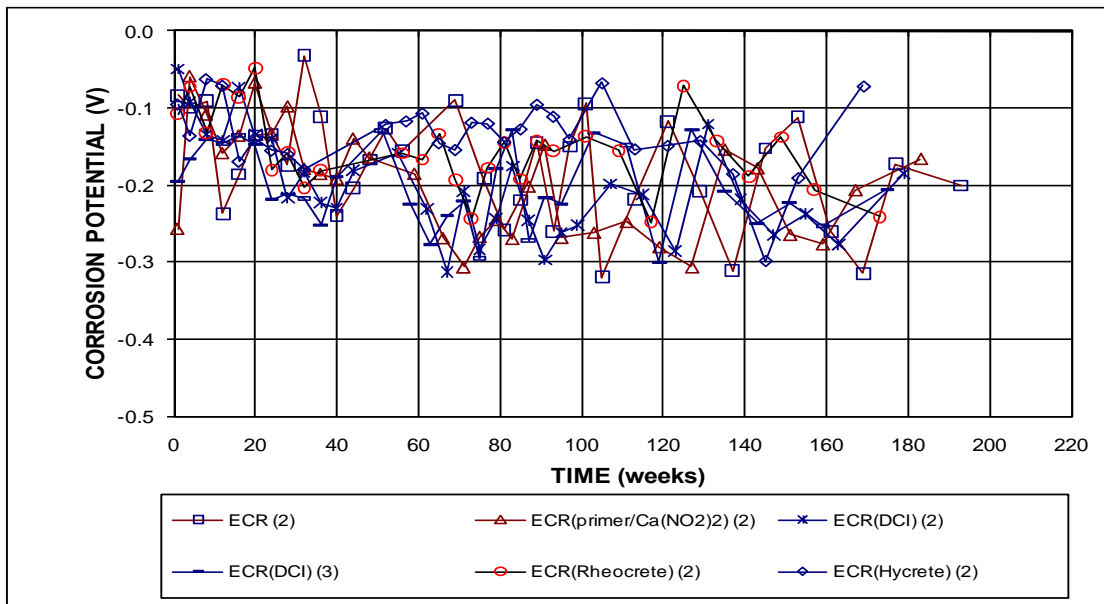


Figure 3.58d – Field Test. Average bottom mat corrosion potentials with respect to a copper-copper sulfate electrode for specimens with ECR, ECR with a primer containing calcium nitrite, and ECR with corrosion inhibitors in concrete, without cracks, specimen No. 2 and 3. (ECR with 16 holes through the epoxy)

more positive than -0.350 V throughout the test period; while the other specimens had corrosion potentials that were occasionally below -0.350 V. For the bottom mat, only conventional ECR (1) had a corrosion potential between -0.350 and -0.400 V at week 189 only, while the corrosion potentials for all other specimens were consistently above -0.350 V.

Figure 3.59 shows the average mat-to-mat resistance for inhibitor specimens without cracks. The ECR(Hycrete) specimens had the highest resistances during a majority of the test period, with values between 5,000 and 10,000 ohms from week 40 to 69 and between 10,000 to 18,000 ohms from week 73 to 140. After week 140, the values dropped to a range of between 6,000 to 11,000 ohms, but were still higher than the majority of the other specimens. ECR(Rheocrete) (1) had several high “spike” values of resistance at weeks 61 (9,458 ohms), 101 (9,794 ohms), and 149 (19,723 ohms).

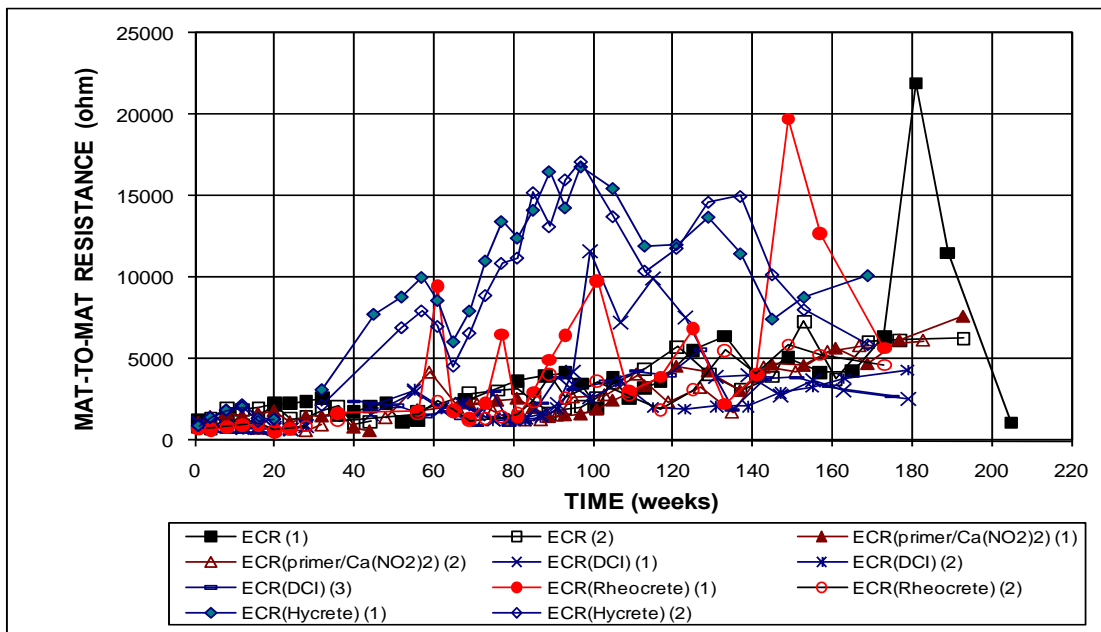


Figure 3.59 – Field Test. Average mat-to-mat resistances for specimens with ECR, ECR with a primer containing calcium nitrite, and ECR with corrosion inhibitors in concrete, without cracks (ECR with 16 holes through the epoxy).

ohms). The resistance of ECR(DCI) (1) had a sharp increase between week 99 and 123. ECR (1) had “spike” values of resistance, 21,941 and 11,518 ohms at weeks 173 and 199, respectively. The resistances for the other specimens increased progressively from 1,000 to 6,000 ohms during their test period.

3.3.2.2 Field Specimens with Cracks

The average corrosion rates for the specimens with simulated cracks are shown in Figures 3.60 and 3.61. Most specimens had values ranging from -0.02 to 0.04 $\mu\text{m}/\text{yr}$ based on total area, and from -5.00 to 15.00 $\mu\text{m}/\text{yr}$ based on exposed area. ECR(DCI) (2) had the highest corrosion rate, 20.38 $\mu\text{m}/\text{yr}$ based on exposed area at week 24, followed by ECR(primer/Ca(NO₂)₂) (1) with 18.48 $\mu\text{m}/\text{yr}$ at week 161, ECR (2) with 17.40 $\mu\text{m}/\text{yr}$ at week 101, and ECR(Rheocrete) (2) with 16.94 $\mu\text{m}/\text{yr}$ at

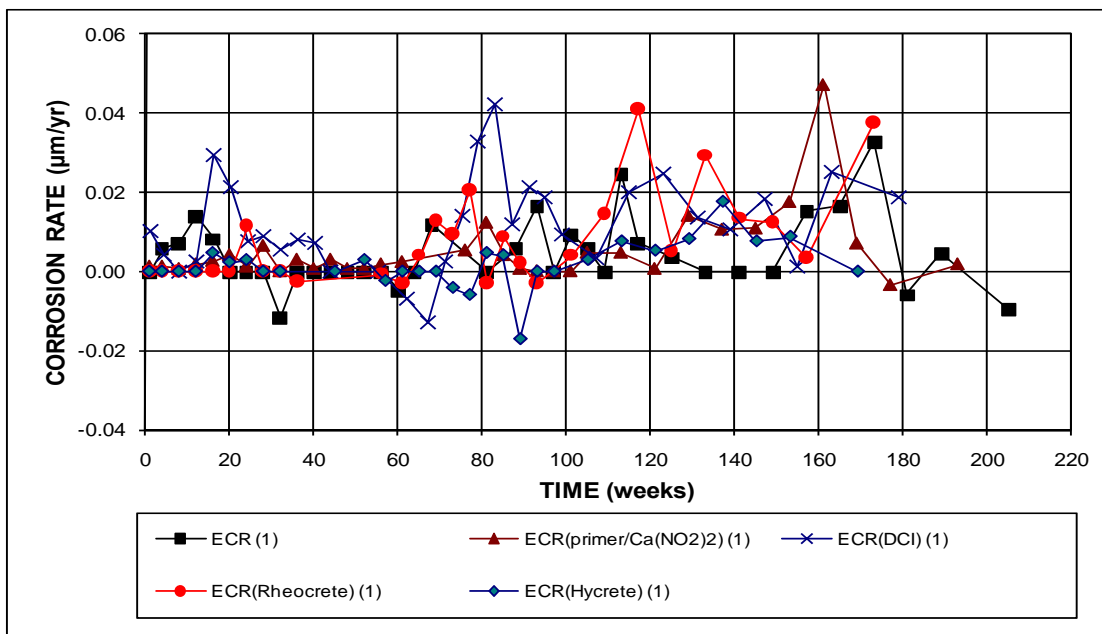


Figure 3.60a – Field Test. Average corrosion rates for specimens with ECR, ECR with a primer containing calcium nitrite, and ECR with corrosion inhibitors in concrete, with cracks, specimen No. 1. (ECR with 16 holes through the epoxy)

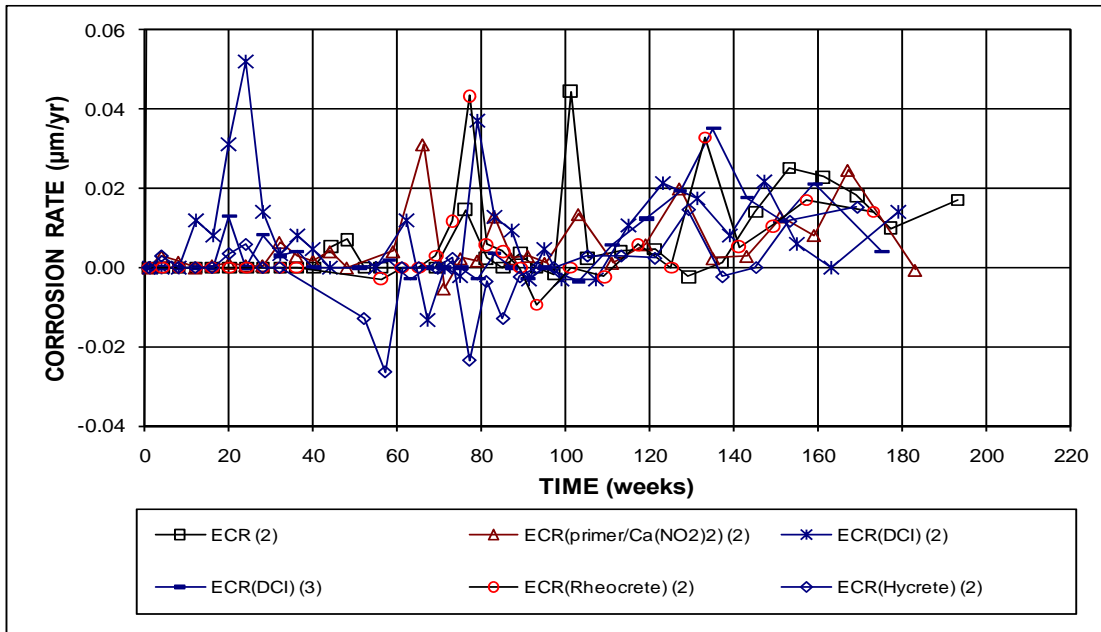


Figure 3.60b – Field Test. Average corrosion rates for specimens with ECR, ECR with a primer containing calcium nitrite, and ECR with corrosion inhibitors in concrete, with cracks, specimen No. 2 and 3. (ECR with 16 holes through the epoxy)

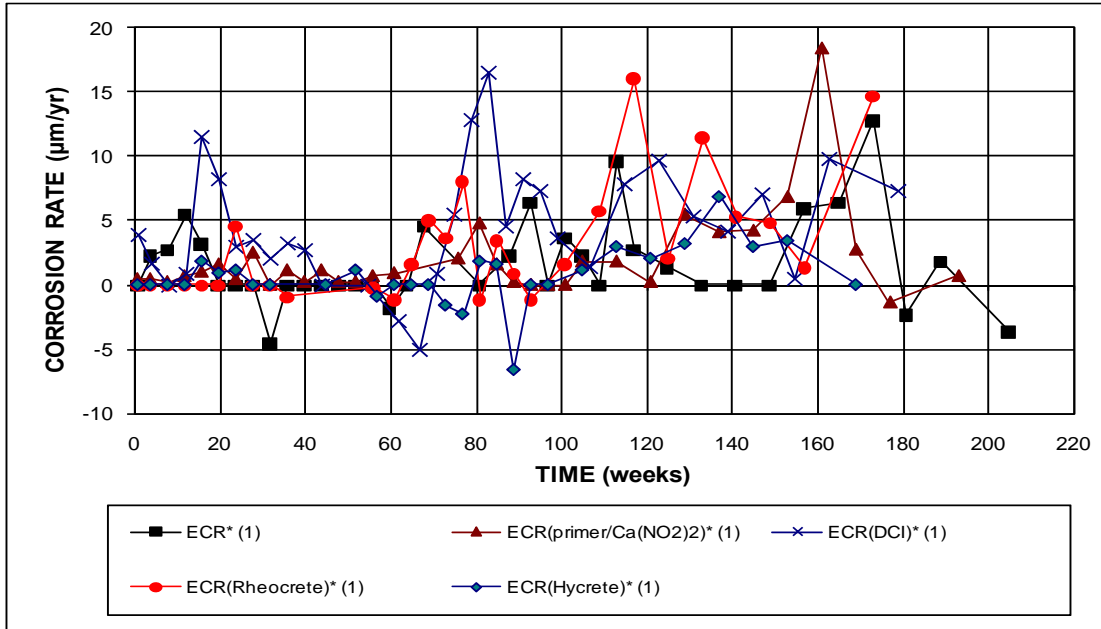


Figure 3.61a – Field Test. Average corrosion rates for specimens with ECR, ECR with a primer containing calcium nitrite, and ECR with corrosion inhibitors in concrete, with cracks, specimen No. 1. * Based on exposed area (ECR with 16 holes through the epoxy)

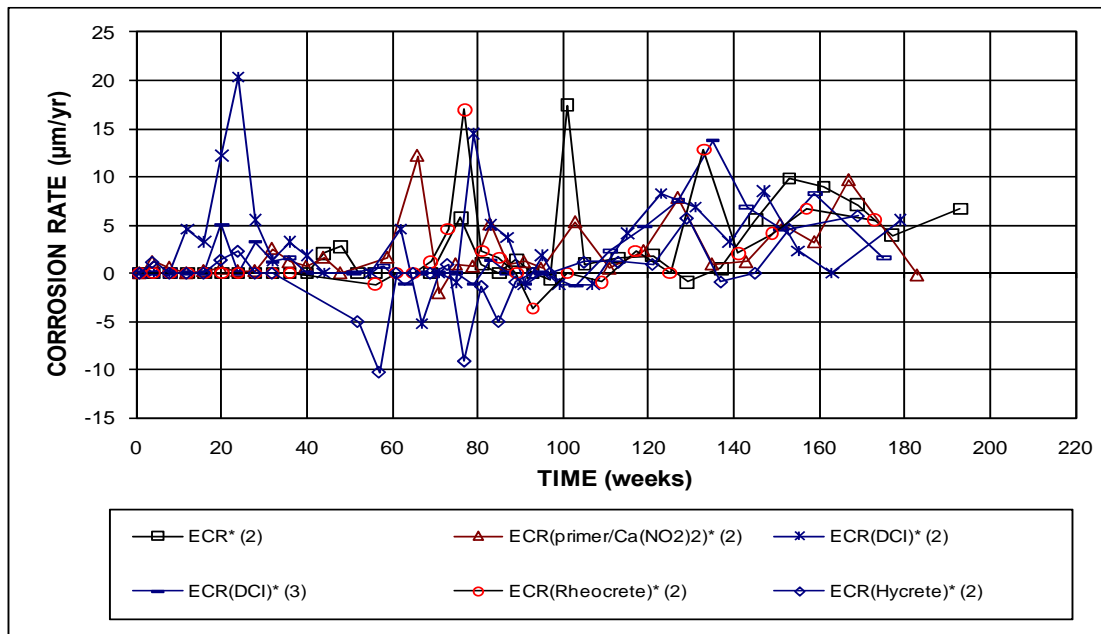


Figure 3.61b – Field Test. Average corrosion rates for specimens with ECR, ECR with a primer containing calcium nitrite, and ECR with corrosion inhibitors in concrete, with cracks, specimen No. 2 and 3. * Based on exposed area (ECR with 16 holes through the epoxy)

week 77. Negative corrosion rates were observed for some specimens, especially ECR(Hycrete) (1) and (2), and ECR(DCI) (1) during the test period between week 52 and 89.

The average corrosion losses are shown in Figures 3.62 and 3.63, based on total and exposed area, respectively, and summarized in Table 3.9. ECR(DCI) (1) and (2), ECR(primer/Ca(NO₂)₂) (2), and ECR(Rheocrete) (1) had higher corrosion losses than ECR after weeks 20, 60, and 110, respectively, except ECR(primer/Ca(NO₂)₂) (2) had a slightly lower value than ECR(2) at week 183. The corrosion losses of ECR(DCI) (3), ECR(primer/Ca(NO₂)₂) (1), and ECR(Rheocrete) (2) were about the same as ECR during the test period, while those of Hycrete (1) and (2) were lower than ECR. ECR(Hycrete) (2) exhibited negative corrosion losses for all times after initiating at week 52, becoming first more negative and then less negative, and reaching 0 at week 169 (the last date for which data was recorded). The average corrosion losses for the

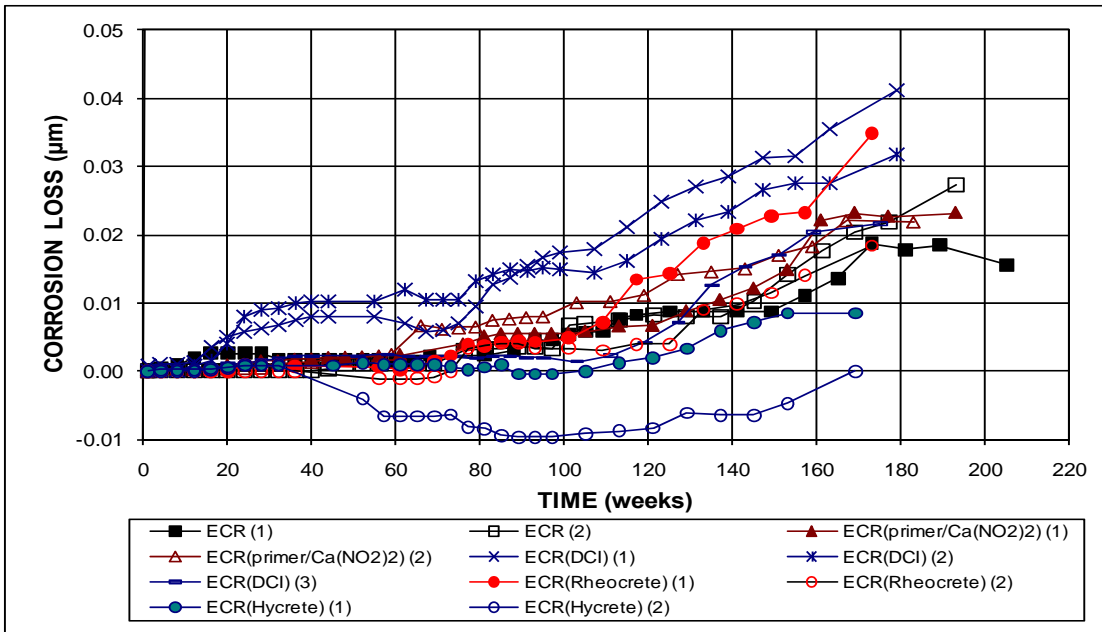


Figure 3.62 – Field Test. Average corrosion losses for specimens with ECR, ECR with a primer containing calcium nitrite, and ECR with corrosion inhibitors in concrete, with cracks (ECR with 16 holes through the epoxy).

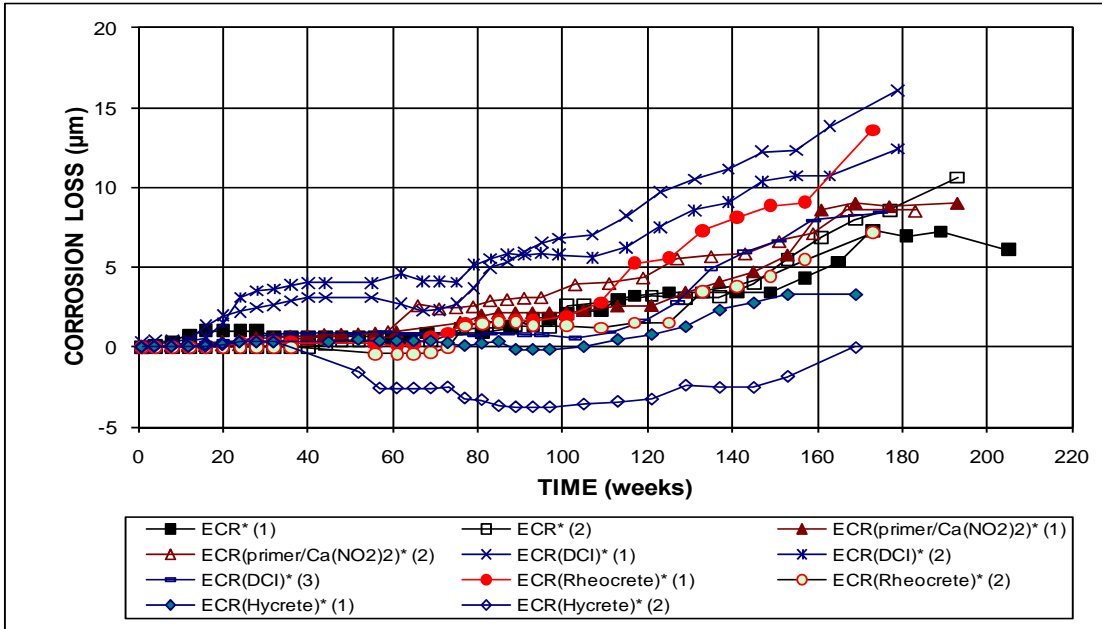


Figure 3.63 – Field Test. Average corrosion losses for specimens with ECR, ECR with a primer containing calcium nitrite, and ECR with corrosion inhibitors in concrete, with cracks. * Based on exposed area (ECR with 16 holes through the epoxy).

Table 3.9 – Corrosion losses for ECR with a primer containing calcium nitrite and ECR with corrosion inhibitors in the field test, with simulated cracks

Corrosion Inhibitors with Cracks							
Steel Designation ^a	Exposure time (weeks)	Test Bar Corrosion Losses (µm)				Average	Standard Deviation
		1	2	3	4		
Based on Total Area							
ECR(primer/Ca(NO ₂) ₂) (1)	169	0.01	0.02	0.04	0.02	0.02	0.01
ECR(primer/Ca(NO ₂) ₂) (2)	167	0.01	0.02	0.02	0.04	0.02	0.01
ECR(DCI) (1)	163	0.03	0.04	0.04	0.03	0.04	0.01
ECR(DCI) (2)	163	0.02	β	0.05	0.05	0.03	0.02
ECR(DCI) (3)	175	0.06	0.03	β	0.01	0.02	0.03
ECR(Rheocrete) (1)	173	0.04	0.07	0.02	0.02	0.03	0.02
ECR(Rheocrete) (2)	173	0.01	0.02	0.03	0.02	0.02	0.01
ECR(Hycrete) (1)	169	0.03	0.01	-0.01	β	0.01	0.02
ECR(Hycrete) (2)	169	-0.01	0.02	-0.01	-0.01	β	0.02
Based on Exposed Area							
ECR(primer/Ca(NO ₂) ₂)* (1)	169	2.84	9.67	14.72	8.95	9.04	4.87
ECR(primer/Ca(NO ₂) ₂)* (2)	167	2.99	8.61	8.37	14.55	8.63	4.72
ECR(DCI)* (1)	163	11.06	14.57	16.33	13.35	13.83	2.21
ECR(DCI)* (2)	163	6.60	-0.88	18.46	18.74	10.73	9.59
ECR(DCI)* (3)	175	21.70	10.92	-1.06	2.18	8.44	10.19
ECR(Rheocrete)* (1)	173	15.64	25.68	6.80	6.25	13.59	9.13
ECR(Rheocrete)* (2)	173	3.80	7.04	9.79	8.03	7.17	2.51
ECR(Hycrete)* (1)	169	11.41	4.91	-2.61	-0.49	3.31	6.26
ECR(Hycrete)* (2)	169	-1.99	9.26	-4.91	-2.40	-0.01	6.32

^a ECR = conventional epoxy-coated reinforcement.

All ECRs have 16 3-mm (¹/₈-in.) diameter holes through the epoxy.

ECR(primer/Ca(NO₂)₂) = ECR with a primer containing calcium nitrite.

ECR(DCI) = conventional ECR with DCI inhibitor in concrete.

ECR(Rheocrete) = conventional ECR with Rheocrete inhibitor in concrete.

ECR(Hycrete) = conventional ECR with Hycrete inhibitor in concrete.

* Based on exposed area.

β Corrosion loss (absolute value) less than 0.005 µm.

majority of specimens with cracks were slightly higher than those of specimens without cracks, with the highest value of 0.04 µm for ECR(DCI) (1) at week 163 based on total area and 13.83 µm based on exposed area, followed by ECR(Rheocrete) (1) with 0.03 and 13.59 µm at week 173, and ECR(DCI) (2) with 0.02 and 10.73 µm at week 163 based on total and exposed area, respectively. Only specimen, ECR(Hycrete) (2), showed negative average corrosion loss during the test

period and reached 0 and $-0.01 \mu\text{m}$ at week 169 based on total and exposed area, respectively.

The average corrosion potentials with respect to CSE are shown in Figure 3.64. Specimens with cracks had more negative top mat corrosion potentials than specimens without cracks, with a majority of values ranging between -0.050 and -0.400 V before week 60 and between -0.200 and -0.600 V after that. ECR(Rheocrete) (1) had the most negative top mat corrosion potential with a value of -0.769 V at week 149. The majority of the bottom mat corrosion potentials ranged from -0.100 and -0.400 V, except ECR(Rheocrete) (1) at week 157 and conventional ECR (1) at weeks 97, 101 and 105 had more negative corrosion potentials than -0.400 V for the bottom mats of steel.

Figure 3.65 shows the average mat-to-mat resistance for specimens with cracks.

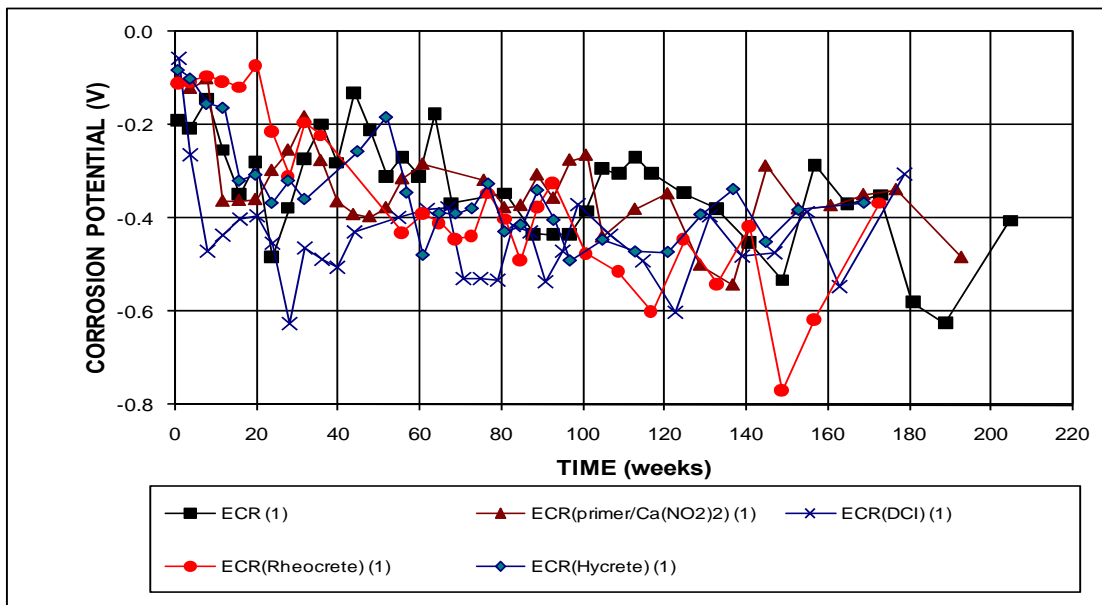


Figure 3.64a – Field Test. Average top mat corrosion potentials with respect to a copper-copper sulfate electrode for specimens with ECR, ECR with a primer containing calcium nitrite, and ECR with corrosion inhibitors in concrete, with cracks, specimen No. 1. (ECR with 16 holes through the epoxy)

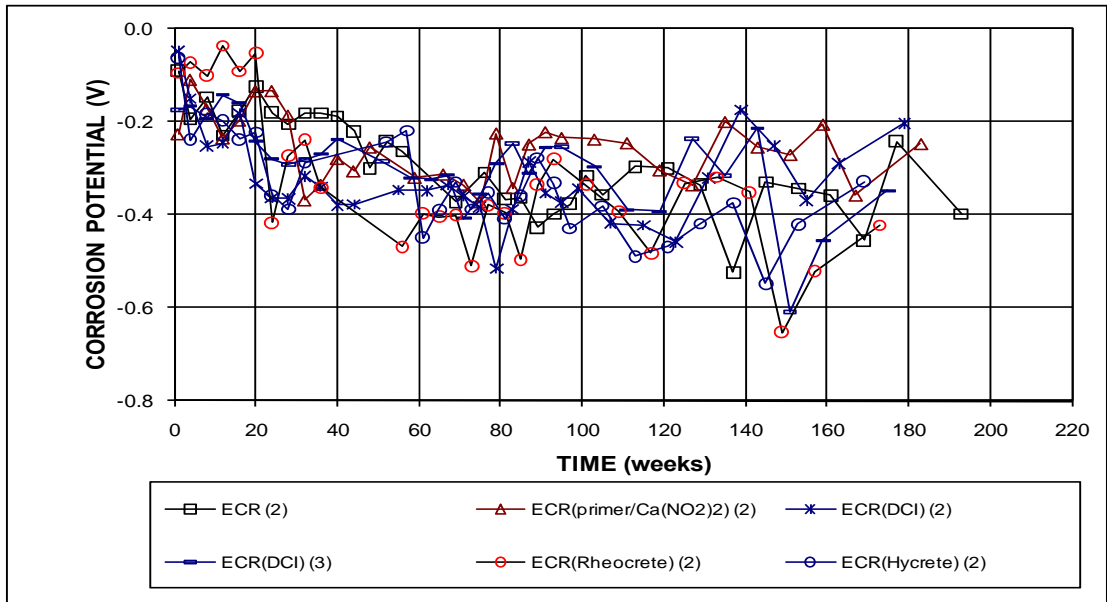


Figure 3.64b – Field Test. Average top mat corrosion potentials with respect to a copper-copper sulfate electrode for specimens with ECR, ECR with a primer containing calcium nitrite, and ECR with corrosion inhibitors in concrete, with cracks, specimen No. 2 and 3. (ECR with 16 holes through the epoxy)

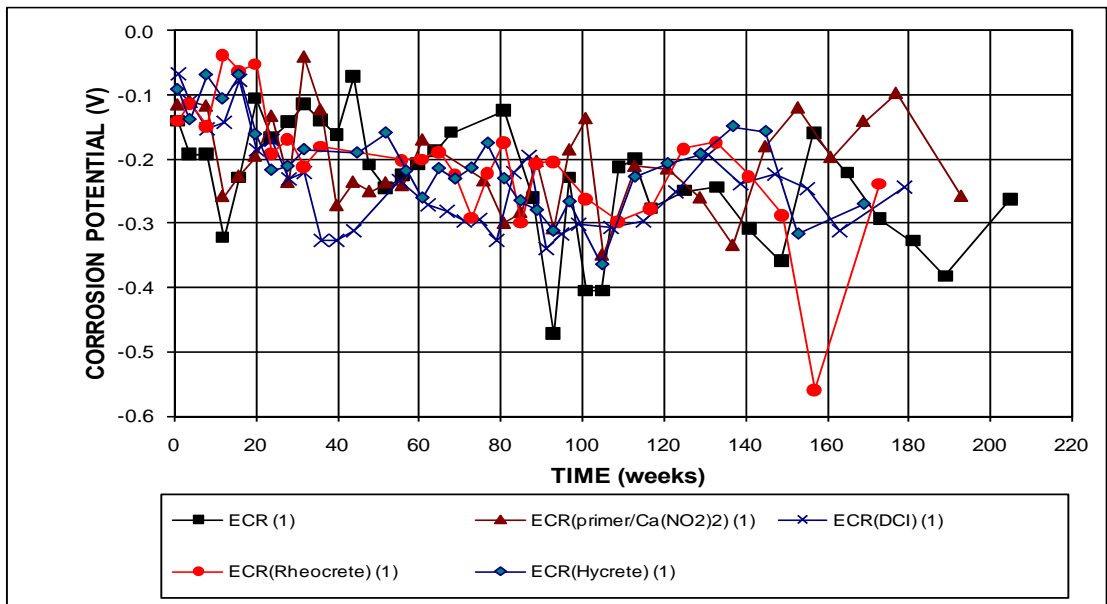


Figure 3.64c – Field Test. Average bottom mat corrosion potentials with respect to a copper-copper sulfate electrode for specimens with ECR, ECR with a primer containing calcium nitrite, and ECR with corrosion inhibitors in concrete, with cracks, specimen No. 1. (ECR with 16 holes through the epoxy)

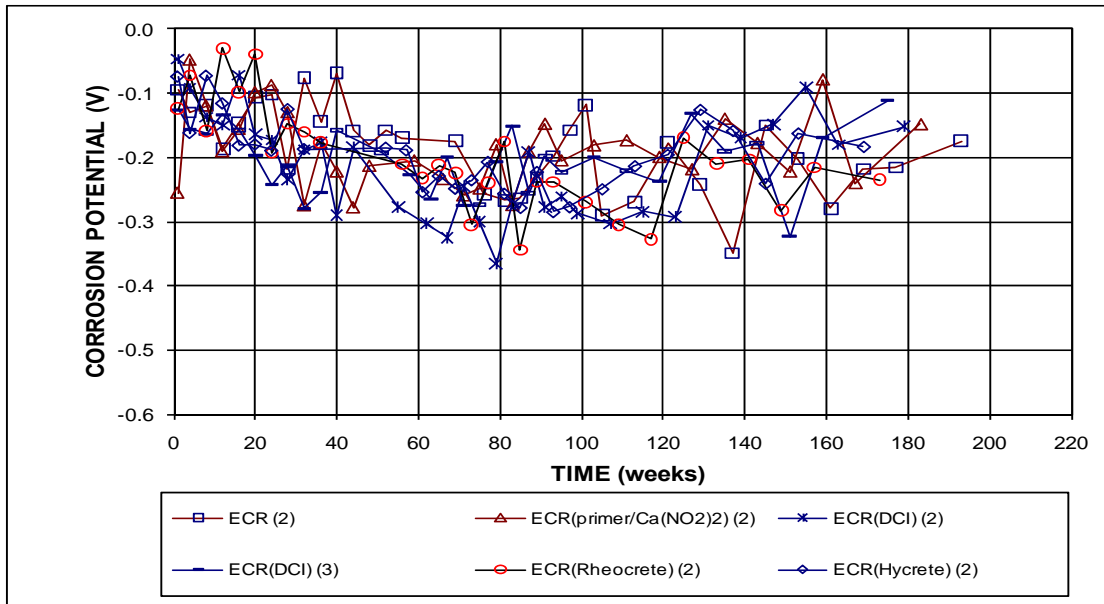


Figure 3.64d – Field Test. Average bottom mat corrosion potentials with respect to a copper-copper sulfate electrode for specimens with ECR, ECR with a primer containing calcium nitrite, and ECR with corrosion inhibitors in concrete, with cracks, specimen No. 2 and 3. (ECR with 16 holes through the epoxy)

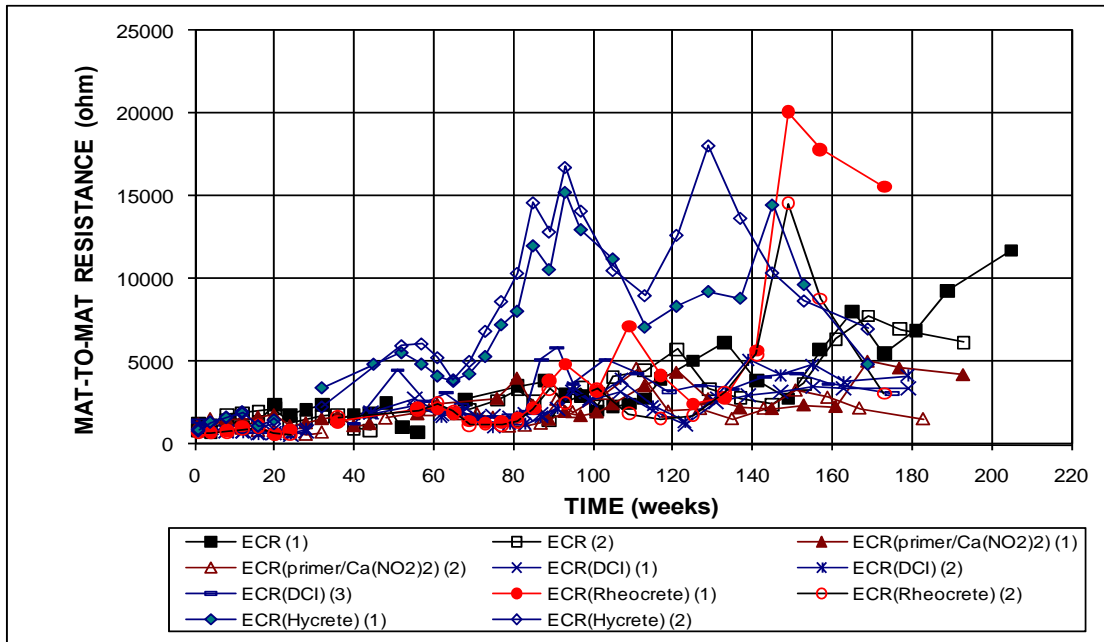


Figure 3.65 – Field Test. Average mat-to-mat resistances for specimens with ECR, ECR with a primer containing calcium nitrite, and ECR with corrosion inhibitors in concrete, with cracks (ECR with 16 holes through the epoxy).

ECR(Hycrete) had the highest resistances between weeks 32 and 145, with values around 5,000 ohms during weeks 45 and 73. After week 73, the resistance progressively increased to a peak value of 18,087 ohms at week 129 and then dropped to values around 5,000 ohms at week 169. ECR(Rheocrete) (1) and (2) had spikes of 20,100 and 14,563 ohms, respectively, both at week 149. The resistances for the other specimens were similar, increasing progressively from about 1,000 ohms at the beginning of the test to 5,000 ohms at ages ranging from 169 to 193 weeks.

Overall, the corrosion inhibitors did not improve corrosion resistance of ECR. Most specimens without simulated cracks had average corrosion rates of less than 0.04 and 15.00 $\mu\text{m}/\text{yr}$ based on total and exposed area, respectively, average corrosion losses less than 0.02 and 6.00 μm for ages ranging from 163 to 175 weeks, and corrosion potentials for both top and bottom mat bars more positive than -0.350 V. Most specimens with simulated cracks had corrosion rates ranging between -0.02 and 0.04 $\mu\text{m}/\text{yr}$ based on total area and between -5.00 and 15.00 $\mu\text{m}/\text{yr}$ based on exposed area, corrosion losses less than 0.04 and 15.00 μm for ages ranging from 163 to 175 weeks, and corrosion potentials more positive than -0.600 V for top mat bars and -0.400 V for bottom mat bars. The average mat-to-mat resistances for most specimens without and with cracks were below 7,000 ohms, except for Hycrete specimens, which had resistances above 7,000 ohms during the majority test period and the “peak” values of about 17, 000 ohms. For specimens both without and with cracks, corrosion activity increased after week 60, with higher corrosion rates and more negative corrosion potentials. The performance of all the specimens with ECR and corrosion inhibitors was similar.

3.3.3 Multiple-Coated Reinforcement

This section includes the test results for specimens with the multiple-coated (MC) reinforcement. The average results are presented in Figures 3.66 through 3.77 and the individual test results are included in Appendices A and B.

3.3.3.1 Field Specimens without Cracks

The average corrosion rates for specimens without simulated cracks are shown in Figures 3.66 and 3.67. The MC specimens had corrosion rates similar to those of the conventional ECR specimens, with values less than $0.02 \mu\text{m}/\text{yr}$ based on total area, but with several exceptions as noted next. MC (1) had an average corrosion rate of about $0.03 \mu\text{m}/\text{yr}$ at weeks 4, 151, and 199 based on total area. Based on exposed area, the corrosion rates of MC were below $10.00 \mu\text{m}/\text{yr}$, except MC (1) had values of 13.61 , 10.06 , and $13.02 \mu\text{m}/\text{yr}$ at weeks 4, 151, and 199, respectively. MC (1) also exhibited the highest negative corrosion rate, -0.05 and $-20.52 \mu\text{m}/\text{yr}$ at week 82 based on total and exposed area, respectively.

The average corrosion losses are shown in Figures 3.68 and 3.69 and summarized in Table 3.10. ECR (1) had positive corrosion losses throughout the test period, increasing gradually after corrosion initiation at week 80 and reached a corrosion loss of 0.02 and $8.96 \mu\text{m}$ at week 205 based on total and exposed area, respectively. The average corrosion losses of MC (2) fluctuated around 0 and remained below 0.005 and $1.18 \mu\text{m}$ at week 183. MC (1) had negative corrosion losses between weeks 82 and 159, which became positive and increased gradually to a value of below 0.005 and $0.61 \mu\text{m}$ at week 167, reaching a value of 0.01 and $5.53 \mu\text{m}$ at week 199, based on total and exposed area, respectively. The ECR (2) specimen exhibited negative corrosion after initiating after week 69 and reached a

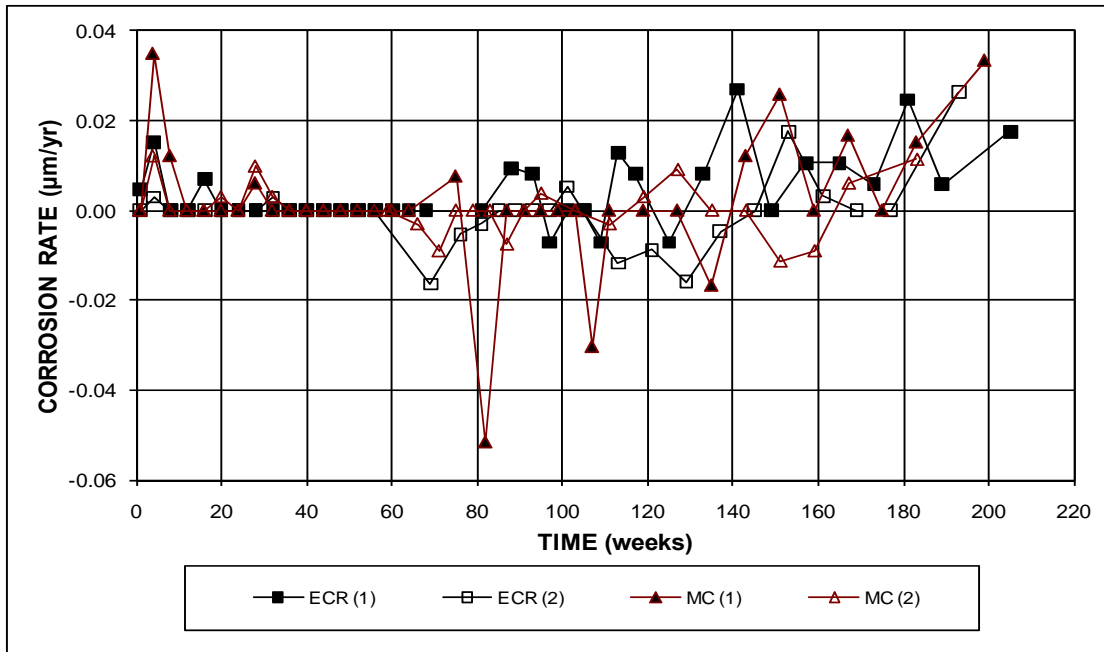


Figure 3.66 – Field Test. Average corrosion rates for specimens with ECR and multiple-coated bars, without cracks (ECR with 16 holes through the coating).

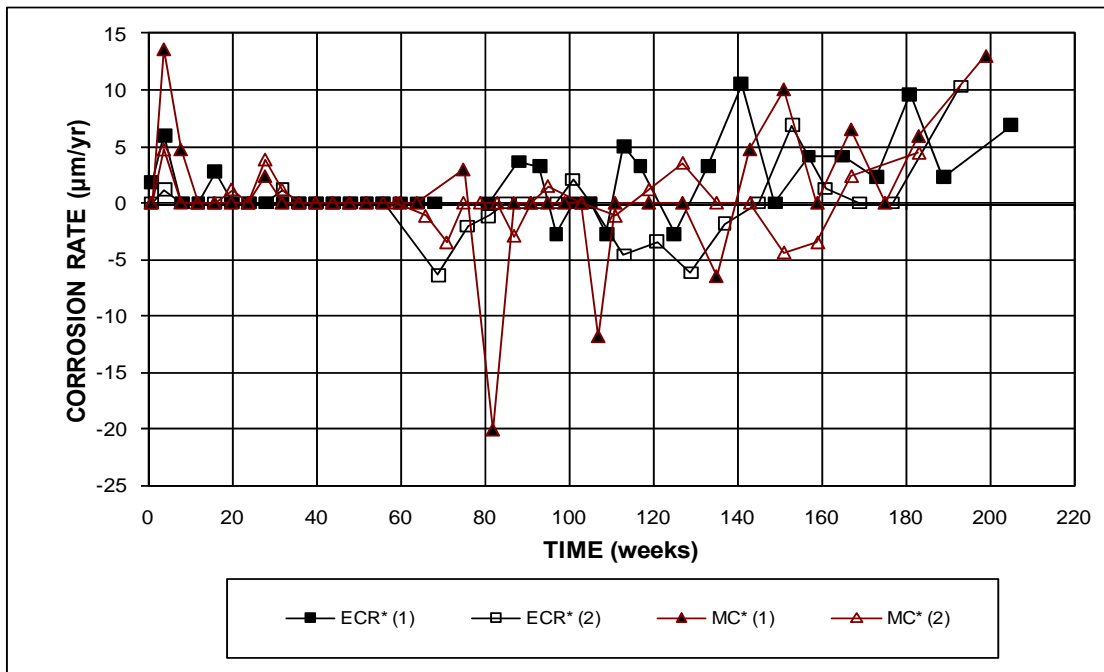


Figure 3.67 – Field Test. Average corrosion rates for specimens with ECR and multiple-coated bars, without cracks. * Based on exposed area (ECR with 16 holes through the coating).

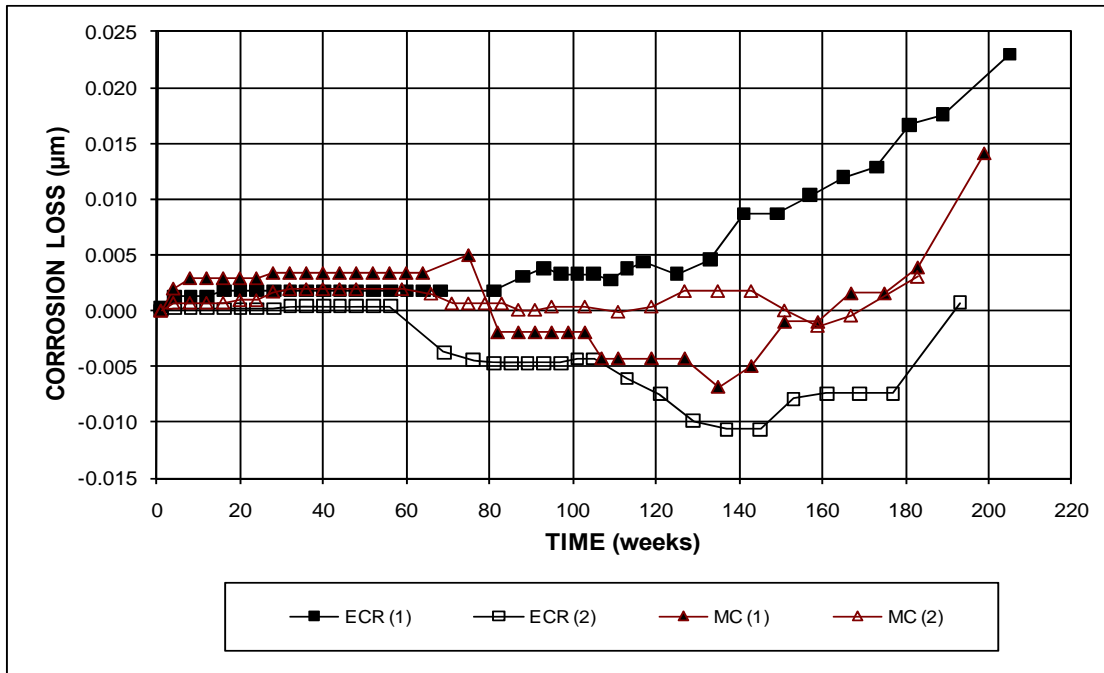


Figure 3.68 – Field Test. Average corrosion losses for specimens with ECR and multiple-coated bars, without cracks (ECR with 16 holes through the coating).

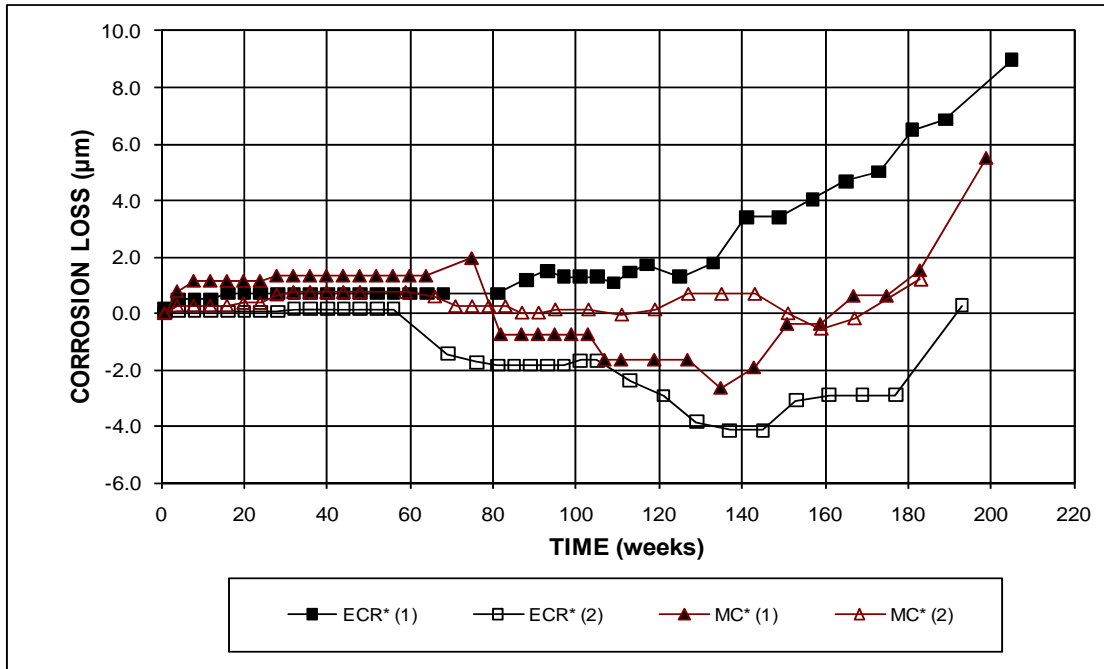


Figure 3.69 – Field Test. Average corrosion losses for specimens with ECR and multiple-coated bars, without cracks. * Based on exposed area (ECR with 16 holes through the coating).

Table 3.10 – Corrosion losses for multiple-coated bars in the field test, without cracks

Multiple Coated Bars without Cracks							
Steel Designation ^a	Exposure time (weeks)	Test Bar Corrosion Losses (μm)				Average	Standard Deviation
		1	2	3	4		
Based on Total Area							
MC (1)	167	β	β			β	β
MC (2)	167	0.00	-0.01	β	0.01	β	0.01
Based on Exposed Area							
MC* (1)	167	0.98	0.25			0.61	0.51
MC* (2)	167	0.00	-3.80	0.34	2.73	-0.18	2.70

^a MC = multiple coated bars.

Both zinc and epoxy layers are penetrated with 16 3-mm ($1/8$ -in.) diameter holes.

* Based on exposed area.

β Corrosion loss (absolute value) less than $0.005 \mu\text{m}$.

corrosion loss of 0 at week 193.

The average corrosion potentials with respect to a CSE are shown in Figure 3.70. The MC specimens had more negative corrosion potentials than the conventional ECR specimens. The top mat corrosion potentials of the MC bars ranged between -0.300 and -0.550 V, except for MC(2) with -0.282 V at week 143 and MC(1) with -0.206 V at week 175; while those of the ECR bars were between -0.100 and -0.355 V, except ECR(2) had values of -0.032 V at week 32 and -0.092 V at week 69. The bottom mat corrosion potentials of the MC bars were between -0.400 and -0.200 V before week 167. After week 167, the bottom mat potential values for the MC specimens shifted to less negative values, similar to that observed for the conventional ECR specimens, with the majority of the values ranging from -0.300 to -0.100 V. The performance of the MC specimens was primarily due to the active zinc layer protecting the underlying steel. Zinc is a more active metal than iron, and generally provides galvanic protection to the less active metal. When zinc corrodes, it exhibits a more negative half-cell potential than iron.

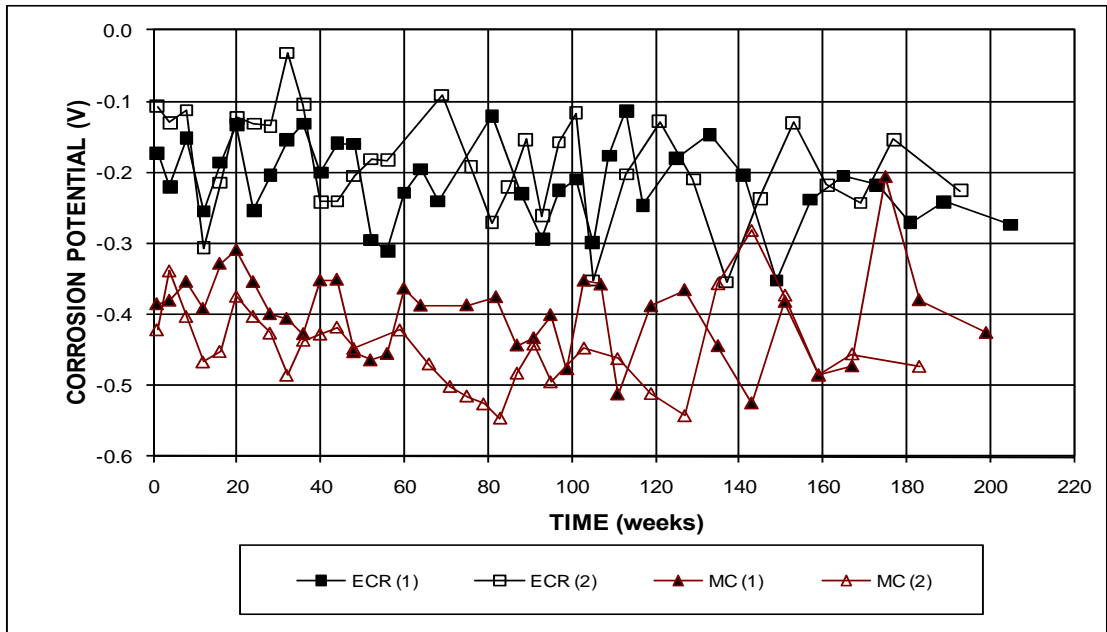


Figure 3.70a – Field Test. Average top mat corrosion potentials with respect to a copper-copper sulfate electrode for specimens with ECR and multiple-coated bars, without cracks (ECR with 16 holes through the coating).

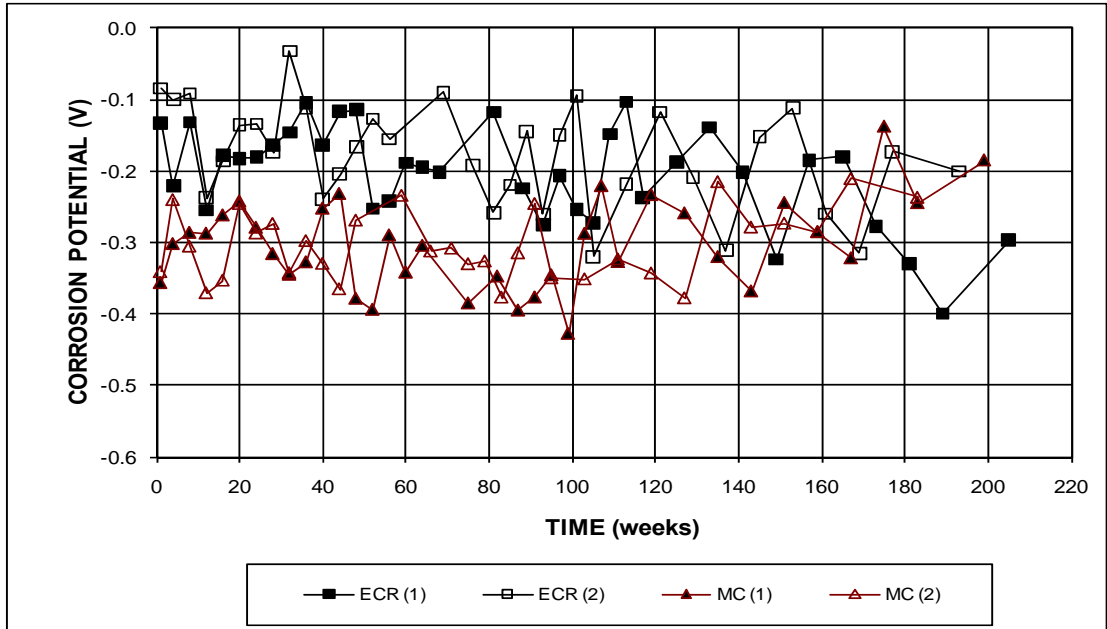


Figure 3.70b – Field Test. Average bottom mat corrosion potentials with respect to a copper-copper sulfate electrode for specimens with ECR and multiple-coated bars, without cracks (ECR with 16 holes through the coating).

Figure 3.71 shows the average mat-to-mat resistance for the MC specimens without cracks. The resistances of the MC specimens were similar to those of the ECR specimens, increasing progressively from values of around 1,000 to 7,000 ohms during the test period.

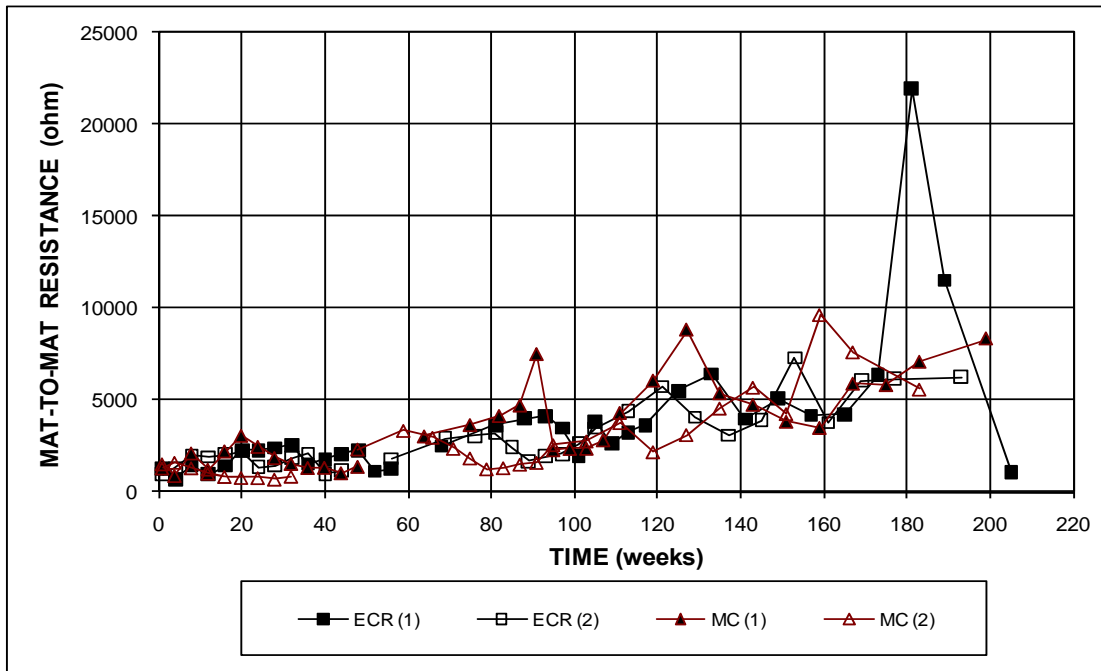


Figure 3.71 – Field Test. Average mat-to-mat resistances for specimens with ECR and multiple-coated bars, without cracks (ECR with 16 holes through the coating).

3.3.3.2 Field Specimens with Cracks

Figures 3.72 and 3.73 present the average corrosion rates for specimens with cracks. The MC specimens had similar corrosion rates to the ECR specimens. The corrosion rates for specimens with cracks were slightly higher than those of specimens without cracks, with the highest value, $0.05 \mu\text{m}$, occurring for specimen MC (1) at week 167. Negative corrosion rates appeared occasionally, with the most negative value, $-0.02 \mu\text{m}$, for specimen MC (1) at weeks 99 and 107. The corrosion

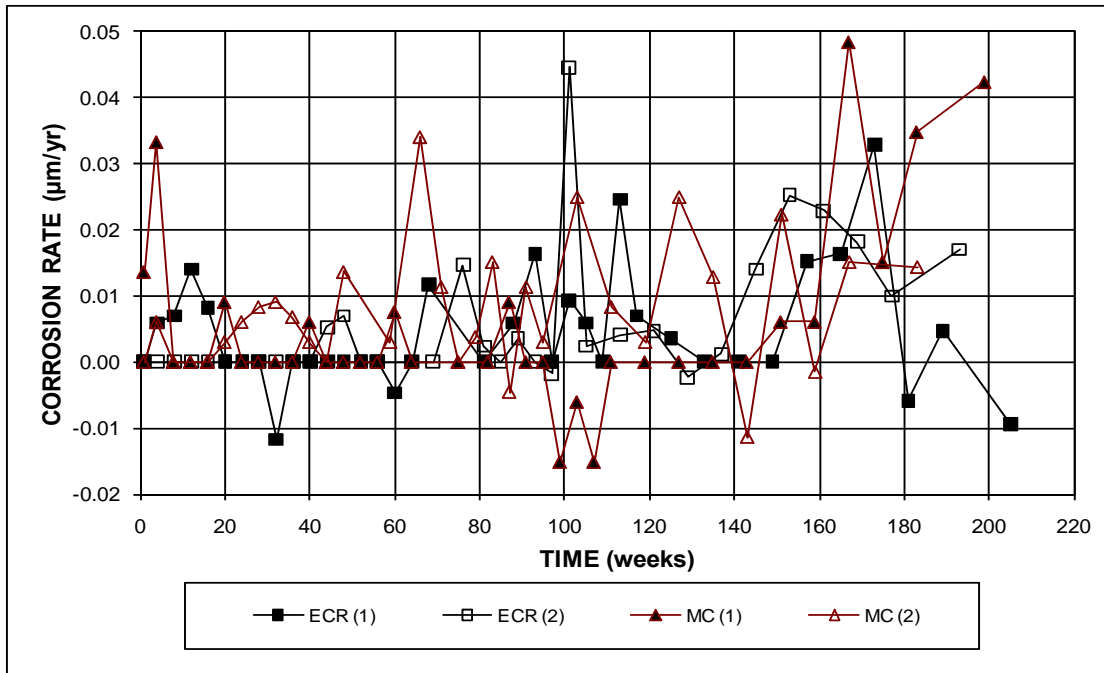


Figure 3.72 – Field Test. Average corrosion rates for specimens with ECR and multiple-coated bars, with cracks (ECR with 16 holes through the coating).

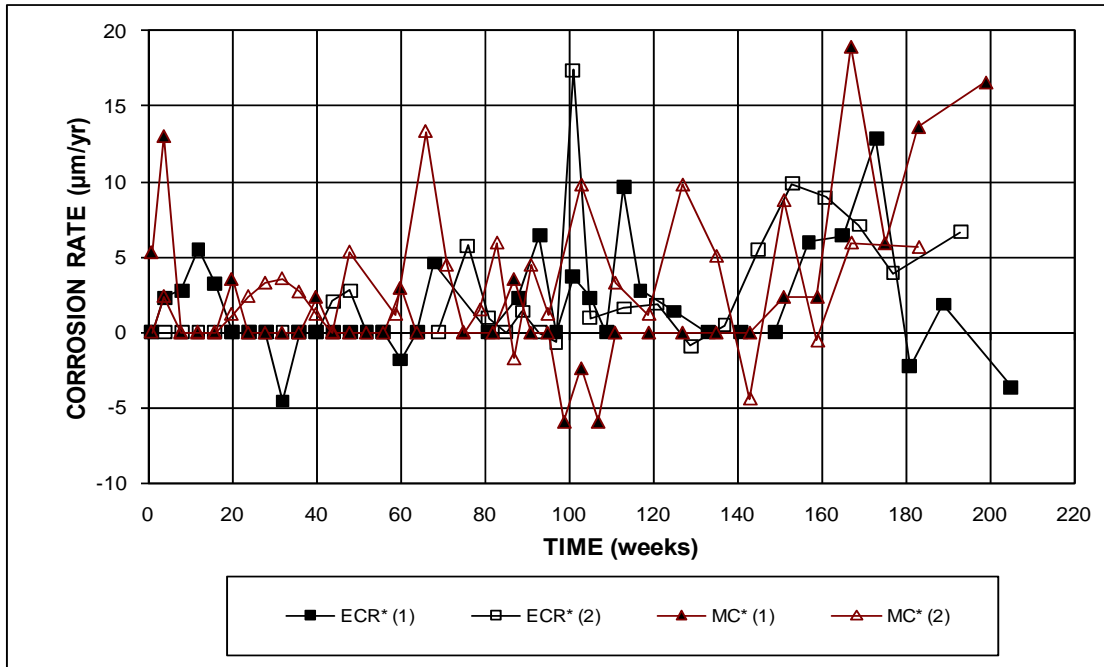


Figure 3.73 – Field Test. Average corrosion rates for specimens with ECR and multiple-coated bars, with cracks. * Based on exposed area (ECR with 16 holes through the coating).

rates based on exposed area for the MC specimens were as high as $18.94 \mu\text{m}$ for MC (1) at week 167 and as negative as $-5.92 \mu\text{m}$ for MC (1) at weeks 99 and 107.

As shown in Figure 3.74 and 3.75, specimen MC (2) had much higher corrosion losses than the other specimens after week 60, while MC (1) had corrosion losses lower than the other specimens before week 160. After week 160, losses increased rapidly. As of May 31, 2008, specimens MC (1) and (2) and ECR (2) had corrosion losses of about $0.03 \mu\text{m}$ based on total area, compared to a loss of $0.02 \mu\text{m}$ observed for specimen ECR (1). Specimen MC (2) had the highest total corrosion loss, $10.91 \mu\text{m}$, based on exposed area at week 167, followed by ECR (2) with $7.97 \mu\text{m}$ at week 169, and ECR (1) with $7.29 \mu\text{m}$ at week 173. Specimen MC (1) had the lowest corrosion loss, $4.73 \mu\text{m}$, at week 167 based on exposed area, although it had passed the ECR specimens by week 199.

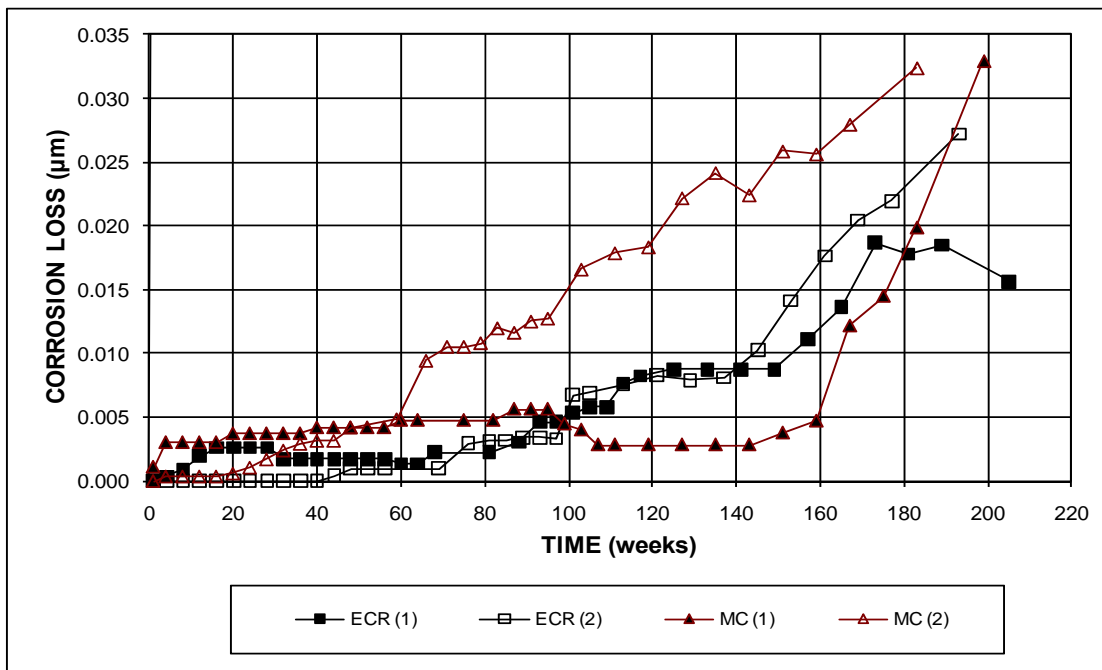


Figure 3.74 – Field Test. Average corrosion losses for specimens with ECR and multiple-coated bars, with cracks (ECR with 16 holes through the coating).

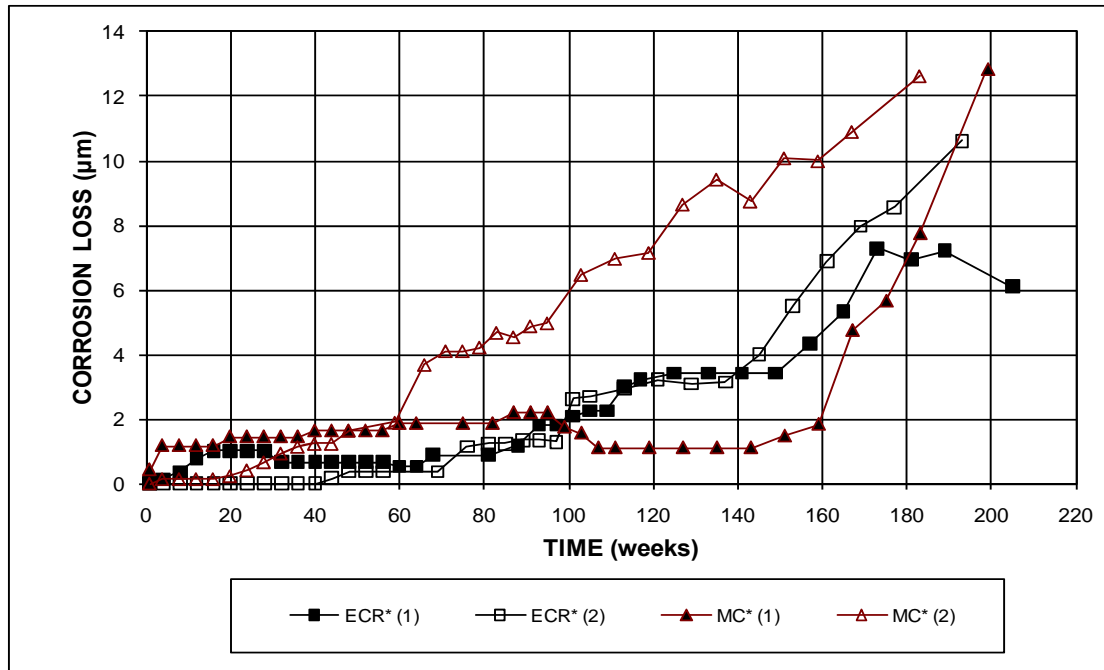


Figure 3.75 – Field Test. Average corrosion losses for specimens with ECR and multiple-coated bars, with cracks. * Based on exposed area (ECR with 16 holes through the coating).

Table 3.11 – Corrosion losses for multiple-coated bars in the field test, with simulated cracks

Multiple Coated Bars with Cracks							
Steel Designation ^a	Exposure time (weeks)	Test Bar Corrosion Losses (µm)				Average	Standard Deviation
		1	2	3	4		
Based on Total Area							
MC (1)	167	0.01	0.01			0.01	β
MC (2)	167	0.04	-0.02	0.06	0.03	0.03	0.03
Based on Exposed Area							
MC* (1)	167	3.85	5.62			4.73	1.26
MC* (2)	167	16.89	-6.40	21.64	11.52	10.91	12.26

^a MC = multiple coated bars.

Both zinc and epoxy layers are penetrated with 16 3-mm ($1/8$ -in.) diameter holes.

* Based on exposed

β Corrosion loss (absolute value) less than 0.005 µm.

As shown in Figure 3.76, the top mat corrosion potentials were more negative for the MC specimens than for ECR specimens, with the majority of the values more negative than -0.400 V with respect to a CSE, but with several exceptions as noted

next. Specimen MC (1) had a top mat corrosion potential of -0.700 V at week 48 and -0.721 V at week 143. These low corrosion potentials were not accompanied by an increase of the corrosion rate, suggesting that they might be aberrant readings. The bottom corrosion potentials of the MC specimens were more negative than those of ECR specimens before week 91, except for ECR (1) having -0.323 V at week 12. After week 91, MC and ECR specimens had similar bottom mat corrosion potentials.

Mat-to-mat resistance results for specimens with cracks are shown in Figure 3.77. The MC specimens had mat-to-mat resistances similar to those of the ECR specimens, increasing from 1,000 to 6,000 ohms during the test period ending of May 31, 2008. The mat-to-mat resistance of specimen MC (1) decreased from 6,000 ohms at week 135 to 2,000 ohms at week 199, while the resistance of specimens MC (2) increased slowly from 1,500 to 5,600 ohms during the same period.

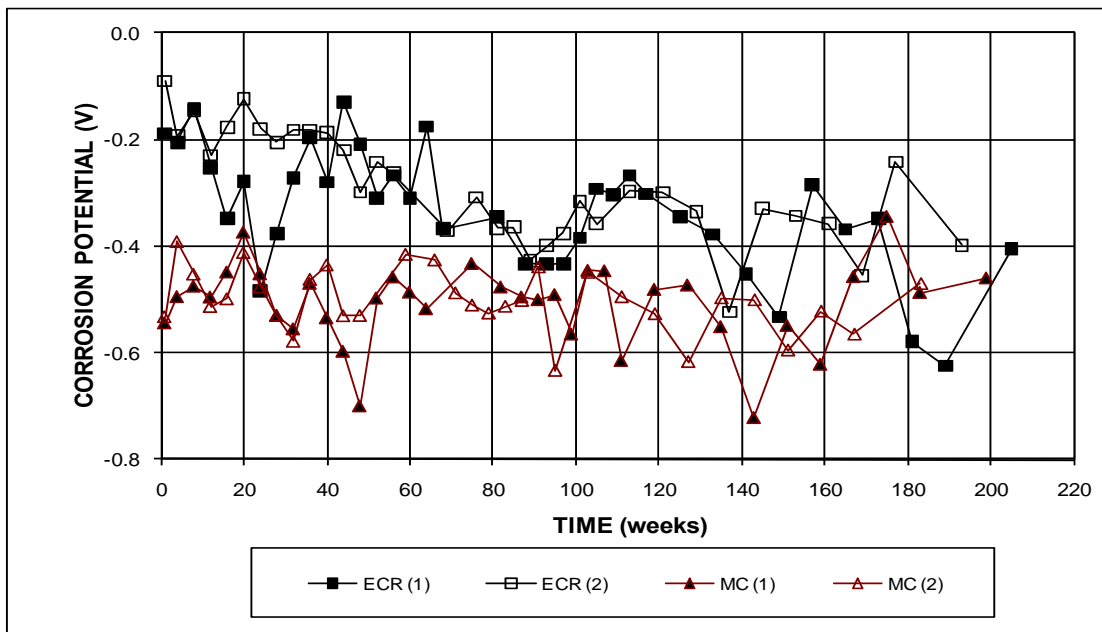


Figure 3.76a – Field Test. Average top mat corrosion potentials with respect to a copper-copper sulfate electrode for specimens with ECR and multiple-coated bars, with cracks (ECR with 16 holes through the coating).

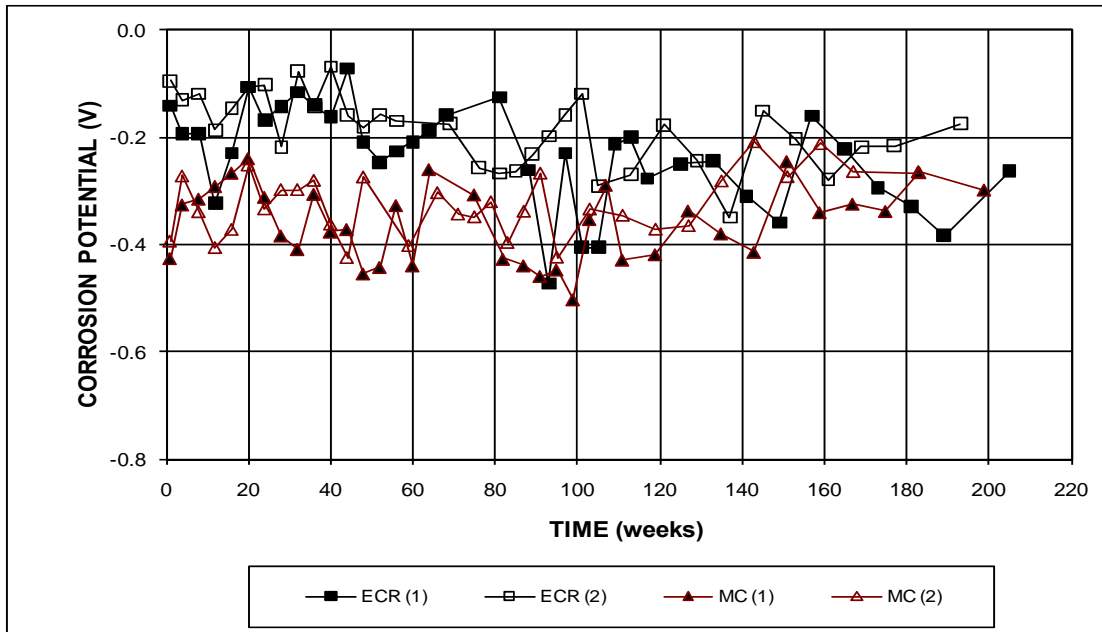


Figure 3.76b – Field Test. Average bottom mat corrosion potentials with respect to a copper-copper sulfate electrode for specimens with ECR and multiple-coated bars, with cracks (ECR with 16 holes through the coating).

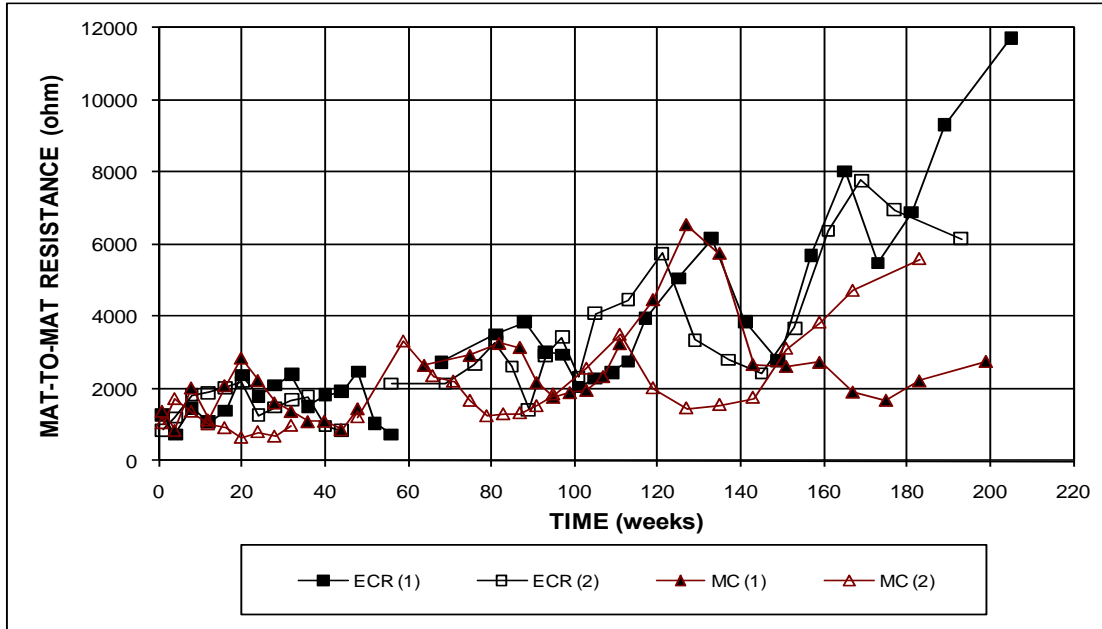


Figure 3.77 – Field Test. Average mat-to-mat resistances for specimens with ECR and multiple-coated bars, with cracks (ECR with 16 holes through the coating).

In summary, the average corrosion losses of the MC bars were comparable to those of the ECR bars, and both types of reinforcement exhibited significantly better corrosion resistance compared to bare reinforcement. Similar to the results for the specimens in the ASTM G109 test, the specimens containing ECR and MC demonstrated very low corrosion losses compared to specimens containing conventional steel due to the limited access of oxygen, moisture, and chloride ions and the high resistance of the epoxy coating. The corrosion losses of the MC specimens with cracks were higher than those of specimens without cracks.

3.3.4 ECR with Increased Adhesion

This section includes the test results for field test specimens containing ECR with increased adhesion, including ECR with chromate pretreatment, ECR the DuPont coating, and ECR with the Valspar coating. Average results as of May 31, 2008 are presented in Figures 3.78 through 3.89. The individual test results are included in Appendix A and B.

3.3.4.1 Field Specimens without Cracks

The average corrosion rates for specimens without simulated cracks are shown in Figures 3.78 and 3.79. All specimens had similar corrosion rates, stabilizing around 0 before week 60 and fluctuating between -0.03 and 0.04 $\mu\text{m}/\text{yr}$ based on total area after that, and between -10.00 and 15.00 $\mu\text{m}/\text{yr}$ based on exposed area, but with exceptions as noted next. Specimen ECR(Valspar) (2) had the highest corrosion rate, 0.07 and 29.08 $\mu\text{m}/\text{yr}$ at week 85 based on total and exposed area, respectively. Some specimens exhibited negative corrosion, especially the ECR(Chromate) specimens during the test period from week 60 to 140. ECR(Chromate) (1) had the most

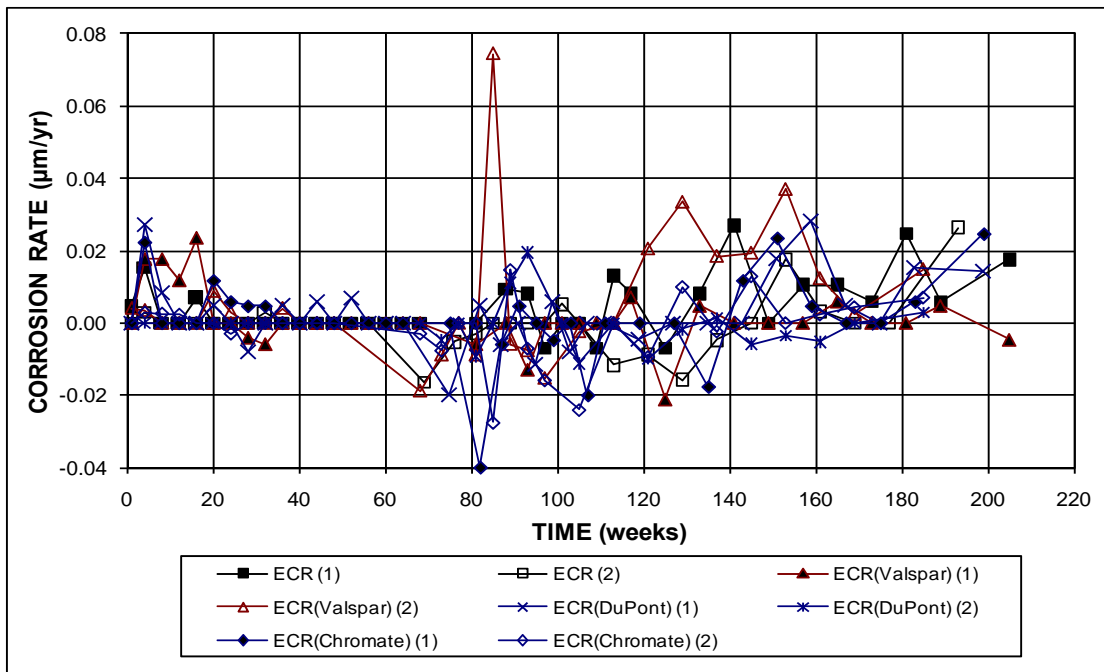


Figure 3.78 – Field Test. Average corrosion rates for specimens with ECR and ECR with increased adhesion, without cracks (ECR with 16 holes through the epoxy).

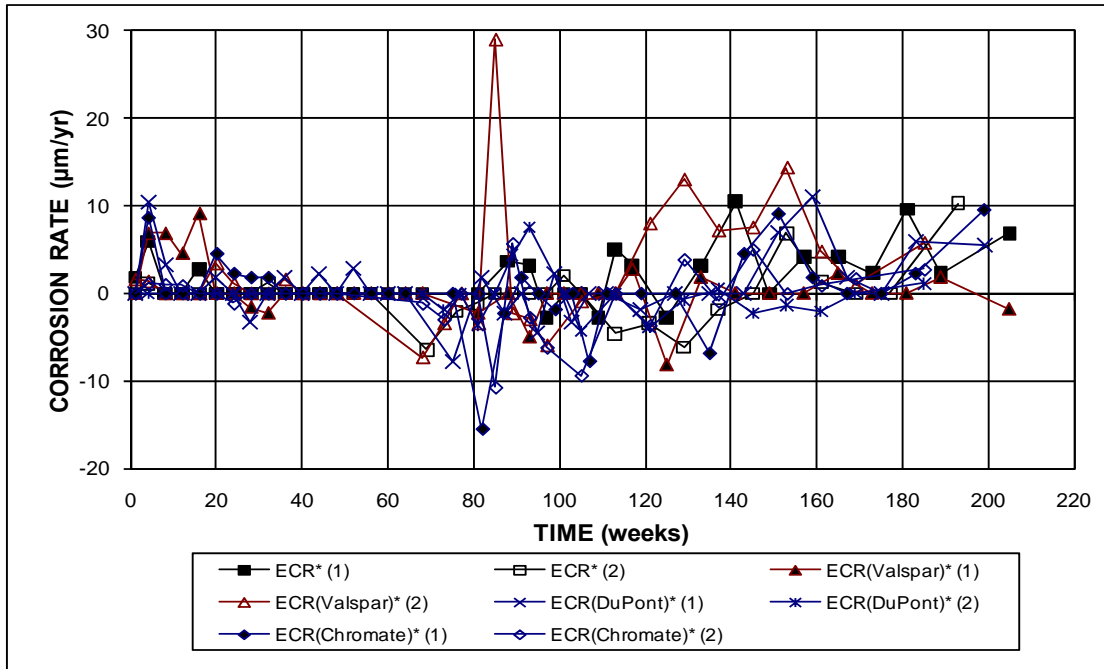


Figure 3.79 – Field Test. Average corrosion rates for specimens with ECR and ECR with increased adhesion, without cracks. * Based on exposed area (ECR with 16 holes through the epoxy).

negative corrosion rate, -0.04 and -15.57 $\mu\text{m}/\text{yr}$ at week 82 based on total and exposed area, respectively. However, these corrosion rates were not accompanied by sharp corrosion potential shifts and might be aberrant readings.

The average corrosion losses are shown in Figures 3.80 and 3.81 and summarized in Table 3.12. Most specimens exhibited negative corrosion losses during the test period, except for specimen ECR (1), for which the losses increased gradually to 0.02 and 8.96 μm at week 205 based on total and exposed area, respectively, and ECR(Valspar) (1), for which the losses remained near 0. The corrosion losses for specimens ECR(Valspar) (2), ECR(DuPont) (1), and ECR(Chromate) (1) shifted gradually from negative to positive values after weeks 121, 143, and 175, respectively. The corrosion losses of ECR(DuPont) (2) and ECR(Chromate) (2) remained negative, while that of ECR(2) just exceeded 0 at week 193. As of May 31, 2008, all of the specimens had average corrosion losses of no more than 0.02 μm at weeks ranging from 165 to 169 weeks based on total area, and no more than 7.11 μm based on exposed area. Specimen ECR(Valspar) (2) exhibited the highest corrosion loss, 7.11 μm based on exposed area at week 169, followed by specimen ECR(DuPont) (1) with 1.98 μm at week 167 and specimen ECR(Valspar) (1) with 0.20 μm at week 165. The other increased adhesion specimens had negative average corrosion losses with an extreme value of -2.04 μm for ECR(Chromate) (2) at week 169.

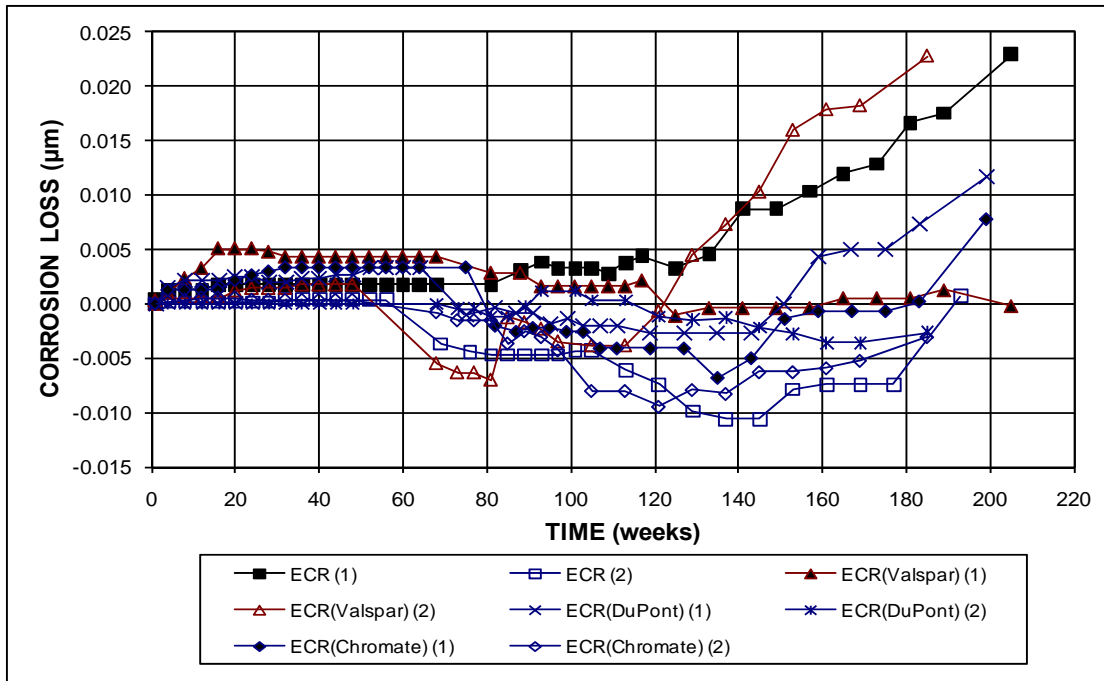


Figure 3.80 – Field Test. Average corrosion losses for specimens with ECR and ECR with increased adhesion, without cracks (ECR with 16 holes through the epoxy).

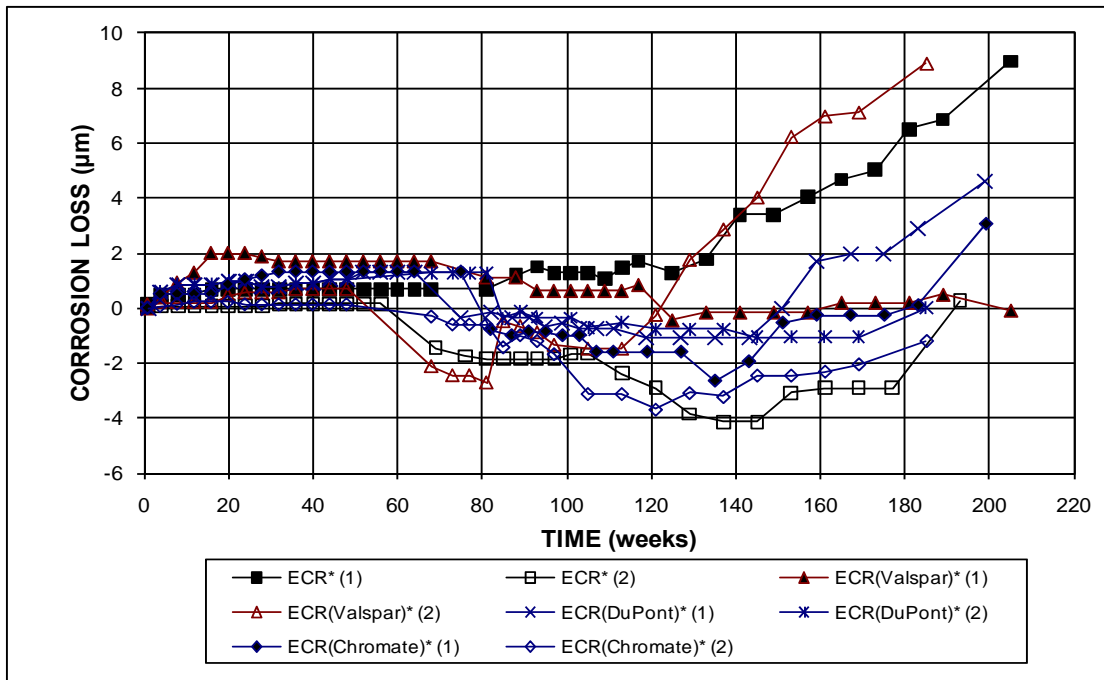


Figure 3.81 – Field Test. Average corrosion losses for specimens with ECR and ECR with increased adhesion, without cracks. * Based on exposed area (ECR with 16 holes through the epoxy).

Table 3.12 – Corrosion losses for ECR with increased adhesion in the field test, without cracks

Increased Adhesion without Cracks							
Steel Designation ^a	Exposure time (weeks)	Test Bar Corrosion Losses (µm)				Average	Standard Deviation
		1	2	3	4		
Based on Total Area							
ECR(Valspar) (1)	165	β	β			β	β
ECR(Valspar) (2)	169	-0.02	-0.01	0.06	0.04	0.02	0.04
ECR(DuPont) (1)	167	0.01	β			0.01	β
ECR(DuPont) (2)	169	β	β	-0.01	β	β	β
ECR(Chromate) (1)	167	β	β			β	0.01
ECR(Chromate) (2)	169	-0.01	β	-0.02	0.01	-0.01	0.01
Based on Exposed Area							
ECR(Valspar*) (1)	165	-0.32	0.72			0.20	0.73
ECR(Valspar)* (2)	169	-5.86	-3.49	22.40	15.39	7.11	13.94
ECR(DuPont)* (1)	167	3.05	0.92			1.98	1.51
ECR(DuPont)* (2)	169	-1.22	0.33	-2.85	-1.83	-1.39	1.33
ECR(Chromate)* (1)	167	-1.74	1.22			-0.26	2.09
ECR(Chromate)* (2)	169	-5.42	-1.04	-6.71	5.00	-2.04	5.29

^a ECR = conventional epoxy-coated reinforcement.

All ECRs have 16 3-mm (¹/₈-in.) diameter holes through the epoxy.

ECR(Valspar) = ECR with increased adhesion produced by Valspar.

ECR(DuPont) = ECR with increased adhesion produced by DuPont.

ECR(Chromate) = ECR with the zinc chromate pretreatment.

* Based on exposed area.

The average corrosion potentials with respect to a CSE are shown in Figure 3.82. The corrosion potentials for all the specimens were similar, with both the top and bottom mat corrosion potentials ranging between -0.025 and -0.300 V before week 44 and fluctuating between -0.100 and -0.400 V after that. The majority of the potential readings of all of the specimens were less negative than -0.350 V, indicating a low probability of corrosion.

The mat-to-mat resistances of the increased adhesion specimens were similar and increased with time from 1,000 to 9,000 ohms, as shown in Figure 3.83. There are several spikes on the plot. The resistances of ECR(DuPont) (2) and conventional ECR(1) were around 22,000 ohms at weeks 161 and 181, respectively, and ECR(DuPont) (1) had high values near 14,000 ohms at weeks 137 and 145.

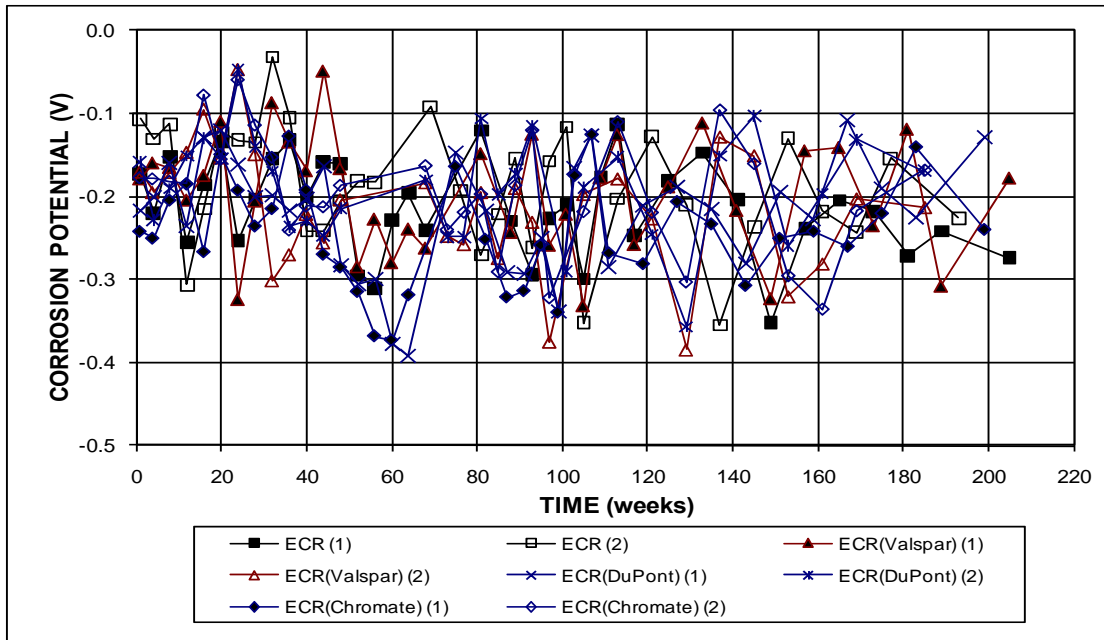


Figure 3.82a – Field Test. Average top mat corrosion potentials with respect to a copper-copper sulfate electrode for specimens with ECR and ECR with increased adhesion, without cracks (ECR with 16 holes through the epoxy).

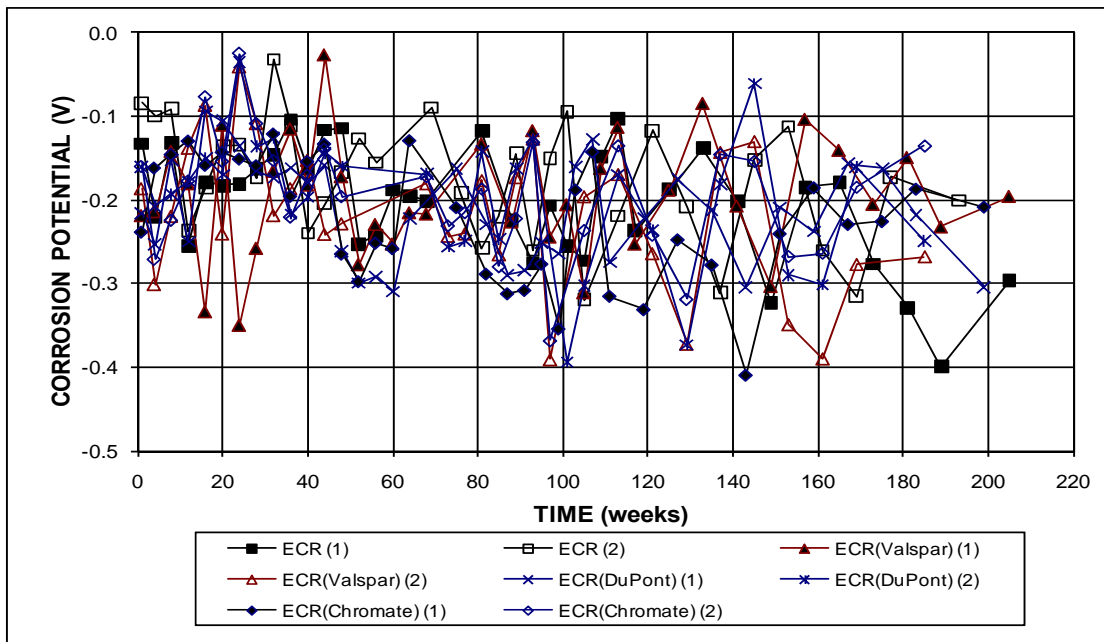


Figure 3.82b – Field Test. Average bottom mat corrosion potentials with respect to a copper-copper sulfate electrode for specimens with ECR and ECR with increased adhesion, without cracks (ECR with 16 holes through the epoxy).

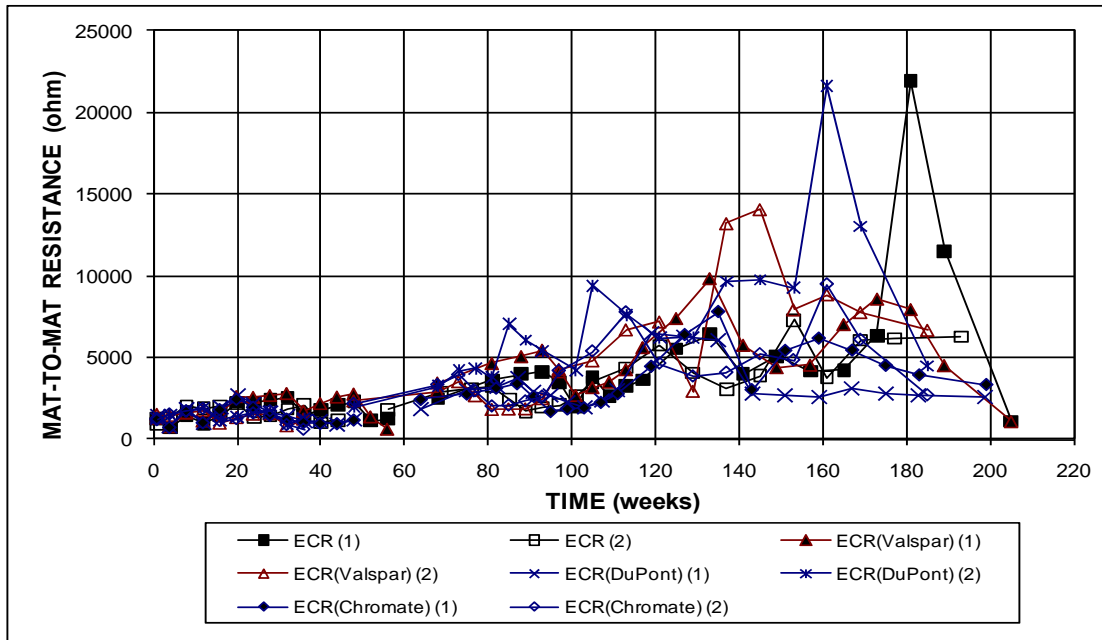


Figure 3.83 – Field Test. Average mat-to-mat resistances for specimens with ECR and ECR with increased adhesion, without cracks (ECR with 16 holes through the epoxy).

3.3.4.2 Field Specimens with Cracks

The test results as of May 31, 2008 for the increased adhesion ECR field test specimens with simulated cracks are shown in Figures 3.84 through 3.89. The average corrosion losses are summarized in Table 3.13.

Figures 3.84 and 3.85 show the average corrosion rates for the specimens with cracks. The majority of the corrosion rates calculated for the increased adhesion specimens were less than $0.03 \mu\text{m}/\text{yr}$ based on total area. Specimen ECR(DuPont) (2) had the highest corrosion rate, 0.14 and $53.58 \mu\text{m}/\text{yr}$ at week 185 based on total and exposed area, respectively, followed by specimen ECR(Valspar) (1) with 0.08 and $29.31 \mu\text{m}/\text{yr}$ at week 52. These values were not accompanied by sharp drops of the corresponding corrosion potentials and may be aberrant readings.

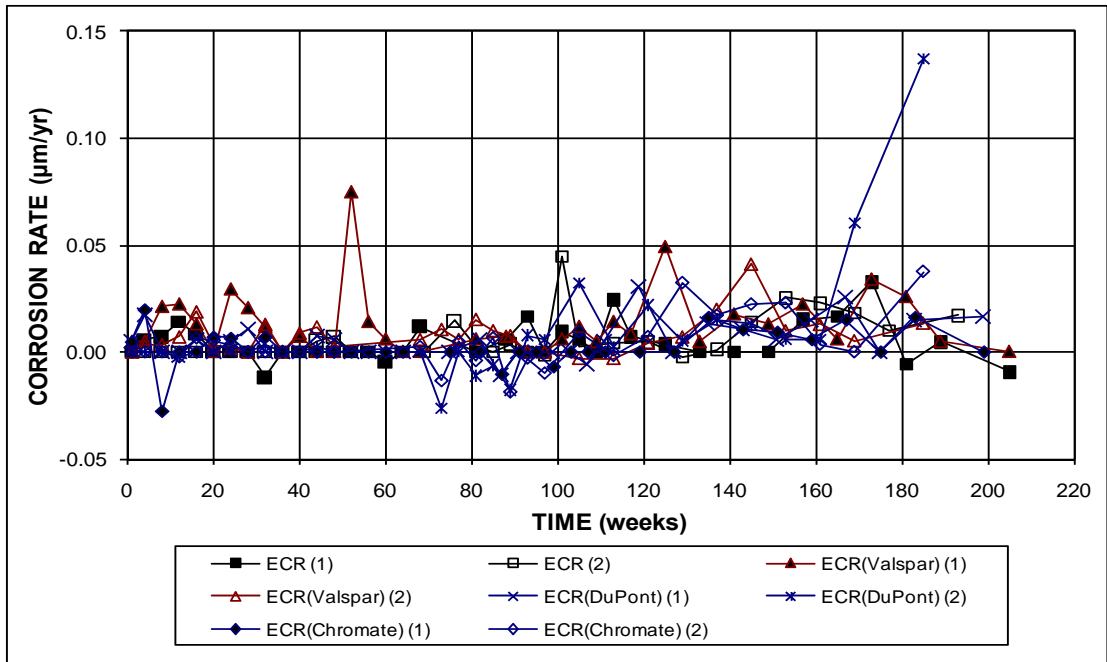


Figure 3.84 – Field Test. Average corrosion rates for specimens with ECR and ECR with increased adhesion, with cracks (ECR with 16 holes through the epoxy).

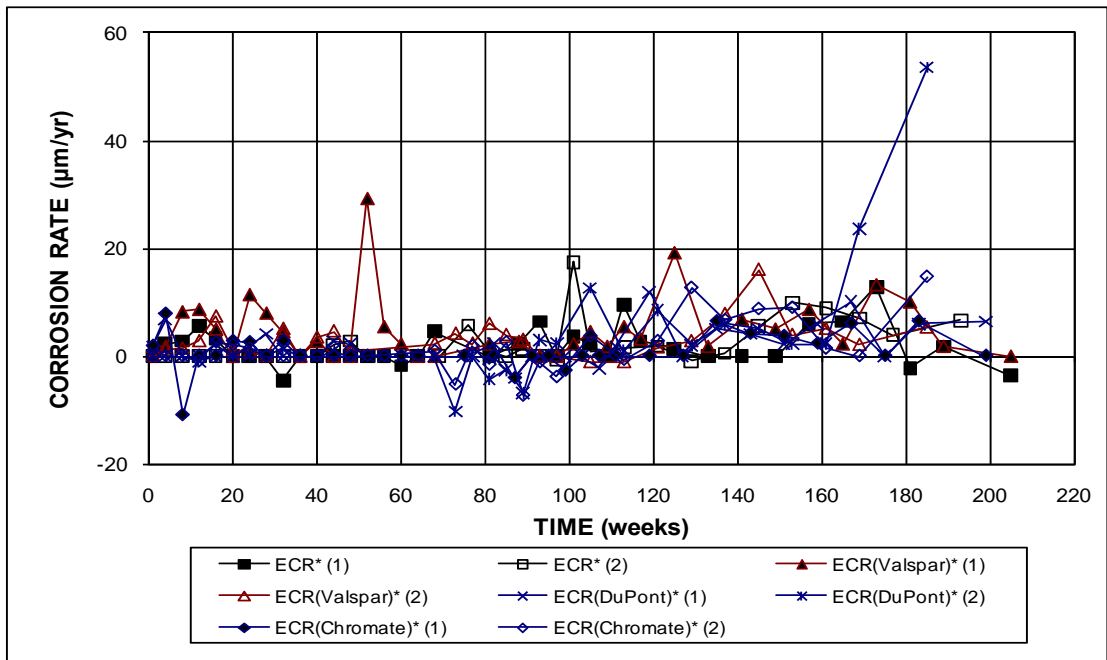


Figure 3.85 – Field Test. Average corrosion rates for specimens with ECR and ECR with increased adhesion, with cracks. * Based on exposed area (ECR with 16 holes through the epoxy).

The average corrosion losses are plotted in Figures 3.86 and 3.87 and summarized in Table 3.13. The corrosion losses for all the specimens increased gradually after initiating. Specimen ECR(Valspar) had the highest corrosion losses during most of the test period but was surpassed by specimen ECR(DuPont) (2) at week 185. Specimen ECR(Chromate) (1) had the lowest average corrosion loss after initiating at week 135. The other specimens had corrosion losses similar to those of the ECR specimens. Specimen ECR(Valspar) (1) exhibited the greatest corrosion loss, averaging 0.04 and 15.89 μm at week 165, based on total and exposed area, respectively, followed by specimen ECR(Valspar) (2) with an average corrosion loss of 0.03 and 10.27 μm at week 169. The average corrosion losses for specimens ECR(DuPont) (2) and (1) and ECR(Chromate) (2) were 0.02 μm at weeks of 169, 167, and 169 based on total area, and 8.19, 7.49, and 6.26 μm based on exposed area, respectively, which were about the same as those of ECR(1) and (2) at weeks 173 and 169. ECR(Chromate) (1) exhibited the lowest corrosion loss, 0.01 μm at week 167 based on total area and 3.21 μm based on exposed area, equal to one-fifth of the corrosion loss for ECR(Valspar) (1) (0.04 and 15.89 μm) at week 165. The average corrosion losses for specimens with cracks were about twice those of specimens without cracks.

The corrosion potential readings with respect to a CSE are shown in Figure 3.88. All specimens exhibited similar corrosion potentials. The corrosion potentials for the top mat bars ranged from -0.100 to -0.400 V before week 16 and shifted to more negative values after week 64, with corrosion potentials being more negative than -0.350 V for all the specimens. In the bottom mat, the corrosion potentials of all specimens ranged between -0.050 to -0.277 V before week 44, except for ECR(1), which had a corrosion potential of -0.323 V at week 12. After week 44, the corrosion

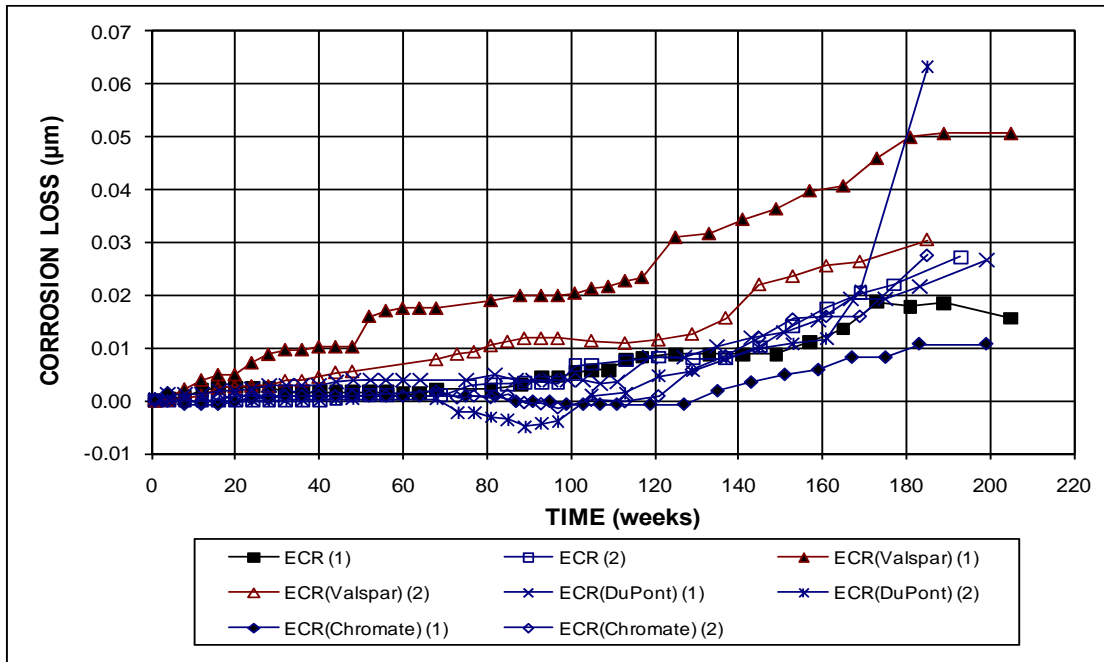


Figure 3.86 – Field Test. Average corrosion losses for specimens with ECR and ECR with increased adhesion, with cracks (ECR with 16 holes through the epoxy).

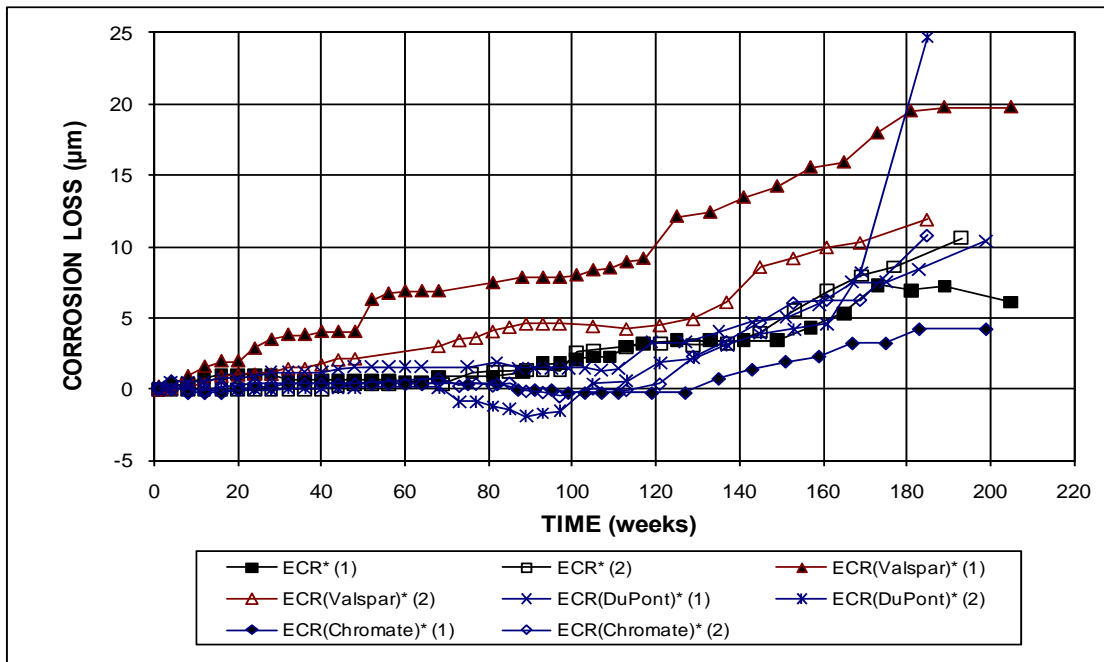


Figure 3.87 – Field Test. Average corrosion losses for specimens with ECR and ECR with increased adhesion, with cracks. * Based on exposed area (ECR with 16 holes through the epoxy).

Table 3.13 – Corrosion losses for ECR with increased adhesion in the field test, with simulated cracks

Increased Adhesion with Cracks							
Steel Designation ^a	Exposure time (weeks)	Test Bar Corrosion Losses (µm)				Average	Standard Deviation
		1	2	3	4		
Based on Total Area							
ECR(Valspar) (1)	165	0.03	0.05			0.04	0.01
ECR(Valspar) (2)	169	0.03	0.02	β	0.05	0.03	0.02
ECR(DuPont) (1)	167	0.02	0.02			0.02	0.01
ECR(DuPont) (2)	169	β	0.03	0.01	0.05	0.02	0.02
ECR(Chromate) (1)	167	0.02	β			0.01	0.01
ECR(Chromate) (2)	169	β	0.02	0.03	0.01	0.02	0.01
Based on Exposed Area							
ECR(Valspar*) (1)	165	13.17	18.62			15.89	3.85
ECR(Valspar)* (2)	169	12.12	9.23	1.14	18.60	10.27	7.24
ECR(DuPont)* (1)	167	6.11	8.88			7.49	1.96
ECR(DuPont)* (2)	169	-0.44	11.31	3.87	18.00	8.19	8.15
ECR(Chromate)* (1)	167	5.97	0.44			3.21	3.91
ECR(Chromate)* (2)	169	1.53	9.30	11.59	2.61	6.26	4.94

^a ECR = conventional epoxy-coated reinforcement.

All ECRs have 16 3-mm (¹/₈-in.) diameter holes through the epoxy.

ECR(Valspar) = ECR with increased adhesion produced by Valspar.

ECR(DuPont) = ECR with increased adhesion produced by DuPont.

ECR(Chromate) = ECR with the zinc chromate pretreatment.

* Based on exposed area.

β Corrosion loss (absolute value) less than 0.005 µm.

potentials exhibited bigger fluctuations, between -0.058 and -0.475 V, except for ECR(Chromate) (1), which had a corrosion potential of -0.514 V at week 52.

The mat-to-mat resistances for the specimens with simulated cracks were similar to the specimens without cracks, increasing from 1,000 to 9,000 ohms during the test, as shown in Figure 3.89. The resistance of specimen ECR(DuPont) (2) exhibited big fluctuations between weeks 105 and 153, varying from 4, 000 to 12,000 ohms. Specimen ECR(Chromate) (1) exhibited a decrease in corrosion resistance after week 159, which dropped to values around 3,000 ohms.

The test results in both cracked and uncracked concrete demonstrated that increased adhesion between the epoxy and reinforcing steel provided no improvement

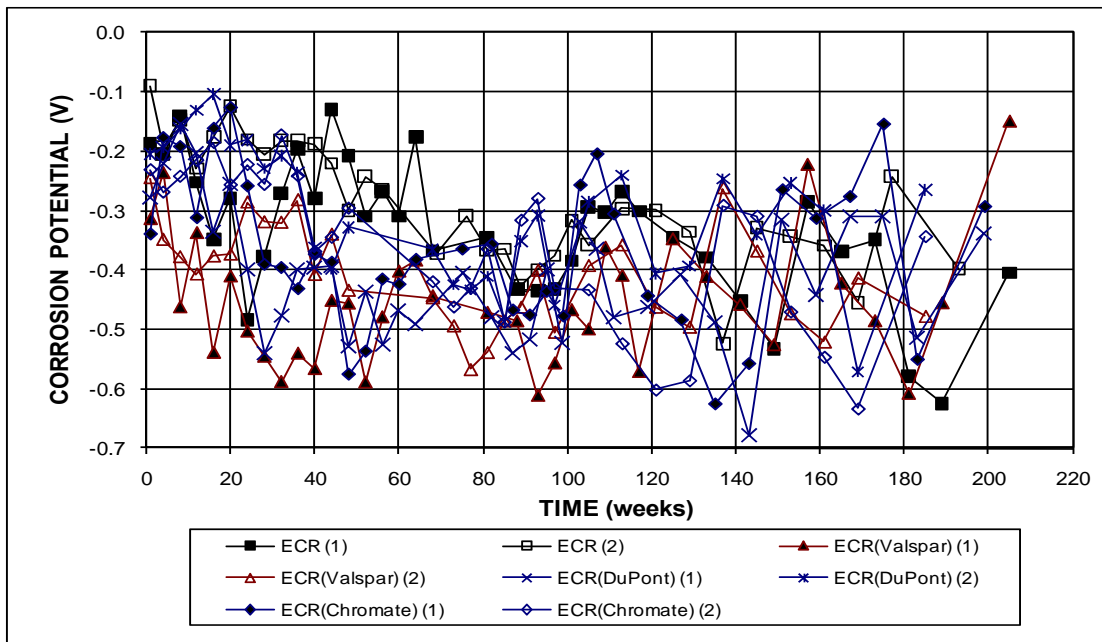


Figure 3.88a – Field Test. Average top mat corrosion potentials with respect to a copper-copper sulfate electrode for specimens with ECR and ECR with increased adhesion, with cracks (ECR with 16 holes through the epoxy).

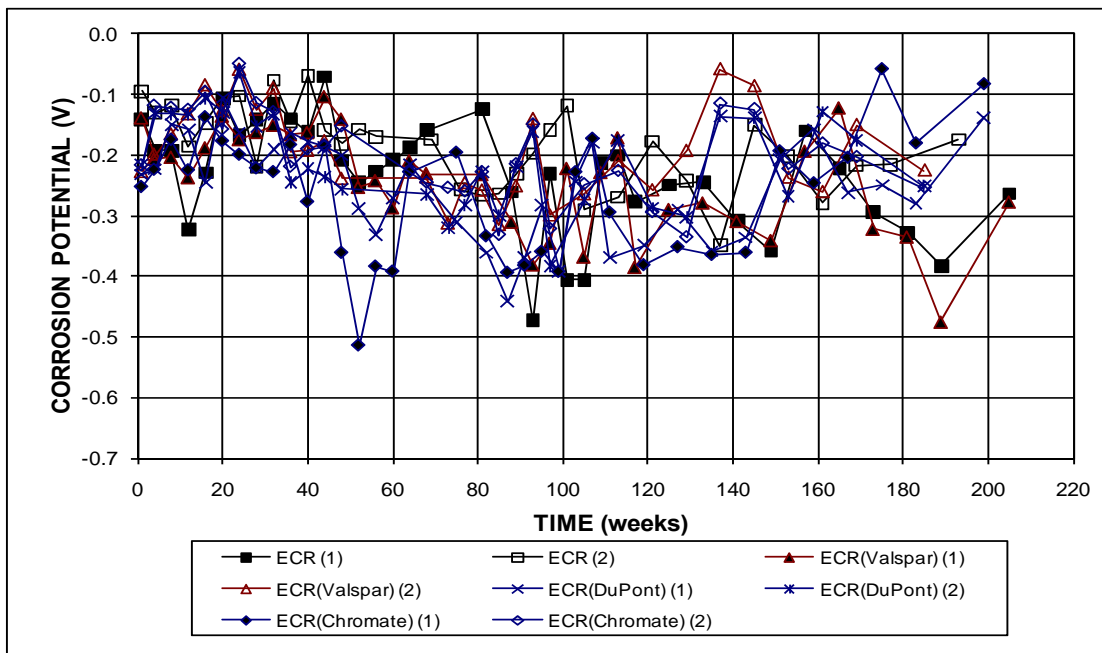


Figure 3.88b – Field Test. Average bottom mat corrosion potentials with respect to a copper-copper sulfate electrode for specimens with ECR and ECR with increased adhesion, with cracks (ECR with 16 holes through the epoxy).

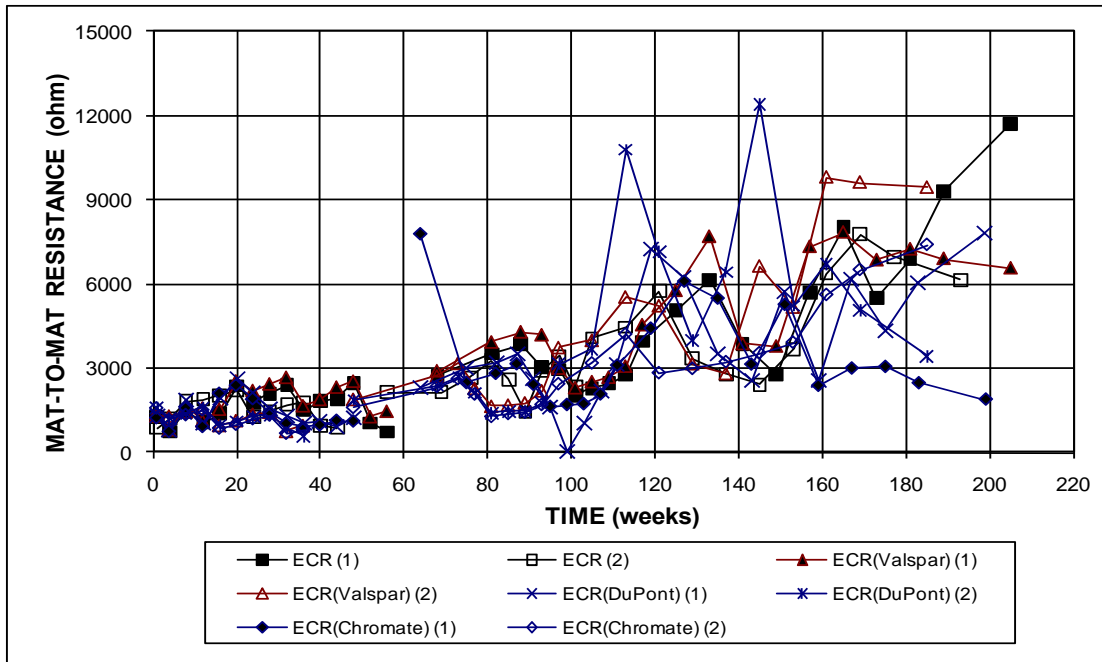


Figure 3.89 – Field Test. Average mat-to-mat resistances for specimens with ECR and ECR with increased adhesion, with cracks (ECR with 16 holes through the epoxy).

to the corrosion resistance of ECR under the exposure conditions provided by the field tests. For specimens without cracks, most specimens exhibited negative corrosion losses during the test period, except specimen ECR (1), for which the losses increased gradually, and specimen ECR(Valspar) (1), for which the losses remained near 0. As of May 31, 2008, all of the specimens had average corrosion losses of no more than 0.02 μm at ages ranging from 165 to 173 weeks based on total area, and no more than 7.11 μm based on exposed area. Specimen ECR(Valspar) (2) exhibited the highest corrosion loss, 7.11 μm based on exposed area at week 169, followed by specimen ECR(1) with 5.02 μm at week 173, ECR(DuPont) (1) with 1.98 μm at week 167, and specimen ECR(Valspar) (1) with 0.20 μm at week 165. The other specimens had negative average corrosion losses, with an extreme value of $-2.89 \mu\text{m}$ for ECR (2) at week 169. For specimens with simulated cracks, the corrosion losses for all the specimens increased gradually after initiating. Specimen ECR(Valspar) had the

highest corrosion losses during most of the test period but was surpassed by specimen ECR(DuPont) (2) at week 185. Specimen ECR(Chromate) (1) had the lowest average corrosion loss after initiating at week 135. The other specimens had corrosion losses similar to those of the ECR specimens.

3.3.5 Visual Inspection

The field test specimens were visually inspected for staining and cracking as of the cutoff date. The specimens with conventional steel showed heavy staining on the top surface, with the exception of specimen DCB-Conv. (2) without simulated cracks. Of the specimens that had heavy staining on the concrete top surface, some also exhibited cracking and spalling of the concrete, as shown in Figure 3.90. Uncracked specimens ECR(Rheocrete) (2) at week 173 and DCB-Conv. (2) at week 215, and cracked specimens ECR(Valspar) (1) at week 205, ECR(DuPont) (2) at week 185, and ECR(DCI) (1) and (2) at week 179 were observed to have slight staining on the surface (Figure 3.91). All of the specimens fabricated with the inhibitor Hycrete exhibited scaling on the top surface (Figure 3.92). All of the other specimens were observed to have sound concrete, showing no staining, cracking, or scaling (Figure 3.93).



Figure 3.90 – Field test specimen Conv. (1) at week 205, showing cracking, spalling, and heavy staining on portions of the surface.



Figure 3.91 – Field test specimen ECR(DCI) (1) with simulated cracks at week 179, showing light staining on the surface.



Figure 3.92 – Field test specimen ECR(Hycrete) (2) with simulated cracks at week 169, showing scaling on the surface.



Figure 3.93 – Field test specimen ECR (1) at week 205, showing no cracking or staining of the surface.

3.3.6 Summary

To summarize the field tests for different corrosion protection systems, conventional steel corroded at much higher rates and exhibited greater losses than any of the systems containing ECR or MC reinforcement. The corrosion losses were no more than 0.01 and 5.02 μm for the ECR specimens without cracks and no more than 0.02 and 7.97 μm for the ECR specimens with cracks based on total and exposed area, respectively, at ages ranging from 169 to 173 weeks.

The corrosion inhibitors did not improve corrosion resistance of ECR in the field tests. Most specimens without simulated cracks had average corrosion losses less than 0.02 and 6.00 μm based on total and exposed area, respectively, for ages ranging from 163 to 175 weeks. Most specimens with simulated cracks had average corrosion losses less than 0.04 and 15.00 μm based on total and exposed area, respectively, for ages ranging from 163 to 175 weeks. The corrosion performance for all of the specimens with ECR and corrosion inhibitors was similar.

The average corrosion losses of the MC bars were comparable to those of the ECR bars, and both types of reinforcement exhibited significantly better corrosion resistance compared to bare reinforcement. The corrosion losses of the MC specimens with cracks were higher than those of specimens without cracks.

The test results in both cracked and uncracked concrete demonstrated that increased adhesion between the epoxy and reinforcing steel provided no improvement to the corrosion resistance of ECR under the exposure conditions provided by the field tests. For specimens without cracks, all of the specimens had average corrosion losses of no more than 0.02 μm at ages ranging from 165 to 173 weeks based on total area, and no more than 7.11 μm based on exposed area. For specimens with simulated cracks, the corrosion losses for all the specimens increased gradually after initiating,

with average corrosion losses of no more than 0.04 μm at ages ranging from 165 to 173 weeks based on total area, and no more than 15.89 μm based on exposed area.

Overall, the ECR and MC specimens had similar corrosion performance. The corrosion resistance was significantly improved for the ECR and MC reinforcement compared to conventional steel due to the high resistance of the epoxy coating. The corrosion inhibitors provided no improvement in corrosion resistance for the specimens containing ECR. The increased adhesion between the epoxy and reinforcing steel provided no benefits in corrosion performance of ECR under the exposure conditions provided by the tests.

The results presented in this section will be discussed further in Chapter 4, along with comparisons of the corrosion protection systems and test methods.

3.4 KDOT BRIDGE PROJECTS

The section covers the test results for two bridges reinforced with pickled 2205 stainless steel, the Doniphan County Bridge (DCB) and the Mission Creek Bridge (MCB). The results include corrosion potential maps of the bridge decks and the corrosion performance of the accompanying bench-scale and field test specimens as of May 31, 2008. The bench-scale specimens were reinforced with pickled 2205 stainless steel, and the field test specimens were reinforced with conventional, epoxy-coated, or pickled 2205 stainless steel.

3.4.1 Bench-scale Tests

The test results for the Southern Exposure (SE) and cracked beam (CB) specimens containing pickled 2205 stainless steel and concrete with the same mixture proportions and materials as placed in the corresponding bridge decks are presented in this section (test setup is described in Section 2.5.5).

Southern Exposure Test

The SE tests have been underway, and the test period for those specimens is greater than 96 weeks due to the high corrosion resistance of 2205 stainless steel. The average results are based on six and five specimens for DCB and MCB bridges, respectively. The average test results for the SE specimens are presented in Figures 3.94 through 3.97 and the corrosion losses as of May 31, 2008 are summarized in Table 3.14. The individual test results are presented in Appendix A (corrosion rates, corrosion losses, and top and bottom corrosion potentials) and Appendix B (mat-to-mat resistance).

Figure 3.94 shows the average corrosion rates for SE specimens for both bridges. The corrosion rates of the DCB-2205p specimens ranged between -0.036

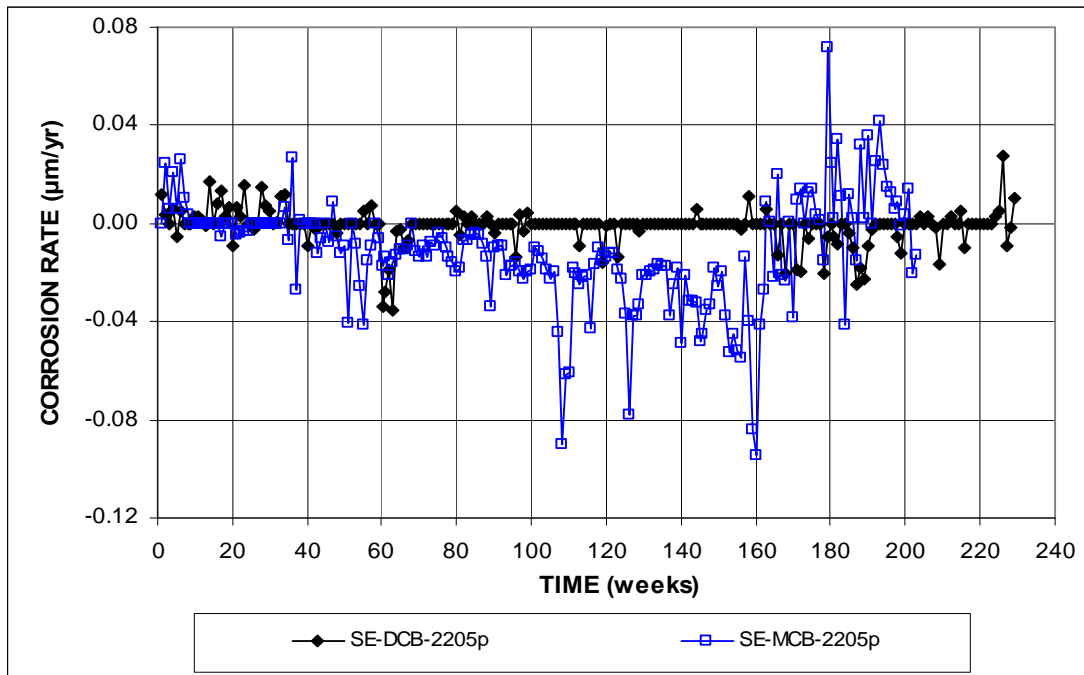


Figure 3.94 – Southern Exposure Test. Average corrosion rates for specimens with pickled 2205 stainless steel for the DCB and MCB.

and $0.028 \mu\text{m/yr}$ during the test period, while the corrosion rates of the MCB-2205p specimens were both higher and lower than those of the DCB-2205p specimens, ranging between -0.094 and $0.072 \mu\text{m/yr}$. The MCB-2205p specimens exhibited negative corrosion rates during weeks 40 to 180, which gradually shifted to positive values after week 180. The DCB-2205p specimens occasionally had negative corrosion rates during the test period. The negative corrosion rates were corroborated by the measured corrosion potentials for the bottom mats steel, which were more negative than the top mats.

The average corrosion losses for the SE specimens cast for the two bridges are shown in Figure 3.95 and summarized in Table 3.14. In both cases, the losses were very low. The DCB-2205p specimens had corrosion losses around zero, with the maximum positive corrosion losses below $0.003 \mu\text{m}$ before week 62 and negative corrosion losses below $-0.005 \mu\text{m}$ after week 190, while the MCB-2205p specimens

exhibited negative corrosion that increased progressively, reaching a value of about $-0.05 \mu\text{m}$ at week 170, decreasing thereafter.

Table 3.14 – Corrosion losses at 203 weeks for pickled 2205 stainless steel in bench-scale tests for the DCB and MCB

Steel Designation ^a	Specimen Corrosion Losses (μm)						Average	Standard Deviation
	1	2	3	4	5	6		
Southern Exposure Test								
DCB-2205p	β	β	β	-0.01	-0.01	-0.01	β	0.01
MCB-2205p	-0.16	-0.07	-0.01	-0.04	0.04		-0.05	0.07
Cracked Beam Test								
DCB-2205p	0.01	0.09	-0.02				0.03	0.05
MCB-2205p	-0.09	-0.04	-0.30	0.61	-0.20	0.03	β	0.32

^a DCB = Doniphan County Bridge. MCB = Mission Creek Bridge.
 2205p = Pickled 2205 stainless steel.
 β Corrosion loss (absolute value) less than $0.005 \mu\text{m}$.

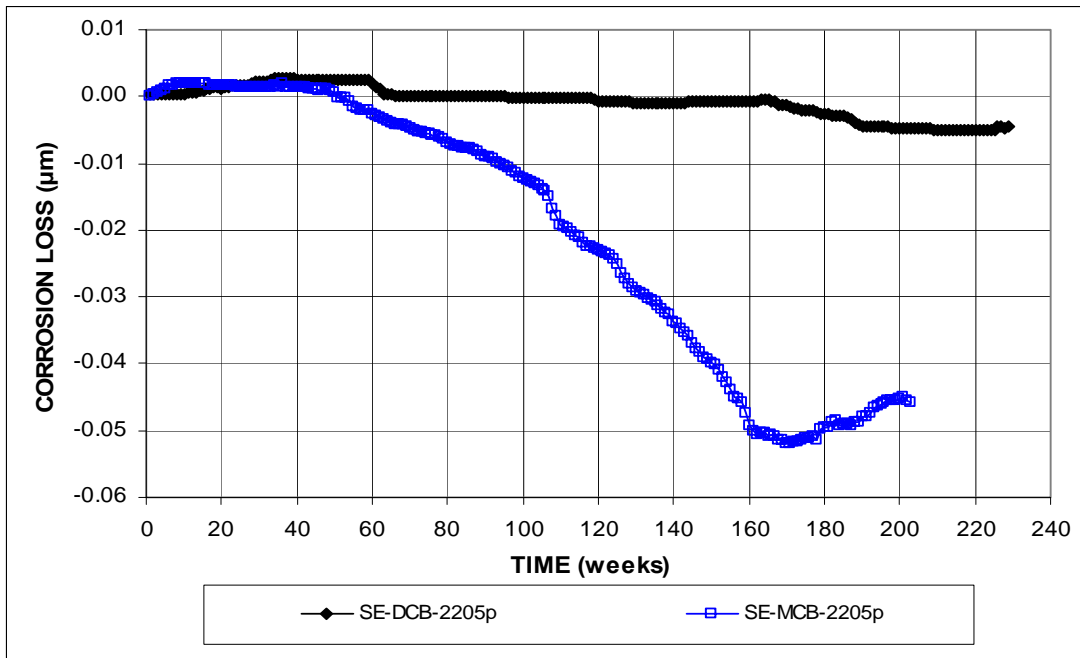


Figure 3.95 – Southern Exposure Test. Southern Exposure Test. Average corrosion losses for specimens with pickled 2205 stainless steel for the DCB and MCB.

The average corrosion potentials with respect to a CSE are shown in Figure 3.96. Both the top and bottom corrosion potentials for the two bridges were relatively stable, with values more positive than -0.300 V, except in week 154 for the top mat of DCB-2205p (top corrosion potential of -0.351 V) and week 227 for the bottom mat (bottom corrosion potential of -0.305 V).

Figure 3.97 shows the average mat-to-mat resistances for specimens with pickled 2205 stainless steel for both bridges. The mat-to-mat resistance for the MCB-2205p specimens ranged from 85 to 556 ohms, which were much lower than those of the DCB-2205p specimens, with values ranging from 130 to 13,000 ohms. The mat-to-mat resistances for the MCB-2205p specimens were also much more stable than those of the DCB-2205p specimens.

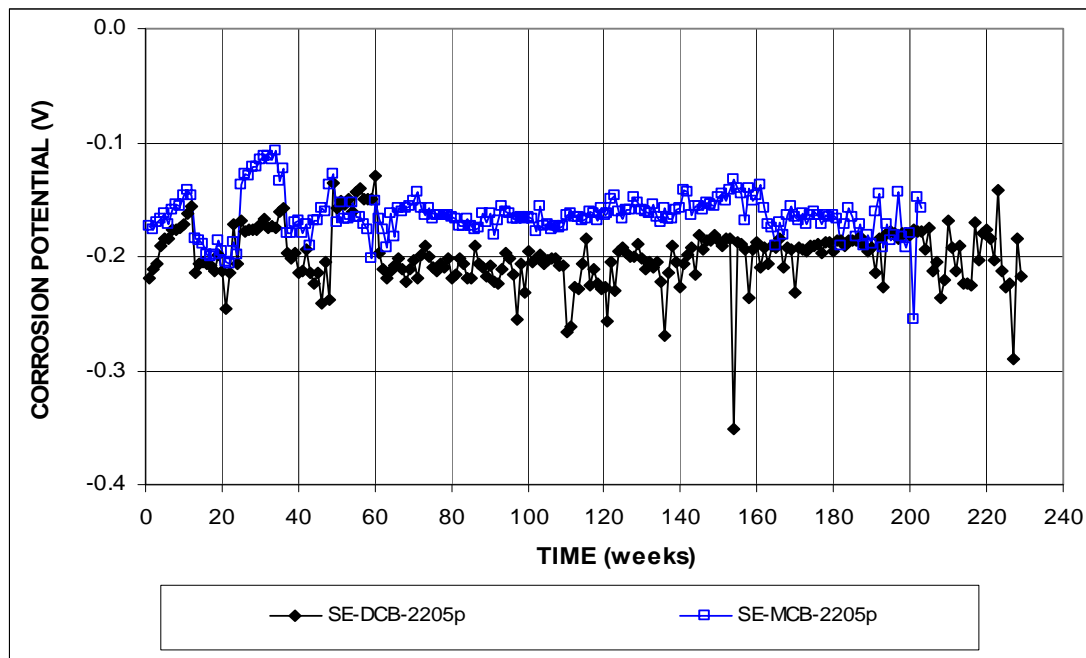


Figure 3.96a – Southern Exposure Test. Average top mat corrosion potentials with respect to a copper-copper sulfate electrode for specimens with pickled 2205 stainless steel for the DCB and MCB.

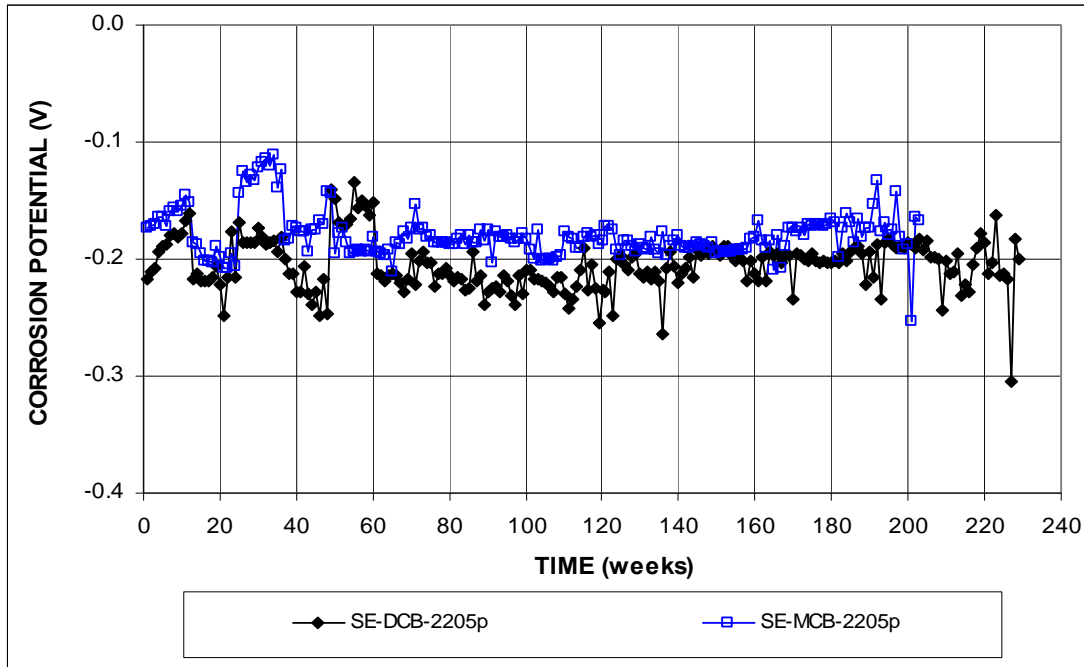


Figure 3.96b – Southern Exposure Test. Average bottom mat corrosion potentials with respect to a copper-copper sulfate electrode for specimens with pickled 2205 stainless steel for the DCB and MCB.

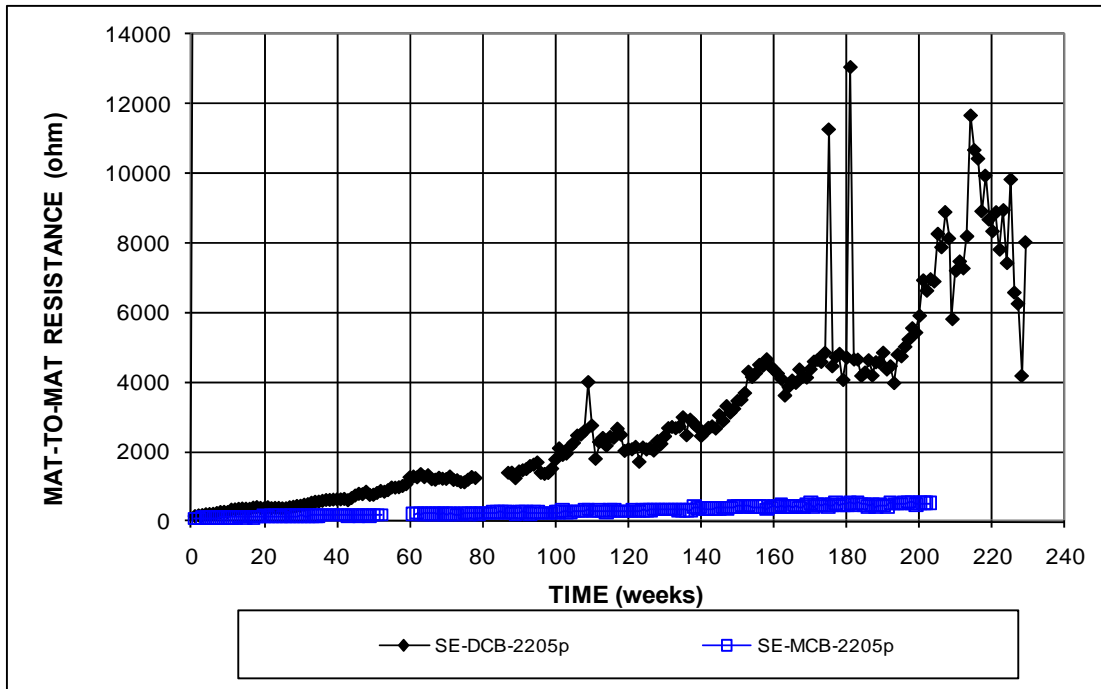


Figure 3.97 – Southern Exposure Test. Average mat-to-mat resistances for specimens with pickled 2205 stainless steel for the DCB and MCB.

Cracked Beam Test

The average results for the cracked beam tests are presented in Figures 3.98 through 3.101 and the corrosion losses at 203 weeks are summarized in Table 3.14. The average results are based on three and five specimens for DCB and MCB bridges, respectively. The individual results are included in Appendices A and B.

Figure 3.98 shows the average corrosion rates for the cracked beam specimens for both bridges. The corrosion rates for the CB specimens were about twice the rates for SE specimens, ranging between -0.114 and 0.084 $\mu\text{m}/\text{yr}$ for the specimens cast for the Doniphan County Bridge and between -0.093 and 0.177 $\mu\text{m}/\text{yr}$ for the specimens cast for the Mission Creek Bridge. As with the SE specimens, some specimens for both bridges exhibited negative corrosion rates, especially the MCB-2205p specimens between weeks 20 and 55, 140 and 173, and after week 198, indicating that the bottom mats were more active than the corresponding top mats during those periods.

The average corrosion losses for the CB specimens for the two bridges are shown in Figure 3.99 and summarized in Table 3.14. The losses were again very low; they fluctuated at a higher frequency for the CB specimens than for the SE specimens for both bridges due to the greater variation of corrosion rate. The DCB-2205p specimens had positive corrosion losses for the entire test period, with values around 0.01 μm between weeks 29 and 119 and near 0.03 μm after week 160, while the MCB-2205p specimens had negative corrosion losses during a majority of the test period, with values around 0 between weeks 135 and 147 and remained above 0 after week 186 with a high value of 0.008 μm at week 191.

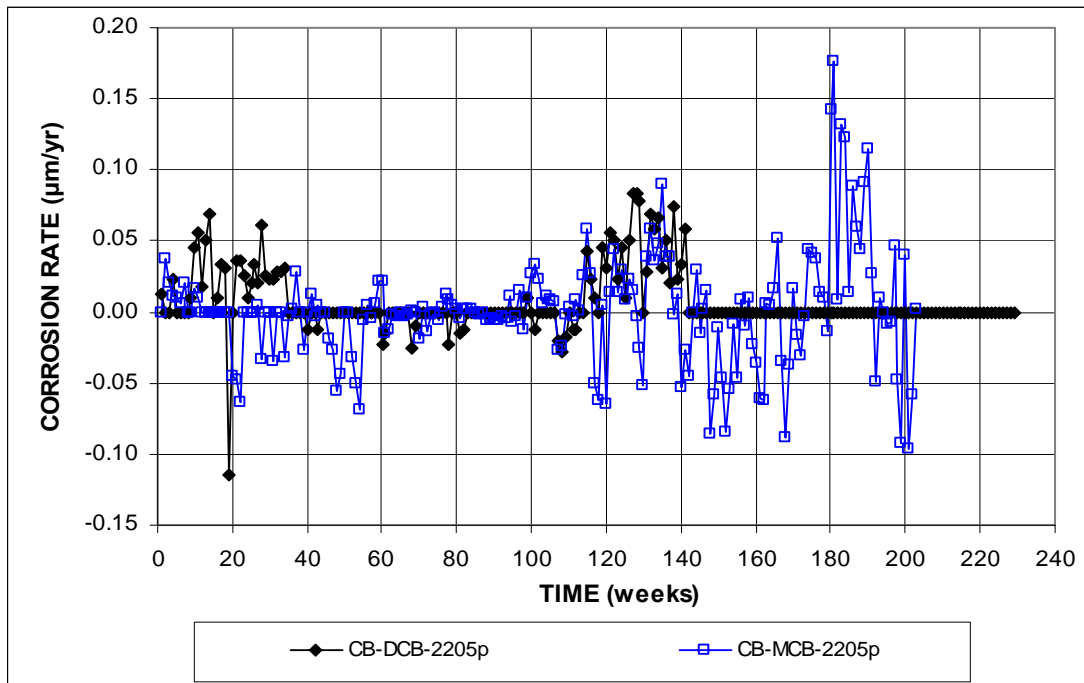


Figure 3.98 – Cracked Beam Test. Average corrosion rates for specimens with pickled 2205 stainless steel for the DCB and MCB.

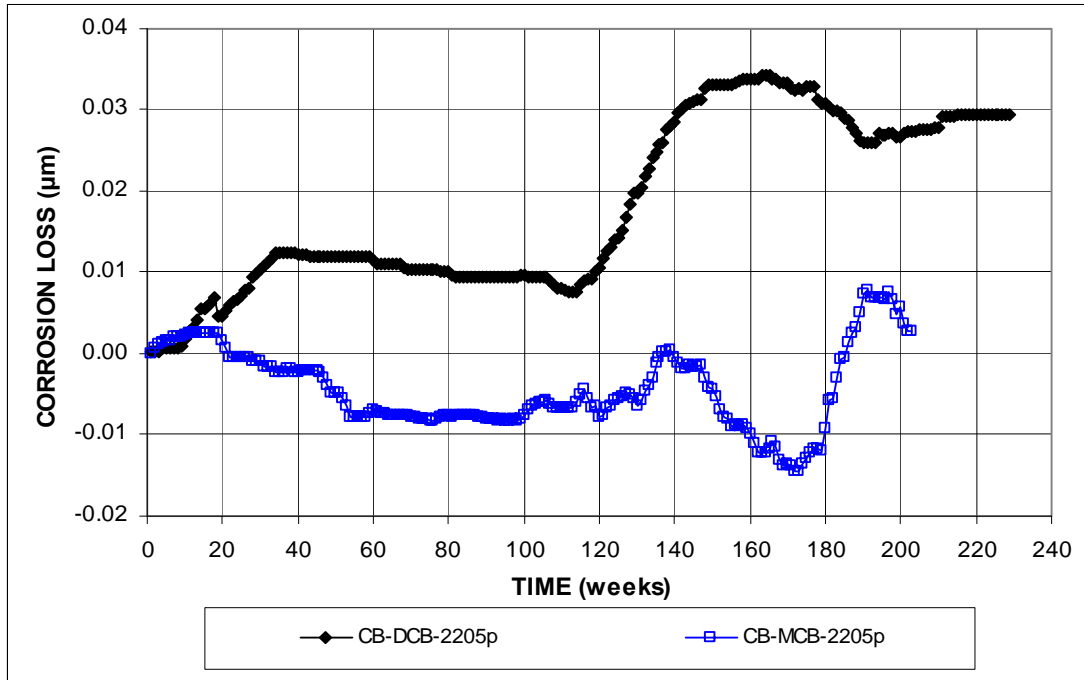


Figure 3.99 – Cracked Beam Test. Average corrosion losses for specimens with pickled 2205 stainless steel for the DCB and MCB.

The average corrosion potentials for the CB specimens are shown in Figure 3.100. The plots of the top mat corrosion potentials for both bridges show slight trends shifting in the negative direction. The DCB-2205p specimens had slightly more negative top mat corrosion potentials than the MCB-2205p specimens, but the corrosion potential remained more positive than -0.350 V, except for -0.354 V at week 208; while the top mat corrosion potentials for MCB-2205p were consistently above -0.300 V by week 203. The bottom mat corrosion potentials for both bridges were relatively stable, with values fluctuating around -0.200 V. Similar to the top mats, the bottom mat corrosion potentials of the DCB-2205p specimens were slightly more negative than those of the MCB-2205p specimens, but with values that were more positive than -0.300 V throughout the test period.

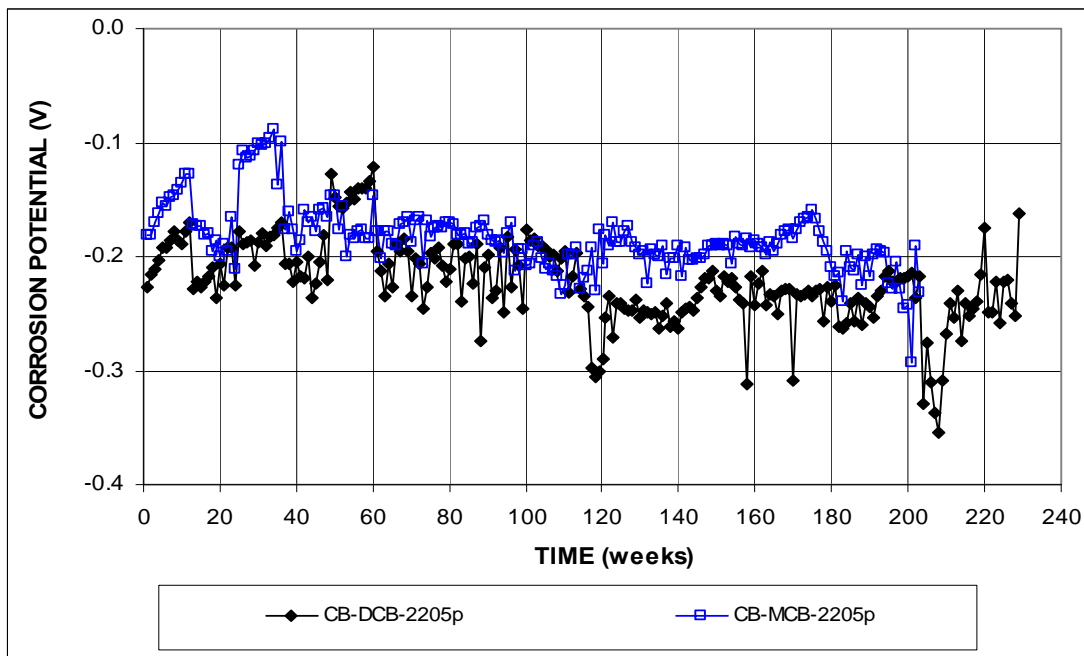


Figure 3.100a – Cracked Beam Test. Average top mat corrosion potentials with respect to a copper-copper sulfate electrode for specimens with pickled 2205 stainless steel for the DCB and MCB.

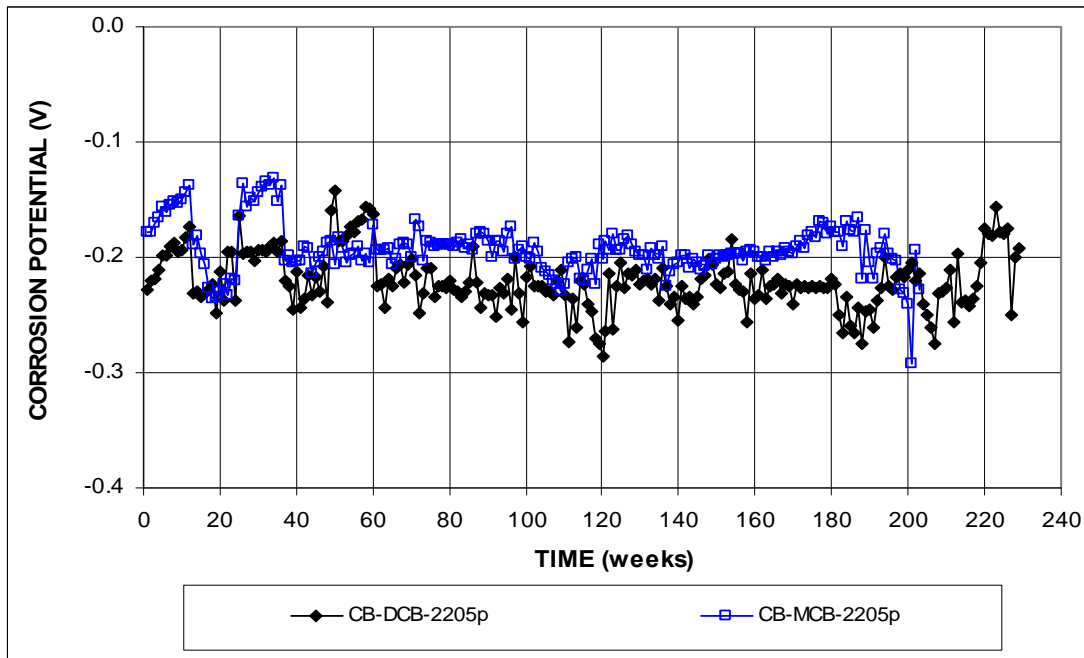


Figure 3.100b – Cracked Beam Test. Average bottom mat corrosion potentials with respect to a copper-copper sulfate electrode for specimens with pickled 2205 stainless steel for the DCB and MCB.

Figure 3.101 shows the average mat-to-mat resistances for specimens with pickled 2205 stainless steel in the CB test. The mat-to-mat resistances for the MCB-2205p specimens increased from 200 to 5,000 ohms, while that of DCB-2205p increased from 300 to 17,000 ohms. The MCB-2205p specimens demonstrated more stable mat-to-mat resistances than did of the DCB-2205p specimens. The mat-to-mat resistance plots for both DCB-2205p and MCB-2205p specimens exhibited more fluctuations and higher resistances in the CB test than in the SE test. For the DCB-2205p specimens, the average mat-to-mat resistance was around 8,000 ohms in the SE test and 13,000 ohms in the CB test at weeks around 220 as of May 31, 2008, while the MCB-2205p specimens had average mat-to-mat resistance of approximately 500 and 1,600 ohms at week 200 in the SE and CB test, respectively.

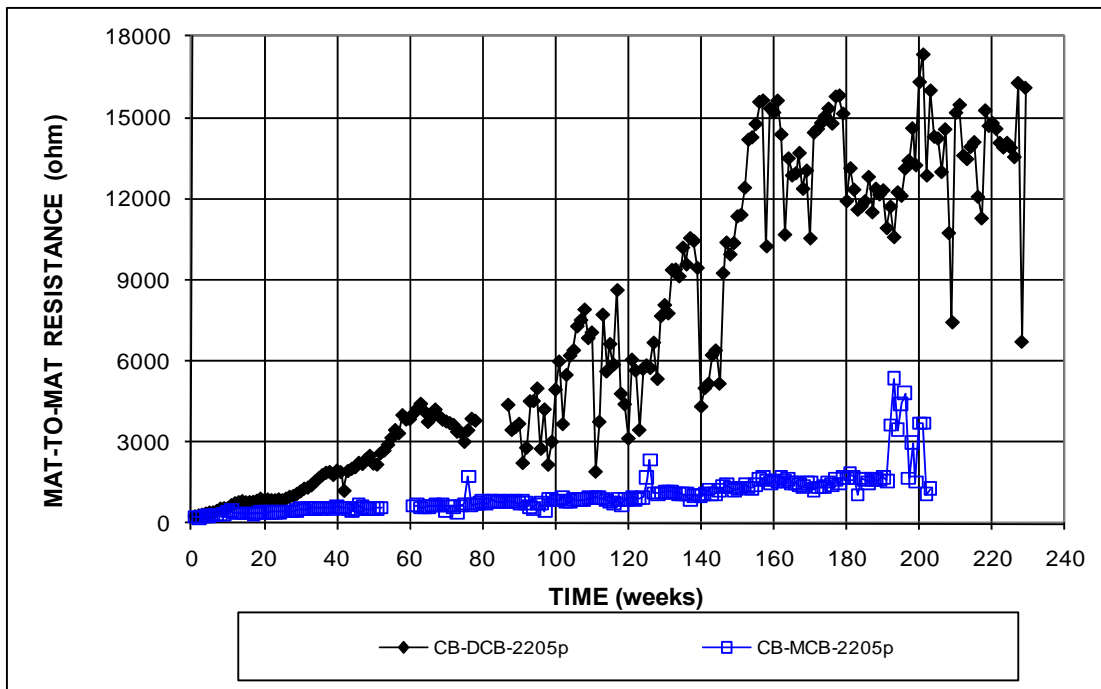


Figure 3.101 – Cracked Beam Test. Average mat-to-mat resistances for specimens with pickled 2205 stainless steel for the DCB and MCB.

3.4.2 Field Test

This section presents the test results for the field test specimens containing conventional, epoxy-coated, and pickled 2205 stainless steel cast with concrete with the same mixture proportions and materials as the corresponding decks for the Doniphan County Bridge and the Mission Creek Bridge (test setup is described in Section 2.5.4). For the Doniphan County Bridge, all of the specimens were cast without simulated cracks and the ECR bars were placed without intentional holes in the epoxy coating. For the Mission Creek Bridge, one of the two specimens for each system (specimen No. 2) contained simulated cracks and all of the ECR bars had 16 3-mm ($\frac{1}{8}$ -in.) diameter holes in the epoxy coating.

The corrosion rates and corrosion losses for specimens with conventional and pickled 2205 stainless steel are based on the total area of the top mat bars due to

electrical connection between the bars in these specimens, while those of the specimens with the epoxy-coated bars are based on the total area of one test bar and the exposed area of the drilled holes (Mission Creek Bridge). The readings for field specimens exhibited larger fluctuations than those of the bench-scale specimens due the changes in outdoor temperatures and concrete moisture content. As described in Section 1.2, for corrosion to occur, four elements must be present – an anode, a cathode, an electrolyte, and an electron path. Changing temperature and moisture can affect the electron transport efficiency in electrolyte and, therefore, affect corrosion activity.

3.4.2.1 Doniphan County Bridge

The average results for the field test specimens for the Doniphan County Bridge are presented in Figures 3.102 through 3.105 and the corrosion losses at week 215 are summarized in Table 3.15. The individual results are presented in Appendix A (corrosion rates, corrosion losses, and corrosion potentials) and Appendix B (mat-to-mat resistance).

As shown in Figure 3.102, conventional steel had the highest corrosion rates, which increased over time and reached a high value of 1.818 $\mu\text{m}/\text{yr}$ for DCB-Conv. (1) at week 175 and 1.615 $\mu\text{m}/\text{yr}$ for DCB-Conv. (2) at week 215. The corrosion rates for specimens with the epoxy-coated steel and 2205 stainless steel fluctuated around 0, with values ranging between -0.032 and 0.027 $\mu\text{m}/\text{yr}$ and between -0.004 and 0.005 $\mu\text{m}/\text{yr}$, respectively. The corrosion rates of conventional steel were on an order of 300 times the corrosion rates of the stainless steel and 60 times the corrosion rates of the epoxy-coated steel. Both epoxy-coated specimens exhibited negative corrosion rates at a very low amplitude during portions of the test period.

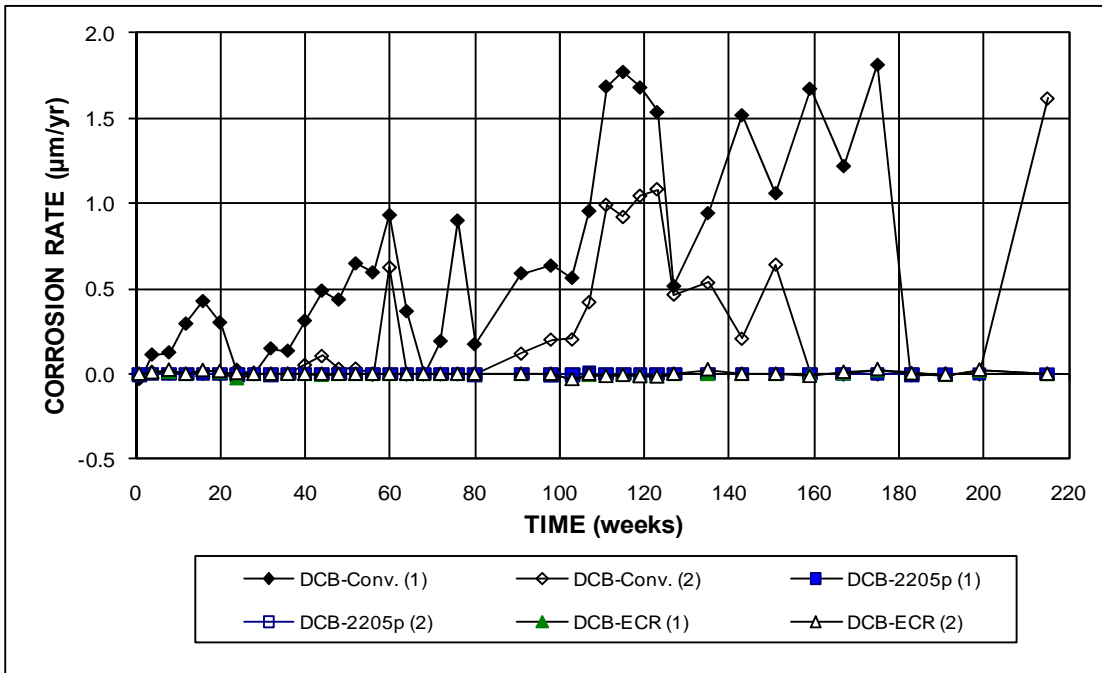


Figure 3.102a – Field Test. Average corrosion rates for specimens with conventional steel, pickled 2205 stainless steel, and ECR for the Doniphan County Bridge.

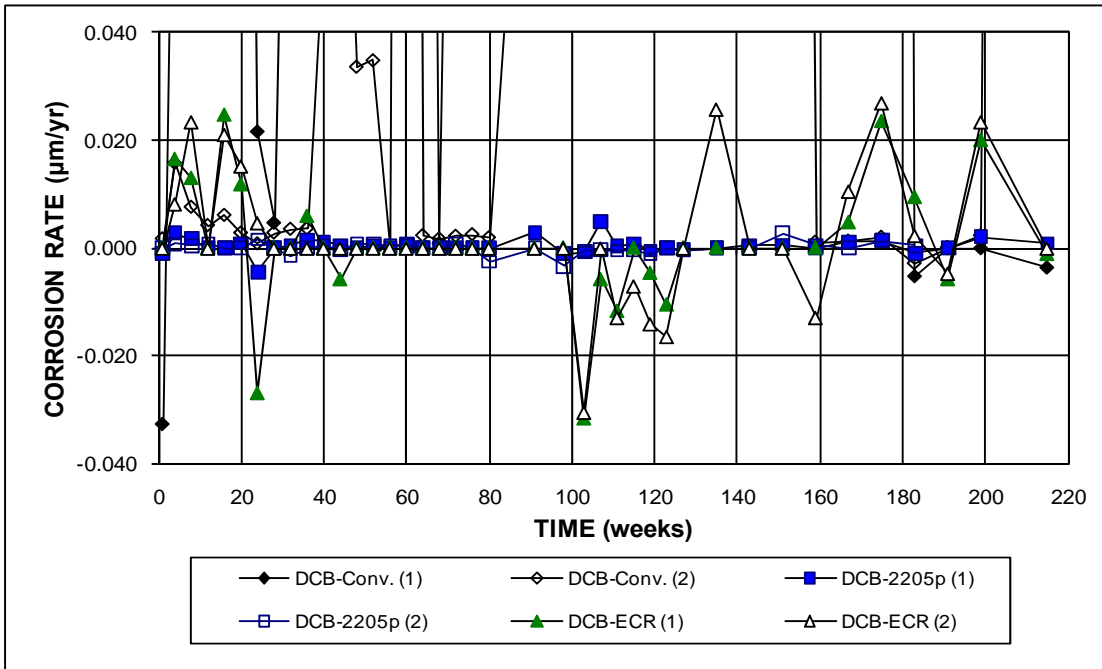


Figure 3.102b – Field Test. Average corrosion rates for specimens with conventional steel, pickled 2205 stainless steel, and ECR for the Doniphan County Bridge. (Different scale)

The average corrosion losses are shown in Figure 3.103 and summarized in Table 3.15. The corrosion losses of conventional steel increased progressively over time and reached 2.66 μm for DCB-Conv. (1) and 1.24 μm for DCB-Conv. (2) at week 215; while those of the 2205 stainless steel and epoxy-coated steel were much lower throughout the test period, with values ranging between -0.003 and 0.01 μm .

Table 3.15 – Corrosion losses at 215 weeks for conventional steel, pickled 2205 stainless steel, and ECR in field test for the Doniphan County Bridge

Steel Designation ^a	Test bar Corrosion Losses (μm) ^b		Average	Standard Deviation
	1	2		
DCB-Conv. (1)	3.56	1.77	2.66	1.26
DCB-Conv. (2)	1.51	0.96	1.24	0.39
DCB-2205p (1)	β	β	β	β
DCB-2205p (2)	β	β	β	β
DCB-ECR (1)	β	0.01	β	0.01
DCB-ECR (2)	0.01	0.01	0.01	β

^a DCB = Doniphan County Bridge.

Conv. = Conventional steel. 2205p = pickled 2205 stainless steel.

ECR = Conventional epoxy-coated reinforcement.

^b Values for Conv. and 2205p are based on total area of top mat bars. Values for ECR are based on total area of one ECR bar and there are no drilled holes on the epoxy coating.

β Corrosion loss (absolute value) less than 0.005 μm .

The average corrosion potentials with respect to a CSE are shown in Figure 3.104. Conventional specimens exhibited more negative corrosion potentials than specimens with epoxy-coated and 2205 stainless steel. The top mat corrosion potentials were more negative than -0.350 V, indicating active corrosion for DCB-Conv. (1) after week 60 and for DCB-Conv. (2) between weeks 98 and 167, except at week 123. The bottom mat corrosion potentials for conventional steel fluctuated around -0.350 V after week 72, indicating a slight tendency to corrode. The corrosion potentials for the ECR and the 2205 stainless steel specimens were similar, with values more positive than -0.350 V, except for the top mat of DCB-ECR (1) with

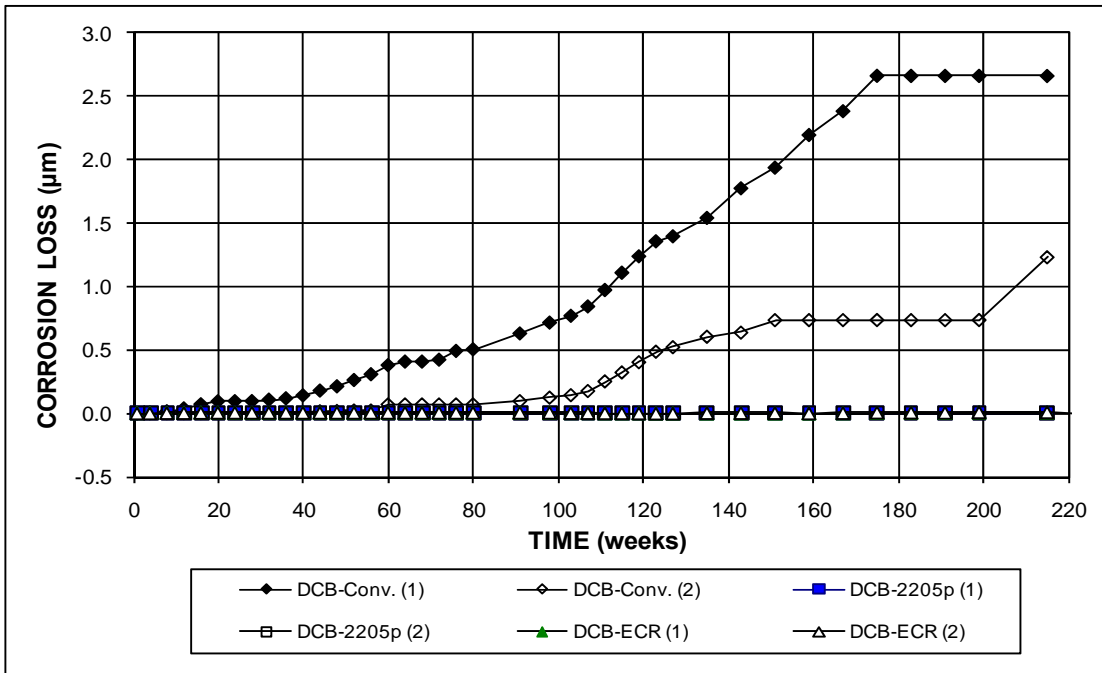


Figure 3.103a – Field Test. Average corrosion losses for specimens with conventional steel, pickled 2205 stainless steel, and ECR for the Doniphan County Bridge.

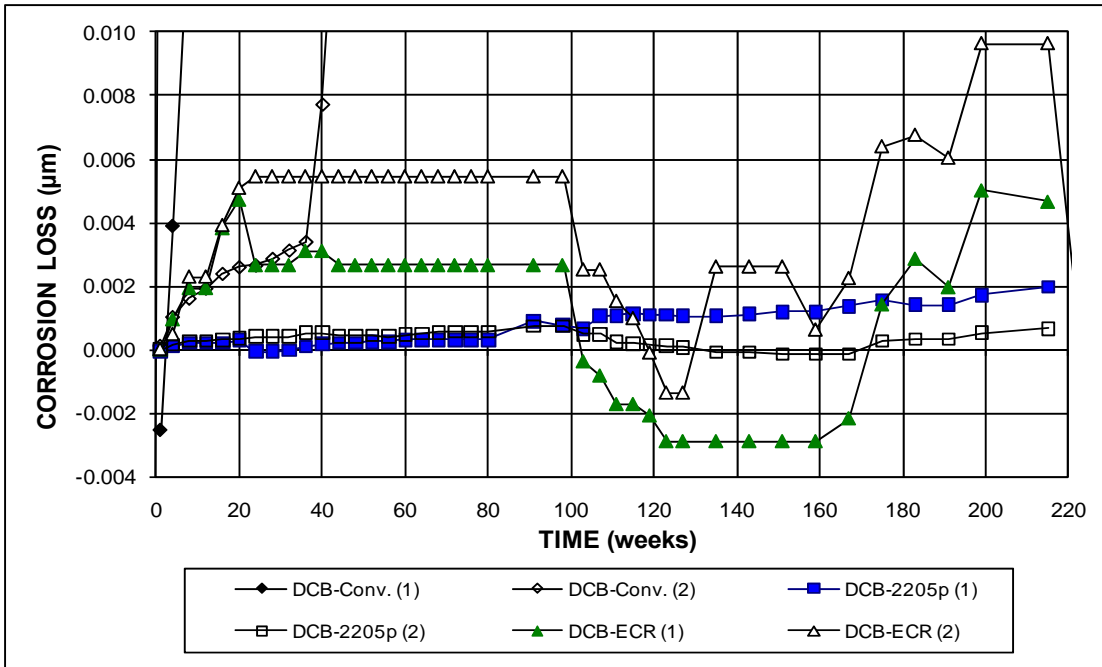


Figure 3.103b – Field Test. Average corrosion losses for specimens with conventional steel, pickled 2205 stainless steel, and ECR for the Doniphan County Bridge. (Different scale)

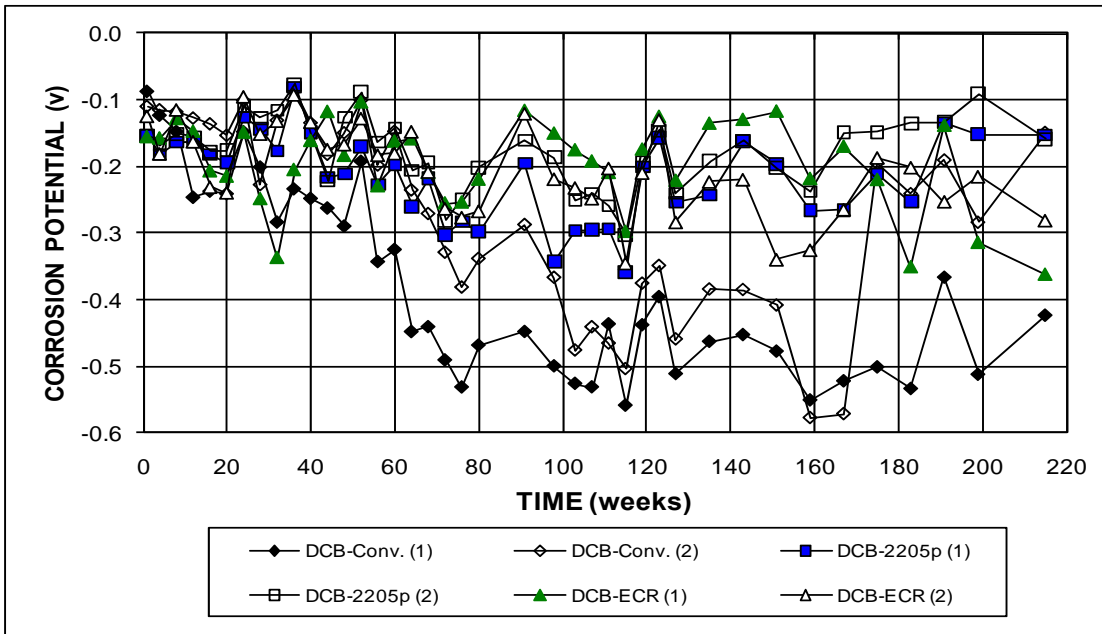


Figure 3.104a – Field Test. Average top mat corrosion potentials with respect to a copper-copper sulfate electrode for specimens with conventional steel, pickled 2205 stainless steel, and ECR for the Doniphan County Bridge.

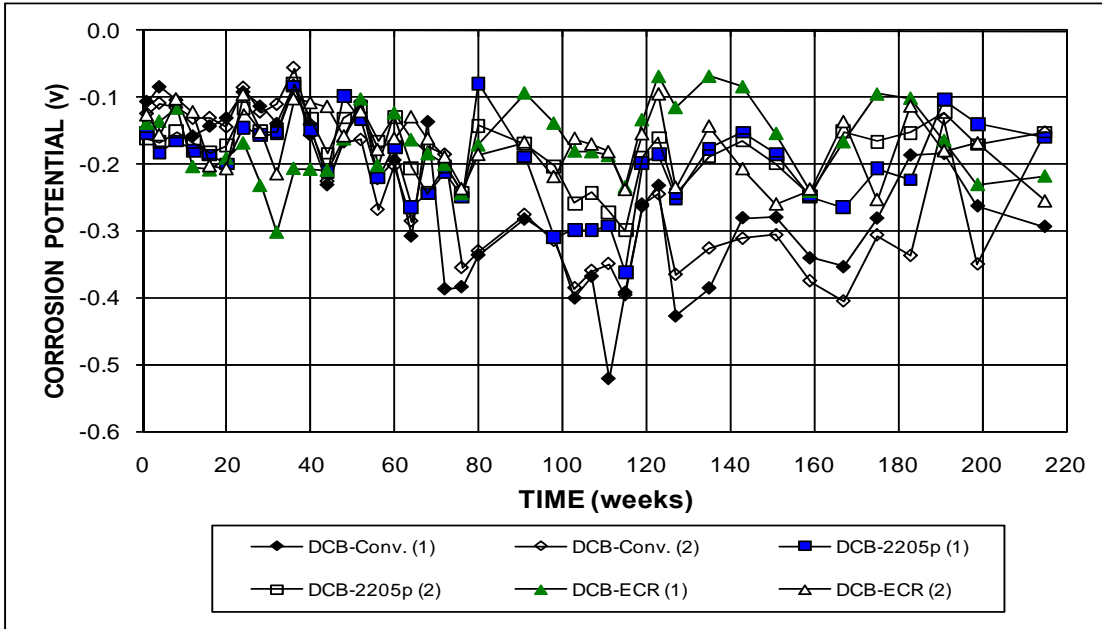


Figure 3.104b – Field Test. Average bottom mat corrosion potentials with respect to a copper-copper sulfate electrode for specimens with conventional steel, pickled 2205 stainless steel, and ECR for the Doniphan County Bridge.

corrosion potentials -0.352 and -0.363 V at weeks 183 and 215, respectively, and the bottom mat of DCB-2205p (1) with a corrosion potential of -0.362 V at week 115.

As shown in Figure 3.105, the mat-to-mat resistances for the epoxy-coated bar specimens ranged from 1,200 to 15,000 ohms, while those of the conventional steel and 2205 stainless steel were below 120 ohms, except for DCB-2205p (1) with an increase during the period between weeks 115 and 135 to a peak value as high as 7,845 ohms.

3.4.2.2 Mission Creek Bridge

The average test results for the Mission Creek Bridge specimens are presented in Figures 3.106 through 3.109 and the corrosion losses at week 189 are summarized in Table 3.16. The individual test results are presented in Appendices A and B.

As shown in Figure 3.106, the specimens with conventional steel initiated corrosion activity around week 65 and had much higher corrosion rates than the other specimens. The specimens with simulated cracks (No. 2 specimens) showed more active corrosion than specimens without cracks, with higher corrosion rates and more negative top mat corrosion potentials. Specimen MCB-Conv. (2) had the highest corrosion rate, $9.37 \mu\text{m/yr}$ at week 89. Specimen MCB-2205p (2) showed active corrosion after week 117 with corrosion rates ranging between -0.82 and $0.32 \mu\text{m/yr}$. The corrosion rates of the MCB-2205p (1) and both ECR specimens were less than $0.08 \mu\text{m/yr}$, indicating that these specimens remained in a passive state during the test period.

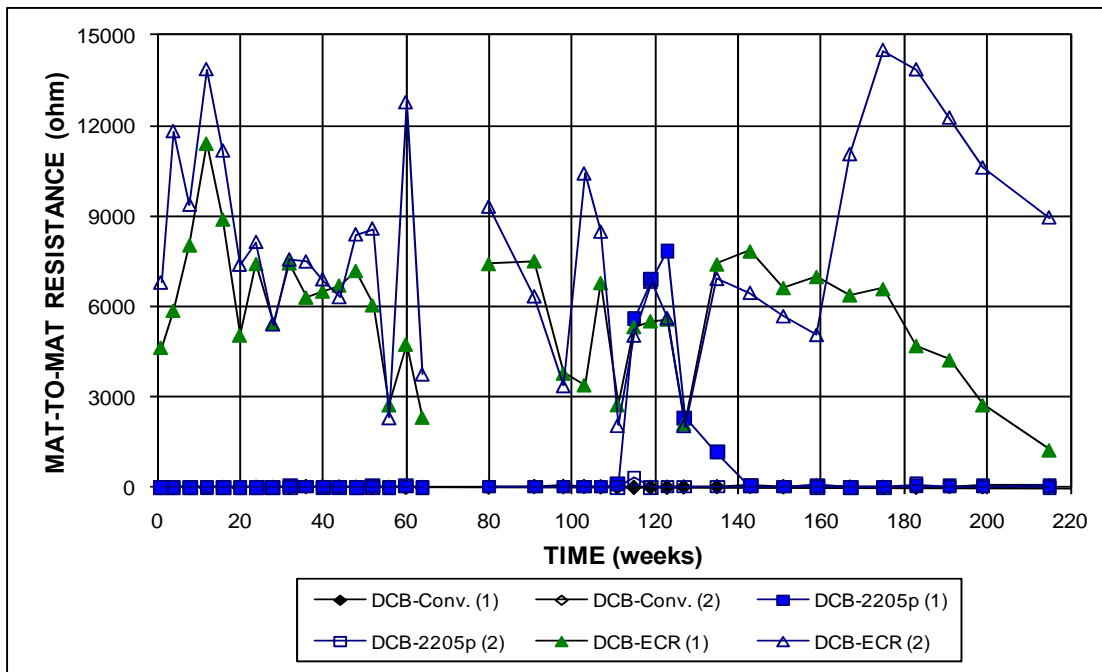


Figure 3.105a – Field Test. Average mat-to-mat resistances for specimens with conventional steel, pickled 2205 stainless steel, and ECR for the Doniphan County Bridge.

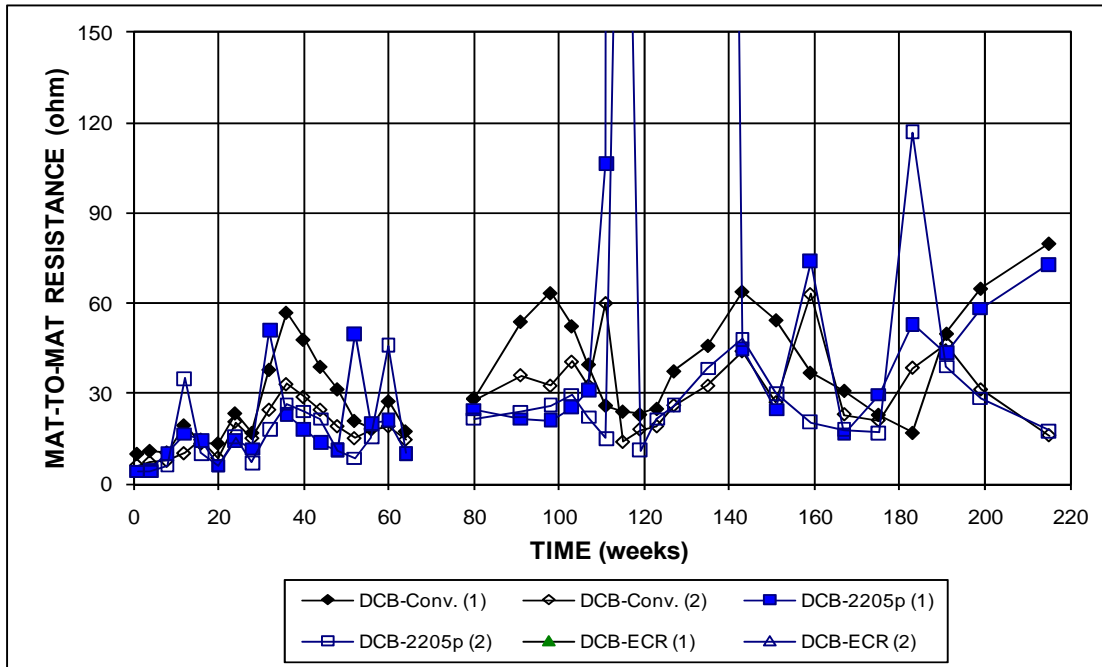


Figure 3.105b – Field Test. Average mat-to-mat resistances for specimens with conventional steel, pickled 2205 stainless steel, and ECR for the Doniphan County Bridge. (Different scale)

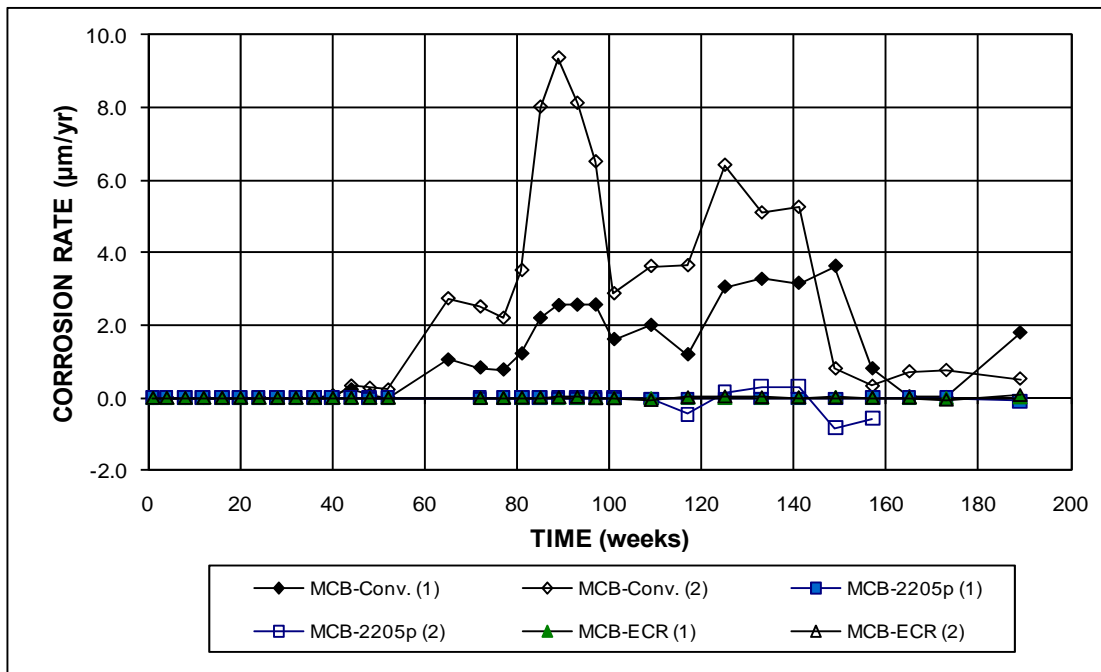


Figure 3.106a – Field Test. Average corrosion rates for specimens with conventional steel, pickled 2205 stainless steel, and ECR for the Mission Creek Bridge.

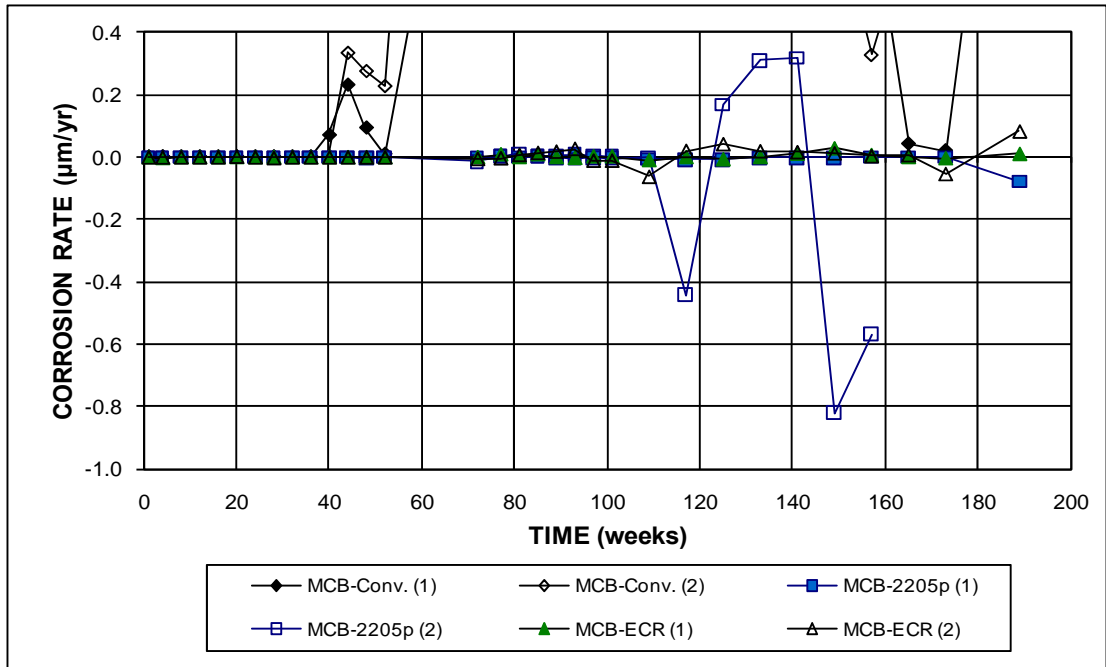


Figure 3.106b – Field Test. Average corrosion rates for specimens with conventional steel, pickled 2205 stainless steel, and ECR for the Mission Creek Bridge. (Different scale)

The average corrosion losses for the specimens for the Mission Creek Bridge are shown in Figure 3.107. The corrosion losses for conventional steel specimens increased gradually after initiating at week 65 and remained around 8 μm for specimen MCB-Conv. (2) and 4 μm for specimen MCB-Conv. (1) after week 140, while those of the 2205 stainless steel and epoxy-coated specimens remained near zero throughout the test. As shown in Table 3.16, Specimen MCB-Conv. (2) had the highest corrosion loss, 8.53 μm at week 189, followed by specimen MCB-Conv. (1) with 4.67 μm . Specimens MCB-ECR (2) and (1) had respective corrosion losses of 0.03 and 0.01 μm at week 189 based on total area and 10.57 and 1.52 μm based on exposed area. The specimens with pickled 2205 stainless steel exhibited small negative corrosion values, $-0.03 \mu\text{m}$ for MCB-2205p (1) and $-0.25 \mu\text{m}$ for MCB-2205p (2), which are comparable to those of the matching bench-scale specimens, $-0.05 \mu\text{m}$ and less than $0.005 \mu\text{m}$, respectively.

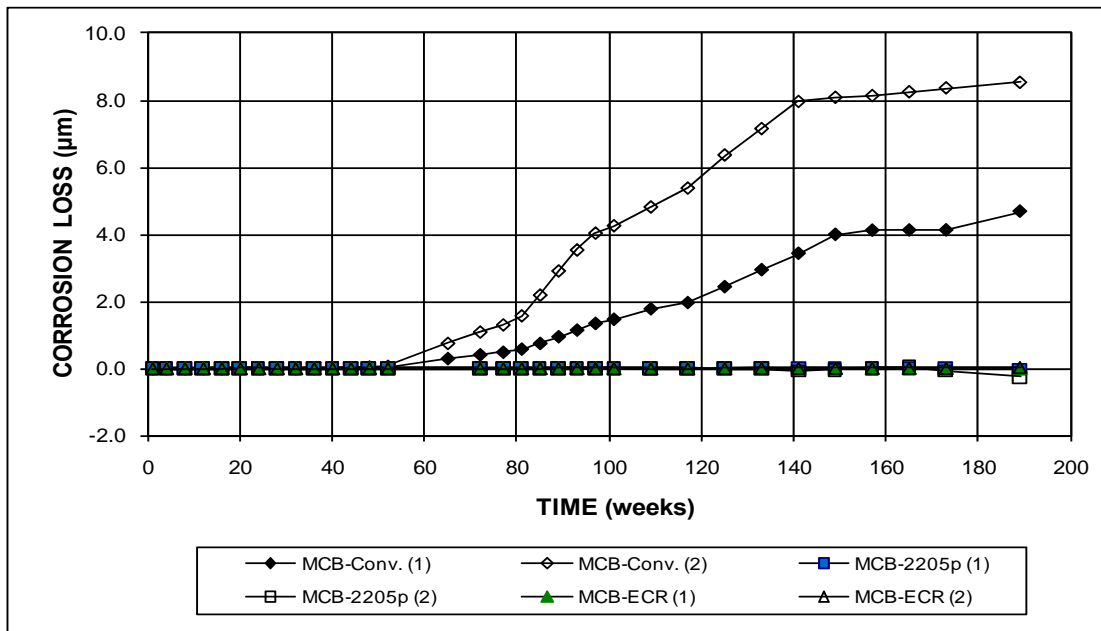


Figure 3.107a – Field Test. Average corrosion losses for specimens with conventional steel, pickled 2205 stainless steel, and ECR for the Mission Creek Bridge.

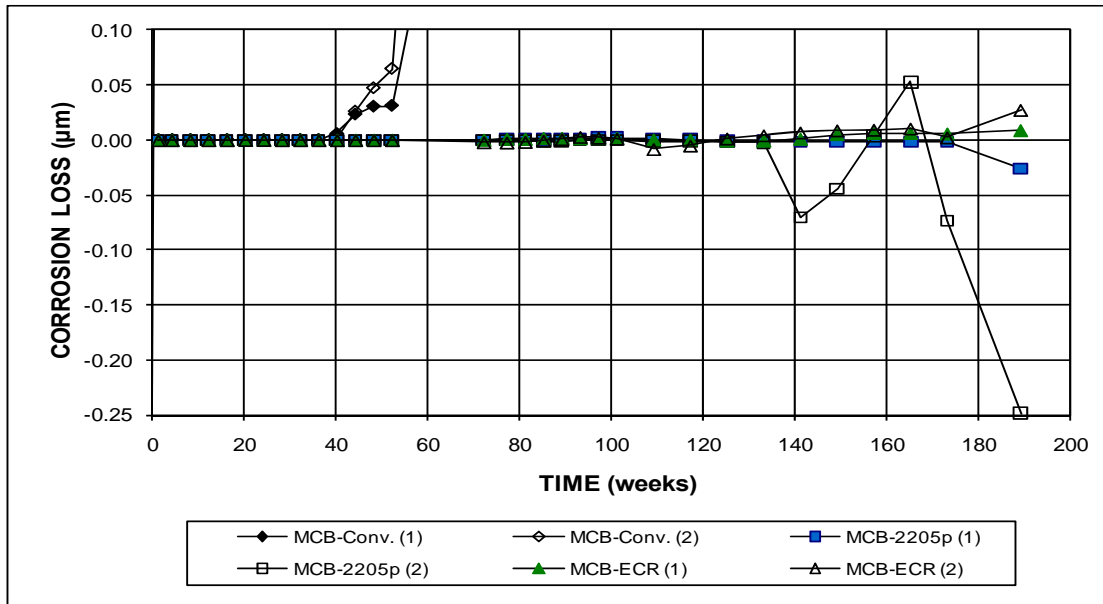


Figure 3.107b – Field Test. Average corrosion losses for specimens with conventional steel, pickled 2205 stainless steel, and ECR for the Mission Creek Bridge. (Different scale)

Table 3.16 – Corrosion losses at 189 weeks for conventional steel, pickled 2205 stainless steel, and ECR in field test for the Mission Creek Bridge

Steel Designation ^a	Test bar Corrosion Losses (µm) ^b				Average	Standard Deviation
	1	2	3	4		
Based on Total Area						
MCB-Conv. (1)	3.40	5.94			4.67	1.79
MCB-Conv. (2)	7.53	9.52			8.53	1.41
MCB-2205p (1)	β	-0.05			-0.03	0.04
MCB-2205p (2)	β	-0.50			-0.25	0.35
MCB-ECR (1)	0.01	0.01	0.02	β	0.01	0.01
MCB-ECR (2)	0.03	0.05	-0.02	0.05	0.03	0.03
Based on Exposed Area						
MCB-ECR (1)*	2.85	2.11	0.02	1.09	1.52	1.23
MCB-ECR (2)*	13.37	18.45	-6.92	18.17	10.77	12.02

^a MCB = Mission Creek Bridge.

Conv. = Conventional steel. 2205p = pickled 2205 stainless steel.

ECR = Conventional epoxy-coated reinforcement, with coating penetrated with 16 3-mm (1/8-in.) holes .

All No. 2 specimens have simulated cracks.

^b For corrosion losses based on total area, Conv. and 2205p are based on total area of top mat bars and ECR are based on total area of one ECR bar.

* Values based on exposed area.

β Corrosion loss (absolute value) less than 0.005 µm.

The average corrosion potentials with respect to CSE are shown in Figure 3.108. The corrosion potentials for the top mats of the conventional steel specimens were between -0.110 and -0.400 V before week 36 and slightly shifted to more negative values after that, with values ranging between -0.400 and -0.650 V after week 72, except for MCB-Conv. (1) with a corrosion potential of -0.376 V at week 97. Top mat corrosion potentials for specimen MCB-ECR (2) fluctuated around -0.400 V, while the top mat corrosion potential of specimen MCB-ECR (1) and the stainless steel specimens were more positive than -0.350 V throughout the test, except for MCB-ECR (1) with corrosion potentials -0.357 and -0.395 V at weeks 85 and 97, respectively. The bottom mat corrosion potentials were similar for all of the specimens, fluctuating around -0.200 V with a range between -0.050 and -0.270 V before week 60 and a range between -0.070 and -0.385 V thereafter.

As shown in Figure 3.109, specimen MCB-ECR (2) had the highest mat-to-mat resistances, followed by specimen MCB-ECR (1). The mat-to-mat resistance of specimen MCB-ECR (2) was 43,024 ohms at week 125 and 32,867 ohms at week 165, much higher than the high of 14,494 ohms for either DCB-ECR specimen. The mat-to-mat resistances of specimen MCB-ECR (1) were lower than those of specimen MCB-ECR (2), ranging from 1,000 to 10,000 ohms, similar to those of DCB-ECR specimens, while those of the conventional steel and pickled 2205 stainless steel specimens were below 1,100 ohms.

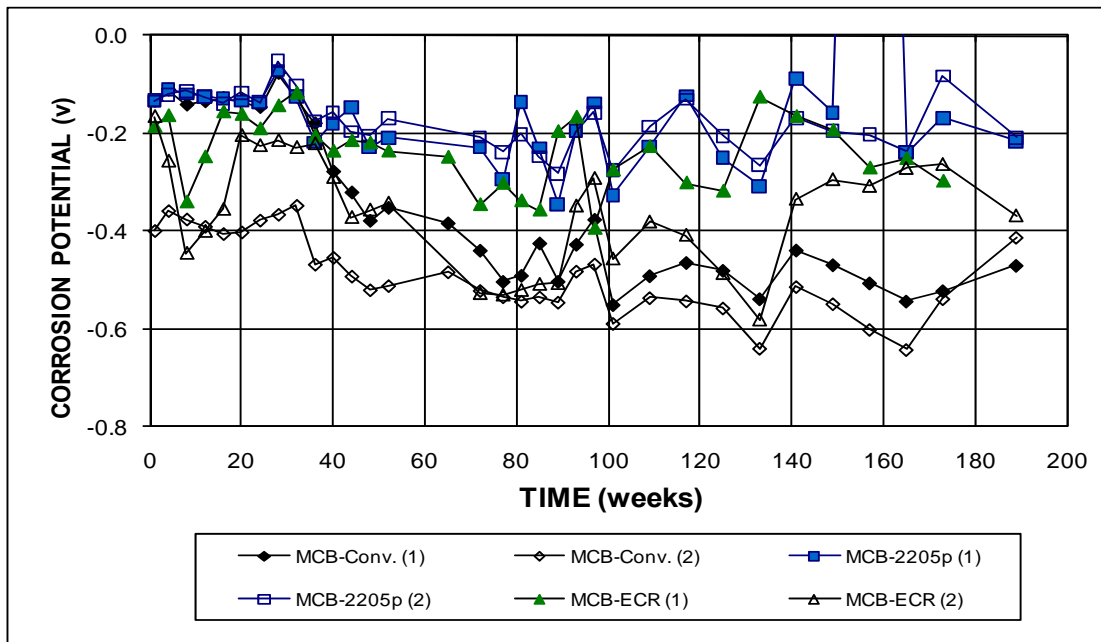


Figure 3.108a – Field Test. Average top mat corrosion potentials with respect to a copper-copper sulfate electrode for specimens with conventional steel, pickled 2205 stainless steel, and ECR for the Mission Creek Bridge.

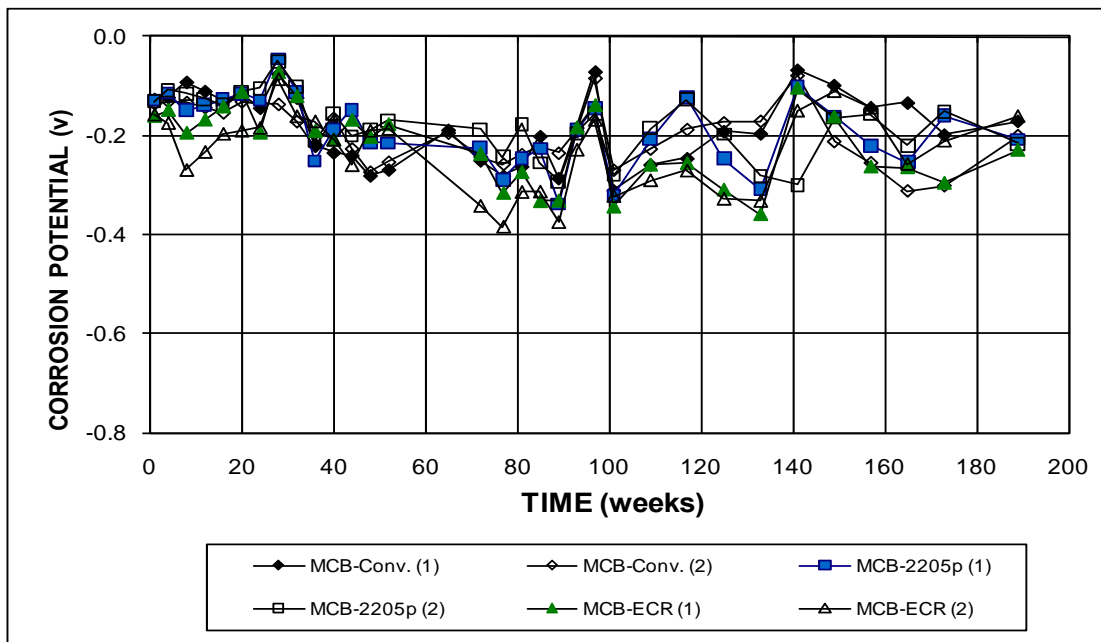


Figure 3.108b – Field Test. Average bottom mat corrosion potentials with respect to a copper-copper sulfate electrode for specimens with conventional steel, pickled 2205 stainless steel, and ECR for the Mission Creek Bridge.

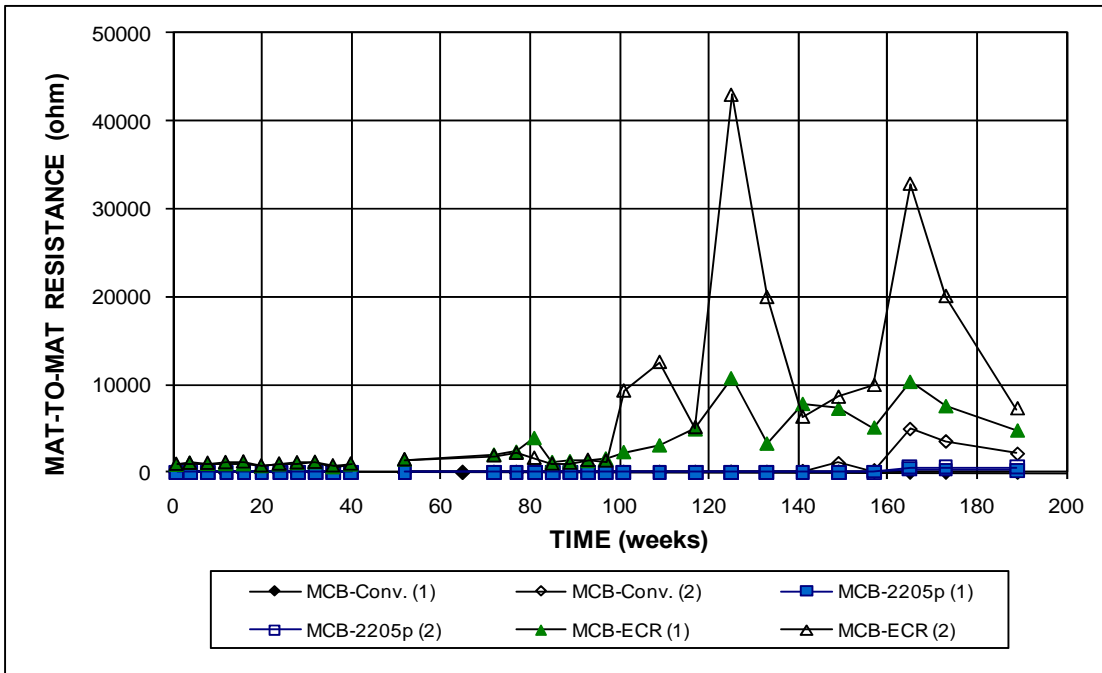


Figure 3.109a – Field Test. Average mat-to-mat resistances for specimens with conventional steel, pickled 2205 stainless steel, and ECR for the Mission Creek Bridge.

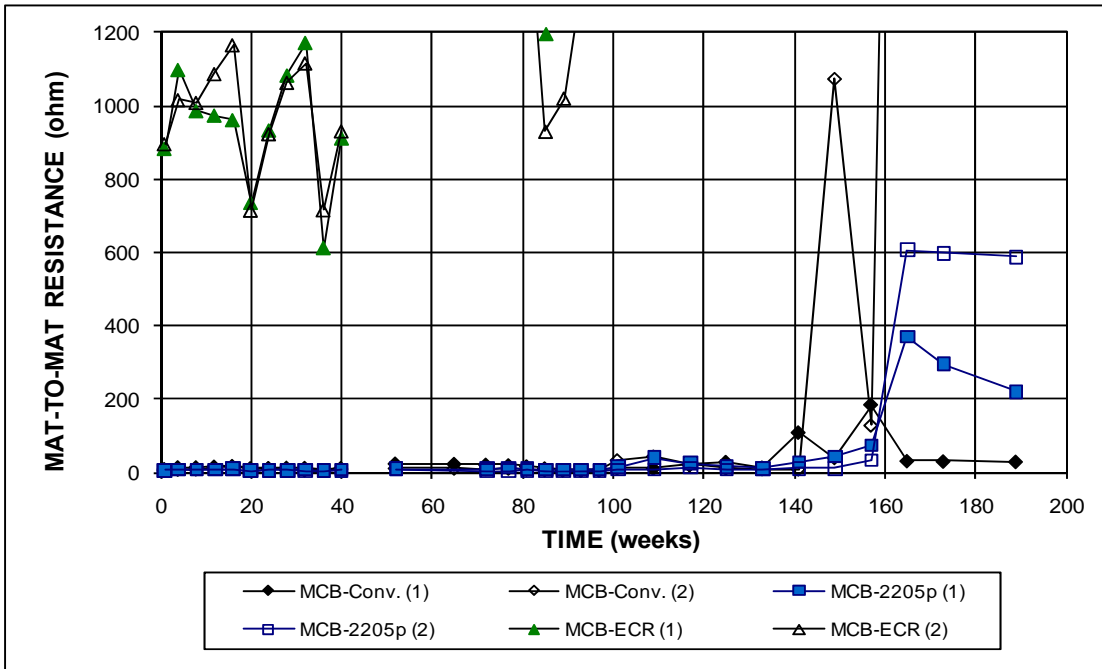


Figure 3.109b – Field Test. Average mat-to-mat resistances for specimens with conventional steel, pickled 2205 stainless steel, and ECR for the Mission Creek Bridge. (Different scale)

3.4.3 Bridge Corrosion Potential Mapping

To monitor the corrosion performance of pickled 2205 stainless steel reinforcement in the Doniphan County and Mission Creek Bridges, test bars were installed in both bridge decks. The measured resistance between the top and bottom test bars was zero, indicating that an electrical connection existed between the top and bottom mat bars. Therefore, corrosion potentials, rather than corrosion current, were used to monitor the long-term corrosion performance of the 2205 stainless steel in both bridge decks.

Every six months, corrosion potentials were measured with respect to a CSE on a fixed grid following procedures described in Section 2.5. The measurements were used to map the corrosion potential contours. Since the first round of the potential surveys was performed in September 2004, eight sets of readings had been recorded for both bridges as of the cutoff date of May 31, 2008. Due to the excellent corrosion performance of stainless steel, the corrosion potentials have not changed very much in four years (current ages of bridges). Therefore, the potential maps of the 1st, 5th, and 8th surveys for both bridges are presented in this section, while all of the maps are included in Appendix C.

3.4.3.1 Doniphan County Bridge

The Doniphan County Bridge (Bridge No. 7-22-18.21(004)) is located on K-7 over the Wolf River in Northeast Kansas. It is a 75.8-m (249-ft) long, three-span continuous composite steel girder bridge. The bridge deck was cast on February 26, 2004 to replace the previous deck, which had deteriorated due to corrosion of the reinforcing steel. Measuring points are distributed on a 2.5×2.5 m (8.2×8.2 ft) grid across the full bridge length (not including the abutments), making 4 rows of 31 and a

total of 124 potential measuring points. As described in Section 2.5.3, the potential was measured at least one hour after the concrete surface was wetted.

Figure 3.110 shows the corrosion potential map for the Doniphan County Bridge as measured on September 17, 2004 during the first survey (seven months after casting). The corrosion potentials in the middle region of the bridge, 3 to 73 m (10 to 240 ft) from the west end, ranged from -0.050 to -0.100 V, while both ends, close to the abutments, were slightly more negative, between -0.100 and -0.200 V. Overall, the bridge had corrosion potentials that were more positive than -0.200 V, indicating a low probability of corrosion activity according to ASTM C876.

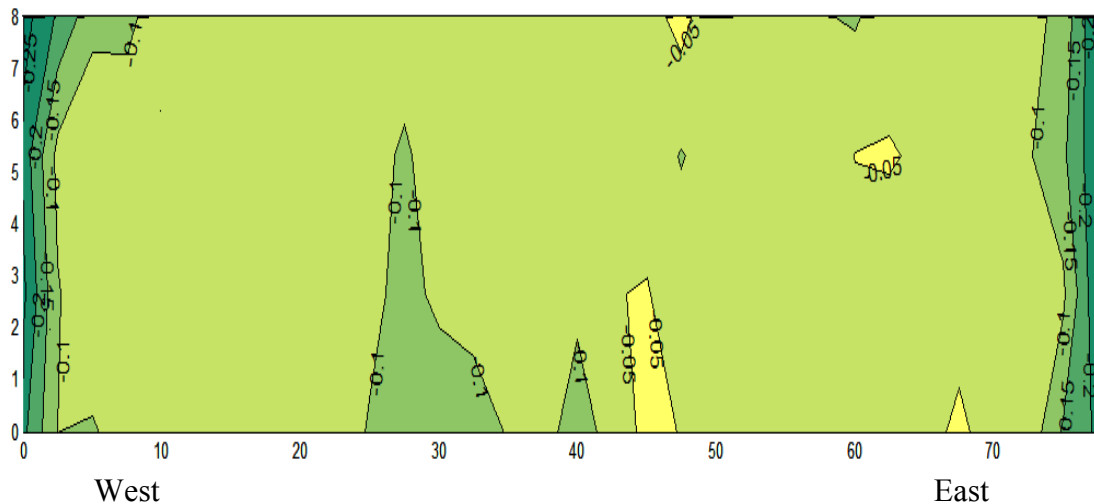


Figure 3.110 – Corrosion potential map for the Doniphan County Bridge (1st survey, September 17, 2004).

The corrosion potential map for the Doniphan County Bridge as measured on October 9, 2006, the fifth survey (two and half years after casting), is shown in Figure 3.111. The middle region, 37 to 65 m (121 to 213 ft) away from the west side, had corrosion potentials more positive than -0.200 V, but somewhat more negative than the potentials measured during the first survey (-0.050 to -0.100 V), at an age of six months, but still in the passive state. The corrosion potentials in the regions close to

both abutments dropped from -0.200 V for the first survey to -0.350 to -0.500 V. Since mild steel form ties had been used in both abutments (of the type shown as in Figure 3.316), the very negative corrosion potentials may be due to corrosion of the form ties. In addition, the bridge is buried in the earth at both ends (the west and east side), and the concrete sections are thick at those location (much thicker than the deck), which would restrict oxygen penetration. As mentioned in Section 1.4.1, steel in structures buried in the earth often have very negative potentials due to restricted access of oxygen; here, the more negative potentials on both ends could also be due to the low oxygen concentration.

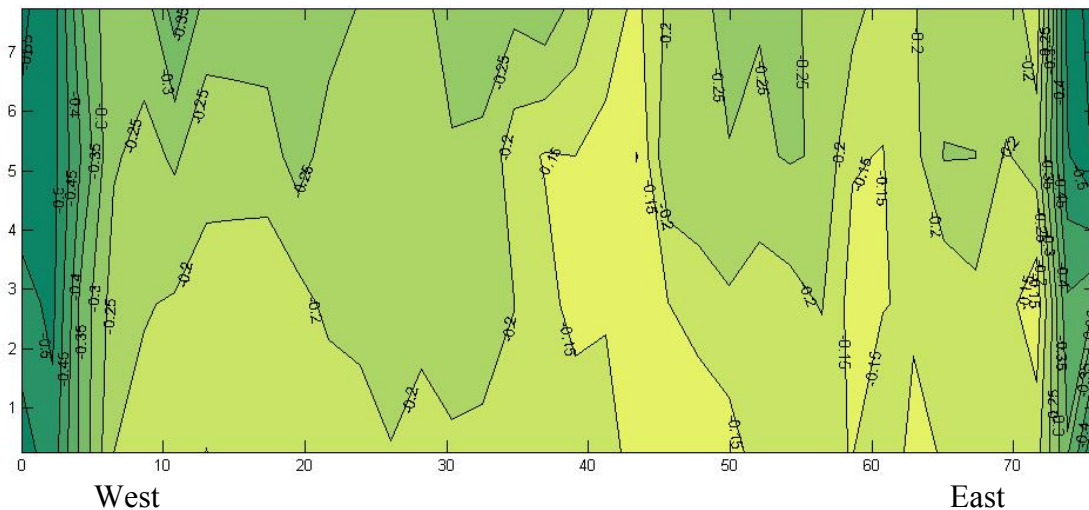


Figure 3.111 – Corrosion potential map for the Doniphan County Bridge (5th survey, October 9, 2006).

The eighth survey was performed on April 11, 2008 (four years after casting), and the corrosion potential map is shown in Figure 3.112. The corrosion potentials in the middle regions of the bridges, 5 to 71 m (16 to 233 ft) from the west end, were -0.150 V, while several small areas on the north and south sides of the bridge had corrosion potentials between -0.250 and -0.350 V. The corrosion potentials on both ends were more negative than those in the middle. This is mainly because the steel

girders on both sides (the north and south side) have mild steel studs penetrating the deck and salt has easier access to the edge girders, therefore causing more negative corrosion potentials on the sides. The mild steel form ties used in the deck can also cause more negative corrosion potentials. The potential readings at the west abutment ranged from -0.300 to -0.450 V, while those at the east abutment ranged from -0.300 to -0.400 V. Overall, the reinforcing steel in the bridge deck appears still to be in the passive state.

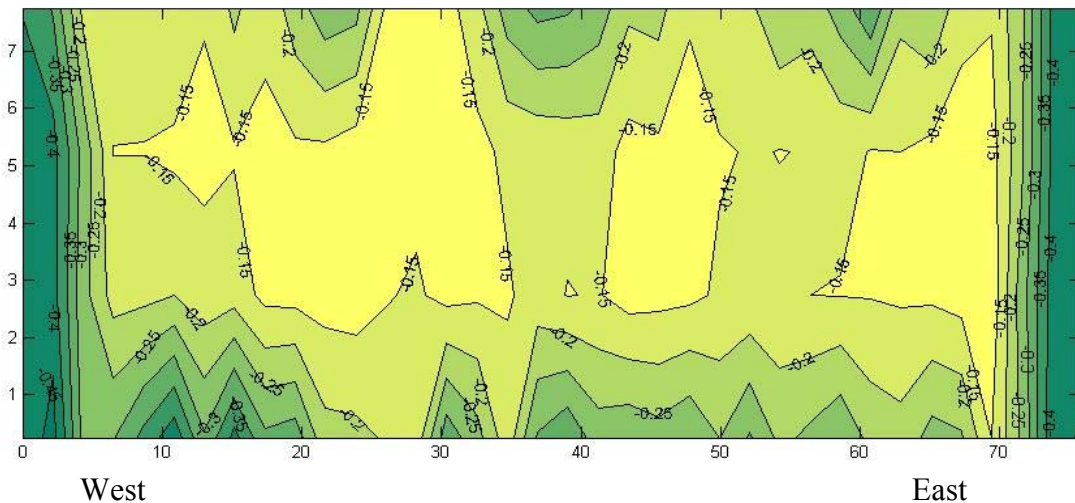


Figure 3.112 – Corrosion potential map for the Doniphan County Bridge (8th survey, April 11, 2008).

3.4.3.2 Mission Creek Bridge

The Mission Creek Bridge (Bridge No. 4-89-4.58(281)) is located on K-4 over Mission Creek in Shawnee County, Kansas. It is a 27.45-m (90-ft) long, one-span composite steel girder bridge. The bridge deck was cast on August 25, 2004. Test points are distributed on a 2.75×2.2 m (9.0×7.2 ft) grid across the full bridge length (not including the abutments), making 4 rows of 13 and a total of 52 test points.

The first survey for the Mission Creek Bridge was conducted on September 1,

2004 (seven days after casting) and the potential map is shown in Figure 3.113. The corrosion potentials on the deck were between -0.100 and -0.200 V, except for two small areas located about 5 m (16 ft) away from the west side of the bridge having corrosion potentials of -0.250 V. The less negative potential readings (above -0.250 V) indicate a passive state of corrosion.

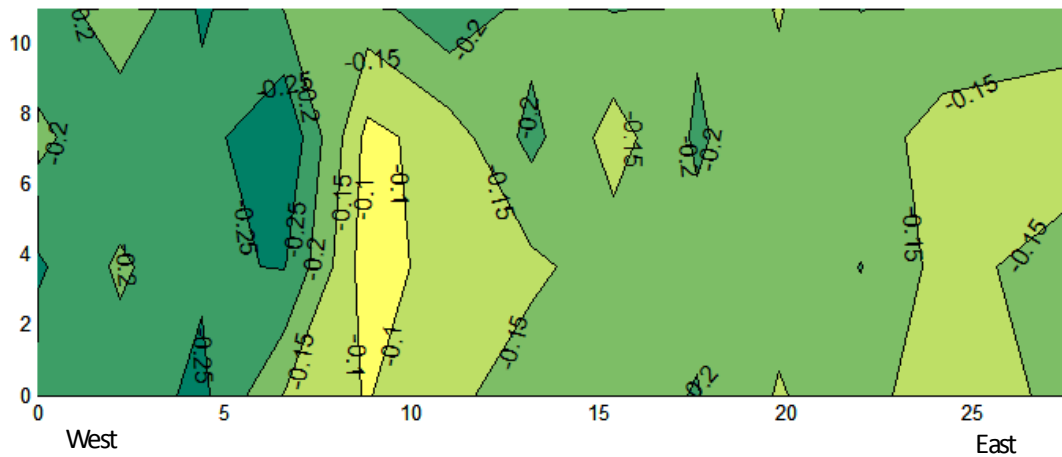


Figure 3.113 – Corrosion potential map for the Mission Creek Bridge (1st survey, September 1, 2004).

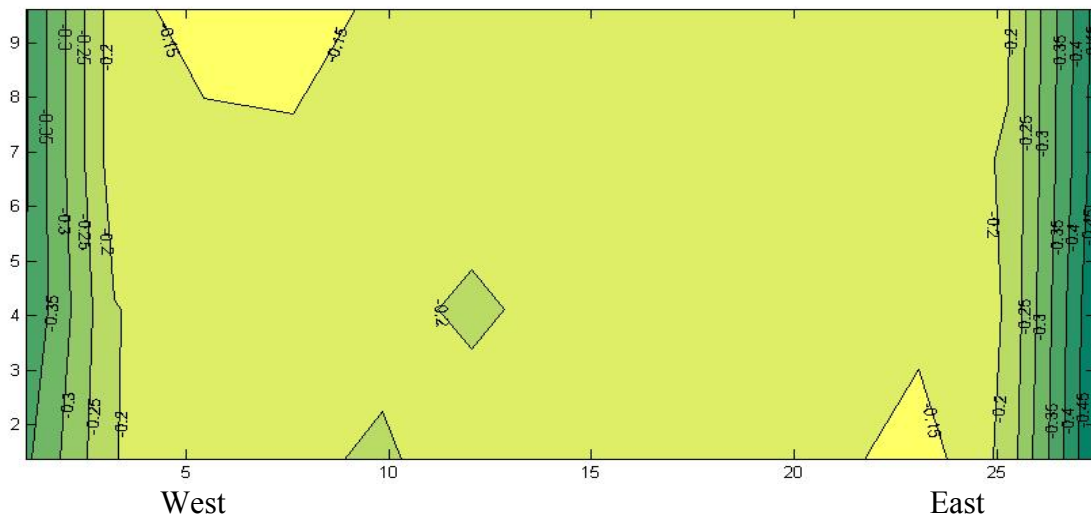


Figure 3.114 – Corrosion potential map for the Mission Creek Bridge (5th survey, October 16, 2006).

Figure 3.114 shows the corrosion potential map based on the fifth survey of the Mission Creek Bridge, conducted on October 16, 2006 (at an age of two years). The corrosion potentials in the middle region, 3 to 26 m (10 to 85 ft) from the west side, were between -0.150 and -0.250 V, while the potential in the regions close to both abutments ranged from -0.300 to -0.450 V.

The eighth survey was taken on April 7, 2008 at an age of about four years. The corrosion potential map is shown in Figure 3.115. The potential in middle region, 3 to 26 m (10 to 85 ft) from the west side, continued to be less negative, with values between -0.100 and -0.250 V, while the potential in the regions close to the abutments ranged from -0.300 to -0.500 V.

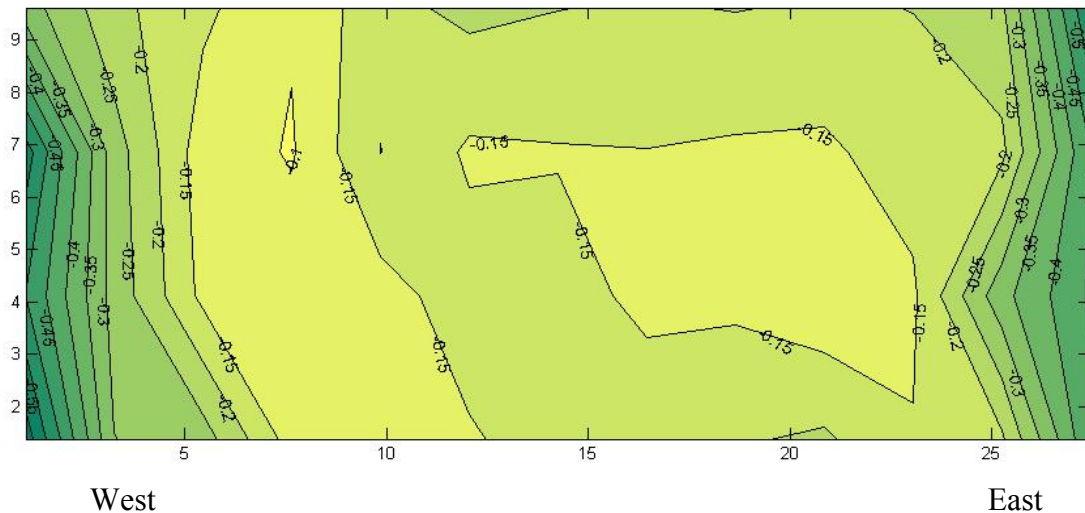


Figure 3.115 – Corrosion potential map for the Mission Creek Bridge (8th survey, April 7, 2008).

As shown in Figure 3.116, form ties were used in the abutments to hold the forms in place. The ties were made of mild steel and remained in the concrete after the forms were removed. Corrosion of the mild steel may be the reason for the low corrosion potentials, i.e., below -0.350 V. As mentioned in the Doniphan County Bridge, however, another possibility could be low oxygen concentrations in the earth

and adjacent concrete, which often results in negative corrosion potentials. Overall, after four years in service, no corrosion activity has been observed for pickled 2205 stainless steel in the two bridge decks.



Figure 3.116 – Reinforcing bar cages at the east abutment for the Mission Creek Bridge, showing mild steel form ties used in the bridge decks.

3.4.4 Summary

Bench-scale and Field Tests

The stainless steel exhibited negative corrosion in the Southern Exposure test and had corrosion losses of no more than $0.03 \mu\text{m}$ in the cracked beam test. The corrosion loss of the pickled 2205 stainless steel was less than 1/300 of the corrosion

loss of the conventional steel and 1/60 of the corrosion loss of the epoxy-coated steel after the four-year field test.

Bridge Corrosion Potential Mapping

The corrosion potential maps demonstrate that the 2205 stainless steels in the two bridge decks still remain in the passive state. The more negative corrosion potentials recorded in the regions near the abutments are likely due to the corrosion of mild steel form ties and the restricted access of oxygen for the structures that have thick concrete sections and are buried in the earth. As mentioned in Section 1.4.1, steel in structures buried in the earth often have very negative potentials due to restricted access of oxygen; here, the more negative potentials on both ends could also be due to the low oxygen concentration. The corrosion potentials on the side of bridge decks were more negative than those in the middle region. This is mainly because the steel girders on the sides have mild steel studs penetrating the deck and salt has easier access to the edge girders, therefore causing more negative corrosion potentials on the sides. The mild steel form ties used in the deck could also contribute to the more negative corrosion potentials,

All of the test results indicate that pickled 2205 stainless steel provides excellent corrosion performance.

3.5 LINEAR POLARIZATION RESISTANCE TEST

Total corrosion current densities, described here as “microcell current densities,” for the bench-scale and field test specimens were measured using the linear polarization resistance (LPR) test. One specimen for each test method and corrosion protection system was selected. The test program is summarized in Tables 2.6 through 2.8 in Chapter 2. The LPR test for bench-scale specimens was performed

every four weeks for both the top and bottom mats of steel and once for field specimens on May 2008, approximately four years after the tests were initiated. This section presents the guidelines used to interpret microcell corrosion current densities obtained from the LPR test along with the corrosion rates and corrosion losses based on the LPR readings. For the bench-scale specimens, the microcell corrosion losses are compared with the macrocell corrosion losses for each corrosion protection system to investigate the relationship between the results obtained using the two test procedures. All of the results are reported as of the cutoff date, May 31, 2008.

Based on studies in the laboratory and in the field, Broomfield developed guidelines to interpret microcell corrosion current densities. A Stern-Geary constant B of 26 mV was used in his tests. Four different corrosion levels are typically defined based on the corrosion current densities measured in the LPR test and are shown in Table 3.17.

Table 3.17 – Guideline for interpretation of corrosion current densities in LPR test (Broomfield 1997)

Corrosion Current Density mA/cm^2	Corrosion Rate, $\mu\text{m}/\text{yr}$		Corrosion Levels
	Based on iron	Based on zinc	
< 0.1	< 1.16	< 1.50	Passive corrosion condition
0.1 to 0.5	1.16 to 5.8	1.50 to 7.50	Low to moderate corrosion
0.5 to 1.0	5.8 to 11.6	7.50 to 15.0	Moderate to high corrosion
> 1.0	> 11.6	< 15.0	High corrosion

A Stern-Geary constant B of 26 mV and the microcell corrosion current densities for the conventional steel was also used in the current study. For ease of comparison with the macrocell results presented earlier in this chapter, the corrosion current densities obtained from the LPR test were converted to corrosion rates, based on iron and zinc, respectively, using Eq. (1.10) and integrated to obtain corrosion losses.

3.5.1 Microcell Corrosion

This section presents the LPR test results for bench-scale and field test specimens. One specimen, specified in Table 2.25, Chapter 2, is tested for each of the corrosion protection systems. The microcell corrosion rates and losses for the top mats in the Southern Exposure and cracked beam specimens are plotted in Figures 3.117 to 3.122, and the corrosion losses are summarized in Table 3.18. The microcell corrosion rates and losses for the bottom mats of steel and the corrosion potentials for both mats of steel for individual specimens from the LPR test are included in Appendix D. Due to the long-term nature of the test, the results as of May 31, 2008 are reported, with an age of 72 weeks for control specimens and 40 weeks for inhibitor specimens. Corrosion losses at 40 weeks are compared for all specimens.

Southern Exposure Test

Figure 3.117 shows the microcell corrosion rates for the control specimens containing conventional steel and ECR in the SE test. Conventional steel exhibited much higher corrosion rates than epoxy-coated steel after corrosion initiation at week 24, which is consistent with corrosion initiation based on the macrocell readings shown in Figure 3.18 in Section 3.2.1. The highest microcell corrosion rate was $53.35\mu\text{m}/\text{yr}$ for conventional steel and 0.08 and $36.42\mu\text{m}/\text{yr}$ for ECR at week 60 based on total and exposed area, respectively.

As shown in Figure 3.118, the total corrosion losses for conventional steel were similar to the corrosion rate, much higher than those for epoxy-coated steel. The corrosion losses increased slowly over time before week 56 and rapidly thereafter. As shown in Table 3.18, the microcell corrosion loss for conventional steel was $0.69\mu\text{m}$ at week 40, while that of epoxy-coated steel was less than 0.005 and $0.46\mu\text{m}$ based on total and exposed area, respectively. By week 72, the microcell corrosion loss

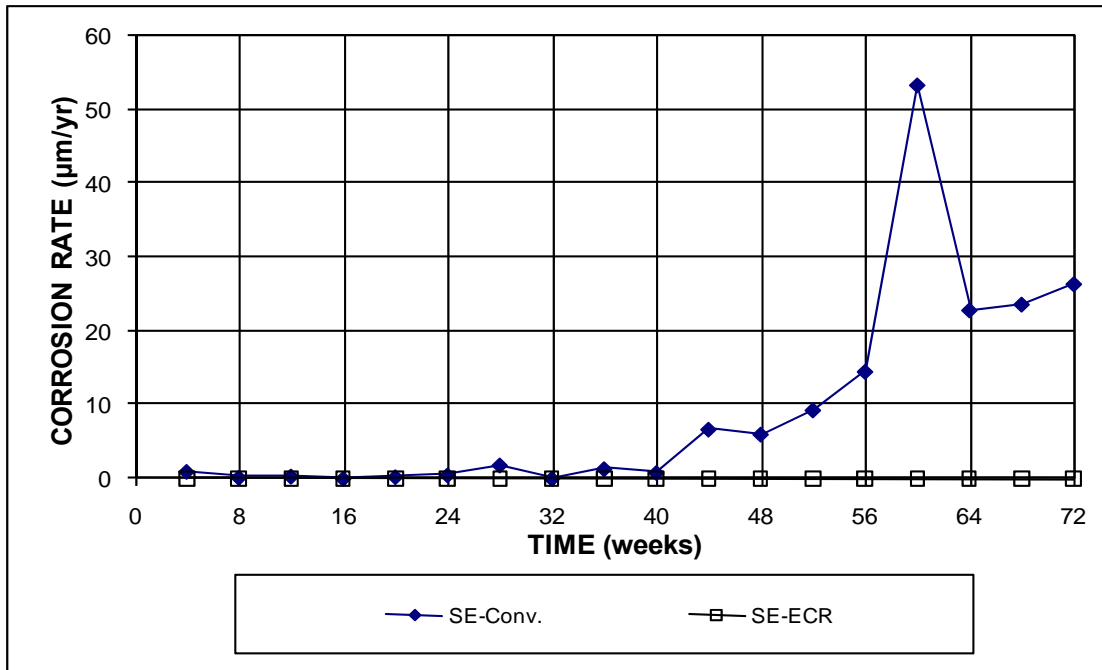


Figure 3.117a – Microcell corrosion rates from LPR method for specimens with conventional steel and ECR in the Southern Exposure test (ECR have four holes through the epoxy).

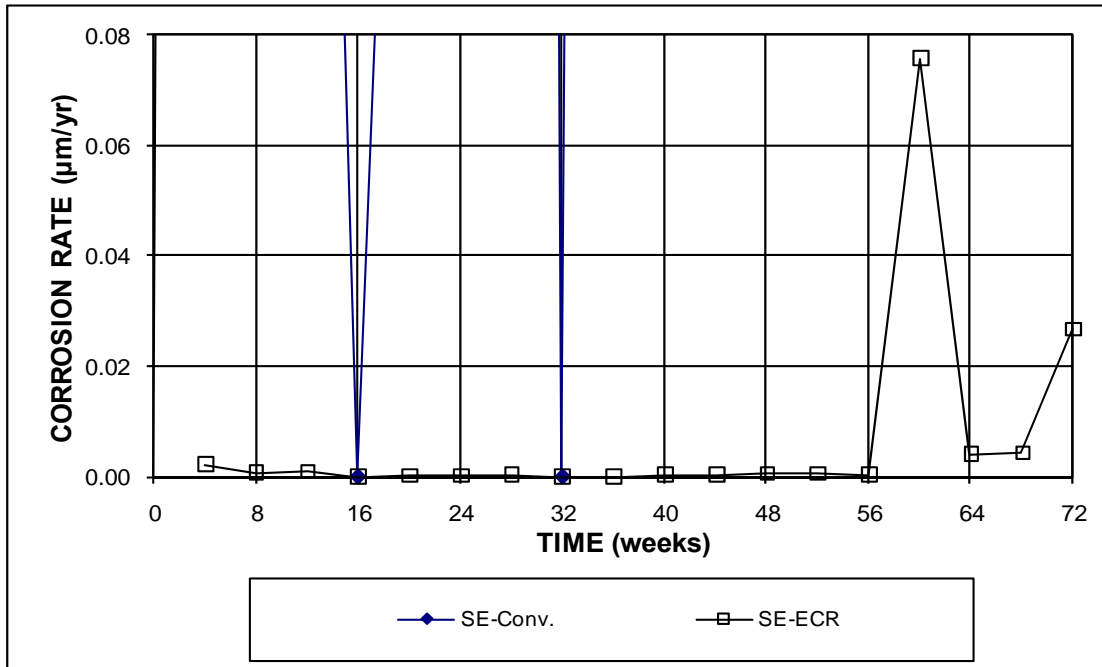


Figure 3.117b – Microcell corrosion rates from LPR method for specimens with conventional steel and ECR in the Southern Exposure test (ECR have four holes through the epoxy). (Different scale)

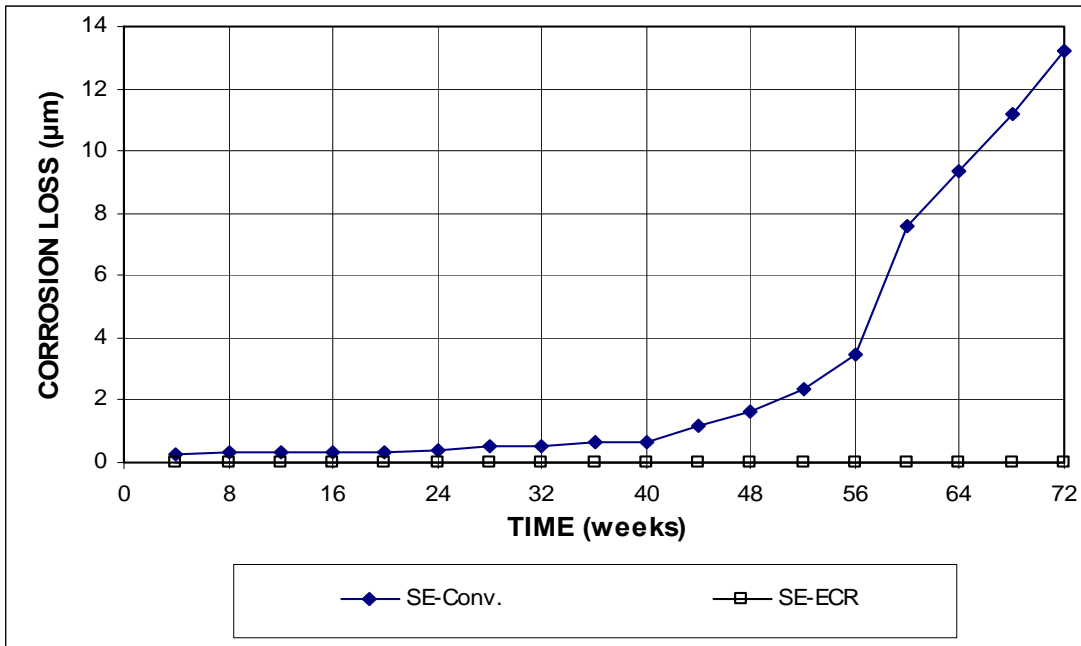


Figure 3.118a – Microcell corrosion losses from LPR method for the top mats in specimens with conventional steel and ECR in the Southern Exposure test (ECR have four holes through the epoxy).

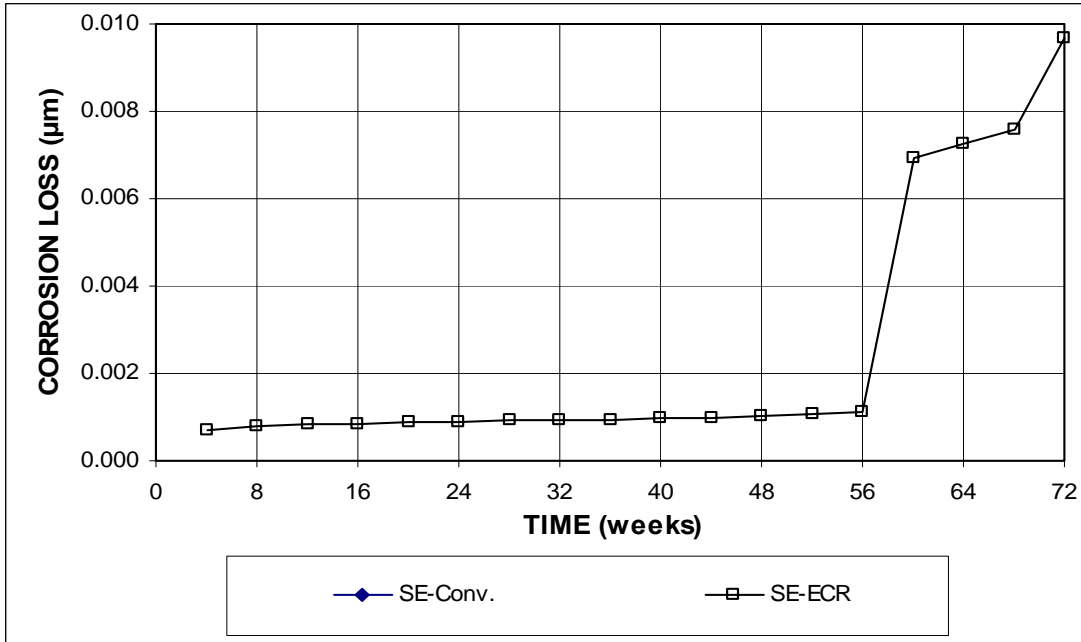


Figure 3.118b – Microcell corrosion losses from LPR method for the top mats in specimens with conventional steel and ECR in the Southern Exposure test (ECR have four holes through the epoxy). (Different scale)

became 13.20 and 0.01 μm for conventional steel and ECR, respectively.

Figures 3.119 and 3.120 present the microcell corrosion results for specimens with conventional steel (N5) cast in concretes containing the various corrosion inhibitors in the Southern Exposure test. As shown in Figure 3.119, the corrosion rates for all the specimens increased over time. The microcell corrosion rates exhibited fluctuations during the test period, indicating the dynamic nature of the corrosion process. The specimen without inhibitors and the specimen with DCI had the same corrosion rates through week 36; at week 40, the corrosion rate of the specimen without inhibitors was 7.41 $\mu\text{m}/\text{yr}$, which is over two times the value of 3.29 $\mu\text{m}/\text{yr}$ for the DCI specimen at week 40, but still lower than moderate corrosion level (5.8 $\mu\text{m}/\text{yr}$) according to Broomfield's guideline as presented in Table 3.17. Specimens with Hycrete and Rhecrete had much lower corrosion rates, with values no more than 0.43 and 0.73 $\mu\text{m}/\text{yr}$ before week 40 and 0.33 and 2.62 $\mu\text{m}/\text{yr}$ at week 40, respectively.

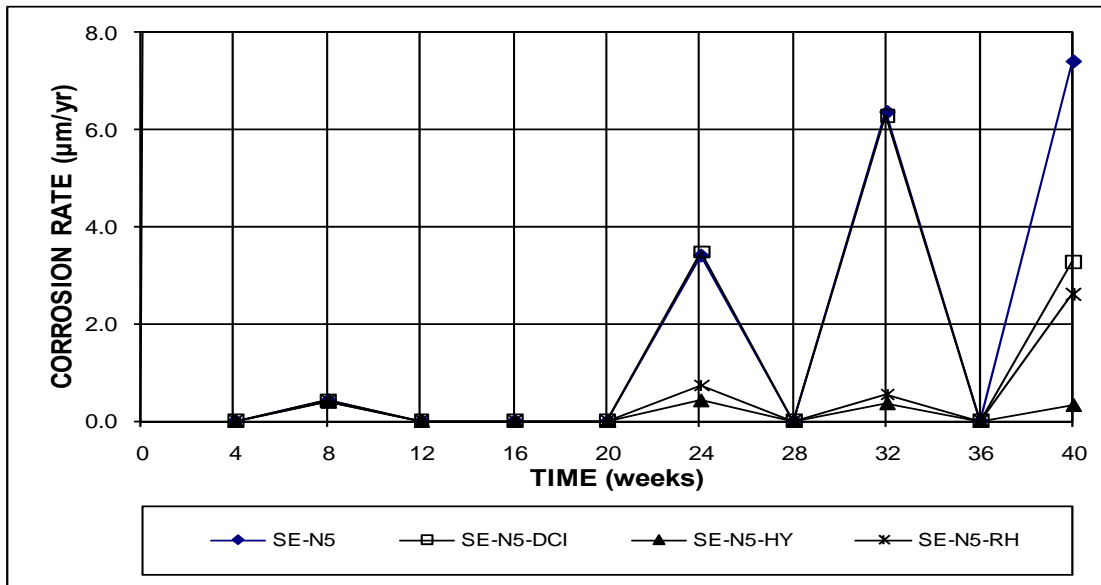


Figure 3.119 – Microcell corrosion rates from LPR method for specimens with conventional steel and different inhibitors in the Southern Exposure test.

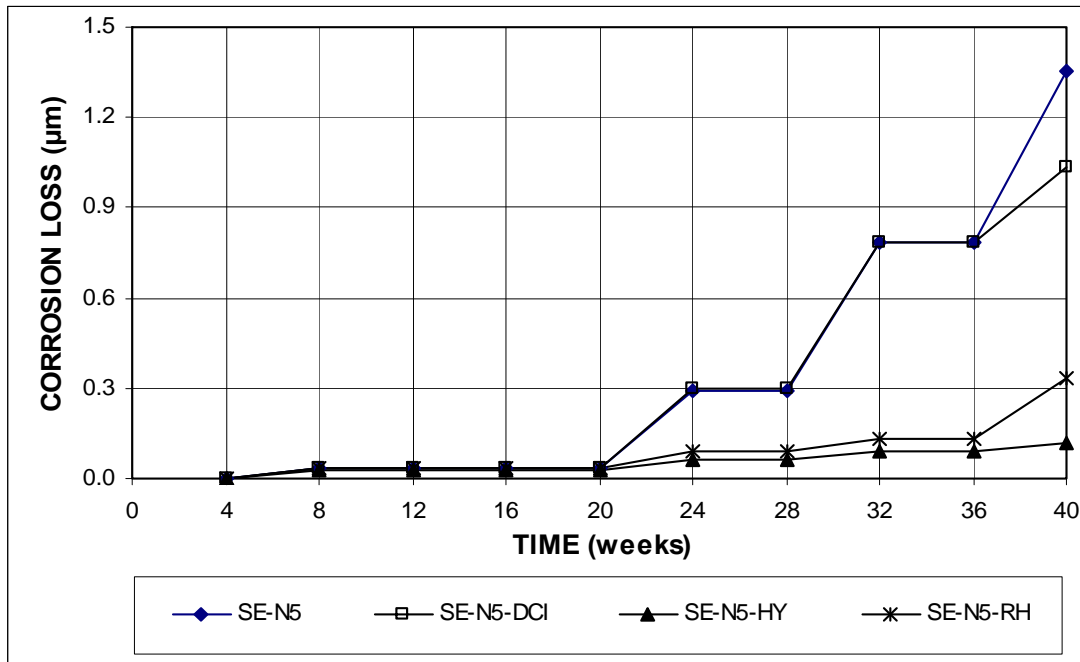


Figure 3.120 – Microcell corrosion losses from LPR method for the top mats in specimens with conventional steel and different inhibitors in the Southern Exposure test.

The corrosion losses for specimens with conventional steel and various corrosion inhibitors are plotted in Figure 3.120 and summarized in Table 3.18. After week 20, the specimen without inhibitors and the specimen with DCI had much higher corrosion losses than the specimens with Hycrete and Rheocrete. At week 40, the specimen without inhibitors had a microcell corrosion loss of 1.35 μm , followed by the DCI specimen with 1.04 μm , and the Hycrete specimen with 0.33 μm . At 0.12 μm , the Rheocrete specimen had the lowest microcell corrosion loss.

The corrosion rates and losses based on the microcell corrosion were consistent with those obtained based on the macrocell corrosion for the inhibitor specimens in the Southern Exposure test (Figure 3.24 in Section 3.2). The conventional steel specimens without inhibitors exhibited the most active corrosion activity, followed by

the DCI specimen. The Hycrete specimen had the lowest active corrosion activity, which was slightly lower than the Rheocrete specimen.

Table 3.18 – Total corrosion losses (μm) at 40 weeks from linear polarization resistance method for the Southern Exposure and cracked beam test

Steel Designation ^a	Corrosion Loss ^b (μm)	
	SE	CB
Control		
Conv.	0.69	
ECR	0.00	
ECR*	0.46	
Corrosion Inhibitors		
N5	1.35	10.16
N5-DCI	1.04	15.02
N5-HY	0.12	6.20
N5-RH	0.33	14.60

^a Conv. = conventional steel.
 ECR = conventional epoxy-coated reinforcement, four 3-mm ($1/8$ -in.) diameter holes through the epoxy coating.
 N5 = conventional steel, different heat.
 DCI = concrete mixed with DCI inhibitor.
 HY = concrete mixed with Hycrete inhibitor.
 RH = concrete mixed with Rheocrete inhibitor.

^b Corrosion losses are based on total area.
 β Absolute values less than 0.005 μm
 * Corrosion loss is based on exposed area.

Cracked Beam Test

Figures 3.121 and 3.122 present the microcell corrosion results for the cracked beam specimens with conventional steel and the three corrosion inhibitors. As shown in Figure 3.121, the corrosion rates for the specimen with DCI increased over time after corrosion initiated at week 24, except at week 36 when the corrosion loss was near zero. The highest rate, 70.20 $\mu\text{m}/\text{yr}$, occurred at week 40. The corrosion rates for the specimens with Hycrete remained relatively low compared to the other specimens, with values of no more than 20 $\mu\text{m}/\text{yr}$ during the test and a rate of 17.96 $\mu\text{m}/\text{yr}$ at

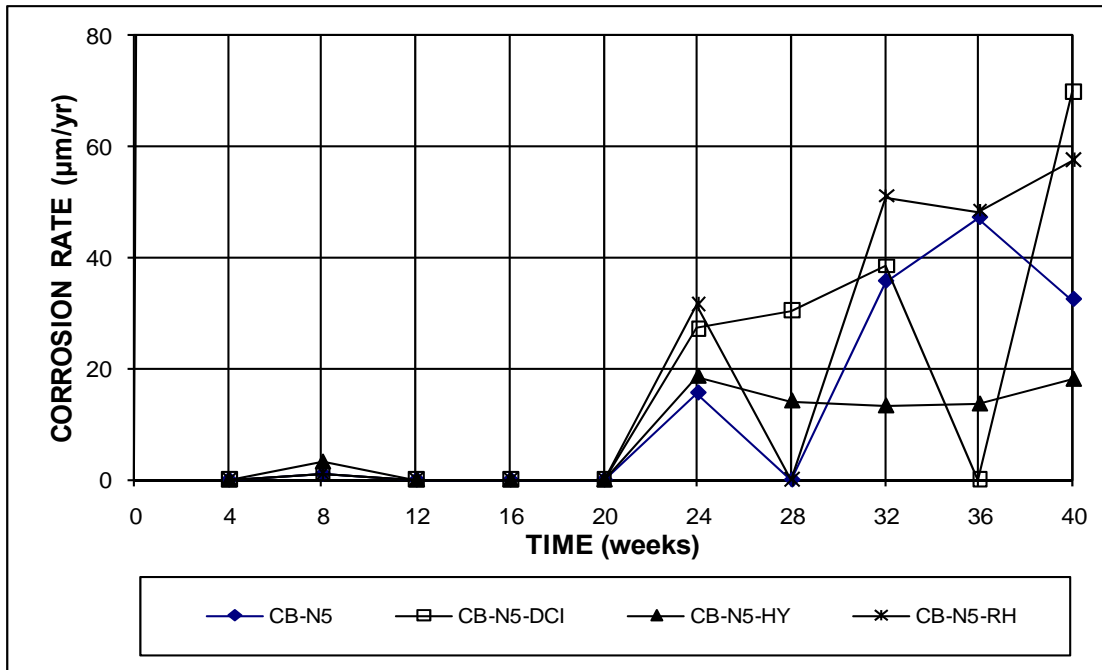


Figure 3.121 – Microcell corrosion rates from LPR method for specimens with conventional steel and different inhibitors in the cracked beam test.

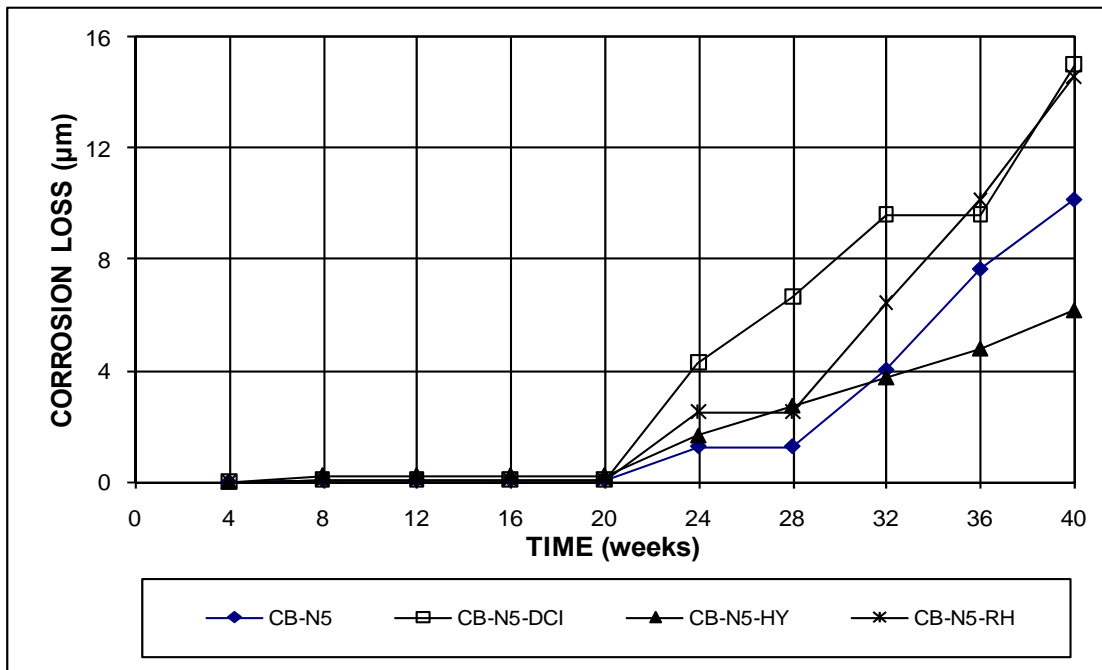


Figure 3.122 – Microcell corrosion losses from LPR method for the top mats in specimens with conventional steel and different inhibitors in the cracked beam test.

week 40. The specimens with Rheocrete and without inhibitors had corrosion rates of 57.59 and 32.48 $\mu\text{m}/\text{yr}$, respectively, at week 40. At week 40, the corrosion activity for all specimens was high according to the Broomfield guideline as presented in Table 3.17.

The corrosion losses for the specimens are plotted in Figure 3.122 and summarized in Table 3.18. After week 20, the DCI specimen had higher corrosion losses than the other specimens except at week 36. As shown in Table 3.18, the DCI specimen had the highest microcell corrosion loss, 15.02 μm , at week 40, followed by the Rheocrete specimen with 14.60 μm and the specimen without inhibitors with 10.16 μm . The Hycrete specimen had the lowest microcell corrosion loss 6.20 μm .

The microcell corrosion losses for the cracked beam specimens are on the order of ten times higher than those for the Southern Exposure specimens. In both the Southern Exposure and cracked beam tests, the Hycrete specimen exhibited the best corrosion performance, indicating that Hycrete improved the corrosion resistance of reinforcing steel not only in uncracked concrete, but also in cracked concrete, while the other inhibitors only improved the corrosion resistance of reinforcing steel in uncracked concrete. The test results are consistent with those obtained in the macrocell corrosion tests (presented in Section 3.2.2).

ASTM G109 Test

Figures 3.123 and 3.124 present the microcell corrosion results for specimens in the ASTM G109 test. As shown in Figure 3.123, specimens with conventional steel had the highest corrosion rates when compared with the other specimens, with a high value of 1.80 $\mu\text{m}/\text{yr}$ at week 157. The corrosion rates for the ECR-4h specimen fluctuated below 0.06 $\mu\text{m}/\text{yr}$ based on total area after initiating at week 129, while the rates for the ECR-10h specimens were below 0.04 $\mu\text{m}/\text{yr}$, except for a value of 0.043

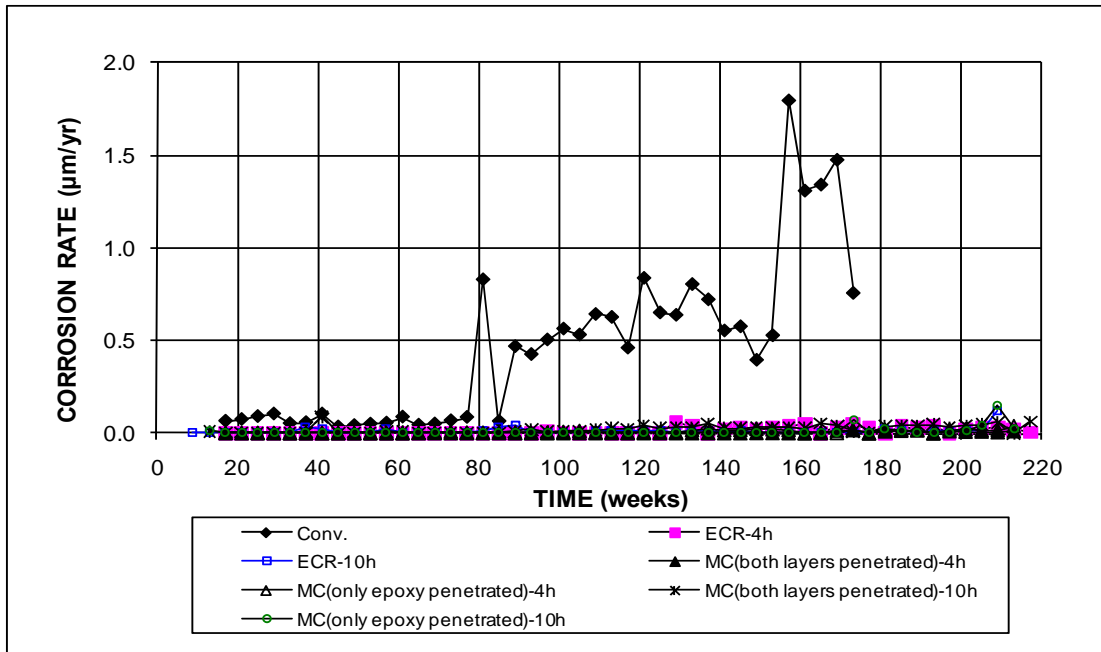


Figure 3.123a – Microcell corrosion rates from LPR method for specimens with conventional steel, ECR, and multiple-coated bars in the ASTM G109 test (ECR have four and ten holes through the epoxy).

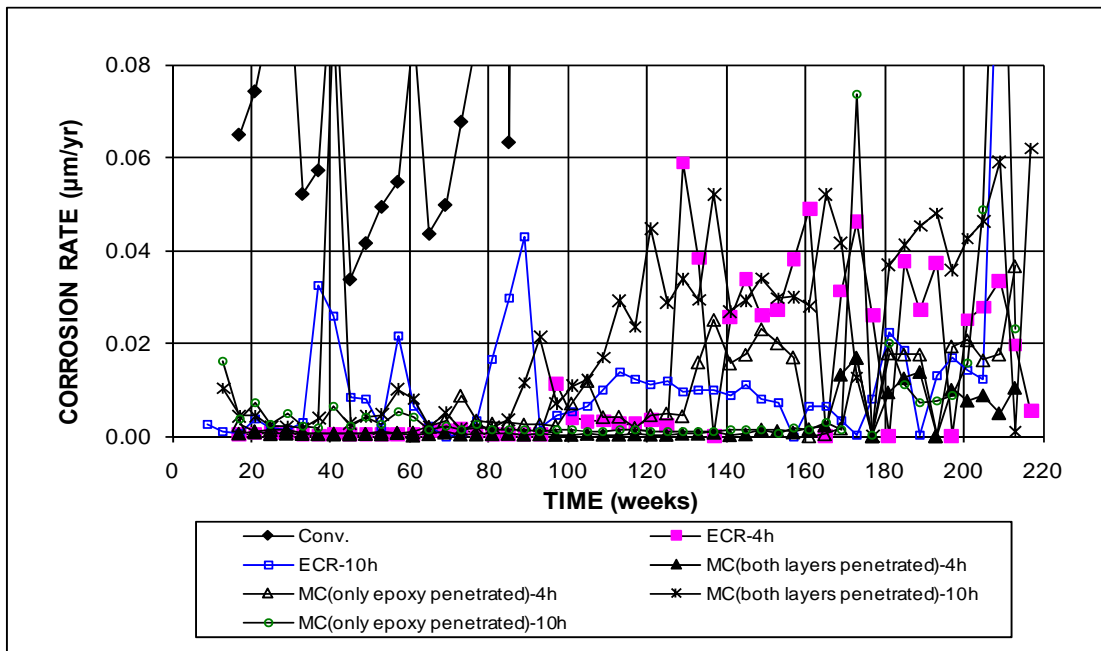


Figure 3.123b – Microcell corrosion rates from LPR method for specimens with conventional steel, ECR, and multiple-coated bars in the ASTM G109 test (ECR have four and ten holes through the epoxy). (Different scale)

$\mu\text{m}/\text{yr}$ at week 89. The corrosion rates of the MC(both layers penetrated)-10h specimens were higher than for the other MC specimens, with a high value of $0.06 \mu\text{m}/\text{yr}$ based on total area at week 217. The MC(both layers penetrated) specimens with four holes had the lowest corrosion losses, with values below $0.02 \mu\text{m}/\text{yr}$ based on total area during the test period.

The microcell corrosion losses for specimens in the ASTM G109 test are plotted in Figure 3.124 and summarized in Table 3.19. The specimen with conventional steel had the highest microcell corrosion losses at all times, with a corrosion loss of $1.43 \mu\text{m}$ at week 173. The microcell corrosion losses for the other specimens were below $0.10 \mu\text{m}$ based on total area at 209 weeks. As shown in Table 3.19, the corrosion loss for the MC(both layers penetrated)-10h specimens was $0.09 \mu\text{m}$ based on total area at week 209, followed by ECR and ECR-10h specimens with $0.05 \mu\text{m}$ at week 209. The conventional ECR specimen with four holes had the highest corrosion loss based on exposed area, with a value of $21.40 \mu\text{m}$ at week 209.

Table 3.19 – Total corrosion losses (μm) from linear polarization resistance method for the ASTM G109 test

Steel Designation ^a	Exposure Time (weeks)	G109	
		Based on Total Area	Based on Exposed Area
Control			
Conv.	173 ^b	1.43	
ECR	209	0.05	21.40
ECR-10h	209	0.05	8.17
Multiple Coated Bars			
MC(both layers penetrated)	209	0.01	4.07
MC(both layers penetrated)-10h	209	0.09	15.08
MC(only epoxy penetrated)	209	0.03	12.27
MC(only epoxy penetrated)-10h	209	0.03	5.76

^a Conv. = conventional steel. ECR = conventional epoxy-coated reinforcement.

MC(both layers penetrated) = multiple coated bars with both the zinc and epoxy layers penetrated.

MC(only epoxy penetrated) = multiple coated bars with only epoxy penetrated.

10h = ECR with 10 holes, otherwise 4 holes.

^b Test was terminated due to cracking.

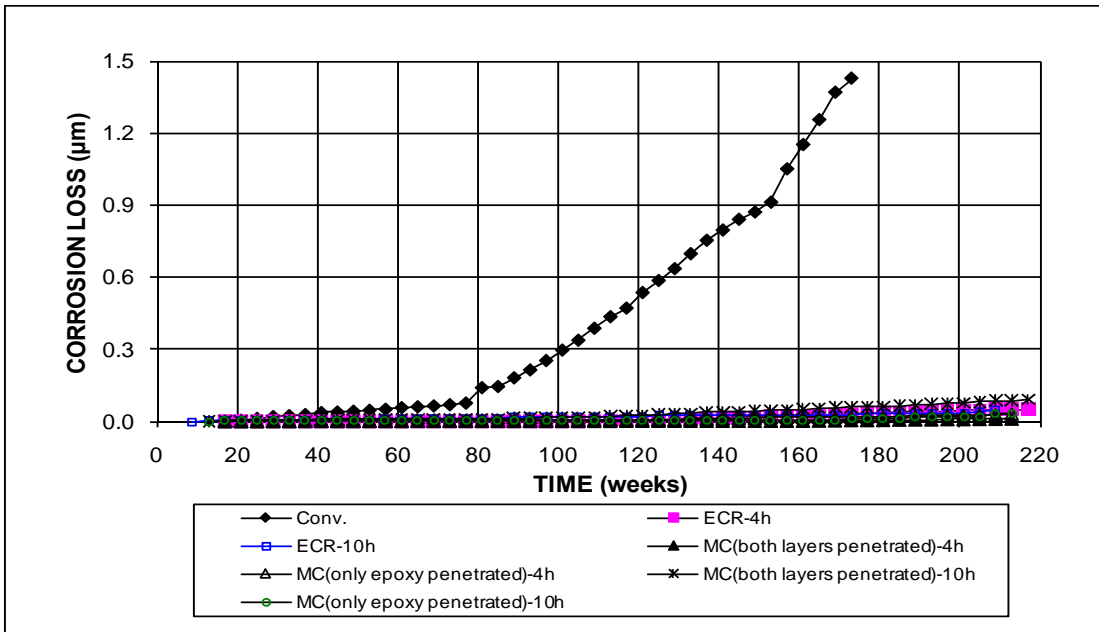


Figure 3.124a – Microcell corrosion losses from LPR method for the top mats in specimens with conventional steel, ECR, and multiple-coated bars in the ASTM G109 test (ECR have four and ten holes through the epoxy).

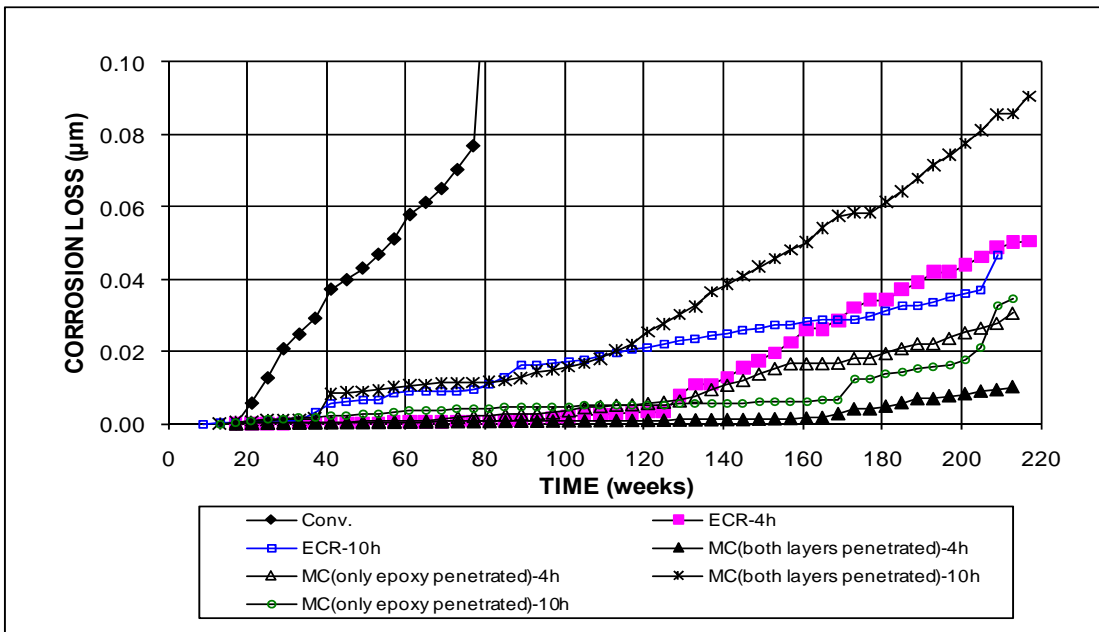


Figure 3.124b – Microcell corrosion losses from LPR method for specimens with conventional steel, ECR, and multiple-coated bars in the ASTM G109 test (ECR have four and ten holes through the epoxy). (Different scale)

The microcell corrosion loss for the specimen with conventional steel was at least 15 times higher than that of any of the specimens with MC and ECR at week 209.

Field Test

For the field test specimens, the LPR test was only performed once; therefore, microcell corrosion rates instead of corrosion losses are reported for these specimens. One specimen (Specimen No. 1) was selected for each system, and the test results are shown in Table 3.20 for specimens without simulated cracks and Table 3.21 for specimens with simulated cracks.

As shown in Table 3.20 for specimens without simulated cracks, the specimen with conventional steel had the highest corrosion rate for the top mat, with a value of $0.318 \mu\text{m/yr}$ based on total area at week 205, which is 50 times the value of $0.006 \mu\text{m/yr}$ for the ECR specimen. The microcell corrosion rate of the ECR(Rheocrete) specimen was $0.005 \mu\text{m/yr}$ at week 173, followed by the MC specimen with $0.004 \mu\text{m/yr}$ at week 199. All of the other specimens showed microcell corrosion rates below $0.002 \mu\text{m/yr}$ based on the total area for the top bars. For the bottom bars, the conventional steel specimen also exhibited the highest corrosion rate, $0.094 \mu\text{m/yr}$; all of the other specimens had bottom bar corrosion rates below $0.01 \mu\text{m/yr}$ based on total area.

Based on exposed area, the microcell corrosion rates ranged from 0.25 to $2.46 \mu\text{m/yr}$. The ECR specimen had a corrosion rate of $2.46 \mu\text{m/yr}$, followed by the ECR(Rheocrete) and MC specimens with 2.12 and $1.74 \mu\text{m/yr}$, respectively. The remaining specimens had corrosion rates between 0.2 and $1 \mu\text{m/yr}$ for the top mat bars. The ECR(DuPont), ECR(primer/ $\text{Ca}(\text{NO}_2)_2$), and ECR(Rheocrete) specimens had corrosion rates of 2.86, 1.18, and $1.04 \mu\text{m/yr}$ for the bottom bars, respectively, while the others had corrosion rates below $1 \mu\text{m/yr}$.

Table 3.20 – Microcell corrosion rates ($\mu\text{m}/\text{yr}$) from linear polarization resistance method for specimens without cracks in the field test

Steel Designation ^a	Exposure time (weeks)	Based on Total Area		Based on Exposed Area	
		Top Mat	Bottom Mat	Top Mat	Bottom Mat
Control					
Conv.	205	3.18E-01	9.35E-02		
ECR	205	6.31E-03	^c	2.46E+00	^c
Corrosion Inhibitors					
ECR(primer/Ca(NO ₂) ₂)	193	1.17E-03	3.02E-03	4.58E-01	1.18E+00
ECR(DCI)	179	1.33E-03	1.05E-03	5.21E-01	4.09E-01
ECR(Rheocrete)	173	5.43E-03	2.65E-03	2.12E+00	1.04E+00
ECR(Hycrete)	169	1.15E-03	9.70E-04	4.50E-01	3.79E-01
Multiple Coated Bars					
MC	199	4.47E-03	1.35E-03	1.74E+00	5.26E-01
Increased Adhesion					
ECR(Valspar)	205	1.50E-03	^c	5.85E-01	^c
ECR(DuPont)	199	6.30E-04	7.33E-03	2.46E-01	2.86E+00
ECR(Chromate)	199	1.85E-03	1.61E-03	7.23E-01	6.26E-01
^a Conv. = conventional steel. ECR = conventional epoxy-coated reinforcement.					
The coating on all epoxy-coated bars is penetrated with 16 3-mm (1/8-in.) diameter holes.					
ECR(primer/Ca(NO ₂) ₂) = ECR with a primer containing calcium nitrite.					
ECR(DCI) = conventional ECR with DCI inhibitor in concrete.					
ECR(Rheocrete) = conventional ECR with Rheocrete inhibitor in concrete.					
ECR(Hycrete) = conventional ECR with Hycrete inhibitor in concrete.					
MC = multiple coated bars.					
ECR(Valspar) = ECR with increased adhesion produced by Valspar.					
ECR(DuPont) = ECR with increased adhesion produced by DuPont.					
ECR(Chromate) = ECR with the zinc chromate pretreatment.					
^b The scan range: +/- 20 mV of corrosion potentials. The scan rate is 0.125 mV/s. Tafel constant β is 0.12 V for the cathode and 0.12 V for the anode. Corrosion current densities are based on total area of bars.					
^c Data not available					

The microcell corrosion rates for specimens with cracks are shown in Table 3.21. Conventional steel had the highest corrosion rate, 0.789 $\mu\text{m}/\text{yr}$ at week 205, followed by the ECR(DCI), ECR(Valspar), and ECR(Hycrete) specimens with 0.085, 0.038, and 0.024 $\mu\text{m}/\text{yr}$, respectively, based on total area. The corrosion rates are more than twice the values of those of the corresponding specimens without cracks. All of the other specimens exhibited corrosion rates less than 0.020 $\mu\text{m}/\text{yr}$ based on

Table 3.21 – Microcell corrosion rates ($\mu\text{m}/\text{yr}$) from linear polarization resistance method for specimens with simulated cracks in the field test

Steel Designation ^a	Exposure time (weeks)	Based on Total Area		Based on Exposed Area	
		Top Mat	Bottom Mat	Top Mat	Bottom Mat
Control					
Conv.	205	7.89E-01	3.18E-01		
ECR	205	1.12E-02	^c	4.37E+00	^c
Corrosion Inhibitors					
ECR(primer/Ca(NO ₂) ₂)	193	1.22E-02	2.20E-03	4.77E+00	8.57E-01
ECR(DCI)	179	8.52E-02	4.44E-03	3.32E+01	1.73E+00
ECR(Rheocrete)	173	^c	9.20E-03	^c	3.59E+00
ECR(Hycrete)	169	2.40E-02	2.96E-03	9.37E+00	1.16E+00
Multiple Coated Bars					
MC	199	1.75E-02	2.48E-03	6.83E+00	9.69E-01
Increased Adhesion					
ECR(Valspar)	205	3.79E-02	5.00E-03	1.48E+01	1.95E+00
ECR(DuPont)	199	1.75E-02	8.65E-04	6.85E+00	3.38E-01
ECR(Chromate)	199	1.08E-02	1.56E-03	4.23E+00	6.09E-01
^a Conv. = conventional steel. ECR = conventional epoxy-coated reinforcement.					
The coating on all epoxy-coated bars is penetrated with 16 3-mm (1/8-in.) diameter holes.					
ECR(primer/Ca(NO ₂) ₂) = ECR with a primer containing calcium nitrite.					
ECR(DCI) = conventional ECR with DCI inhibitor in concrete.					
ECR(Rheocrete) = conventional ECR with Rheocrete inhibitor in concrete.					
ECR(Hycrete) = conventional ECR with Hycrete inhibitor in concrete.					
MC = multiple coated bars.					
ECR(Valspar) = ECR with increased adhesion produced by Valspar.					
ECR(DuPont) = ECR with increased adhesion produced by DuPont.					
ECR(Chromate) = ECR with the zinc chromate pretreatment.					
^b The scan range: +/- 20 mV of corrosion potentials. The scan rate is 0.125 mV/s. Tafel constant β is 0.12 V for the cathode and 0.12 V for the anode. Corrosion current densities are based on total area of bars.					
^c Data not available					

total area. The conventional steel specimen had a corrosion rate of 0.318 $\mu\text{m}/\text{yr}$ for the bottom mat bars, while all of the other specimens had corrosion rates less than 0.01 $\mu\text{m}/\text{yr}$.

Based on exposed area, the ECR(DCI) specimen had the highest corrosion rate, 33.2 $\mu\text{m}/\text{yr}$, followed by the ECR(Valspar) and ECR(Hycrete) specimens with 14.8 and 9.37 $\mu\text{m}/\text{yr}$, respectively. Three specimens – ECR(primer/Ca(NO₂)₂), ECR, and

ECR(Chromate) had low corrosion rates, between 4 and 5 $\mu\text{m}/\text{yr}$ based on exposed area.

3.5.2 Microcell Corrosion versus Macrocell Corrosion

Microcell and macrocell corrosion losses are compared for the Southern Exposure (SE) and cracked beam (CB) specimens tested in this study, along with those in a group reported by Darwin et al. (2007). The corrosion losses at 40 weeks are summarized in Table 3.22 based on total and exposed area. The combined results from these two resources are also included. For comparison, the corrosion losses for conventional steel are based on total area, representing average values for all of the conventional steel, while the losses for ECR are based on exposed area, representing the average values for specimens with four and ten holes through the epoxy coating. For example, the microcell corrosion loss at 40 weeks for the ECR specimens with four holes in the SE test was 0.309 μm , which was the average of those of ECR-r, 0.459 μm , and ECR, 0.159 μm , based on exposed area. The microcell corrosion loss for the ECR specimens with ten holes was 1.348 μm based on exposed area. The average of 0.309 and 1.348 μm was 0.829 μm , which was used as the combined results in Figures 3.125 to represent the average microcell corrosion loss for the ECR specimens for comparison. The calculations of the combined effects for the other systems are similar to those of ECR. All specimens had water-cement ratios of 0.45. The relative corrosion performance of the systems based on the combined results is illustrated in Figures 3.125 and 3.126 – with the data points of the relatively more effective systems closer to the origin.

Table 3.22 – Microcell and macrocell corrosion losses (μm) at 40 weeks for specimens in the Southern Exposure and cracked beam test

Steel Designation ^a	Based on Total Area				Based on Exposed Area			
	SE		CB		SE		CB	
	Microcell	Macrocell	Microcell	Macrocell	Microcell	Macrocell	Microcell	Macrocell
Specimens in Current Study								
Conv.-r	0.687	0.823						
ECR-r	0.001	0.004			0.459	1.701		
N5	1.354	3.261	10.160	15.680				
N5-DCI	1.038	1.608	15.021	10.252				
N5-HY	0.116	0.350	6.195	4.812				
N5-RH	0.333	0.511	14.597	10.098				
Specimens from FHWA Report (Darwin et al. 2007)								
Conv.	0.326	0.208	24.561	5.228				
ECR	0	0.003	0.015	0.024	0.159	1.396	7.252	11.390
ECR(DCI)	0	0.001	0.209	0.006	0.235	0.622	100.575	2.839
ECR(HY)	0.002	0	0.074	0.014	1.018	-0.223	35.741	6.686
ECR(RH)	0.001	0	0.412	0.027	0.451	-0.164	198.108	12.951
ECR(CN)	0.001	0.001	0.283	0.005	0.689	0.598	135.796	2.534
ECR-10h	0.007	0.003	0.107	0.034	1.348	0.610	20.599	6.476
ECR(DCI)-10h	0.001	0.001	0.228	0.017	0.276	0.099	43.750	3.341
ECR(HY)-10h	0.002	0.001	0.413	0.042	0.410	0.169	79.318	8.080
ECR(RH)-10h	0.005	0.001	0.351	0.073	1.019	0.131	67.512	13.983
ECR(CN)-10h	0.003	0	0.168	0.060	0.532	0.084	32.298	11.481
Combined Results^b								
Conv.	0.789	1.431	17.360	10.454				
Conv.-DCI	1.038	1.608	15.021	10.252				
Conv.-HY	0.116	0.350	6.195	4.812				
Conv.-RH	0.333	0.511	14.597	10.098				
ECR-4h and 10h					0.829	1.079	13.926	8.933
ECR(DCI)-4h and 10h					0.255	0.360	72.162	3.090
ECR(HY)-4h and 10h					0.714	-0.027	57.529	7.383
ECR(RH)-4h and 10h					0.735	-0.016	132.810	13.467
ECR(CN)-4h and 10h					0.611	0.341	84.047	7.008
^a Conv. = conventional steel, 4th batch. Conv.-r = repeated test for Conv. N5 = Conventional steel, 5th batch. ECR = conventional epoxy-coated reinforcement, with four 3-mm ($\frac{1}{8}$ -in.) diameter holes through the epoxy. ECR-r = repeated test for ECR. ECR(CN) = ECR with a primer coat containing $\text{Ca}(\text{NO}_2)_2$. DCI = concrete mixed with DCI inhibitor. HY = concrete mixed with Hycrete inhibitor. RH = concrete mixed with Rheocrete inhibitor. 10h = ECR bars with 10 holes through epoxy. All specimens have a water-cement ratio of 0.45.								
^b Losses for Conv. are based on total area, average values of Conv.-r, N5, and Conv. specimens. Losses for ECR specimens are based on exposed area, average values of 4h and 10h specimens. Losses for ECR-4h specimens are based on average values of ECR-r and ECR specimens.								

Figure 3.125 shows the relative performance for specimens in the Southern Exposure test. For specimens with conventional steel and different inhibitors, the relative performance is similar, whether based on the microcell or macrocell corrosion losses, with microcell/macrocell corrosion loss ratios being approximately 0.65. Hycrete specimens had the best corrosion performance, followed by the Rheocrete and the DCI specimens. For specimens with ECR and different inhibitors, losses based on microcell corrosion were higher than those based on macrocell corrosion, with the exception of the DCI specimens. The microcell/macrocell corrosion loss ratio for the ECR with DCI and $\text{Ca}(\text{NO}_2)_2$ primer specimens was 0.7 and 1.8, respectively. The ratios for the ECR with Hycrete and Rheocrete specimens was negative (-26.5 and -44.8 , respectively) due to the negative macrocell corrosion losses, which indicates that the bottom mats of steel had greater losses than the top mats based on the macrocell corrosion. Based on the corrosion losses, the systems with ECR appeared to perform well in intact concrete, with microcell and macrocell corrosion losses less than 0.83 and $1.08 \mu\text{m}$ at 40 weeks based on exposed area, respectively, while conventional steel specimens with and without inhibitors had microcell corrosion losses between 0.12 and $1.04 \mu\text{m}$ and macrocell corrosion losses between 0.35 and $1.61 \mu\text{m}$ based on total area (Table 3.22).

The relative performance of specimens in the cracked beam test is shown in Figure 3.126. Both microcell and macrocell corrosion losses had much higher values with wider scatter than those demonstrated in the Southern Exposure test. The microcell corrosion losses based on the LPR method were, in all cases, higher than those obtained based on macrocell current. For the specimens with conventional steel cast in concrete with an inhibitor, the Hycrete specimens exhibited the best performance based on both microcell and macrocell corrosion losses, 6.20 and 4.81

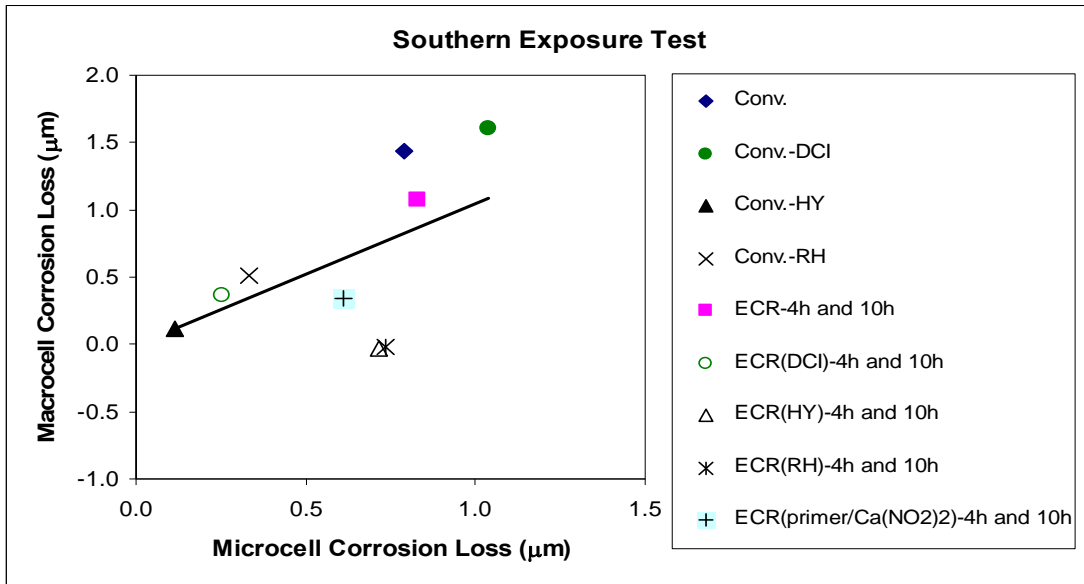


Figure 3.125 – Southern Exposure Test. Microcell versus macrocell corrosion losses for specimens with conventional steel and ECR with different inhibitors, results based on total area for conventional steel and exposed area for ECR, with average values for specimens with four and ten holes.

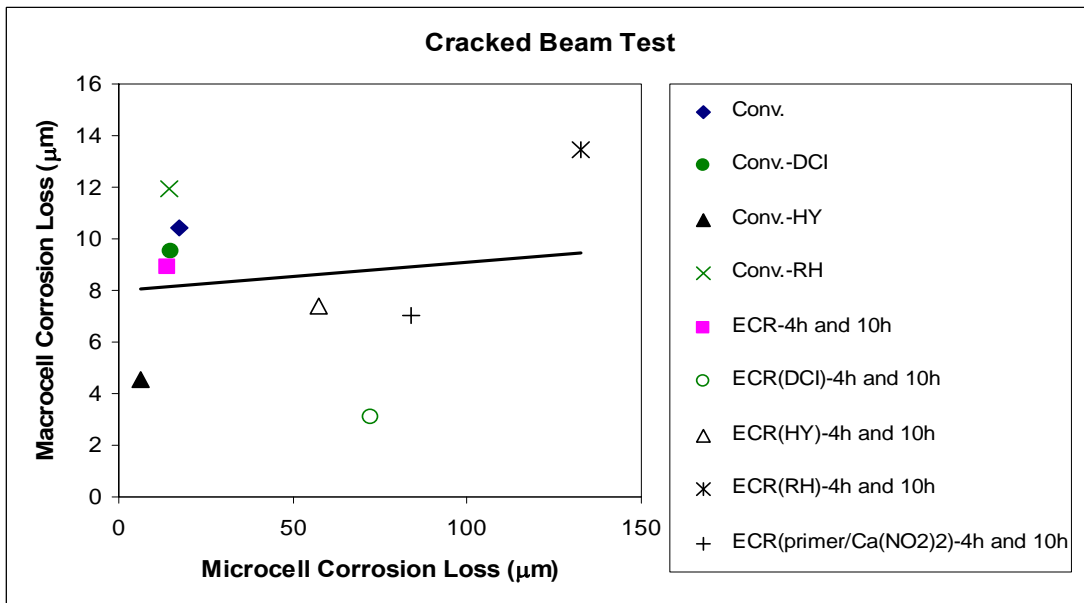


Figure 3.126 – Cracked Beam Test. Microcell versus macrocell corrosion losses for specimens with conventional steel and ECR with different inhibitors, results based on total area for conventional steel and exposed area for ECR, with average values for specimens with four and ten holes.

μm , respectively, at 40 weeks, with a microcell/macrocell corrosion loss ratio of 1.3. The losses for the other conventional steel specimens at 40 weeks ranged from 14.60 to 17.36 μm based on microcell corrosion and from 10.10 to 10.45 μm , based on macrocell corrosion, respectively, with microcell/macrocell corrosion loss ratios ranging from 1.4 to 1.7. For specimens with ECR cast in concrete with an inhibitor, the Hycrete specimens performed better than the other inhibitor specimens based on microcell corrosion losses. At 40 weeks, the microcell/macrocell corrosion loss ratio for the ECR with Hycrete specimens was 7.8. The ECR with DCI specimens had the lowest macrocell corrosion loss, 3.09 μm , but a microcell corrosion loss, 72.16 μm , and a microcell/macrocell ratio of 23.4. The ECR with Rheocrete specimens had the highest microcell and macrocell corrosion losses, 132.81 and 13.47 μm , respectively, with a microcell/macrocell corrosion loss ratio of 9.9. The ECR with $\text{Ca}(\text{NO}_2)_2$ primer specimens had a macrocell corrosion loss similar to ECR with Hycrete, 7.01 μm , with a microcell corrosion loss, 84.05 μm , and a microcell/macrocell loss ratio of 12.0.

In summary, Hycrete had the best performance among the inhibitors tested – DCI, Hycrete, Rheocrete, and ECR with a primer containing $\text{Ca}(\text{NO}_2)_2$. Hycrete improved the corrosion resistance of reinforcing steel not only in uncracked concrete, but also in cracked concrete. At 40 weeks, the microcell and macrocell corrosion losses for the ECR specimens based on exposed area are of the same order of magnitude as those of the specimens with conventional steel based on total area.

3.6 CRITICAL CHLORIDE THRESHOLD TEST

The results of the chloride analyses for conventional steel with different corrosion inhibitors and zinc-coated reinforcing steel are presented in this section.

The results include the time-to-initiation, corrosion rates, corrosion potentials, and individual and average critical chloride contents on a water-soluble basis. To limit the effect of outliers, chloride contents that were more than two standard deviations away from the mean were removed from consideration and the remaining values were again averaged. The outliers are identified by an asterisk in the tables.

As described in Section 2.7.1, corrosion initiation was determined by when the corrosion rate of the specimen reached $0.3 \mu\text{m}/\text{yr}$ or when a sharp drop in corrosion potential of the top mat of reinforcing steel was observed, with the former serving as the primary guide. The test results for individual specimens, shown in Appendix E, demonstrate the sharp drops in the corrosion potentials in many specimens.

The critical chloride thresholds for conventional steel are compared among specimens with different inhibitors and without inhibitors (results from Ji et al. 2005). For zinc-coated reinforcing steel, the critical chloride threshold is compared with the corresponding threshold for conventional steel and MMFX steel (results from Ji et al. 2005).

3.6.1 Conventional Steel with Corrosion Inhibitors

The chloride threshold results for DCI specimens are presented in Table 3.23. Five data points, or 4.2% of the 120 chloride values, were identified as outliers and removed from the analysis. The conventional steel in the DCI specimens had times-to-initiation ranging from 17 to 43 weeks (with an average of 26.5 weeks), with corresponding corrosion rates ranging from 0.30 to $1.68 \mu\text{m}/\text{yr}$ and corrosion potentials ranging from -0.293 to -0.376 V with respect to a CSE for the top mat of steel. The average chloride threshold for the six DCI specimens was $1.59 \text{ kg}/\text{m}^3$ ($2.69 \text{ lb}/\text{yd}^3$), with individual chloride contents ranging from 0.52 to $2.85 \text{ kg}/\text{m}^3$ (0.88 to

Table 3.23 – Critical chloride thresholds for conventional steel with DCI inhibitor in initiation beam test

Specimens ^a		Age (weeks)	Rate ($\mu\text{m}/\text{yr}$)	Top Potential (V)	Water Soluble Cl^- (kg/m^3)				
	Side ^b				1	2	3	4	5
B-N4-DCI-45N-1	1	43	0.95	-0.337	1.35	0.82	2.77	1.76	1.95
	2				2.47	2.47	2.85	1.91	2.21
B-N4-DCI-45N-2	1	31	0.30	-0.293	1.05	1.87	1.35	1.55	1.31
	2				1.31	1.39	1.31	1.42	2.10
B-N4-DCI-45N-3	1	20	1.17	-0.344	0.71	1.50	1.29	1.46	1.83
	2				1.20	1.12	1.24	1.50	1.24
B-N4-DCI-45N-4	1	23	0.82	-0.331	1.72	1.50	1.61	1.54	2.40
	2				1.42	1.95	1.16	1.31	1.01
B-N4-DCI-45N-5	1	25	0.51	-0.362	1.95	1.80	3.13*	2.47	2.02
	2				3.03*	1.57	1.20	3.05*	1.68
B-N4-DCI-45N-6	1	17	1.68	-0.376	1.09	1.31	1.39	1.42	1.05
	2				1.65	1.09	0.75	1.20	1.54
Average		26.5							

Specimens ^a		Water Soluble Cl^- (kg/m^3)					Average (kg/m^3)	SD ^c	COV ^c
	Side ^b	6	7	8	9	10			
B-N4-DCI-45N-1	1	2.02	2.25	2.25	2.70	1.31	2.05	0.56	0.27
	2	1.50	1.54	2.28	2.81	1.87			
B-N4-DCI-45N-2	1	1.27	1.20	1.68	1.46	1.20	1.59	0.40	0.25
	2	2.21	1.54	2.10	2.43	2.13			
B-N4-DCI-45N-3	1	3.65*	1.65	0.82	1.12	0.94	1.27	0.38	0.30
	2	1.09	1.68	0.67	0.94	2.10			
B-N4-DCI-45N-4	1	1.91	1.50	1.95	1.65	1.91	1.63	0.33	0.20
	2	1.27	1.65	1.98	1.50	1.72			
B-N4-DCI-45N-5	1	1.20	1.65	1.80	2.58	3.03*	1.86	0.50	0.27
	2	1.65	1.83	1.12	2.66	2.56			
B-N4-DCI-45N-6	1	1.24	1.16	0.60	1.35	0.60	1.19	0.38	0.32
	2	1.31	0.90	1.95	1.72	0.52			
Average							1.59		

^a Beam Specimens.

^b 10 chloride samples taken from each side of the bar per specimen.

^c SD = Standard Deviation, COV = Coefficient of Variation.

* Outlier sample.

4.79 lb/yd³) and the average chloride values for individual specimens ranging from 1.19 to 2.05 kg/m³ (2.01 to 3.46 lb/yd³). The coefficient of variation (COV) for the average specimen threshold values was 0.27. The scatter is due to the non-homogeneous nature of the concrete, which causes uneven ingress of chlorides through the pores in the concrete.

The chloride threshold results for the Hycrete specimens are presented in Table 3.24. Five data points, or 4.2% of the 120 chloride values, were identified as outliers and removed from the analysis. The conventional steel in the Hycrete specimens had times-to-initiation ranging from 12 to 52 weeks (with an average of 28.5 weeks), which is a wider range than that for the DCI specimens. The corrosion rates at initiation ranged from 0.34 to 1.35 $\mu\text{m}/\text{yr}$ and the top mat corrosion potentials ranged from -0.299 to -0.391 V with respect to a CSE. The average chloride threshold for the six Hycrete specimens was 0.37 kg/m³ (0.62 lb/yd³), which is much lower than that for the DCI specimens. The individual chloride contents for the Hycrete specimens ranged from 0.07 to 1.24 kg/m³ (0.13 to 2.08 lb/yd³), and the average chloride values for individual specimens ranged from 0.24 to 0.58 kg/m³ (0.40 to 0.98 lb/yd³). The coefficient of variation (COV) for the average specimen threshold values was 0.55, which indicates larger scatter relative to the DCI specimens. The very low critical corrosion threshold for the Hycrete specimens has prompted the need to repeat the series of tests. The value of that series will be presented in a later report.

Table 3.25 shows the chloride threshold results for Rheocrete specimens. Four data points, or 3.3% of the 120 chloride values, were removed from the analysis as outliers. The times-to-initiation ranged from 14 to 26 weeks (with an average of 19.5 weeks), with corrosion rates ranging from 0.32 to 2.61 $\mu\text{m}/\text{yr}$ and the top mat

Table 3.24 – Critical chloride thresholds for conventional steel with Hycrete inhibitor in initiation beam test

Specimens ^a		Age (weeks)	Rate ($\mu\text{m}/\text{yr}$)	Top Potential (V)	Water Soluble Cl^- (kg/m^3)				
Side ^b	1				2	3	4	5	
B-N4-HY-45N-1	1	16	0.55	-0.320	0.19	0.15	0.15	0.19	0.19
	2				0.26	0.30	0.22	0.30	0.34
B-N4-HY-45N-2	1	26	1.35	-0.391	0.19	0.15	0.15	0.30	0.19
	2				0.15	0.19	0.22	0.19	0.26
B-N4-HY-45N-3	1	48	0.34	-0.314	0.30	0.07	0.34	0.45	0.19
	2				0.15	0.15	0.49	0.56	0.34
B-N4-HY-45N-4	1	12	0.55	-0.348	0.24	0.34	0.37	0.22	0.22
	2				1.09	0.45	0.41	0.34	0.45
B-N4-HY-45N-5	1	52	1.16	-0.344	1.16	1.83*	1.83*	0.52	0.52
	2				0.41	0.22	0.52	0.34	1.16
B-N4-HY-45N-6	1	17	0.46	-0.299	0.26	0.19	0.15	0.11	0.15
	2				0.56	0.26	0.52	0.49	1.12
Average		28.5							

Specimens ^a		Water Soluble Cl^- (kg/m^3)					Average (kg/m^3)	SD ^c	COV ^c
Side ^b	6	7	8	9	10				
B-N4-HY-45N-1	1	0.60	0.30	0.41	0.22	0.28	0.28	0.12	0.41
	2	0.22	0.49	0.22	0.26	1.33*			
B-N4-HY-45N-2	1	0.30	0.22	0.19	0.28	0.46	0.24	0.08	0.35
	2	0.15	0.26	0.34	0.37	0.21			
B-N4-HY-45N-3	1	0.90	0.56	0.22	0.45	0.71	0.38	0.20	0.53
	2	0.30	0.34	3.59*	0.37	0.37			
B-N4-HY-45N-4	1	0.30	0.15	0.11	0.11	0.11	0.41	0.30	0.72
	2	1.09	0.79	0.64	0.67	0.17			
B-N4-HY-45N-5	1	1.24	0.97	0.67	0.26	0.45	0.58	0.33	0.57
	2	0.56	0.22	0.30	0.49	0.41			
B-N4-HY-45N-6	1	0.41	0.26	0.30	1.35*	0.26	0.32	0.23	0.74
	2	0.22	0.26	0.15	0.22	0.15			
Average						0.37			

^a Beam Specimens.

^b 10 chloride samples taken from each side of the bar per specimen.

^c SD = Standard Deviation, COV = Coefficient of Variation.

* Outlier sample.

Table 3.25 – Critical chloride thresholds for conventional steel with Rheocrete inhibitor in initiation beam test

Specimens ^a		Age (weeks)	Rate ($\mu\text{m}/\text{yr}$)	Top Potential (V)	Water Soluble Cl^- (kg/m^3)				
	Side ^b				1	2	3	4	5
B-N4-RH-45N-1	1	16	0.32	-0.301	0.60	0.37	0.64	1.54	0.86
	2				1.54	0.75	1.80	1.13	2.32
B-N4-RH-45N-2	1	14	2.61	-0.421	0.19	0.19	0.22	0.19	0.19
	2				0.60	1.01	0.56	0.52	0.52
B-N4-RH-45N-3	1	20	0.85	-0.357	0.49	0.56	1.76	0.97	0.52
	2				0.67	0.71	1.61	1.01	0.64
B-N4-RH-45N-4	1	21	0.80	-0.397	1.50	2.08	1.01	0.97	0.94
	2				1.54	1.83	2.51	1.61	1.95
B-N4-RH-45N-5	1	26	0.95	-0.404	1.87	1.76	0.90	2.25	2.12
	2				1.24	2.83	3.44*	1.09	1.50
B-N4-RH-45N-6	1	20	0.98	-0.457	2.02	2.81	1.24	1.87	2.21
	2				1.12	0.45	1.57	2.81	1.46
Average		19.5							

Specimens ^a		Water Soluble Cl^- (kg/m^3)					Average (kg/m^3)	SD ^c	COV ^c
	Side ^b	6	7	8	9	10			
B-N4-RH-45N-1	1	0.64	0.49	0.37	1.39	1.54	1.27	0.65	0.51
	2	2.10	1.24	1.95	2.02	2.10			
B-N4-RH-45N-2	1	0.52	0.34	0.94	0.26	0.30	0.57	0.39	0.68
	2	1.35	0.49	1.09	1.39	0.45			
B-N4-RH-45N-3	1	0.79	1.31	0.67	1.09	0.37	0.94	0.41	0.44
	2	1.72	0.67	1.24	1.09	0.90			
B-N4-RH-45N-4	1	0.82	0.97	0.45	0.71	0.90	1.23	0.54	0.44
	2	0.86	0.90	1.09	0.75	1.16			
B-N4-RH-45N-5	1	2.32	1.76	2.77	1.72	1.83	1.78	0.58	0.32
	2	1.98	1.57	0.82	3.78*	5.09*			
B-N4-RH-45N-6	1	1.65	3.29*	2.17	1.95	2.96	1.69	0.72	0.43
	2	1.50	0.37	1.57	1.20	1.12			
Average							1.23		

^a Beam Specimens.

^b 10 chloride samples taken from each side of the bar per specimen.

^c SD = Standard Deviation, COV = Coefficient of Variation.

* Outlier sample.

corrosion potentials ranging from 0.301 to -0.457 V with respect to a CSE for the top mat of steel. The average chloride threshold content for the six Rheocrete specimens was 1.23 kg/m^3 (2.07 lb/yd^3) with the individual chloride contents ranging from 0.57 to 1.78 kg/m^3 (0.95 to 3.01 lb/yd^3). The coefficient of variation (COV) for the average specimen threshold value was 0.47 .

For comparison, the critical chloride corrosion thresholds for conventional reinforcement as measured by Ji et al. (2005) are presented in Table 3.26. The threshold values were obtained using both beam specimens, as used for conventional steel with inhibitors in this study, and Modified Southern Exposure (MSE) specimens, which were twice the width of the beam specimens and contained two top bars with four bottom bars; the top bars were individually monitored and 10 samples were taken from each side of the specimens once corrosion had initiated in the bar. Because twice as many samples were taken from the beam specimens, they received twice the weight assigned as the MSE specimens when calculating the average chloride corrosion threshold. Five chloride values, or 3.5% of the chloride values, were removed from consideration for conventional steel because the values were more than two standard deviations away from the mean.

As shown in Table 3.26, the conventional steel bars had times-to-initiation ranging from 8 to 23 weeks (with an average of 14.2 weeks), with an average corrosion rate of $1.59 \text{ }\mu\text{m/yr}$ and an average corrosion potential of -0.361 V with respect to a CSE at corrosion initiation. After the removal of outliers, the average chloride threshold for all specimens was 0.96 kg/m^3 (1.63 lb/yd^3). The individual chloride contents ranged from 0.34 to 1.91 kg/m^3 (0.58 to 3.21 lb/yd^3), and the average values for the individual specimens ranged from 0.58 to 1.20 kg/m^3 (0.98 to 2.02 lb/yd^3). The coefficients of variation (COV) for individual bars ranged from 0.32

Table 3.26 – Critical chloride thresholds for conventional steel with no inhibitors in modified Southern Exposure and initiation beam test (results from Ji et al. 2005)

Specimens ^a	Bar No.	Age (weeks)	Rate ($\mu\text{m}/\text{yr}$)	Top Potential (V)	Water Soluble Cl^- (kg/m^3)				
					1	2	3	4	5
MSE-Conv.-1	1 ^b	-	-	-	-	-	-	-	-
	2	8	0.84	-0.273	0.41	0.90	0.99	1.61	0.71
MSE-Conv.-2	1 ^b	-	-	-	-	-	-	-	-
	2	12	2.89	-0.396	0.56	1.42	0.76	2.84*	0.97
MSE-Conv.-3	1	15	1.96	-0.404	0.41	0.49	0.37	0.49	0.56
	2	14	1.79	-0.380	2.17*	1.01	0.60	0.78	1.35
MSE-Conv.-4	1	9	1.76	-0.379	0.46	0.61	0.50	0.51	0.46
	2	9	3.51	-0.421	0.47	0.62	0.99	0.36	0.46
MSE-Conv.-5	1	14	0.82	-0.332	1.01	1.38	1.42	0.97	1.08
	2	9	0.35	-0.280	0.52	0.50	0.39	0.61	0.41
MSE-Conv.-6	1	20	1.52	-0.361	0.90	0.82	1.08	1.57	1.91
	2	17	1.84	-0.379	1.61	1.08	1.08	1.79	1.68
	Side ^c								
B-Conv.-1	1	21	1.17	-0.358	0.90	1.46	0.75	1.35	0.82
	2				2.59*	1.36	1.16	1.37	0.86
B-Conv.-2	1	23	1.17	-0.392	1.35	0.51	1.08	0.99	0.77
	2				0.67	1.61	1.61	1.64	1.53
B-Conv.-3	1	14	1.02	-0.344	1.35	0.62	1.12	1.64	2.35*
	2				1.27	1.83	0.93	1.72	1.31
Average		14.2							

Specimens ^a	Bar No.	Water Soluble Cl^- (kg/m^3)					Average (kg/m^3)	SD ^d	COV ^d
		6	7	8	9	10			
MSE-Conv.-1	1 ^b	-	-	-	-	-	0.92	0.44	0.48
	2	-	-	-	-	-			
MSE-Conv.-2	1 ^b	-	-	-	-	-	0.93	0.37	0.40
	2	-	-	-	-	-			
MSE-Conv.-3	1	1.08	0.75	1.53	-	-	0.78	0.38	0.48
	2	-	-	-	-	-			
MSE-Conv.-4	1	0.46	0.34	0.76	0.46	0.82	0.58	0.19	0.33
	2	0.60	0.50	0.82	0.46	0.97			
MSE-Conv.-5	1	0.67	0.90	0.54	0.43	0.71	0.72	0.32	0.44
	2	0.52	0.43	0.43	0.95	0.56			
MSE-Conv.-6	1	0.79	1.79	0.86	1.35	1.23	1.20	0.40	0.34
	2	0.67	0.69	0.78	1.31	1.01			
	Side ^c								
B-Conv.-1	1	1.83	1.12	0.97	1.16	0.93	1.12	0.35	0.32
	2	1.79	0.56	0.83	1.31	0.72			
B-Conv.-2	1	0.80	0.88	0.92	0.80	0.92	1.15	0.40	0.35
	2	1.69	1.38	0.92	1.76	2.85*			
B-Conv.-3	1	1.49	0.67	1.12	1.49	0.90	1.17	0.39	0.34
	2	0.49	0.71	1.53	1.12	0.93			
Average						0.96			

^a B=Beam Specimens, MSE= Modified Southern Exposure.

^b Sample not available-bar subjected to testing using other trial methods.

^c 10 chloride samples taken from each side of the bar per specimen.

^d SD = Standard Deviation, COV = Coefficient of Variation.

* Outlier sample.

to 0.48, and COV for the average specimen threshold value was 0.38.

Tables 3.23 through 3.25 demonstrate that with an average value of 0.37 kg/m^3 (0.62 lb/yd^3), conventional steel in concrete containing Hycrete had a much lower average critical chloride threshold than conventional steel in concrete with DCI or Rheocrete and conventional steel in concrete without inhibitors, which had average values of 1.59, 1.23, and 0.96 kg/m^3 (2.69, 2.07, and 1.62 lb/yd^3), respectively. The tables also demonstrate that the chloride threshold is not a single value for a system, but rather a range of values. This point is illustrated in Figure 3.127, which shows the ranges of chloride sample values at corrosion initiation for conventional steel in concrete without inhibitors and with DCI, Hycrete, and Rheocrete inhibitors. Of the four, conventional steel in concrete with Hycrete exhibited the narrowest range and the lowest individual sample values with the longest initiation time, while conventional steel in concrete with DCI or Rheocrete exhibited a wider range and higher individual sample values with a longer initiation time than conventional steel in concrete without inhibitors. The long initiation time demonstrated the excellent corrosion performance for the conventional steel with Hycrete inhibitor, while the low chloride threshold may help to explain the way that Hycrete prevents corrosion, that is, by reducing the concrete permeability and forming a film on the surface of the reinforcement. The reason causing the very low threshold, however, will require additional study.

After the test was completed, the specimens were broken and the conventional reinforcement was examined for corrosion products. Corrosion products were observed on the bars on the top mats for all of the specimens, which in most cases, showed slight corrosion (Figure 3.128). Two of six Rheocrete specimens showed severe corrosion on the top bars, one of which is illustrated in Figure 3.129. Of the

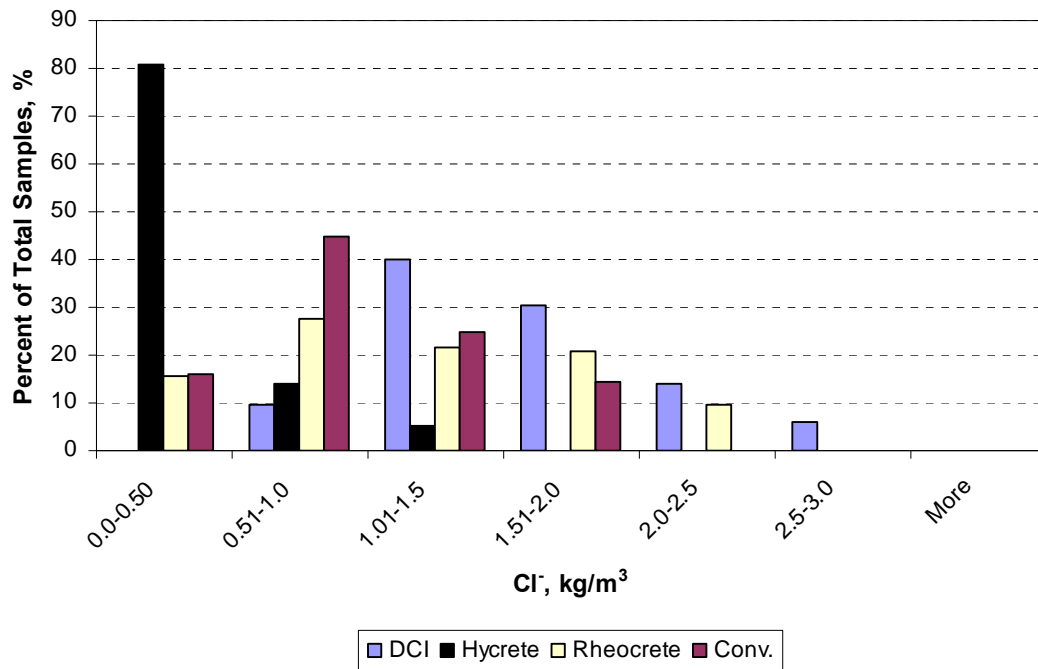


Figure 3.127 – Comparison of the ranges of chloride sample values at corrosion initiation for conventional steel without inhibitors and with DCI, Hycrete, and Rheocrete inhibitor.



Figure 3.128 – Initiation Beam Test. Conventional steel in the top mat (B-N4-Hycrete-45N-3) showing slight corrosion.



Figure 3.129 – Initiation Beam Test. Conventional steel in the top mat (B-N4-Rheocrete-45N-4) showing severe corrosion.

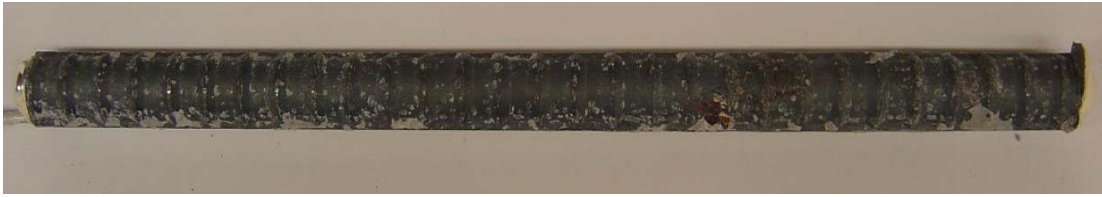


Figure 3.130 – Initiation Beam Test. Conventional steel in the bottom mat (B-N4-Rheocrete-45N-2) showing slight corrosion.

bars on the bottom mats, three showed slight corrosion, including bars in one DCI and two Rheocrete specimens, one of which is shown in Figure 3.130.

3.6.2 Zinc-Coated Reinforcing Steel

This section presents the test results for zinc-coated reinforcement that meets the requirement of ASTM A767, with the exception that bars were not subjected to chromate treatment as required by the specification. The results include the critical chloride threshold and the autopsy results for evidence of the formation of hydrogen at the surface of the bars.

The corrosion rates, corrosion potentials, and mat-to-mat resistance of the 12 beam specimens containing zinc-coated reinforcing steel are shown, respectively, in Figures 3.131 to 3.133. The specimens were exposed to the salt solutions until the corrosion rate reached $0.3 \mu\text{m}/\text{yr}$ or when a sharp change in corrosion potential of the top mat of reinforcing steel (Figure 3.132a) was observed, with the former serving as the primary guide. The figures show that the corrosion rates were variable during the first four to six weeks of the tests, with the corrosion potentials of both the top and bottom mats stabilizing near -0.400 V . The early variations in corrosion rate, including apparently negative values, resulted from the amphoteric nature of zinc. The corrosion rates are based on the macrocell current between the top and bottom mats of steel, and early in the test, before significant quantities of chloride had

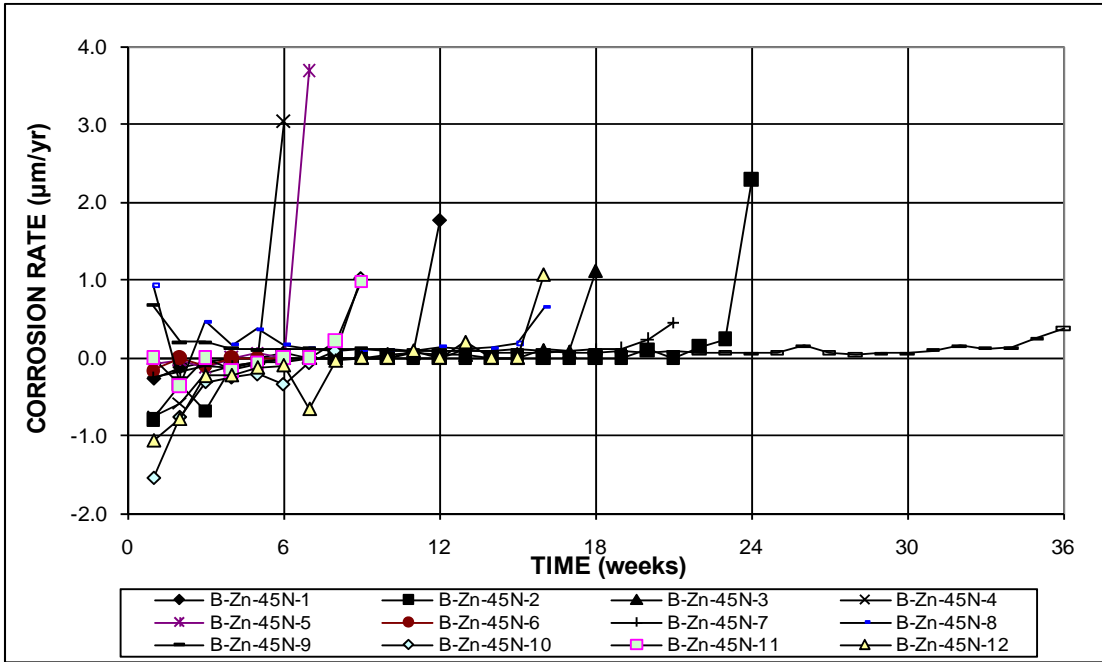


Figure 3.131 – Corrosion rates for specimens with zinc-coated reinforcing steel in initiation beam test.

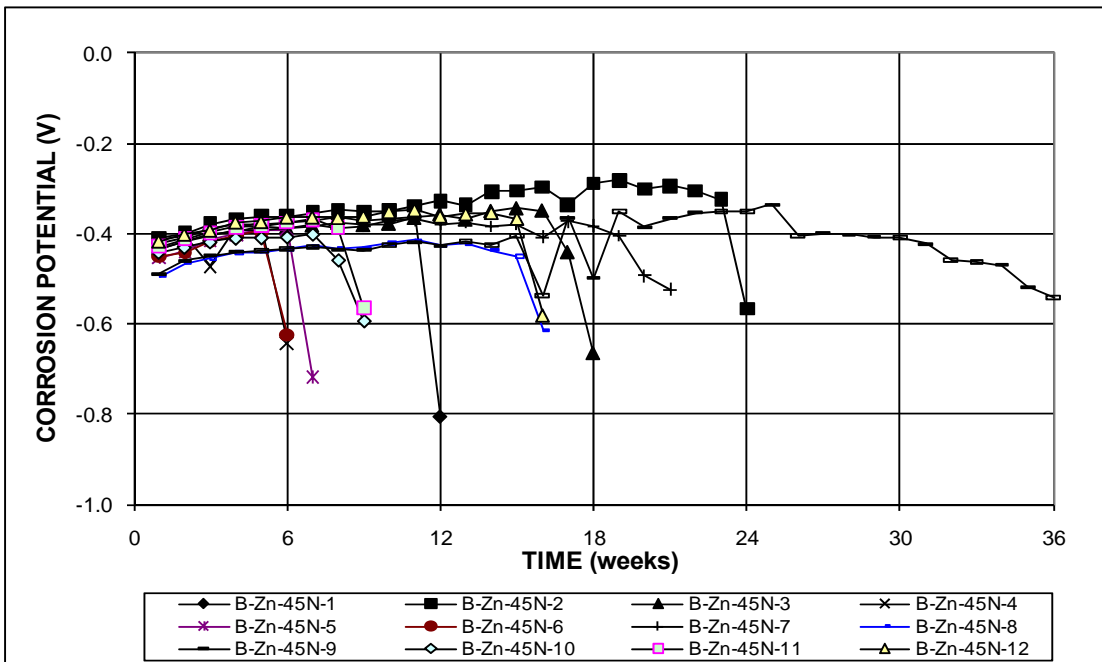


Figure 3.132a – Top bar corrosion potential with respect to a copper-copper sulfate electrode for specimens with zinc-coated reinforcing steel in initiation beam test.

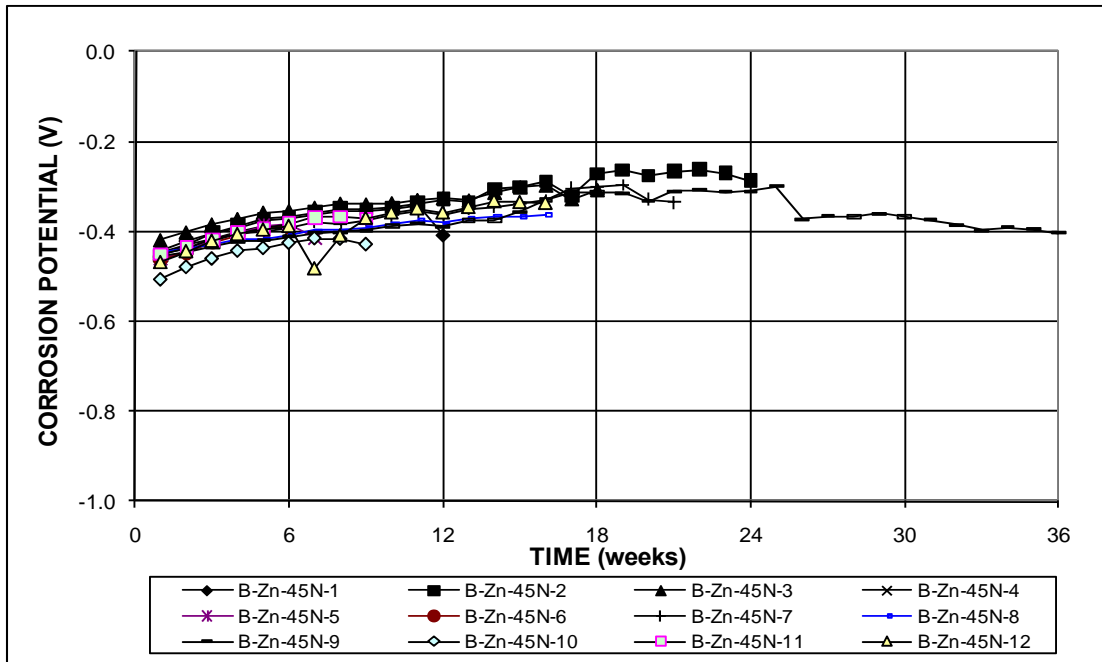


Figure 3.132b – Bottom bar corrosion potential with respect to a copper-copper sulfate electrode for specimens with zinc-coated reinforcing steel in initiation beam test.

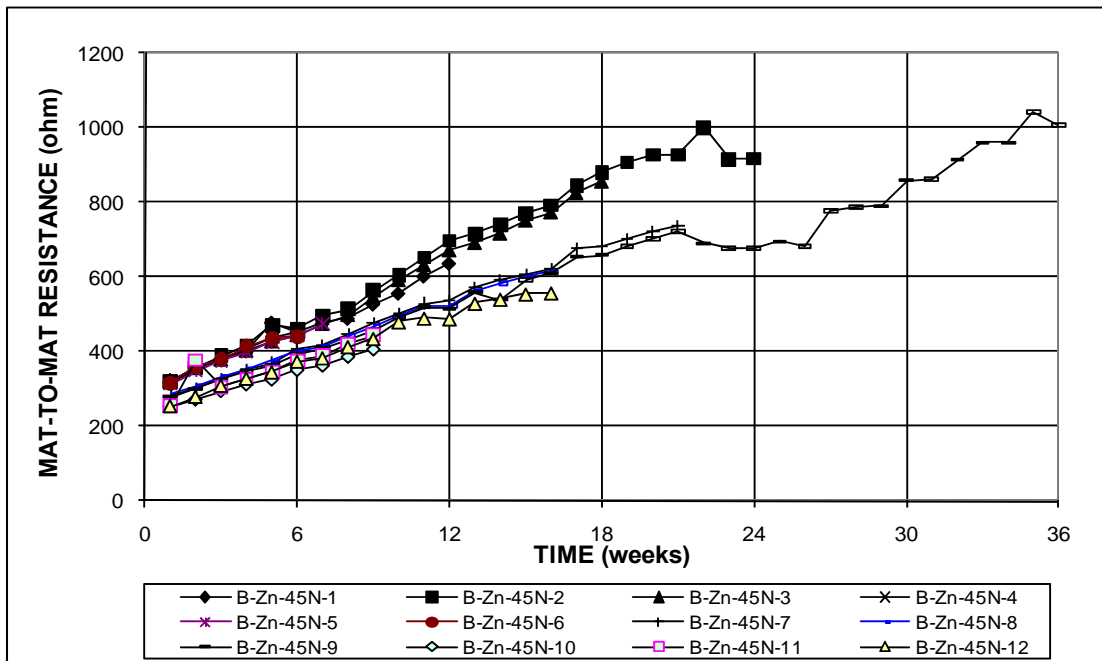


Figure 3.133 – Mat-to-mat resistance for specimens with zinc-coated reinforcing steel in initiation beam test.

reached the top steel, the current was actually more likely to indicate “negative corrosion” because the bottom mat contained two bars, as compared to the single bar in the top mat.

Upon the initiation of corrosion, the corrosion rates turned sharply positive (usually from one week to the next, Figure 3.131) and the corrosion potentials of the top mat changed sharply to more negative values (Figure 3.132a). This was true, except for specimens 7 and 9. The corrosion rate of specimen 7 increased from zero to a value above $0.3 \mu\text{m/yr}$ over a two-week period, while the corrosion rate for specimen 9 increased gradually between weeks 24 and 36. The mat-to-mat resistances increased steadily from 250 to 1,000 ohms over time (Figure 3.133).

Following corrosion initiation, the tests were terminated, samples were taken for chloride analysis, and the specimens were autopsied. These procedures are described in Section 2.7.1.

Critical Chloride Threshold

The results of the chloride analyses for the zinc-coated bars are presented in Table 3.27. Twelve data points, or 5% of the 240 chloride values, were removed for the zinc-coated bars because the values were more than two standard deviations away from the mean. They are identified by an asterisk in Table 3.27.

The bars had times-to-initiation ranging from 6 to 36 weeks (with an average of 15.0 weeks), with an average corrosion rate of $1.37 \mu\text{m/yr}$ and an average corrosion potential of -0.619 V with respect to CSE at corrosion initiation. After the removal of outliers, the average chloride threshold for all 12 specimens was 1.52 kg/m^3 (2.57 lb/yd^3). The individual chloride contents ranged from 0.13 to 4.64 kg/m^3 (0.22 to 7.82 lb/yd^3), and the average values for the individual specimens ranged from 0.59 to 2.92 kg/m^3 (1.00 to 4.93 lb/yd^3). The coefficients of variation (COV) for individual bars

Table 3.27– Critical chloride thresholds for zinc-coated steel in initiation beam test

Specimens ^a		Age (weeks)	Rate ($\mu\text{m}/\text{yr}$)	Top Potential (V)	Water Soluble Cl ⁻ (kg/m^3)				
	Side ^b				1	2	3	4	5
B-Zn-45N-1	1	12	1.77	-0.81	1.72	3.37	1.78	4.22	3.08
	2				3.03	4.57	2.55	5.77*	2.77
B-Zn-45N-2	1	24	2.30	-0.57	2.85	1.91	1.31	1.46	2.51
	2				2.92	2.66	3.48	2.58	2.88
B-Zn-45N-3	1	18	1.12	-0.66	4.38	5.13*	3.89	1.39	1.35
	2				0.60	4.08	3.65	4.42	3.18
B-Zn-45N-4	1	6	3.04	-0.64	0.19	0.56	0.22	0.62	0.52
	2				0.34	0.51	0.90	0.27	1.39
B-Zn-45N-5	1	7	3.69	-0.72	1.50	2.43	0.34	1.35	1.46
	2				4.27	2.90	0.75	0.67	1.12
B-Zn-45N-6	1	6	0.00	-0.62	0.64	0.71	0.82	0.37	0.60
	2				0.82	0.26	0.15	0.30	0.34
B-Zn-45N-7	1	21	0.44	-0.52	1.87	4.64	0.86	1.50	1.76
	2				0.64	0.86	1.61	2.28	1.83
B-Zn-45N-8	1	16	0.65	-0.61	0.64	2.28	0.49	0.60	0.71
	2				2.66	2.88	2.96	4.31	3.11
B-Zn-45N-9	1	36	0.37	-0.54	3.29	1.05	1.61	2.10	1.20
	2				4.04	4.42	6.44*	4.72*	4.98*
B-Zn-45N-10	1	9	1.02	-0.59	0.75	0.30	0.32	0.19	0.21
	2				0.30	0.15	0.30	0.52	1.42
B-Zn-45N-11	1	9	0.98	-0.56	0.90	0.94	0.22	0.30	0.30
	2				0.67	1.27	1.27	0.82	1.24
B-Zn-45N-12	1	16	1.06	-0.58	0.52	1.16	1.98	0.64	0.62
	2				3.28	0.28	1.01	0.22	2.66
Average		15.0							

Specimens ^a		Water Soluble Cl ⁻ (kg/m^3)					Average (kg/m^3)	SD ^c	COV ^c
	Side ^b	6	7	8	9	10			
B-Zn-45N-1	1	2.32	3.07	3.56	1.80	1.50	2.92	0.89	0.31
	2	3.03	4.49	3.22	2.51	2.96			
B-Zn-45N-2	1	2.28	1.87	0.90	2.55	1.91	2.04	0.79	0.38
	2	0.75	2.21	1.05	1.95	0.86			
B-Zn-45N-3	1	1.01	1.09	1.38	1.60	0.85	2.36	1.35	0.57
	2	2.73	1.12	2.58	4.87*	3.26			
B-Zn-45N-4	1	0.82	1.05	1.01	0.41	0.82	0.63	0.34	0.53
	2	0.34	0.64	0.41	1.20	0.49			
B-Zn-45N-5	1	0.75	1.01	0.39	1.61	1.24	1.34	0.97	0.73
	2	0.82	1.46	0.22	1.83	0.60			
B-Zn-45N-6	1	0.22	0.13	0.24	1.39	0.22	0.61	0.47	0.77
	2	0.88	0.49	0.64	2.06	0.94			
B-Zn-45N-7	1	5.20*	2.81	1.65	1.05	1.01	1.91	1.16	0.61
	2	1.65	3.89	1.05	1.12	4.12			
B-Zn-45N-8	1	0.52	1.78	2.77	1.24	1.31	2.30	1.34	0.58
	2	4.46	2.96	4.38	3.67	2.32			
B-Zn-45N-9	1	0.94	1.42	1.68	0.94	0.97	2.15	1.35	0.63
	2	5.65*	5.77*	5.58*	6.70*	4.23			
B-Zn-45N-10	1	1.98	1.09	0.64	0.37	0.26	0.59	0.47	0.79
	2	0.82	0.71	0.45	0.22	0.86			
B-Zn-45N-11	1	0.26	1.20	0.52	0.30	0.49	0.70	0.37	0.53
	2	0.56	1.05	0.71	0.45	0.45			
B-Zn-45N-12	1	0.75	0.64	0.71	1.16	0.52	1.09	1.06	0.97
	2	0.26	3.74	5.17*	0.22	0.34			
Average							1.52		

^a Beam Specimens.^b 10 chloride samples taken from each side of the bar per specimen.^c SD = Standard Deviation, COV = Coefficient of Variation.

* Outlier sample.

ranged from 0.31 to 0.97, and the COV for the average specimen threshold value was 0.62.

Comparisons to Conventional and MMFX Steel

For comparison, the critical chloride corrosion thresholds for conventional and MMFX microcomposite reinforcement as measured by Ji et al. (2005) are presented, respectively, in Tables 3.26 and 3.28.

Three chloride values, or 2.1% of the chloride values, were removed from the MMFX steel sample because the values were more than two standard deviations away from the mean.

As shown in Table 3.28, the MMFX bars had times-to-initiation ranging from 17 to 51 weeks (with an average of 28.8 weeks), with an average corrosion rate of 0.89 $\mu\text{m}/\text{yr}$ and an average corrosion potential of -0.365 V with respect to a CSE at corrosion initiation. After the removal of outliers, the average chloride threshold for all specimens was 3.76 kg/m^3 (6.34 lb/yd^3). The individual chloride contents ranged from 1.27 to 6.58 kg/m^3 (2.14 to 11.08 lb/yd^3) and the average values for the individual specimens ranged from 2.78 to 5.04 kg/m^3 (4.69 to 8.49 lb/yd^3). The coefficients of variation (COV) for individual bars ranged from 0.19 to 0.47, and COV for the average specimen threshold value was 0.31.

Tables 3.26 through 3.28 demonstrate that with an average value of 1.52 kg/m^3 (2.57 lb/yd^3), zinc-coated steel had a higher critical corrosion threshold than conventional steel, which had an average value of 0.96 kg/m^3 (1.63 lb/yd^3), and a lower threshold than MMFX steel, which had an average value of 3.76 kg/m^3 (6.34 lb/yd^3). Figure 3.134 shows the ranges of chloride sample values at corrosion initiation for zinc-coated, conventional, and MMFX reinforcement. Zinc-coated and MMFX steel exhibited wider ranges than conventional steel. Of the three, zinc-coated

Table 3.28 – Critical chloride thresholds for MMFX microcomposite steel in modified Southern Exposure and initiation beam test (from Ji et al. 2005)

Specimens ^a	Bar No.	Age (weeks)	Rate ($\mu\text{m}/\text{yr}$)	Top Potential (V)	Water Soluble Cl^- (kg/m^3)				
					1	2	3	4	5
MSE-MMFX-1	1	23	0.50	-0.390	3.21	3.55	3.38	4.71	5.83
	2	17	0.60	-0.362	1.57	1.76	2.32	2.20	2.76
MSE-MMFX-2	1	23	0.41	-0.333	3.47	2.88	5.98	5.34	6.32
	2	28	0.01	-0.363	4.41	5.19	5.57	5.42	5.98
MSE-MMFX-3	1 ^b	-	-	-	-	-	-	-	-
	2	17	1.95	-0.460	1.49	2.43	2.56	2.99	3.40
MSE-MMFX-4	1	30	0.57	-0.348	1.87	3.03	3.14	3.74	3.36
	2	29	2.00	-0.367	2.91	2.35	2.05	3.96	3.03
MSE-MMFX-5 ^c	-	-	-	-	-	-	-	-	-
MSE-MMFX-6	1	26	1.20	-0.359	2.99	1.61	2.09	2.54	2.54
	2	39	0.68	-0.368	2.51	2.91	3.32	3.18	3.09
	Side ^d								
B-MMFX-1	1	51	1.02	-0.36	4.33	5.49	5.72	5.11	5.53
	2				5.90	5.88	6.24	6.01	4.79
B-MMFX-2	1	26	1.22	-0.341	1.27	1.46	1.87	1.85	3.14
	2				2.28	2.84	3.36	3.29	3.06
B-MMFX-3	1	36	0.56	-0.329	3.81	3.74	4.02	4.76	4.36
	2				4.97	3.66	2.73	3.51	3.18
Average		28.8							

Specimens ^a	Bar No.	Water Soluble Cl^- (kg/m^3)					Average (kg/m^3)	SD ^e	COV ^e
		6	7	8	9	10			
MSE-MMFX-1	1	6.09	6.58	6.84*	6.28	6.98*	3.88	1.54	0.40
	2	4.37	3.66	3.89	4.30	3.33			
MSE-MMFX-2	1	-	-	-	-	-	5.04	0.94	0.19
	2	5.19	7.77*	4.97	4.89	4.97			
MSE-MMFX-3	1 ^b	-	-	-	-	-	3.23	0.98	0.30
	2	4.48	3.70	4.86	2.99	3.44			
MSE-MMFX-4	1	3.36	2.28	-	-	-	2.78	0.81	0.29
	2	1.27	1.57	3.85	3.33	2.24			
MSE-MMFX-5 ^c	-	-	-	-	-	-	-	-	-
MSE-MMFX-6	1	4.28	2.24	2.73	3.62	2.88	4.15	1.25	0.30
	2	3.36	4.04	3.50	1.84	3.32			
	Side ^d								
B-MMFX-1	1	6.16	6.16	4.29	4.33	4.82	3.89	1.84	0.47
	2	5.90	5.72	4.93	6.09	3.85			
B-MMFX-2	1	1.61	2.24	2.43	3.51	3.14	3.88	1.00	0.26
	2	3.40	4.52	5.57	4.45	3.89			
B-MMFX-3	1	3.10	3.10	4.63	6.46	2.95	3.69	1.02	0.28
	2	4.74	4.93	1.72	3.88	3.60			
Average						3.76			

^a B=Beam Specimens, MSE= Modified Southern Exposure

^b Sample not available-bar subjected to testing using other trial methods

^c Specimen contaminated from the outside

^d 10 chloride samples taken from each side of the bar per specimen

^e SD = Standard Deviation, COV = Coefficient of Variation

* Outlier sample

steel exhibited the lowest individual sample value, although this may be a function of variability in the concrete within individual specimens. On the low side, zinc-coated steel also exhibited low average values of the chloride threshold that match those exhibited by conventional steel. For example, the three lowest values of the critical chloride corrosion threshold for zinc-coated bars ranged from 0.59 to 0.64 kg/m³ (1.00 to 1.07 lb/yd³), which were similar to the three lowest values for conventional steel, which ranged from 0.58 to 0.78 kg/m³ (0.98 to 1.32 lb/yd³) (Tables 3.26 and 3.28).

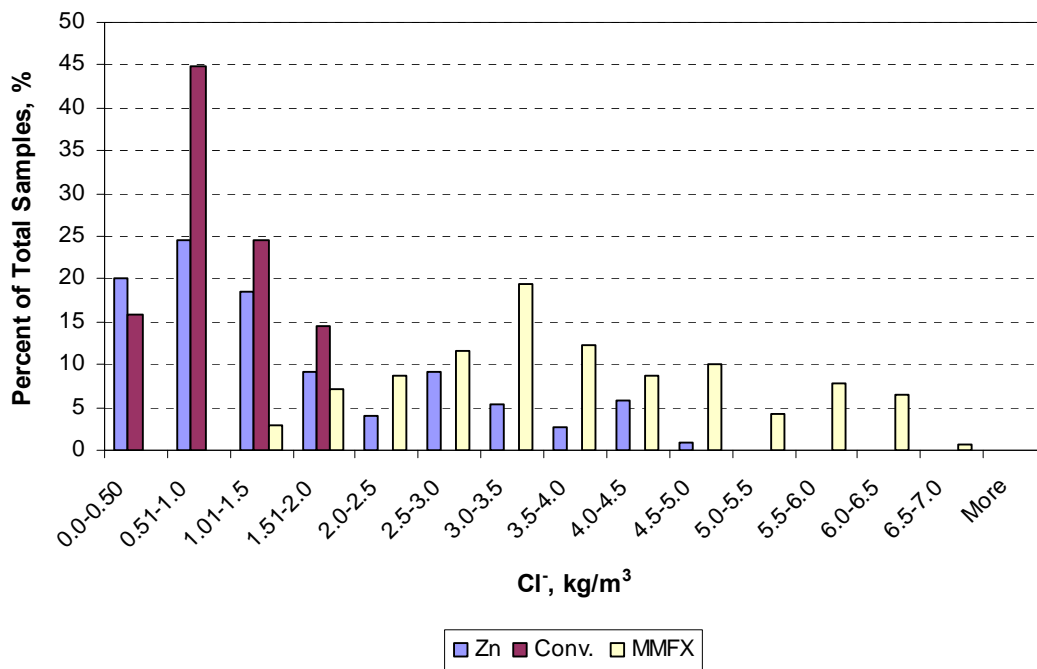


Figure 3.134 – Comparison of the ranges of chloride sample values at corrosion initiation for zinc-coated (Zinc), conventional (Conv.), and MMFX reinforcement.

In contrast, on the high side, the three highest values of the critical chloride corrosion threshold for the zinc-coated bars ranged from 2.30 to 2.93 kg/m³ (3.88 to 4.93 lb/yd³), which were far greater than the three highest values for conventional steel, which ranged from 1.15 to 1.20 kg/m³ (1.94 to 2.02 lb/yd³). This wide range in

critical chloride values may help explain the widely varying level of performance reported for zinc-coated reinforcement in concrete. The lowest three and highest three values for MMFX steel, respectively, ranged from 2.78 to 3.69 kg/m³ (4.69 to 6.22 lb/yd³) and 3.89 to 5.04 kg/m³ (6.56 to 8.49 lb/yd³) (Table 3.28).

Autopsy Results

Following the tests, the zinc-coated specimens were examined to determine the degree of corrosion of the reinforcing bars and for signs of staining and increased porosity due to hydrogen formation. For all twelve zinc-coated steel test specimens, a white crystalline corrosion product was visible on the top bar. A typical example is shown in Figure 3.135. The crystals were large, indicating that the pH of the concrete was above 13.3 (Andrade and Macias 1988, Bentur et. al. 1997) and that the zinc had not been passivated. Seven of the twelve specimens had sufficient local corrosion losses on the top bar to result in the loss of the outer pure zinc layer, exposing the outer zinc-iron intermetallic layer, which appears as a black area centered in the white zinc corrosion product (Figure 3.136). Three of twelve specimens exhibited bottom bar corrosion in addition to the top bar corrosion (Figure 3.137). On two of the specimens with bottom bar corrosion, the corrosion was sufficient to expose the intermetallic zinc-iron layer (Figure 3.138). Corrosion initiation of the bottom bar is unlikely due to chlorides. The presence of bottom bar corrosion may be due to reduced passivity of zinc without the chromate treatment in plastic concrete or due to loss of metal in presence of high-pH concrete pore solution. All specimens exhibited localized corrosion on the bar comparable in area to the localized corrosion at initiation observed on conventional bars (Figure 3.139).



(a)



(b)

Figure 3.135 – Initiation Beam Test. (a) Top bar (top) and bottom bars (bottom) for specimens with zinc-coated reinforcement after autopsy (B-Zn-45N-8). (b) Corrosion product on top bar, showing large white crystalline corrosion product.



(a)



(b)

Figure 3.136 – Initiation Beam Test. (a) Top bar (top) and bottom bars (bottom) for specimens with zinc-coated reinforcement after autopsy (B-Zn-45N-3). (b) Corrosion product on top bar showing exposure of underlying steel.

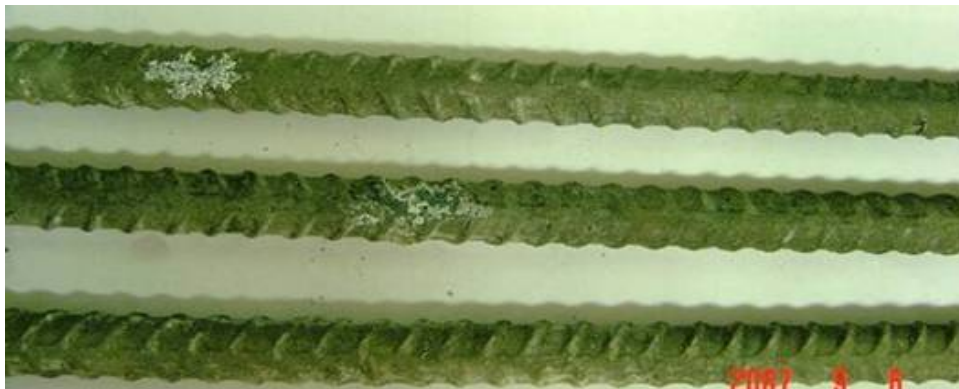


Figure 3.137 – Initiation Beam Test. Zinc-coated reinforcement after autopsy (B-Zn-45N-11) showing corrosion on top bar (top) and bottom bars (bottom).



Figure 3.138 – Initiation Beam Test. Zinc-coated reinforcement after autopsy (B-Zn-45N-4) showing corrosion on the bottom bar exposing underlying steel.



Figure 3.139 – Typical corrosion at initiation on conventional steel.

Measurements of total coating thickness using a pull-off gage produced values ranging from 173 to 254 μm , (6.8 to 10 mils), with an average of 193 μm (7.6 mils), with no more than a 51- μm (2-mil) loss. This occurred on a bar with a coating thickness of 254 μm (10 mils) at regions in which the pure zinc layer had been lost, suggesting that, at the time of the autopsy, only the pure layer of zinc had been lost. This loss, however, does not bode well for the long-term performance of the bars because, without the outer layer of pure zinc, the intermetallic layers tend to break down very rapidly because the protective layer of calcium hydroxyzincate cannot form (Andrade and Macias 1988).

During the autopsy, the concrete was also examined for signs of staining and increased porosity due to hydrogen formation. No exterior staining of the concrete was visible on any of the specimens; however, specimen B-Zn-45N-10 exhibited visible interior staining of the concrete after autopsy (Figure 3.140). Increased

porosity of the concrete was noted in all specimens, with the concrete below the bar exhibiting increased porosity relative to the concrete above the bar (Figures 3.141 and 3.142). It should be noted, however, that this effect is likely due to entrained air (used in the concrete), as increased porosity under the bar was also noted in concrete cast with conventional steel reinforcement (Figure 3.143). Thus, the increase in local porosity observed in the zinc-coated specimens was comparable to that observed in specimens containing conventional steel reinforcement.



Figure 3.140 – Initiation Beam Test. Specimen with zinc-coated reinforcement after autopsy (B-Zn-45N-10) showing visible interior staining of the concrete.



(a)



(b)

Figure 3.141 – Initiation Beam Test. Specimen with zinc-coated reinforcement after autopsy (B-Zn-45N-2) showing increased porosity of concrete below the bar relative to the concrete above the bar. (a) Above and (b) Below the bar.



(a)



(b)

Figure 3.142 – Initiation Beam Test. Specimen with zinc-coated reinforcement after autopsy (B-Zn-45N-2, another bar) showing increased porosity of concrete below the bar relative to the concrete above the bar. (a) Above and (b) Below the bar.



(a)



(b)

Figure 3.143 – Initiation Beam Test. Specimen with conventional reinforcement after autopsy showing increased porosity of concrete below the bar relative to the concrete above the bar. (a) Above and (b) Below the bar.

Summary

The average critical chloride thresholds for conventional steel with different corrosion inhibitors and zinc-coated, conventional, and MMFX reinforcement are shown in Table 3.29. The Hycrete specimens exhibited a lower chloride threshold and longer time to corrosion initiation than DCI, Rheocrete, or the conventional steel specimens, suggesting that its ability to improve the corrosion resistance of reinforcement is likely due to its ability to reduce concrete permeability rather than

any effect on the corrosion threshold. The DCI and Rheocrete specimens had higher chloride threshold values than the conventional steel specimens. The specimens containing the three inhibitors had an extended time to corrosion initiation as compared to the specimens containing conventional steel without inhibitors. Corrosion products were observed on the top bars of all inhibitor specimens.

Table 3.29 – Comparison of the average critical chloride thresholds

Specimens ^a	Age	Corrosion Rate	Top Potential	Cl ⁻ average	Cl ⁻ Median	SD ^c	COV ^c	Removed Outliers ^d
	(weeks)	($\mu\text{m}/\text{yr}$)	(V)	(kg/m^3)	(kg/m^3)			
Conv. (DCI)	26.5	0.90	-0.341	1.59	1.54	0.42	0.27	4.17%
Conv. (Hycrete)	28.5	0.73	-0.336	0.37	0.30	0.21	0.55	4.17%
Conv. (Rheocrete)	19.5	1.09	-0.390	1.23	1.10	0.55	0.47	3.33%
Conv.	14.2	1.59	-0.361	0.96	0.90	0.36	0.38	3.62%
Average^b		1.08	-0.357					
Zinc	15.0	1.37	-0.619	1.52	1.09	0.88	0.62	5.00%
MMFX	28.8	0.89	-0.365	3.76	3.51	1.17	0.31	2.11%

^a Conv. = Conventional steel. Zinc = Zinc-coated steel. MMFX = MMFX microcomposite steel.

Conv. (DCI) = Conv. with DCI inhibitor in concrete. Conv. (Hycrete) = Conv. with Hycrete inhibitor.

Conv. (Rheocrete) = Conv. with Rheocrete inhibitor in concrete.

^b Average values for conventional steel.

^c SD = Standard Deviation, based on the average of specimen threshold values.

COV = Coefficient of Variation, based on the average of specimen threshold values.

^d Chloride samples that are two standard deviations away from the mean are removed as outliers.

The average critical corrosion threshold for zinc-coated reinforcement was higher than the observed critical corrosion threshold of conventional steel and lower than the value for MMFX steel. The average top mat corrosion potential for zinc-coated reinforcement at corrosion initiation, -0.619 V, was more negative than those of conventional and MMFX steel, with average values of about -0.357 and -0.365 V, respectively. The coefficient of variation in the critical corrosion threshold for zinc reinforcement was larger than those for conventional and MMFX reinforcement, potentially indicating a greater variation in the performance of zinc-coated reinforcement. Zinc corrosion products were observed on the top bar of all twelve specimens. Increased porosity was noted in the concrete directly beneath the

reinforcement, but the increase was comparable to that observed for specimens containing conventional reinforcement. Zinc corrosion products were also observed on some bottom bars, which may be due to a reduction in the passivity of the zinc without a chromate pretreatment in plastic concrete or due to loss of metal in the presence of high-pH concrete pore solution.

The results in Table 3.29 can be used to estimate the time to corrosion initiation for the three types of inhibitors and steel. This can be done in conjunction with chloride surveys reported by Miller and Darwin (2000) and Lindquist, Darwin and Browning (2005, 2006) for bridge decks in northeast Kansas, as will be described in detail in the Section 4.3.

CHAPTER 4

SUMMARY OF RESULTS AND ECONOMIC ANALYSIS

This chapter summarizes the test results presented in Chapter 3, including discussion, comparison, and analysis of various corrosion protection systems and different test methods. An economic analysis for bridges built with different corrosion protection systems is also performed based on the experience of the Kansas Department of Transportation of Kansas (KDOT) and other states in conjunction with the laboratory results obtained in this study.

4.1 SUMMARY OF TEST RESULTS

This section presents a summary of the test results covered in Chapter 3. At this writing, the rapid macrocell tests are completed, while the bench-scale and field tests are still underway. The results obtained to date, however, provide a useful comparison of the relative performance of the systems and the overall performance of the epoxy-coated reinforcement, corrosion inhibitors, and 2205 stainless steel.

The rapid macrocell test imposes a severe exposure condition on the specimens and therefore provides distinguishable results in a relatively short time (usually 15 to 25 weeks). The Southern Exposure (SE) and cracked beam (CB) tests use a higher salt concentration for the ponding solution and more aggressive ponding and drying cycles than the ASTM G109 and field tests. Therefore, the average corrosion rates and losses for specimens in the SE and CB tests are higher than those obtained for the corresponding specimens in the ASTM G109 and field tests.

The test results for the corrosion protection systems evaluated in this study are summarized in the following sections.

4.1.1 Conventional Steel and Epoxy-Coated Reinforcement

Conventional steel and epoxy-coated reinforcement (ECR) were evaluated as control specimens in the rapid macrocell, bench-scale, and field tests. The test results for these specimens, in combination with past experience testing the systems, indicate that ECR improves the corrosion resistance of conventional steel significantly under all test conditions. The following paragraphs summarize this behavior.

In the rapid macrocell test, conventional steel was evaluated using mortar-wrapped specimens, which had mortar water-cement (w/c) ratios of 0.45 or 0.35, exposed to a 1.6-molal ion concentration of NaCl in simulated concrete pore solution. Conventional steel had an average total corrosion loss of 1.80 μm for a w/c ratio of 0.45 at 15 weeks, while the average total corrosion loss for specimens with a w/c ratio of 0.35 was 0.39 μm (22% of that observed for conventional steel in mortar with a w/c ratio of 0.45, Table 3.2). Guo et al. (2006) evaluated ECR in a 1.6-molal ion NaCl and simulated concrete pore solution using mortar-wrapped specimens and a w/c ratio of 0.50. Results from Guo's tests showed that the average total corrosion of ECR was less than 0.005 μm based on total area at 15 weeks compared to that for conventional steel in the same tests (4.82 μm). The corrosion loss of ECR is, thus, far less than that of conventional steel.

In the SE test, six specimens containing conventional steel and six specimens containing conventional ECR bars (with four holes through the epoxy coating), each with a w/c ratio of 0.45, were evaluated as controls. The average corrosion losses were 0.96 and 3.42 μm for conventional steel and no more than 0.005 and 0.01 μm for ECR based on total area at 42 and 67 weeks, respectively (Table 3.3). The corrosion loss of ECR was 0.5% of that of the conventional steel. Based on exposed area, the average corrosion losses for ECR were 1.95 and 3.04 μm at 42 and 67 weeks,

respectively, which are on the same order of magnitude as the average corrosion loss of the uncoated conventional steel, indicating that very high corrosion activity can occur at localized areas of ECR.

Three specimens in the SE test and three specimens in the CB test, each containing conventional steel, with a w/c ratio of 0.45 were evaluated as inhibitor controls (Table 3.4). The average total corrosion loss of the conventional steel in the CB test was 16.35 μm at 42 weeks, which when compared to SE results is 4.5 times the average corrosion loss of conventional steel (3.60 μm) and over 3,000 times the average corrosion loss of ECR with four holes (less than 0.005 μm).

In the ASTM G109 test, five out six specimens with conventional steel were removed from the test at week 174 because of cracking caused by corrosion. Based on the average of six specimens (final corrosion losses were included for the removed specimens), the average corrosion loss of conventional steel was 2.05 μm , while those of both ECR with four and ten holes were slightly negative at week 209 (Table 3.5), indicating that the bottom mat of steel exhibited more corrosion losses than the top mat.

In the field test, two specimens each without (Table 3.6) and two specimens each with simulated cracks (Table 3.7) were evaluated for conventional steel and ECR (ECR has 16 intentional holes through the epoxy coating), using a 10% rock salt solution applied every four weeks. At about 170 weeks, the total corrosion losses of ECR were 2% and 0.9% of the corrosion losses of the conventional steel for specimens without and with simulated cracks in the concrete, respectively. The corrosion losses of the cracked specimens were twice the corrosion losses of the uncracked specimens.

4.1.2 Corrosion Inhibitors and Low Water-Cement Ratios

Conventional steel in concrete containing DCI, Hycrete, or Rheocrete were evaluated in the rapid macrocell and bench-scale tests. In the rapid macrocell test, mortar-wrapped specimens with w/c ratios of 0.45 and 0.35 were used. ECR in concrete with the three inhibitors, along with ECR with a primer containing microencapsulated calcium nitrite were evaluated in the field test. In general, the results from the tests indicate that corrosion inhibitors improve the corrosion resistance of conventional steel in both cracked and uncracked concrete. The inhibitors tend to delay the onset of corrosion in uncracked concrete but not in cracked concrete. For specimens cast with ECR, the addition of a corrosion inhibitor in concrete provides limited improvement to the corrosion resistance. The effect of using a corrosion inhibitor with ECR is difficult to measure because of the effectiveness of ECR by itself as a corrosion protection system. The following paragraphs summarize the data that support these conclusions.

In the SE test, specimens with conventional steel and Hycrete had the lowest average corrosion loss, 0.38 μm , followed by specimens with Rheocrete with 0.59 μm , and DCI with 1.82 μm , compared to specimens without inhibitors, which had an average corrosion loss of 3.60 μm at 42 weeks. The corrosion loss of conventional steel was reduced 90% by Hycrete, 84% by Rheocrete, and 49% by DCI, when compared to specimens without inhibitors.

In the CB test, specimens with conventional steel and Hycrete had the lowest average corrosion loss, 4.93 μm , followed by specimens with Rheocrete with 10.51 μm , and DCI with 10.63 μm , compared to specimens without inhibitors, which had an average corrosion loss of 16.35 μm at 42 weeks. The corrosion loss of conventional steel was reduced 70% by Hycrete, 36% by Rheocrete, and 35% by DCI,

when compared to specimens without inhibitors.

In the field tests of specimens containing ECR (Tables 3.8 and 3.9), the average corrosion losses for the inhibitor specimens were no more than 0.02 μm for ages ranging from 163 to 175 weeks based on total area, except for ECR(DCI) (1), which had an average corrosion loss of 0.04 μm , and ECR(DCI) (2) and ECR(Rheocrete) (1), which had average corrosion losses of 0.03 μm .

Bench-scale specimens with conventional steel and Hycrete exhibited a lower chloride threshold and a longer time to corrosion initiation than specimens with Rheocrete, DCI, and specimens without inhibitors. After corrosion initiation, specimens with Hycrete corroded at very low corrosion rates in both cracked and uncracked concrete, which resulted in low corrosion losses, as demonstrated by the SE and CB specimens. The reason that Hycrete was effective in cracked concrete may be explained by the mechanism by which Hycrete limits corrosion. Hycrete prevents corrosion primarily by reducing the permeability of concrete. The decision to use Hycrete in concrete mixes must be approached cautiously, however, because of evidence of low strength and durability. The concrete properties shown in Table 2.26 indicate that Hycrete reduces the 28-day compressive strength of concrete, and therefore, modifications of concrete mixes, such as adding extra cement, will be needed to compensate for the strength loss. The field specimens containing Hycrete exhibited scaling across the upper surface, the only ones to do so in this study.

Conventional steel cast in concrete with Rheocrete had an increased critical chloride threshold and extended time to corrosion initiation compared to conventional steel specimens without inhibitors. After corrosion initiation, CB specimens with Rheocrete exhibited average corrosion losses similar to those for the CB specimens with DCI (Figure 3.29), which were higher than those for the CB specimens with

Hycrete. SE specimens with Rheocrete exhibited average corrosion losses similar to those for the SE specimens with Hycrete, which were lower than those for the SE specimens with DCI (Figure 3.25). Specimens cast with Rheocrete showed significant improvement in corrosion resistance in uncracked concrete as measured by the average corrosion losses in the SE test, but very limited improvement in cracked concrete as measured by average corrosion losses in the CB test.

Conventional steel cast in concrete with DCI had an increased critical chloride threshold and extended time to corrosion initiation as compared to conventional steel specimens without inhibitors. The average corrosion rates for the SE specimens with DCI were higher than those for specimens with Hycrete or Rheocrete after initiation, and resulted in relatively high average corrosion losses in the SE test. In the CB test, the corrosion rates and losses for specimens with DCI were similar to those for specimens with Rheocrete, but higher than those for specimens with Hycrete. These trends may be explained by the mechanism of DCI in preventing corrosion. As described in Section 1.6.4, DCI [$\text{Ca}(\text{NO}_2)_2$] can help to form a passive $\gamma\text{-FeOOH}$ film on the steel surface. When the chloride concentration level is relatively high, however, the passive film becomes unstable and corrosion initiates. Once corrosion has initiated, the passive protection promoted by DCI is greatly diminished.

4.1.3 Multiple-Coated Reinforcement

Multiple-coated reinforcement (MC) was evaluated using the ASTM G109 and field tests. In the ASTM G109 test, MC bars with four and ten holes through the epoxy coating were tested in two forms: (1) with only the epoxy layer penetrated, and (2) with both the zinc and epoxy layers penetrated. In the field test, MC bars with 16 holes were tested with both layers penetrated. In this study, MC bars exhibited similar

average corrosion losses as those of ECR with several exceptions as noted below.

In the ASTM G109 test (Table 3.5), MC bars with only the epoxy layer penetrated with 10 holes had the highest average corrosion loss, 0.10 μm , based on total area, while the average corrosion losses for ECR and the other MC specimens were less than 0.005 μm at 209 weeks.

In the field test, the average corrosion losses for MC specimens were less than 0.002 μm in uncracked concrete (Table 3.10) and were 0.01 and 0.03 μm in the two cracked concrete specimens (Table 3.11) based on total area at 167 weeks, compared to conventional ECR, which had average corrosion losses of no more than 0.02 μm .

In a study conducted by Darwin et al. (2007), however, MC specimens were evaluated in the SE and CB tests, and the results showed that the highest corrosion losses were attained by the MC bars with both layers penetrated followed by those with only the epoxy layer penetrated and, in turn, by conventional ECR. The high corrosion losses of MC result because the zinc coating provides protection to the underlying steel by acting as a sacrificial anode. The inconsistent results noted above in the ASTM G109 and field tests in this study maybe due to the influence of the high resistance provided by the epoxy coating and the mild exposure condition provided in these tests.

4.1.4 Epoxy-Coated Reinforcement with Increased Adhesion

Three types of ECR with increased adhesion were evaluated in the field test, including ECR with zinc chromate pretreatment prior to the application of epoxy coating and ECR with the high adhesion epoxy coatings produced by DuPont and Valspar. The results showed that ECR with increased adhesion provided no improvement in the corrosion resistance of the bars.

Based on total area, specimens with increased adhesion ECR had average corrosion losses of no more than 0.02 μm in uncracked concrete (Table 3.12), compared to specimens with conventional ECR that had an average corrosion loss of no more than 0.01 μm . In cracked concrete (Table 3.13), the two specimens with ECR(Valspar) had average corrosion losses of 0.03 and 0.04 μm , and the other specimens had average corrosion losses of 0.01 to 0.02 μm , compared to specimens with conventional ECR that had an average corrosion loss of 0.02 μm .

The results in this study were consistent with those reported by Darwin et al. (2007), in which the three types of ECR with increased adhesion were evaluated in SE and CB tests. The results demonstrate that increased adhesion between the epoxy and the reinforcing steel provide no advantage with respect to conventional ECR.

4.1.5 KDOT Bridge Projects

Pickled 2205 stainless steel used in two KDOT bridges, the Doniphan County Bridge (DCB) and Mission Creek Bridge (MCB), were evaluated in bench-scale tests, field tests, and through corrosion potential surveys of the bridge decks. The test results indicate that the pickled 2205 stainless steel had excellent corrosion resistance and that the pickled 2205 stainless steel in the two bridge decks remains in a passive state.

The pickled 2205 stainless steel remained passive in the SE test, and while total average corrosion losses for specimens of 0.027 and 0.003 μm were recorded in the CB tests for the Doniphan County Bridge and the Mission Creek Bridge, respectively (Table 3.14). For the field test specimens associated with the Doniphan County Bridge (Table 3.15), specimens with conventional steel had the highest average corrosion losses, 2.66 μm , at 215 weeks in uncracked concrete, while specimens with

pickled 2205 stainless steel and ECR exhibited average corrosion losses of no more than 0.01 μm , equal to less than 0.4% of the corrosion losses of specimens with conventional steel.

For the field test specimens associated the Mission Creek Bridge (Table 3.16), specimens with pickled 2205 stainless steel exhibited negative average corrosion losses, $-0.25 \mu\text{m}$, in the cracked concrete, indicating that the bottom mat of steel had more corrosion activity than the top mat. Specimens with ECR had average corrosion losses of no more than 0.03 μm in the cracked specimen, while specimens with conventional steel had the highest average corrosion losses, with a maximum of 8.53 μm in the cracked specimen. The corrosion losses for the uncracked specimens were lower than those of the cracked specimens for all three types of reinforcement.

Bi-annual bridge surveys were performed on both bridge decks to obtain corrosion potential contours. The corrosion potentials of the majority of the bridge decks were below -0.200 V (Figures 3.112 and 3.115), indicating a very low probability of corrosion activity. The regions near the two abutments had corrosion potentials between -0.300 and -0.500 V . Since mild steel form ties were used in both abutments (as shown in Figure 316), the more negative corrosion potentials may be due to corrosion of the form ties. As mentioned in Section 1.4.1, steel in structures buried in the earth often have very negative potentials due to the restricted access of oxygen, and thus the more negative corrosion potentials could be due to a low oxygen concentration, as well.

4.2 COMPARISON OF TEST METHODS

This section presents the comparisons between the results obtained in the rapid macrocell, SE, and CB tests. The comparisons are based on the results for specimens

with conventional steel and corrosion inhibitors in the rapid macrocell test at 15 weeks and in the SE and CB tests at 42 weeks, including results expressed as average corrosion rates and corrosion losses. Although water-cement ratios of 0.45 and 0.35 were used in the rapid macrocell test, results of the rapid macrocell test used for comparisons will be solely based on the results for specimens with a w/c ratio of 0.35. The results for specimens with a w/c ratio of 0.45 are not used because, as described in Section 3.1, they did not exhibit a significant difference among different inhibitors. To better illustrate the comparisons, error bars with one standard deviation are included for all the data points in the plots. The results for the rapid macrocell test are based on six specimens, while the results of the SE and CB specimens are based on three specimens.

The corrosion rates and losses used for comparing the test methods are summarized in Tables 4.1 and 4.2. The specimens in the rapid macrocell test had the lowest average corrosion rates and losses at 15 weeks, followed by the corresponding specimens in the SE and CB tests at 42 weeks, except that specimens with Hycrete had a slightly higher average corrosion loss in the rapid macrocell test than that in the SE test. The specimens in the rapid macrocell test had the highest coefficients of variation (COV) for corrosion rate and loss at 15 weeks, followed by the corresponding specimens in the SE and CB tests at 42 weeks, except that the specimens without an inhibitor and the specimens with DCI had slightly lower COVs for corrosion rate in the SE test than those in the CB test. The average corrosion losses in the rapid macrocell test did not show a distinguishable difference among all the specimens. Specimens with conventional steel without inhibitors had the highest average corrosion losses in the SE and CB tests, followed by specimens with DCI and Rheocrete. Specimens with Hycrete had the lowest average corrosion losses in the SE

and CB tests.

A linear regression analysis is performed to investigate whether there is a linear relationship between the results of two different test methods. If results are consistent between two test methods, the best fit line through a set of results obtained using the least squares method will have a positive slope with a relatively high coefficient of determination, R^2 (R^2 , with values between 0 and 1). R^2 represents the proportion of variability in one data set that is predictable by a second data set. It measures how well a fitted regression line approximates real data points. A value of 0 means there is no linear relationship between the two methods being compared and a value of 1 means there is a perfect linear relationship between the two methods. Values of R^2 greater than 0.65 generally indicate a strong linear relationship between the two data sets being compared.

Table 4.1 – Average corrosion rates ($\mu\text{m}/\text{yr}$) for specimens in the rapid macrocell test (at 15 weeks) and the bench-scale tests (at 42 weeks)

Specimen Designation	Macrocell $w/c=0.35$			SE			CB		
	Average	Standard Deviation	COV ^a	Average	Standard Deviation	COV ^a	Average	Standard Deviation	COV ^a
Conv.	5.28	8.20	1.55	9.06	3.77	0.42	17.85	15.07	0.84
Conv. (DCI)	4.52	4.17	0.92	5.74	0.67	0.12	10.20	1.39	0.14
Conv. (Hycrete)	0.46	1.46	3.17	0.87	0.94	1.09	3.33	0.24	0.07
Conv. (Rheocrete)	0.83	1.50	1.80	2.09	2.20	1.05	10.29	2.12	0.21

^a COV = Coefficient of variation.

Table 4.2 – Average corrosion losses (μm) for specimens in the rapid macrocell test (at 15 weeks) and the bench-scale tests (at 42 weeks)

Specimen Designation	Macrocell $w/c=0.35$			SE			CB		
	Average	Standard Deviation	COV ^a	Average	Standard Deviation	COV ^a	Average	Standard Deviation	COV ^a
Conv.	0.39	0.52	1.34	3.60	2.45	0.68	16.35	6.12	0.37
Conv. (DCI)	0.53	0.43	0.81	1.82	0.43	0.24	10.63	1.02	0.10
Conv. (Hycrete)	0.42	0.99	2.36	0.38	0.34	0.88	4.93	0.89	0.18
Conv. (Rheocrete)	0.25	0.34	1.33	0.59	0.68	1.15	10.51	1.74	0.17

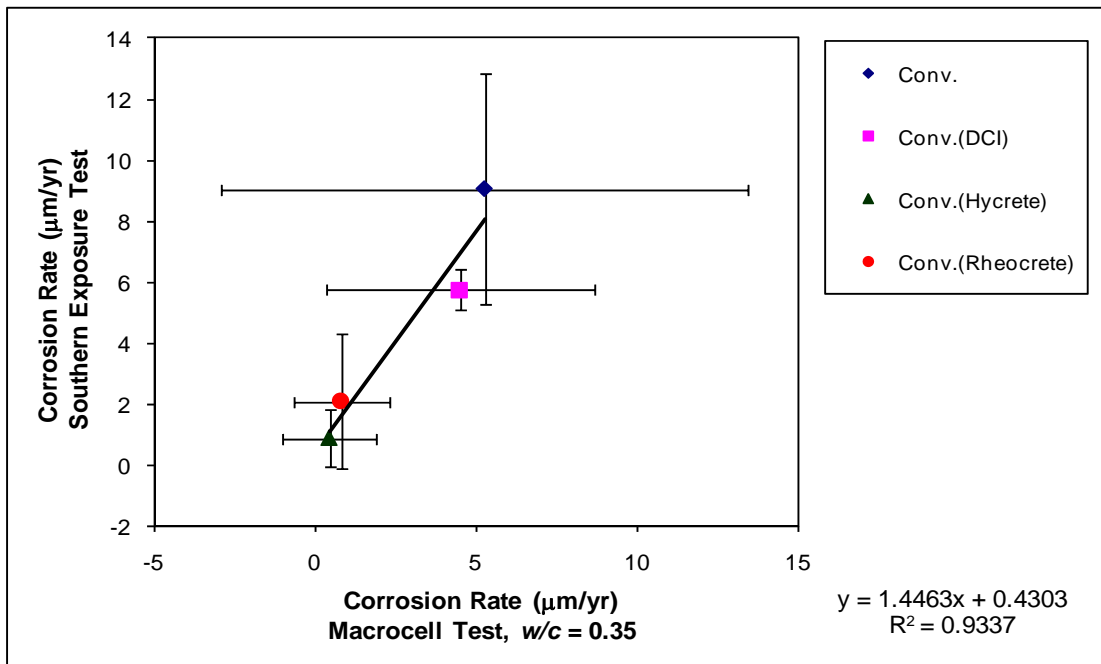
^a COV = Coefficient of variation.

4.2.1 Southern Exposure Test versus Rapid Macrocell Test

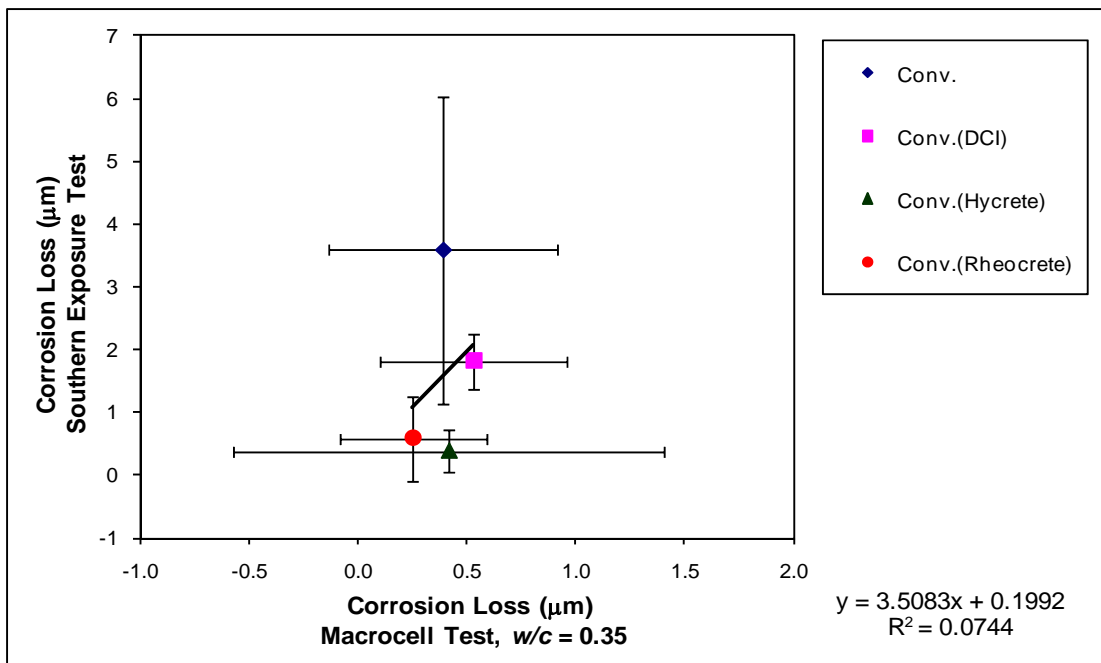
Results for specimens with a w/c ratio of 0.35 are used to represent the results in the rapid macrocell test. The comparisons of the corrosion rates and total corrosion losses between the SE and the rapid macrocell test with the w/c of 0.35 are presented in Figures 4.1 (a) and (b), respectively.

As shown in Figure 4.1 (a), the trends noted for corrosion rates in the SE test at 42 weeks were consistent with those in the rapid macrocell test at 15 weeks. The coefficient of determination R^2 is 0.93, indicating that 93% of the total variation in the corrosion rates for one test is predicted by variations in the corrosion rate from the other test. Specimens with conventional steel without inhibitors had the highest corrosion rates, followed by specimens with DCI. Specimens with Hycrete exhibited the lowest corrosion rates in both tests. The results indicate that the correlation is significant for corrosion rate at the specific ages in the rapid macrocell and SE tests and there is a good linear relationship between the test results obtained using the two test methods. This plot also demonstrates that the variations in the corrosion rates in the macrocell test were much higher than those in the SE test.

The comparisons of the corrosion losses between the SE test and the rapid macrocell test are shown in Figure 4.1 (b). The coefficient of determination R^2 is only 0.07, indicating that only 7% of the total variation in the corrosion losses obtained using the two test methods can be explained by the fitted trendline. The results, thus, show that there is no correlation between corrosion losses in the rapid macrocell and the SE tests. This is largely because the corrosion losses obtained with different inhibitors do not differ significantly in the rapid macrocell test.



(a)



(b)

Figure 4.1 – (a) Comparison of average corrosion rates and (b) corrosion losses for the Southern Exposure test (at 42 weeks) versus the rapid macrocell test with mortar-wrapped specimens with a w/c ratio of 0.35 (at 15 weeks).

4.2.2 Cracked Beam Test versus Rapid Macrocell Test

Comparisons of corrosion rates and total corrosion losses obtained using the CB and the rapid macrocell tests with the w/c of 0.35 are presented in Figures 4.2 (a) and (b), respectively.

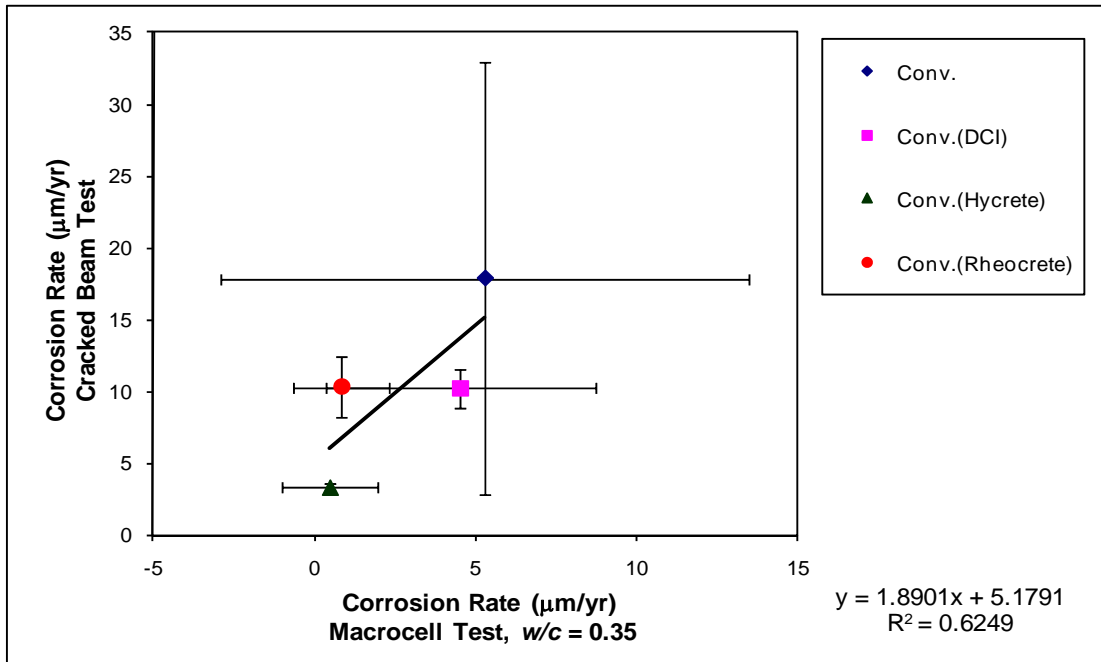
As shown in Figure 4.2 (a), the corrosion rates in the CB test at 42 weeks exhibit a linear relationship with those of the rapid macrocell test at 15 weeks. The coefficient of determination R^2 is 0.62. Specimens with conventional steel without inhibitors had the highest corrosion rate, while the Hycrete specimens exhibited the lowest corrosion rates in both tests. The COVs for the corrosion rates in the macrocell test are much higher than for the CB test.

The comparisons of the corrosion losses between the CB test and the rapid macrocell test are shown in Figure 4.2 (b). The coefficient of determination R^2 is only 0.01, indicating that there is no correlation between the corrosion losses in the rapid macrocell and CB tests. Once again, this is largely due to the inability of the rapid macrocell test to distinguish between the corrosion inhibitors based on total corrosion loss. The limited number of data points (four) used in the regression analysis may also contribute to the poor linear relationship between the corrosion losses.

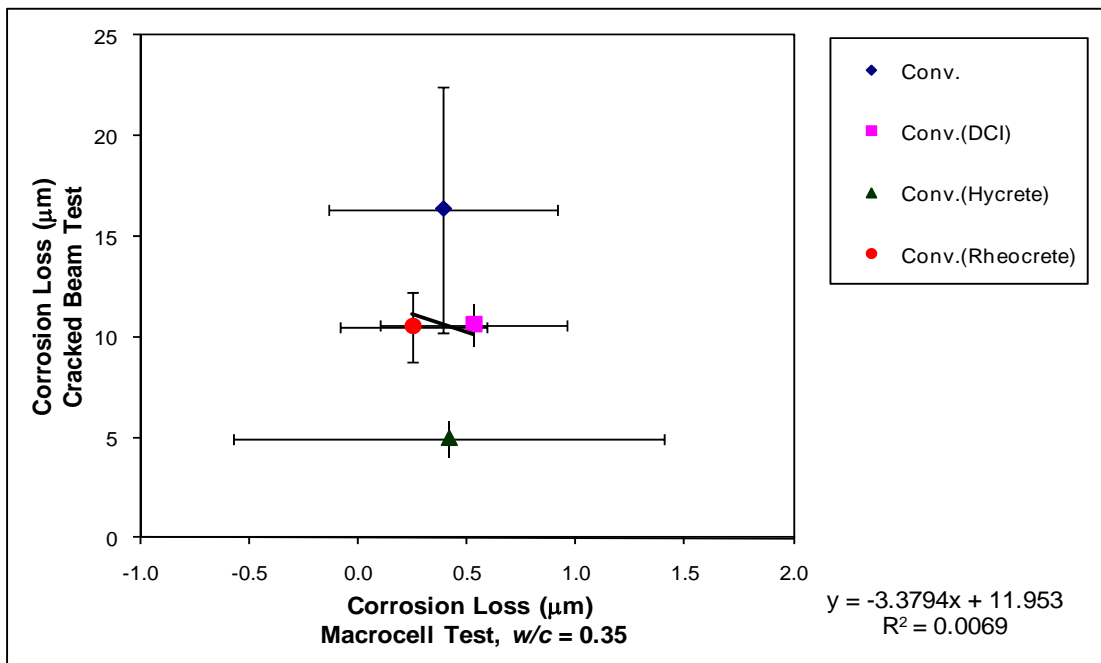
4.2.3 Cracked Beam Test versus Southern Exposure Test

Comparisons of corrosion rates and total corrosion losses between the CB and SE tests are presented in Figures 4.3 (a) and (b), respectively.

As shown in Figure 4.3 (a), the corrosion rates measured in the CB test at 42 weeks had a strong linear relationship to those obtained using the SE test at 42 weeks. The coefficient of determination R^2 is 0.82, indicating that 82% of the total variation in the corrosion rate for one test method can be explained by the variation in

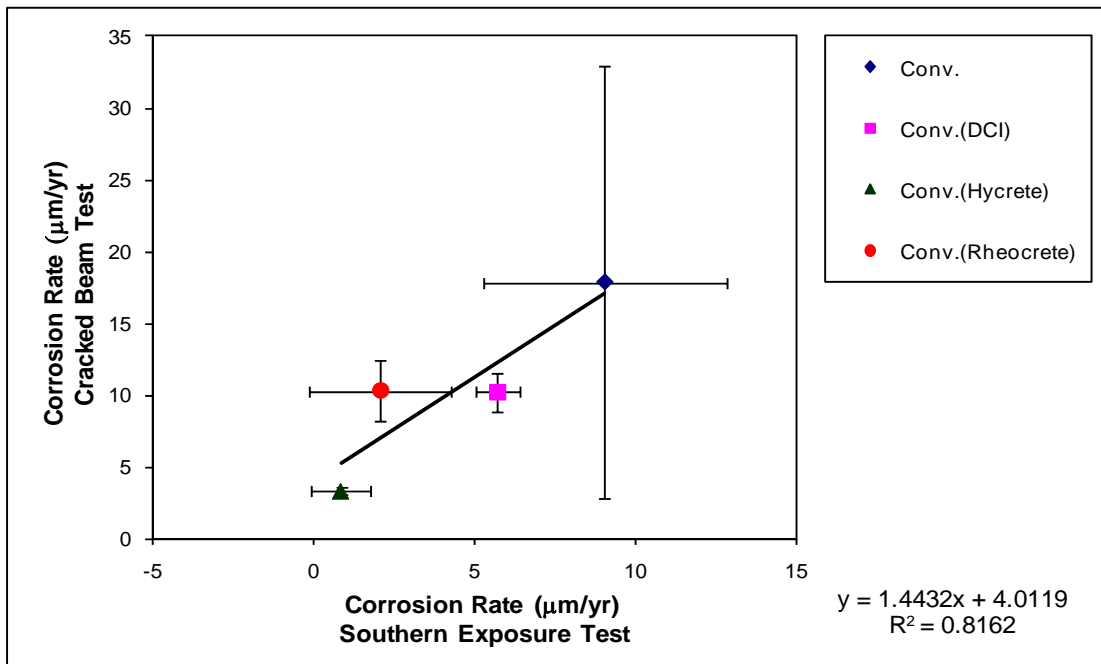


(a)

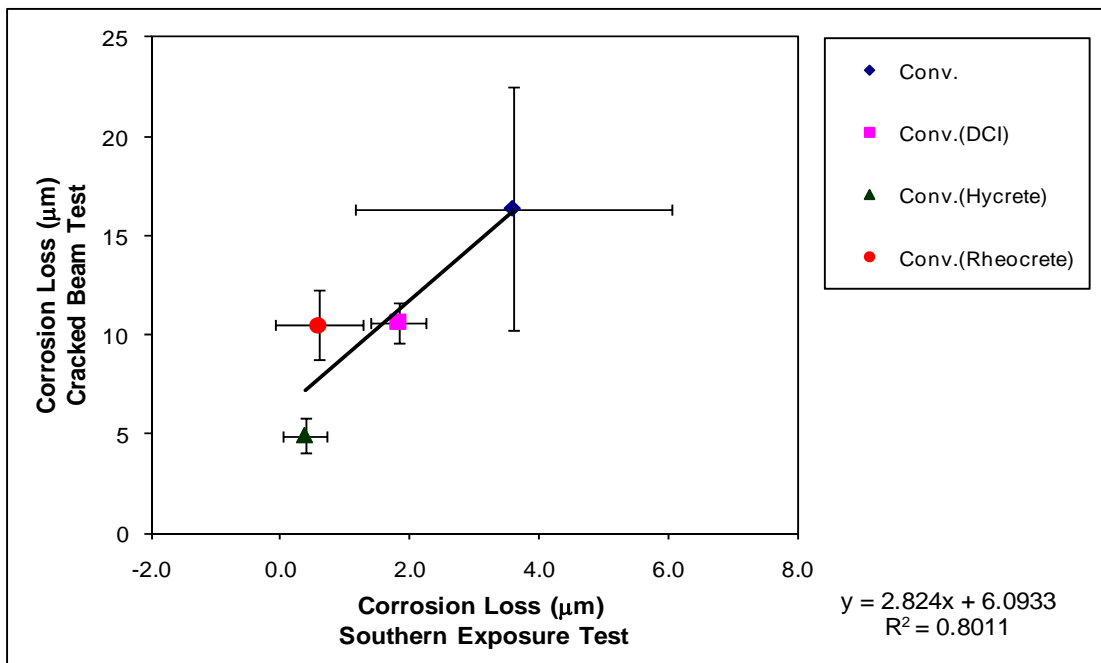


(b)

Figure 4.2 – (a) Comparison of average corrosion rates and (b) corrosion losses for the cracked beam test (at 42 weeks) versus the rapid macrocell test with mortar-wrapped specimens with a w/c ratio of 0.35 (at 15 weeks).



(a)



(b)

Figure 4.3 – (a) Comparison of average corrosion rates and (b) corrosion losses for the cracked beam test (at 42 weeks) versus the Southern Exposure test (at 42 weeks).

corrosion rate for the other. Specimens with conventional steel without inhibitors had the highest corrosion rates, while those with Hycrete exhibited the lowest corrosion rates in both tests.

The comparisons of the corrosion losses between the CB test and the SE test at 42 weeks are shown in Figure 4.3 (b). The corrosion losses in the CB test had a strong linear relationship to those in the SE test. The coefficient of determination R^2 is 0.80. As for the corrosion rates, the specimens with conventional steel and without inhibitors had the highest corrosion losses, while the Hycrete specimens exhibited the lowest corrosion losses in both tests.

The specimens with Rheocrete exhibited corrosion rates and losses that were similar to those of the specimens with DCI in the CB test but lower in the SE test. Overall, the comparisons between the results in the CB and the SE tests exhibited a strong linear relationship.

4.2.4 Summary

The coefficients of determination between test methods for conventional steel without and with different corrosion inhibitors are summarized in Table 4.3. Based on the comparisons, there is a good linear relationship between the results obtained in the rapid macrocell test and those obtained in the SE and CB tests in terms of corrosion rate, with coefficients of determination of 0.93 and 0.62, but no correlation in terms of corrosion loss. This is because the rapid macrocell test did not produce corrosion losses that were distinctly different for the different corrosion protection systems. The comparisons between the SE and the CB test methods show strong linear relationships, with high coefficients of determination, R^2 in terms for both corrosion rate and corrosion loss (0.82 and 0.80, respectively).

Table 4.3 – Coefficients of determination R^2 between results using different test methods for conventional steel in mortar or concrete without and with different inhibitors

Test Method	Macrocell ^c		SE ^d	
	CR ^a	CL ^b	CR ^a	CL ^b
Macrocell ^c	–	–	–	–
SE ^d	0.93	0.07	–	–
CB ^d	0.62	0.01	0.82	0.80

^a CR = Corrosion rate. ^b CR = Corrosion loss.

^c Results are based on rapid macrocell test with a water-cement ratio of 0.35 at 15 weeks.

^d Results are based on the Southern Exposure and cracked beam test at 42 weeks.

4.3 LIFE EXPECTANCY AND COST EFFECTIVENESS

This section covers the economic analysis of bridge decks containing three types of corrosion protection systems, including corrosion inhibitors, alternative forms of reinforcement, and ECR with increased adhesion. The corrosion inhibitor systems include conventional steel or ECR cast in concrete with corrosion inhibitors, DCI, Hycrete, and Rheocrete, along with ECR containing a calcium nitrite primer. The multiple-coated reinforcement (MC) and pickled 2205 stainless steel are compared as alternative reinforcements to conventional steel and ECR. ECR with increased adhesion systems include ECR with a zinc chromate pretreatment before the application of epoxy coating, as well as ECR with the high adhesion epoxy coatings by DuPont and Valspar. Results for systems with conventional steel and ECR are included for comparison. The economic analysis includes comparisons of the life expectancy and cost effectiveness for different corrosion protection systems.

The bridge decks used in the comparisons include (1) a typical monolithic bridge deck with a total deck thickness of 216 mm (8.5 in.) and concrete cover over the top layer of reinforcing steel of 76 mm (3 in.) for all of the systems, and (2) a concrete subdeck with a thickness of 178 mm (7 in.) and silica fume concrete overlay

of 38 mm (1.5 in.) for systems containing conventional steel and ECR.

The estimate of life expectancy is based on the time to first repair and the time between repairs. The time to first repair or “initial repair” is the sum of the time required for corrosion to initiate and the subsequent propagation period required to cause concrete delamination and cracking due to corrosion. This section presents the methods used to determine the time to first repair based on field experience and the laboratory results obtained in this study. The total cost of a new bridge deck and subsequent repair costs over a 75-year service life are compared on a present-cost basis.

4.3.1 Life Expectancy

The life expectancy of bridge decks is based on estimates of the time to first repair and the time between repairs, which are based on both experience in practice and analysis. Based on the experience of the Department of Transportation in South Dakota (SDDOT) (Gilsrud 2007), the time to first repair for bridge decks containing conventional steel is estimated to be 10 years under harsh environmental conditions and 25 years in arid conditions. The 25-year estimate matches that estimated by KDOT (Kepler et al. 2000). For bridge decks containing ECR, the time to first repair is estimated to be 35 years by KDOT and 40 years by SDDOT. The estimates for ECR are based on the fact that bridge decks containing ECR have never required repair due to corrosion-induced damage since the first used in the late 1970s in Kansas and South Dakota (Kepler et al. 2000 and Gilsrud 2007).

Estimates of time to first repair are based on (1) the chloride content that is required for corrosion to initiate on the reinforcing steel, (2) the time required for the amount of chlorides to reach that chloride initiation threshold, and (3) the time

required for corrosion products to cause cracking and spalling of the concrete cover. Time to first repair is the sum of the time to corrosion initiation and the time to cracking.

Time to Corrosion Initiation

The time to corrosion initiation is estimated based on the critical chloride thresholds (water-soluble chloride content) for conventional reinforcing steel obtained in the current study (Section 3.6) and the chloride concentrations measured at crack locations on bridge decks in Kansas (Miller and Darwin 2000, Lindquist, Darwin, and Browning 2005).

Chloride contents were measured at varying depths in reinforced concrete bridge decks at cracks and in uncracked regions. Because surveys for bridge decks with ages ranging from several months to 20 years demonstrate that reinforced concrete bridge decks exhibit significant cracking parallel to and above the reinforcing bars, chloride contents at crack locations are used to estimate the time to corrosion initiation in this study. Figure 4.4 shows the relationship between the average chloride content and time at crack locations at a depth of 76.2 mm (3 in.) for bridges with an average annual daily traffic (AADT) greater than 7500 (high traffic bridges) (Lindquist et al. 2006). The chloride data included in the figure are based on studies by Miller and Darwin (2000) and Lindquist, Darwin, and Browning (2005).

Based on the data shown in Figure 4.4, the chloride concentrations appear to increase linearly with time with a relationship of chloride concentration C versus time T that can be described by the trendline:

$$C = 0.0187 T + 0.4414 \quad (4.1)$$

The average time to reach a specific critical chloride threshold can be expressed as

$$T_c = (C_c - 0.4414) / 0.0187 \quad (4.2)$$

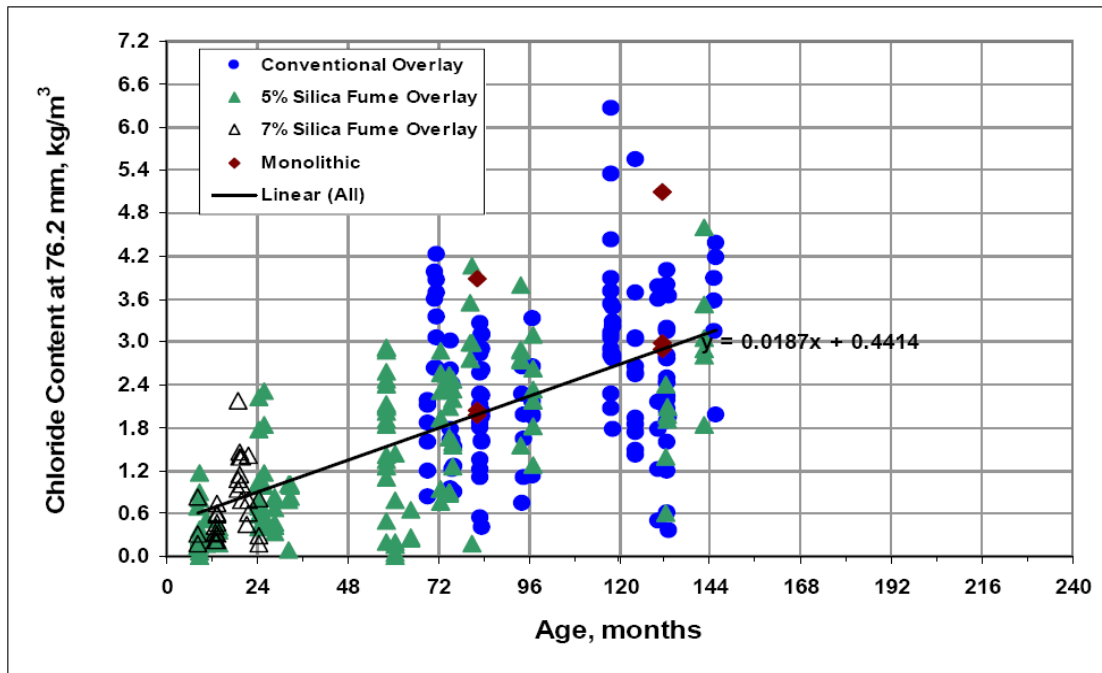


Figure 4.4 – Chloride content taken at cracks interpolated at a depth of 76.2 mm (3 in.) versus placement age for bridges with an AADT greater than 7500.

where

C_c = critical chloride threshold, kg/m^3 , based on water-soluble method; and

T_c = time to reach the critical chloride threshold, months.

For example, the chloride content required for corrosion initiation of conventional steel is 0.96 kg/m^3 (1.62 lb/yd^3 , from Table 3.29). The average time to reach this chloride concentration is $(0.96 - 0.4414) / 0.0187 = 27.7$ months (2.3 years), which is taken as the time to corrosion initiation at crack locations for conventional steel cast in concrete without inhibitors.

The critical chloride thresholds and the times to corrosion initiation for the different corrosion protection systems in the study [calculated using Eq. (4.2)] are listed in Table 4.4. The critical chloride thresholds for conventional steel without and with inhibitors are based on the results from the chloride threshold test described in Section 3.6 and summarized in Table 3.29. Because specimens with conventional

Table 4.4 – Time to corrosion initiation for bridge decks with different corrosion protection systems

Steel Designation ^a	Chloride Corrosion Threshold		Time to Corrosion Initiation
	kg/m ³	lb/yd ³	years
Conv.	0.96	1.63	2.3
ECR	0.96	1.63	2.3
Corrosion Inhibitors			
Conv. (DCI)	1.59	2.69	5.1
Conv. (Hycrete)	0.96	1.63	2.3
Conv. (Rheocrete)	1.23	2.07	3.5
ECR (DCI)	1.59	2.69	5.1
ECR(Hycrete)	0.96	1.63	2.3
ECR(Rheocrete)	1.23	2.07	3.5
Increased Adhesion			
ECR(Chromate)	0.96	1.63	2.3
ECR(DuPont)	0.96	1.63	2.3
ECR(Valspar)	0.96	1.63	2.3
Alternative Reinforcement			
MC	1.52	2.57	4.8

^a Conv. = conventional steel.

ECR = conventional epoxy-coated reinforcement, all epoxy coatings are assumed damaged.

Conv.(DCI) = Conv. with DCI inhibitor in concrete. Conv.(Hycrete) = Conv. with Hycrete inhibitor.

Conv. (Rheocrete) = Conv. with Rheocrete inhibitor.

ECR(DCI) = ECR with DCI inhibitor in concrete. ECR(Hycrete) = ECR with Hycrete inhibitor.

ECR (Rheocrete) = ECR with Rheocrete inhibitor in concrete.

ECR(Chromate) = ECR with Chromate pretreatment.

ECR(DuPont) = ECR with increased adhesion DuPont coating.

ECR(Valspar) = ECR with increased adhesion Valspar coating.

MC = multiple-coated reinforcement.

steel and Hycrete had a lower chloride threshold (0.37 kg/m³ or 0.62 lb/yd³) and a longer time to corrosion initiation (28.5 weeks) than specimens without inhibitors (0.96 kg/m³ or 1.63 lb/yd³ and 14.2 weeks, respectively), Eq. (4.2) is not used to estimate the time to corrosion initiation for bridge decks containing conventional steel and Hycrete. Rather, the same chloride threshold as used for the specimens without inhibitors is used here for steel in cracked concrete containing Hycrete. For ECR with a damaged coating, the same critical chloride threshold is used as for the

corresponding conventional steel, since the underlying conventional steel bars are exposed to similar concrete environments. For ECR with increased adhesion and ECR with a calcium nitrite primer, the same critical chloride thresholds as used for the conventional ECR are used, since the field test results (Figure 3.78) do not demonstrate a distinguishable difference between the times to corrosion initiation for the two cases. For MC steel with a damaged coating, the critical chloride threshold for zinc (1.52 kg/m³ or 2.57 lb/yd³) (see Section 3.6.2) is used since zinc is exposed to the concrete environment after the coating is damaged. For pickled 2205 stainless steel, none of the SE specimens in this study has corroded in the four years of test period, and therefore no critical chloride threshold is available at this point.

The time to first repair is estimated as the sum of the time to corrosion initiation and time to cracking after corrosion has initiated, as shown in Table 4.5. For uncoated steel, corrosion occurs along the length of the reinforcing bar, and a time to cracking is estimated based on an average corrosion loss of 25 μm (Pfeifer 2000). For coated steel, corrosion is limited to regions of damage in the protective epoxy coating, and a time to cracking is estimated using an expression developed by Torres-Acosta and Sagues (2004):

$$x_{crit} = 11 \left(\frac{C}{\phi} \right) \left(\frac{C}{L} + 1 \right)^2 \quad (4.3)$$

where

x_{crit} = corrosion loss in thickness needed to crack concrete cover, μm;

C = concrete cover, mm, $C = 25$ mm (1 in.) for the Southern Exposure specimens;

ϕ = diameter of reinforcing bar, mm, $\phi = 15.875$ mm ($\frac{5}{8}$ in.) for No. 16 (No.5) bars;

Table 4.5 – Time to first repair for bridge decks containing different corrosion protection systems

Steel Designation ^a	Average Corrosion Rate ^b (µm/yr)	Total Corrosion Loss to Crack Concrete (µm)	Corrosion Initiation Time (years)	Time to Cracking after Initiation (years)	Time to First Repair (years)
Conv.	2.96	25	2.3	8.4	11 25*
ECR	2.09	2852	2.3	1365	35* 40* >75
Corrosion Inhibitors					
Conv. (DCI-S)	2.91	25	5.1	8.6	14 25*
Conv. (Hycrete)	0.87	25	2.3	28.7	31
Conv. (Rheocrete)	2.36	25	3.5	10.6	14 25*
ECR (DCI)	2.06	2852	5.1	1384	35* 40* >75
ECR(Hycrete)	0.62	2852	2.3	4600	35* 40* >75
ECR(Rheocrete)	1.67	2852	3.5	1708	35* 40* >75
Increased Adhesion					
ECR(Chromate)					35*
ECR(DuPont)					40*
ECR(Valspar)	2.09	2852	2.3	1365	>75
Alternative Reinforcement					
MC	28.45	2852	4.8	100	35* 40* >75
Pickled 2205 stainless steel	0.04	25	— ^c	625	>75

^a Conv. = conventional steel.

ECR = conventional epoxy-coated reinforcement, all epoxy coatings are assumed damaged.

Conv.(DCI) = Conv. with DCI inhibitor in concrete. Conv.(Hycrete) = Conv. with Hycrete inhibitor.

Conv. (Rheocrete) = Conv. with Rheocrete inhibitor.

ECR(DCI) = ECR with DCI inhibitor in concrete. ECR(Hycrete) = ECR with Hycrete inhibitor.

ECR (Rheocrete) = ECR with Rheocrete inhibitor in concrete.

ECR(Chromate) = ECR with Chromate pretreatment.

ECR(DuPont) = ECR with increased adhesion DuPont coating.

ECR(Valspar) = ECR with increased adhesion Valspar coating.

MC = multiple-coated reinforcement.

^b Half of the average values of the Southern Exposure and Cracked Beam specimens based on corrosion loss slopes.

Values for all epoxy-coated specimens are based on exposed area of four holes.

^c Data is not available due to no Southern Exposure specimen has initiated corrosion by the cutoff date in this study.

* Time to first repair based on estimation by bridge management engineers.

L = length of exposed anodic ring region, where local corrosion occurs on the bar, mm, $L = 3.2$ mm (0.125 in.) for drilled holes in the epoxy coating in this study.

For the ECR bars used in SE specimens, with the epoxy coating damaged by a 3.2-mm (0.125-in.) wide ring, a clear concrete cover of 25 mm (1 in.), and a bar diameter of 16 mm ($\frac{5}{8}$ in.), the calculated critical corrosion loss according to Eq. (4.3) is 1426 μm . For the ECR bars in the field, the local corrosion occurs at specific damaged regions, rather than on a ring-shaped region. The tensile stress produced by the increased volume of the corrosion product from the one hole on one side of an ECR bar [taken here as 3.2 mm (0.125 in.) in diameter] should be at most equal to one-half of that produced by a ring-shaped region with a length equal to the drilled hole diameter of 3.2 mm (0.125 in.). Therefore, the corrosion loss needed to crack the concrete cover of SE specimens with ECR bars is estimated to be 2852 μm , which is twice the value of the corrosion loss calculated using Eq. (4.3) based on a ring-shaped region. Although this value is based on a cover of 25 mm (1 in.), it will be used as to conservatively estimate the corrosion losses needed to crack concrete on a bridge deck.

The time needed to reach a specific corrosion loss is calculated based on the corrosion rate after initiation. The rate used, half of the average corrosion rate of the SE and CB specimens, is selected because it matches the time to first cracking for conventional steel in bridge decks in Kansas. For ECR bars, the corrosion rates are based on exposed area.

The corrosion rates used to calculate time to cracking are determined from the corrosion loss graphs rather than directly from corrosion rate plots. As shown in the corrosion rate and loss figures in Chapter 3, corrosion rates vary from week to week,

but these values average out, producing corrosion losses with similar rates of increase for the specimens in the same system. The corrosion rate used to determine a time to cracking for each system is taken as the average slope of the corrosion loss plots for all specimens over the period in which the rate of corrosion loss is stable. This period is not the same for all specimens.

For conventional steel and ECR without inhibitors, specimens from previous tests are included in the calculation, including specimens with conventional steel N and N3 from Ji et al. (2005) at 96 weeks and specimens with conventional steel N4 and ECR from Darwin et al. (2007) at 96 weeks. For conventional steel with inhibitors, corrosion rates obtained from the SE and CB tests in this study are not directly used to represent that system, but rather to calculate ratios of corrosion rates of systems without corrosion inhibitors to corrosion rates of systems with corrosion inhibitors, as will be described in the following paragraphs. This approach is taken because the short exposure age (42 weeks), the small number of specimen samples (three for each system), and variations in concrete and conventional steel (N5) properties result in considerable differences among specimens in a single system. Corrosion rates for specimens with ECR and different corrosion inhibitors are also calculated based on these ratios. For MC steel, specimens from Darwin et al. (2007) at 96 weeks are used in the calculation of the corrosion rate, based on the average of the values for specimens with both layers penetrated and only the epoxy layer penetrated. Because zinc corrodes sacrificially to protect the underlying steel when both steel and zinc are exposed, the calculated corrosion rate for the MC bars with both layers penetrated represents the corrosion rate of a mixture of zinc and steel rather than steel alone.

For pickled 2205 stainless steel, the corrosion rate is obtained from the SE and

the only two corroded CB specimens (CE-DCB-2205p-2 and CE-DCB-2205p-4). Because the SE specimens showed only negative corrosion, a value of zero was chosen to represent their contribution.

For bridge decks containing conventional steel, the corrosion rate is calculated as

$$[(3.64 + 8.21) / 2] / 2 = 2.96 \mu\text{m/yr}$$

(3.64 $\mu\text{m/yr}$ for the SE and 8.21 $\mu\text{m/yr}$ for the CB specimens). For bridge decks containing ECR, the corrosion rate based on exposed area is

$$[(1.55 + 6.82) / 2] / 2 = 2.09 \mu\text{m/yr}$$

(1.55 $\mu\text{m/yr}$ for the SE and 6.82 $\mu\text{m/yr}$ for the CB specimens).

For SE specimens with conventional steel, the corrosion rate for specimens without inhibitors is 4.23 $\mu\text{m/yr}$, while corrosion rates for specimens with DCI, Hycrete, and Rheocrete are 4.15, 1.24, and 3.37 $\mu\text{m/yr}$, respectively, giving ratios for specimens with DCI, Hycrete, and Rheocrete of

$$4.15 / 4.23 = 0.98,$$

$$1.24 / 4.23 = 0.29, \text{ and}$$

$$3.37 / 4.23 = 0.80,$$

respectively. Therefore, corrosion rates for bridge decks containing conventional steel and the inhibitors DCI, Hycrete, and Rheocrete are expected to be

$$2.96 \times 0.98 = 2.91 \mu\text{m/yr},$$

$$2.96 \times 0.29 = 0.87 \mu\text{m/yr}, \text{ and}$$

$$2.96 \times 0.80 = 2.36 \mu\text{m/yr},$$

respectively. Corrosion rates based on exposed area for bridge decks containing ECR and the inhibitors DCI, Hycrete, and Rheocrete are estimated as

$$2.09 \times 0.98 = 2.06 \mu\text{m/yr},$$

$$2.09 \times 0.29 = 0.62 \text{ } \mu\text{m/yr, and}$$

$$2.09 \times 0.80 = 1.67 \text{ } \mu\text{m/yr,}$$

respectively.

For bridge decks containing MC steel, the corrosion rate based on exposed area is

$$[(19.91 + 93.90) / 2] / 2 = 28.45 \text{ } \mu\text{m/yr}$$

(19.91 $\mu\text{m/yr}$ for the SE specimens and 93.90 $\mu\text{m/yr}$ for the CB specimens based on averages in each case for specimens with both layers penetrated and specimens with only the epoxy layer penetrated).

For bridge decks containing pickled 2205 stainless steel, the corrosion rate is calculated as

$$[(0 + 0.17) / 2] / 2 = 0.04 \text{ } \mu\text{m/yr}$$

(SE specimens remained passive and 0.17 $\mu\text{m/yr}$ for the CB specimens).

The corrosion rates used to calculate time to first repair for the different corrosion protection systems are summarized in Table 4.5.

Using the calculated corrosion rates shown in Table 4.5 and a required corrosion loss of 25 μm for uncoated steel and 2852 μm for coated steel, the time from corrosion initiation to first repair is calculated as follows:

Conventional steel	$25 / 2.96 = 8.4$ years
ECR	$2852 / 2.09 = 1365$ years > 75 years
Conventional steel with DCI	$25 / 2.91 = 8.6$ years
Conventional steel with Hycrete	$25 / 0.87 = 28.7$ years
Conventional steel with Rheocrete	$25 / 2.36 = 10.6$ years
Multiple-coated steel	$2852 / 28.45 = 100$ years > 75 years
Pickled 2205 stainless steel	$25 / 0.04 = 625$ years > 75 years

Because bridge decks containing ECR with corrosion inhibitors have lower corrosion rates than bridge decks containing ECR without inhibitors and they will also not require repair during a 75-year service life based on the corrosion losses needed to crack concrete. Bridge decks containing ECR with increased adhesion are treated as having the same time to first repair as bridge decks containing ECR and do not require repair during a 75-year service life, again based on the corrosion losses needed to crack concrete.

Time to First Repair

The time to first repair is estimated by adding the time to corrosion initiation and time to cracking after initiation. For bridge decks containing conventional steel without inhibitors, the time to corrosion initiation is 2.3 years, and the time to cracking after initiation is 8.4 years. Therefore, the time to first repair is

$$\text{Conventional steel} \quad 2.3 + 8.4 = 10.7 \text{ years}$$

which is rounded to 11 years. Similarly, the times to first repair for conventional steel with corrosion inhibitors are

$$\text{Conventional steel with DCI} \quad 5.1 + 8.6 = 13.7 \text{ years (14 years)}$$

$$\text{Conventional steel with Hycrete} \quad 2.3 + 28.7 = 31.0 \text{ years (31 years)}$$

$$\text{Conventional steel with Rheocrete} \quad 3.5 + 10.6 = 14.1 \text{ years (14 years)}$$

As mentioned before, the time to first repair for bridge decks containing conventional steel is estimated by SDDOT and KDOT to be between 10 and 25 years based on the experience. In this study, the recommended time to first repair for bridge decks containing conventional steel based on analysis of the laboratory results (11 years) is within the range estimated by bridge maintenance engineers (10 to 25 years). For bridge decks containing ECR and pickled 2205 stainless steel, the calculated time to first repair is beyond the 75-year service life. However, adhesion loss between the

epoxy and the steel may reduce the time to first repair of ECR (Sagues et al. 1994, *Adhesion* 1995). Based on test results of field specimens, ECR with increased adhesion provided no advantage in corrosion resistance with respect to conventional ECR. To account for the potential effect of adhesion loss, 35 and 40 years as times to first repair for bridges decks containing ECR are considered in the economic analysis based on recommendations by KDOT and SDDOT, respectively. The time to first repair for bridge decks with different corrosion protection systems tested in this study are summarized in Table 4.5.

4.3.2 Cost Effectiveness

The cost effectiveness of conventional steel, ECR, and pickled 2205 stainless steel are compared over a 75-year service cycle. Two types of bridge decks are included in the cost analysis, a 216-mm (8.5-in.) thick concrete bridge deck for all the systems and a 178-mm (7-in.) thick subdeck with a 38-mm (1.5-in.) silica fume concrete overlay for systems containing conventional steel and ECR. Cost estimates include new construction costs and the subsequent repair costs at 25-year cycles over a 75-year service life. For bridge decks containing conventional steel, the times to first repair are based on the times calculated from the test results, 11 years, and the recommendations from KDOT and SDDOT, 10 and 25 years. For bridge decks containing epoxy-coated steel, the time to first repair are based on estimates of 35 and 40 years by KDOT and SDDOT and 75 years from analysis. In all cases where repair is needed, additional repairs based on 25-year cycles are used in the analysis for the 75-year service life.

New Bridge Deck Costs

Current costs for new bridge decks are calculated considering the in-place costs

of concrete, silica fume overlays, the various types of reinforcing steel, and the corrosion inhibitors. Based on the average bid costs on ten KDOT bridge projects for the years 2004 through 2007 (<http://www.ksdot.org>) and the price changes in July 2008 (Engineering News Record, 2008), the in-place cost of the concrete is \$735.74/m³ (562.51/yd³), and the in-place cost of the silica fume overlay is \$44.49/m² (37.20/yd²) for a thickness of 38 mm (1.5 in.).

For some steels, such as MC and stainless steel, there are no bid costs to estimate the placement costs. To account for the missing cost information, the in-place costs of these steels are estimated considering the base cost at the mill and the placement cost, including fabrication, delivery, and placement on the bridge decks. For conventional steel, the base cost is \$0.93/kg (\$0.42/lb) based on a 20-city average price in July 2008 (Engineering News Record, 2008), and the total cost is \$2.08/kg (\$0.94/lb) based on average bid costs of KDOT bridge projects and the associated price change. The placement cost, \$1.16/kg (\$0.52/lb), is the difference between these two values. For ECR, the base cost is \$1.28/kg (\$0.58/lb) and the total cost is \$2.25/kg (\$1.02/lb), giving a placement cost of \$0.97/kg (\$0.44/lb). Here, the calculated placement cost for conventional steel is higher than ECR, mainly because a much smaller quantity of conventional steel is used in the bridge projects used in this study and therefore the sample size contains bias.

For ECR with increased adhesion, the same price as used for conventional ECR is used, with a total in-place cost of \$2.25/kg (\$1.02/lb) for all three types of increased adhesion ECR.

For MC bars, a base cost of \$1.87/kg (\$0.85/lb) is used based on the manufacturer's price in 2008. The placement cost of conventional steel, \$1.16/kg (\$0.52/lb), is used for MC steel. This gives a total in-place cost of \$3.02/kg (\$1.37/lb)

for MC steel.

For pickled 2205 stainless steel, a base cost of \$5.19/kg (\$2.35/lb) is used based on the analysis by Balma et al. (2005). The same placement cost of \$1.16/kg (\$0.52/lb) as conventional steel is used for pickled 2205 stainless steel. This gives a total in-place cost of \$6.34/kg (\$2.88/lb) for pickled 2205 stainless steel.

The costs of corrosion inhibitors provided by the manufacturers are used in the analysis: \$2.11/L (\$8.00/gal) for DCI-S, \$4.95/L (\$18.75/gal) for Hycrete, and \$6.08/L (\$23.00/gal) for Rheocrete 222+. The dosage rates of 15 L/m³ (3 gal/yd³) for DCI-S, 7.5 L/m³ (1.5 gal/yd³) for Hycrete, and 5 L/m³ (1 gal/yd³) for Rheocrete, respectively, are used in the analysis. For bridge decks containing Hycrete, 35.6 kg/m³ (60 lb/yd³) extra Type I/II portland cement is included in the cost to compensate for the strength loss caused by the Hycrete inhibitor. A price of \$0.13/kg (\$0.06/lb) for Type I/II portland cement is provided by a local ready-mix plant.

The construction costs for new bridge decks are summarized in Table 4.6. Based on average bids for 12 monolithic KDOT bridge decks constructed during the four-year period 2004 through 2007, an average density of reinforcing steel of 163 kg/m³ (275 lb/yd³) is used in the calculations. All costs are expressed in dollars per square meter and are calculated as follows:

$$\text{216-mm concrete deck} \quad \frac{\$735.74}{\text{m}^3} \times \frac{0.216 \text{ m}^3}{\text{m}^2} = \$158.92 / \text{m}^2$$

178-mm concrete subdeck + 38-mm silica fume overlay

$$\begin{aligned} & \frac{\$735.74}{\text{m}^3} \times \frac{0.178 \text{ m}^3}{\text{m}^2} + \$44.49 / \text{m}^2 \\ & = \$130.96 / \text{m}^2 + \$44.49 / \text{m}^2 = \$175.45 / \text{m}^2 \end{aligned}$$

$$\text{Conventional steel} \quad \frac{\$2.08}{\text{kg}} \times \frac{163 \text{ kg}}{\text{m}^3} \times \frac{0.216 \text{ m}^3}{\text{m}^2} = \$73.23 / \text{m}^2$$

Table 4.6 – In-place cost for different construction items in new bridge decks

Items	In-place Cost		Cost per Area ^a	
	SI Unit	Inch-Pound Unit	\$/m ²	\$/yd ²
216-mm (8.5-in.) concrete deck	\$735.74/m ³	\$562.51/yd ³	158.92	132.82
178-mm (7-in.) concrete subdeck	\$735.74/m ³	\$562.51/yd ³	130.96	109.38
38-mm (1.5-in.) silica fume overlay (SFO)	\$44.49/m ²	\$37.20/yd ²	44.49	37.20
Conventional steel	\$2.08/kg	\$0.94/lb	73.23	61.03
Epoxy-coated reinforcement	\$2.25/kg	\$1.02/lb	79.22	66.23
DCI-S	\$2.11/L	\$8.00/gal	6.84	5.67
Hycrete	\$4.95/L	\$18.75/gal	8.02	6.64
Cement	\$0.13/kg	\$0.06/lb	1.00	0.85
Rheocrete	\$6.08/L	\$23.00/gal	6.57	5.43
Three types of ECR with increased adhesion	\$2.25/kg	\$1.02/lb	79.22	66.23
Multiple-coated reinforcement	\$3.02/kg	\$1.37/lb	106.33	88.95
Pickled 2205 stainless steel	\$6.34/kg	\$2.88/lb	223.22	187.00

^a The costs per area for reinforcements are based on an average amount of reinforcing steel of 163 kg/m³ (275 lb/yd³). The costs per area for corrosion inhibitors are based on the dosage rates of 15 L/m³ (3 gal/yd³) for DCI-S, 7.5 L/m³ (1.5 gal/yd³) for Hycrete, and 5 L/m³ (1 gal/yd³) for Rheocrete. 35.60 kg/m³ (60 lb/yd³) extra type I/II cement is considered to add to concrete mixes to compensate the loss in strength for concrete containing Hycrete inhibitor.

$$\text{Epoxy-coated steel} \quad \frac{\$2.25}{\text{kg}} \times \frac{163 \text{ kg}}{\text{m}^3} \times \frac{0.216 \text{ m}^3}{\text{m}^2} = \$79.22 / \text{m}^2$$

$$\text{Corrosion inhibitor DCI-S} \quad \frac{\$2.11}{\text{L}} \times \frac{15 \text{ L}}{\text{m}^3} \times \frac{0.216 \text{ m}^3}{\text{m}^2} = \$6.84 / \text{m}^2$$

$$\begin{aligned} \text{Corrosion inhibitor Hycrete} + 35.60 \text{ kg/m}^3 \text{ (60 lb/yd}^3\text{) Type I/II cement} \\ \frac{\$4.95}{\text{L}} \times \frac{7.5 \text{ L}}{\text{m}^3} \times \frac{0.216 \text{ m}^3}{\text{m}^2} + \frac{\$0.13}{\text{kg}} \times \frac{35.6 \text{ kg}}{\text{m}^3} \times \frac{0.216 \text{ m}^3}{\text{m}^2} \\ = \$8.02 / \text{m}^2 + \$1.00 / \text{m}^2 = \$9.02 / \text{m}^2 \end{aligned}$$

$$\text{Corrosion inhibitor Rheocrete} \quad \frac{\$6.08}{\text{L}} \times \frac{5 \text{ L}}{\text{m}^3} \times \frac{0.216 \text{ m}^3}{\text{m}^2} = \$6.57 / \text{m}^2$$

Three types of ECR with increased adhesion

$$\frac{\$2.25}{\text{kg}} \times \frac{163 \text{ kg}}{\text{m}^3} \times \frac{0.216 \text{ m}^3}{\text{m}^2} = \$79.22 / \text{m}^2$$

$$\text{Multiple-coated reinforcement} \quad \frac{\$3.02}{\text{kg}} \times \frac{163 \text{ kg}}{\text{m}^3} \times \frac{0.216 \text{ m}^3}{\text{m}^2} = \$106.33 / \text{m}^2$$

$$\text{Pickled 2205 stainless steel} \quad \frac{\$6.34}{\text{kg}} \times \frac{163 \text{ kg}}{\text{m}^3} \times \frac{0.216 \text{ m}^3}{\text{m}^2} = \$223.22/\text{m}^2$$

Repair Costs

Repair costs for bridge decks are based on information provided by SDDOT (Gilsrud 2007) and the analysis by Darwin et al. (2007). A typical bridge deck used for analysis has a depth of 216 mm (8.5 in.), a width of 11 m (36 ft), and a total length of 46 m (150 ft). Bridge deck repair projects typically include removing deteriorated concrete and replacing it with a low-slump dense concrete overlay, bridge rail modification, replacement of approach guard rails, approach pavement work, mobilization, traffic control, and other miscellaneous work. Bridge decks reinforced with ECR built since the late 1970s have not required repairs to date, and therefore the repair costs are estimated based on values for decks with conventional steel. This is adequate because the repair costs for bridge decks with ECR should be similar to those of bridge decks with conventional steel based on the construction items typically involved in the repair. A total repair cost of \$349/m² (\$292/yard²) is used for the corrosion protection systems in this study based on the analysis by Darwin et al. (2007). For a 75-year service life of bridge decks, 25-year repair cycles are used for all the systems that require repair.

Cost Effectiveness

Comparisons of the cost effectiveness for bridge decks containing different corrosion protection systems are based on the present value of the costs using discount rates of 2, 4, and 6%. The present values of the repair costs are calculated as:

$$P = F \times (1+i)^{-n} \quad (4.4)$$

where P = present worth, F = cost of repair, i = discount rate (%), 2, 4, and 6% are used in this study, and n = time to repair (in years).

For example, for monolithic bridge decks with a thickness of 216 mm (8.5 in.),

the present cost based on a discount rate of 2% for bridge decks containing conventional steel in a harsh environment over a 75-year service life can be calculated as follows:

$$\begin{aligned}
 \text{Present cost} &= \text{Initial cost of deck} + \text{Repair cost} \times (1+i)^{-n} \\
 &= \frac{\$158.92}{\text{m}^2} + \frac{\$73.23}{\text{m}^2} + \frac{\$349}{\text{m}^2} \times [(1+2\%)^{-11} + (1+2\%)^{-36} + (1+2\%)^{-61}] \\
 &= \$232.15/\text{m}^2 + \$556.06/\text{m}^2 \\
 &= \$788/\text{m}^2
 \end{aligned}$$

The life cycle costs for bridge decks containing different corrosion protection systems are summarized in Table 4.7a for monolithic decks and Table 4.7b for silica fume decks.

As shown in Table 4.7a, based on new bridge deck costs for a 216-mm (8.5-in.) thick monolithic bridge deck, a bridge deck containing conventional steel has the lowest new deck cost of \$232.15/m², followed by bridge decks containing ECR and ECR with increased adhesion epoxy at \$238.14/m². The new bridge costs for conventional steel with corrosion inhibitor Rheocrete, DCI-S, and Hycrete are \$238.72/m², \$238.99/m², and \$241.17/m², respectively. Decks containing pickled 2205 stainless steel have the highest new deck cost at \$382.14/m², followed by the cost of bridge decks containing MC steel at \$265.25/m². The use of a silica fume overlay increases the total bridge costs by \$16.53/m² for all systems.

Based on present values, the life cycle costs decrease significantly as the discount rate increases from 2%, to 4%, and 6%. Based on cracking analysis, no repairs are needed during a service life of 75 years for bridge decks containing ECR. At a discount rate of 2%, the lowest cost option is a 216-mm (8.5-in.) thick monolithic bridge deck containing ECR or ECR with increased adhesion with a

Table 4.7a – Economic analysis for bridge decks containing different corrosion protection systems - monolithic decks

Option	Type of deck	Type of steel	Type of corrosion inhibitor	Cost of deck	Cost of steel	Cost of inhibitor	Initial cost	Time to repair 1	Cost of repair 1	Time to repair 2	Cost of repair 2	Time to repair 3	Cost of repair 2	Present cost		
				(\$ /m ²)	(\$ /m ²)	(\$ /m ²)		(\$ /m ²)	(years)	(\$ /m ²)	(years)	(\$ /m ²)	(years)	(\$ /m ²)	<i>i</i> = 2%	<i>i</i> = 4%
1	216-mm	Conv.	-	158.92	73.23	-	232.15	11	349	36	349	61	349	788	576	469
2								25	349	50	349	-		575	412	332
3	216-mm	ECR	-	158.92	79.22	-	238.14	35	349	60	349	-		519	360	294
4								40	349	65	349	-		493	338	280
5								>75	349	-			238	238	238	
6	216-mm	Conv.	DCI-S	158.92	73.23	6.84	238.99	14	349	39	349	64	349	763	544	438
7								25	349	50	349	-		581	419	339
8	216-mm	Conv.	Hycrete	158.92	73.23	9.02	241.17	31	349	56	349	-		545	383	312
9	216-mm	Conv.	Rheocrete	158.92	73.23	6.57	238.72	14	349	39	349	64	349	763	544	437
10								25	349	50	349	-		581	419	339
11	216-mm	ECR	DCI-S	158.92	79.22	6.84	244.98	35	349	60	349	-		526	367	301
12								40	349	65	349	-		499	345	287
13								>75	349	-			245	245	245	
14	216-mm	ECR	Hycrete	158.92	79.22	9.02	247.16	35	349	60	349	-		528	369	303
15								40	349	65	349	-		502	347	289
16								>75	349	-			247	247	247	
17	216-mm	ECR	Rheocrete	158.92	79.22	6.57	244.71	35	349	60	349	-		526	366	301
18								40	349	65	349	-		499	345	287
19								>75	349	-			245	245	245	
20	216-mm	ECR(Chromate)	-	158.92	79.22	-	238.14	35	349	60	349	-		519	360	294
21		ECR(DuPont)						40	349	65	349	-		493	338	280
22		ECR(Valspar)						>75	349	-			238	238	238	
23	216-mm	MC	-	158.92	106.33	-	265.25	35	349	60	349	-		546	387	321
24								40	349	65	349	-		520	365	307
25								>75	349	-			265	265	265	
26	216-mm	2205p	-	158.92	223.22	-	382.14	>75	349	-				382	382	382

Table 4.7b – Economic analysis for bridge decks containing different corrosion protection systems - silica fume overlay decks

Option	Type of deck	Type of steel	Type of corrosion inhibitor	Cost of deck	Cost of steel	Cost of inhibitor	Initial cost	Time to repair 1	Cost of repair 1	Time to repair 2	Cost of repair 2	Time to repair 3	Cost of repair 2	Present cost		
				(\$ /m ²)	(\$ /m ²)	(\$ /m ²)		(\$ /m ²)	(years)	(\$ /m ²)	(years)	(\$ /m ²)	(years)	(\$ /m ²)	<i>i</i> = 2%	<i>i</i> = 4%
27	178-mm + 38-mm SFO	Conv.	-	175.45	73.23	-	248.68	11	349	36	349	61	349	805	592	485
28								25	349	50	349	-		591	429	349
29	178-mm + 38-mm SFO	ECR	-	175.45	79.22	-	254.67	35	349	60	349	-		536	376	311
30								40	349	65	349	-		509	355	297
31								>75	349	-			255	255	255	
32	178-mm + 38-mm SFO	Conv.	DCI-S	175.45	73.23	6.84	255.52	14	349	39	349	64	349	780	561	454
33								25	349	50	349	-		598	436	356
34	178-mm + 38-	Conv.	Hycrete	175.45	73.23	9.02	257.70	31	349	56	349	-		562	400	328
35	178-mm + 38-mm SFO	Conv.	Rheocrete	175.45	73.23	6.57	255.25	14	349	39	349	64	349	779	561	454
36								25	349	50	349	-		598	435	356
37	178-mm + 38-mm SFO	ECR	DCI-S	175.45	79.22	6.84	261.51	35	349	60	349	-		542	383	317
38								40	349	65	349	-		516	361	303
39								>75	349	-			262	262	262	
40	178-mm + 38-mm SFO	ECR	Hycrete	175.45	79.22	9.02	263.69	35	349	60	349	-		545	385	320
41								40	349	65	349	-		518	364	306
42								>75	349	-			264	264	264	
43	178-mm + 38-mm SFO	ECR	Rheocrete	175.45	79.22	6.57	261.24	35	349	60	349	-		542	383	317
44								40	349	65	349	-		516	361	303
45								>75	349	-			261	261	261	
46	178-mm + 38-mm SFO	ECR(Chromate)	-	175.45	79.22	-	254.67	35	349	60	349	-		536	376	376
47		ECR(DuPont)						40	349	65	349	-		509	355	355
48		ECR(Valspar)						>75	349	-			255	255	255	
49	178-mm + 38-mm SFO	MC	-	175.45	106.33	-	281.78	35	349	60	349	-		563	403	338
50								40	349	65	349	-		536	382	324
51								>75	349	-			282	282	282	

present cost of \$238/m², followed by a 216-mm (8.5-in.) thick deck containing ECR and DCI-S or Rheocrete with a present cost of \$245/m², and Hycrete with \$247/m² for a service life of 75 years for bridge decks without repairs. At discount rates of 4% and 6%, the lowest cost options are the same as those at the discount rate of 2%.

Based on the experience of SDDOT and KDOT, repairs are needed during a service life of 75-years for bridge decks containing ECR. At a discount rate of 2%, the lowest cost option is a 216-mm (8.5-in.) thick deck containing pickled 2205 stainless steel with a present cost of \$382/m², followed by a 216-mm (8.5-in.) thick deck containing ECR or ECR with increased adhesion with the first repair at 40 years (\$493/m²). When a corrosion inhibitor is used, the costs for a 216-mm (8.5-in.) bridge deck containing ECR and DCI-S, Rheocrete, or Hycrete are \$499/m², \$499/m², and \$502/m², respectively, when the first repair occurs at 40 years. At a discount rate of 4%, the lowest cost option is a 216-mm (8.5-in.) deck containing ECR and ECR with increased adhesion with the first repair at 40 years (\$338/m²), followed by a 216-mm (8.5-in.) deck containing ECR and DCI-S or Rheocrete with a cost of \$345/m², and ECR with Hycrete with a cost of \$347/m². At a discount rate of 6%, the lowest cost options are the same as those at a discount rate of 4%.

The lowest cost options for a 178-mm (7-in.) concrete bridge deck with a 38-mm (1.5-in.) silica fume overlay are the same as those for a 216-mm (8.5-in.) thick monolithic concrete deck, plus \$16.53/m² for all systems for all discount rates.

In summary, for the economic analysis of different corrosion protection systems, based on cracking analysis, the lowest cost option is a 216-mm (8.5-in.) thick monolithic bridge deck containing ECR or ECR with increased adhesion with a present cost of \$238/m² for discount rates of 2%, 4%, and 6%,

Based on the experience of the SDDOT and KDOT, the lowest cost option is a

216-mm (8.5-in.) thick deck containing pickled 2205 stainless steel with a present cost of \$382/m² at a discount rate of 2%. For discount rates of 4% and 6%, the lowest cost option is a 216-mm (8.5-in.) deck containing ECR or ECR with increased adhesion with the first repair at 40 years (\$338/m² and \$280/m², respectively). Considering all cases, the use of ECR or ECR with increased adhesion is the most cost-effective option at a discount rate of 2%. The use of the silica fume overlay increases the total bridge costs by \$16.53/m² for all systems.

CHAPTER 5

CONCLUSIONS AND RECOMMENDATIONS

5.1 SUMMARY

The corrosion performance of different corrosion protection systems for conventional reinforcing steel, epoxy-coated reinforcement, and pickled 2205 stainless steel in Kansas bridge decks is evaluated. The corrosion protection systems involved in this study include:

- Conventional reinforcing steel with or without one of the three corrosion inhibitors, DCI-S, Rheocrete 222+, or Hycrete DSS,
- Conventional epoxy-coated reinforcement (ECR) with or without DCI-S, Rheocrete 222+, or Hycrete DSS, and ECR with a primer coating containing microencapsulated calcium nitrite [$\text{Ca}(\text{NO}_2)_2$],
- Multiple-coated reinforcement with a zinc layer underlying DuPont 8-2739 epoxy coating,
- ECR with a zinc chromate pretreatment before the application of a epoxy coating to improve the adhesion, and ECR with improved adhesion epoxy coatings produced by DuPont and Valspar,
- Pickled 2205 duplex stainless steel,
- Zinc-coated (galvanized) reinforcement without chromate treatment, and
- Concrete with conventional steel and water-cement ratios of 0.45 or 0.35.

Rapid macrocell tests of mortar-wrapped specimens were used to evaluate the corrosion performance of conventional steel with the three different corrosion inhibitors in a 1.6-molal ion concentration of NaCl and simulated concrete pore solution. Three bench-scale tests, including the Southern Exposure (SE), cracked

beam (CB), and ASTM G109 tests, were used to test the conventional, epoxy-coated, and multiple-coated reinforcement in the laboratory. Specimens without and with simulated cracks in the concrete were placed in the field to measure the performance of multiple corrosion protection systems under realistic exposure conditions. The performance of pickled 2205 stainless steel in two bridge decks of the Kansas Department of Transportation (KDOT) was evaluated based on corrosion potential maps obtained in bi-annual bridge surveys on the decks. Specimens cast with the same concrete mix were also evaluated using the SE, CB, and field tests. Comparisons between the rapid macrocell and the SE and CB tests, and between the SE and CB tests were performed to investigate the relationship between the performance of the corrosion protection systems in those test methods.

The critical chloride thresholds were evaluated for beam specimens containing conventional steel and different corrosion inhibitors and zinc-coated reinforcement based on water-soluble chloride. The results were compared with the corresponding thresholds for MMFX microcomposite steel. The time to corrosion initiation in bridge decks was estimated based on critical chloride thresholds for the different corrosion protection systems.

Linear polarization resistance tests were performed on bench-scale and field test specimens to measure total corrosion for the systems. Microcell and macrocell corrosion rates and losses were compared to investigate their relationship for the different corrosion protection systems.

The results obtained from the laboratory tests in this study were used in conjunction with KDOT and South Dakota Department of Transportation (SDDOT) experience to estimate the cost effectiveness of the different corrosion protection systems in bridge decks over a 75-year life cycle at discount rates of 2, 4, and 6%.

5.2 CONCLUSIONS

The following conclusions are based on the results and analyses presented in this report.

1. Of the systems tested, conventional steel has the lowest corrosion resistance. In concrete (bench-scale and field tests), the corrosion loss for epoxy-coated reinforcement is less than 2% of the corrosion loss for conventional steel based on the total surface area. Based on the exposed region in the damaged epoxy coating, the corrosion rate and corrosion loss for the epoxy-coated reinforcement are comparable to those of the conventional steel.
2. The use of a reduced water-cement ratio in concrete significantly improves the corrosion performance of conventional steel in uncracked concrete when compared to concrete with a higher water-cement ratio.
3. The use of a corrosion inhibitor improves the corrosion resistance of conventional steel in both cracked and uncracked concrete, and delays the onset of corrosion in uncracked concrete.
4. The average chloride threshold for conventional steel, on a water-soluble basis, is 1.59 kg/m^3 (2.69 lb/yd^3) for concrete containing DCI, 0.37 kg/m^3 (0.62 lb/yd^3) for concrete containing Hycrete, and 1.23 kg/m^3 (2.07 lb/yd^3) for concrete containing Rheocrete, compared to the average chloride threshold of 0.96 kg/m^3 (1.63 lb/yd^3) for conventional steel in concrete without inhibitors. Concrete with Hycrete exhibits a lower chloride threshold but a longer time to corrosion initiation than concrete containing DCI-S, or Rheocrete, or without inhibitors.
5. For concrete containing conventional steel, specimens with Hycrete perform better than specimens with DCI-S or Rheocrete in both uncracked and cracked

- concrete. Specimens with Rheocrete perform better than those with DCI-S in uncracked concrete but perform in a similar manner when cast in cracked concrete.
6. The use of corrosion inhibitors in concrete provides no significant improvement in the corrosion resistance of epoxy-coated reinforcement due to the high resistance of the epoxy coating itself. The corrosion performance of epoxy-coated reinforcement is similar in concretes containing the three different types of corrosion inhibitors.
 7. Concrete containing Hycrete exhibits strength loss, as well as scaling in the field test specimens.
 8. The average chloride threshold for the zinc-coated (galvanized) reinforcement, on a water-soluble basis, is 1.52 kg/m^3 (2.57 lb/yd^3), which is higher than the average chloride threshold of 0.96 kg/m^3 (1.63 lb/yd^3) for conventional steel and lower than the average chloride threshold of 3.76 kg/m^3 (6.34 lb/yd^3) for MMFX steel.
 9. The range of the chloride threshold for zinc-coated reinforcement is greater than that of conventional steel. On the low side, zinc-coated reinforcement exhibits threshold values that are similar in magnitude to those exhibited by conventional steel. This may explain some of the variation in performance exhibited in the field by zinc-coated reinforcement.
 10. The concrete adjacent to zinc-coated reinforcement that does not have chromate treatment reveals no evidence of an increase in porosity due to hydrogen gas evolution during curing when compared to conventional reinforcing steel in air-entrained concrete. Some galvanized bars, however, showed signs of corrosion, indicating exposure of the intermetallic layer. The loss of the zinc layer may be due to the lack of chromate treatment or due to the loss of metal in the presence of a high-pH concrete pore solution.

11. In the field tests, the epoxy-coated bars with the primer containing microencapsulated calcium nitrite show no improvement in the corrosion resistance compared to conventional epoxy-coated reinforcement.
12. Increased adhesion between the epoxy coating and reinforcing steel provides no significant improvement in the corrosion resistance of epoxy-coated reinforcement.
13. The corrosion losses of multiple-coated reinforcement are comparable with those of conventional epoxy-coated reinforcement for uncracked and cracked concrete. The corrosion potentials show that the zinc is corroded preferentially, providing protection for the underlying steel. The degree of protection needs to be evaluated further based on the visual inspection of the corrosion products upon the completion of the test.
14. Pickled 2205 stainless steel demonstrates excellent performance in corrosion resistance after four years in the SE and CB tests, field test, and bridge corrosion potential mapping.
15. Corrosion potential maps from the bi-annual surveys for the Doniphan County and Mission Creek Bridge decks reveals that no corrosion activity is observed over the majority of the two deck surfaces. More negative corrosion potentials observed near the two abutments for both bridges are possibly due to mild steel form ties used in the abutments and the restricted access of oxygen for the portion of the structures that is buried in the earth.
16. At 42 weeks, the microcell corrosion losses measured in the LPR test for the CB test specimens are on the order of ten times higher than the corresponding microcell losses for the SE test specimens. In the ASTM G109 test, the microcell

corrosion losses for multiple-coated and epoxy-coated reinforcement are less than 6% of that for conventional steel.

17. The relative microcell corrosion losses of SE specimens containing conventional steel and different inhibitors are similar to the macrocell corrosion losses for the same specimens. For CB specimens, the average microcell corrosion losses are higher than those obtained from the macrocell corrosion.
18. For the same corrosion protection system, much lower corrosion rates and corrosion losses are observed in the ASTM G109 and field tests than in the SE and CB tests due to the less severe exposure conditions.
19. Comparisons of corrosion rates and losses for the specimens containing conventional steel and inhibitors in the SE and CB tests exhibit a strong linear relationship between corrosion measured using the two test methods. Comparisons between the rapid macrocell test and SE and CB tests demonstrated a good linear relationship between those methods based on corrosion rate (at 15 weeks for the rapid macrocell test and 42 weeks for the SE and CB tests), but not for corrosion loss, because the corrosion losses in the rapid macrocell test at 15 weeks do not distinguish between these systems.
20. For a 216-mm (8.5-in.) thick monolithic bridge deck constructed using various corrosion protection systems over a 75-year design life, pickled 2205 stainless steel is the most cost-effective option based on experience in practice for a discount rate of 2%. ECR and ECR with increased adhesion are the most cost-effective options based on analysis for a discount rate of 2% and based on both experience and analysis for discount rates of 4% and 6%. For a 178-mm (7-in.) thick subdeck with a 38-mm (1.5-in.) silica fume concrete overlay, ECR and ECR

with increased adhesion are the most cost-effective options based on both experience and analysis for discount rates of 2%, 4%, and 6%.

5.3 RECOMMENDATIONS

1. Based on the economic analysis, decks containing ECR, or ECR with increased adhesion, or pickled 2205 stainless steel are the most cost-effective options.
2. For a better estimate of the cost effectiveness, coating disbondment needs to be evaluated for the epoxy-coated reinforcement with increased adhesion. This must await the end of the tests.
3. Pickled 2205 stainless steel exhibits excellent corrosion resistance, which suggests its use in very important structures in aggressive chloride-exposure environments.
4. The corrosion inhibitor Hycrete improves the corrosion resistance of the conventional steel significantly in both uncracked and cracked concrete, but because it causes strength loss, it is not recommended for use in structural concrete without modifications to increase strength, possibly by using more cement in the mix. In that case, the effect of using concrete with a high paste content must be considered. Scaling of concrete also needs to be considered.
5. The zinc-coating on the multiple-coated bars corrodes sacrificially to protect the underlying steel. Steel corrosion starts before the zinc layer is completely corroded away. The degree of protection and the influence of the corrosion products to stress the surrounding concrete remains unknown and needs to be investigated further.
6. Using a lower water-cement ratio significantly improves the corrosion resistance of conventional steel in uncracked concrete, but not in cracked concrete.

7. To estimate the time to first repair, corrosion rates should be based on the slopes of the corrosion loss graphs. Due to variations in the corrosion performance among the specimens in a single system, more specimens and longer exposure time (three specimens for a majority of the systems and 42 weeks for inhibitor specimens was used in this study) should be used to provide a better understanding of their behaviors.

REFERENCES

AASHTO T 260-97 (2001). "Standard Method of Test for Sampling and Testing for Chloride Ion in Concrete and Concrete Raw Materials," American Association of State Highway and Transportation Officials.

Allyn, M., and Frantz, G. C. (2001a). "Corrosion Tests with Concrete Containing Salts of Alkenyl-Succinic Acid," *ACI Materials Journal*, Vol. 98 No. 3, pp. 224-232.

Allyn, M., and Frantz, G. C. (2001b). "Strength and Durability of Concrete Containing Salts of Alkenyl-Succinic Acid," *ACI Materials Journal*, Vol. 98, No. 1, pp. 52-58.

Alonso, C., Andrade, C., Castellote, M., and Castro, P. (2000). "Chloride Threshold Values to Depassivate Reinforcing Bars Embedded in a Standard OPC Mortar," *Cement and Concrete Research*, Vol. 30, No. 7, pp. 1047-1055.

Andrade, C., and Alonso, C. (2001). "On-site Measurements of Corrosion Rate of Reinforcements," *Construction and Building Materials*, Vol. 15, No. 2-3, pp.141-145.

Andrade, M. C. and Macias, A. (1988). "Galvanized Reinforcements in Concrete," in *Surface Coatings-2*, A. D. Wilson, J. W. Nicolson, and H. J. Prosser, eds., Elsevier Applied Science, London and New York, pp. 137-182.

Arya, C. and Newman, J. B. (1990). "Problem of Predicting Risk of Corrosion of Steel in Chloride Contaminated Concrete," *Proceedings of the Institute of Civil Engineers Part 1*, Vol. 88, pp. 875-888.

ASTM A 615/A 615M. (2001). "Standard Specification for Deformed and Plain Carbon-Steel Bars for Concrete Reinforcement," ASTM International, West Conshohocken, PA.

ASTM A 767/A 767M (2005). "Standard Specification for Zinc-Coated (Galvanized) Steel Bars for Concrete Reinforcement," ASTM International, West Conshohocken, PA.

ASTM A 775-04a (2004). "Standard Specification for Epoxy-Coated Steel Reinforcing Bars," ASTM International, West Conshohocken, PA.

ASTM A 955-07a (2007). "Standard Specification for Deformed and Plain Stainless-Steel Bars for Concrete Reinforcement," ASTM International, West Conshohocken, PA.

ASTM A 1035/A 1035M (2009). "Standard Specification for Deformed and Plain, Low-carbon, Chromium, Steel Bars for Concrete Reinforcement," ASTM International, West Conshohocken, PA.

ASTM C 192/C 192-07 (2007). "Standard Practice for Making and Curing Concrete Test Specimens in the Laboratory," ASTM International, West Conshohocken, PA.

ASTM C 305-06 (2006). "Standard Practice for Mechanical Mixing of Hydraulic Cement Pastes and Mortars of Plastic Consistency," ASTM International, West Conshohocken, PA.

ASTM C 876-91 (1999). "Standard Test Method for Half-cell Potentials of Uncoated Reinforcing Steel in Concrete," ASTM International, West Conshohocken, PA.

ASTM G 109-99a (1999). "Standard Test Method for Determining the Effects of Chemical Admixtures on the Corrosion of Embedded Steel Reinforcement in Concrete Exposed to Chloride Environments," ASTM International, West Conshohocken, PA.

Balma, J., Darwin, D., Browning, J. P., and Locke, C. E. (2005). "Evaluation of Corrosion Protection Systems and Corrosion Testing Methods for Reinforcing Steel in Concrete," *SM Report* No. 76, University of Kansas Center for Research, Inc., Lawrence, KS, 517 pp.

Bautista, A., and Gonzalez, J. A. (1996). "Analysis of the Protective Efficiency of Galvanizing against Corrosion of Reinforcements Embedded in Chloride Contaminated Concrete," *Cement and Concrete Research*, Vol. 26, No. 2, pp. 215-224.

Bellezze, T., Coppola, L., and R. Fratesi. (2000). "Evaluation of Hexavalent Chromium-free Passivation Treatment of Galvanized Bars for Reinforced Concrete," *SP 192-35*, American Concrete Institute, Farmington Hills, MI, pp. 573-589.

Bentur, A., Diamond, S., and Berke, N.S. (1997). *Steel Corrosion in Concrete*, E & FN Spon, New York, 133 pp.

Berke, N. S., Pfeifer, D. W., and Weil, T. G. (1988). "Protection against Chloride-induced Corrosion," *Concrete International*, Vol. 10, No. 12, pp. 45-55.

Berman, H. A. (1974). "The Effects of Sodium Chloride on the Corrosion of Concrete Reinforcing Steel and on the pH of Calcium Hydroxide Solution," *Report* No. FHWA-RD-74-1, Federal Highway Administration, Washington, D.C.

Bertolini, L., Bolzoni, F., Pastore, T., and Pedefferri, P. (2004). "Effectiveness of a Conductive Cementitious Mortar Anode for Cathodic Protection of Steel in Concrete," *Cement and Concrete Research*, Vol. 34, No. 4, pp. 681-694.

Broomfield, J. (1997). *Corrosion of Steel in Concrete: Understanding, Investigation and Repair*, E & FN Spon, UK, 240 pp.

Brown, M. C., Weyers, R. E., and Sprinkel, M. M. (2006). "Service Life Extension of Virginia Bridge Decks Afforded by Epoxy-coated Reinforcement," *Journal of ASTM International*, Vol. 3, No. 2, pp. 2-13.

Callahan, M. R. (1989). "Deicing Salt Corrosion with and without Inhibitors," *Transportation Research Record* No. 1211, pp. 12-17.

Cherry, B. W. (2007). "How to Make It Last a Little Bit Longer," *Corrosion & Materials*, Vol. 32, No. 5, pp. 16-22.

Civjan, S. A., and Crellin, B. J. (2006). "A New Admixture to Mitigate Corrosion Problems," *Concrete International*, Vol. 28, No. 8, pp. 78-82.

Civjan, S. A., LaFave, J. M., Lovett, D., Sund, D. J., and Trybulski, J. (2003). "Performance Evaluation and Economic Analysis of Combination of Durability Enhancing Admixtures (Minerals and Chemical) in Structural Concrete for Northeast U.S.A.," *Report No. NETCR36*, New England Transportation Consortium (NETC), 166 pp.

Civjan, S. A., LaFave, J. M., Trybulski, J., Lovett, D., Lima, J., and Pfeifer, D. W. (2005). "Effectiveness of Corrosion Inhibiting Admixture Combinations in Structural Concrete," *Cement and Concrete Composites*, Vol. 27, No. 6, pp. 688-703.

Clear, K. C. (1976). "Time-to-Corrosion of Reinforcing Steel in Concrete Slabs," *Report No. FHWA-RD-76-70*, Federal Highway Administration, Washington, D.C.

Clemeña, G. G. (2003). "Investigation of the Resistance of Several New Metallic Reinforcing Bars to Chloride-Induced Corrosion in Concrete," *Report No. VTRC 04-R7*, Virginia Transportation Research Council, 24 pp.

Cody, R. D., Cody, A. M., Spry, P. G., and Gan, G. (1996). "Concrete Deterioration by Deicing Salts: An Experimental Study," *Semisequicentennial Transportation Conference Proceedings*, May, Ames, IA.

Corderoy, D. J. H., Ford, P. R., and Herzog, H. (1977). "Corrosion Behavior of Galvanized Steel in Concrete," *Preprinted Papers, Annual Conference - Australasian Corrosion Association*, Paper No. J2, 11 pp.

Cusson, D., Qian, S., Chagnon, N., and Baldock, B. (2008). "Corrosion-Inhibiting Systems for Durable Concrete Bridges. I: Five-Year Field Performance Evaluation," *Journal of Materials in Civil Engineering*, Vol. 20, No. 1, pp. 20-28.

Daigle, L., Lounis, A., and Cusson, D. (2004). "Numerical Prediction of Early-Age Cracking and Corrosion in High Performance Concrete Bridges – Case Study," *2004 Annual Conference of the Transportation Association of Canada*, Québec City, Québec, 20 pp.

Daniel, M. (2004). Lawrence Maintenance Office, Kansas Department of Transportation, Lawrence, KS. Personal communication.

Darwin, D., Browning, J., Gong, L., and Hughes, S. R. (2007). "Effects of Deicers on Concrete Deterioration," *SL Report 07-3*, University of Kansas Center for Research, Inc., Lawrence, KS, 28 pp.

Darwin, D., Browning, J.P., Locke, C.E. and Nguyen, T. V. (2007) "Multiple Corrosion Protection Systems for Reinforced Concrete Bridge Components," *Publication No. FHWA-HRT-07-043*, Federal Highway Administration, also *SM Report 84*, University of Kansas Center for Research, Inc., Lawrence, KS, July, 116 pp.

Darwin, D., Browning, J. P., Nguyen, T. V., and Locke, C. E. (2007). "Evaluation of Metallized Stainless Steel Clad Reinforcement," *South Dakota Department of Transportation Report*, SD2002-16-F, also *SM Report No. 90*, University of Kansas Center for Research, Inc., Lawrence, KS, 156 pp.

Darwin, D., Locke, C. E., Balma, J., and Kahrs, J. T. (1999). "Evaluation of Stainless Steel Clad Reinforcing Bars," *SL Report 99-3*, University of Kansas Center for Research, Inc., Lawrence, KS, 17 pp.

Diamond, S. (1986). "Chloride Concentrations in Concrete Pore Solutions Resulting From Calcium and Sodium Chloride Admixtures," *Cement, Concrete, and Aggregates*, Vol. 8, No. 2, pp. 97-102.

Du, R., Hu, R., Huang, R., and Lin, C. (2006). "In Situ Measurement of Cl- Concentrations and pH at the Reinforcing Steel/Concrete Interface by Combination Sensors," *Analytical Chemistry*, Vol. 78, No. 9, pp. 3179-3185.

Escalante, E. (1990). "Effectiveness of potential measurements for estimating corrosion of steel in concrete," *Corrosion of Reinforcement in Concrete*, Page, C. L., Treadaway, K. W. J., and Bamforth, P. B., eds., Elsevier Applied Science, London, pp. 281-292.

Farzammehr, H. (1985). "Pore Solution Analysis of Sodium Chloride and Calcium Chloride Containing Cement Pastes," *Master of Science Thesis*, University of Oklahoma, Norman, OK, 101 pp.

Feliu, S., Gonzalez, J. A., Andrade, C., and Feliu, V. (1988). "On-site Determination of the Polarization Resistance in a Reinforced Concrete Beam," *Corrosion*, Vol. 44, No. 10, pp. 761-765.

Feliu, S., Gonzalez, J. A., and Andrade, C. (1994). "Errors in the On-site Measurements of Rebar Corrosion Rates Arising From Signal Un Confinement," *SP 151*, American Concrete Institute, Farmington Hills, MI, pp. 183-196.

Flis, J., Pickering, H. W., and Osseo-Asare, K. (1998). "Interpretation of Impedance Data for Reinforcing Steel in Alkaline Solution Containing Chlorides and Acetates," *Electrochim. Acta*, Vol. 43 No. 12-13, pp. 1921-1929.

Frankel, G. S. (2008). "Electrochemical Techniques in Corrosion: Status, Limitations, and Needs," *Journal of ASTM International*, Vol. 5, No. 2, 27pp.

French, C., Leon, R., and Lorentz, T. (1992). "Corrosion of Coated and Uncoated Steel in Concrete," *Structural Engineering Report No. 92-03*, University of Minnesota Center of Transportation Studies, Minneapolis, Minnesota, 204 pp.

Funahashi, M. (1990). "Predicting Corrosion-free Service Life of a Concrete Structure in a Chloride Environment," *ACI Materials Journal*, Vol. 87, No. 6, pp. 581-587.

Gaidis, J. M. (2004). "Chemistry of Corrosion Inhibitors," *Cement and Concrete Composites*, Vol. 26, No. 3, pp. 181-189.

Gaidis, J. M., and Rosenberg, A. M. (1987). "Inhibitor of Chloride-induced Corrosion in Reinforced Concrete by Calcium Nitrite," *Cement, Concrete, and Aggregates*, Vol. 9, No. 1, pp. 30-33.

Gamry (1999). *Electrochemical Measurement System Software Installation Manuals, Revision 3.1*, Gamry Instruments Inc.

Gartner, E. M. and Gaidis, J. M. (1989). "Hydration Mechanisms, I." *Materials Science of Concrete I*, American Ceramic Society, Westerville, OH, pp. 95-125.

Ge, B., Darwin, D., Locke, C. E., and Browning, J. P. (2004). "Evaluation of Corrosion Protection Systems and Testing Methods for Conventional Steel," *SM*

Report No. 73, University of Kansas Center for Research, Inc., Lawrence, KS, 213 pp.

Gilsrud, T. (2007) South Dakota Department of Transportation. Personal communication.

Glass, G. K., and Buenfeld, N. R. (1997). "The Presentation of the Chloride Threshold Level for Corrosion of Steel in Concrete," *Corrosion Science*, Vol. 39, No. 5, pp. 1001-1013.

Gong, L., Darwin, D., Browning, J. P., and Locke, C. E. (2006). "Evaluation of Multiple Corrosion Protection Systems and Stainless Steel Clad Reinforcement for Reinforced Concrete," *SM Report No. 82*, University of Kansas Center for Research, Inc, Lawrence, KS, 504 pp.

Goni, S., and Andrade, C. (1990). "Synthetic Concrete Pore Solution Chemistry and Rebar Corrosion Rate in the Presence of Chlorides" *Cement and Concrete Research*, Vol. 20, No. 4, pp. 525-539.

Gouda, V. K. (1970). "Corrosion and Corrosion Inhibition of Reinforcing Steel. I. Immersed in Alkaline Solutions," *British Corrosion Journal*, Vol. 5, No. 5, pp. 198-203.

Gowers, K. R., Millard, S. G., and Bungey, J. H. (1997) "Experimental Studies on the Use of a Guard Ring For Current Confinement During Linear Polarization Resistance Measurement On Reinforced Concrete," *International Conference on Non Destructive Testing in Civil Engineering 97*, British Institute of N.D.T. Vol. 1, pp. 361-382.

Griffith, A., and Laylor, H. M. (1999). "Epoxy Coated Reinforcement Study," *Report No. OR-RD-99-25*, Oregon Department of Transportation Research Group, Salem, Oregon, 47 pp.

Gu, P., and Beaudoin, J. J. (1998). "Obtaining Effective Half-Cell Potential Measurements in Reinforced Concrete Structures," *Construction Technology Updates*, No. 18, National Research Council of Canada, 4 pp.

Gu, P., Elliott, S., Hristova, R., Beaudoin, J. J., Brousseau, R., and Baldock, B. (1997). "A Study of Corrosion Inhibitor Performance in Chloride Contaminated Concrete by Electrochemical Impedance Spectroscopy," *ACI Materials Journal*, Vol. 94, No. 5, pp. 385-395.

Guo, G., Darwin, D., Browning, J. P., and Carl E. Locke, J. (2006). "Laboratory and Field Tests of Multiple Corrosion Protection Systems for Reinforced Concrete Bridge

Components and 2205 Pickled Stainless Steel,” *SM Report* No. 85, University of Kansas Center for Research, Inc., Lawrence, KS, 776 pp.

Hansson, C. M., Mammoliti, L., and Hope, B. B. (1998). “Corrosion Inhibitors in Concrete – Part1: The Principles,” *Cement and Concrete Research*, Vol. 28, No. 12, pp. 1775-1781.

Hasan, H. O., Ramirez, J. A., Cleary, D. B. (1995). “Field Evaluation of Concrete Bridge Decks Reinforced with Epoxy-coated Steel in Indiana,” *Transportation Research Record* No. 1476, Washington, D. C., pp. 155-161.

Hausmann, D. A. (1967). “Steel Corrosion in Concrete,” *Materials Protection*, No. 6, pp. 19-23.

Higgins, R. J. (1987). “Fusion Bonded Epoxy Powder Coating Chosen for Rebar Protection in Prestigious New Development in Dubai” *Anti-Corrosion Methods and Materials*, Vol. 34, No. 4, pp. 14-15.

Hill, G. A., Spellman, D. L., and Stratfull, R. F. (1976). “Laboratory Corrosion Tests of Galvanized Steel in Concrete,” *Transportation Research Record*, No. 604, pp. 25-37.

Hime, W. G., and Machin, M. (1993). “Performance Variances of Galvanized Steel in Mortar and Concrete,” *Corrosion*, Vol. 49, No. 10, pp. 856-860.

Hofsoy, A., and Gukild, I. (1969). “Bond Studies on Hot-dip-galvanized Reinforcement in Concrete,” *ACI Journal, Proceedings* Vol. 66, No. 3, pp. 174-184.

Hope, B. B., Page, J. A., and Ip, A. K. C. (1986). “Corrosion Rates of Steel in Concrete,” *Cement and Concrete Research*, Vol. 16, No. 5, pp. 771-786.

Husain, A., Al-Bahar, S., Salam, S. A., and Al-Shamali, O. (2004). “Accelerated AC Impedance Testing for Prequalification of Marine Construction Materials,” *Desalination*, No. 165, pp. 377-384.

Iverson, W. P. (1968). “Transient Voltage Changes Produced in Corroding Metals and Alloys,” *Journal of the Electrochemical Society*, Vol. 115, No. 6, pp. 617-618.

Jamil, H. E., Shrirri, A., Boulif, R., Bastos, C., Montemor, M. F., and Herreira, M. G. S. (2004). “Electrochemical Behaviour of Amino-alcohol Based Inhibitor Used to Control Corrosion of Reinforcing Steel,” *Electrochim Acta*, No. 49, pp. 2753-2760.

Jones, D. A. (1996). *Principles and Prevention of Corrosion*, Macmillan Publishing Company, New York, 572 pp.

Kahrs, J. T., Darwin, D., and Locke, C. E. (2001). "Evaluation of Corrosion Resistance of Type 304 Stainless Steel Clad Reinforcing Bars," *SM Report No. 65*, University of Kansas Center for Research, Inc., Lawrence, KS, 76 pp.

Kansas Department of Transportation. (2001). *Snow & Ice Control & Other Motorist Services*, KDOT Maintenance Manual, Chapter 7, Topeka, KS, 38 pp.

Kayyali, O. A., and Haque, M. N. (1995). "The Cl-/OH- Ratio in Chloride-Contaminated Concrete – a Most Important Criterion," *Magazine of Concrete Research*, Vol. 47, No. 172, pp. 235-242.

Kelestemur, O., and Yildiz, S. (2006). "Effect of Various NaCl Concentration on Corrosion of Steel in Concrete Produced by Addition of Styrofoam," *Gazi University Journal of Science*, Vol. 19, No. 3, pp. 163-172.

Kepler, J. L., Darwin, D., Locke, C. E. (2000). "Evaluation of Corrosion Protection Methods for Reinforced Concrete Structures," *SM Report No. 58*, The University of Kansas Center for Research, Inc., Lawrence, KS, 221 pp.

Kilareski, W. P. (1977). "Epoxy Coatings for Corrosion Protection of Reinforcement Steel," *ASTM Special Technique Publication 629*, Chloride Corrosion of Steel in Concrete, pp. 82-88.

Kobayashi, K., and Takewaka, K. (1984). "Experimental Studies on Epoxy-coated Reinforcing Steel for Corrosion Protection," *International Journal of Cement composites and Lightweight Concrete*, Vol. 6, No. 2, pp. 99-116.

Lambert, P., Page, C. L., and Vassie, P. R. W. (1991). "Investigation of Reinforcement Corrosion. 2. Electrochemical Monitoring of Steel in Chloride-contaminated Concrete," *Materials and Structures*, Vol. 24, No. 143, pp. 351-358.

Lee, H., Cody, A. M., Cody, R. D., and Spry, P. G. (2000). "Effects of Various Deicing Chemicals on Pavement Concrete Deterioration," *Proceedings, Mid-Continent Transportation Symposium*, Center for Transportation Research and Education, Iowa State University, Ames, Iowa, pp. 151-155.

Legat, A., and Zevnik, C. (1993). "The Electrochemical Noise of Mild and Stainless Steel in Various Water Solutions," *Corrosion Science*, Vol. 35, No. 3-8, pp. 1661-1666.

Legat, A., Leban, M., and Bajt, Ž. (2004). "Corrosion Processes of Steel in Concrete Characterized by Means of Electrochemical Noise," *Electrochimica Acta*, Vol. 49, pp.2741-2751.

Lewis, D. A. (1965). "Some Aspects of the Corrosion of Steel in Concrete," *Proceeding of the First International Congress on Metallic Corrosion*, pp. 547-555.

Lindquist, W. D., Darwin, D., Browning, J. P. (2005) "Cracking and Chloride Content in Reinforced Concrete Bridge Decks," *SM Report No. 78*, The University of Kansas Center for Research, Inc., Lawrence, KS, 453 pp.

Lindquist, W. D., Darwin, D., Browning, J. P., and Miller, G. G., (2006) "Effect of Cracking on Chloride Content in Concrete Bridge Decks," *ACI Materials Journal*, Vol. 103, No. 6, pp. 467-473.

Liu, Y., and Weyers, R. E. (1998). "Modeling the Time-to-Corrosion Cracking in Chloride-contaminated Reinforced Concrete Structures," *ACI Materials Journal*, Vol. 95, No. 6, pp. 675-681.

MacDonald, D. D. (2006). "Reflections on the History of Electrochemical Impedance Spectroscopy," *Electrochimica Acta*, Vol. 51, No. 8-9, pp. 1376-1388.

MacDonald, D. D., and Mckube, M. C. H. (1981). "Electrochemical Impedance Techniques in Corrosion Science," *ASTM Special Technical Publication*, No. 727, pp. 110-49.

Malik, A. U., Ismail, A., Al-Moaili, F., and Ozair, G. (2004). "Studies on the Performance of Migratory Corrosion Inhibitors in Protection of Rebar Concrete in Gulf Seawater Environment," *Cement and Concrete Composites*, No. 26, pp. 235-242.

Manning, D. G. (1996). "Corrosion Performance of Epoxy-Coated Reinforcing Steel: North American Experience," *Construction and Building Materials*, Vol. 10, No.5, pp. 349-365.

Manning, D. G., Escalante, E., and Whiting, D. (1982). *Panel Report-Galvanized Rebars as Long-Term Protective System*, Washington, D. C.

Mansfeld, F., and Xiao, H. (1993). "Electrochemical Noise Analysis of Iron Exposed to NaCl Solutions of Different Corrosivity," *Journal of Electrochemical Society*, Vol. 140, No. 8, pp. 2205-2209.

Mariaca, L., Bautista, A., Rodriguez, P., and González, J. A. (1997). "Use of Electrochemical Noise for Studying the Rate of Corrosion of Reinforcements Embedded in Concrete," *Materials and Structures*, Vol. 30, pp.613-617.

Martinez, S. L., Darwin, D., McCabe, S. L., and Locke, C. E. (1990). "Rapid Test for Corrosion Effects of Deicing Chemicals in Reinforced Concrete," *SL Report No. 90-4*, University of Kansas Center for Research, Inc., Lawrence, KS, 61 pp.

McCrum, L., and Arnold, C. J. (1993). "Evaluation of Simulated Bridge Deck Slabs Using Uncoated, Galvanized, and Epoxy Coated Reinforcing Steel," *Research Report No.R-1320*, Michigan Department of Transportation, Lansing, MI.

McDonald, D. B., Pfeifer, D. W., and Sherman, M. R. (1998). "Corrosion Evaluation of Epoxy-Coated, Metallic-Clad and Solid Metallic Reinforcing Bars in Concrete," *Publication No. FHWA-RD-98-153*, Federal Highway Administration, McLean, VA, 127 pp.

Mehta, P. K., and Monteiro, P. J. M. (2006). *Concrete Microstructure, Properties, and Materials*, The McGraw-Hill Companies, 659 pp.

Miller, G. and Darwin, D. (2000). "Performance and Constructability of Silica Fume Bridge Deck Overlays," *SM Report No. 57*, The University of Kansas Center for Research, Inc., Lawrence, KS, 423 pp.

Mindess, S., Young, J. F., and Darwin, D. (2003). *Concrete*, 2nd Ed., Pearson Education Inc., Upper Saddle River, NJ, 644 pp.

Minerals website (2008) – <http://minerals.usgs.gov>.

Moreno, M., Morris, W., Alvarez, M. G., and Duffo, G. S. (2004). "Corrosion of Reinforcing Steel in Simulated Concrete Pore Solutions. Effect of Carbonation and Chloride Content," *Corrosion Science*, Vol. 46, No. 11, pp. 2681-2699.

Naish, C. C., Harker, A., and Carney, R. F. A. (1990). "Concrete Inspection: Interpretation of Potential and Resistivity Measurements," *Corrosion of Reinforcement in Concrete*, Page, C. L., Treadaway, K. W. J., and Bamforth, P. B., eds., Elsevier Applied Science, London, pp. 314-332.

Nmai, C. K., Stephens, A. F., and Bobrowski, G. S. (1992). "Organic-based Corrosion-inhibiting Admixture for Reinforced Concrete," *Concrete International*, Vol. 14, No. 4, pp. 45-51.

Nurnberger, U. (1996). "Stainless Steel in Concrete - State of the Art Report," *European Federation of Corrosion Publications No. 18*, the Institute of Materials, London, 30 pp.

Oh, B. H., Jang, S. Y., and Shin, Y. S. (2003). "Experimental Investigation of the Threshold Chloride Concentration for Corrosion Initiation in Reinforced Concrete Structures," *Magazine of Concrete Research*, Vol. 55, No. 2, pp. 117-124.

Perenchio, W. F. (1992). "Corrosion of Reinforcing Bars in Concrete," *Annual Seminar*, Master Builders Technology, Cleveland, OH.

Pfeifer, D. W. (2000). "High Performance Concrete and Reinforcing Steel with a 100-year Service Life." *PCI Journal*, May-June, pp. 46-54.

Pfeifer, D. W., Landgren, J. R., and Zoob, A. (1987). "Protective Systems for New Prestressed and Substructure Concrete," *Publication No. FHWA-RD-86-193*, Federal Highway Administration, McLean, VA, 127 pp.

Pfeifer, D. W., and Scali, M. J. (1981). "Concrete Sealers for Protection of Bridge Structures," *National Cooperative Highway Research Board Program Report No. 244*, Transportation Research Board, National Research Council, Washington, D.C., 138 pp.

Pianca, F. and Schell, H (2005). "The Long Term Performance of Three Ontario Bridges Constructed with Galvanized Reinforcement," *Report*, Ontario Ministry of Transportation (MTO), Downsview, Ontario, Canada, 30 pp.

Pyc, W. A., Demajtis, J., Weyers, R. E., and Sprinkel, M. M. (1999). "Evaluating Corrosion-inhibiting Admixtures." *Concrete International*, Vol. 21, No. 4, pp. 39-44.

Qiao, G. and Ou, J. (2007). "Corrosion Monitoring of Reinforcing Steel in Cement Mortar by EIS and ENA," *Electrochimica Acta*, No. 52, pp. 8008-8019

Rasheeduzzafar, Dakhil, F. H., Bader, M. A., and Khan, M. M. (1992). "Performance of Corrosion-Resisting Steels in Chloride-Bearing Concrete," *ACI Materials Journal*, Vol. 89, No. 5, pp. 439-448.

Roberge, P. R., Beaudoin, R., and Sastri, V. S. (1989). "Electrochemical Noise Measurements for Field Applications," *Corrosion Science*, Vol. 29, No. 10, pp. 1231-1233.

Sagues, A. A. (1994). "Corrosion of Epoxy-Coated Rebar in Florida Bridges," *WPI No. 0510603*, University of South Florida, Tampa, FL, 70 pp.

Salt Institute website (2008). – <http://www.saltinstitute.org>.

Schiessl, P. (1992). "Review of the KC, Inc. Reports on Effectiveness of Epoxy-Coated Reinforcing Steel," Canadian Strategic Highway Research Program, Ottawa, ON, 15 pp.

Schwensen, S. M., Darwin, D., and Locke, C. E. (1995). "Rapid Evaluation of Corrosion-Resistant Concrete Reinforcing Steel in the Presence of Deicers," *SL Report* No. 95-6, University of Kansas Center for Research, Inc., Lawrence, KS, 90 pp.

Searson, P. C., and Dawson, J. L. (1988). "Analysis of Electrochemical Noise Generated by Corroding Electrodes under Open-circuit Conditions." *Journal of Electrochemical Society*, Vol. 38, No. 2, pp. 1908-1914.

Senecal, M. R., Darwin, D., and Locke, C. E., Jr. (1995). "Evaluation of Corrosion-Resistant Steel Reinforcing Bars," *SM Report* No. 40, University of Kansas Center for Research, Inc., Lawrence, KS, 142 pp.

Simoës, A. M. P., and Ferreira, M. G. S. (1987). "Crevice Corrosion Studies on Stainless Steel Using Electrochemical Noise Measurements," *British Corrosion Journal*, Vol. 22, No. 1, pp. 21-25.

Smith, J. L., Darwin, D., and Locke, C. E. (1995). "Corrosion-Resistant Steel Reinforcing Bars Initial Tests," *SL Report* No. 95-1, University of Kansas Center for Research, Inc., Lawrence, KS, 43 pp.

Smith, F. N. and Tullman, M. (1999). "Using Stainless Steel as Long-Lasting Rebar Material," *Materials Performance*, Vol. 38, No. 5, pp. 72-76.

Smith, J. L., and Virmani, Y. P. (2000). "Materials and Methods for Corrosion Control of Reinforced and Prestressed Concrete Structures in New Construction," *Report* No. FHWA-RD-00-081, Federal Highway Administration, Washington, D.C. 82 pp.

Smulko, J. M., Darowicki, K., and Zieliński, A. (2006). "Evaluation of Reinforcement Corrosion Rate in Concrete Structures by Electrochemical Noise Measurements," *Russian Journal of Electrochemistry*, Vol. 42, No. 5, pp. 546-550.

So, H. S., and Millard, S. G. (2007). "On-Site Measurements on Corrosion Rate of Steel in Reinforced Concrete," *ACI Materials Journal*, Nov.-Dec., pp. 638-642.

Song, H., Saraswathy, V. (2007). "Corrosion Monitoring of Reinforced Concrete Structures – A Review," *International Journal of Electrochemical. Science*, Vol. 2, No. 1, pp. 1- 28.

Soylev, T. A., and Richardson, M. G. (2008). "Corrosion Inhibitors for Steel in Concrete: State-of-the-art Report." *Construction and Building Materials*, Vol. 22, No. 4, 609 pp.

Stainless Steel (2008). – http://www.outokumpu.com/pages/Page_____38366.aspx.

Steinbach, O. F., and King, C. V. (1950). *Experiments in Physical Chemistry*, American Book Company, New York, 250 pp.

Stern, M. and Weisert, E. D. (1958). "Experimental Observations on the relations between Polarization Resistance and Corrosion Rate," *Proceedings of the American Society for Testing Materials*, Vol. 59, pp. 1280-1290.

Thomas, M. (1996). "Chloride Thresholds in Marine Concrete," *Cement and Concrete Research*, Vol. 26, No. 4, pp. 513-519.

Tonini, D. E., and Dean, S. W. (1976). "Chloride Corrosion of Steel in Concrete," American Society for Testing and Materials, Philadelphia, PA.

Torres-Acosta, A. A., and Sagües, A. A. (2004). "Concrete Cracking by Localized Steel Corrosion - Geometric Effects." *ACI Materials Journal*, Vol. 101, No. 6, pp. 501-507.

Tourney, P., and Berke, N. (1993). "A Call for Standardized Tests for Corrosion-Inhibiting Admixtures," *Concrete International*, Vol. 15, No. 4, pp. 57-62.

Treadaway, K. W. J., Brown, B. L., and Cox, R. N. (1980). "Durability of Galvanized Steel in Concrete," *ASTM Special Technical Publication 713*, Corrosion of Reinforcing Steel in Concrete, pp. 102-131.

Trejo, D. (2002). "Evaluation of the Critical Chloride Threshold and Corrosion Rate for Different Steel Reinforcement Types," *Interim Report*, Texas Engineering Experimental Station, Jul., 38 pp.

Trépanier, S. M., Hope, B. B., and Hansson, C. M. (2001). "Corrosion inhibitors in concrete – Part III: Effect on Time to Chloride-Induced Corrosion Initiation and Subsequent Corrosion Rates of Steel in Mortar," *Cement and Concrete Research*, Vol. 31, No. 5, pp. 713-718.

Turgoose, S., and Cottis, R. A. (1991). "The Impedance Response of Imcovered Metals, Conference Proceedings: Electrochemical Impedance Analysis and Interpretation," *STP 1188*, ASTM, Philadelphia, PA.

U.S. Department of Transportation (2007). *2006 Status of the Nation's Highways, Bridges, and Transit: Conditions & Performance*, Jan., 2007, pp. 7-17.

Verbeck, G. J. (1975). "Mechanisms of Corrosion of Steel in Concrete," *Corrosion of Metals in Concrete*, SP 49-3, American Concrete Institute, Farmington Hills, MI, pp.21-38.

Vinod, K. (1988). "Protection of Steel Reinforcement for Concrete – A Review," *Corrosion Review*, Vol.16, No. 4, pp. 317-358.

Virmani, Y. P. (1990). "Effectiveness of Calcium Nitrite Admixture as a Corrosion Inhibitor," *Public Roads*, Vol. 544, No. 1, pp. 171-182.

Virmani, Y. P., Clear, K. C., and Pasko., T. J. (1983). "Time-to-Corrosion of Reinforcing Steel in Concrete Slabs – Vol. V: Calcium Nitrite Admixture or Epoxy Coated Reinforcing Bars as Corrosion Protection Systems," *Publication No. FHWA-RD-83-012*, Federal Highway Administration, McLean, VA, 76 pp.

Weyers, R. E., and Cady, P. D. (1987), "Deterioration of Concrete Bridge Decks from Corrosion of Reinforcing Steel," *Concrete International*, Vol. 9, No. 1, pp. 15-20.

Weyers, R. E., Pyc, W., Zemajtis, J., Liu, Y., Mokarem, D., and Sprinkel, M. M. (1998). "Field Investigation of Corrosion-Protection Performance of Bridge Decks Constructed with Epoxy-Coated Reinforcing Steel in Virginia," VTRC 98-R4, Virginia Transportation Research Council, 38 pp.

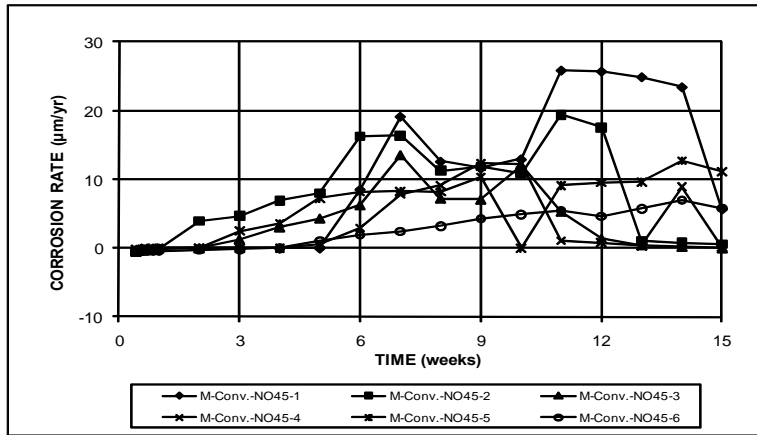
Yeomans, S. R. (1994). "Performance of Black, Galvanized, and Epoxy-coated Reinforcing Steels in Chloride-contaminated Concrete," *Corrosion*, Vol. 50, No. 1, pp. 72-81.

Yonezawa, T., Ashworth, V., Procter, R. P. M. (1988). "Study of the Pore Solution Composition and Chloride Effects in the Corrosion of Steel in Concrete," *Corrosion*, Vol. 44, No. 7, pp. 489-499.

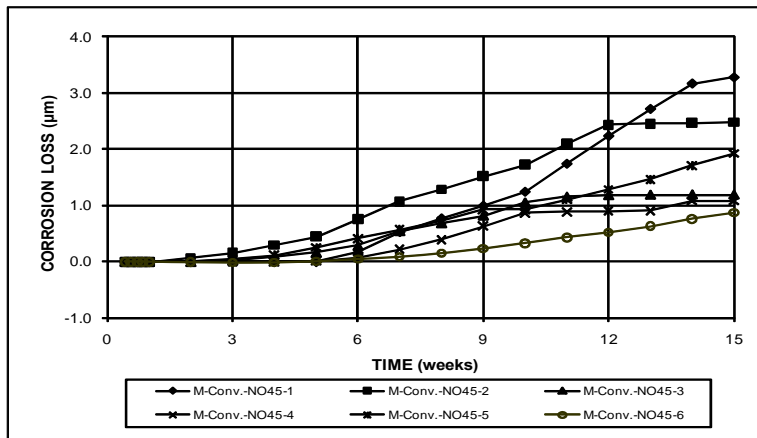
Yoon, I. (2007). "Deterioration of Concrete Due to Combined Reaction of Carbonation and Chloride Penetration: Experimental Study," *Key Engineering Materials*, Vol. 348-349, pp. 729-732.

Zemajtis, J., Weyers, R. E., and Sprinkel, M. M. (1999). "Corrosion Protection Service Life of Low-Permeable Concretes and Low-Permeable Concrete with a Corrosion Inhibitor," *Transportation Research Record* 98-1328, pp. 51-59.

APPENDIX A

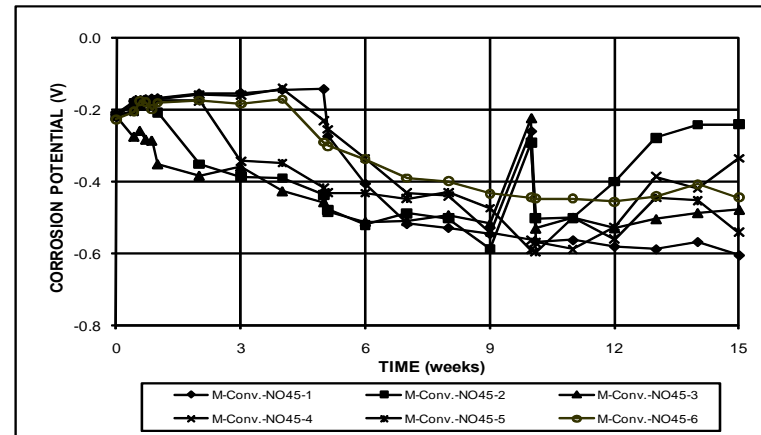


(a)

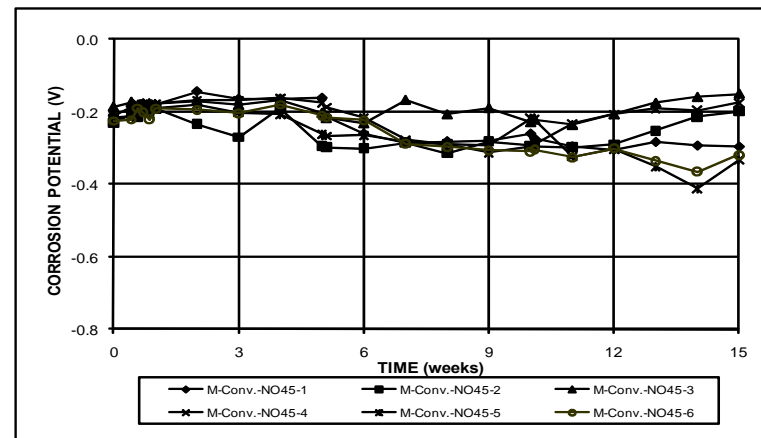


(b)

Figure A.1 – Macrocell Test. (a) Corrosion rates and (b) total corrosion losses for specimens with conventional steel and no inhibitors, $w/c = 0.45$.

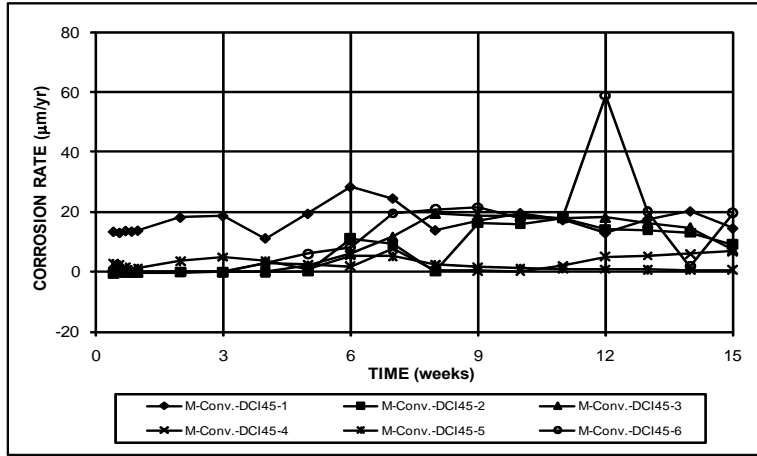


(a)

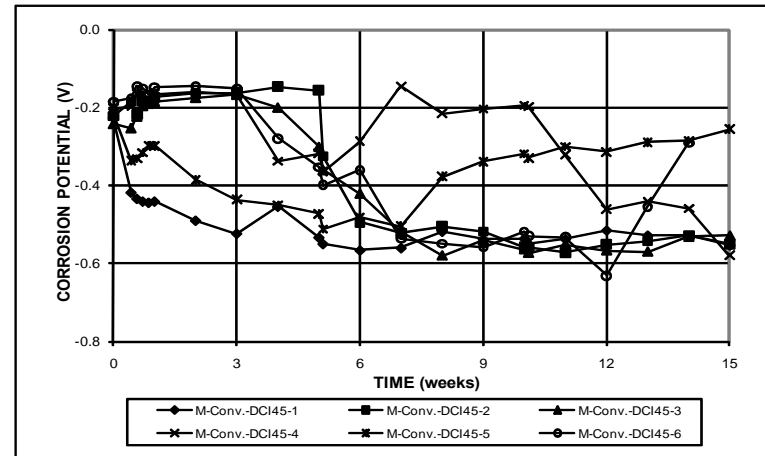


(b)

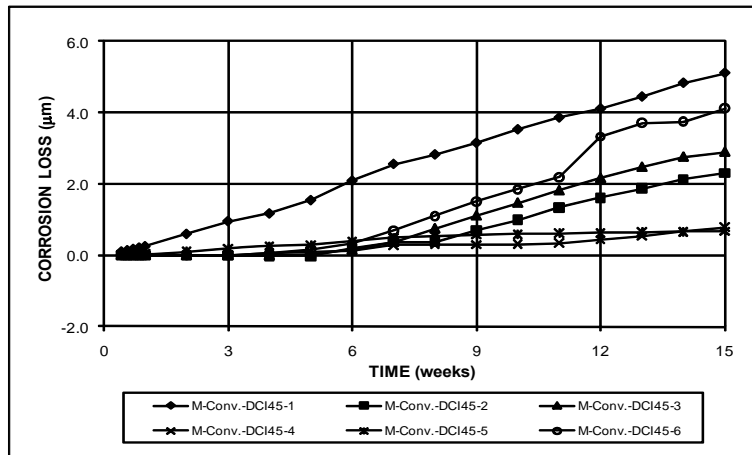
Figure A.2 – Macrocell Test. (a) Anode corrosion potentials and (b) cathode corrosion potentials with respect to a saturated calomel electrode for specimens with conventional steel and no inhibitors, $w/c = 0.45$.



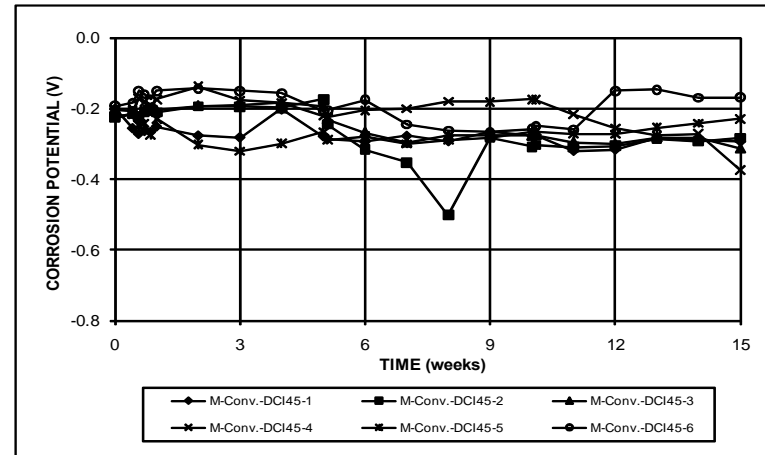
(a)



(a)



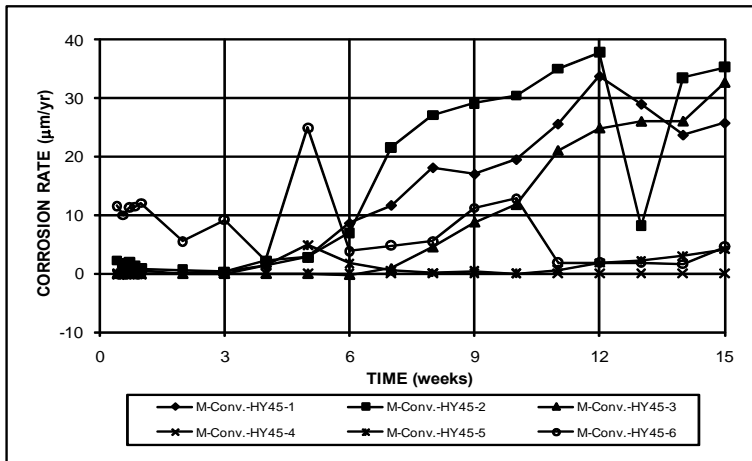
(b)



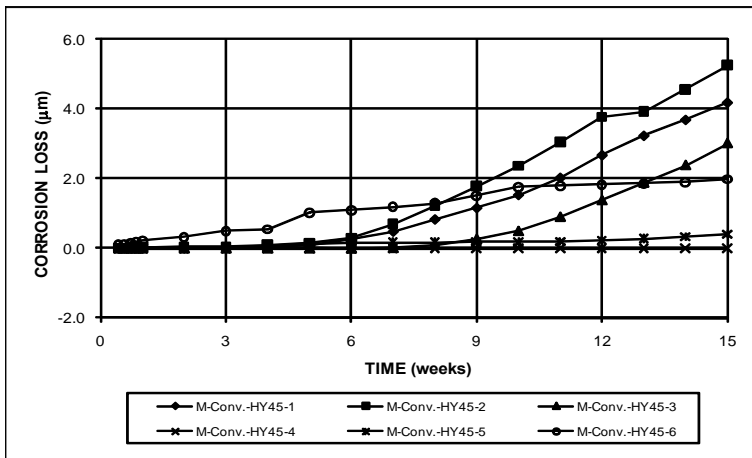
(b)

Figure A.3 – Macrocell Test. (a) Corrosion rates and (b) total corrosion losses for specimens with conventional steel and DCI inhibitor, $w/c=0.45$.

Figure A.4 – Macrocell Test. (a) Anode corrosion potentials and (b) cathode corrosion potentials with respect to a saturated calomel electrode for specimens with conventional steel and DCI inhibitor, $w/c=0.45$.

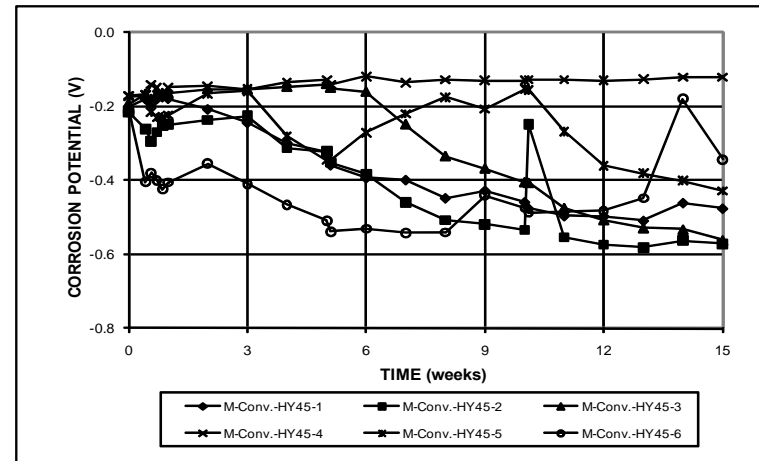


(a)

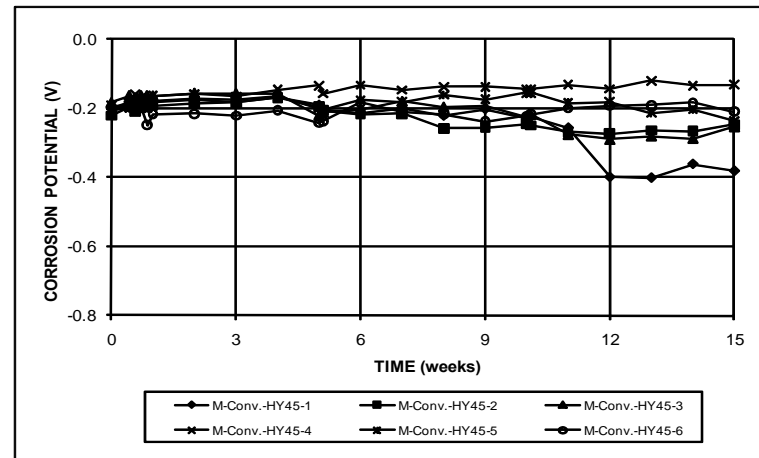


(b)

Figure A.5 – Macrocell Test. (a) Corrosion rates and (b) total corrosion losses for specimens with conventional steel and Hycrete inhibitor, $w/c = 0.45$.

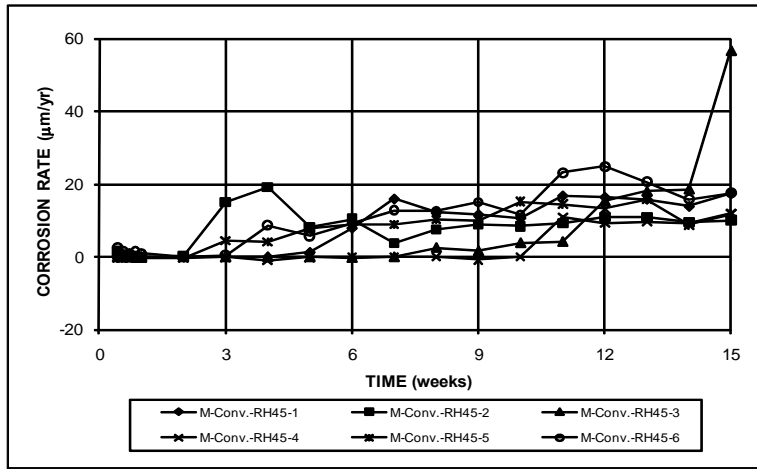


(a)

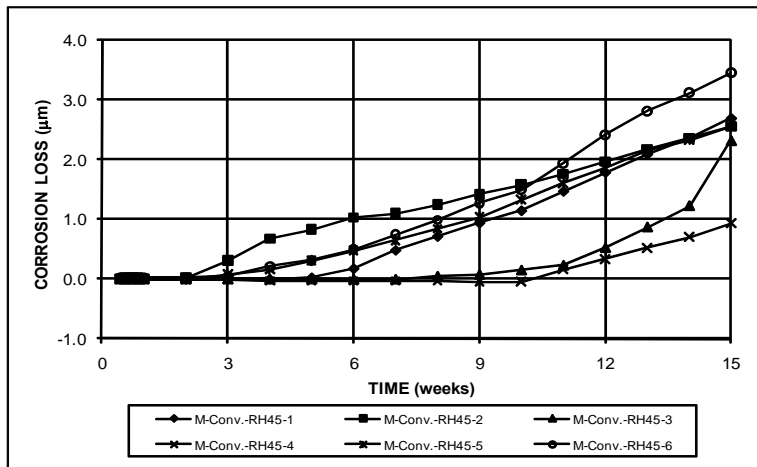


(b)

Figure A.6 – Macrocell Test. (a) Anode corrosion potentials and (b) cathode corrosion potentials with respect to a saturated calomel electrode for specimens with conventional steel and Hycrete inhibitor, $w/c = 0.45$.

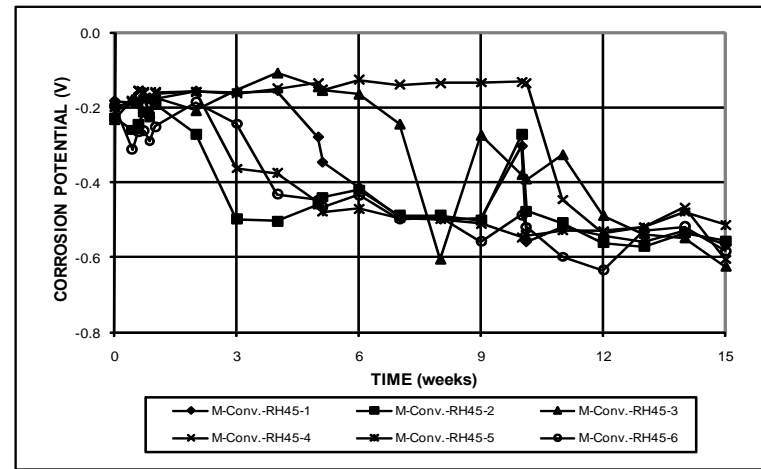


(a)

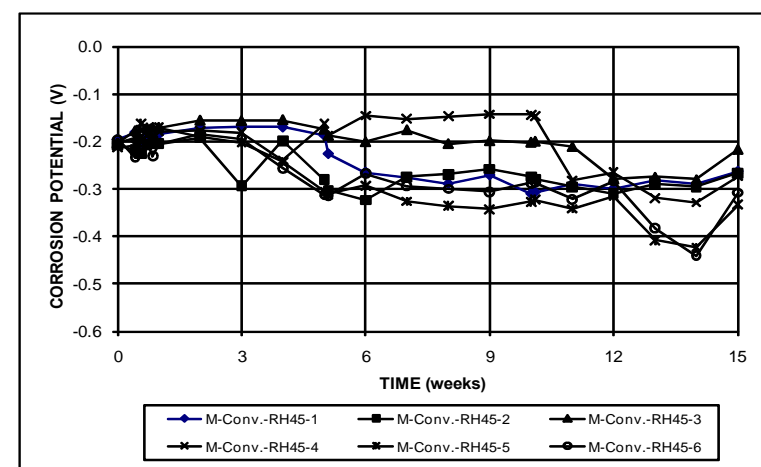


(b)

Figure A.7 – Macrocell Test. (a) Corrosion rates and (b) total corrosion losses for specimens with conventional steel and Rheocrete inhibitor, $w/c=0.45$.

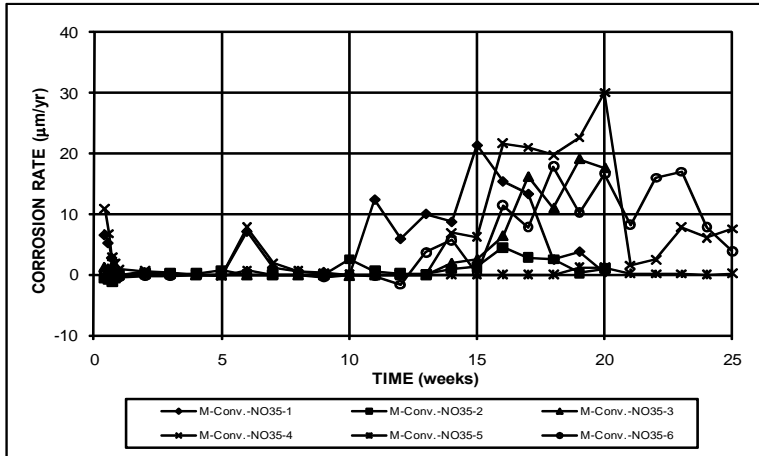


(a)

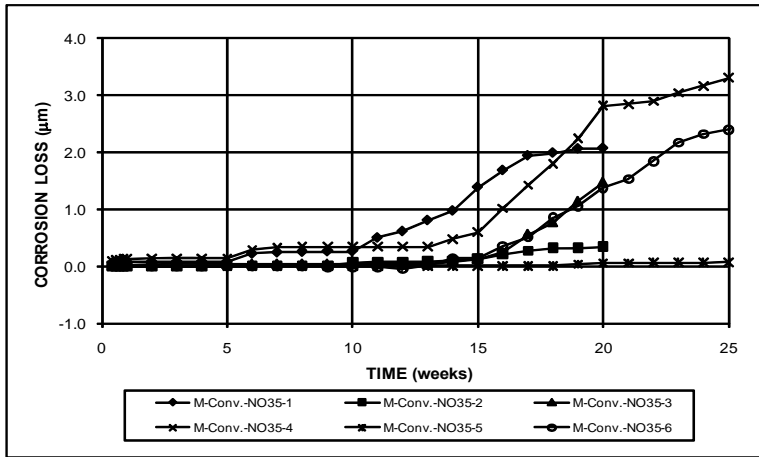


(b)

Figure A.8 – Macrocell Test. (a) Anode corrosion potentials and (b) cathode corrosion potentials with respect to a saturated calomel electrode for specimens with conventional steel and Rheocrete inhibitor, $w/c=0.45$.

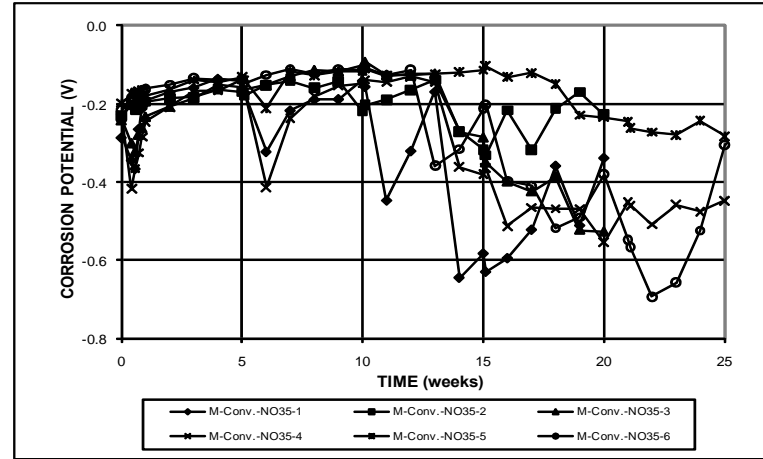


(a)

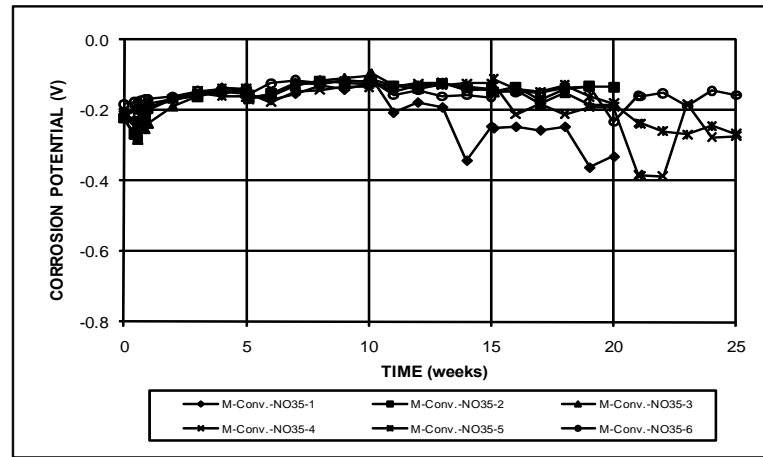


(b)

Figure A.9 – Macrocell Test. (a) Corrosion rates and (b) total corrosion losses for specimens with conventional steel and no inhibitors, $w/c = 0.35$.

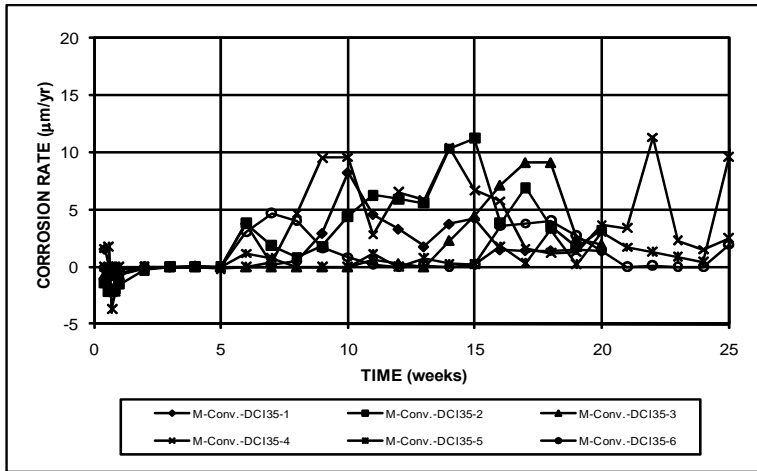


(a)

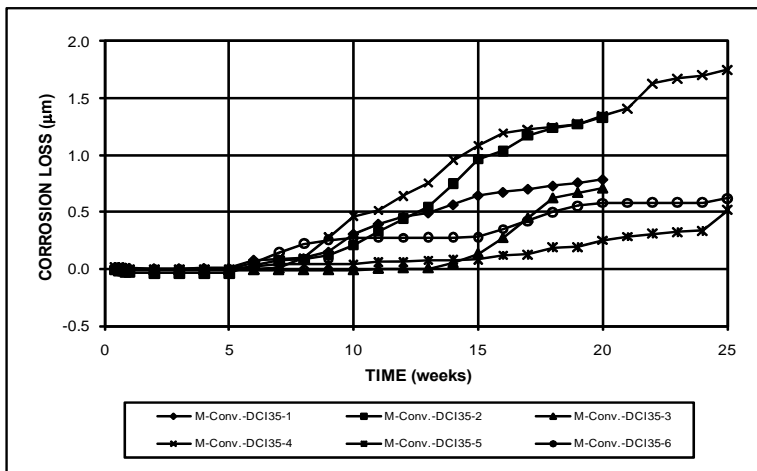


(b)

Figure A.10 – Macrocell Test. (a) Anode corrosion potentials and (b) cathode corrosion potentials with respect to a saturated calomel electrode for specimens with conventional steel and no inhibitors, $w/c = 0.35$.

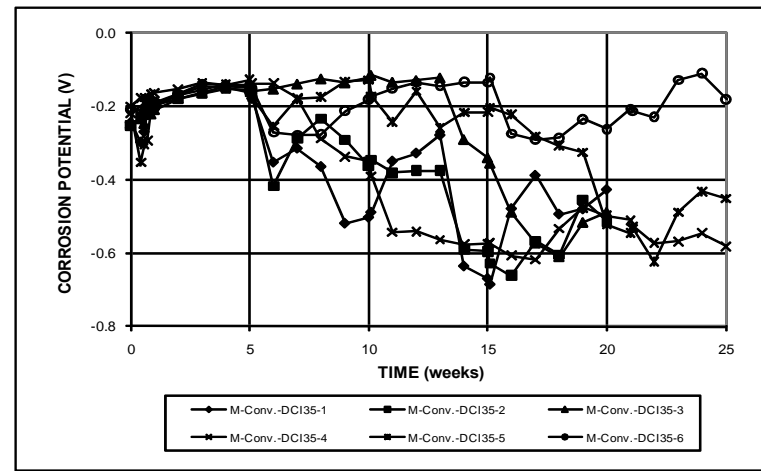


(a)

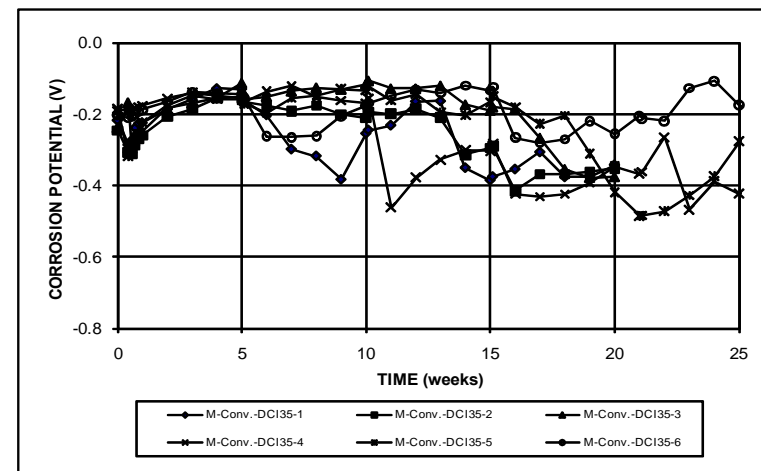


(b)

Figure A.11 – Macrocell Test. (a) Corrosion rates and (b) total corrosion losses for specimens with conventional steel and DCI inhibitor, $w/c=0.35$.

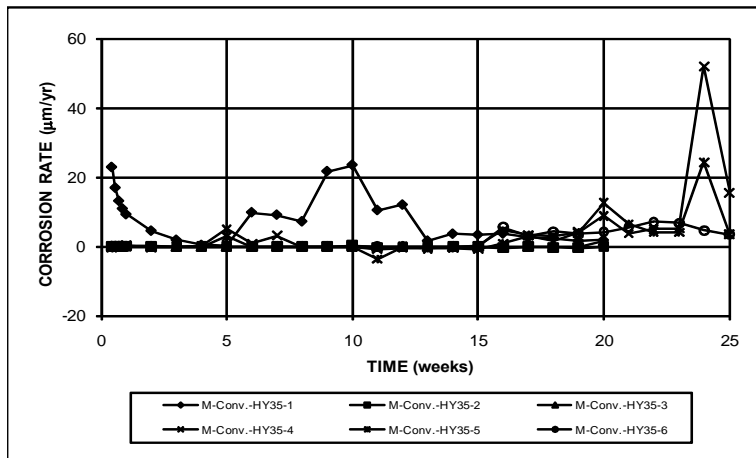


(a)

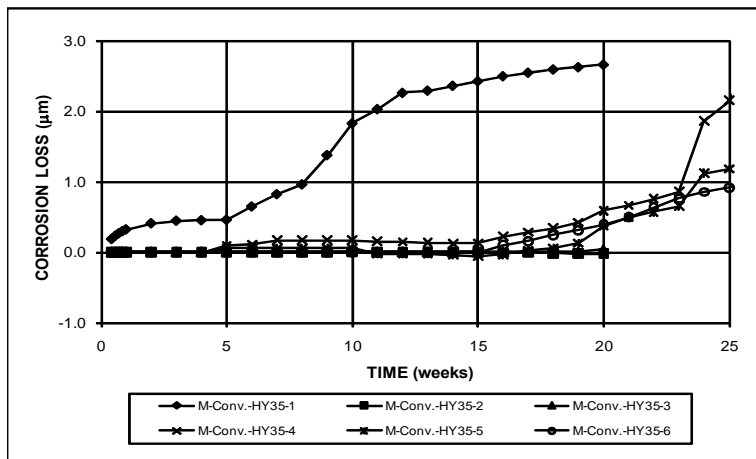


(b)

Figure A.12 – Macrocell Test. (a) Anode corrosion potentials and (b) cathode corrosion potentials with respect to a saturated calomel electrode for specimens with conventional steel and DCI inhibitor, $w/c=0.35$.

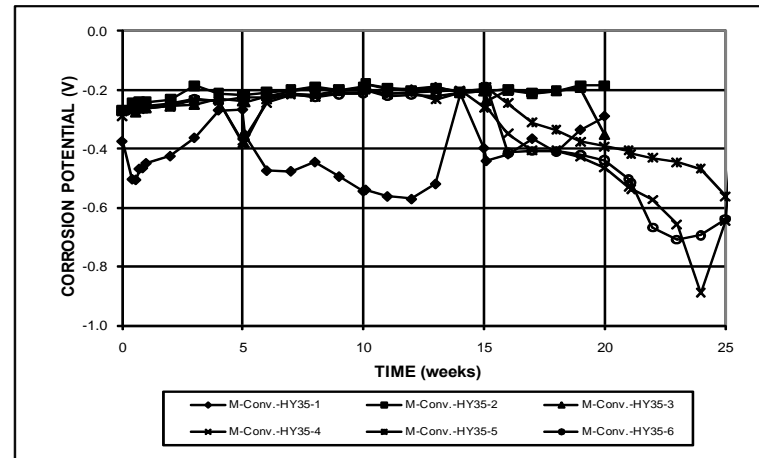


(a)

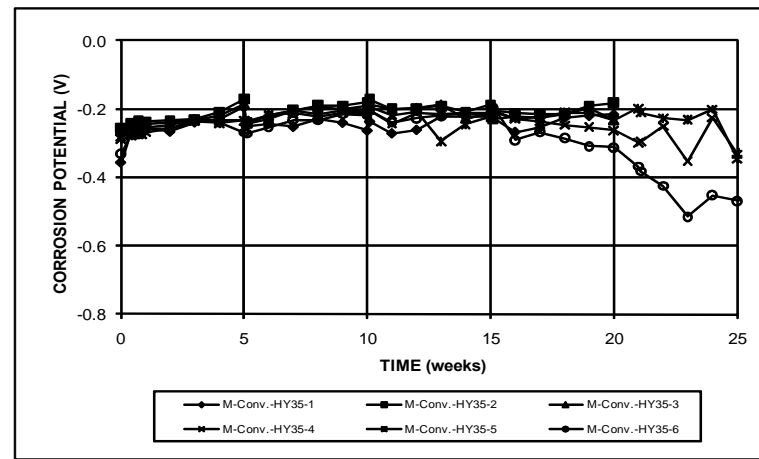


(b)

Figure A.13 – Macrocell Test. (a) Corrosion rates and (b) total corrosion losses for specimens with conventional steel and Hycrete inhibitor, $w/c = 0.35$.

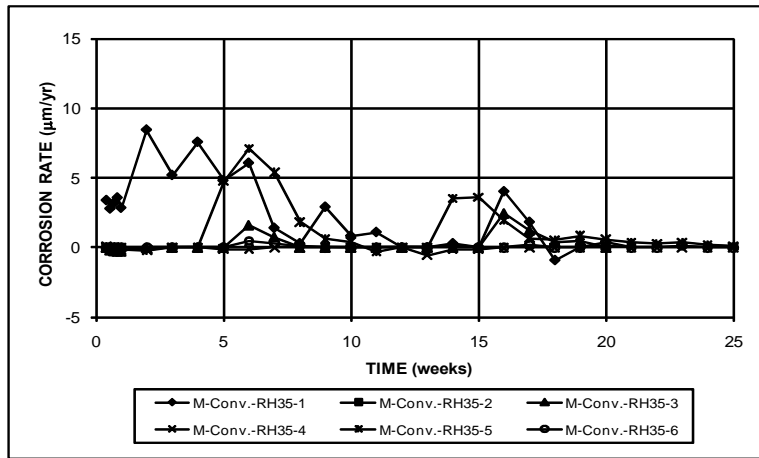


(a)

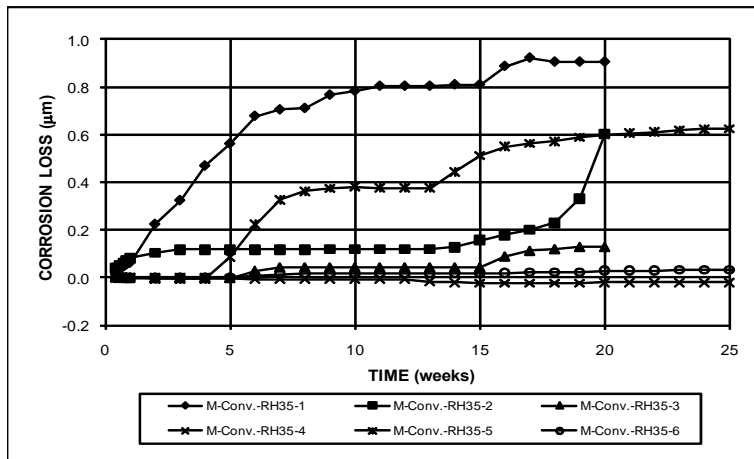


(b)

Figure A.14 – Macrocell Test. (a) Anode corrosion potentials and (b) cathode corrosion potentials with respect to a saturated calomel electrode for specimens with conventional steel and Hycrete inhibitor, $w/c = 0.35$.

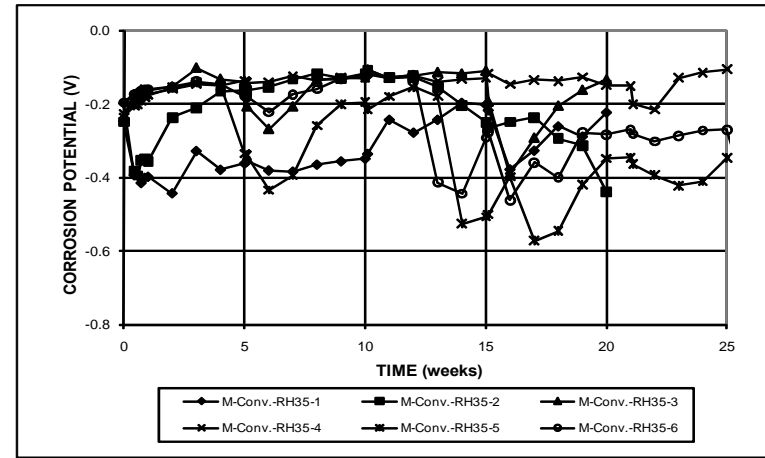


(a)

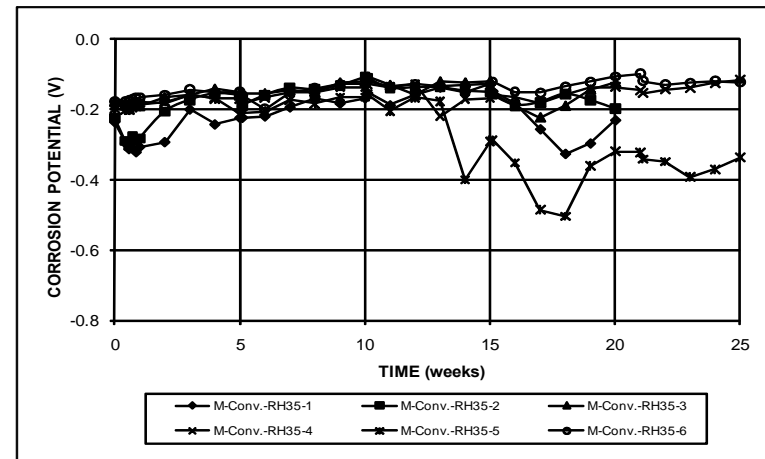


(b)

Figure A.15 – Macrocell Test. (a) Corrosion rates and (b) total corrosion losses for specimens with conventional steel and Rheocrete inhibitor, $w/c = 0.35$.

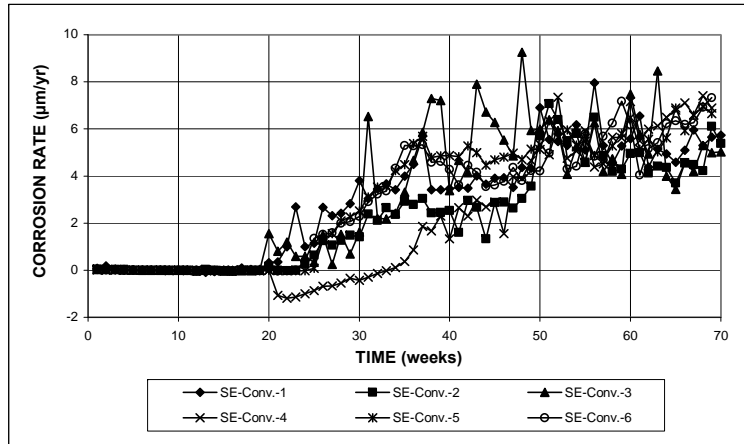


(a)

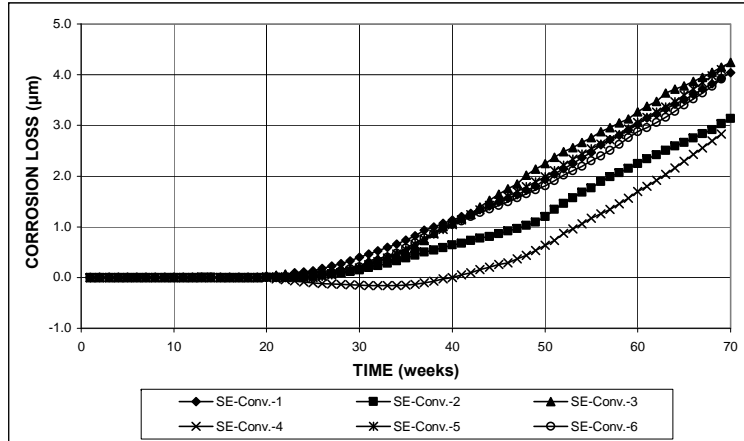


(b)

Figure A.16 – Macrocell Test. (a) Anode corrosion potentials and (b) cathode corrosion potentials with respect to a saturated calomel electrode for specimens with conventional steel and Rheocrete inhibitor, $w/c = 0.35$.

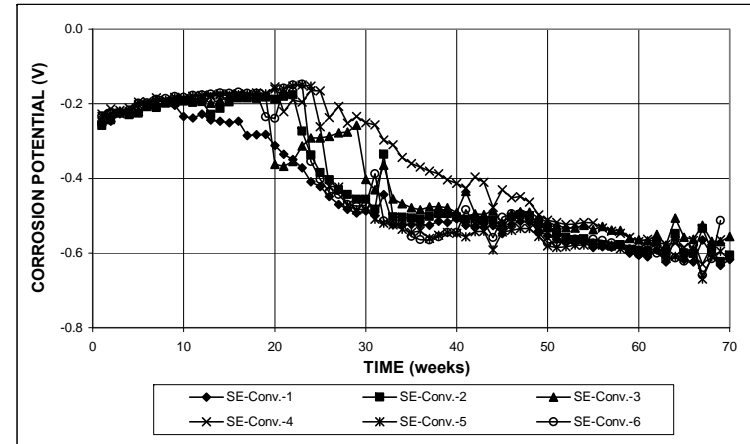


(a)

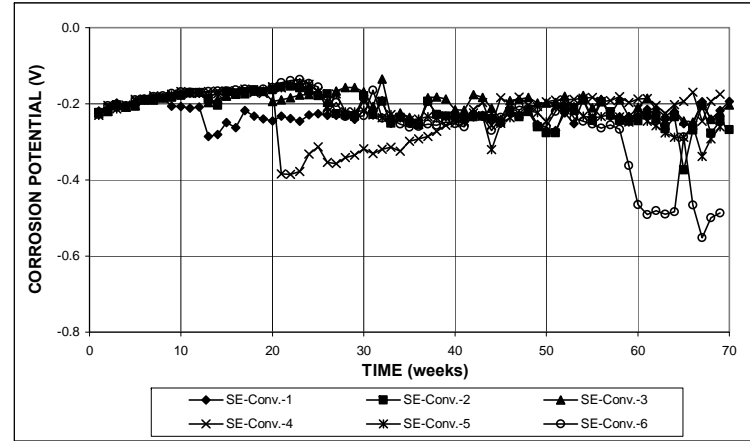


(b)

Figure A.17 – Southern Exposure Test. (a) Corrosion rates and (b) total corrosion losses for specimens with conventional steel.

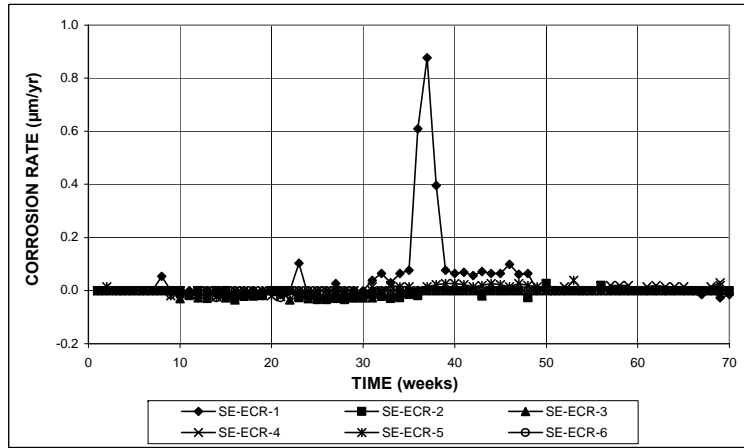


(a)

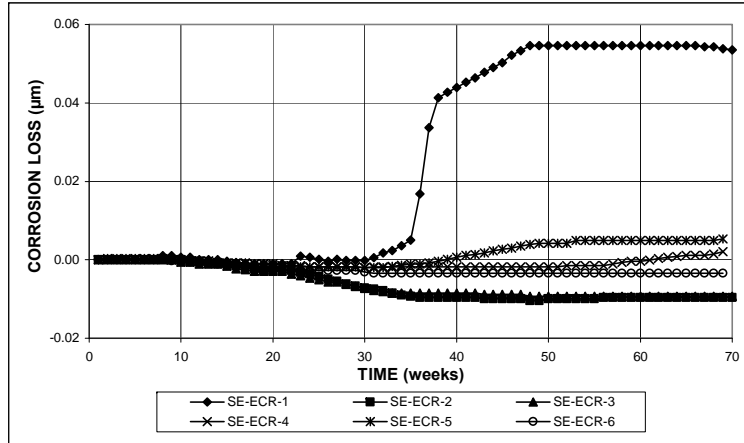


(b)

Figure A.18 – Southern Exposure Test. (a) Top mat corrosion potentials and (b) bottom mat corrosion potentials with respect to a copper-copper sulfate electrode for specimens with conventional steel.

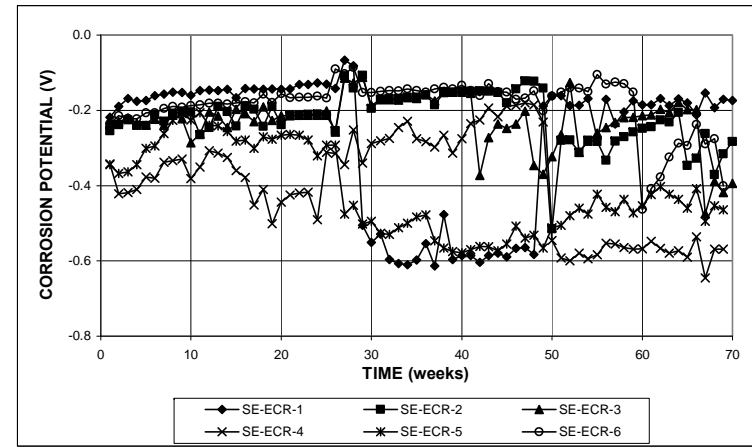


(a)

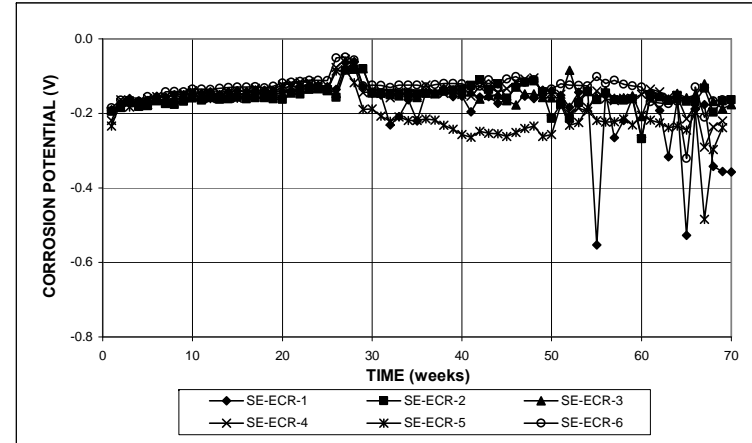


(b)

Figure A.19 – Southern Exposure Test. (a) Corrosion rates and (b) total corrosion losses for specimens with ECR (four holes).

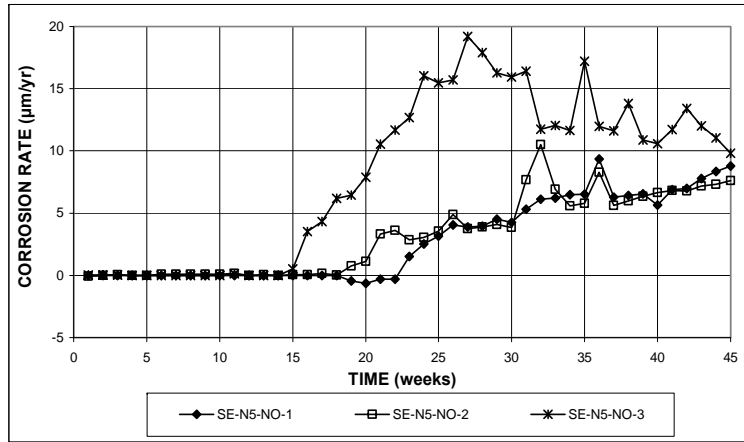


(a)

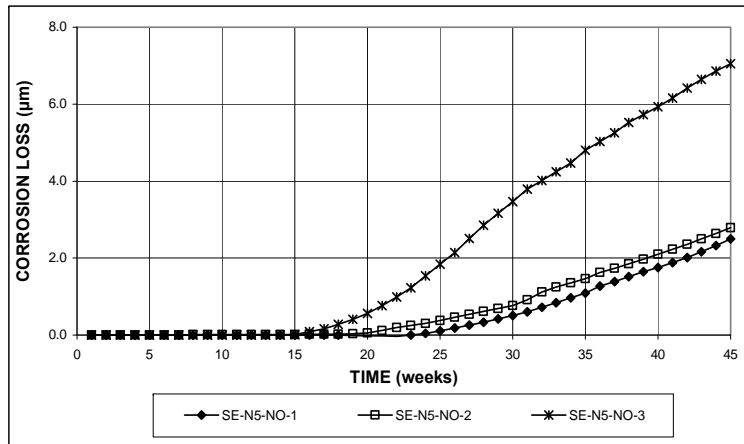


(b)

Figure A.20 – Southern Exposure Test. (a) Top mat corrosion potentials and (b) bottom mat corrosion potentials with respect to a copper-copper sulfate electrode for specimens with ECR (four holes).

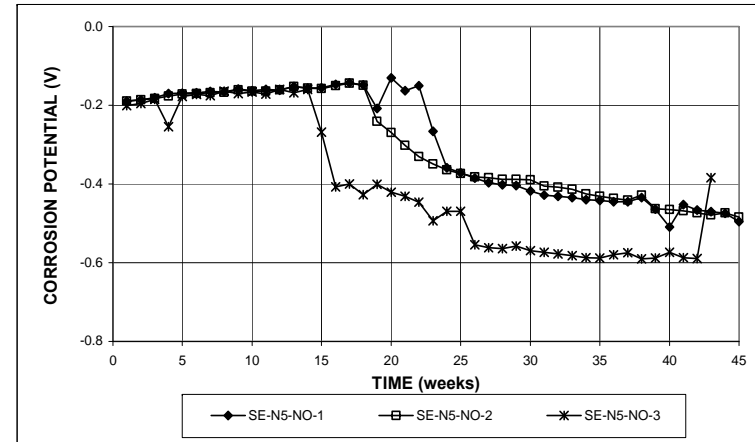


(a)

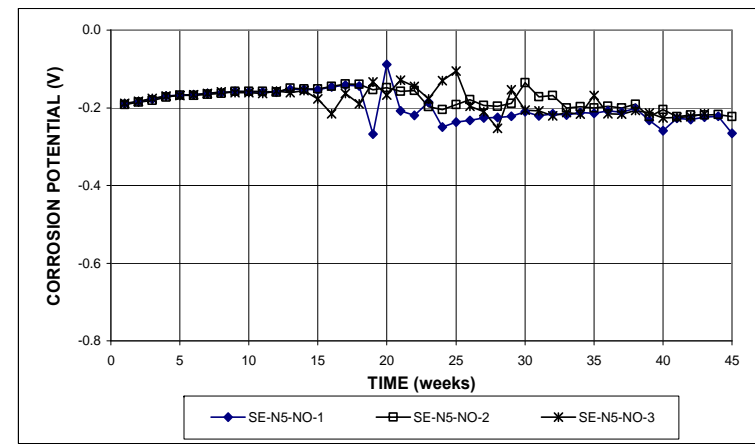


(b)

Figure A.21 – Southern Exposure Test. (a) Corrosion rates and (b) total corrosion losses for specimens with conventional steel and no inhibitor.

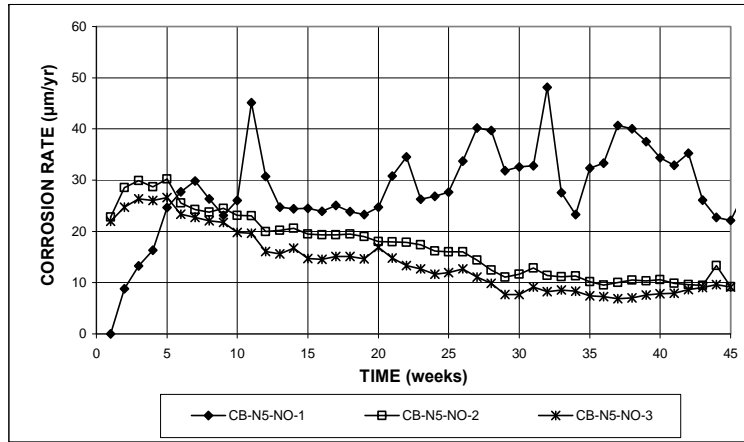


(a)

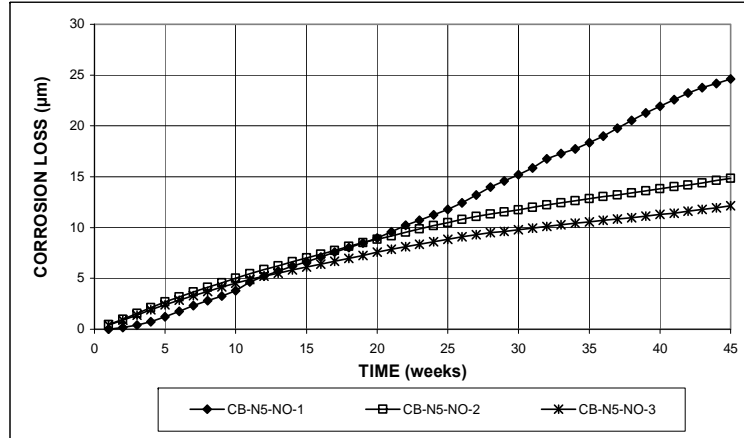


(b)

Figure A.22 – Southern Exposure Test. (a) Top mat corrosion potentials and (b) bottom mat corrosion potentials with respect to a copper-copper sulfate electrode for specimens with conventional steel and no inhibitor.

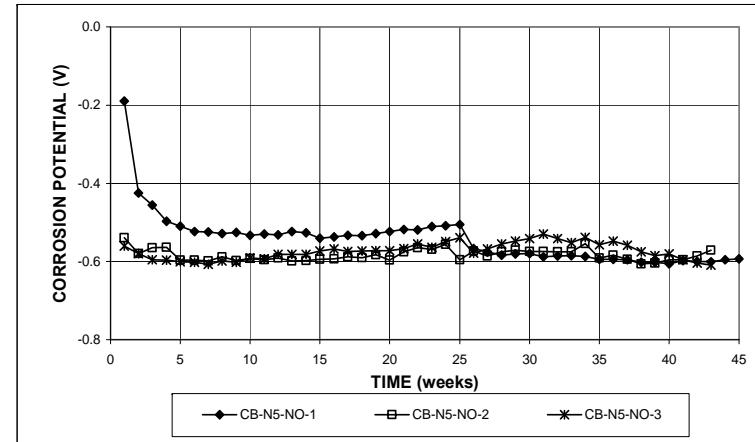


(a)

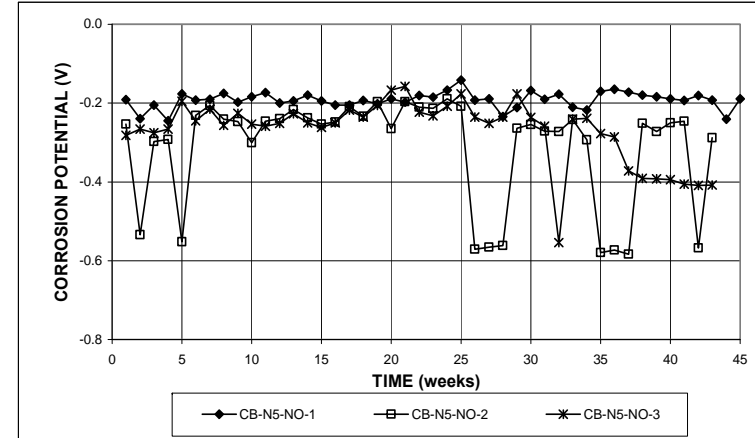


(b)

Figure A.23 – Cracked Beam Test. (a) Corrosion rates and (b) total corrosion losses for specimens with conventional steel and no inhibitor.

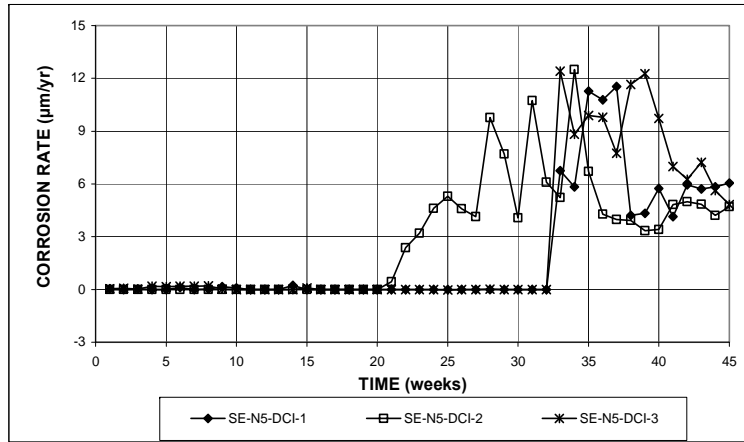


(a)

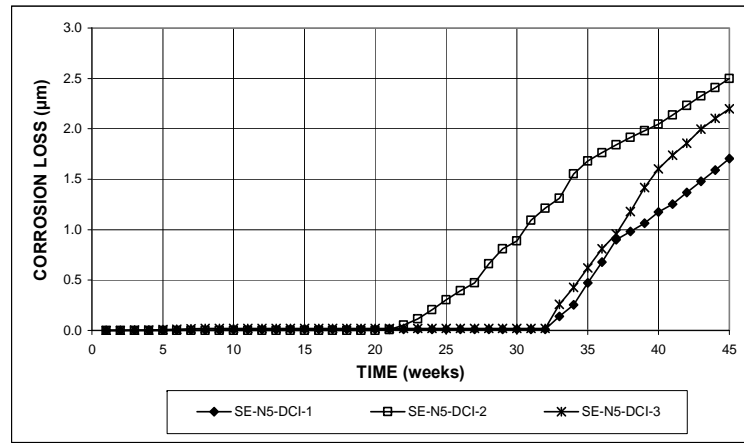


(b)

Figure A.24 – Cracked Beam Test. (a) Top mat corrosion potentials and (b) bottom mat corrosion potentials with respect to a copper-copper sulfate electrode for specimens with conventional steel and no inhibitor.

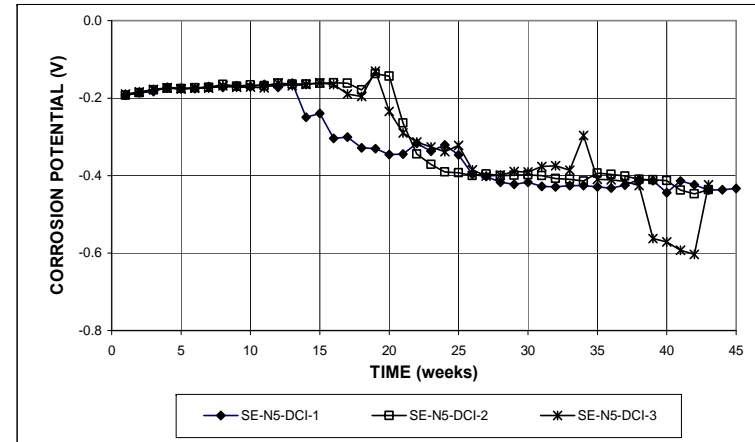


(a)

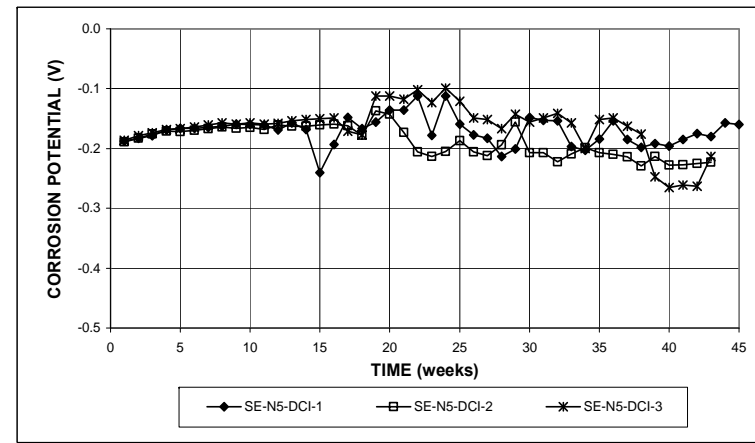


(b)

Figure A.25 – Southern Exposure Test. (a) Corrosion rates and (b) total corrosion losses for specimens with conventional steel and DCI inhibitor.

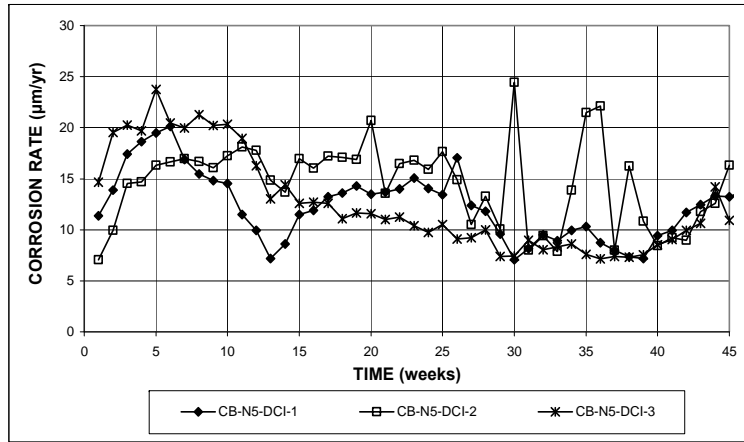


(a)

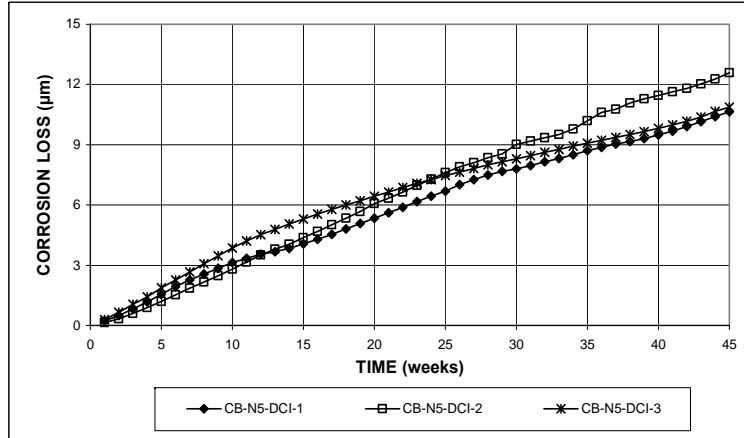


(b)

Figure A.26 – Southern Exposure Test. (a) Top mat corrosion potentials and (b) bottom mat corrosion potentials with respect to a copper-copper sulfate electrode for specimens with conventional steel and DCI inhibitor.

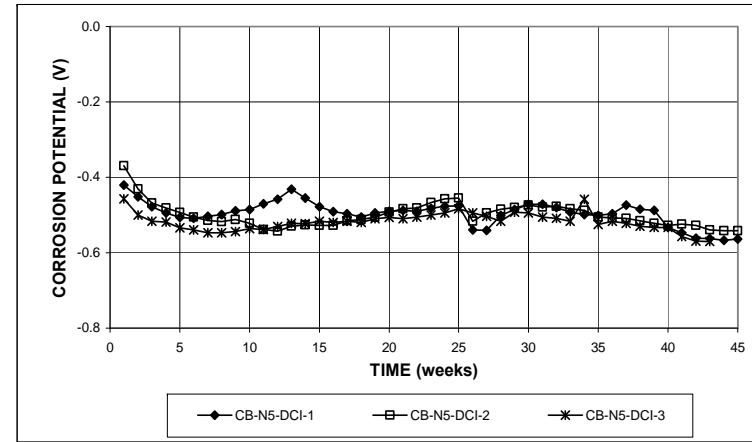


(a)

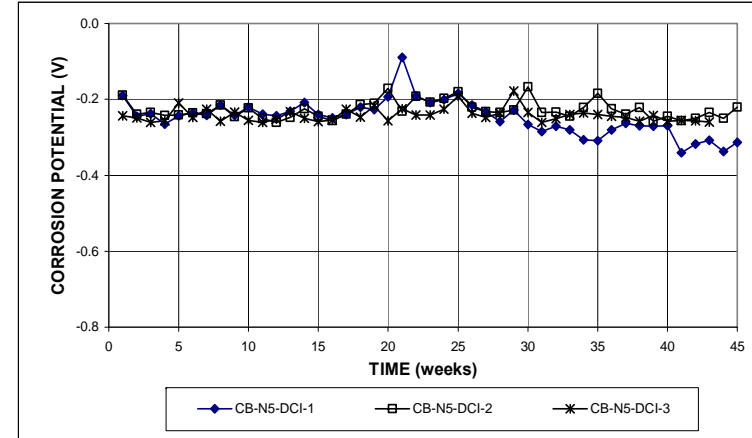


(b)

Figure A.27 – Cracked Beam Test. (a) Corrosion rates and (b) total corrosion losses for specimens with conventional steel and DCI inhibitor.

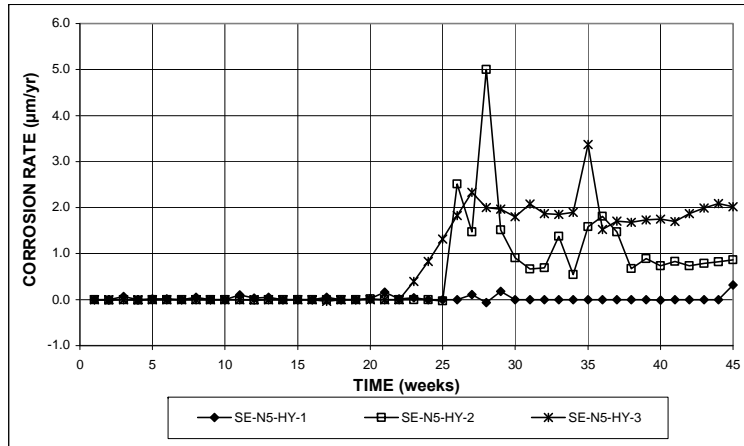


(a)

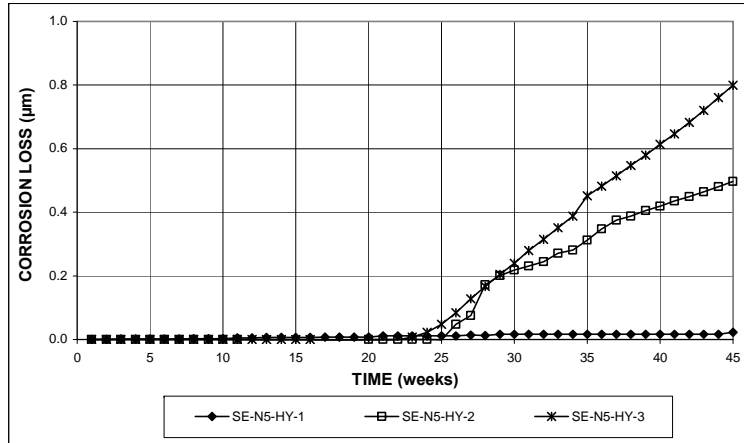


(b)

Figure A.28 – Cracked Beam Test. (a) Top mat corrosion potentials and (b) bottom mat corrosion potentials with respect to a copper-copper sulfate electrode for specimens with conventional steel and DCI inhibitor.

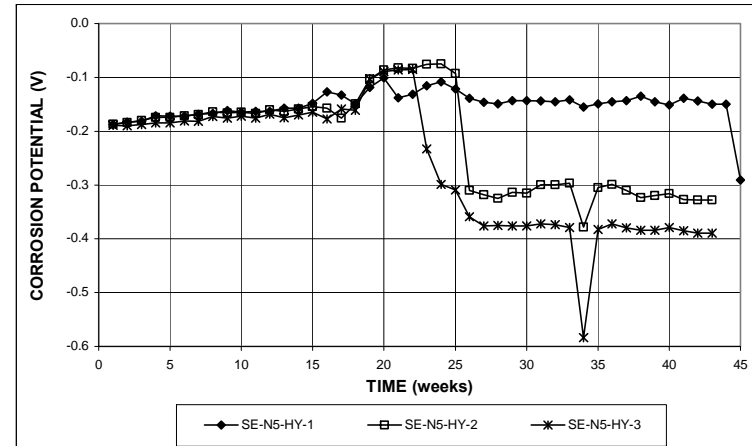


(a)

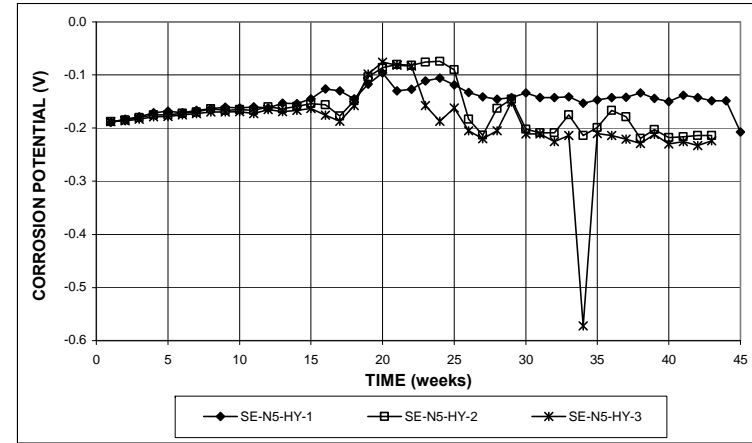


(b)

Figure A.29 – Southern Exposure Test. (a) Corrosion rates and (b) total corrosion losses for specimens with conventional steel and Hycrete inhibitor.

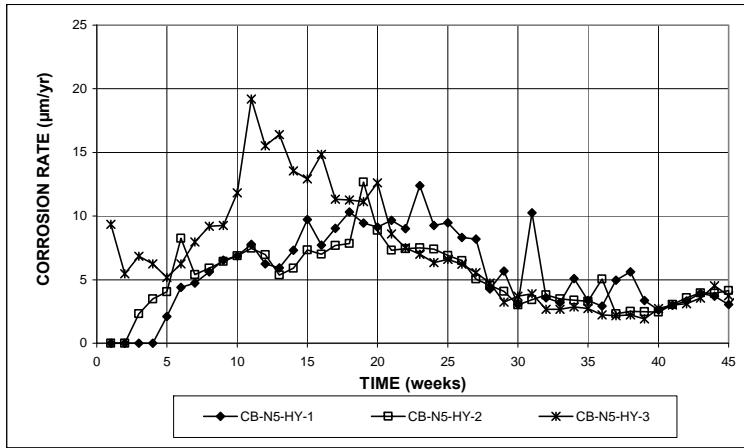


(a)

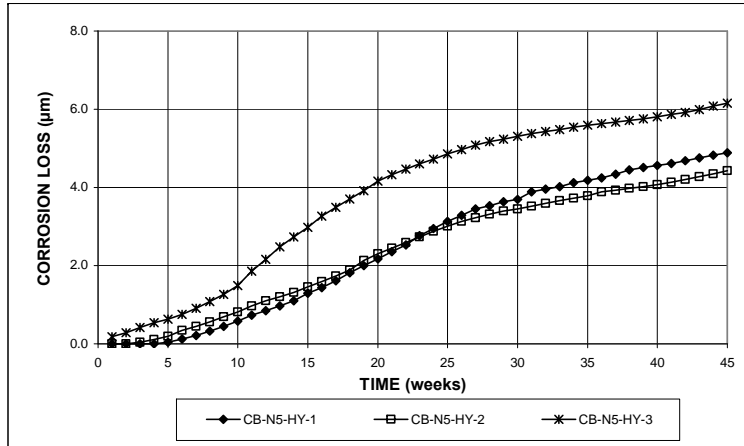


(b)

Figure A.30 – Southern Exposure Test. (a) Top mat corrosion potentials and (b) bottom mat corrosion potentials with respect to a copper-copper sulfate electrode for specimens with conventional steel and Hycrete inhibitor.

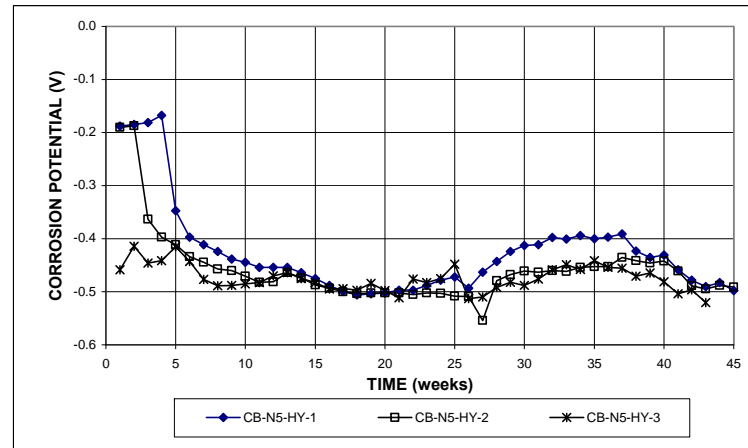


(a)

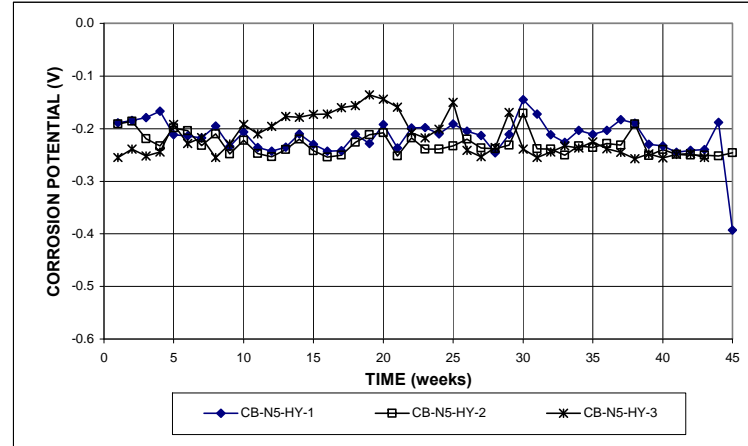


(b)

Figure A.31 – Cracked Beam Test. (a) Corrosion rates and (b) total corrosion losses for specimens with conventional steel and Hycrete inhibitor.

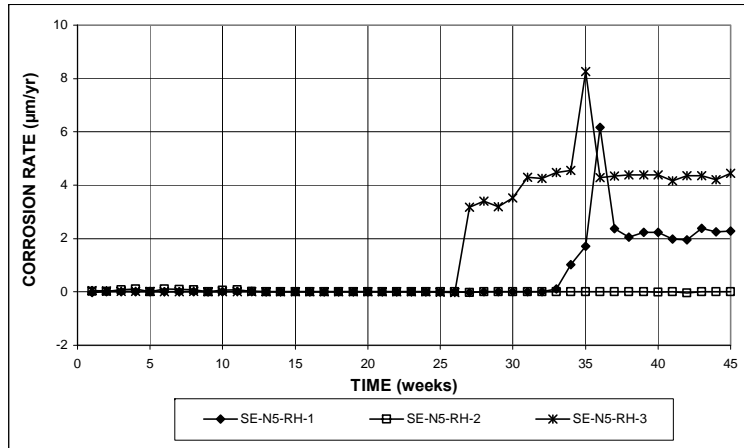


(a)

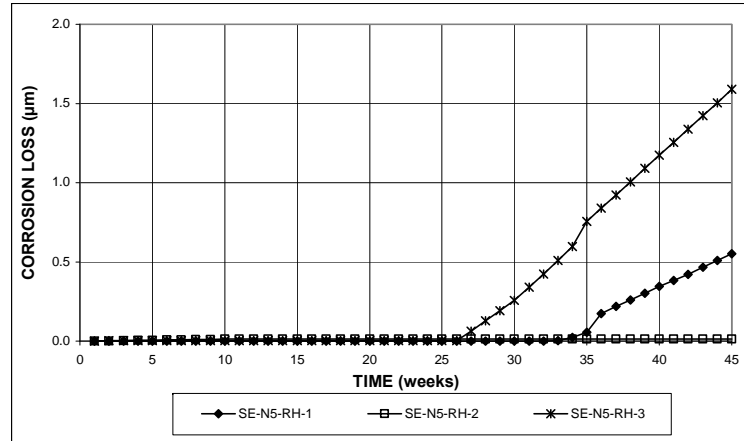


(b)

Figure A.32 – Cracked Beam Test. (a) Top mat corrosion potentials and (b) bottom mat corrosion potentials with respect to a copper-copper sulfate electrode for specimens with conventional steel and Hycrete inhibitor.

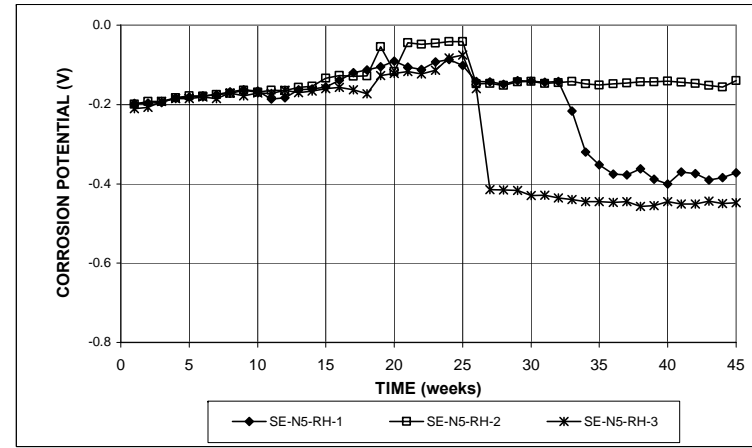


(a)

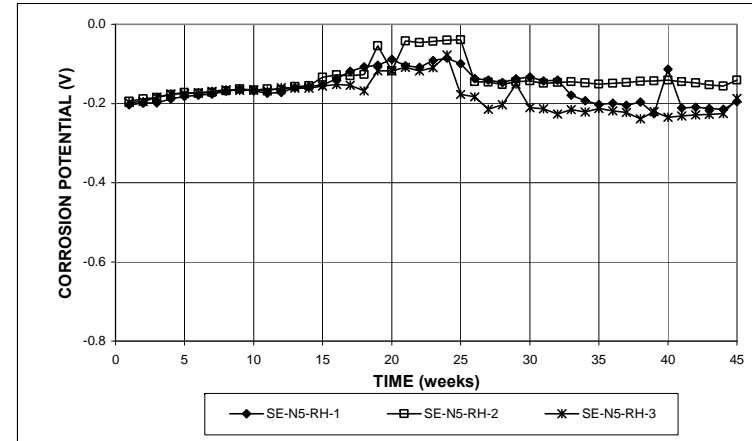


(b)

Figure A.33 – Southern Exposure Test. (a) Corrosion rates and (b) total corrosion losses for specimens with conventional steel and Rheocrete inhibitor.

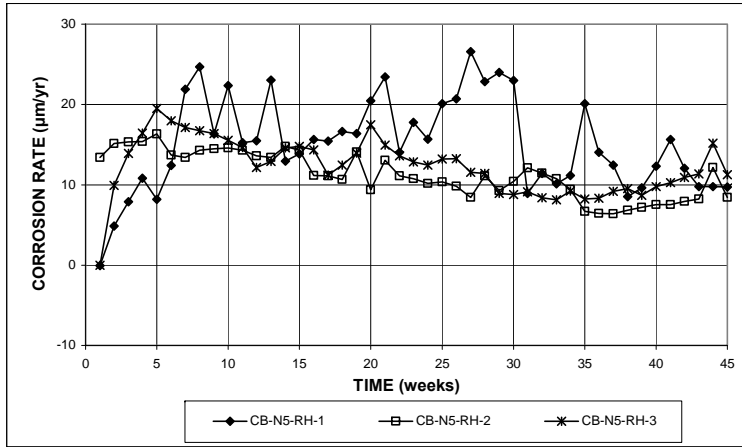


(a)

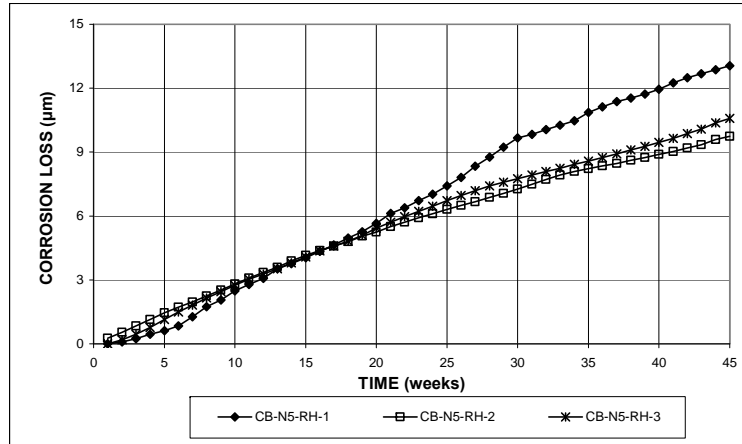


(b)

Figure A.34 – Southern Exposure Test. (a) Top mat corrosion potentials and (b) bottom mat corrosion potentials with respect to a copper-copper sulfate electrode for specimens with conventional steel and Rheocrete inhibitor.

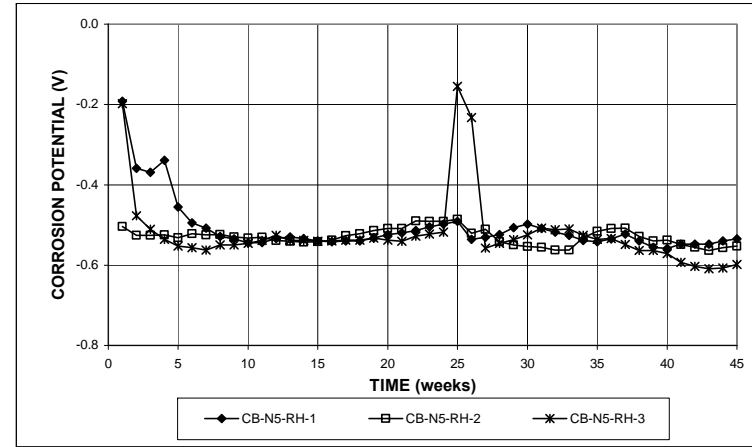


(a)

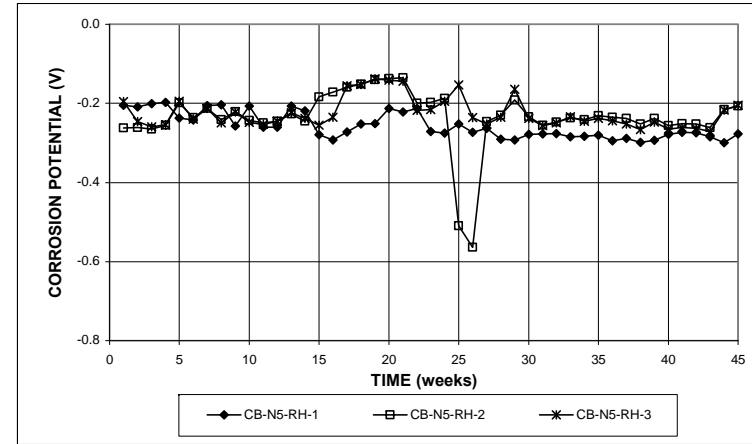


(b)

Figure A.35 – Cracked Beam Test. (a) Corrosion rates and (b) total corrosion losses for specimens with conventional steel and Rheocrete inhibitor.

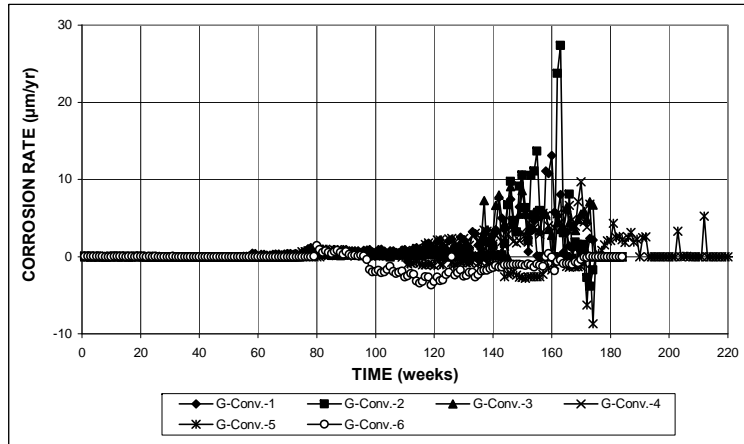


(a)

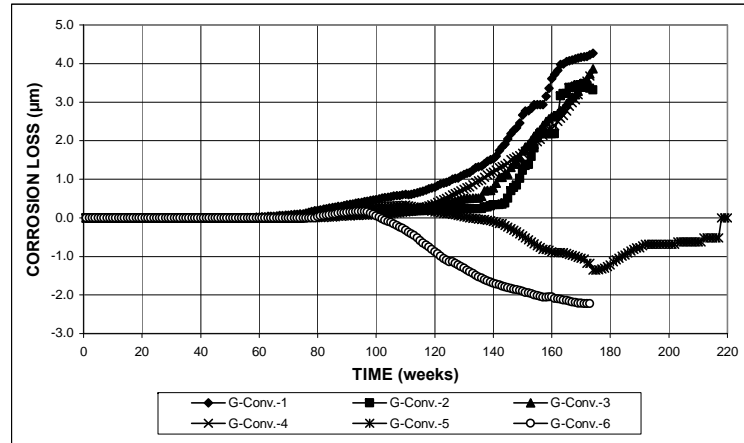


(b)

Figure A.36 – Cracked Beam Test. (a) Top mat corrosion potentials and (b) bottom mat corrosion potentials with respect to a copper-copper sulfate electrode for specimens with conventional steel and Rheocrete inhibitor.

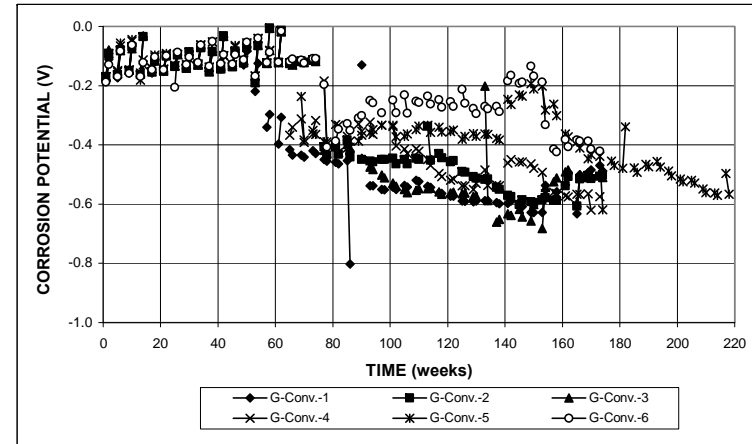


(a)

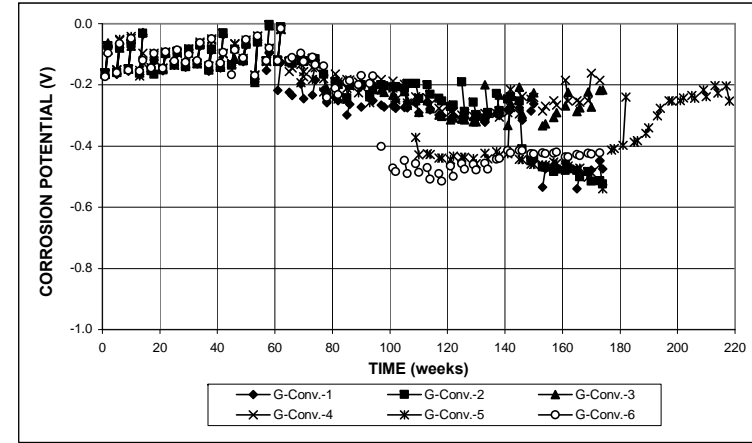


(b)

Figure A.37 – ASTM G109 Test. (a) Corrosion rates and (b) total corrosion losses for specimens with conventional steel.

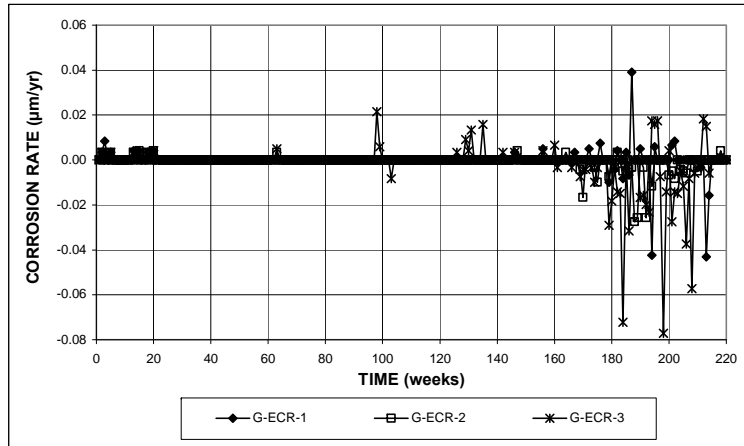


(a)

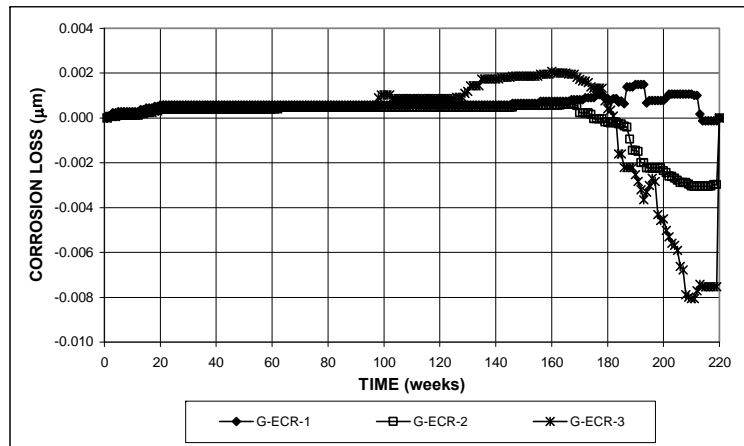


(b)

Figure A.38 – ASTM G109 Test. (a) Top mat corrosion potentials and (b) bottom mat corrosion potentials with respect to a copper-copper sulfate electrode for specimens with conventional steel.

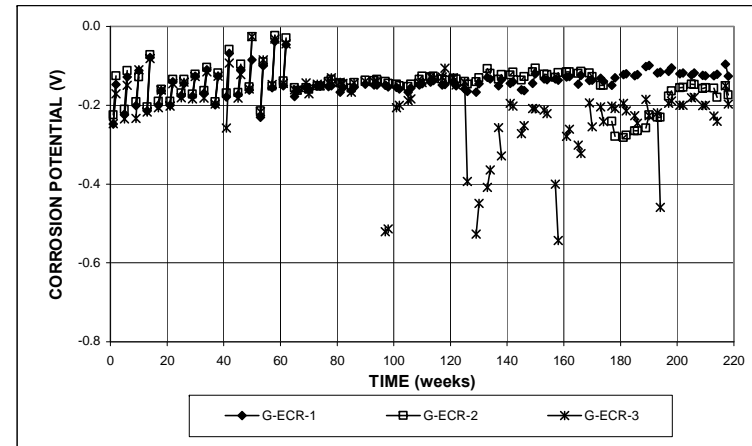


(a)

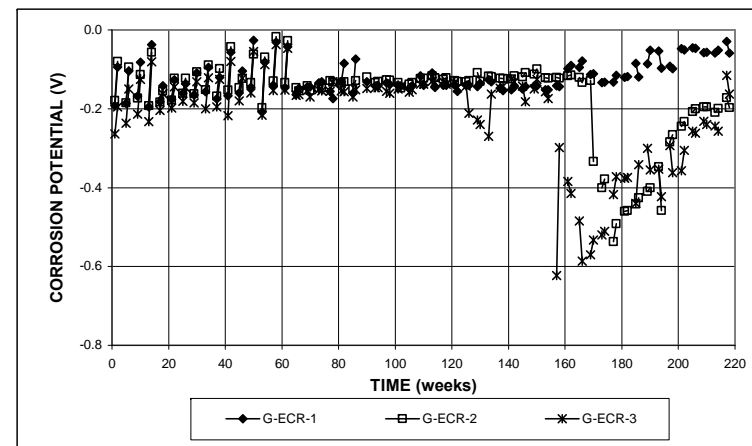


(b)

Figure A.39 – ASTM G109 Test. (a) Corrosion rates and (b) total corrosion losses for specimens with ECR (four holes).

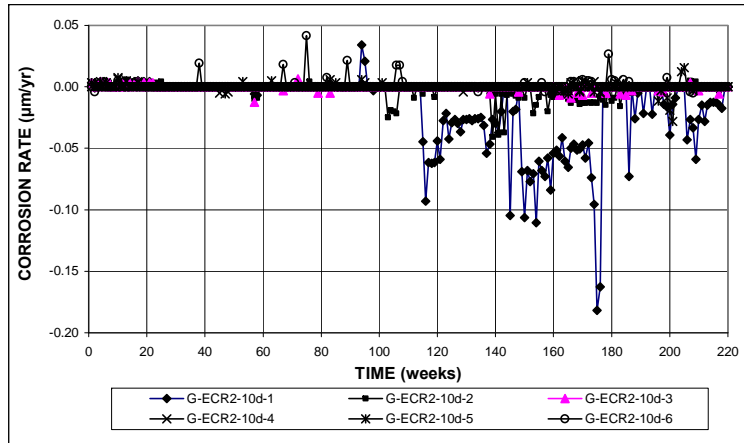


(a)

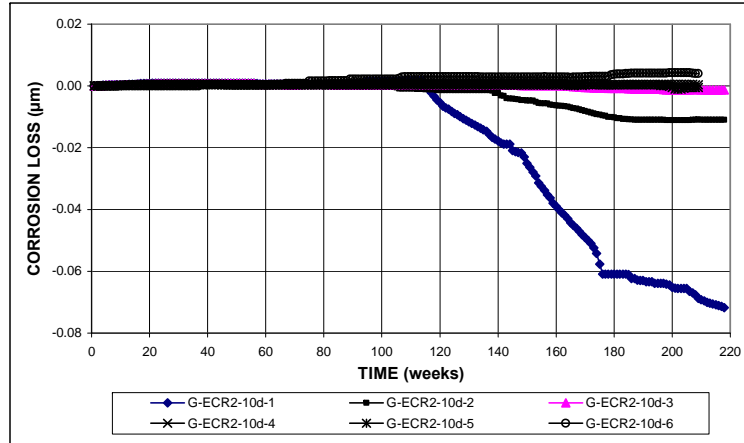


(b)

Figure A.40 – ASTM G109 Test. (a) Top mat corrosion potentials and (b) bottom mat corrosion potentials with respect to a copper-copper sulfate electrode for specimens with ECR (four holes).

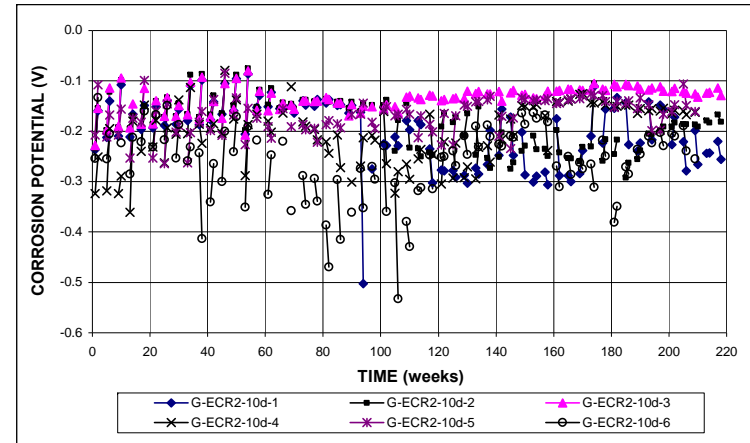


(a)

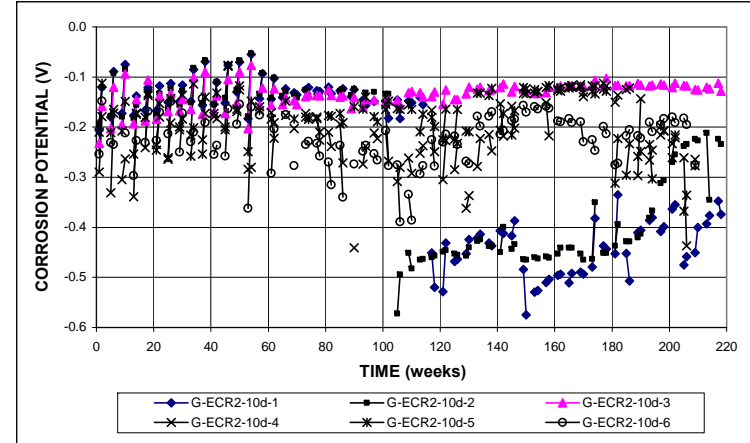


(b)

Figure A.41 – ASTM G109 Test. (a) Corrosion rates and (b) total corrosion losses for specimens with ECR (ten holes).

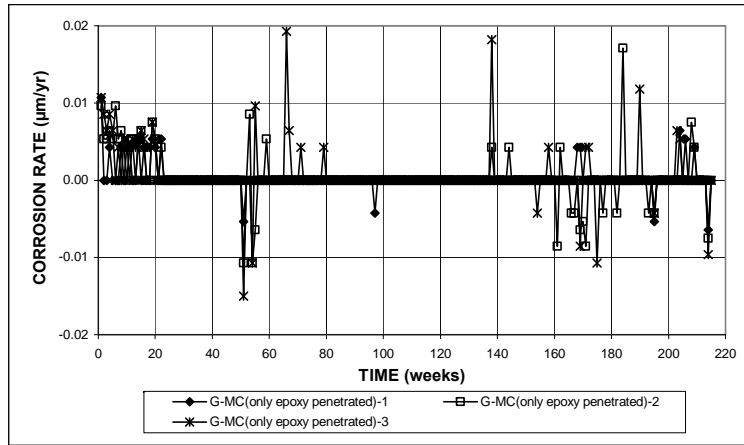


(a)

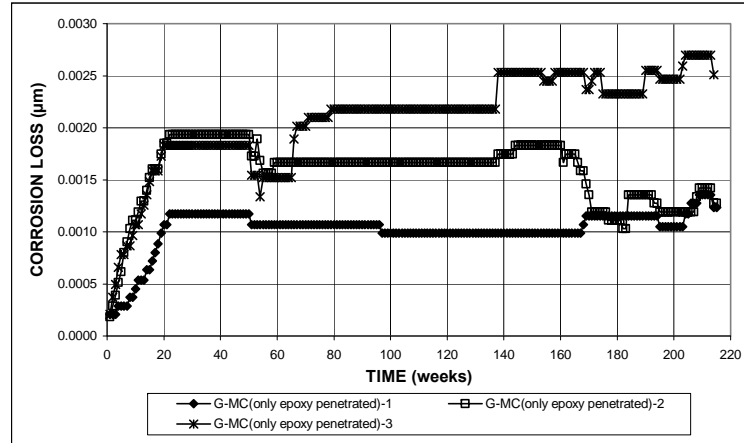


(b)

Figure A.42 – ASTM G109 Test. (a) Top mat corrosion potentials and (b) bottom mat corrosion potentials with respect to a copper-copper sulfate electrode for specimens with ECR (ten holes).

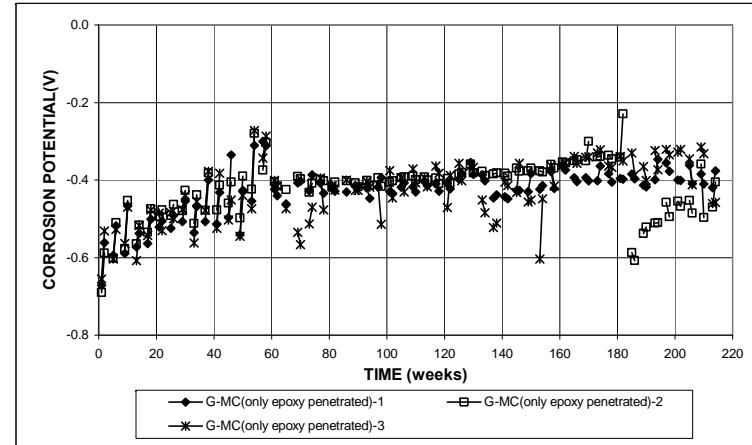


(a)

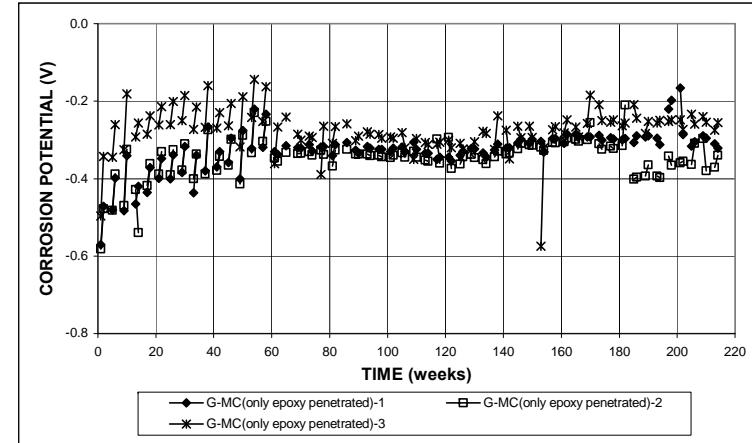


(b)

Figure A.43 – ASTM G109 Test. (a) Corrosion rates and (b) total corrosion losses for specimens with multiple-coated bars (four holes, only epoxy penetrated).

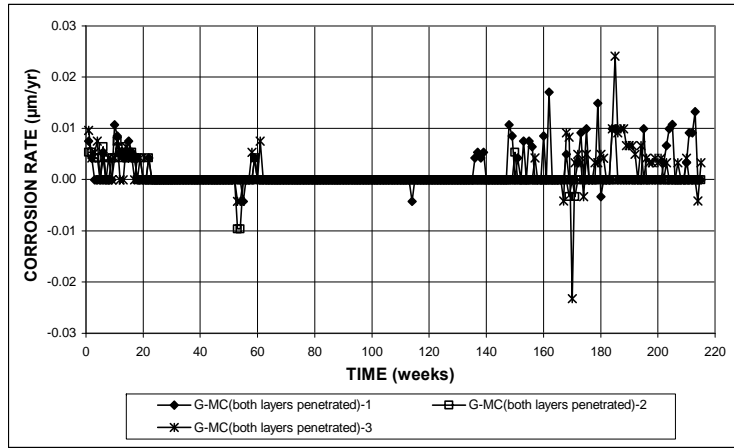


(a)

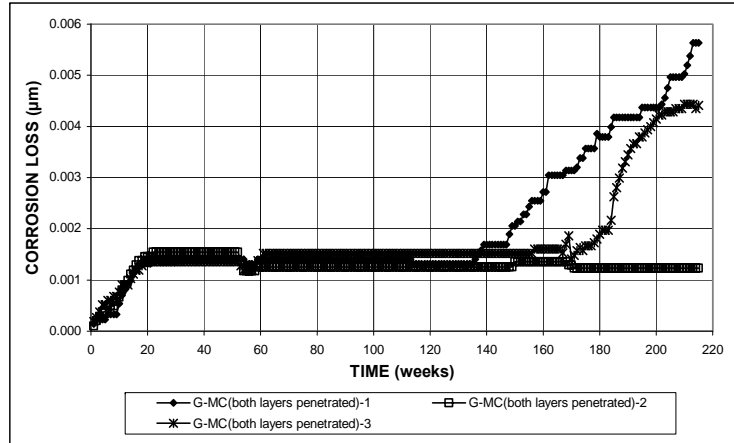


(b)

Figure A.44 – ASTM G109 Test. (a) Top mat corrosion potentials and (b) bottom mat corrosion potentials with respect to a copper-copper sulfate electrode for specimens with multiple-coated bars (four holes, only epoxy penetrated).

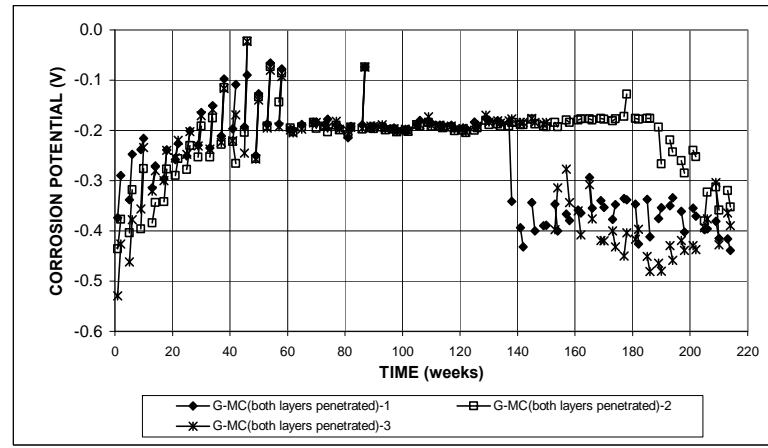


(a)

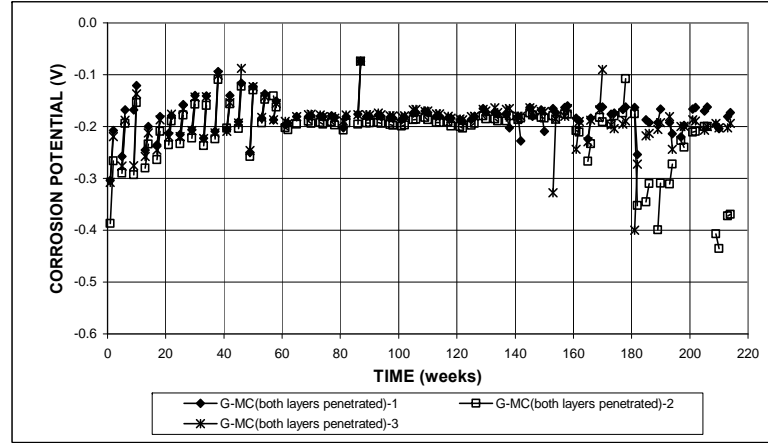


(b)

Figure A.45 – ASTM G109 Test. (a) Corrosion rates and (b) total corrosion losses for specimens with multiple-coated bars (four holes, both layers penetrated).

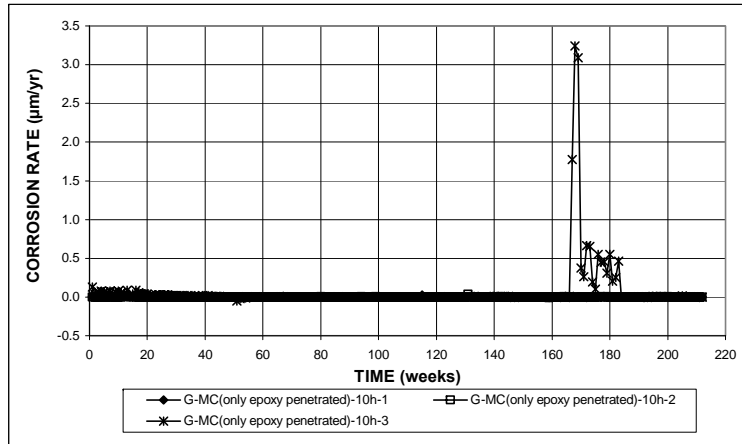


(a)

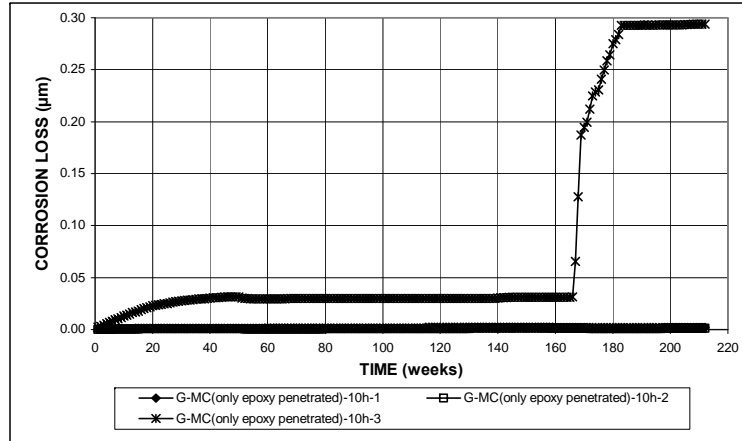


(b)

Figure A.46 – ASTM G109 Test. (a) Top mat corrosion potentials and (b) bottom mat corrosion potentials with respect to a copper-copper sulfate electrode for specimens with multiple-coated bars (four holes, both layers penetrated).

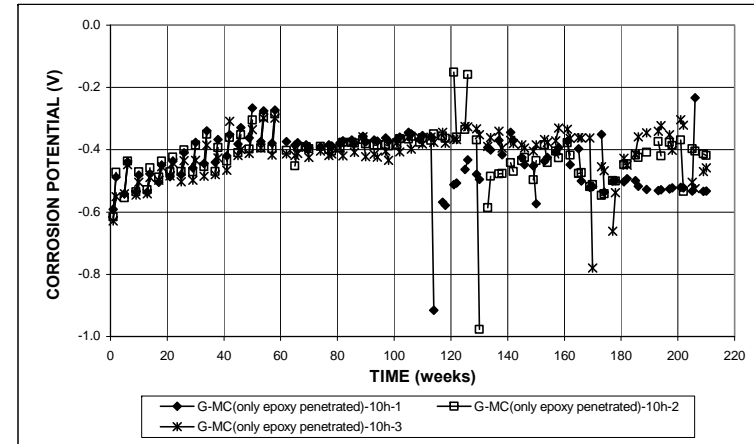


(a)

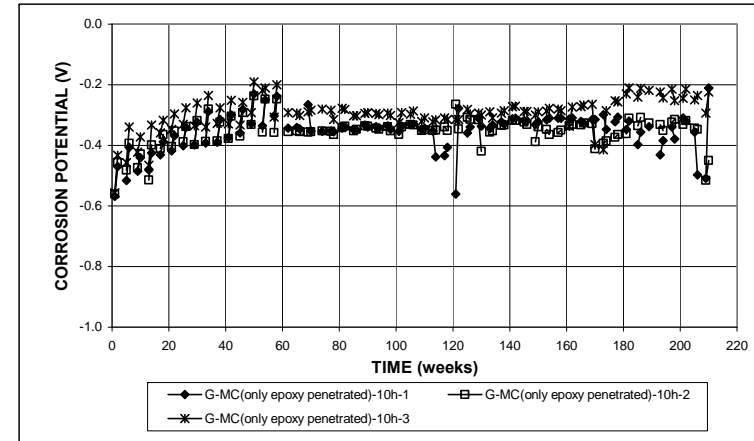


(b)

Figure A.47 – ASTM G109 Test. (a) Corrosion rates and (b) total corrosion losses for specimens with multiple-coated bars (ten holes, only epoxy penetrated).

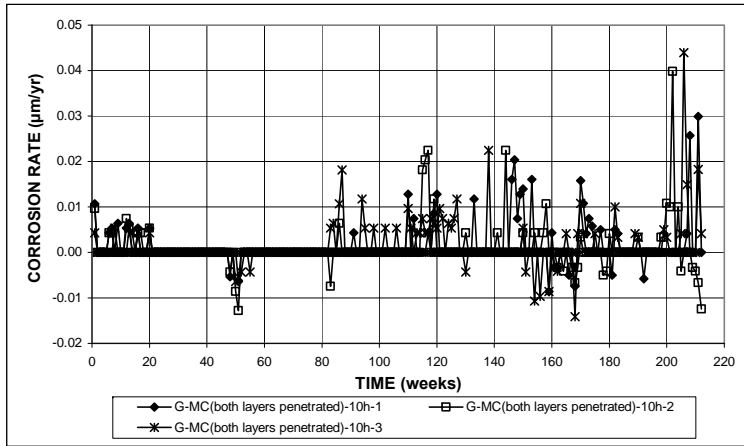


(a)

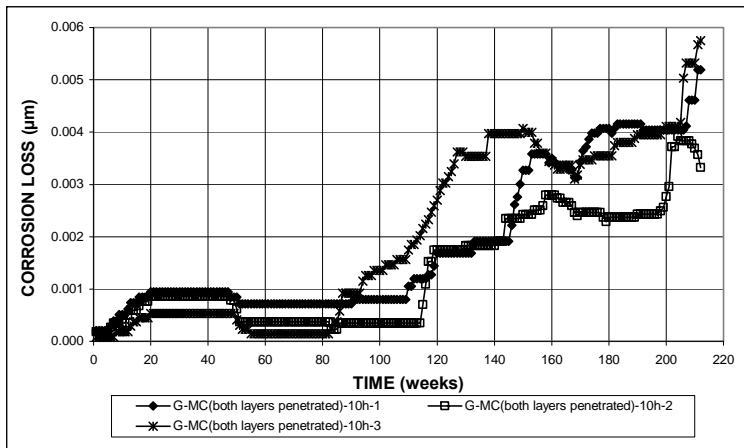


(b)

Figure A.48 – ASTM G109 Test. (a) Top mat corrosion potentials and (b) bottom mat corrosion potentials with respect to a copper-copper sulfate electrode for specimens with multiple-coated bars (ten holes, only epoxy penetrated).

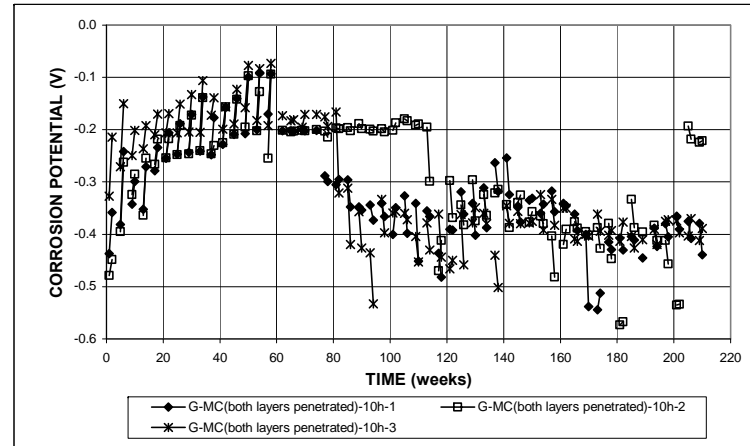


(a)

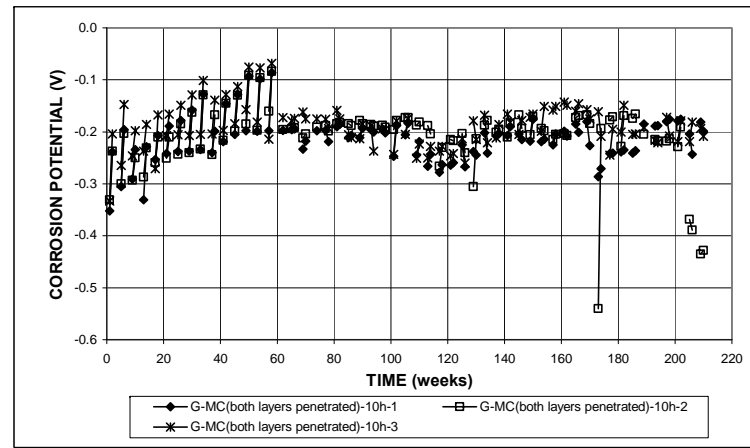


(b)

Figure A.49 – ASTM G109 Test. (a) Corrosion rates and (b) total corrosion losses for specimens with multiple coated bars (ten holes, both layers penetrated).

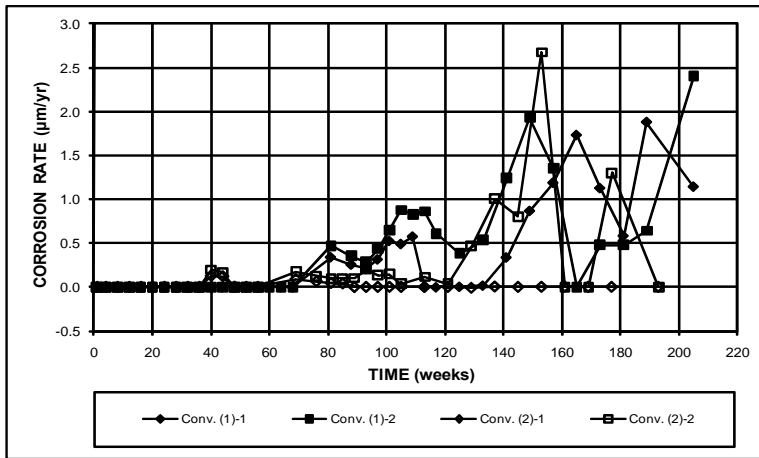


(a)

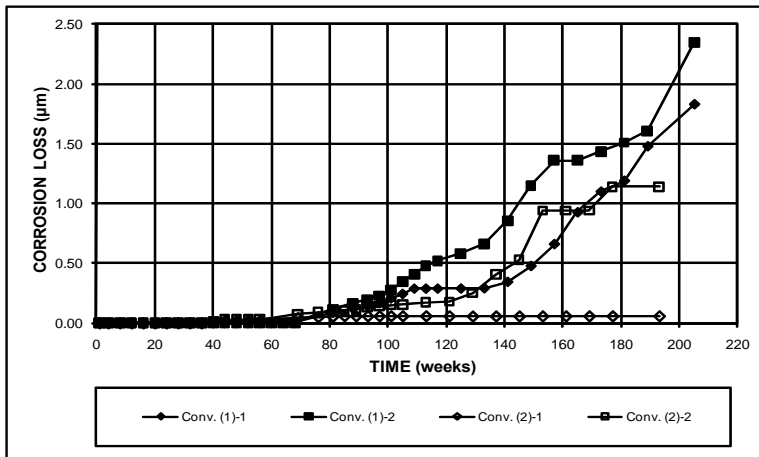


(b)

Figure A.50 – ASTM G109 Test. (a) Top mat corrosion potentials and (b) bottom mat corrosion potentials with respect to a copper-copper sulfate electrode for specimens with multiple coated bars (ten holes, both layers penetrated).

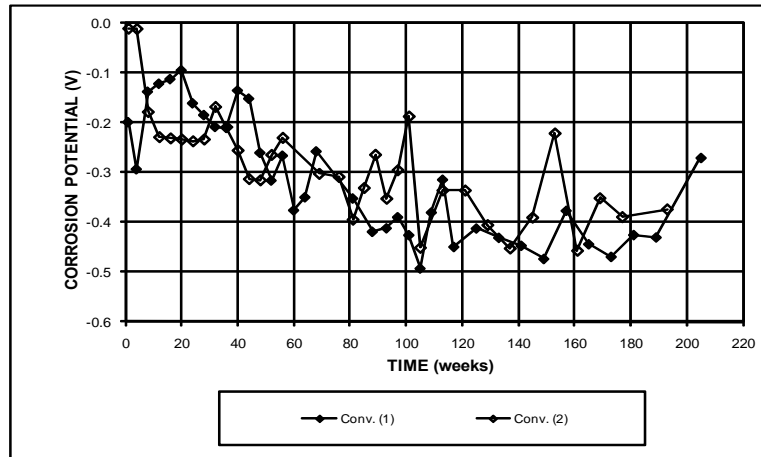


(a)

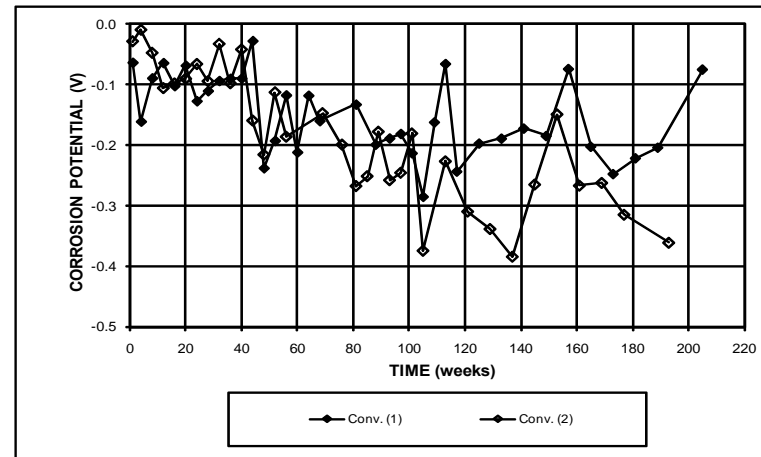


(b)

Figure A.51 – Field Test. (a) Corrosion rates and (b) total corrosion losses for specimens with conventional steel, without cracks.

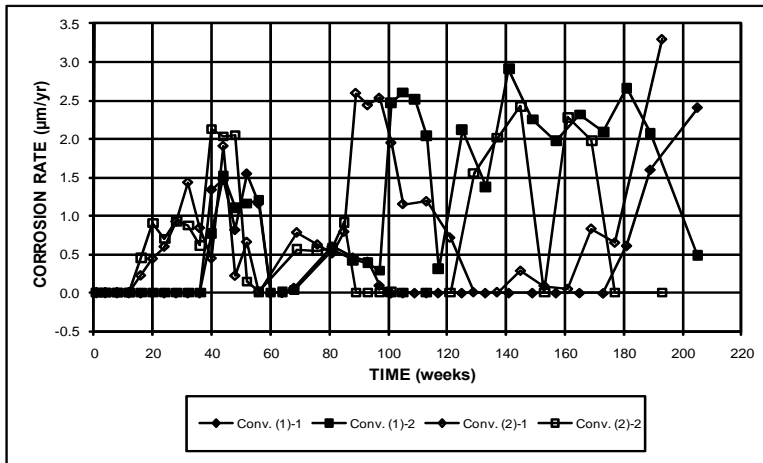


(a)

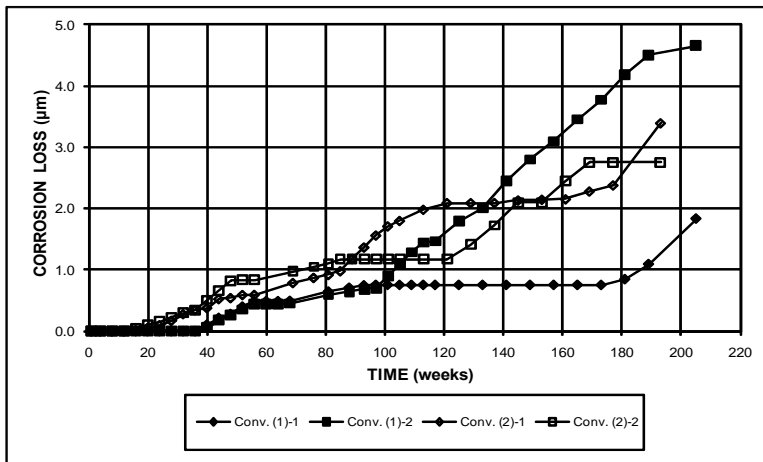


(b)

Figure A.52 – Field Test. (a) Top mat corrosion potentials and (b) bottom mat corrosion potentials with respect to a copper-copper sulfate electrode for specimens with conventional steel, without cracks.

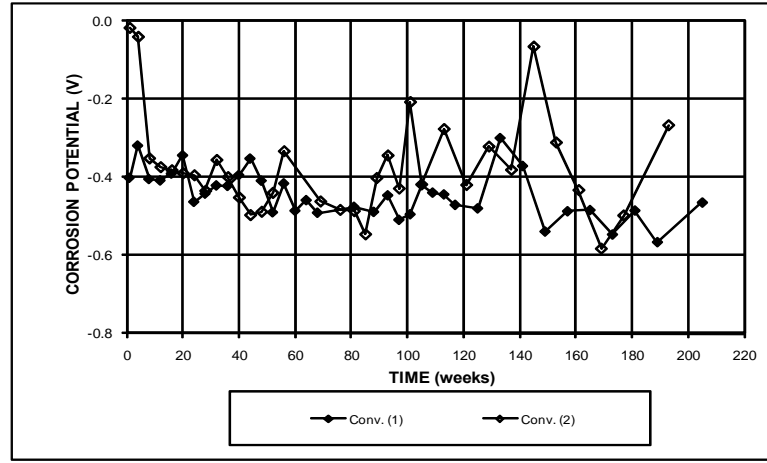


(a)

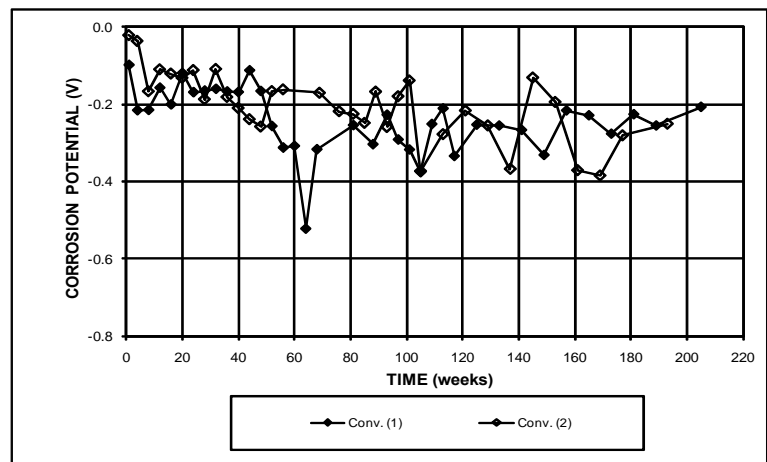


(b)

Figure A.53 – Field Test. (a) Corrosion rates and (b) total corrosion losses for specimens with conventional steel, with cracks.

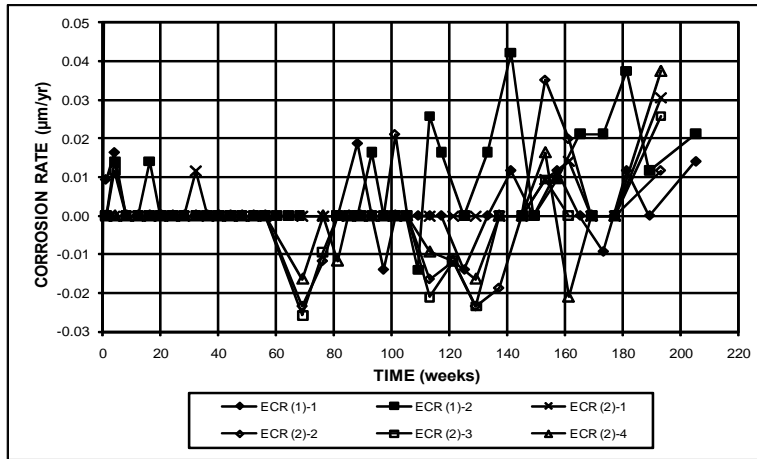


(a)

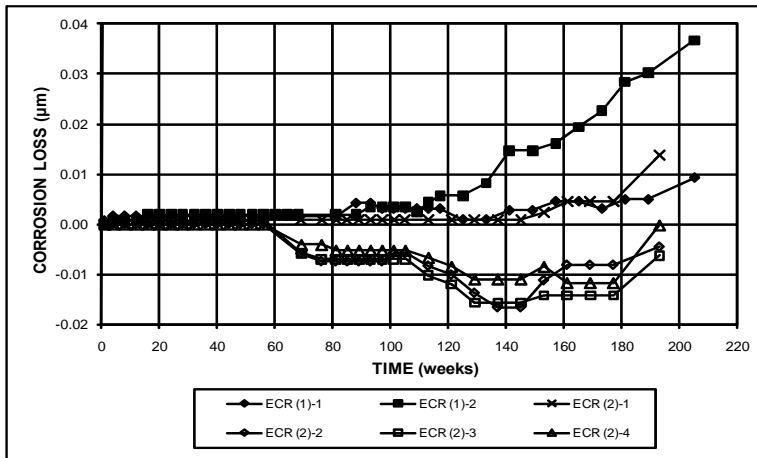


(b)

Figure A.54 – Field Test. (a) Top mat corrosion potentials and (b) bottom mat corrosion potentials with respect to a copper-copper sulfate electrode for specimens with conventional steel, with cracks.

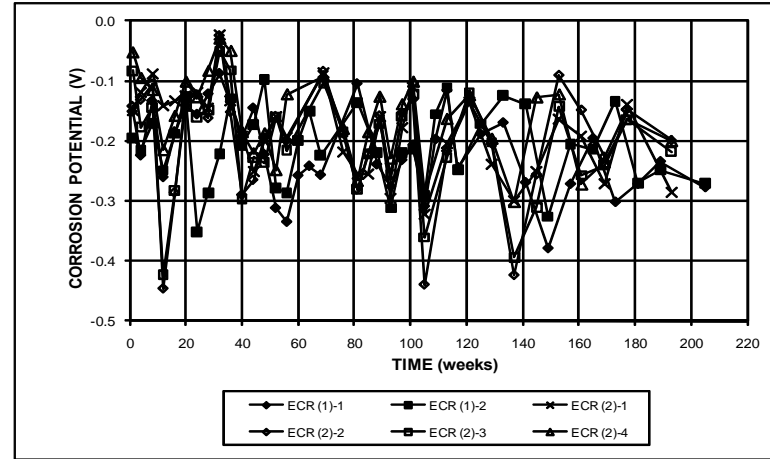


(a)

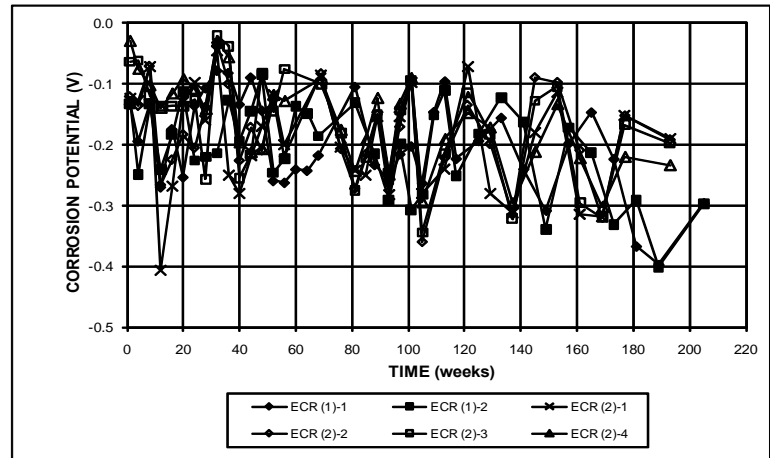


(b)

Figure A.55 – Field Test. (a) Corrosion rates and (b) total corrosion losses for specimens with ECR, without cracks.

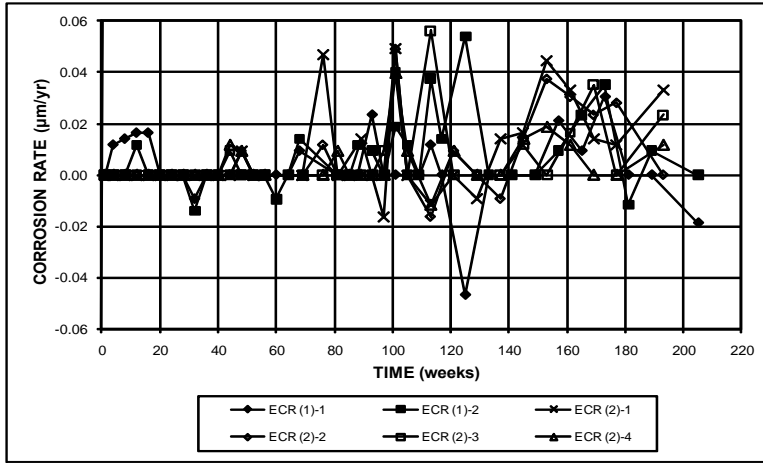


(a)

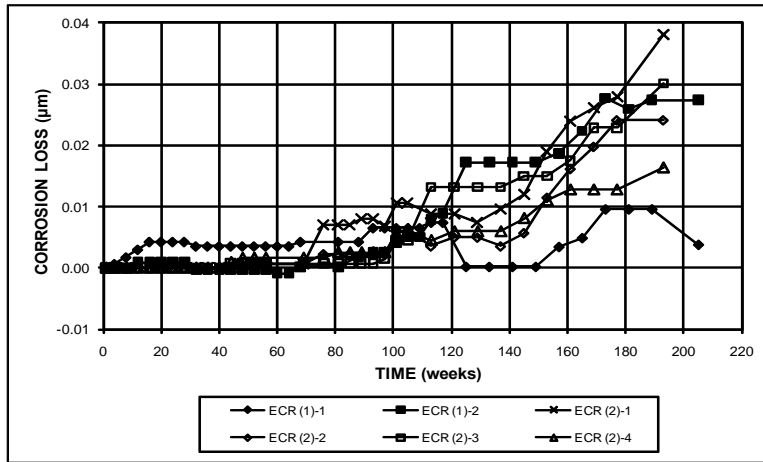


(b)

Figure A.56 – Field Test. (a) Top mat corrosion potentials and (b) bottom mat corrosion potentials with respect to a copper-copper sulfate electrode for specimens with ECR, without cracks.

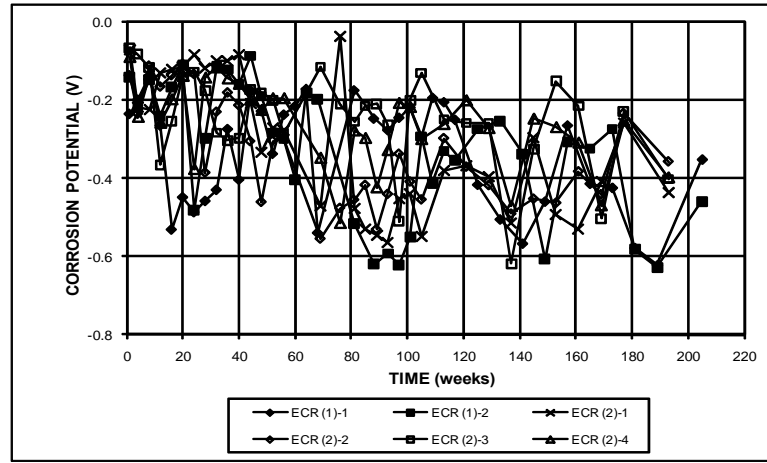


(a)

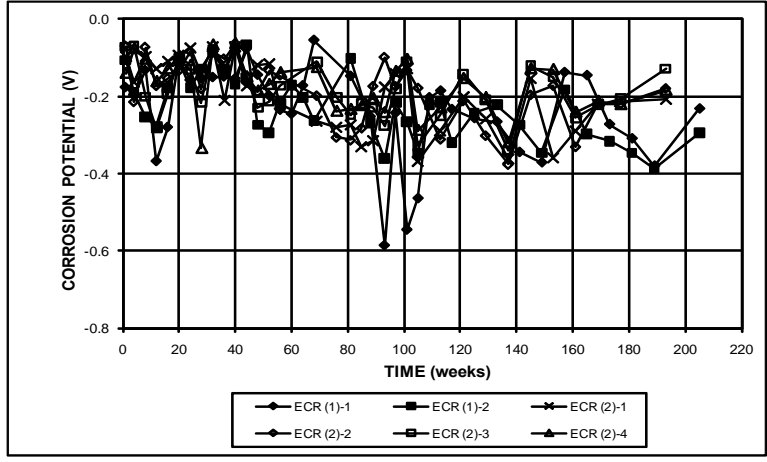


(b)

Figure A.57 – Field Test. (a) Corrosion rates and (b) total corrosion losses for specimens with ECR, with cracks.

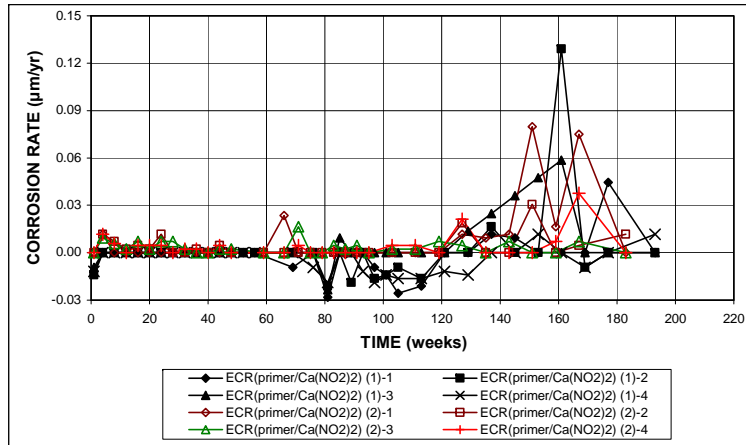


(a)

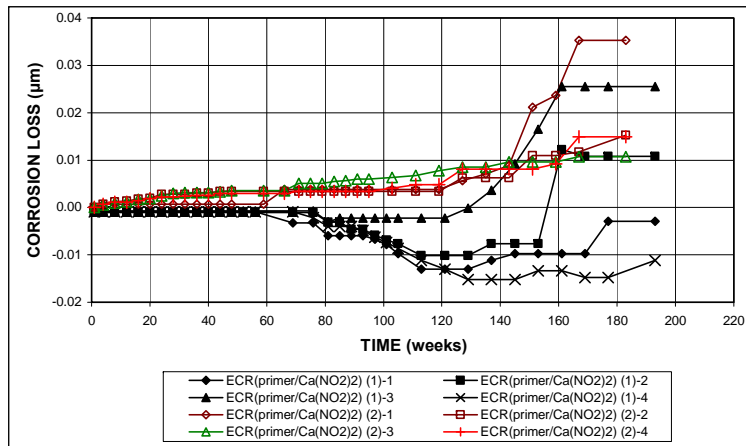


(b)

Figure A.58 – Field Test. (a) Top mat corrosion potentials and (b) bottom mat corrosion potentials with respect to a copper-copper sulfate electrode for specimens with ECR, with cracks.

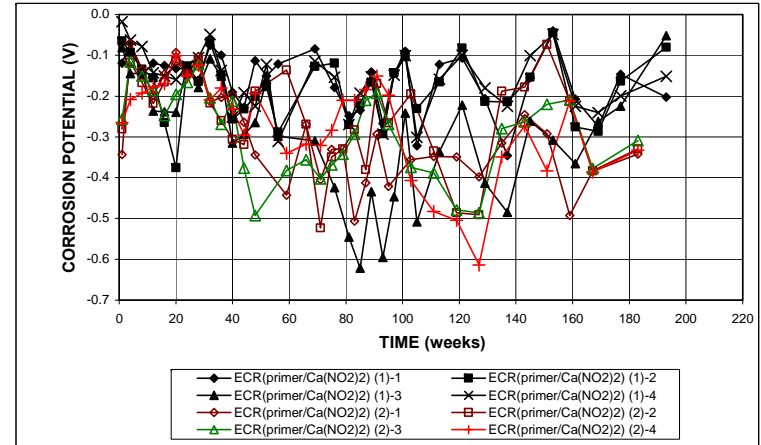


(a)

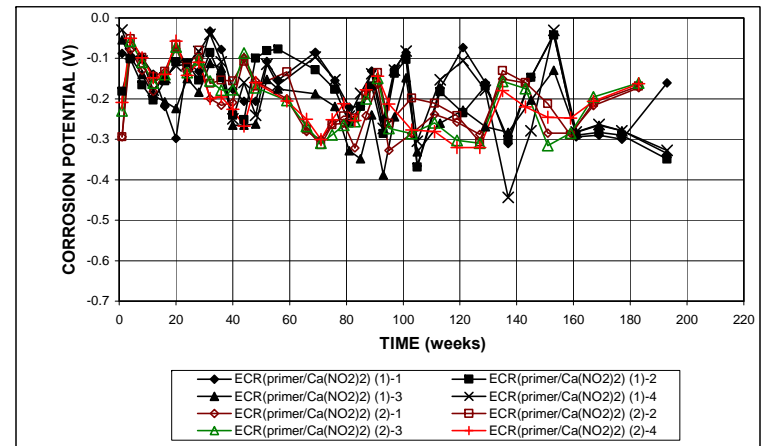


(b)

Figure A.59 – Field Test. (a) Corrosion rates and (b) total corrosion losses for specimens with ECR with a primer containing calcium nitrite, without cracks.

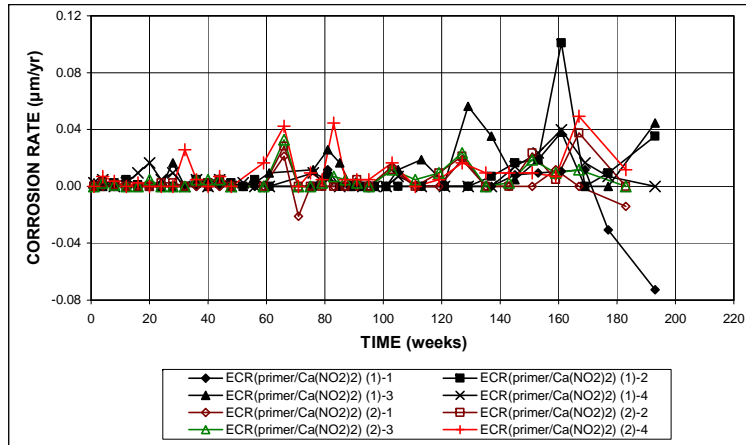


(a)

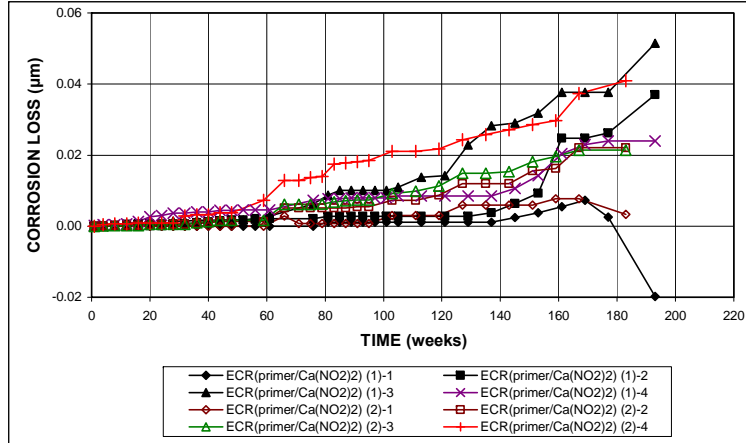


(b)

Figure A.60 – Field Test. (a) Top mat corrosion potentials and (b) bottom mat corrosion potentials with respect to a copper-copper sulfate electrode for specimens with ECR with a primer containing calcium nitrite, without cracks.

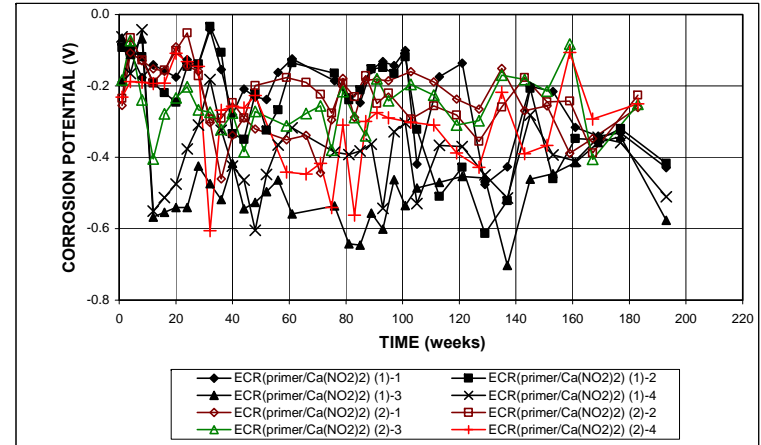


(a)

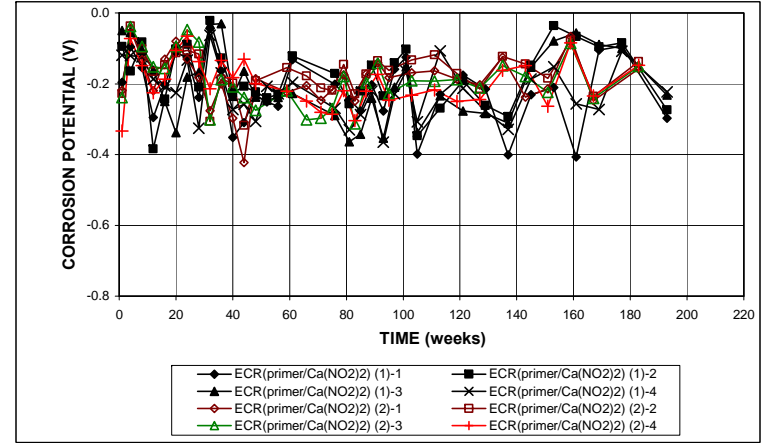


(b)

Figure A.61 – Field Test. (a) Corrosion rates and (b) total corrosion losses for specimens with ECR with a primer containing calcium nitrite, with cracks.

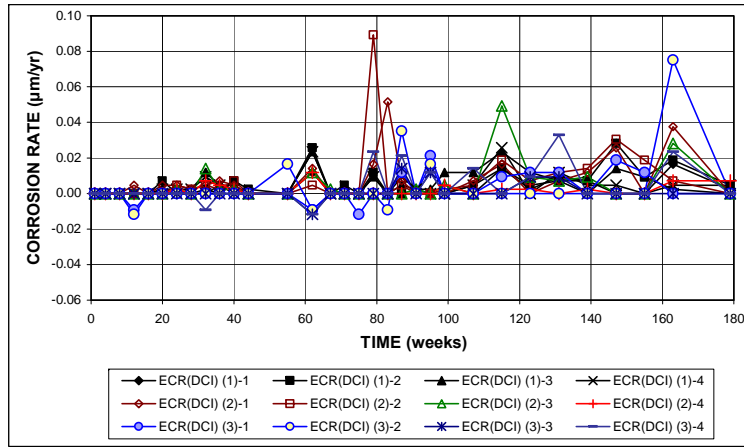


(a)

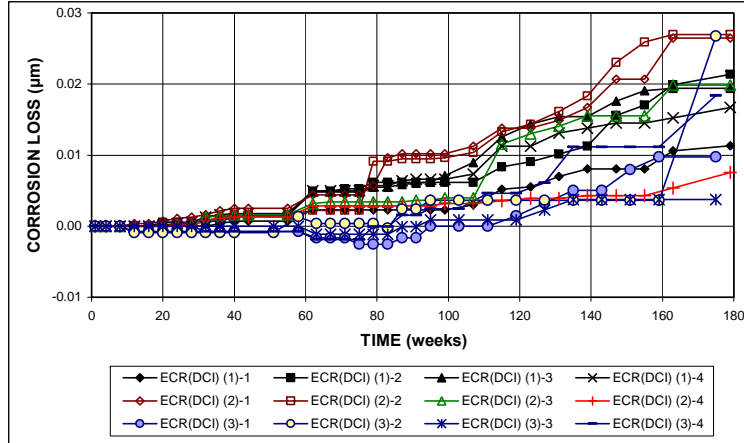


(b)

Figure A.62 – Field Test. (a) Top mat corrosion potentials and (b) bottom mat corrosion potentials with respect to a copper-copper sulfate electrode for specimens with ECR with a primer containing calcium nitrite, with cracks.

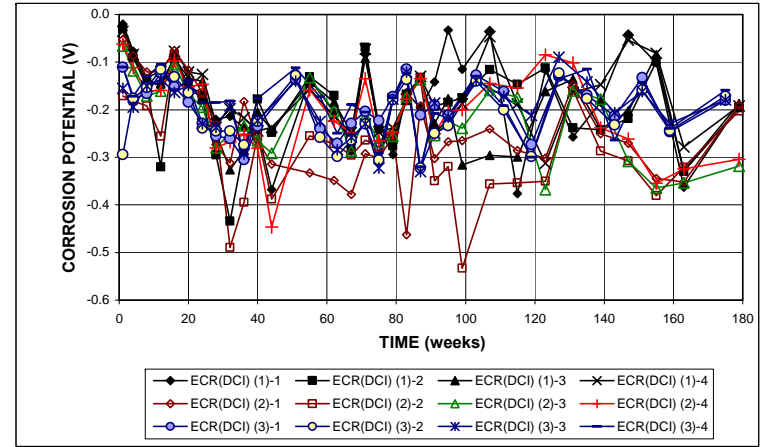


(a)

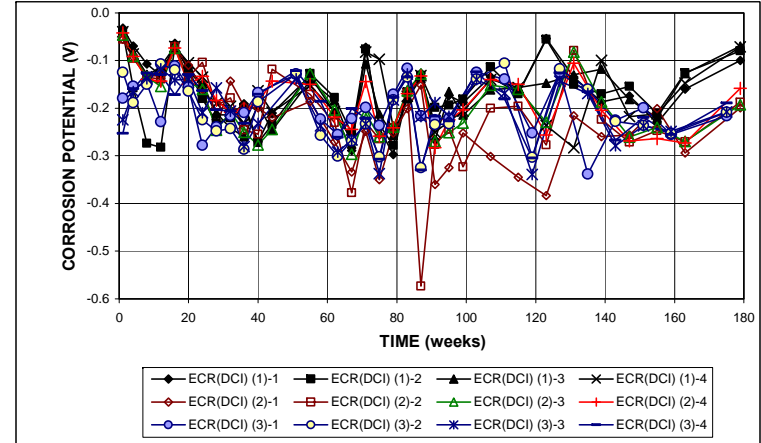


(b)

Figure A.63 – Field Test. (a) Corrosion rates and (b) total corrosion losses for specimens with ECR and DCI inhibitor in concrete, without cracks.

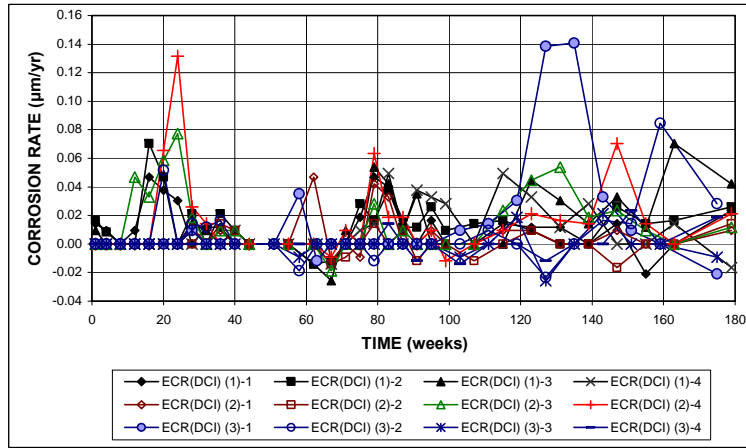


(a)

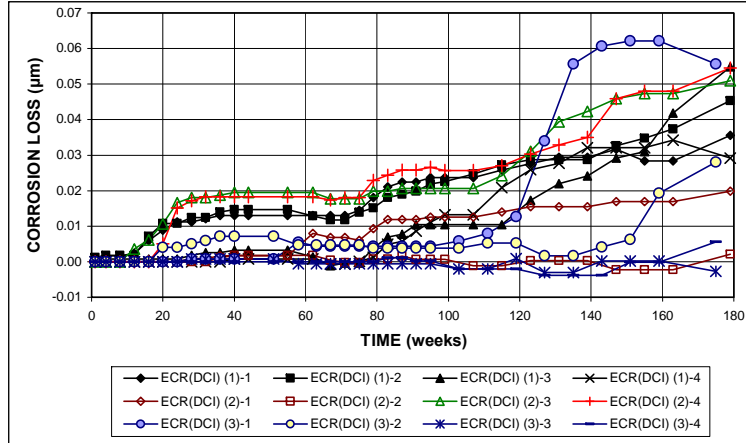


(b)

Figure A.64 – Field Test. (a) Top mat corrosion potentials and (b) bottom mat corrosion potentials with respect to a copper-copper sulfate electrode for specimens with ECR and DCI inhibitor in concrete, without cracks.

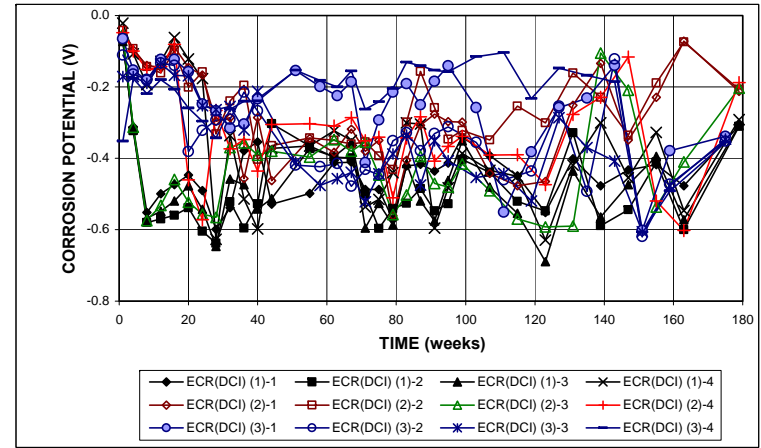


(a)

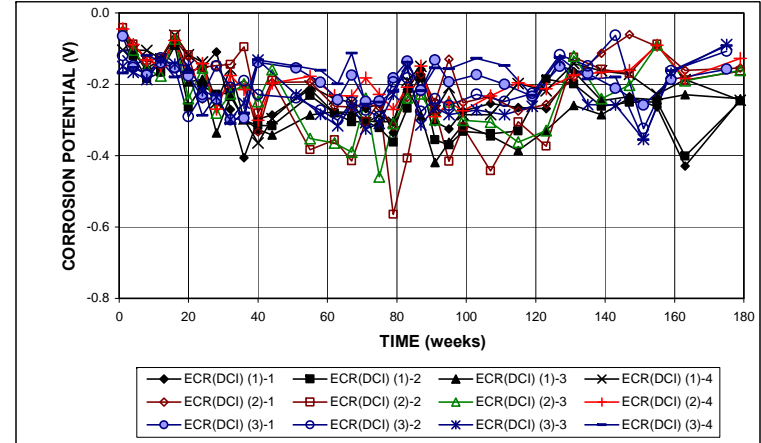


(b)

Figure A.65 – Field Test. (a) Corrosion rates and (b) total corrosion losses for specimens with ECR and DCI inhibitor in concrete, with cracks.

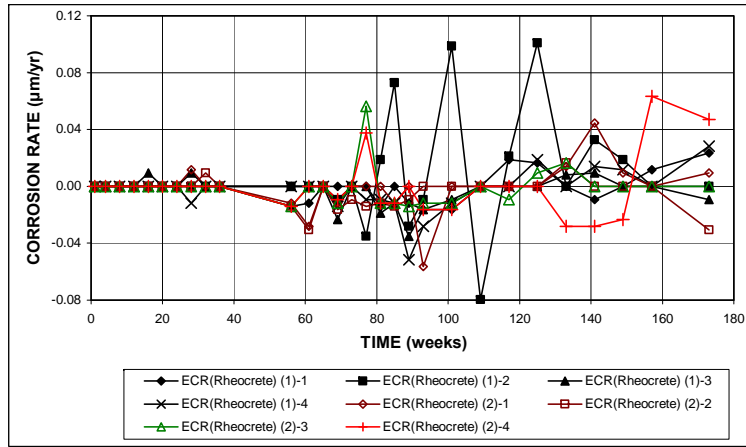


(a)

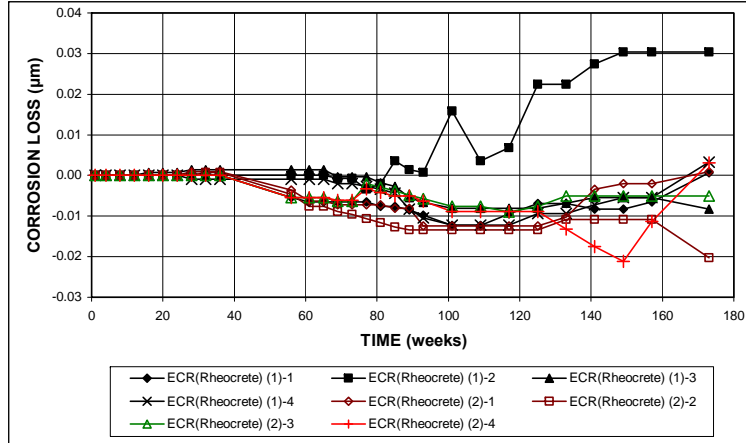


(b)

Figure A.66 – Field Test. (a) Top mat corrosion potentials and (b) bottom mat corrosion potentials with respect to a copper-copper sulfate electrode for specimens with ECR and DCI inhibitor in concrete, with cracks.

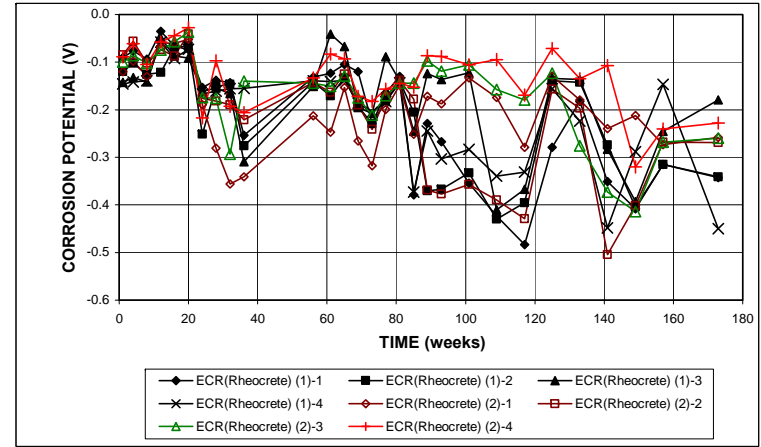


(a)

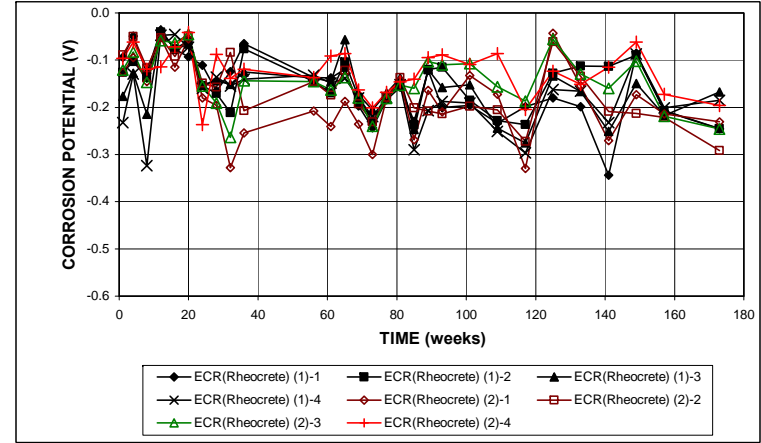


(b)

Figure A.67 – Field Test. (a) Corrosion rates and (b) total corrosion losses for specimens with ECR and Rheocrete inhibitor in concrete, without cracks.

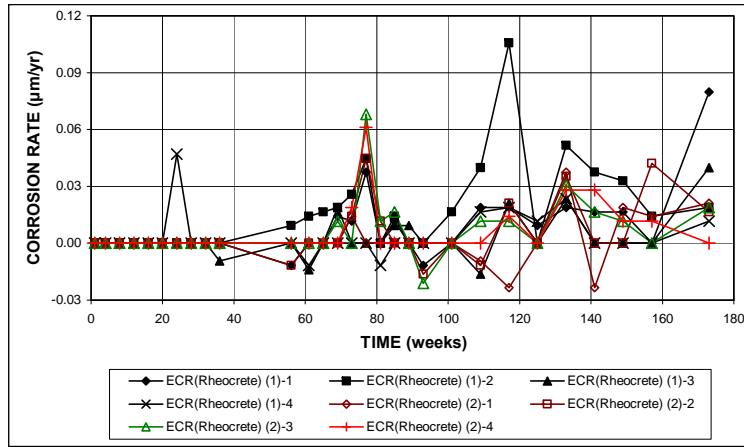


(a)

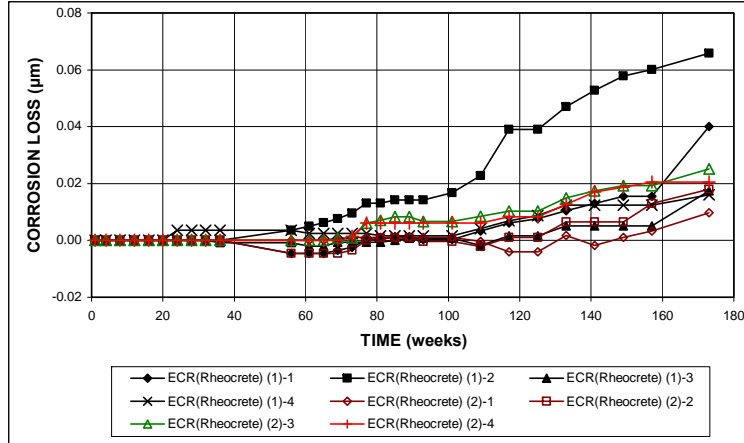


(b)

Figure A.68 – Field Test. (a) Top mat corrosion potentials and (b) bottom mat corrosion potentials with respect to a copper-copper sulfate electrode for specimens with ECR and Rheocrete inhibitor in concrete, without cracks.

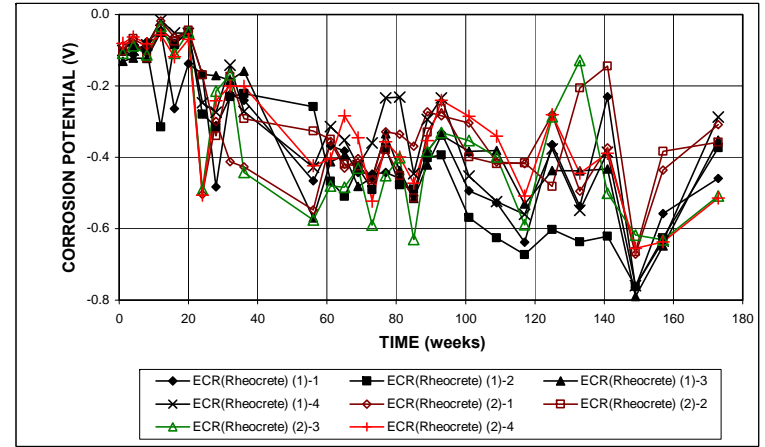


(a)

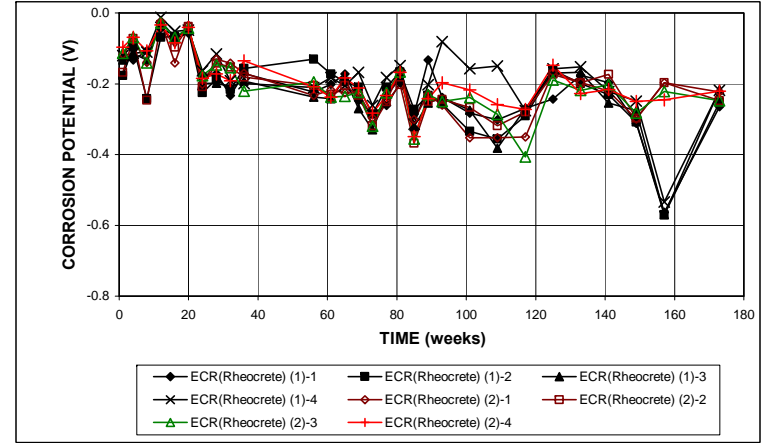


(b)

Figure A.69 – Field Test. (a) Corrosion rates and (b) total corrosion losses for specimens with ECR and Rheocrete inhibitor in concrete, with cracks.

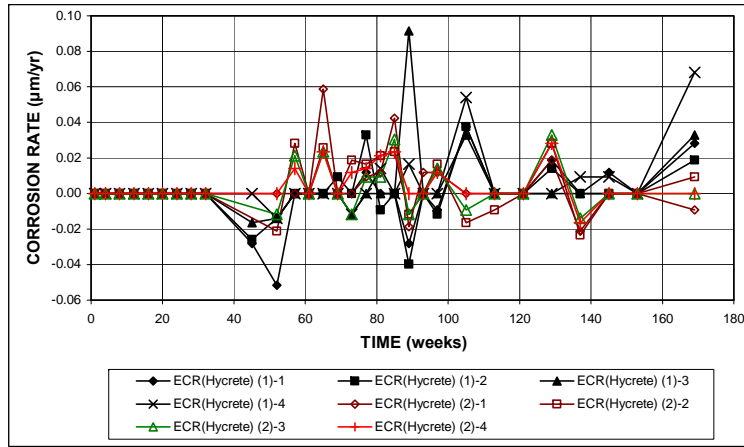


(a)

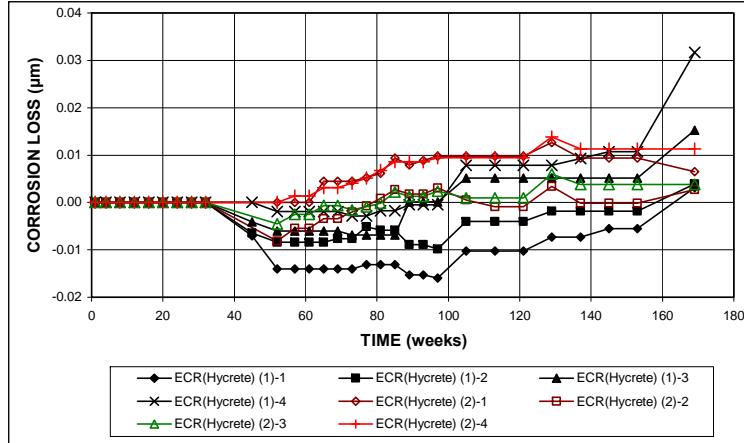


(b)

Figure A.70 – Field Test. (a) Top mat corrosion potentials and (b) bottom mat corrosion potentials with respect to a copper-copper sulfate electrode for specimens with ECR and Rheocrete inhibitor in concrete, with cracks.

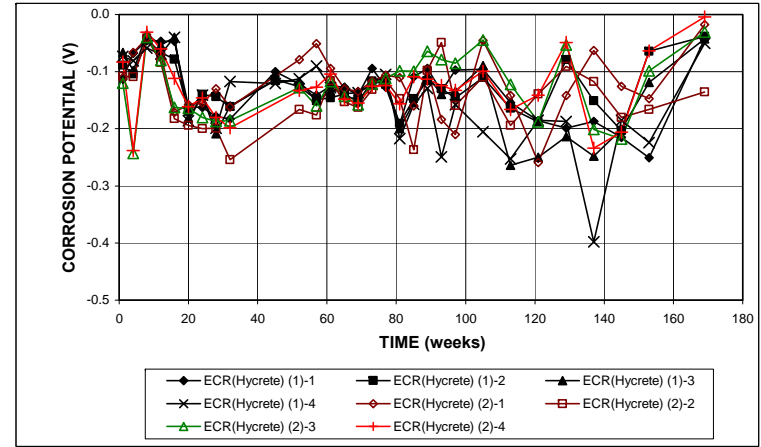


(a)

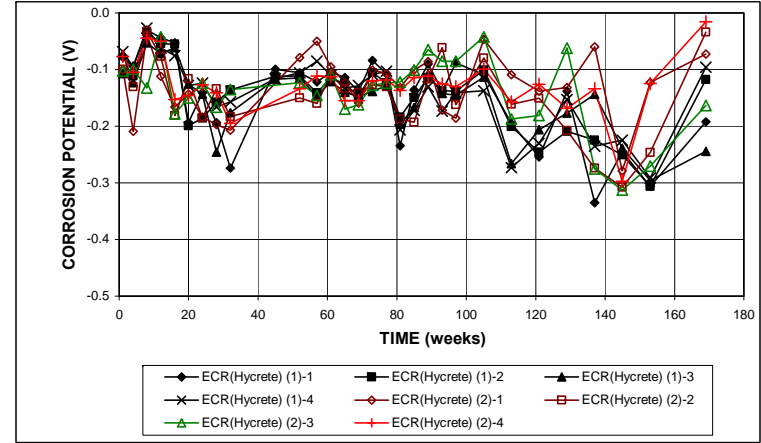


(b)

Figure A.71 – Field Test. (a) Corrosion rates and (b) total corrosion losses for specimens with ECR and Hycrete inhibitor in concrete, without cracks.

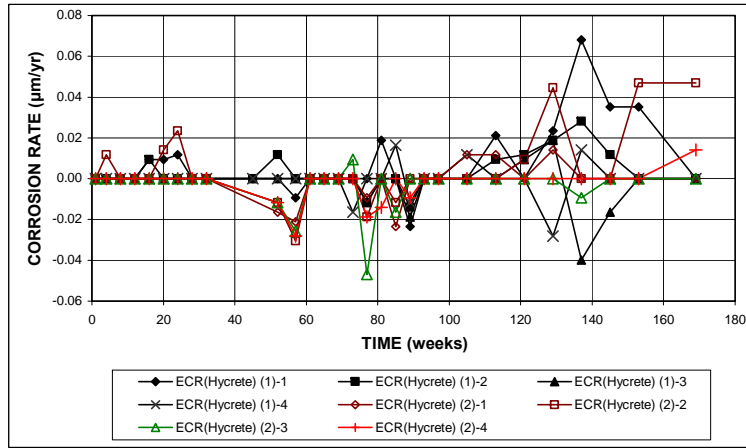


(a)

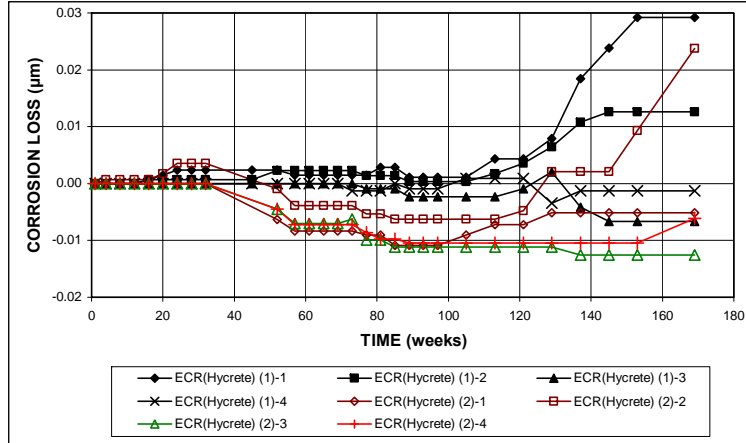


(b)

Figure A.72 – Field Test. (a) Top mat corrosion potentials and (b) bottom mat corrosion potentials with respect to a copper-copper sulfate electrode for specimens with ECR and Hycrete inhibitor in concrete, without cracks.

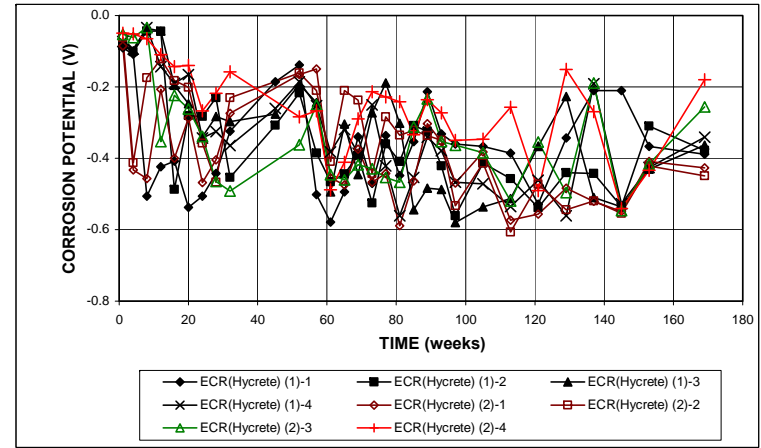


(a)

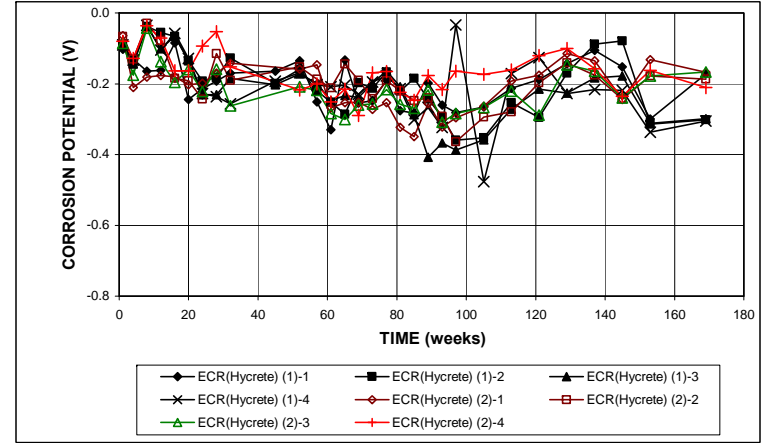


(b)

Figure A.73 – Field Test. (a) Corrosion rates and (b) total corrosion losses for specimens with ECR and Hycrete inhibitor in concrete, with cracks.

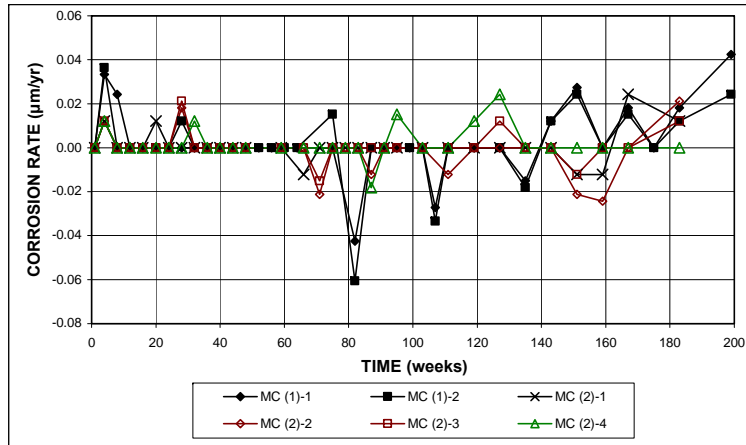


(a)

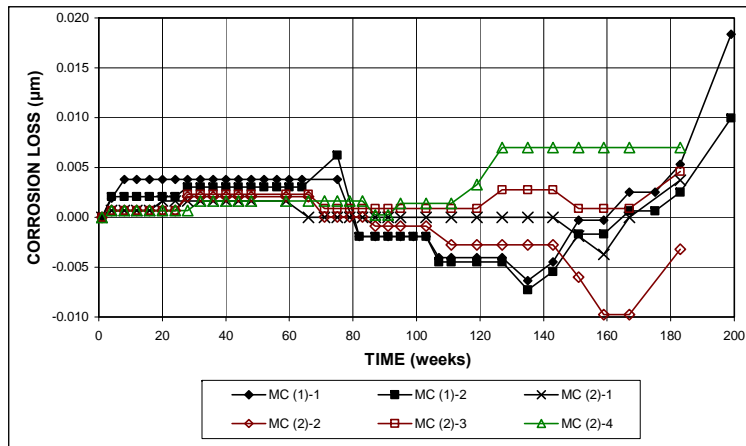


(b)

Figure A.74 – Field Test. (a) Top mat corrosion potentials and (b) bottom mat corrosion potentials with respect to a copper-copper sulfate electrode for specimens with ECR and Hycrete inhibitor in concrete, with cracks.

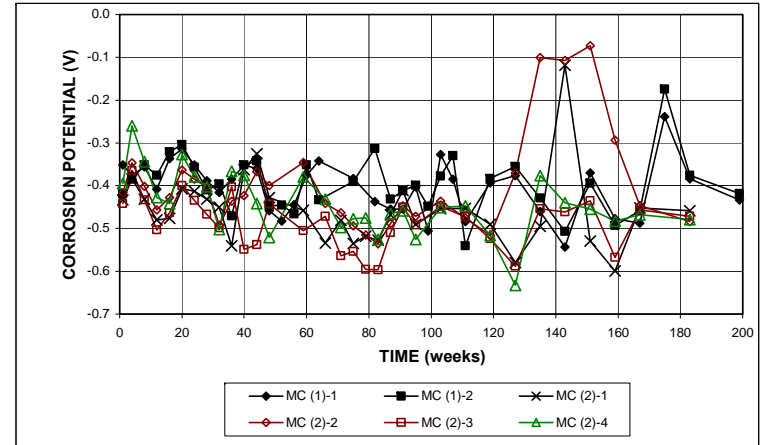


(a)

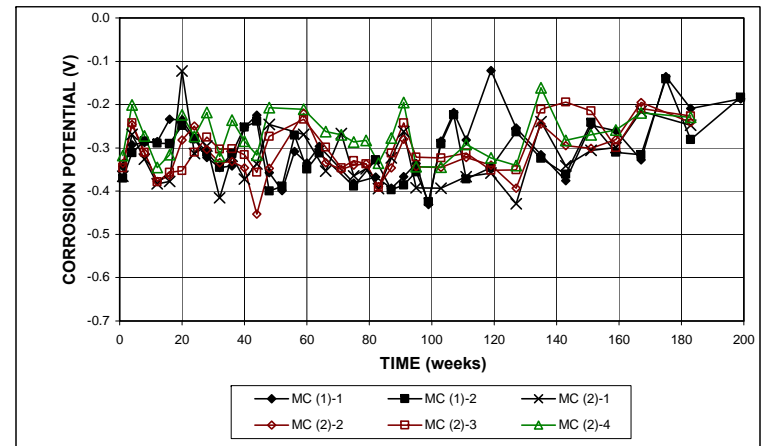


(b)

Figure A.75 – Field Test. (a) Corrosion rates and (b) total corrosion losses for specimens with multiple-coated bars, without cracks.

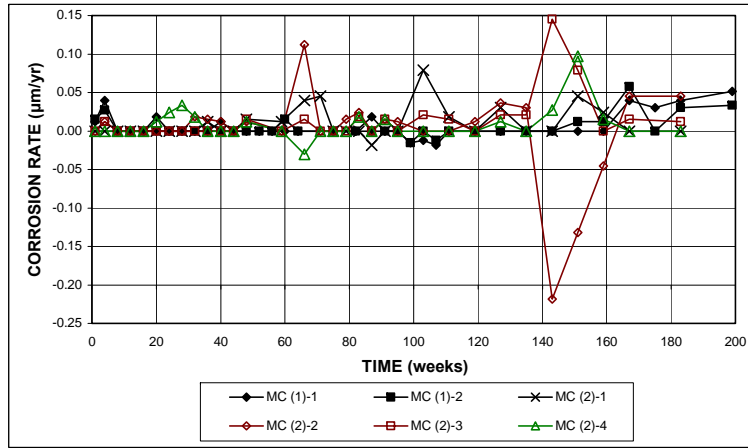


(a)

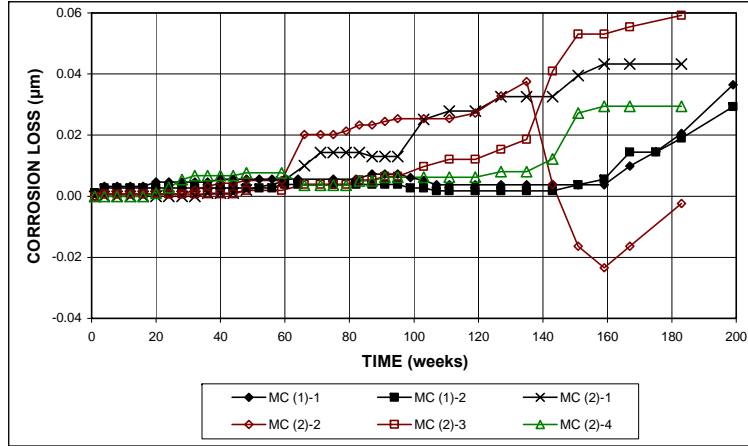


(b)

Figure A.76 – Field Test. (a) Top mat corrosion potentials and (b) bottom mat corrosion potentials with respect to a copper-copper sulfate electrode for specimens with multiple-coated bars, without cracks.

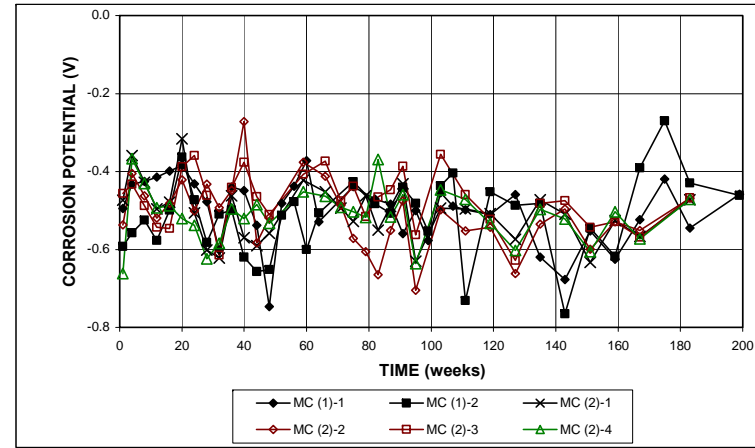


(a)

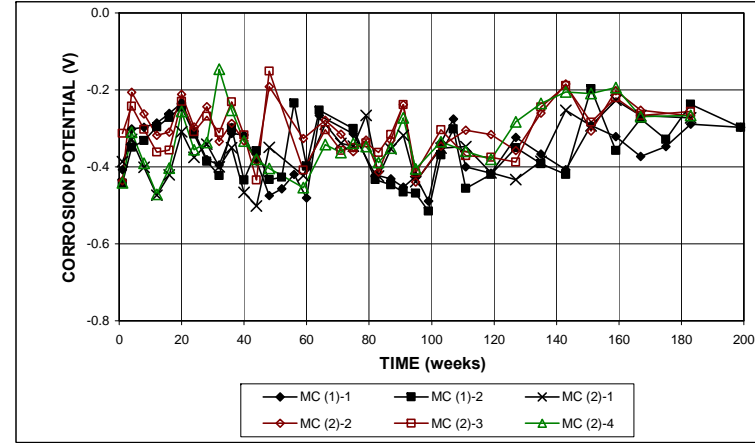


(b)

Figure A.77 – Field Test. (a) Corrosion rates and (b) total corrosion losses for specimens with multiple-coated bars, with cracks.

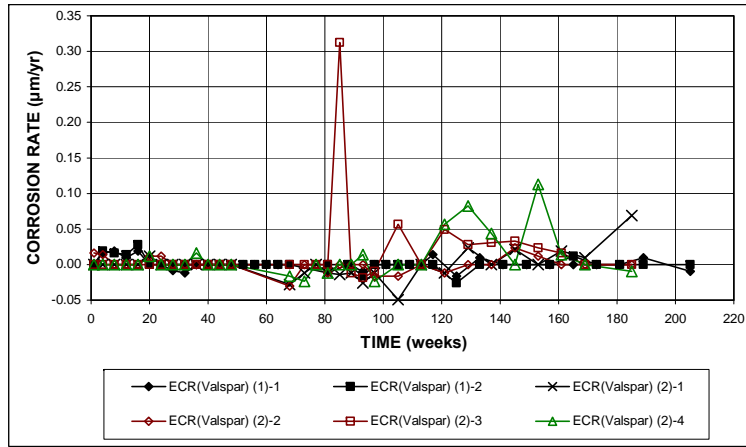


(a)

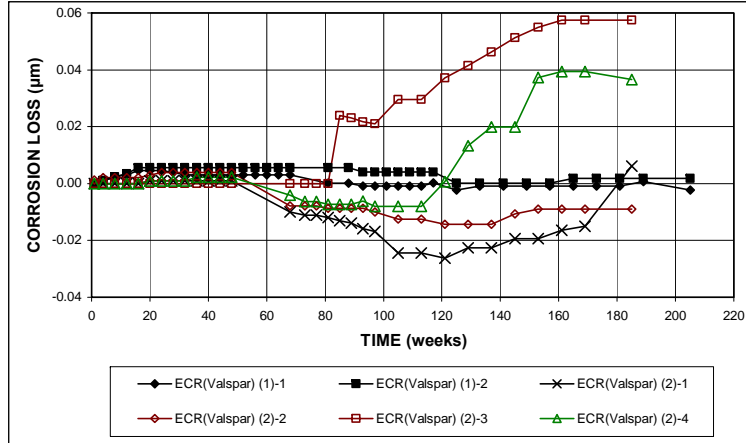


(b)

Figure A.78 – Field Test. (a) Top mat corrosion potentials and (b) bottom mat corrosion potentials with respect to a copper-copper sulfate electrode for specimens with multiple-coated bars, with cracks.

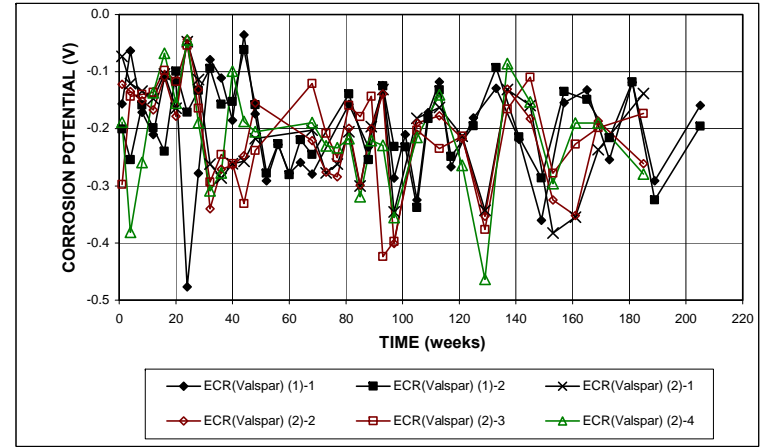


(a)

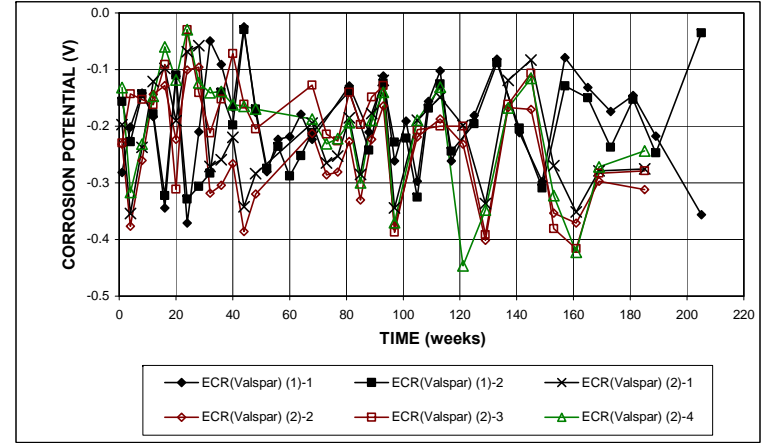


(b)

Figure A.79 – Field Test. (a) Corrosion rates and (b) total corrosion losses for specimens with ECR with increased adhesion Valspar coating, without cracks.

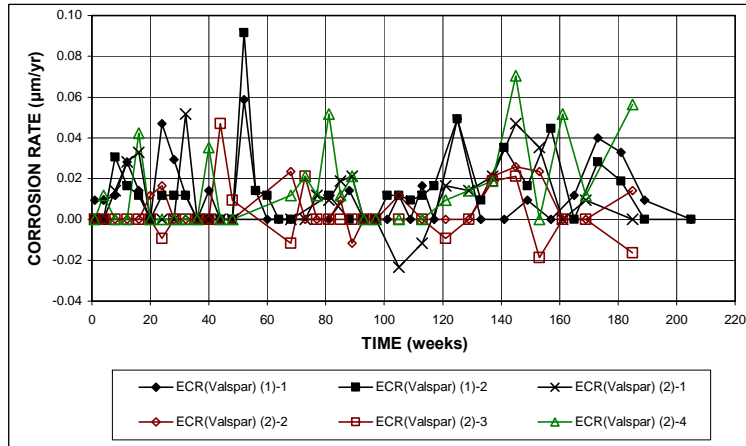


(a)

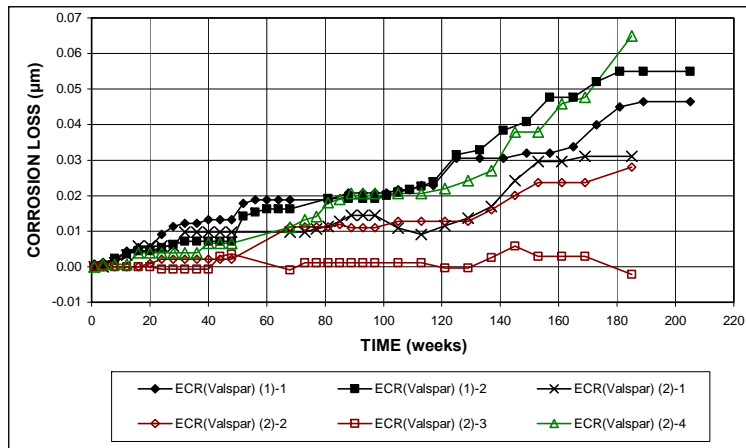


(b)

Figure A.80 – Field Test. (a) Top mat corrosion potentials and (b) bottom mat corrosion potentials with respect to a copper-copper sulfate electrode for specimens with ECR with increased adhesion Valspar coating, without cracks.

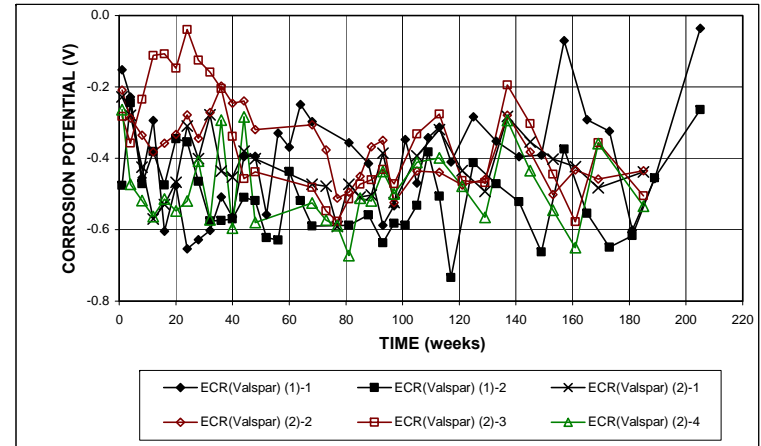


(a)

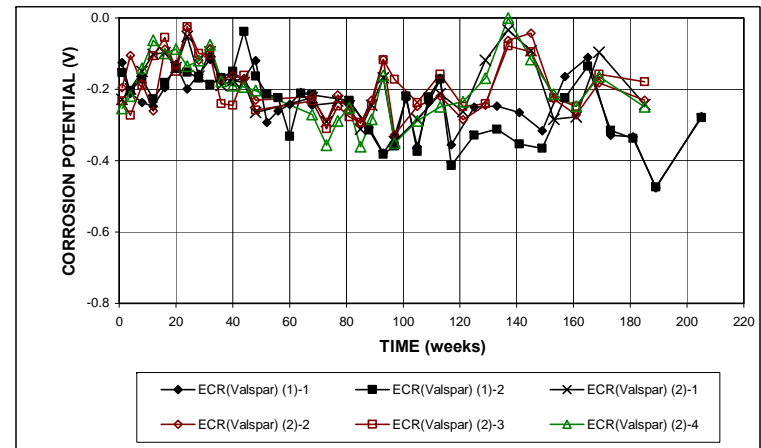


(b)

Figure A.81 – Field Test. (a) Corrosion rates and (b) total corrosion losses for specimens with ECR with increased adhesion Valspar coating, with cracks.

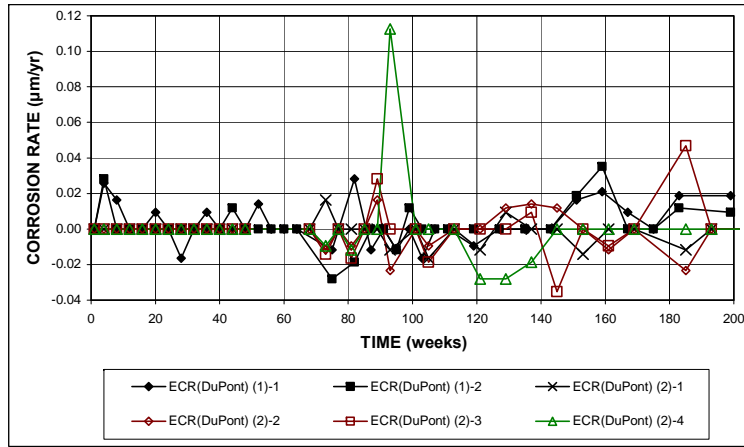


(a)

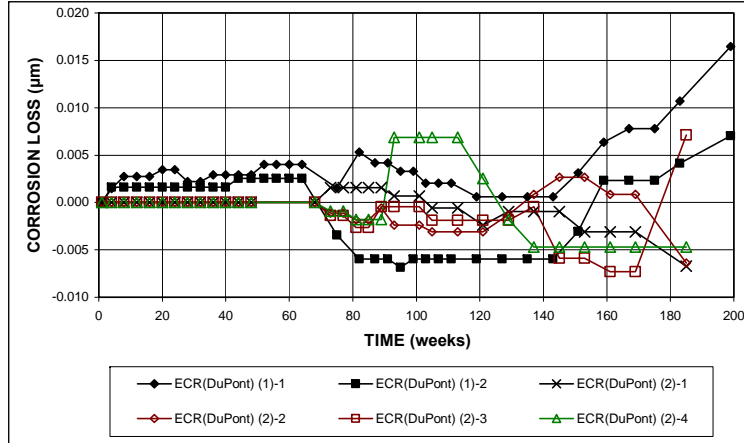


(b)

Figure A.82 – Field Test. (a) Top mat corrosion potentials and (b) bottom mat corrosion potentials with respect to a copper-copper sulfate electrode for specimens with ECR with increased adhesion Valspar coating, with cracks.

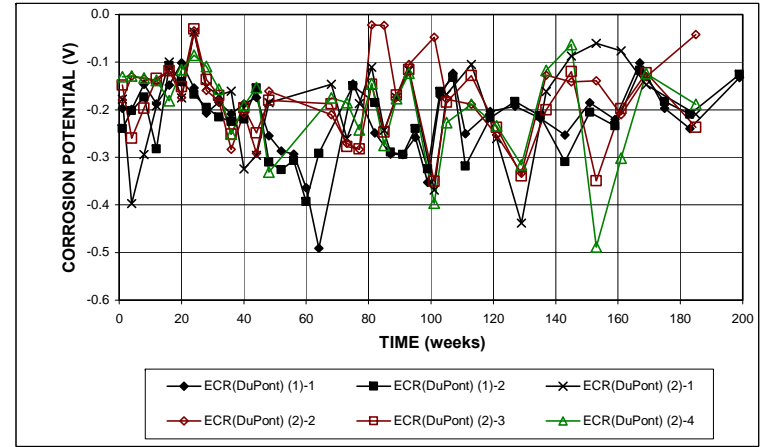


(a)

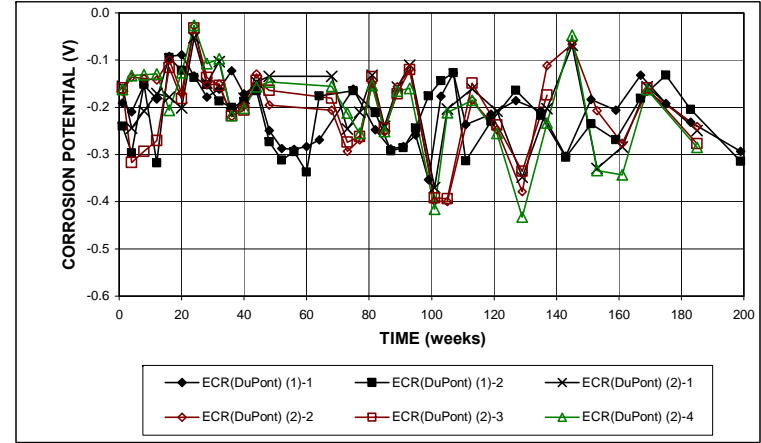


(b)

Figure A.83 – Field Test. (a) Corrosion rates and (b) total corrosion losses for specimens with ECR with increased adhesion DuPont coating, without cracks.

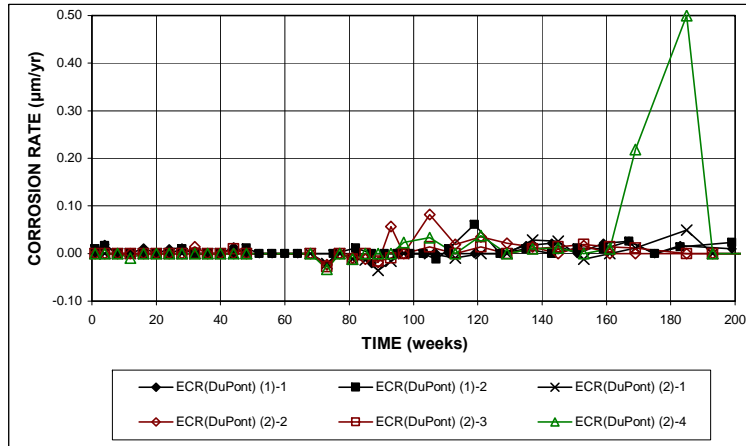


(a)

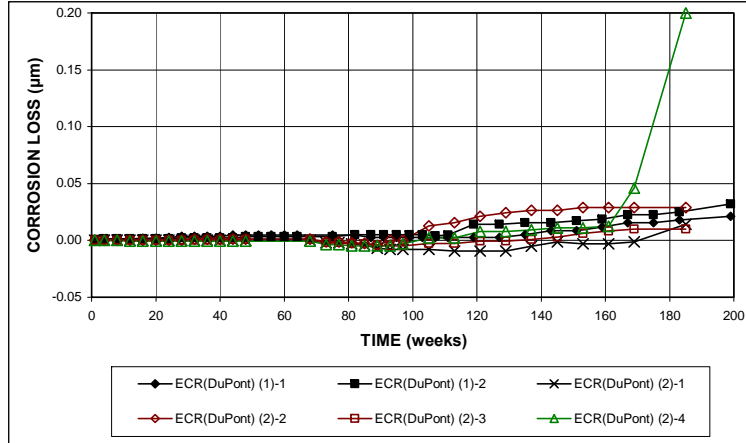


(b)

Figure A.84 – Field Test. (a) Top mat corrosion potentials and (b) bottom mat corrosion potentials with respect to a copper-copper sulfate electrode for specimens with ECR with increased adhesion DuPont coating, without cracks.

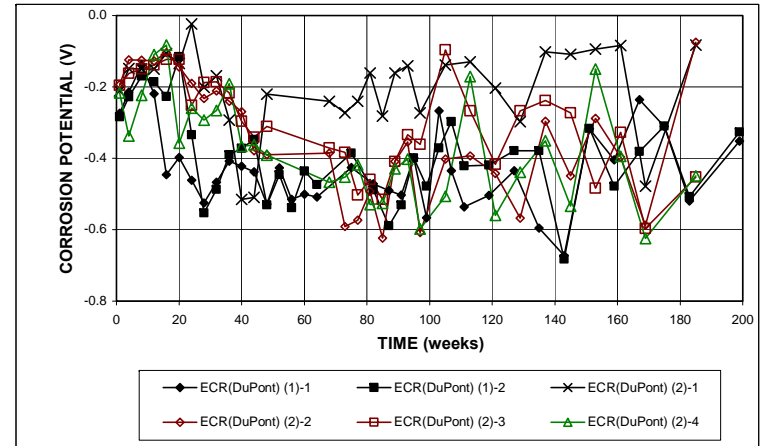


(a)

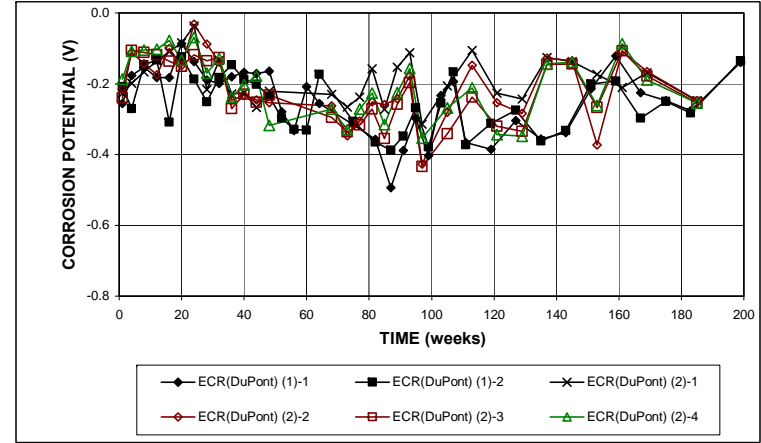


(b)

Figure A.85 – Field Test. (a) Corrosion rates and (b) total corrosion losses for specimens with ECR with increased adhesion DuPont coating, with cracks.

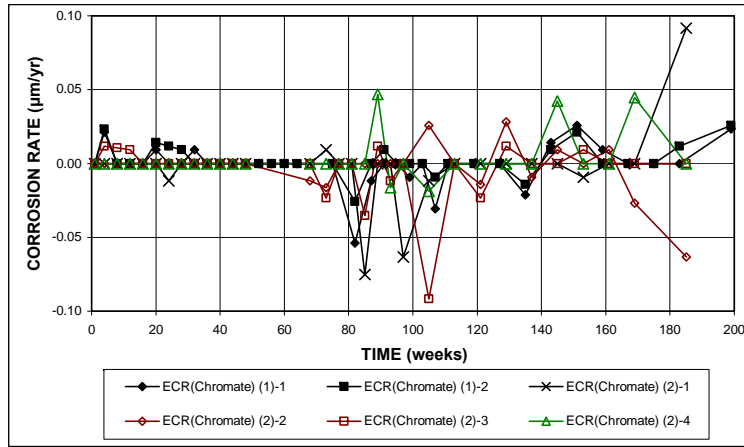


(a)

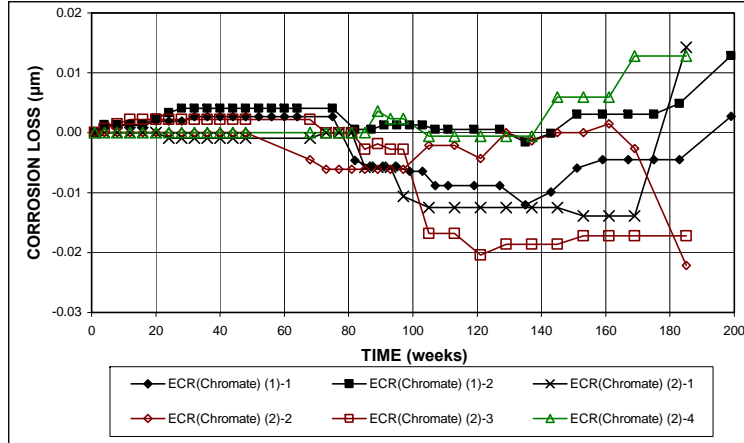


(b)

Figure A.86 – Field Test. (a) Top mat corrosion potentials and (b) bottom mat corrosion potentials with respect to a copper-copper sulfate electrode for specimens with ECR with increased adhesion DuPont coating, with cracks.

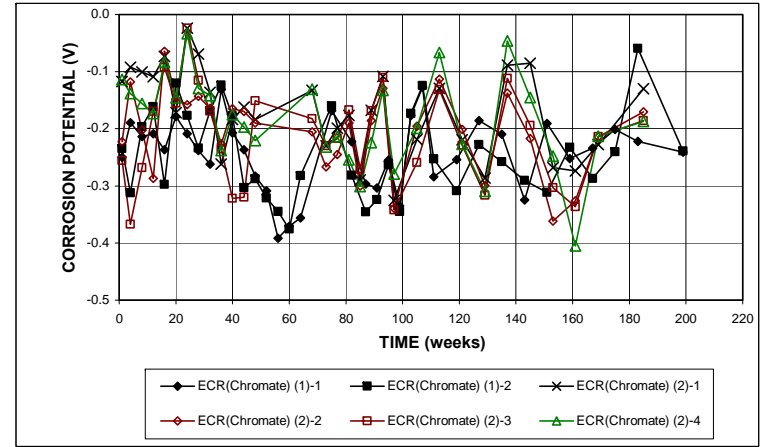


(a)

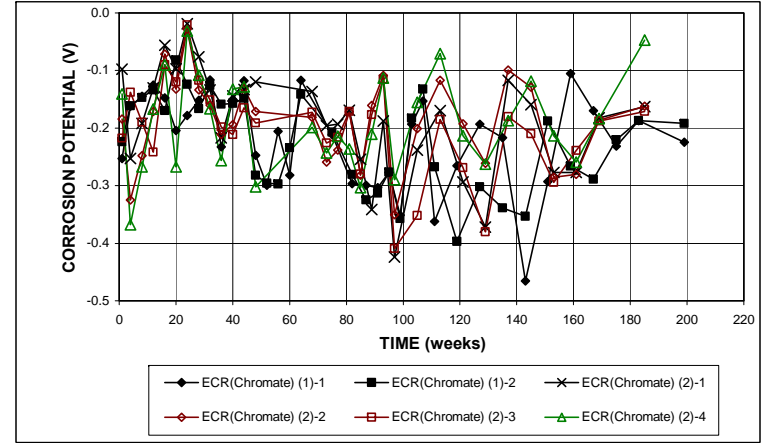


(b)

Figure A.87 – Field Test. (a) Corrosion rates and (b) total corrosion losses for specimens with ECR with zinc chromate pretreatment, without cracks.

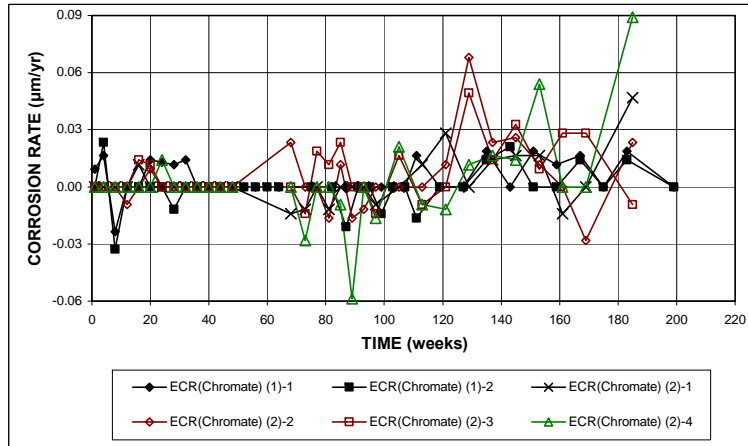


(a)

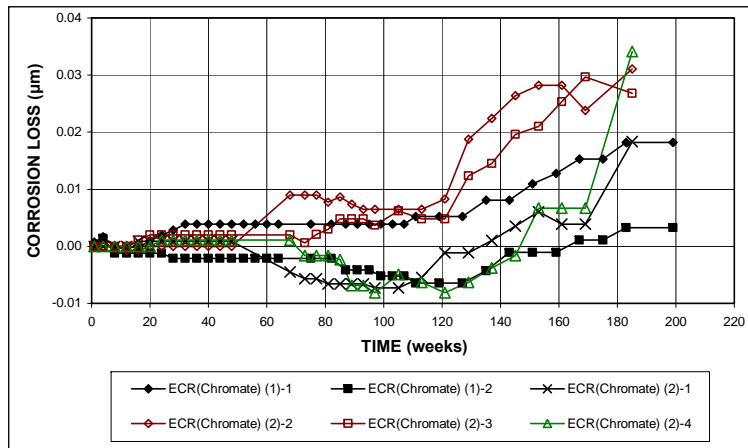


(b)

Figure A.88 – Field Test. (a) Top mat corrosion potentials and (b) bottom mat corrosion potentials with respect to a copper-copper sulfate electrode for specimens with ECR with zinc chromate pretreatment, without cracks.

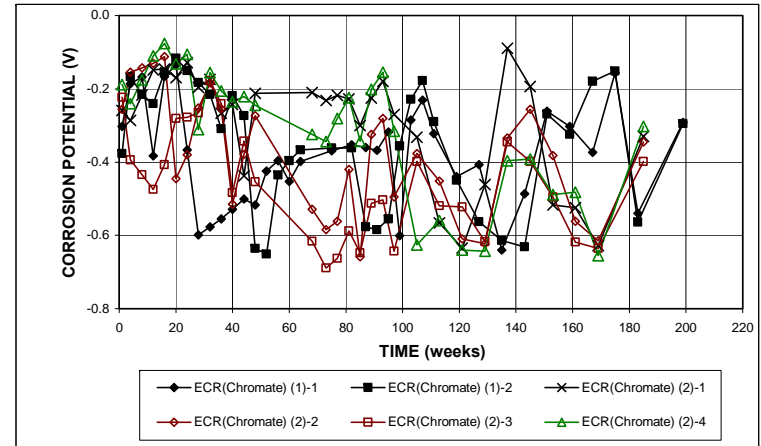


(a)

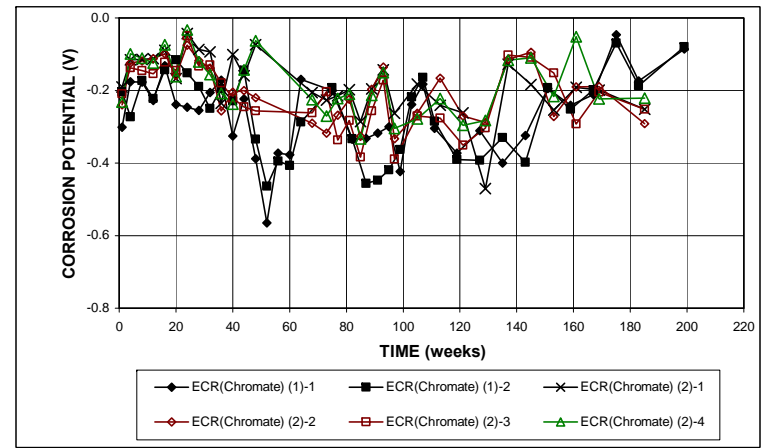


(b)

Figure A.89 – Field Test. (a) Corrosion rates and (b) total corrosion losses for specimens with ECR with zinc chromate pretreatment, with cracks.

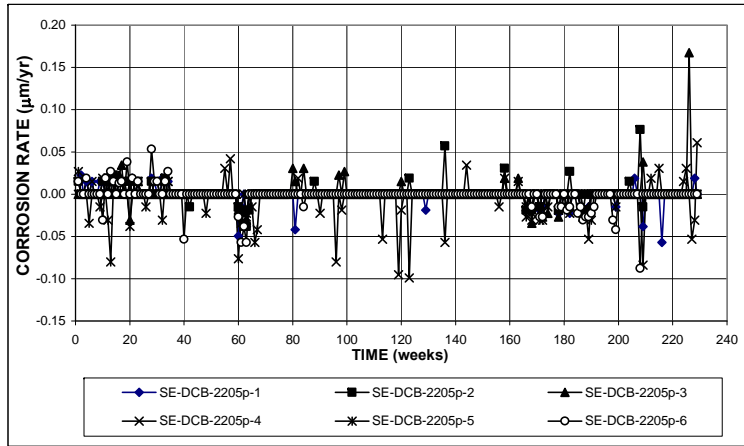


(a)

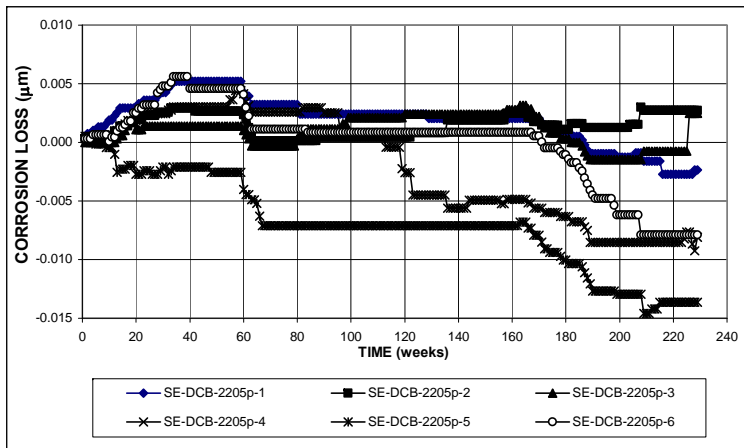


(b)

Figure A.90 – Field Test. (a) Top mat corrosion potentials and (b) bottom mat corrosion potentials with respect to a copper-copper sulfate electrode for specimens with ECR with zinc chromate pretreatment, with cracks.

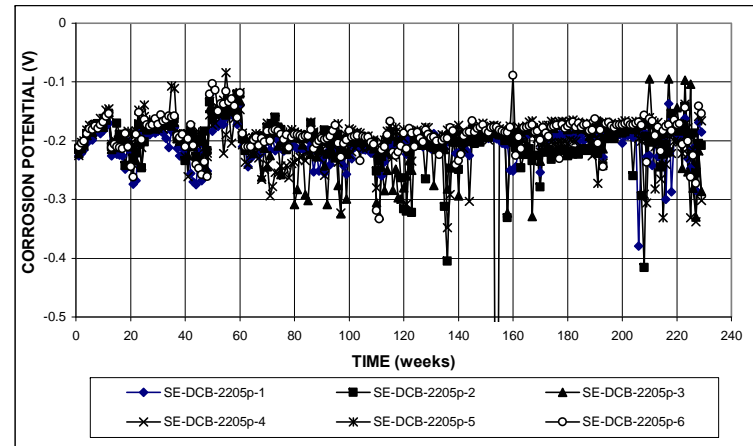


(a)

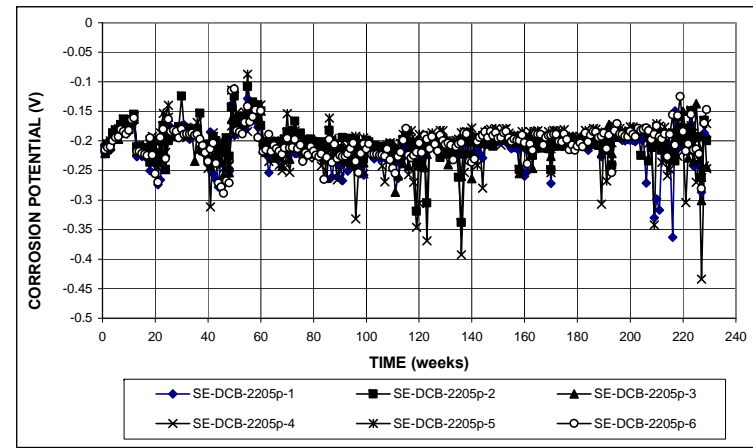


(b)

Figure A.91 – Southern Exposure Test. (a) Corrosion rates and (b) total corrosion losses for specimens with pickled 2205 stainless steel for the Doniphan County Bridge.

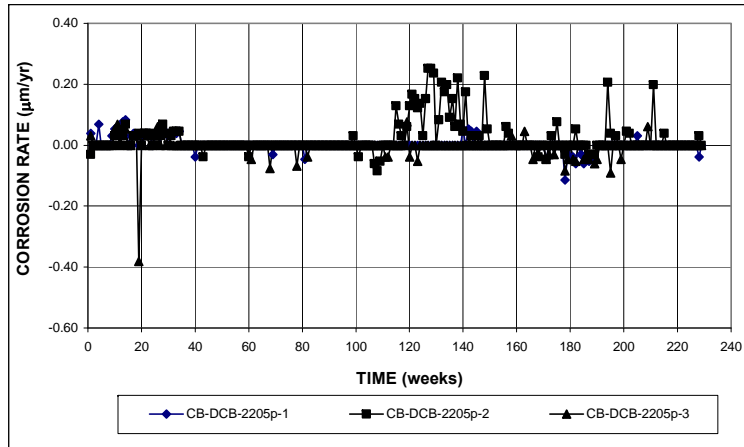


(a)

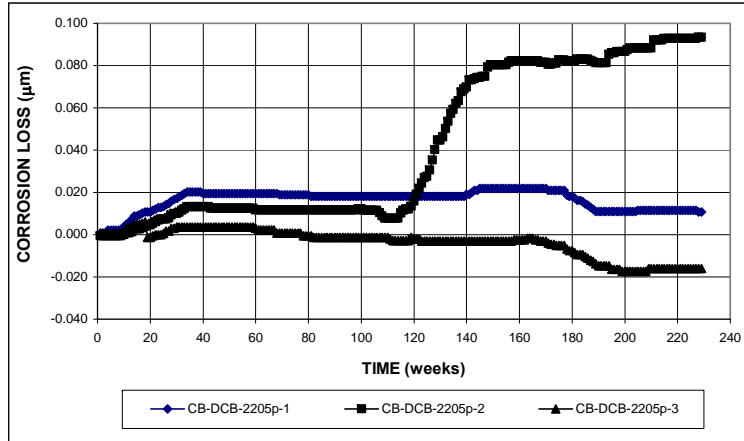


(b)

Figure A.92 – Southern Exposure Test. (a) Top mat corrosion potentials and (b) bottom mat corrosion potentials with respect to a copper-copper sulfate electrode for specimens with pickled 2205 stainless steel for the Doniphan County Bridge.

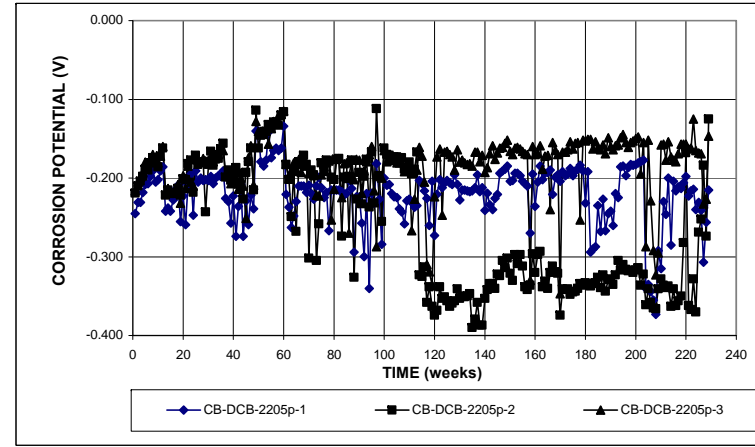


(a)

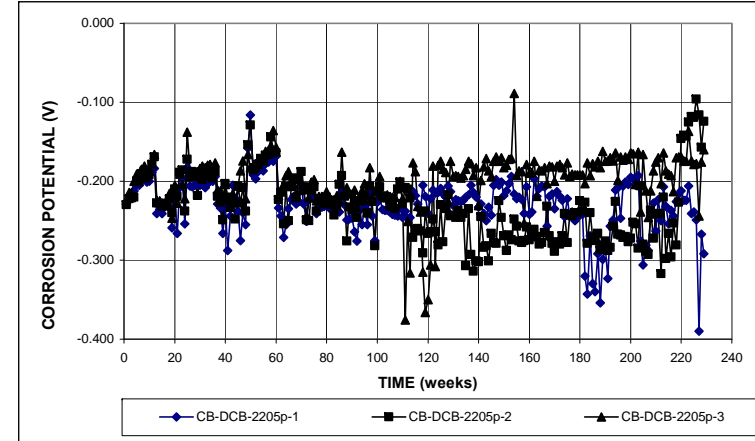


(b)

Figure A.93 – Cracked Beam Test. (a) Corrosion rates and (b) total corrosion losses for specimens with pickled 2205 stainless steel for the Doniphan County Bridge.

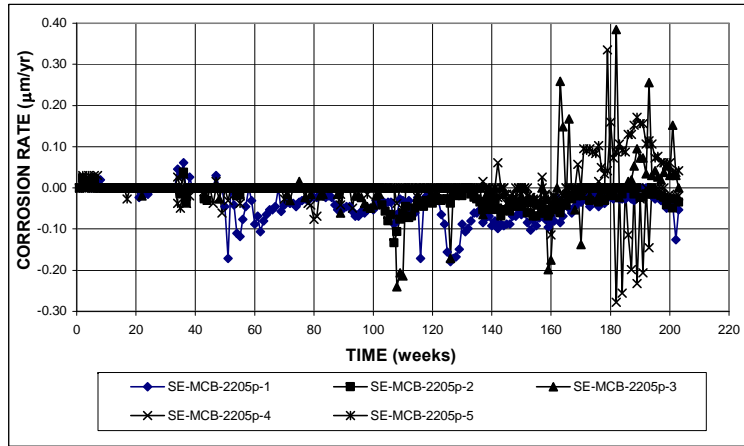


(a)

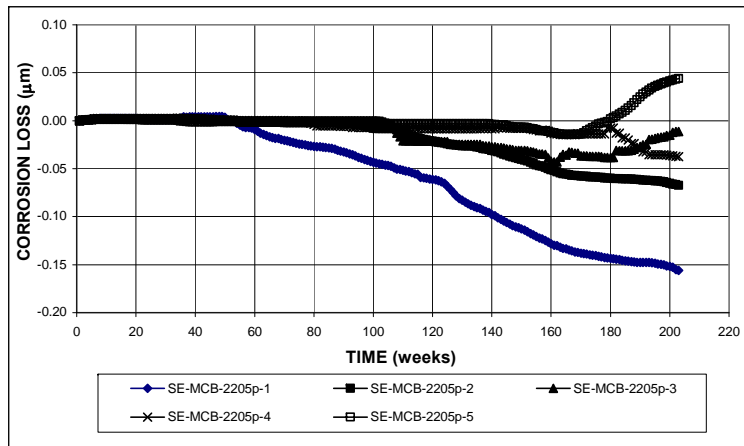


(b)

Figure A.94 – Cracked Beam Test. (a) Top mat corrosion potentials and (b) bottom mat corrosion potentials with respect to a copper-copper sulfate electrode for specimens with pickled 2205 stainless steel for the Doniphan County Bridge.

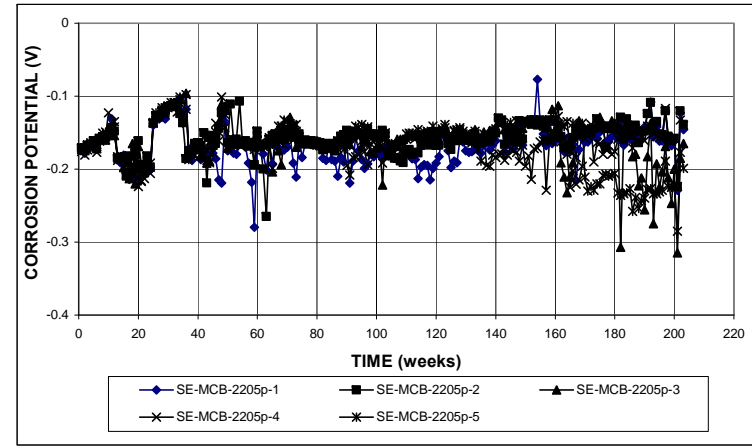


(a)

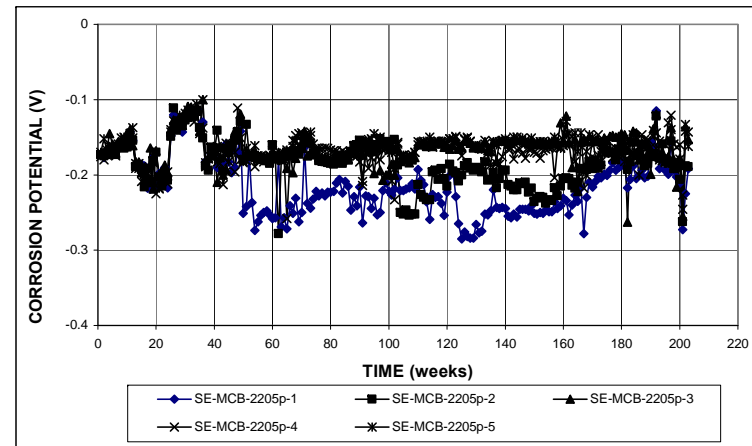


(b)

Figure A.95 – Southern Exposure Test. (a) Corrosion rates and (b) total corrosion losses for specimens with pickled 2205 stainless steel for the Mission Creek Bridge.

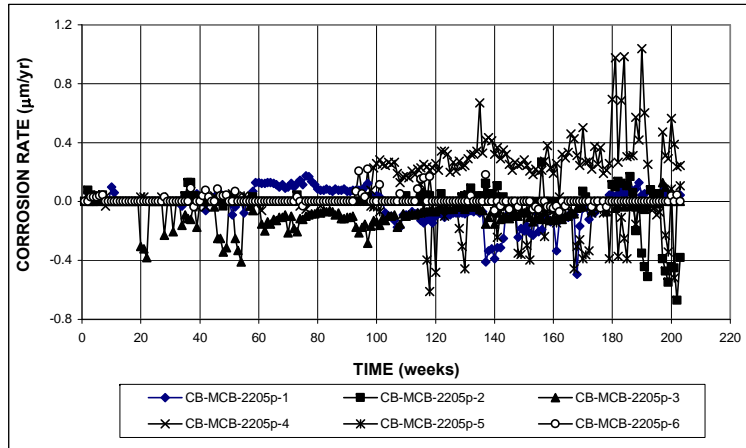


(a)

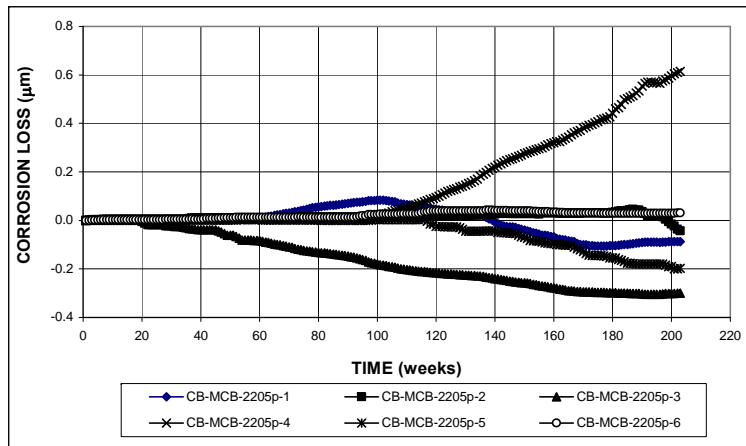


(b)

Figure A.96 – Southern Exposure Test. (a) Top mat corrosion potentials and (b) bottom mat corrosion potentials with respect to a copper-copper sulfate electrode for specimens with pickled 2205 stainless steel for the Mission Creek Bridge.

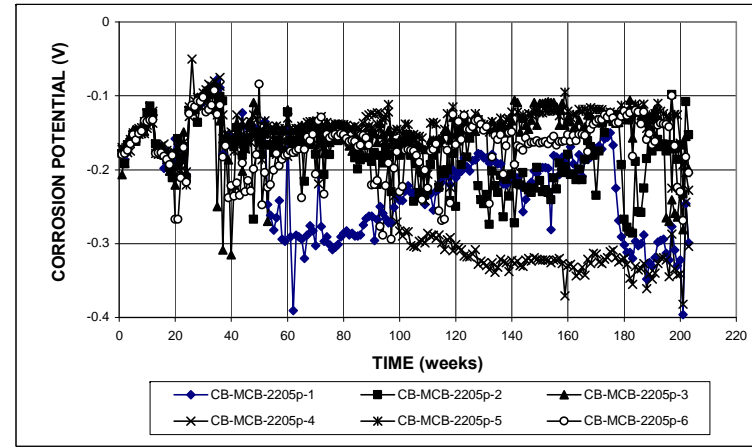


(a)

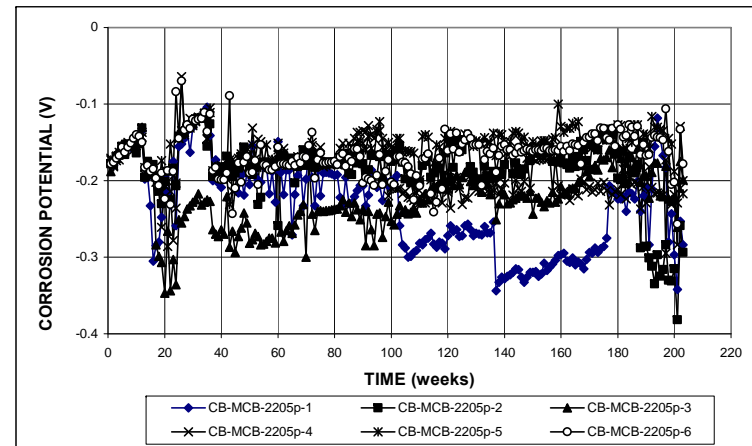


(b)

Figure A.97 – Cracked Beam Test. (a) Corrosion rates and (b) total corrosion losses for specimens with pickled 2205 stainless steel for the Mission Creek Bridge.

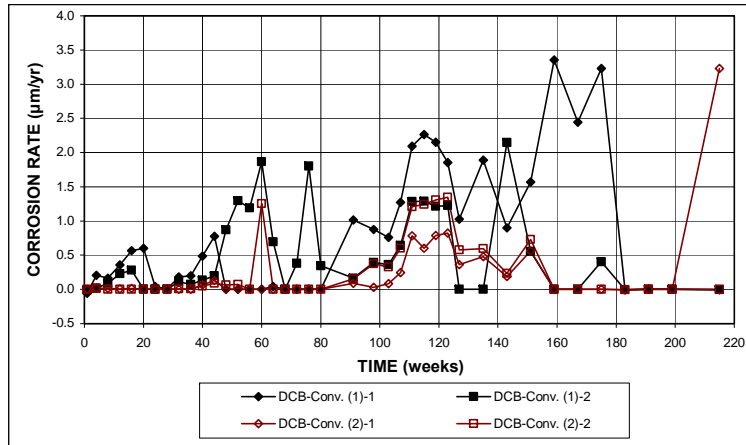


(a)

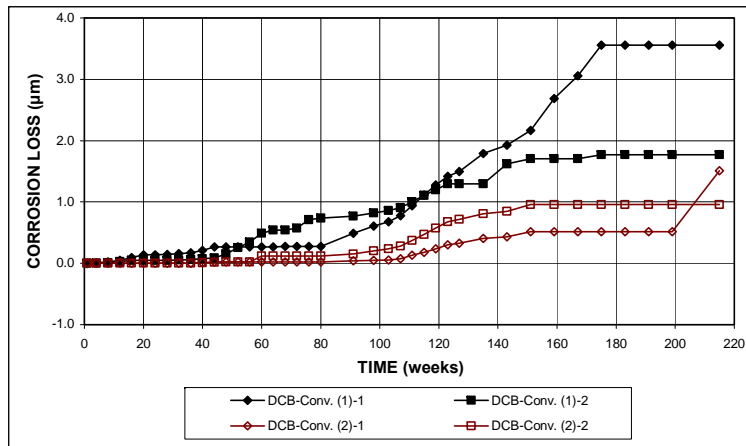


(b)

Figure A.98 – Cracked Beam Test. (a) Top mat corrosion potentials and (b) bottom mat corrosion potentials with respect to a copper-copper sulfate electrode for specimens with pickled 2205 stainless steel for the Mission Creek Bridge.

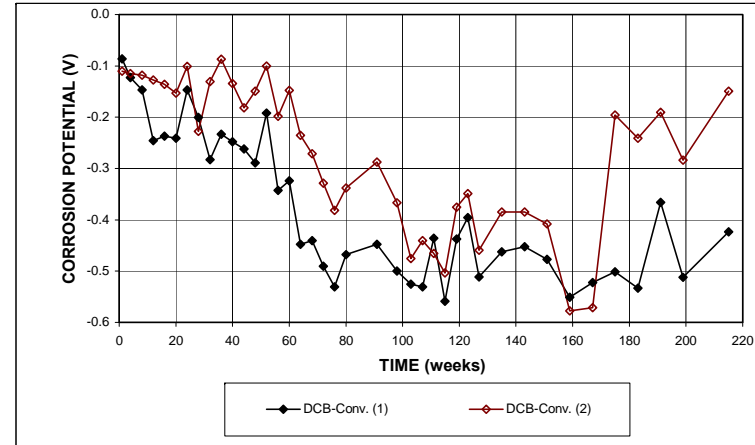


(a)

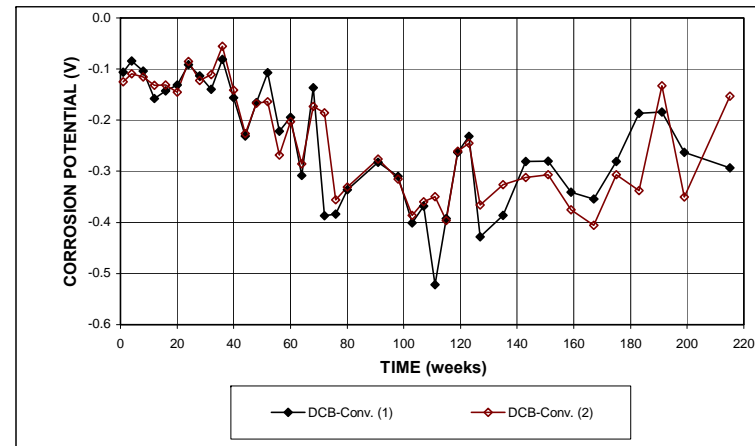


(b)

Figure A.99 – Field Test. (a) Corrosion rates and (b) total corrosion losses for specimens with conventional steel for the Doniphan County Bridge (without cracks).

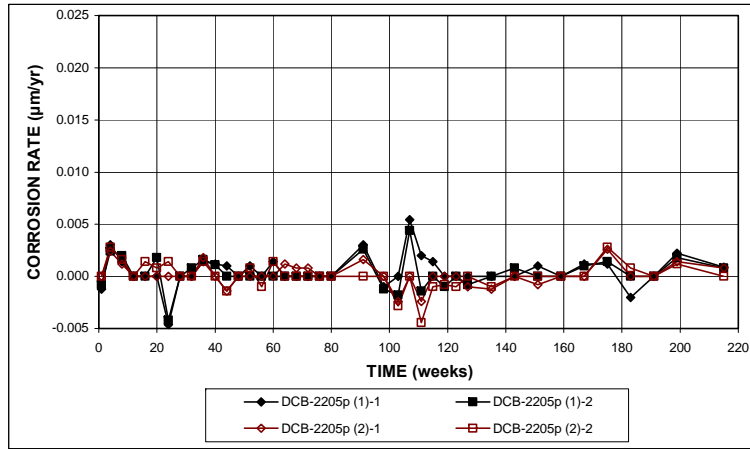


(a)

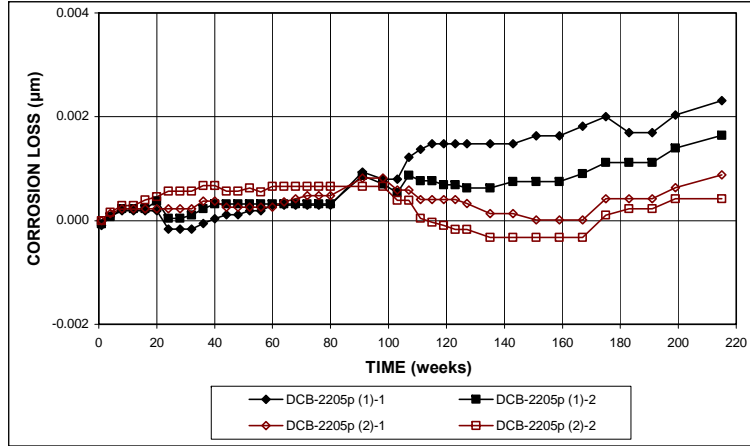


(b)

Figure A.100 – Field Test. (a) Top mat corrosion potentials and (b) bottom mat corrosion potentials with respect to a copper-copper sulfate electrode for specimens with conventional steel for the Doniphan County Bridge (without cracks).

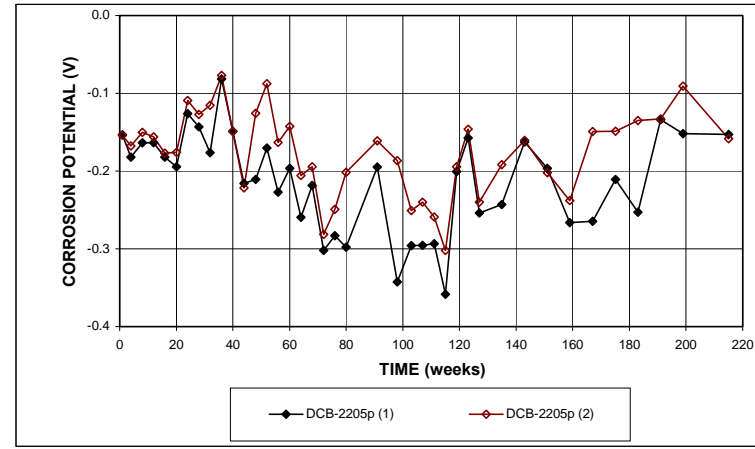


(a)

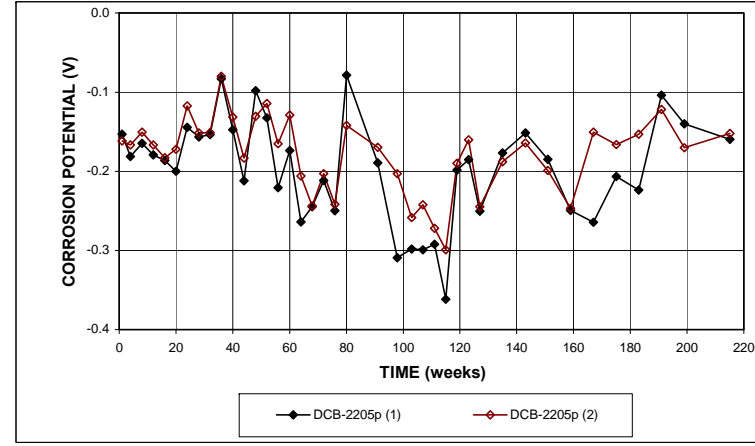


(b)

Figure A.101 – Field Test. (a) Corrosion rates and (b) total corrosion losses for specimens with pickled 2205 stainless steel for the Doniphan County Bridge (without cracks).

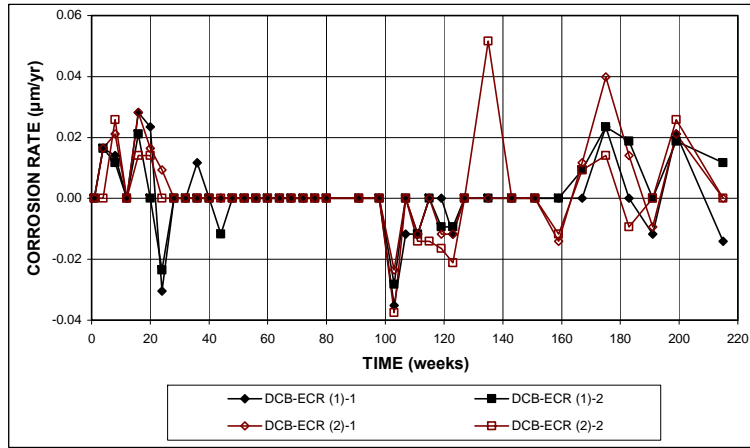


(a)

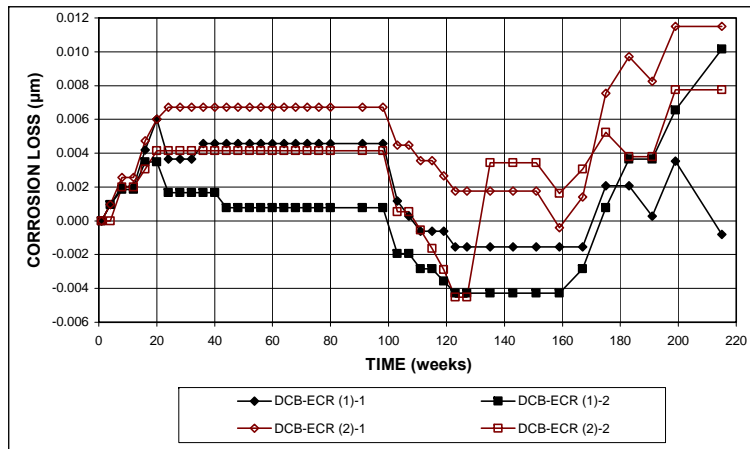


(b)

Figure A.102 – Field Test. (a) Top mat corrosion potentials and (b) bottom mat corrosion potentials with respect to a copper-copper sulfate electrode for specimens with pickled 2205 stainless steel for the Doniphan County Bridge (without cracks).

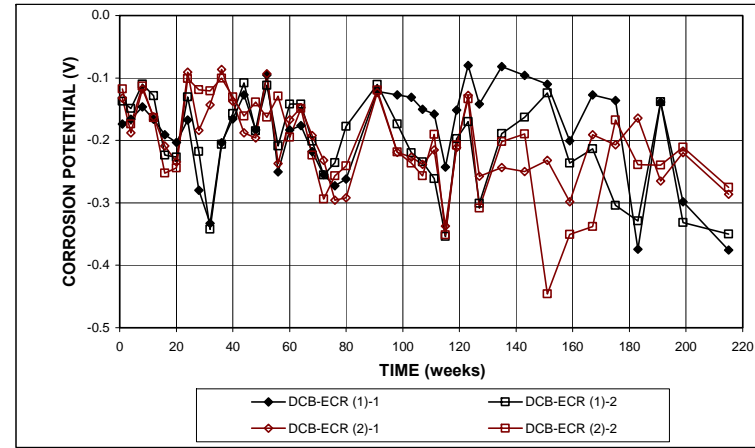


(a)

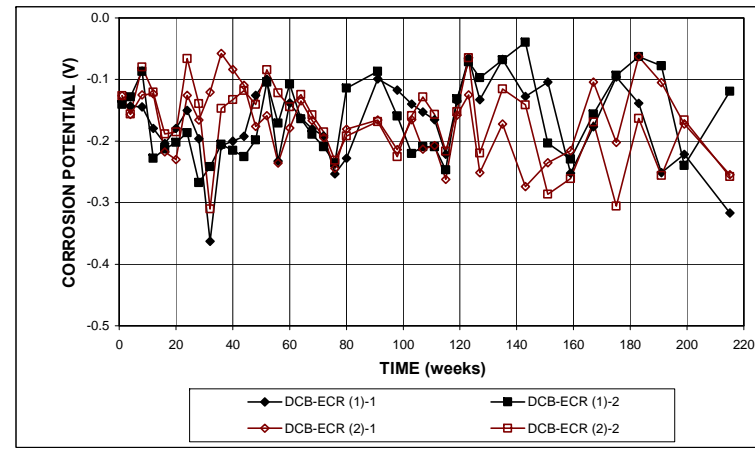


(b)

Figure A.103 – Field Test. (a) Corrosion rates and (b) total corrosion losses for specimens with ECR for the Doniphan County Bridge (without cracks).

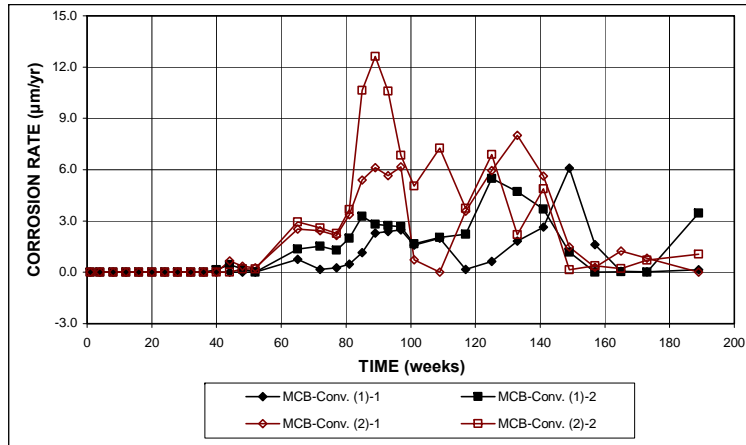


(a)

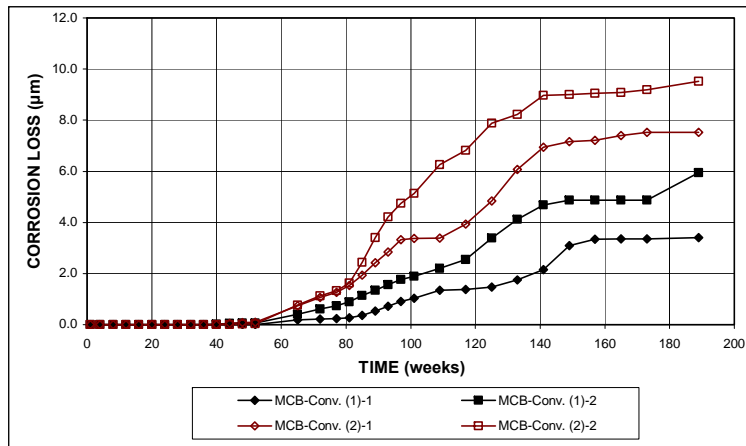


(b)

Figure A.104 – Field Test. (a) Top mat corrosion potentials and (b) bottom mat corrosion potentials with respect to a copper-copper sulfate electrode for specimens with ECR for the Doniphan County Bridge (without cracks).

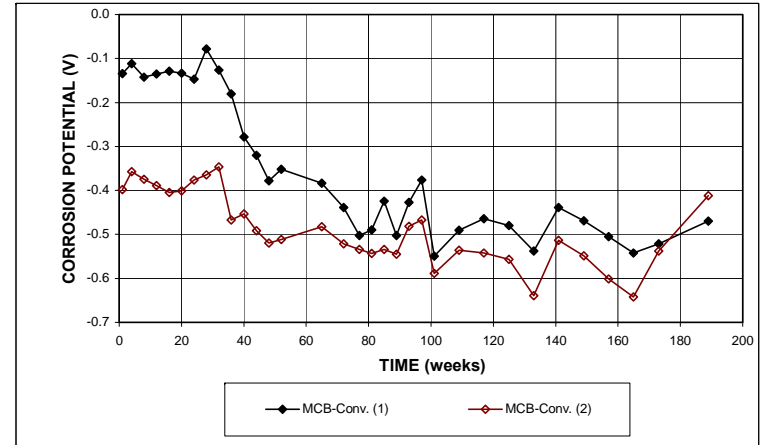


(a)

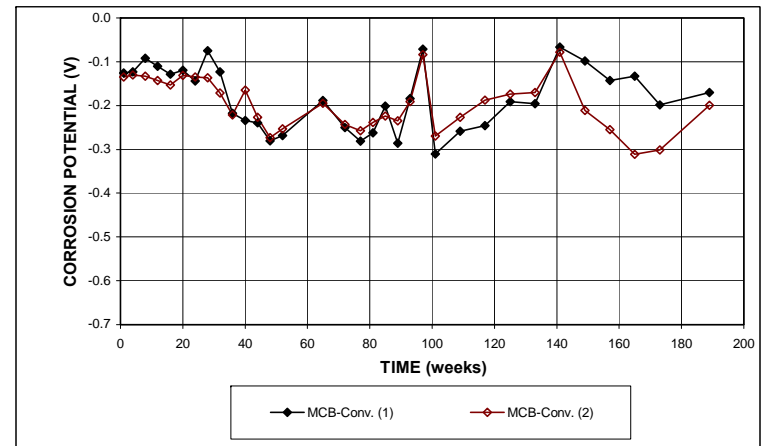


(b)

Figure A.105 – Field Test. (a) Corrosion rates and (b) total corrosion losses for specimens with conventional steel for the Mission Creek Bridge (No. 2 with cracks).

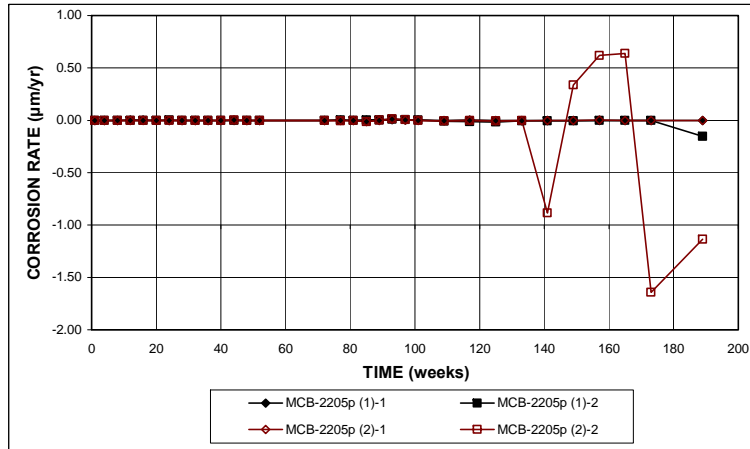


(a)

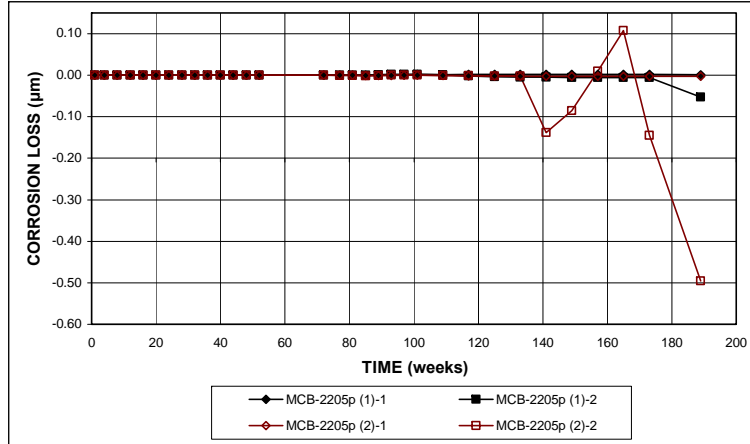


(b)

Figure A.106 – Field Test. (a) Top mat corrosion potentials and (b) bottom mat corrosion potentials with respect to a copper-copper sulfate electrode for specimens with conventional steel for the Mission Creek Bridge (No. 2 with cracks).

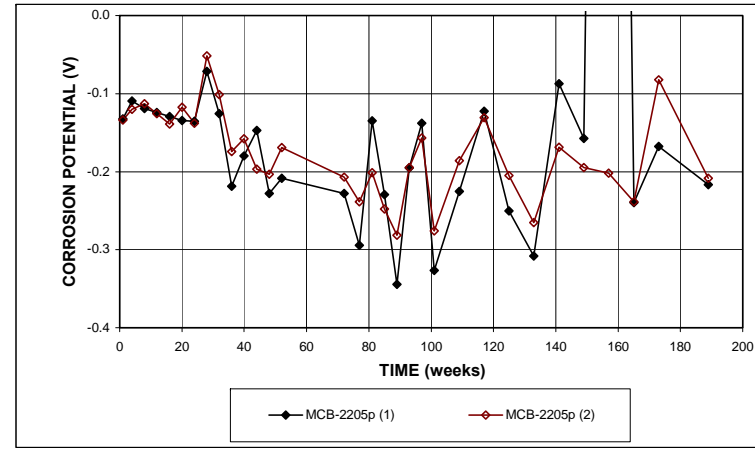


(a)

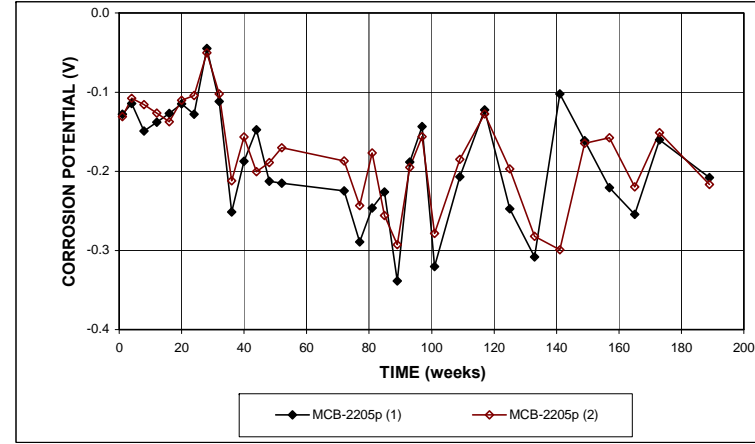


(b)

Figure A.107 – Field Test. (a) Corrosion rates and (b) total corrosion losses for specimens with pickled 2205 stainless steel for the Mission Creek Bridge (No. 2 with cracks).

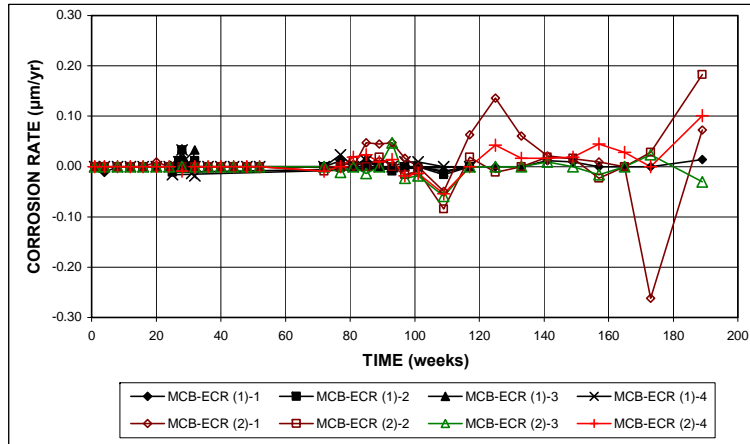


(a)

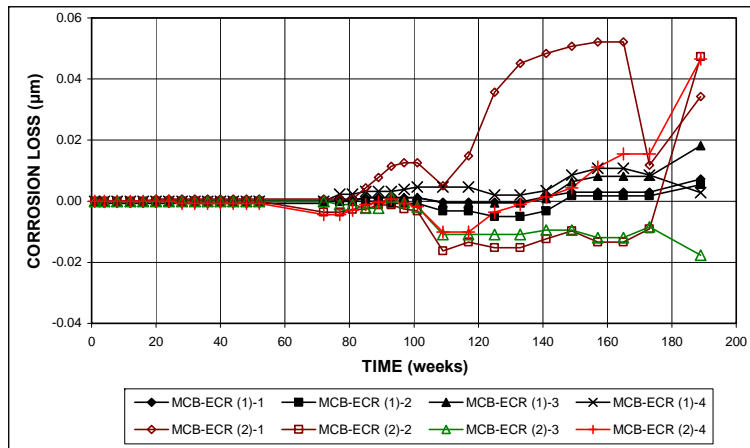


(b)

Figure A.108 – Field Test. (a) Top mat corrosion potentials and (b) bottom mat corrosion potentials with respect to a copper-copper sulfate electrode for specimens with pickled 2205 stainless steel for the Mission Creek Bridge (No. 2 with cracks).

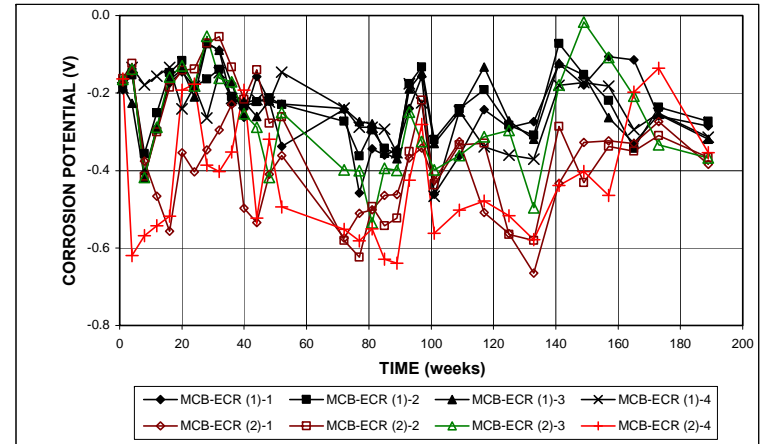


(a)

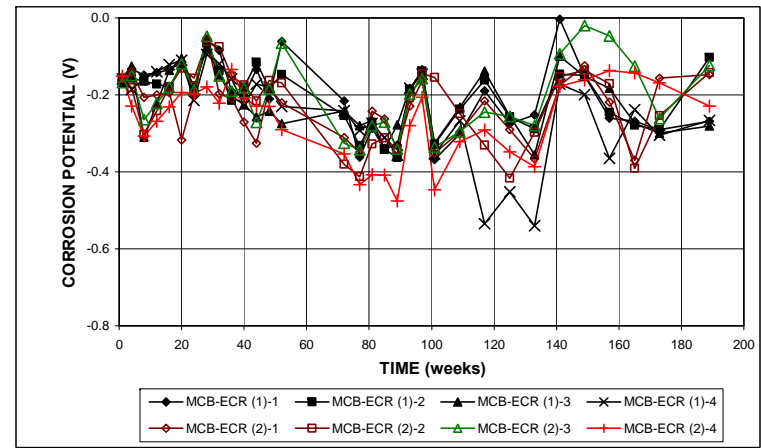


(b)

Figure A.109 – Field Test. (a) Corrosion rates and (b) total corrosion losses for specimens with ECR for the Mission Creek Bridge (No. 2 with cracks).



(a)



(b)

Figure A.110 – Field Test. (a) Top mat corrosion potentials and (b) bottom mat corrosion potentials with respect to a copper-copper sulfate electrode for specimens with ECR for the Mission Creek Bridge (No. 2 with cracks).

APPENDIX B

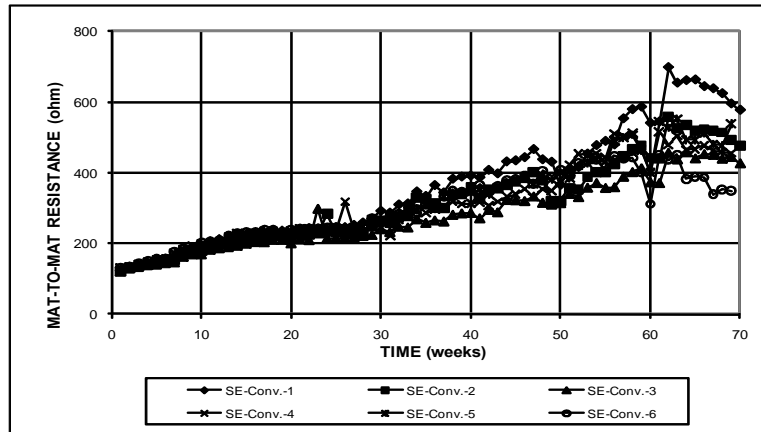


Figure B.1 – Southern Exposure Test. Mat-to-mat resistances for specimens with conventional steel (controls).

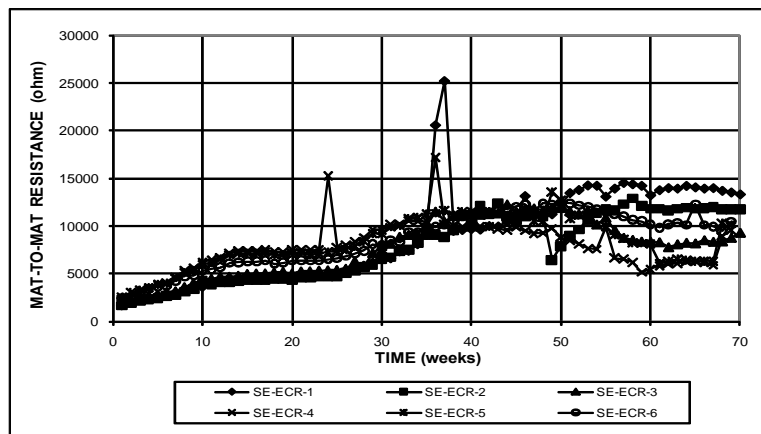


Figure B.2 – Southern Exposure Test. Mat-to-mat resistances for specimens with ECR (ECR with four holes).

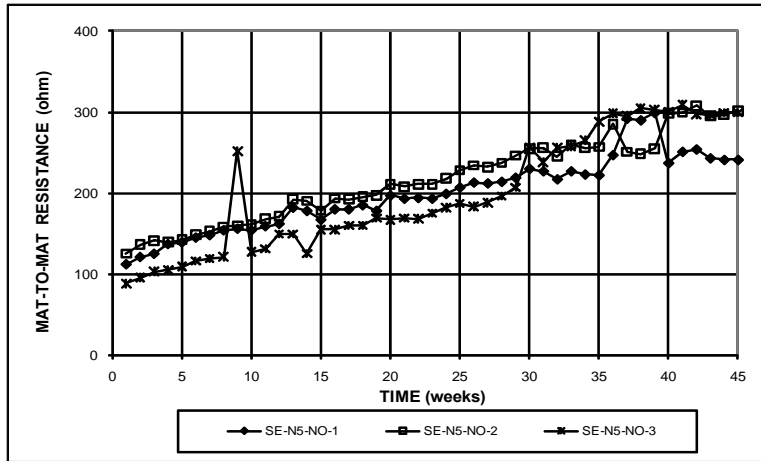


Figure B.3 – Southern Exposure Test. Mat-to-mat resistances for specimens with conventional steel and no inhibitors.

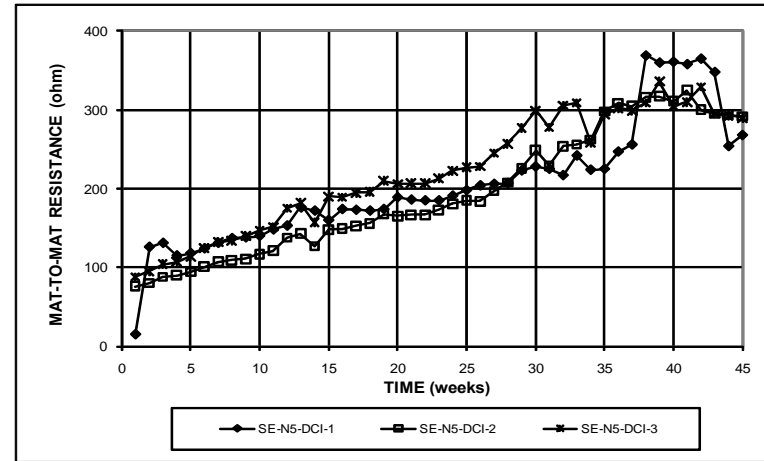


Figure B.5 – Southern Exposure Test. Mat-to-mat resistances for specimens with conventional steel and DCI inhibitor.

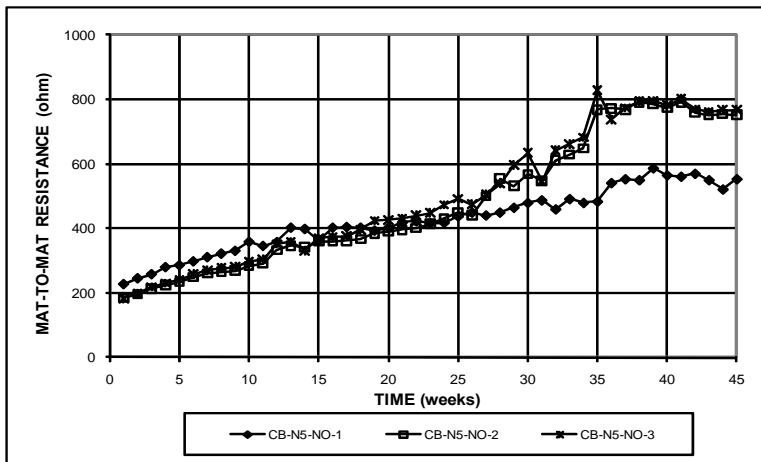


Figure B.4 – Cracked Beam Test. Mat-to-mat resistances for specimens with conventional steel and no inhibitors.

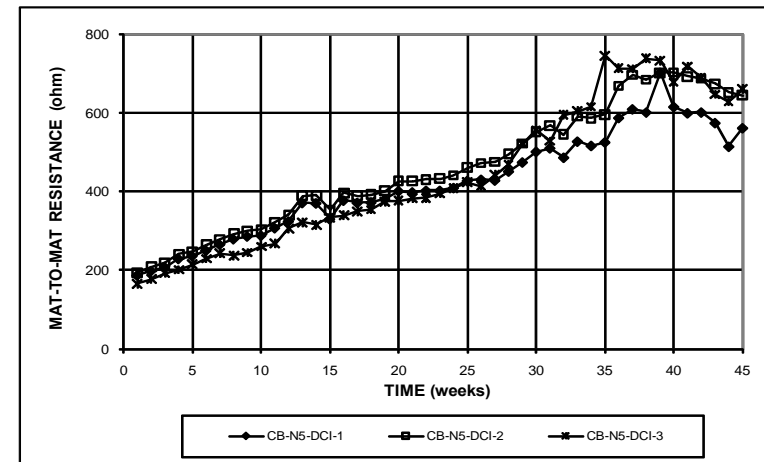


Figure B.6 – Cracked Beam Test. Mat-to-mat resistances for specimens with conventional steel and DCI inhibitor.

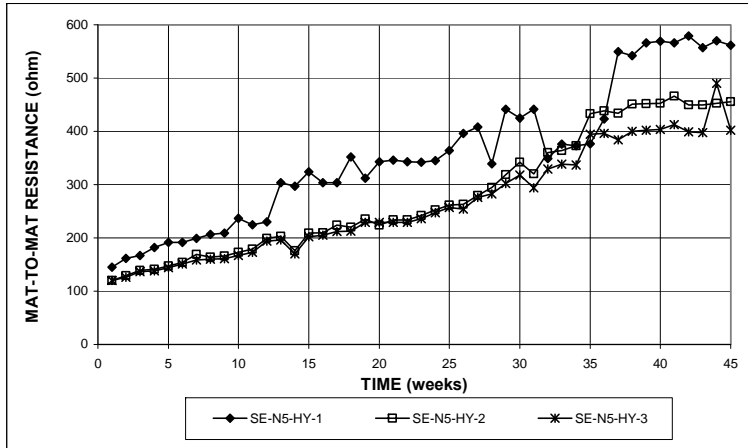


Figure B.7 – Southern Exposure Test. Mat-to-mat resistances for specimens with conventional steel and Hycrete inhibitor.

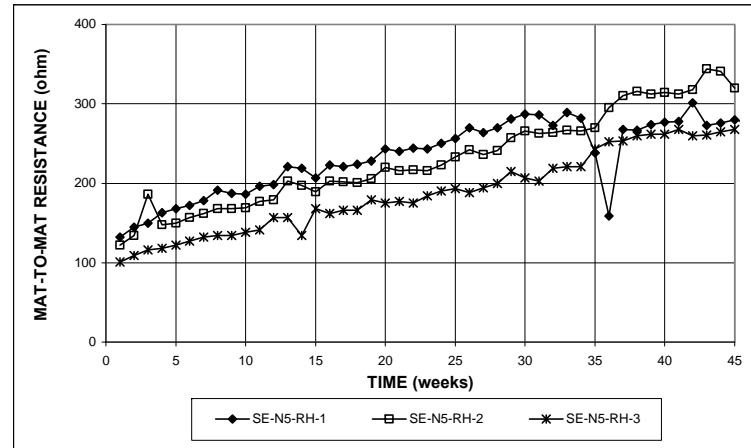


Figure B.9 – Southern Exposure Test. Mat-to-mat resistances for specimens with conventional steel and Rheocrete inhibitor.

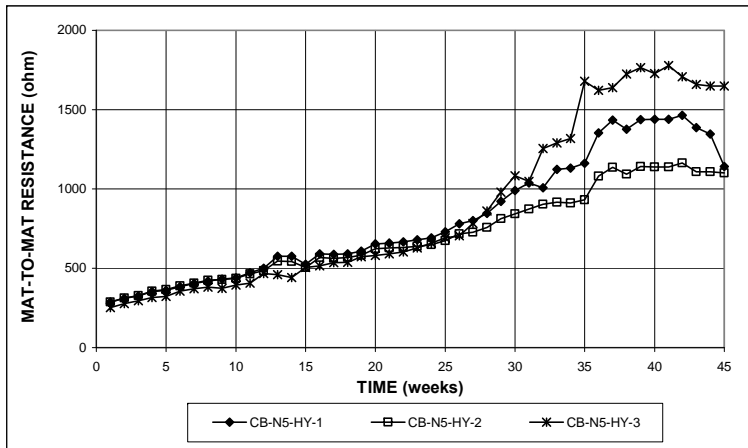


Figure B.8 – Cracked Beam Test. Mat-to-mat resistances for specimens with conventional steel and Hycrete inhibitor.

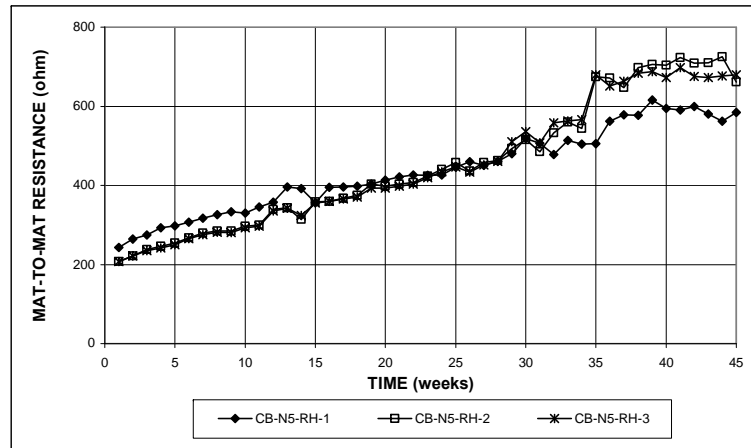


Figure B.10 – Cracked Beam Test. Mat-to-mat resistances for specimens with conventional steel and Rheocrete inhibitor.

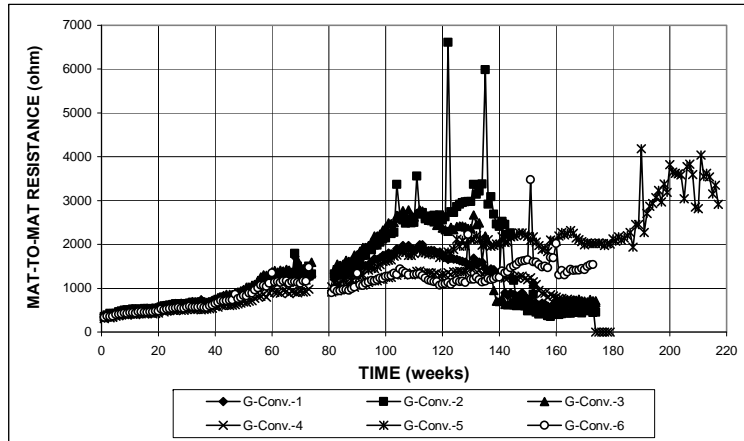


Figure B.11 – ASTM G109 Test. Mat-to-mat resistances for specimens with conventional steel.

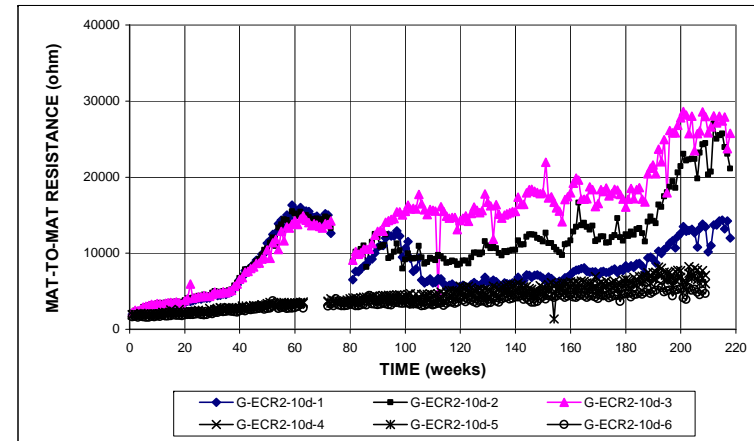


Figure B.13 – ASTM G109 Test. Mat-to-mat resistances for specimens with ECR (ten holes).

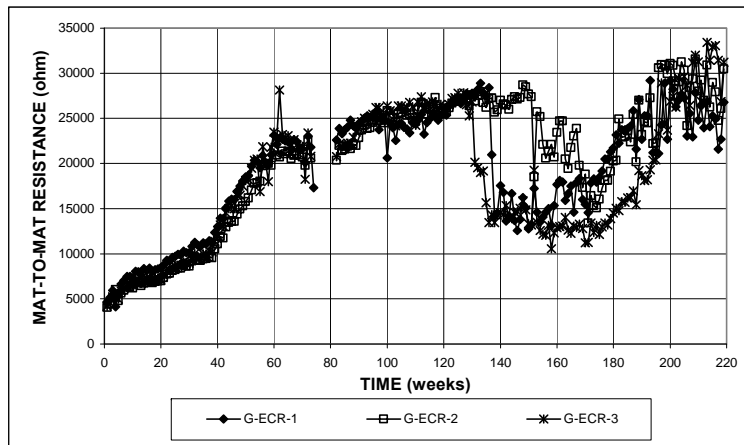


Figure B.12 – ASTM G109 Test. Mat-to-mat resistances for specimens with ECR (four holes).

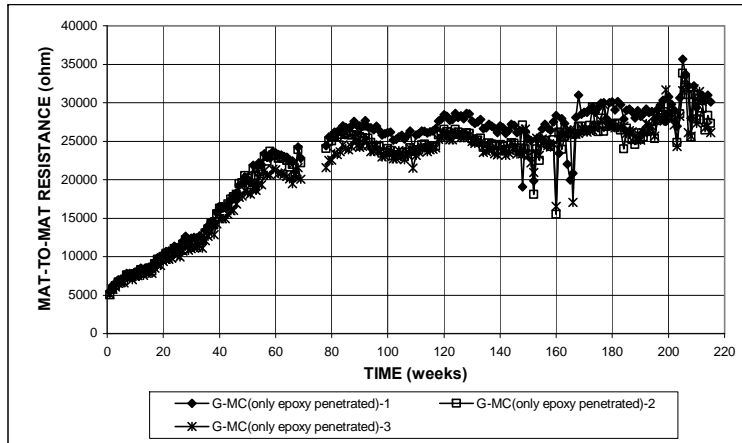


Figure B.14 – ASTM G109 Test. Mat-to-mat resistances for specimens with multiple coated bars (four holes, only epoxy penetrated).

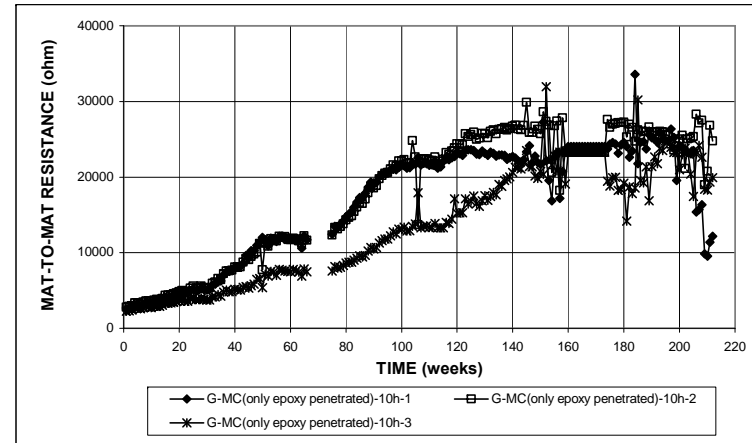


Figure B.16 – ASTM G109 Test. Mat-to-mat resistances for specimens with multiple coated bars (ten holes, only epoxy penetrated).

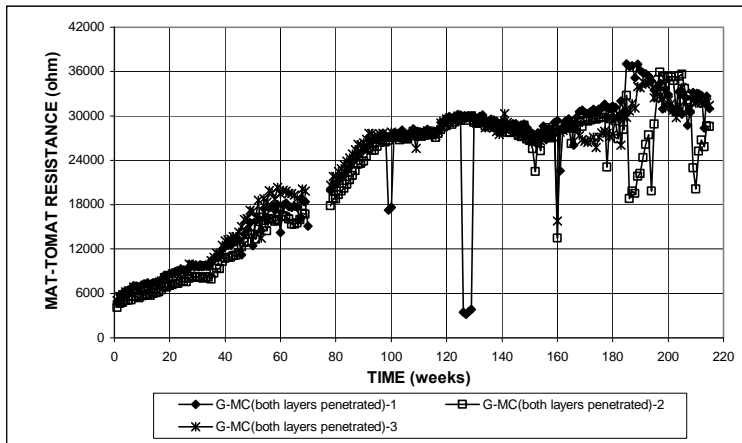


Figure B.15 – ASTM G109 Test. Mat-to-mat resistances for specimens with multiple coated bars (four holes, both layers penetrated).

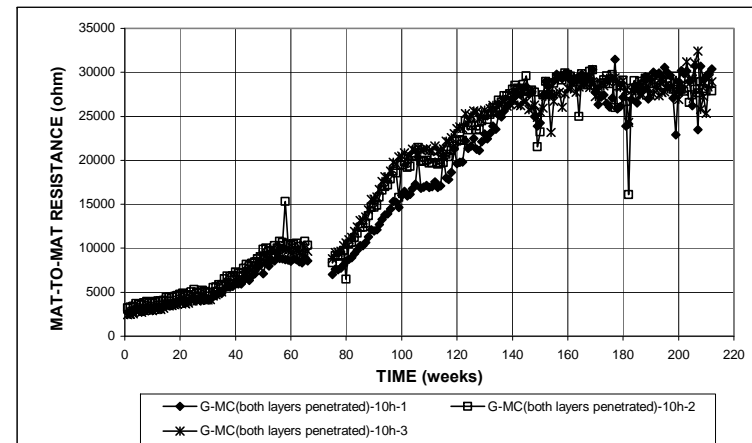


Figure B.17 – ASTM G109 Test. Mat-to-mat resistances for specimens with multiple coated bars (ten holes, both layers penetrated).

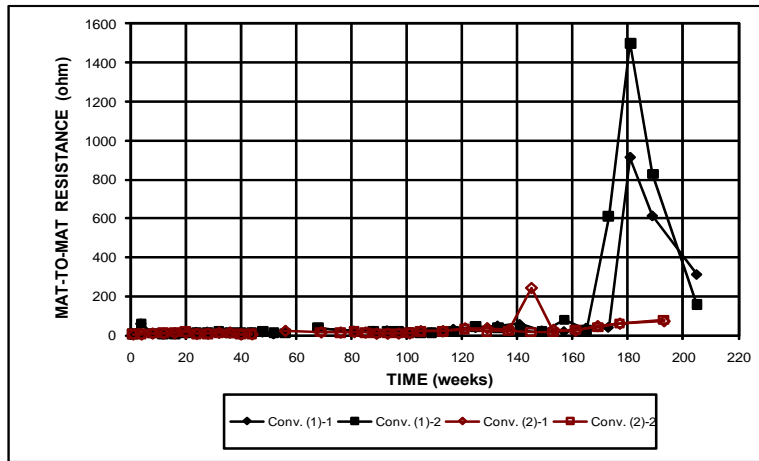


Figure B.18 – Field Test. Mat-to-mat resistances for specimens with conventional steel, without cracks.

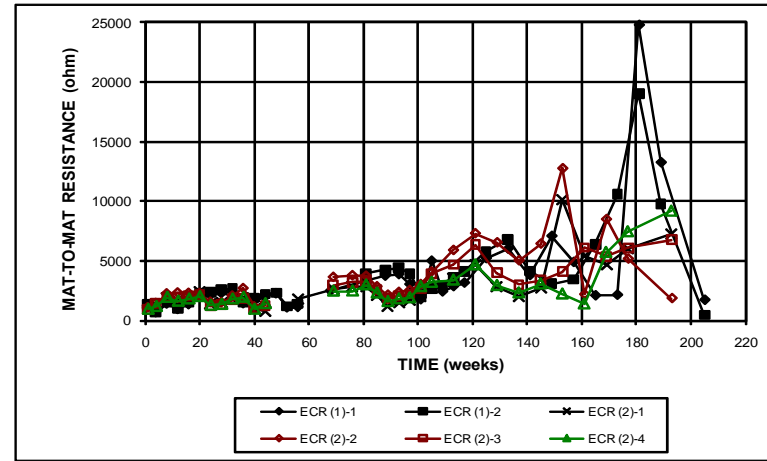


Figure B.20 – Field Test. Mat-to-mat resistances for specimens with ECR, without cracks.

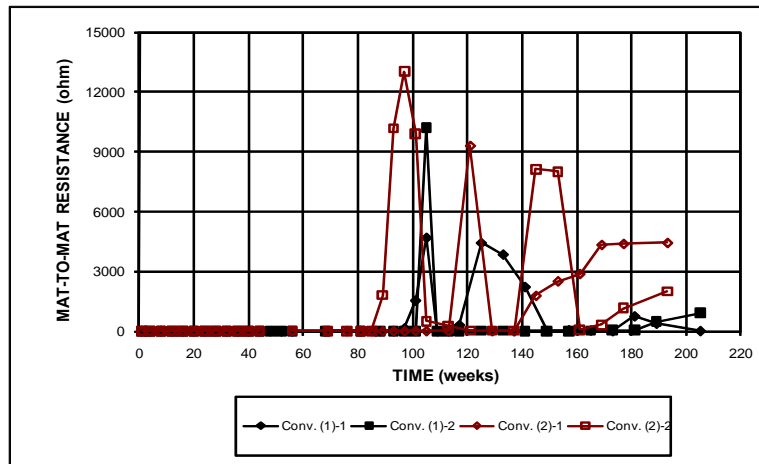


Figure B.19 – Field Test. Mat-to-mat resistances for specimens with conventional steel, with cracks.

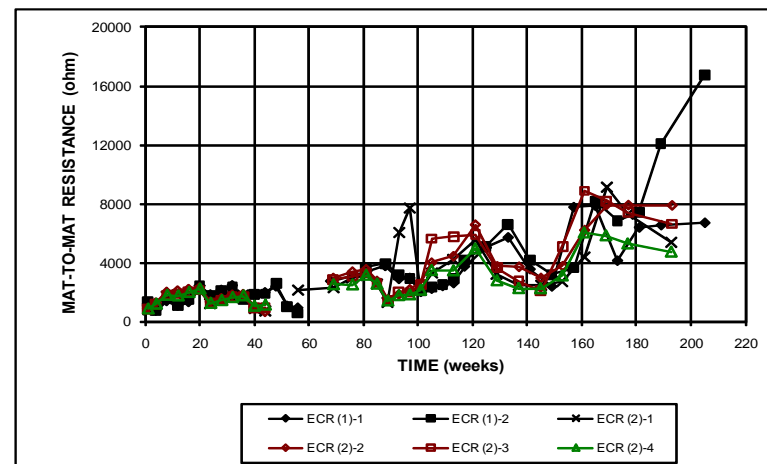


Figure B.21 – Field Test. Mat-to-mat resistances for specimens with ECR, with cracks.

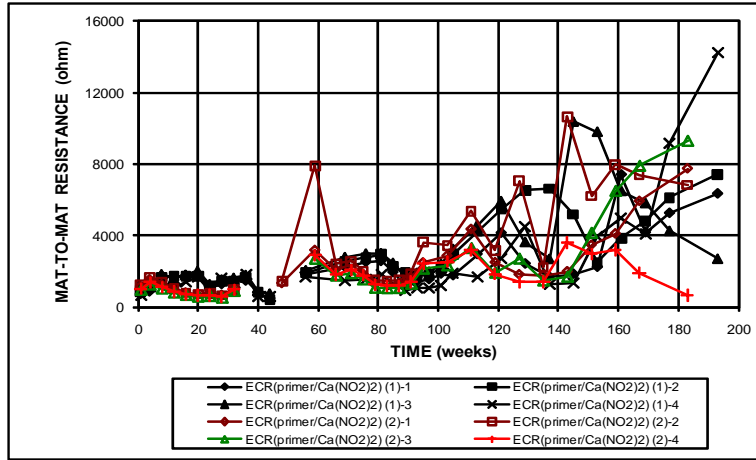


Figure B.22 – Field Test. Mat-to-mat resistances for specimens with ECR with a primer containing calcium nitrite, without cracks.

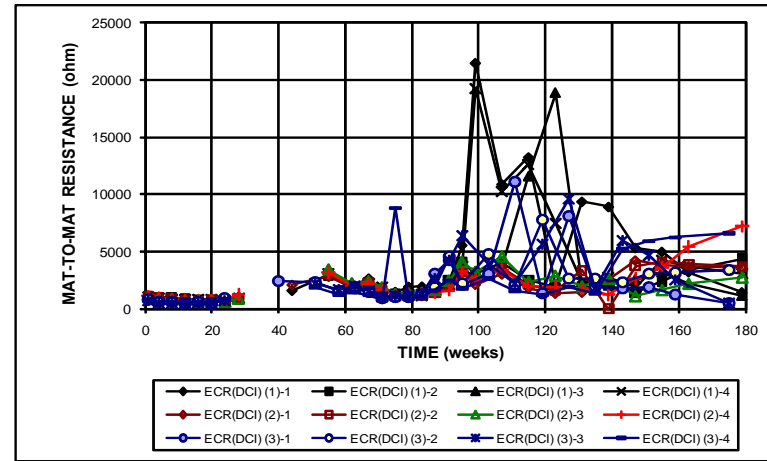


Figure B.24 – Field Test. Mat-to-mat resistances for specimens with ECR and DCI inhibitor, without cracks.

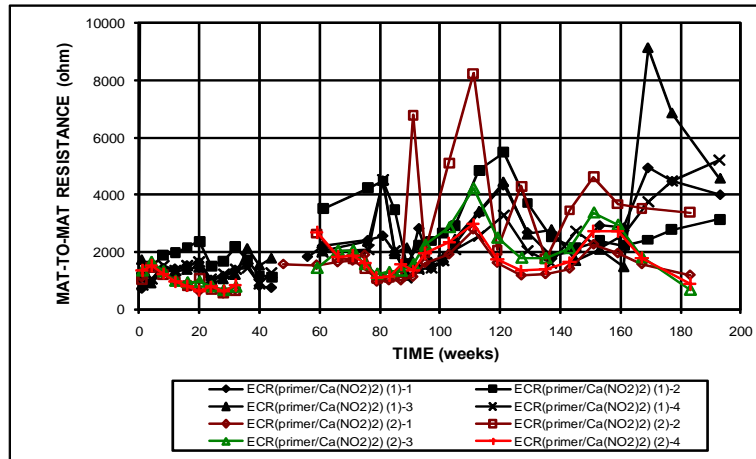


Figure B.23 – Field Test. Mat-to-mat resistances for specimens with ECR with a primer containing calcium nitrite, with cracks.

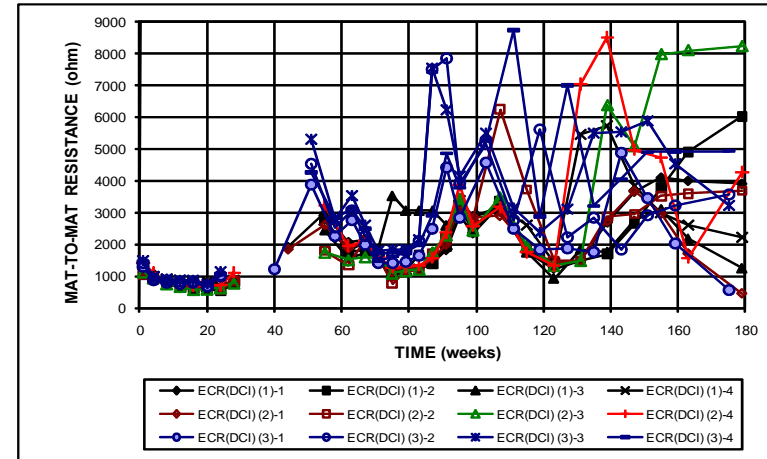


Figure B.25 – Field Test. Mat-to-mat resistances for specimens with ECR and DCI inhibitor, with cracks.

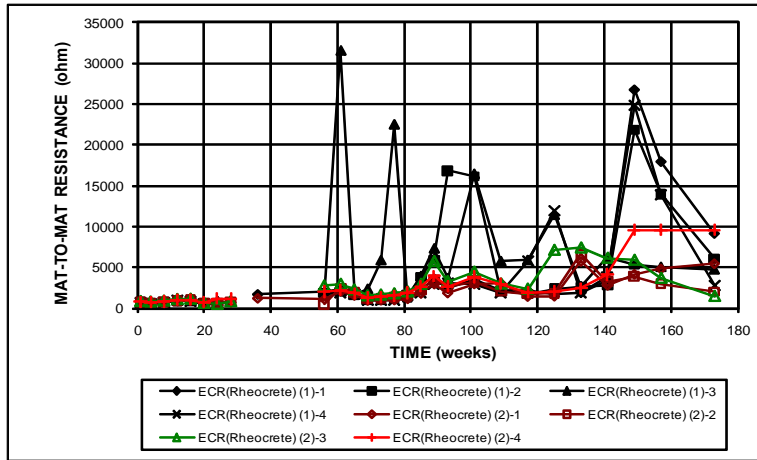


Figure B.26 – Field Test. Mat-to-mat resistances for specimens with ECR and Rheocrete inhibitor, without cracks.

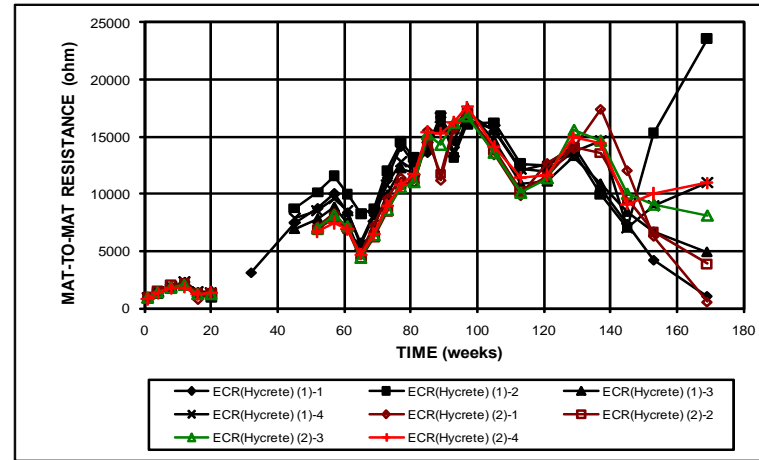


Figure B.28 – Field Test. Mat-to-mat resistances for specimens with ECR and Hycrete inhibitor, without cracks.

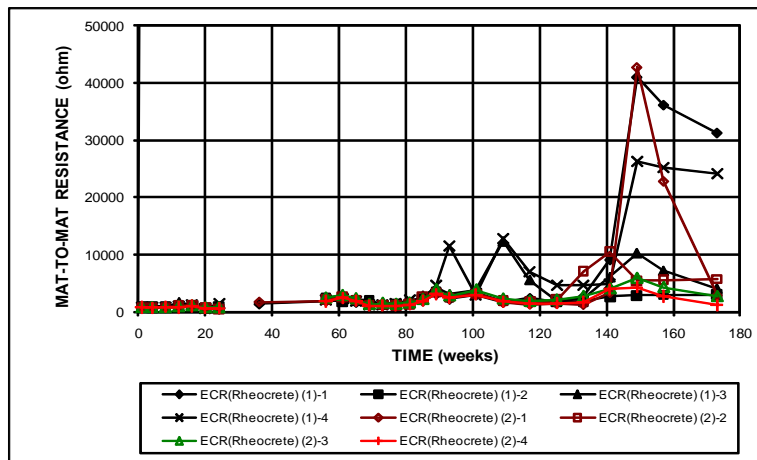


Figure B.27 – Field Test. Mat-to-mat resistances for specimens with ECR and Rheocrete inhibitor, with cracks.

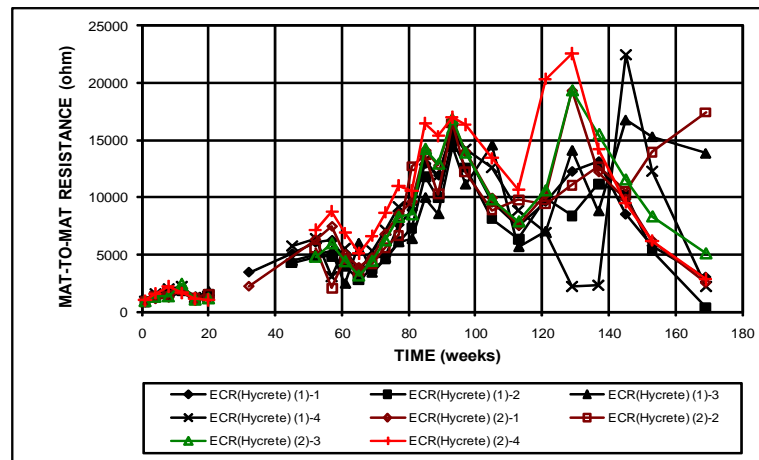


Figure B.29 – Field Test. Mat-to-mat resistances for specimens with ECR and Hycrete inhibitor, with cracks.

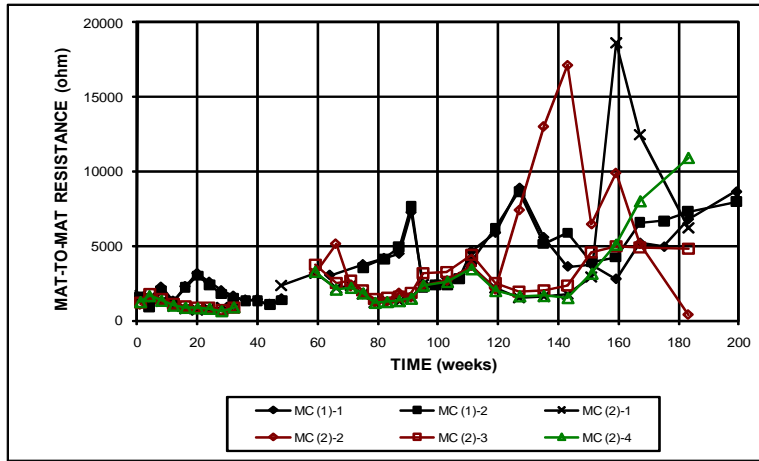


Figure B.30 – Field Test. Mat-to-mat resistances for specimens with multiple-coated bars, without cracks.

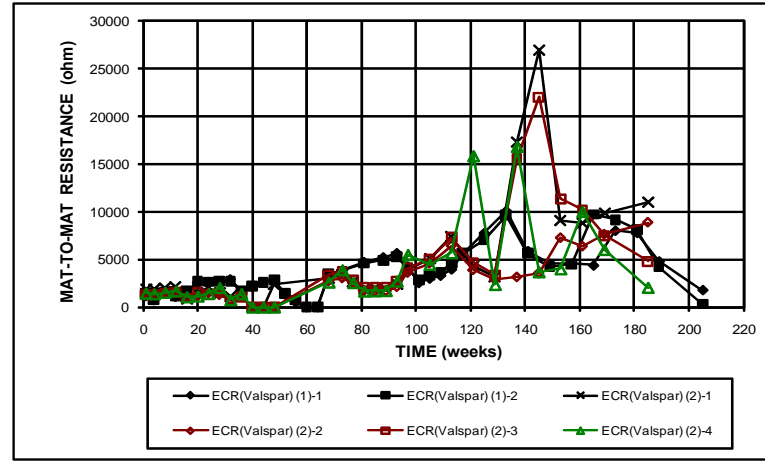


Figure B.32 – Field Test. Mat-to-mat resistances for specimens with ECR with increased adhesion Valspar coating, without cracks.

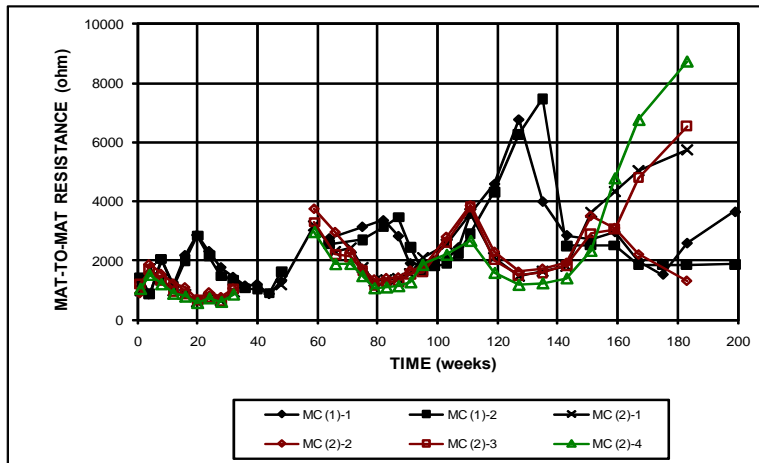


Figure B.31 – Field Test. Mat-to-mat resistances for specimens with multiple-coated bars, with cracks.

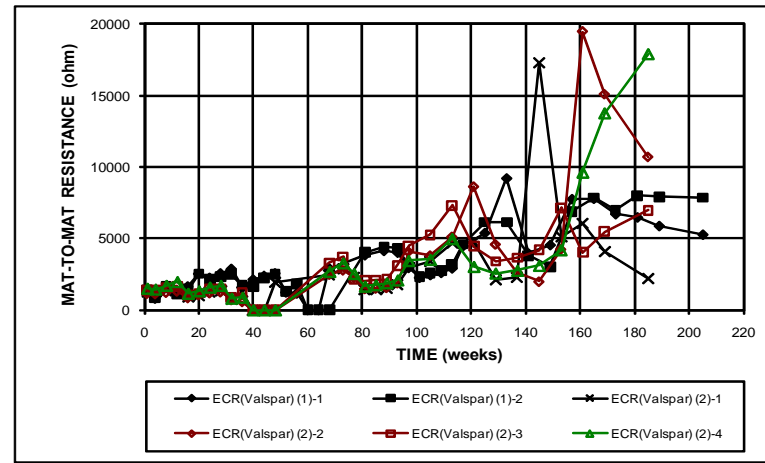


Figure B.33 – Field Test. Mat-to-mat resistances for specimens with ECR with increased adhesion Valspar coating, with cracks.

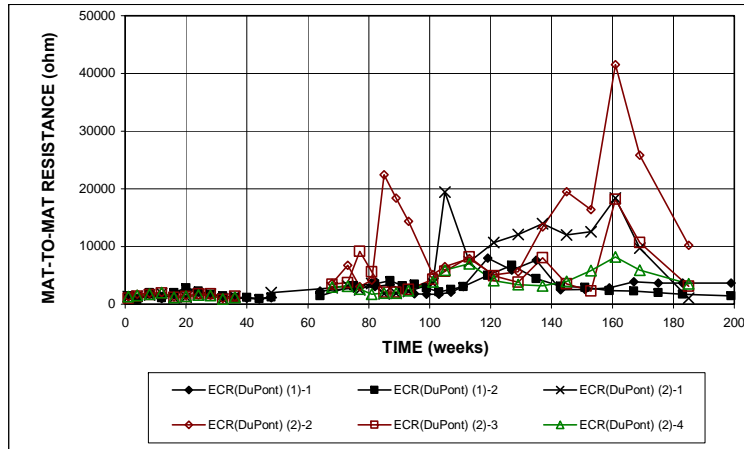


Figure B.34 – Field Test. Mat-to-mat resistances for specimens with ECR with increased adhesion DuPont coating, without cracks.

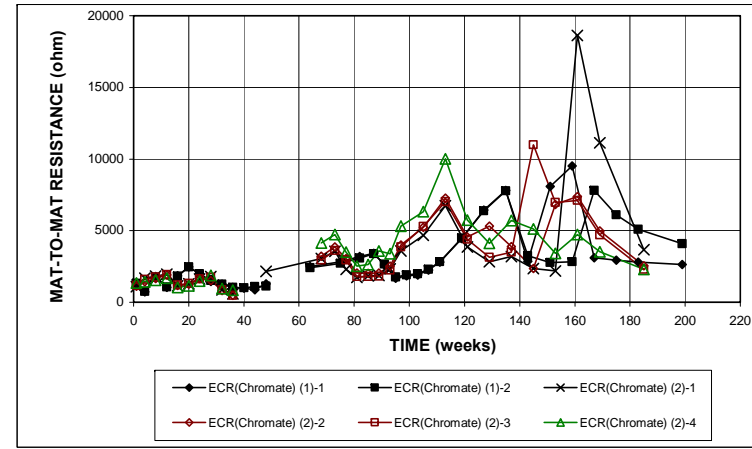


Figure B.36 – Field Test. Mat-to-mat resistances for specimens with ECR with zinc chromate pretreatment, without cracks.

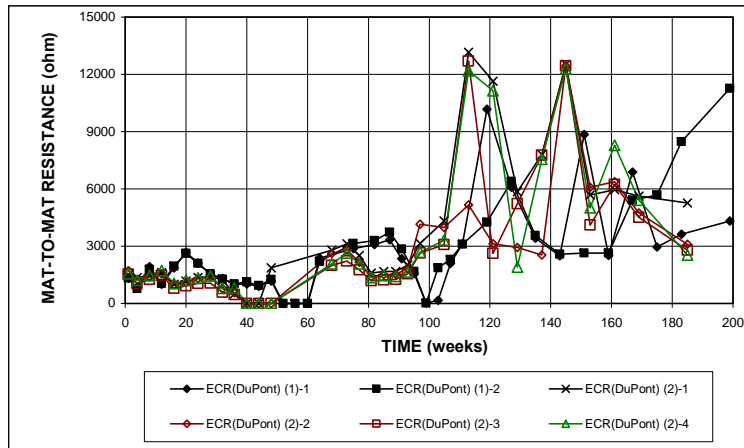


Figure B.35 – Field Test. Mat-to-mat resistances for specimens with ECR with increased adhesion DuPont coating, with cracks

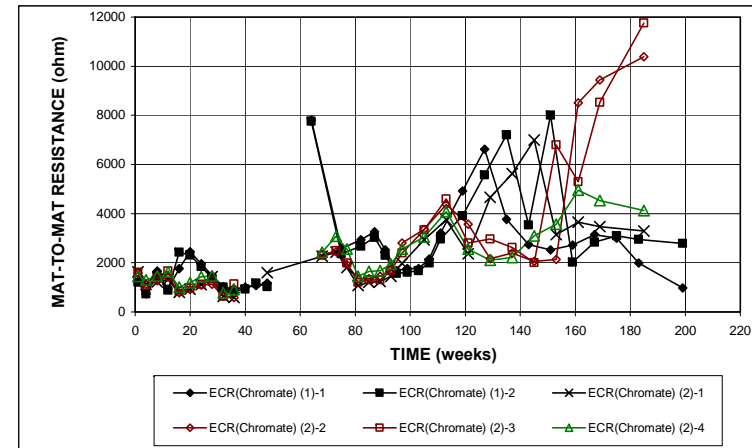


Figure B.37 – Field Test. Mat-to-mat resistances for specimens with ECR with zinc chromate pretreatment, without cracks.

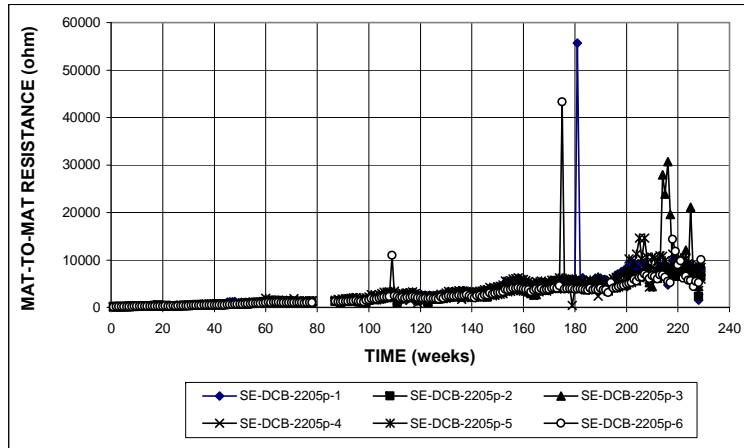


Figure B.38 – Southern Exposure Test. Mat-to-mat resistances for specimens with pickled 2205 stainless steel for the Doniphan County Bridge.

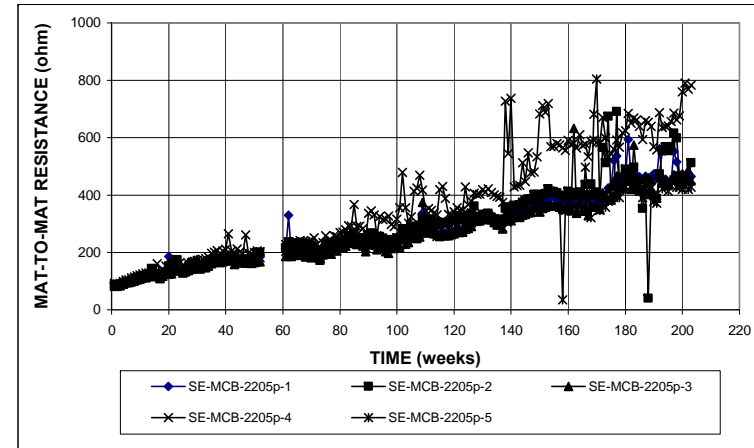


Figure B.40 – Southern Exposure Test. Mat-to-mat resistances for specimens with pickled 2205 stainless steel for the Mission Creek Bridge.

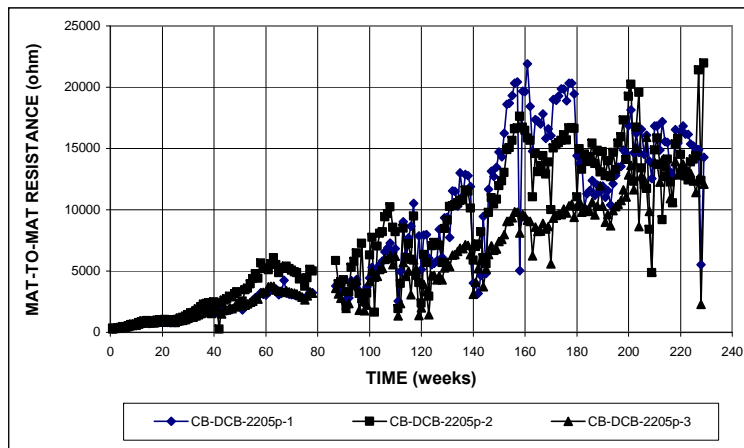


Figure B.39 – Cracked Beam Test. Mat-to-mat resistances for specimens with pickled 2205 stainless steel for the Doniphan County Bridge.

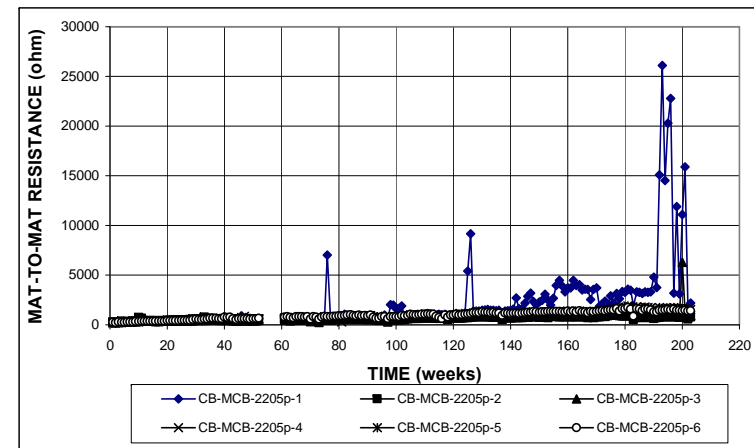


Figure B.41 – Cracked Beam Test. Mat-to-mat resistances for specimens with pickled 2205 stainless steel for the Mission Creek Bridge.

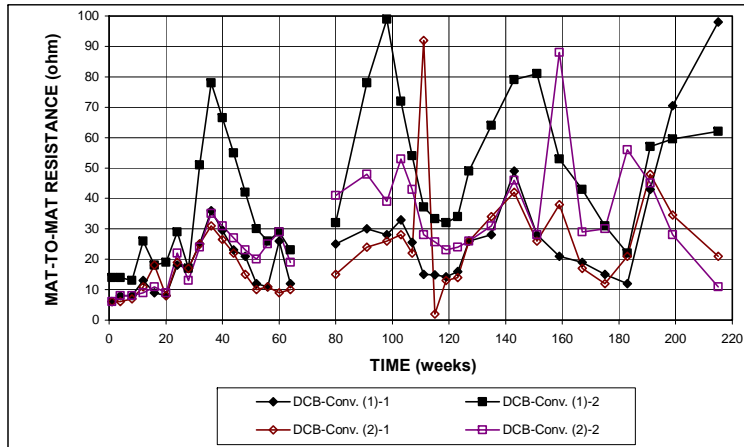


Figure B.42 – Field Test. Mat-to-mat resistances for specimens with conventional steel for the Doniphan County Bridge.

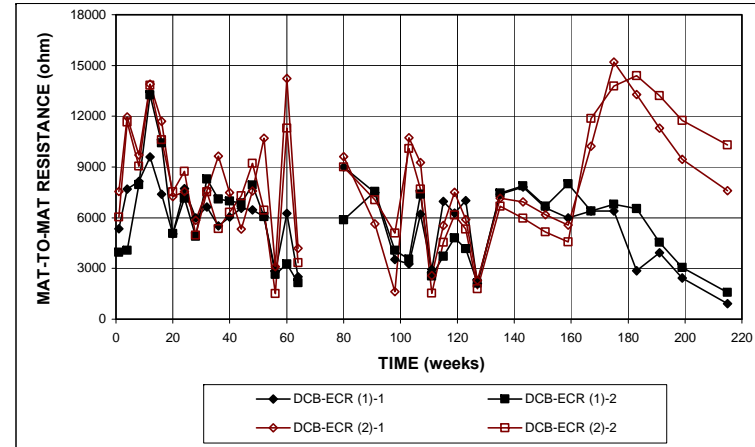


Figure B.44 – Field Test. Mat-to-mat resistances for specimens with ECR for the Doniphan County Bridge.

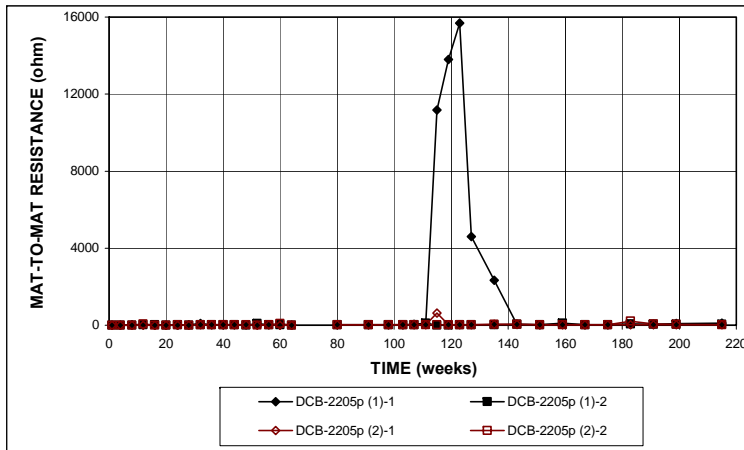


Figure B.43 – Field Test. Mat-to-mat resistances for specimens with pickled 2205 stainless steel for the Doniphan County Bridge.

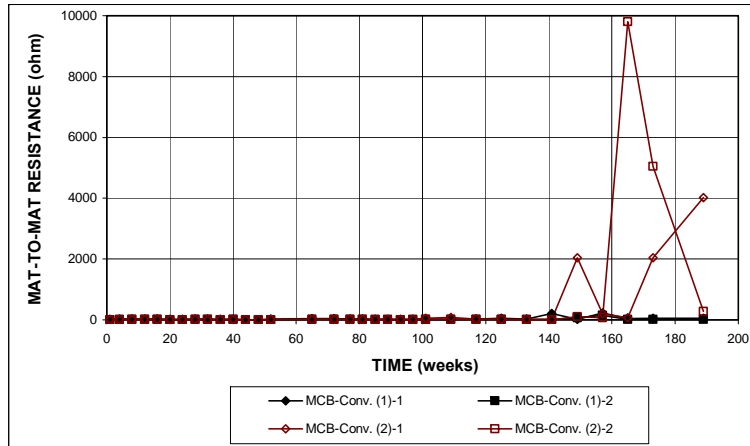


Figure B.45 – Field Test. Mat-to-mat resistances for specimens with conventional steel for the Mission Creek Bridge.

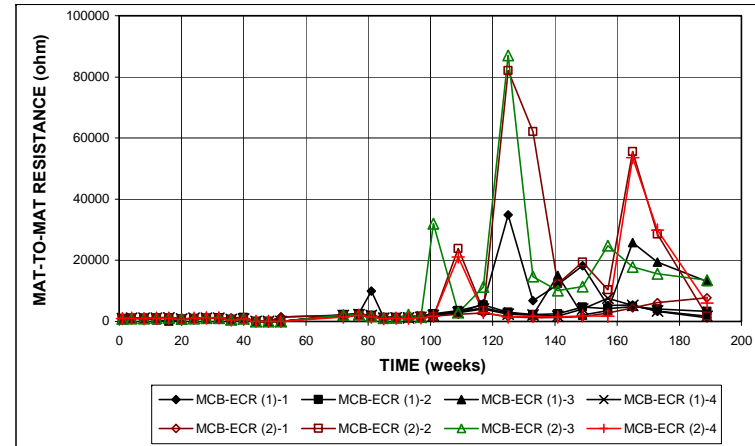


Figure B.47 – Field Test. Mat-to-mat resistances for specimens with ECR for the Mission Creek Bridge.

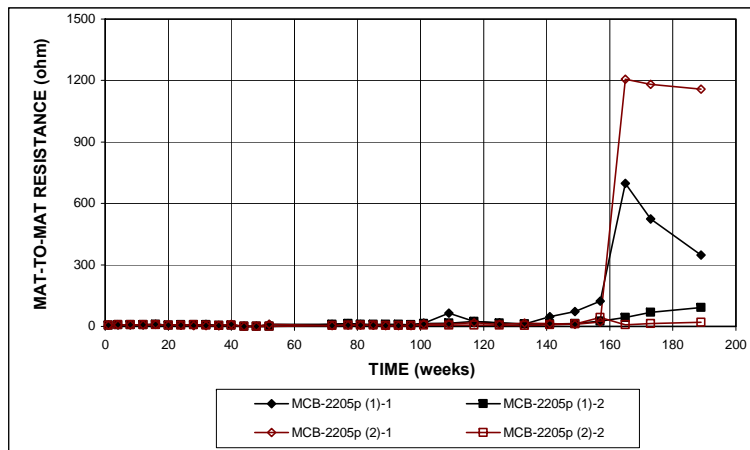


Figure B.46 – Field Test. Mat-to-mat resistances for specimens with pickled 2205 stainless steel for the Mission Creek Bridge.

APPENDIX C

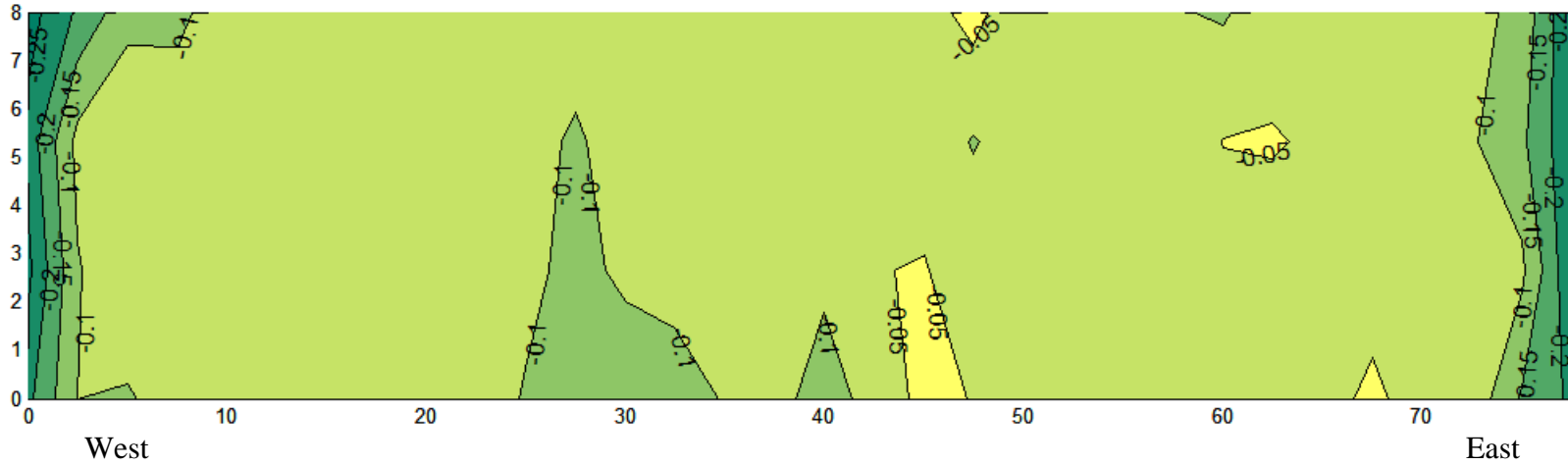


Figure C.1 – Corrosion potential map for the Doniphan County Bridge (September 17, 2004)

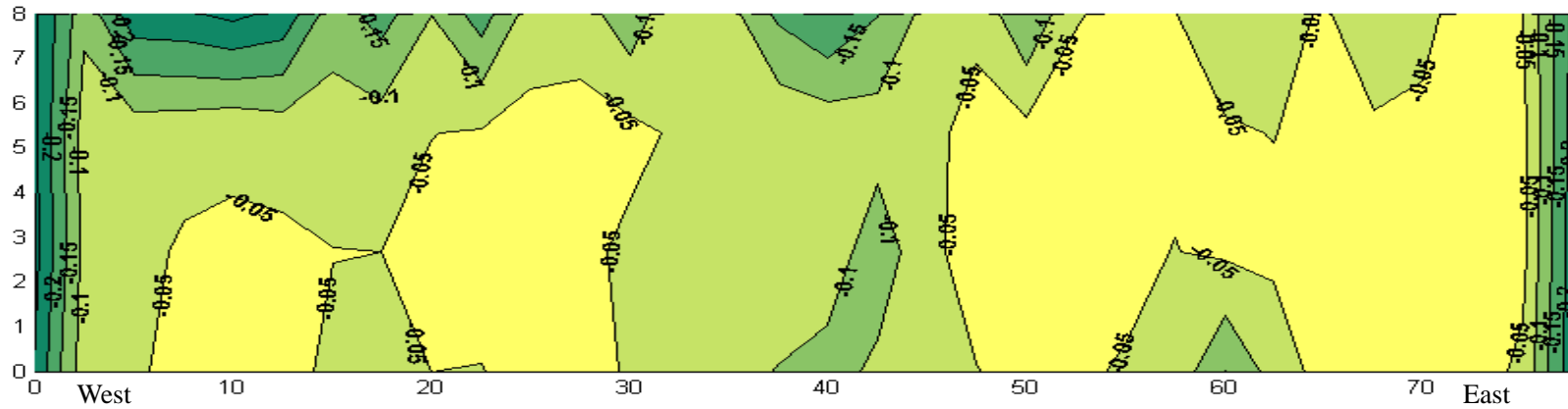


Figure C.2 – Corrosion potential map for the Doniphan County Bridge (April 26, 2005)

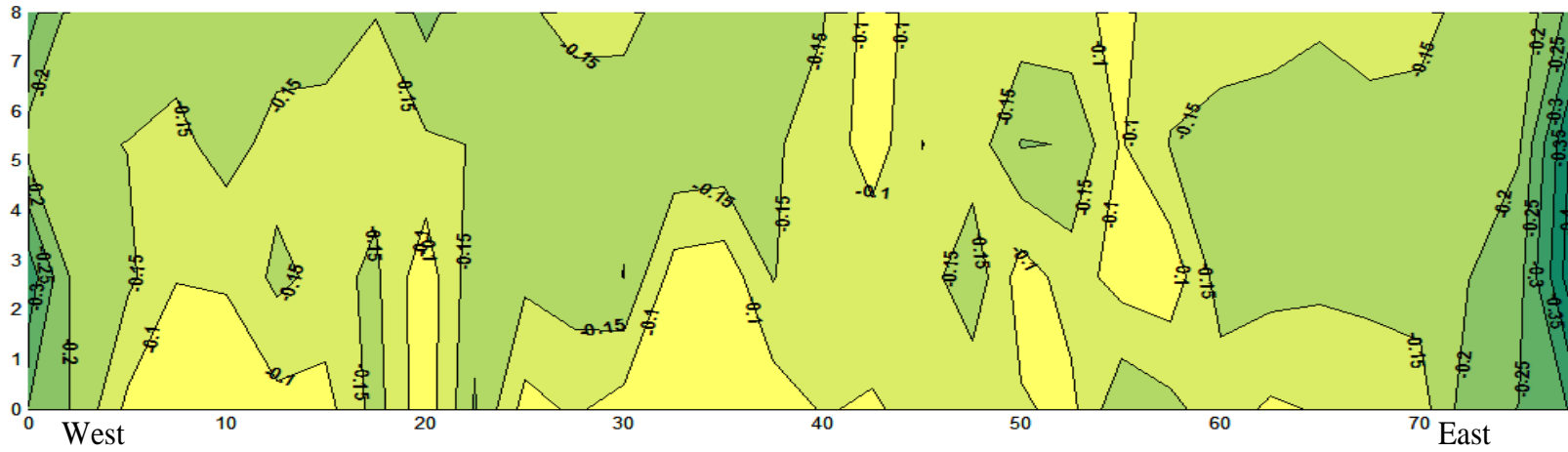


Figure C.3 – Corrosion potential map for the Doniphan County Bridge (October 14, 2005)

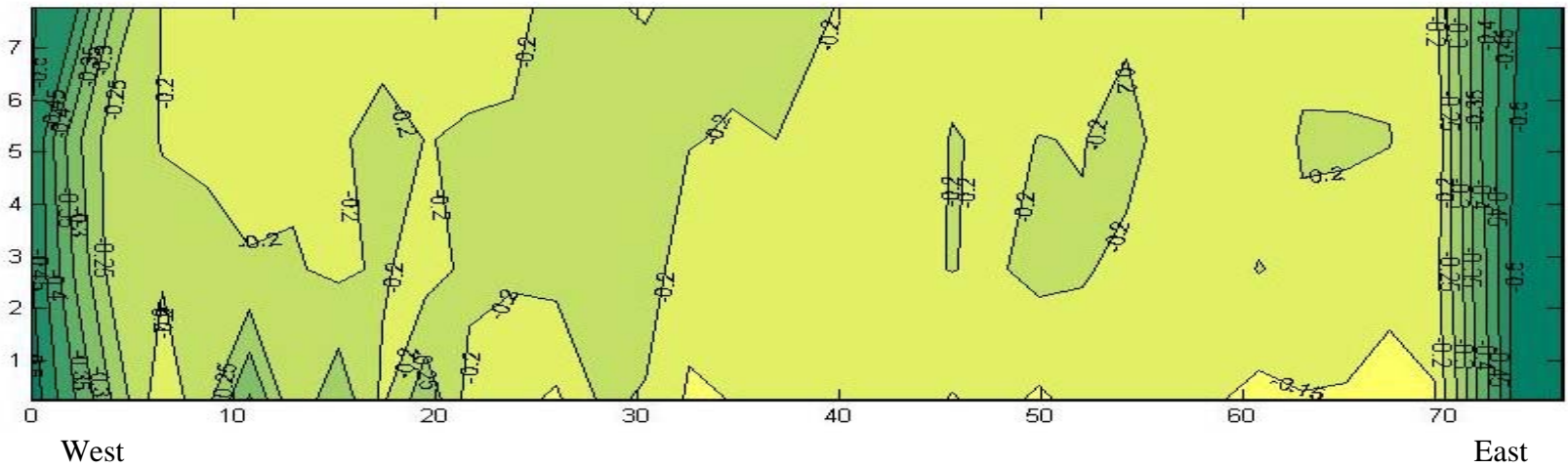


Figure C.4 – Corrosion potential map for the Doniphan County Bridge (June 13, 2006)

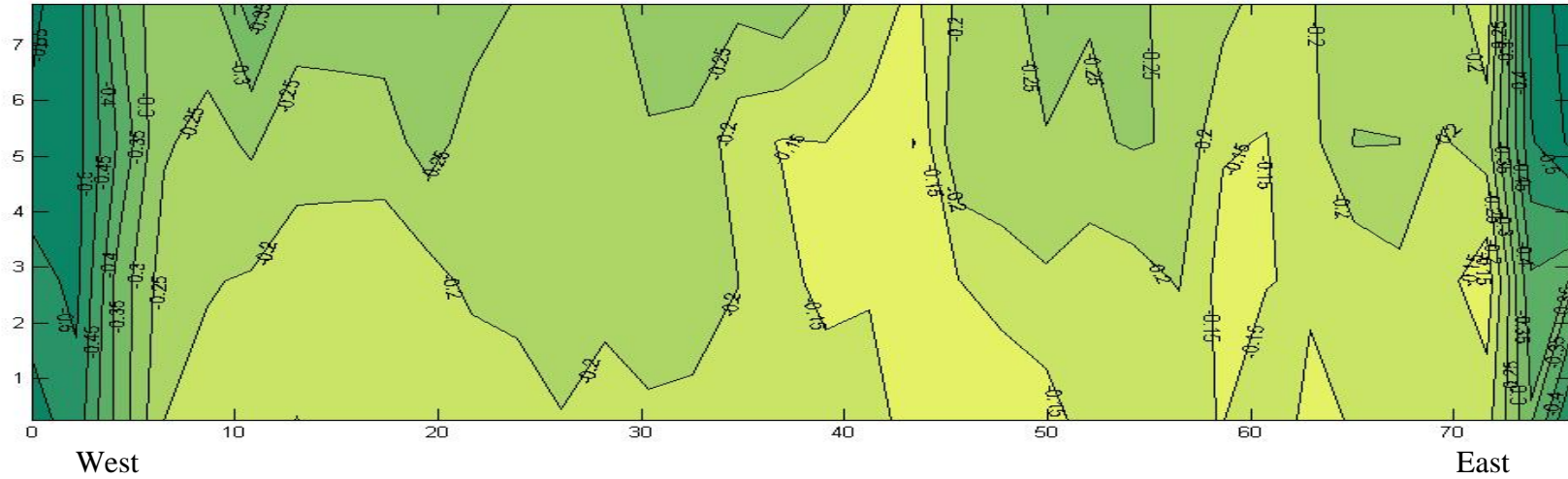


Figure C.5 – Corrosion potential map for the Doniphan County Bridge (October 9, 2006)

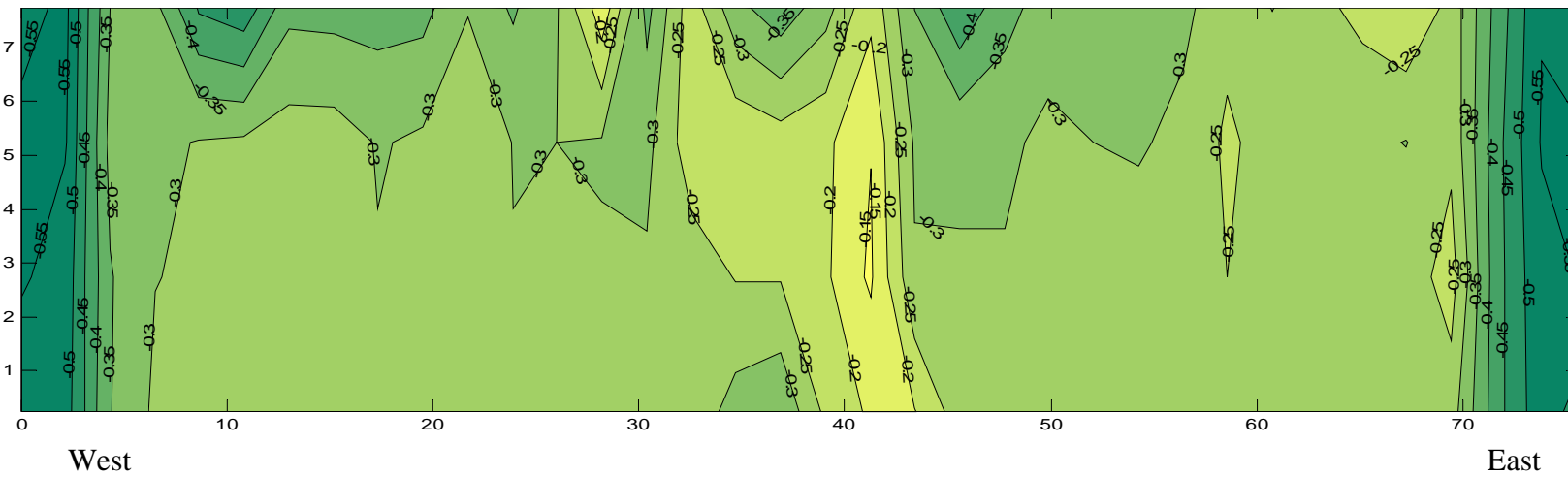


Figure C.6 – Corrosion Potential Mapping for the Doniphan County Bridge (May 11, 2007)

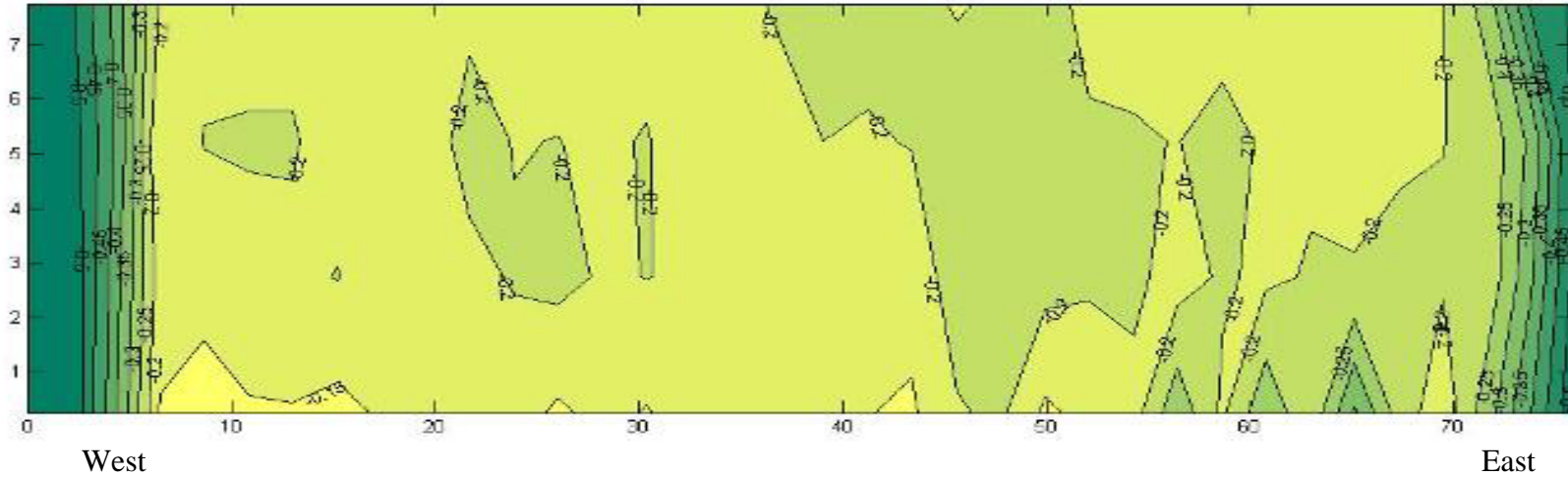


Figure C.7 – Corrosion potential map for the Doniphan County Bridge (October 12, 2007)

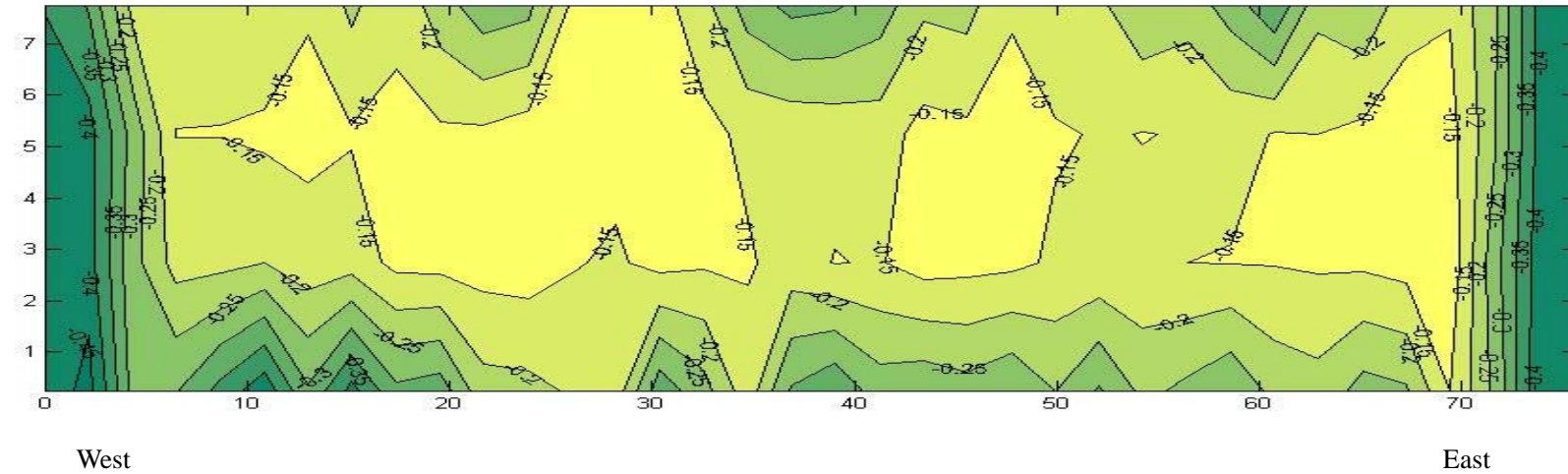


Figure C.8 – Corrosion potential map for the Doniphan County Bridge (April 11, 2008)

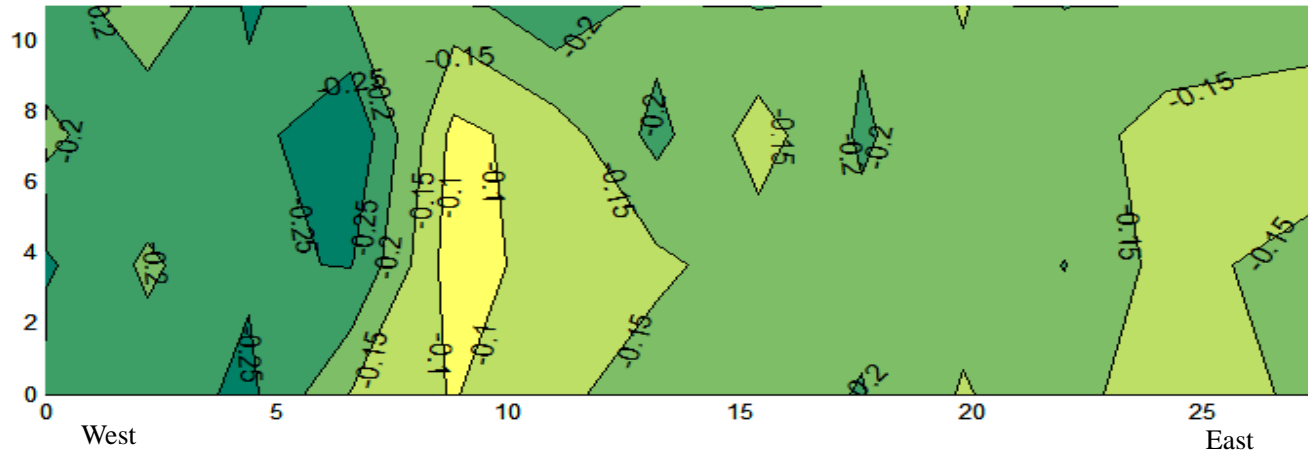


Figure C.9 – Corrosion potential map for the Mission Creek Bridge (September 1, 2004)

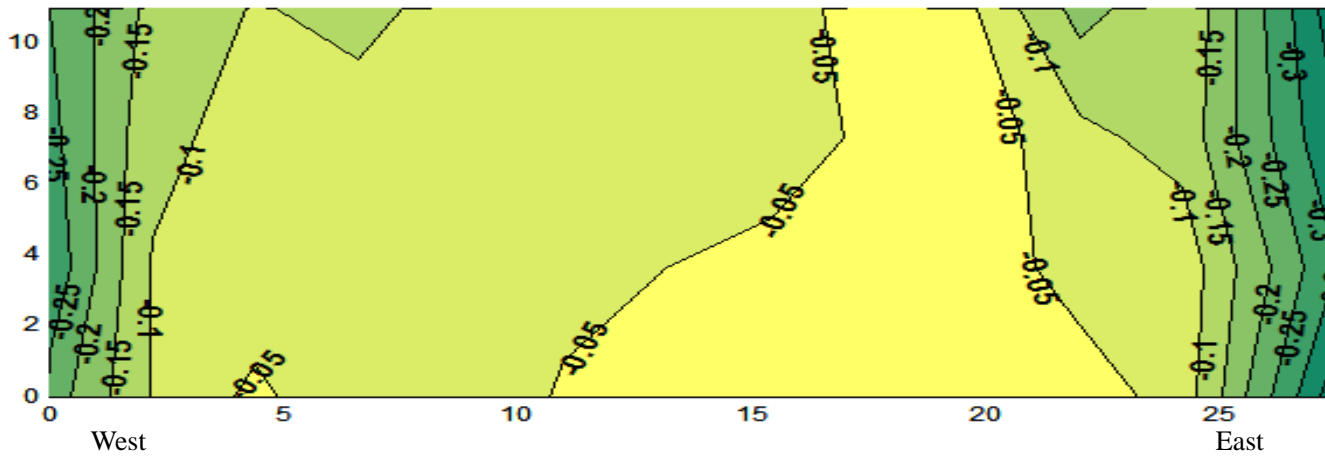


Figure C.10 – Corrosion potential map for the Mission Creek Bridge (April 1, 2005)

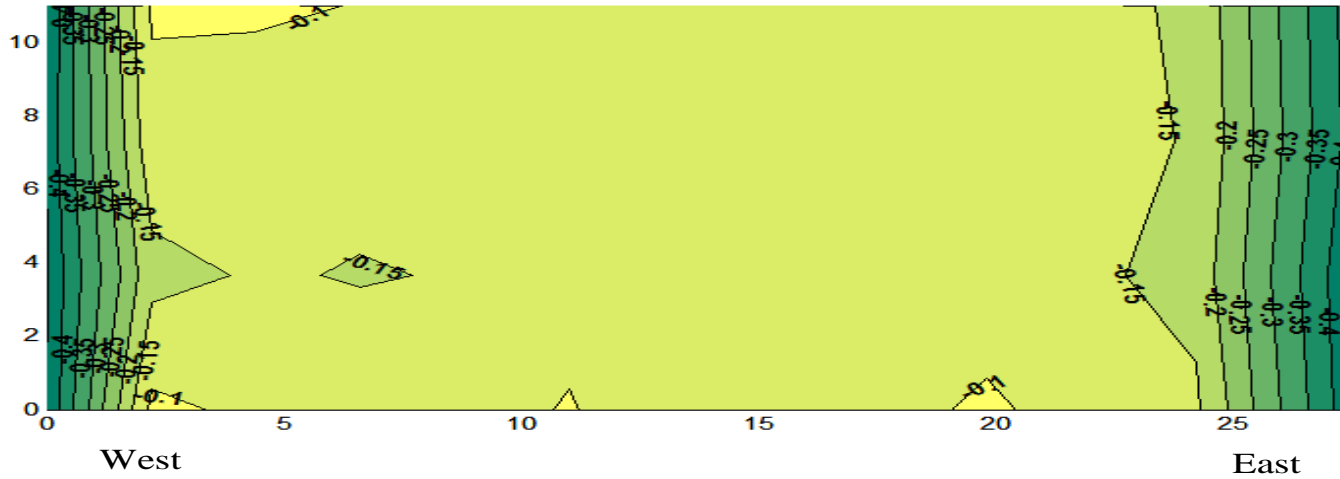


Figure C.11 – Corrosion potential map for the Mission Creek Bridge (September 27, 2005)

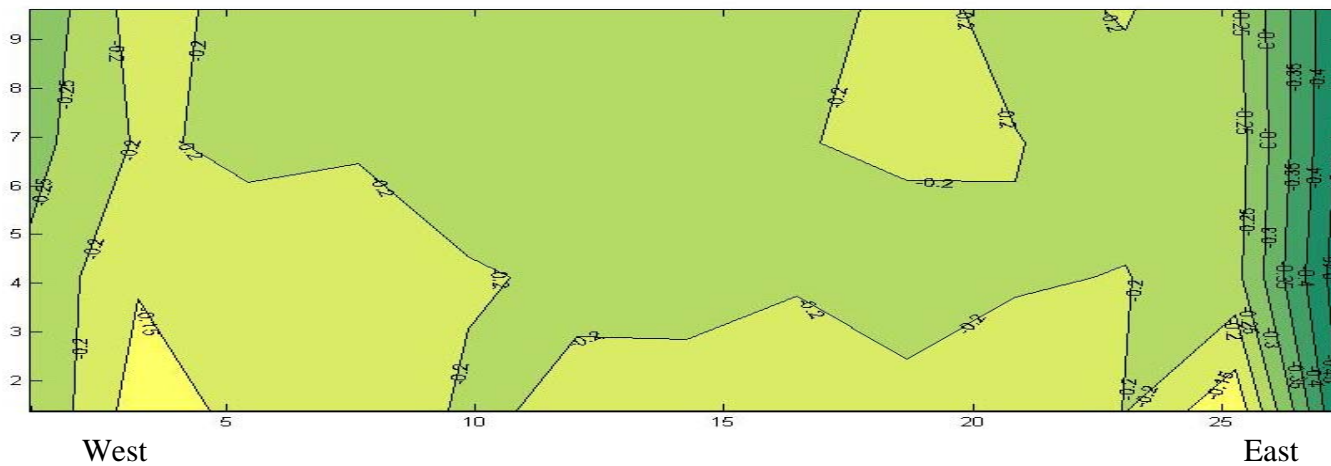


Figure C.12 – Corrosion potential map for the Mission Creek Bridge (June 19, 2006)

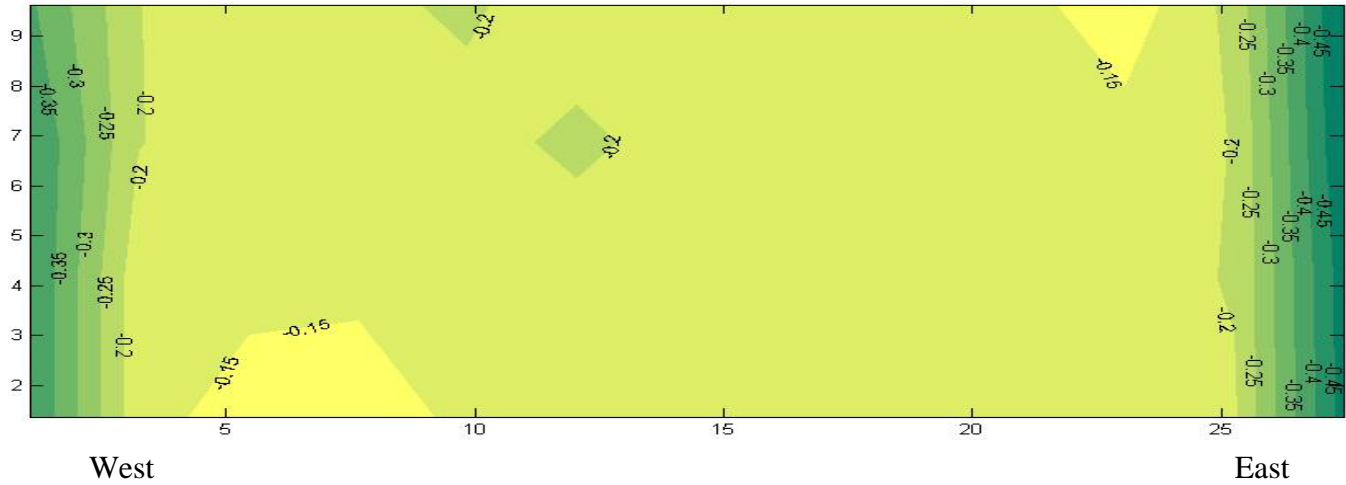


Figure C.13 – Corrosion potential map for the Mission Creek Bridge (October 16, 2006)

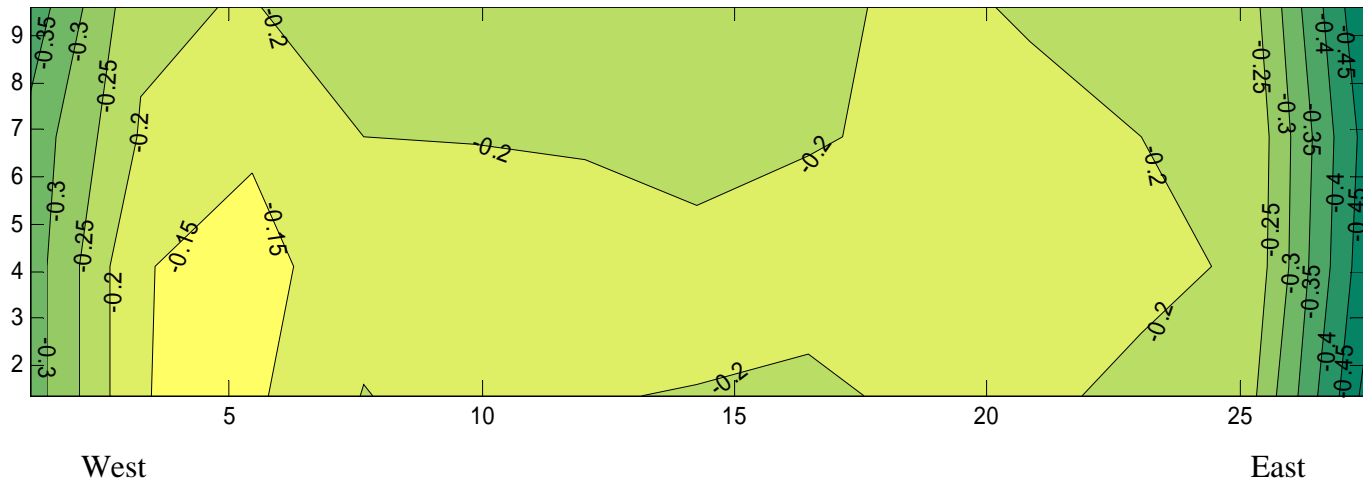
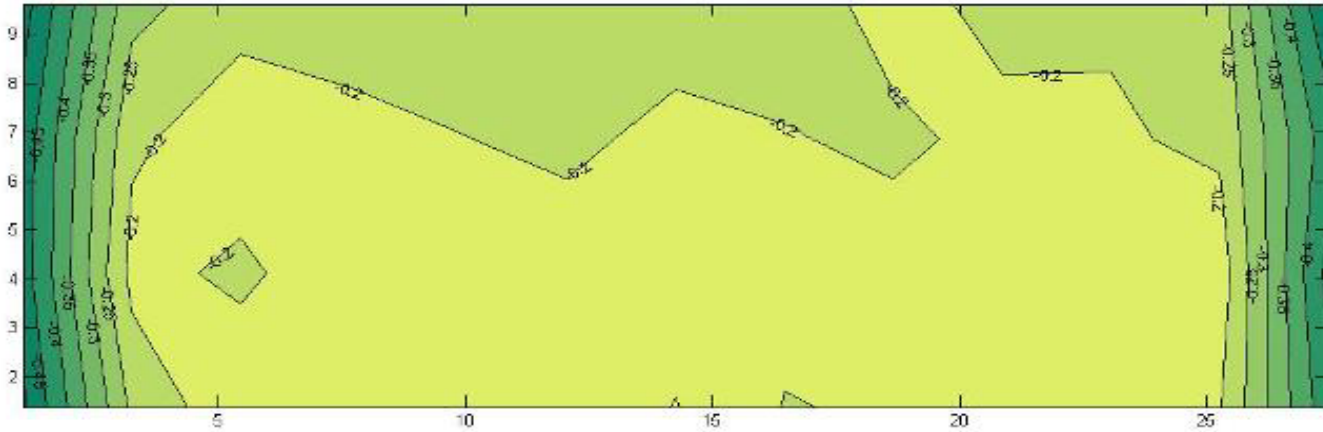
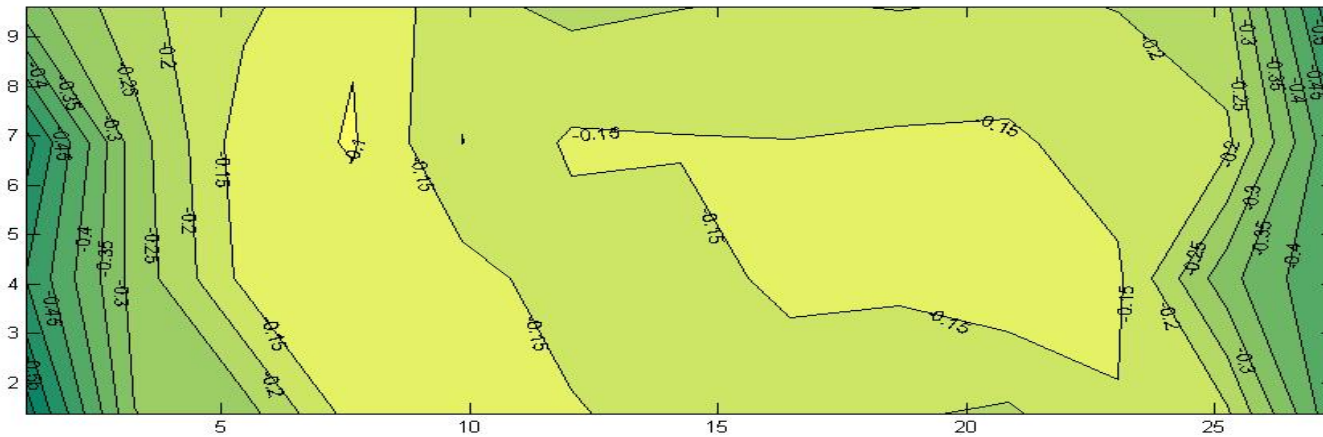


Figure C.14 – Corrosion potential map for the Mission Creek Bridge (May 17, 2007)

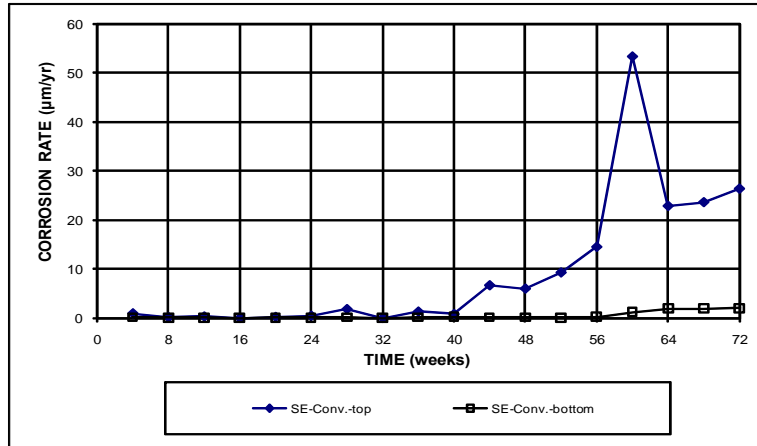


West East
Figure C.15 – Corrosion potential map for the Mission Creek Bridge (October 10, 2007)

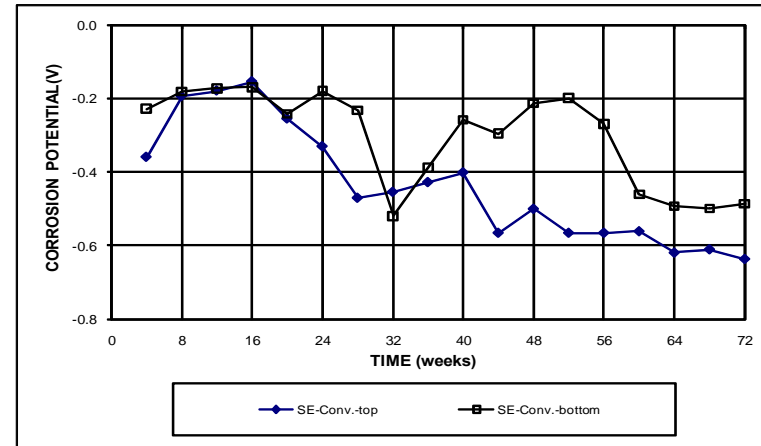


West East
Figure C.16 – Corrosion potential map for the Mission Creek Bridge (April 7, 2008)

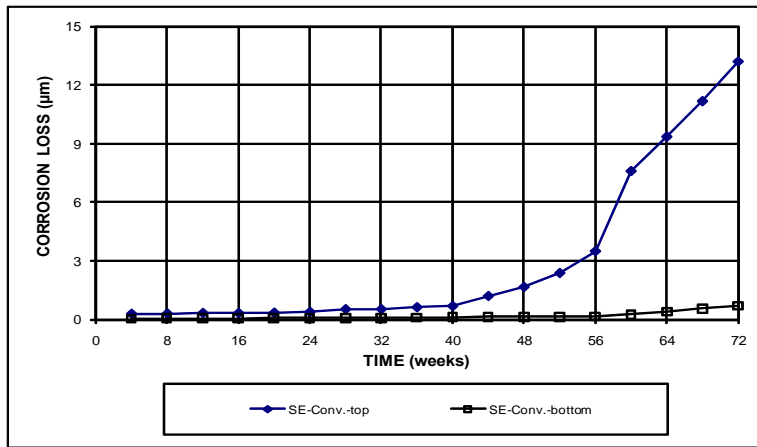
APPENDIX D



(a)

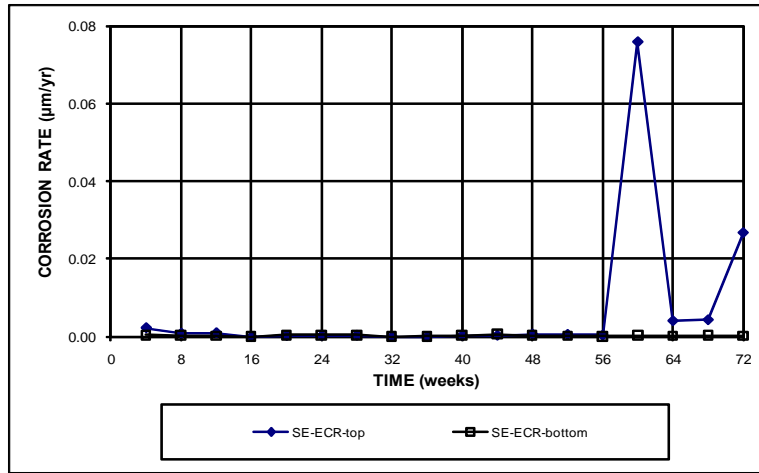


(c)

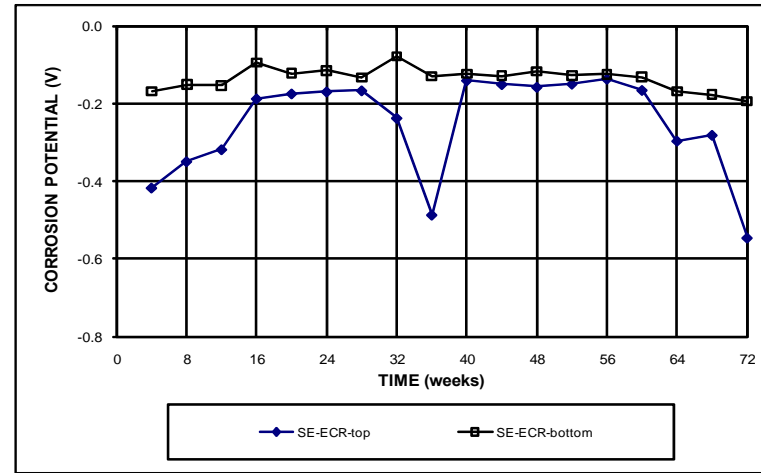


(b)

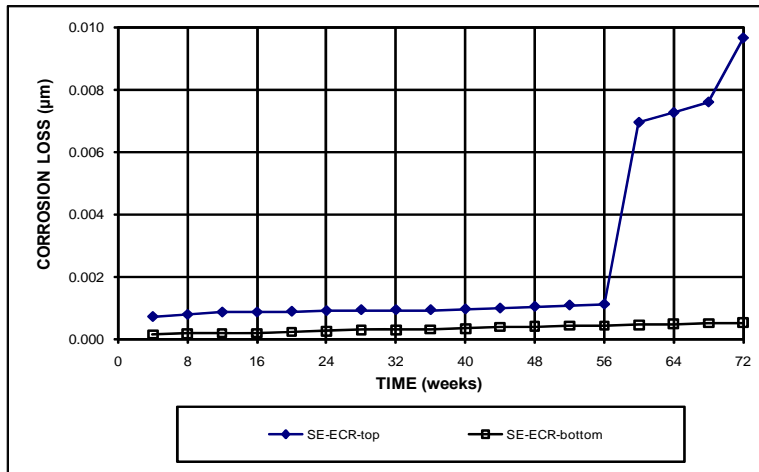
Figure D.1 – LPR Test. (a) Corrosion rates, (b) total corrosion losses, and (c) corrosion potentials with respect to a copper-copper sulfate electrode for Southern Exposure specimens with conventional steel (controls).



(a)

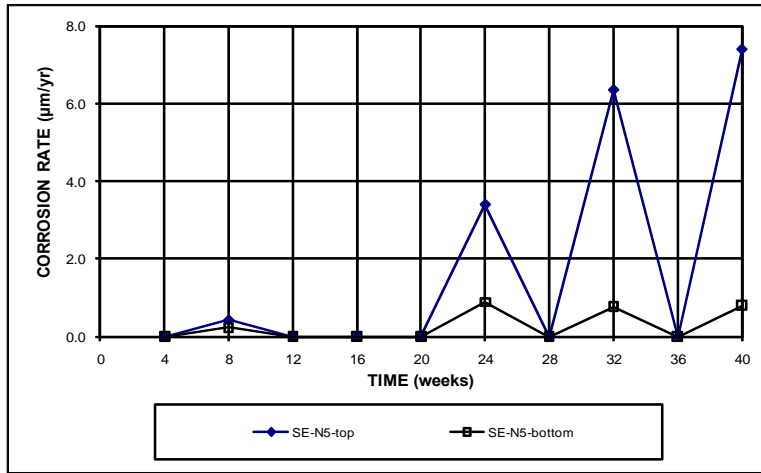


(c)

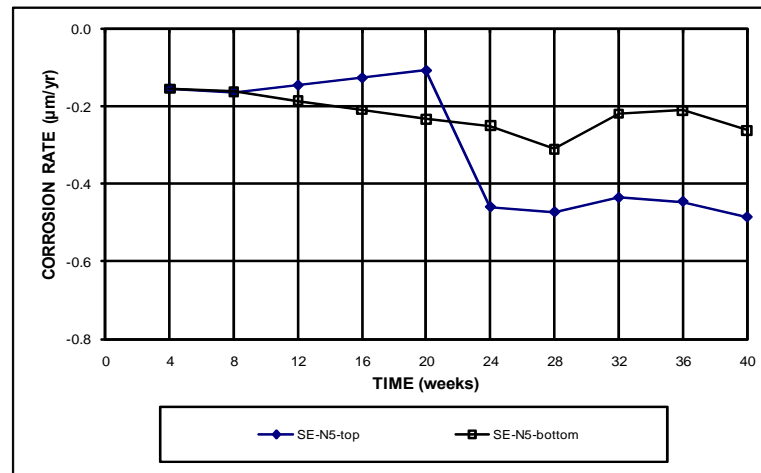


(b)

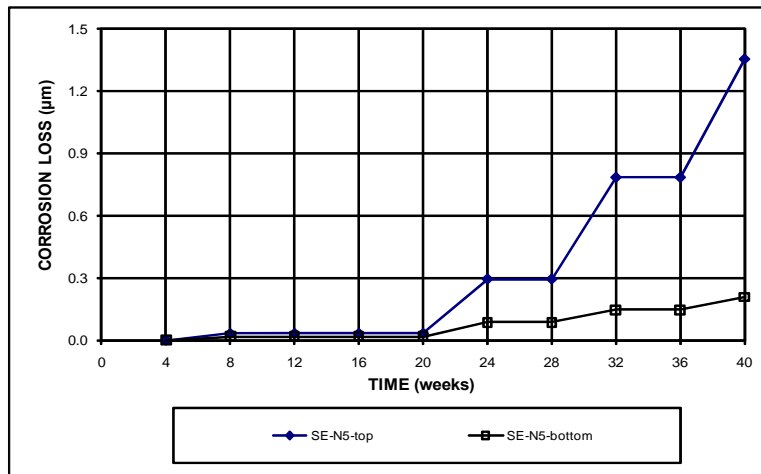
Figure D.2 – LPR Test. (a) Corrosion rates, (b) total corrosion losses, and (c) corrosion potentials with respect to a copper-copper sulfate electrode for Southern Exposure specimens with ECR (four holes).



(a)

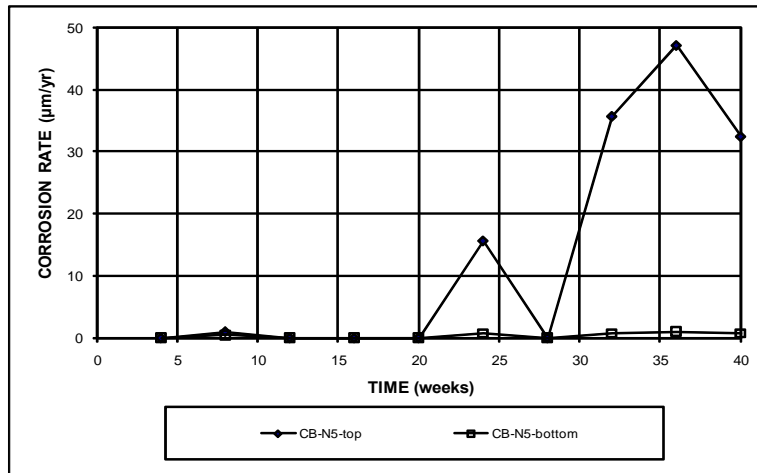


(c)

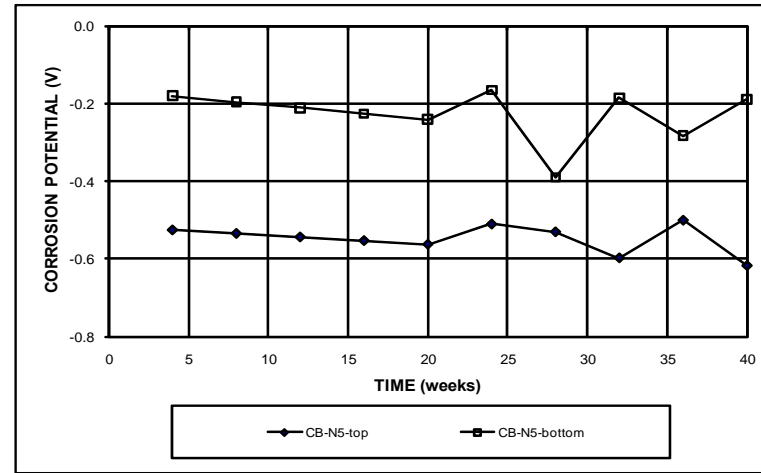


(b)

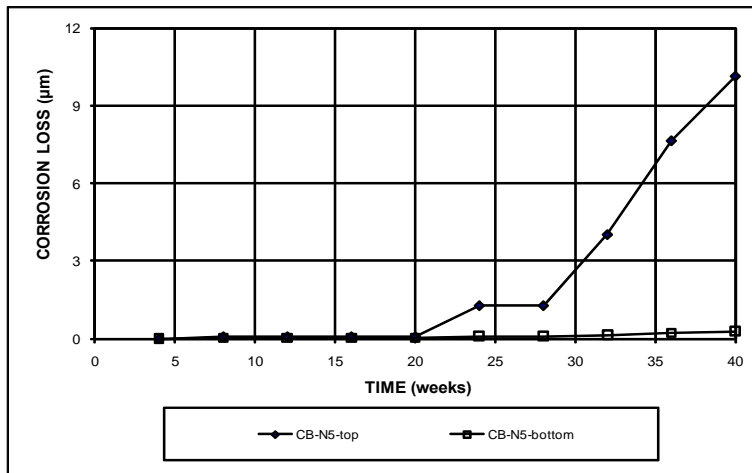
Figure D.3 – LPR Test. (a) Corrosion rates, (b) total corrosion losses, and (c) corrosion potentials with respect to a copper-copper sulfate electrode for Southern Exposure specimens with conventional steel and no inhibitor.



(a)

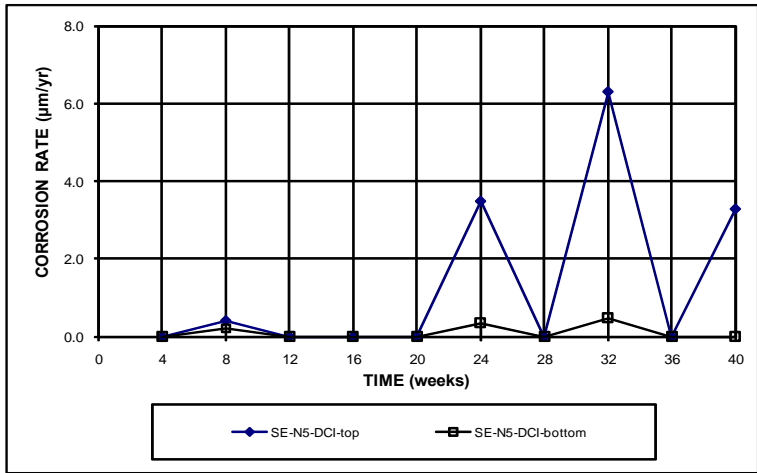


(c)

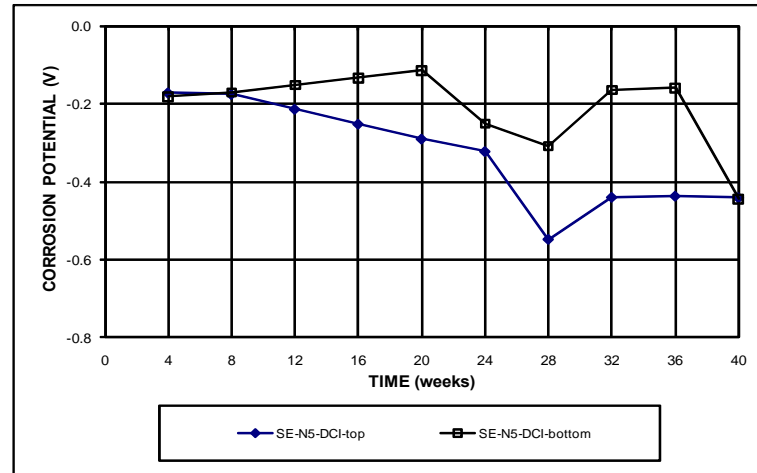


(b)

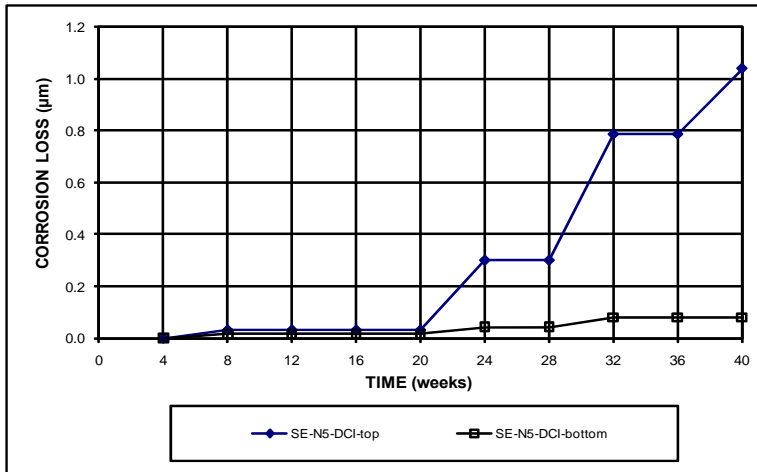
Figure D.4 – LPR Test. (a) Corrosion rates, (b) total corrosion losses, and (c) corrosion potentials with respect to a copper-copper sulfate electrode for cracked beam specimens with conventional steel and no inhibitor.



(a)

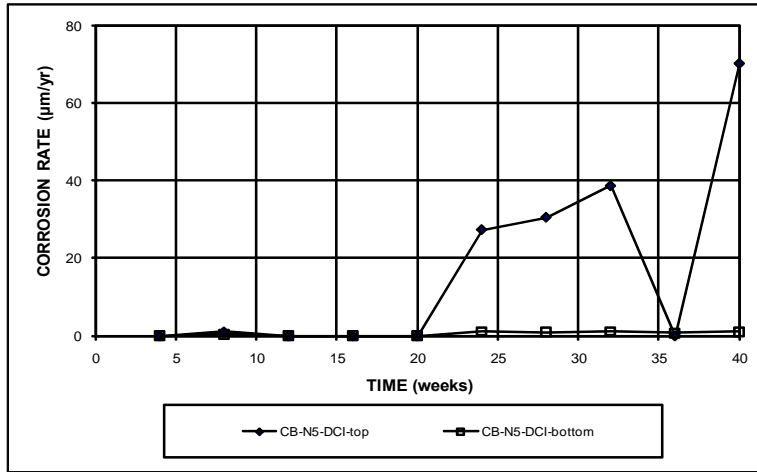


(c)

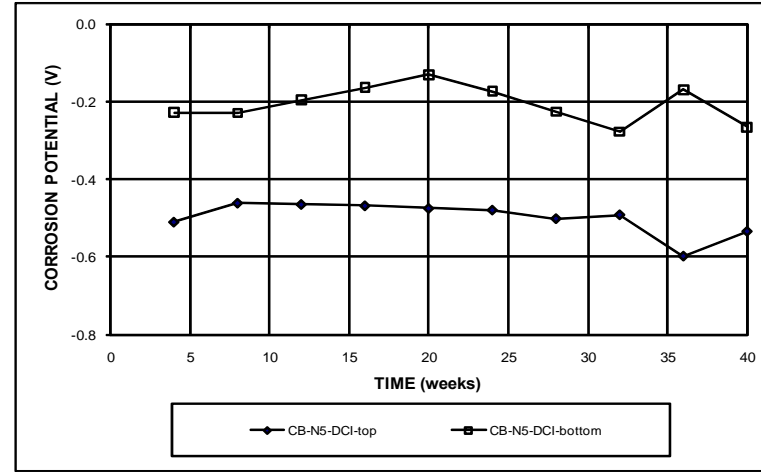


(b)

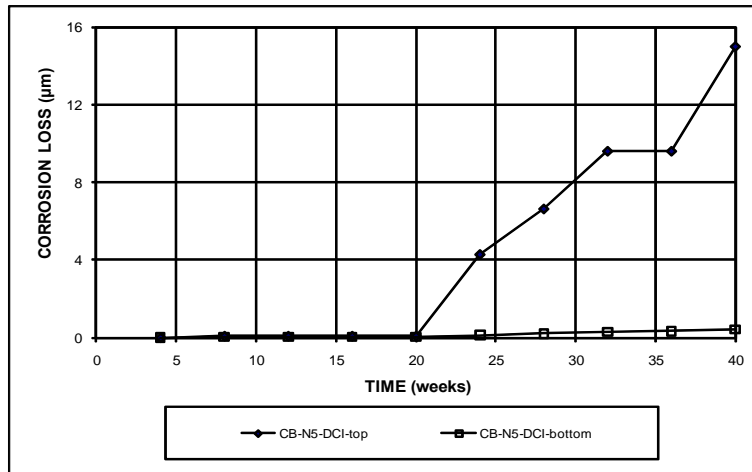
Figure D.5 – LPR Test. (a) Corrosion rates, (b) total corrosion losses, and (c) corrosion potentials with respect to a copper-copper sulfate electrode for Southern Exposure specimens with conventional steel and DCI inhibitor.



(a)

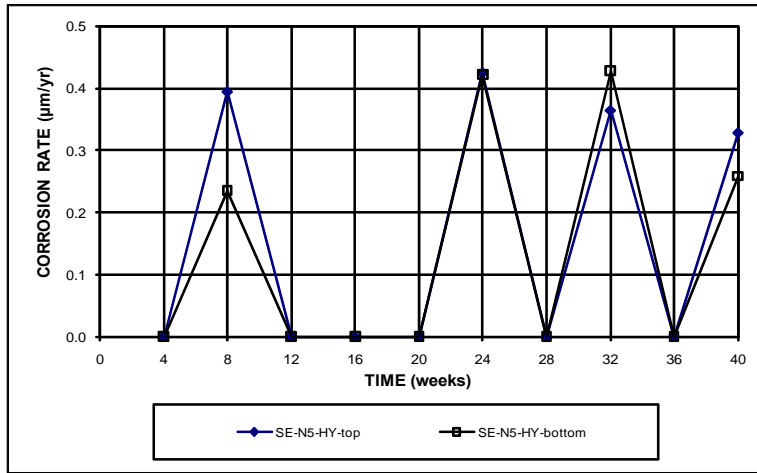


(c)

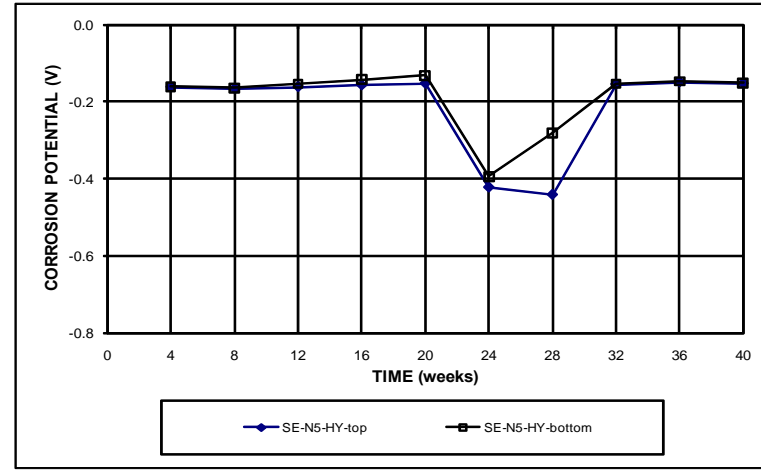


(b)

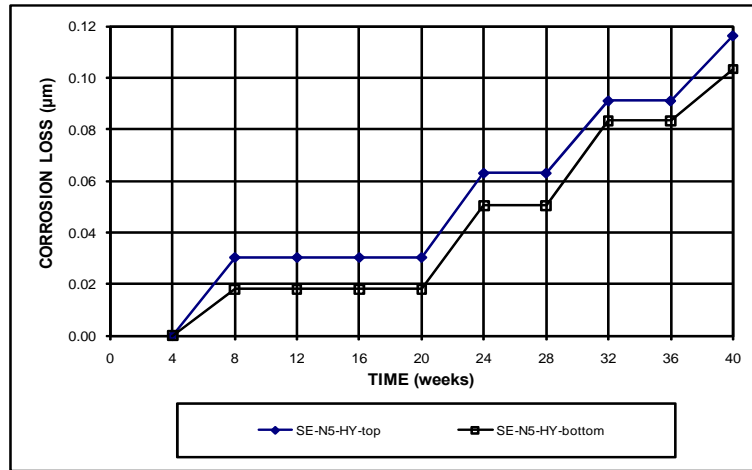
Figure D.6 – LPR Test. (a) Corrosion rates, (b) total corrosion losses, and (c) corrosion potentials with respect to a copper-copper sulfate electrode for cracked beam specimens with conventional steel and DCI inhibitor.



(a)

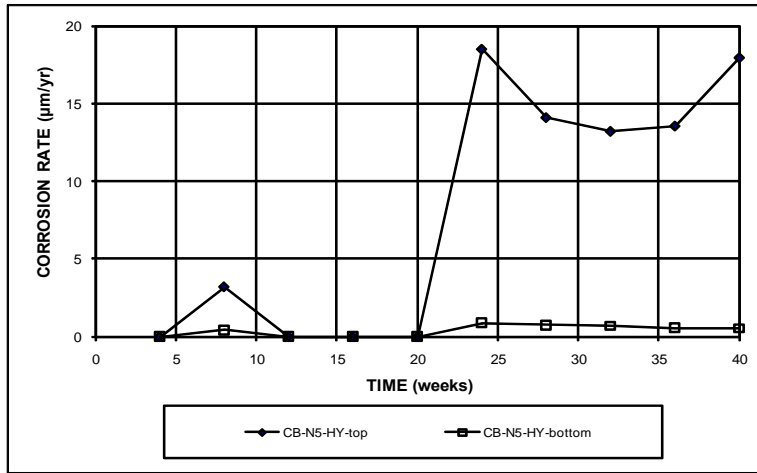


(c)

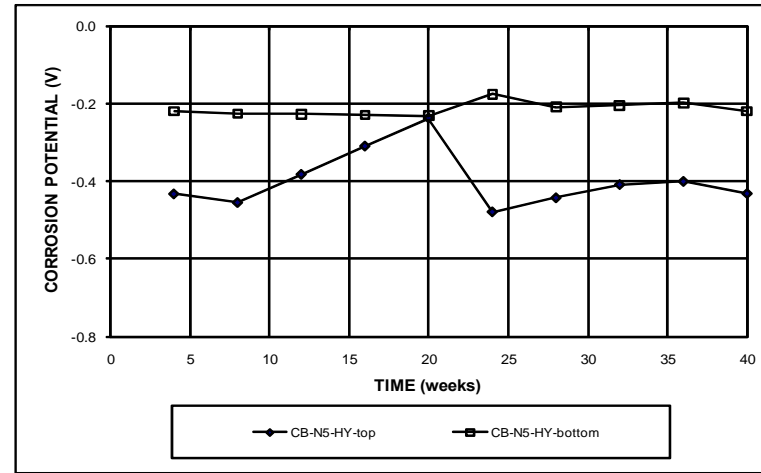


(b)

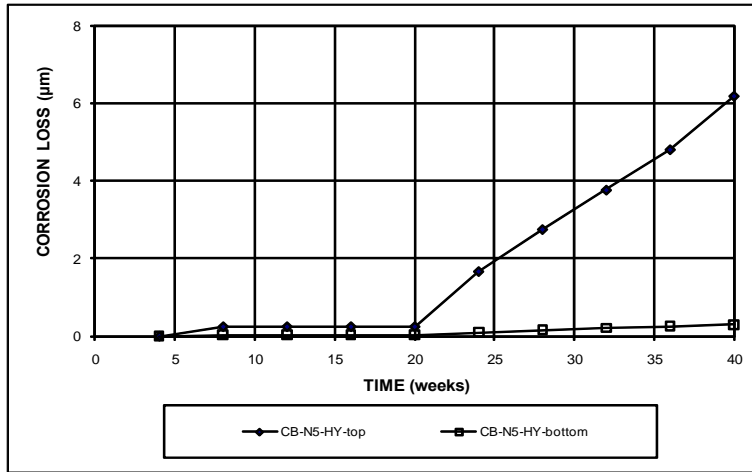
Figure D.7 – LPR Test. (a) Corrosion rates, (b) total corrosion losses, and (c) corrosion potentials with respect to a copper-copper sulfate electrode for Southern Exposure specimens with conventional steel and Hycrete inhibitor.



(a)

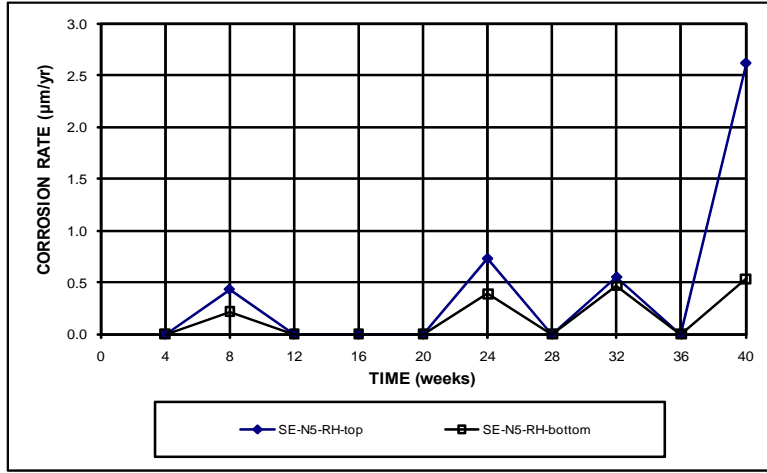


(c)

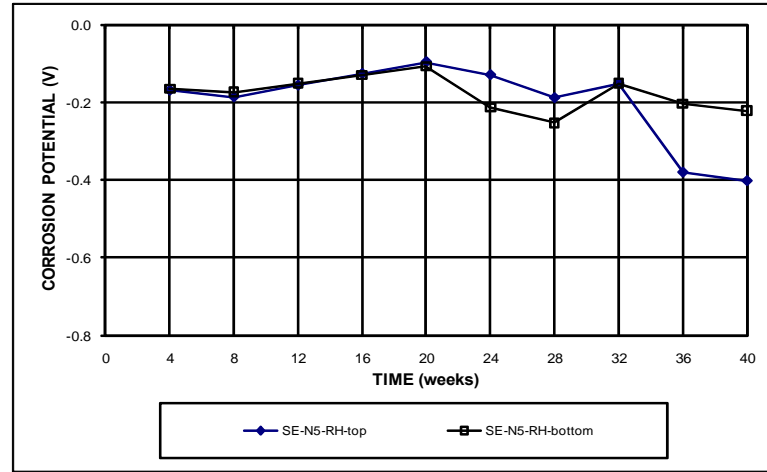


(b)

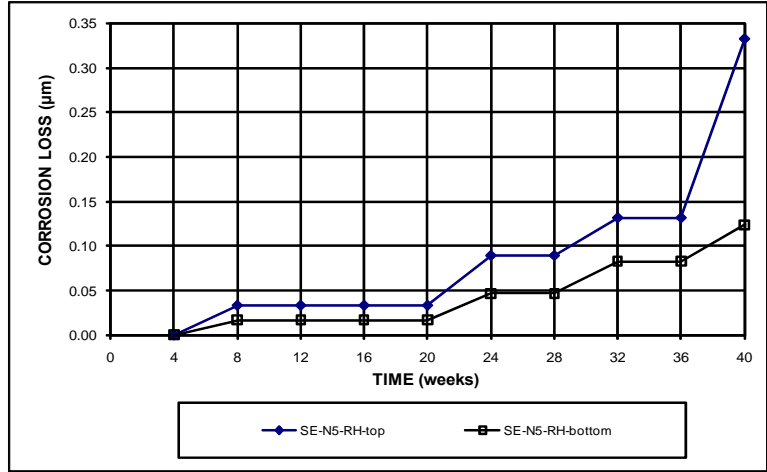
Figure D.8 – LPR Test. (a) Corrosion rates, (b) total corrosion losses, and (c) corrosion potentials with respect to a copper-copper sulfate electrode for cracked beam specimens with conventional steel and Hycrete inhibitor.



(a)

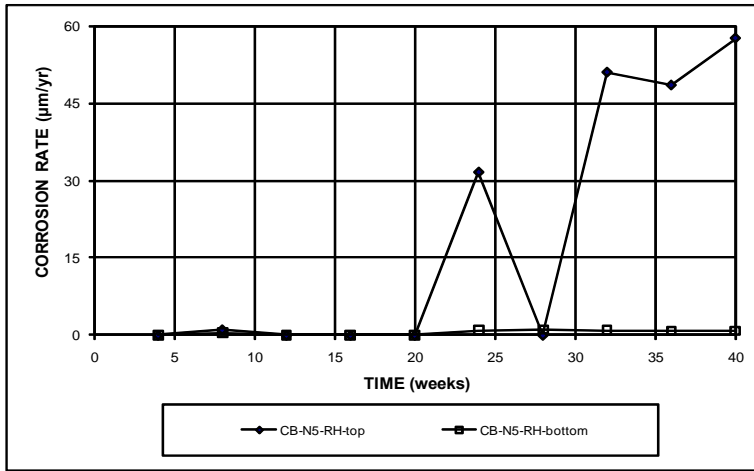


(c)

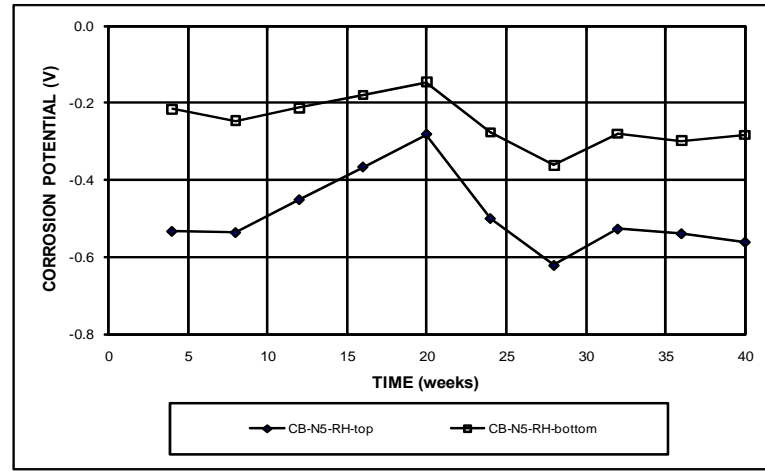


(b)

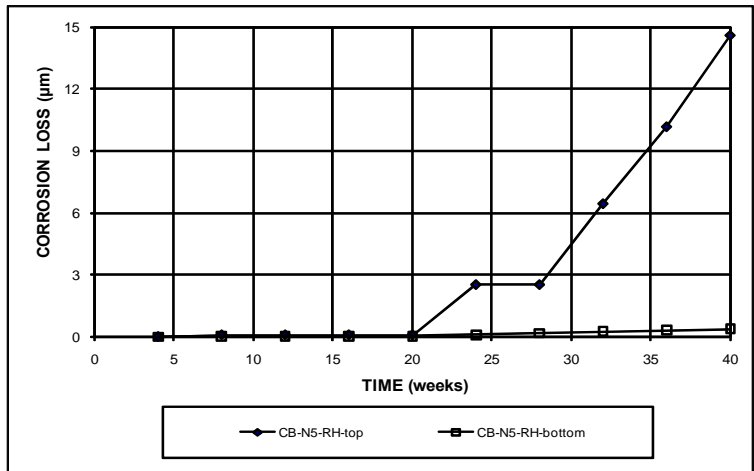
Figure D.9 – LPR Test. (a) Corrosion rates, (b) total corrosion losses, and (c) corrosion potentials with respect to a copper-copper sulfate electrode for Southern Exposure specimens with conventional steel and Rheocrete inhibitor.



(a)

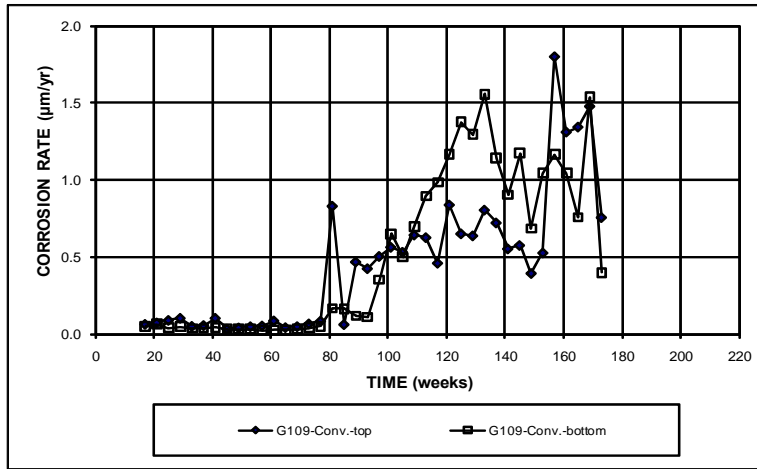


(c)

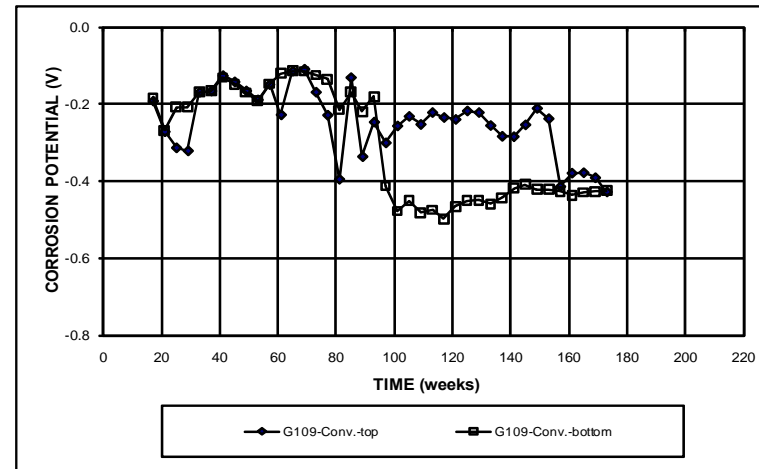


(b)

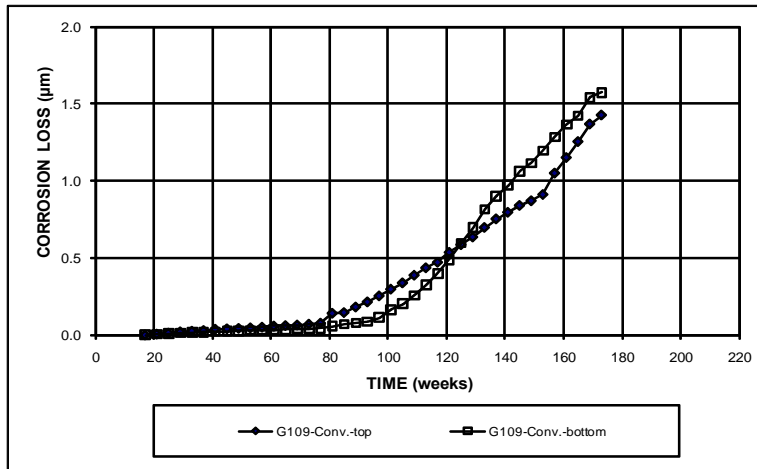
Figure D.10 – LPR Test. (a) Corrosion rates, (b) total corrosion losses, and (c) corrosion potentials with respect to a copper-copper sulfate electrode for cracked beam specimens with conventional steel and Rheocrete inhibitor.



(a)

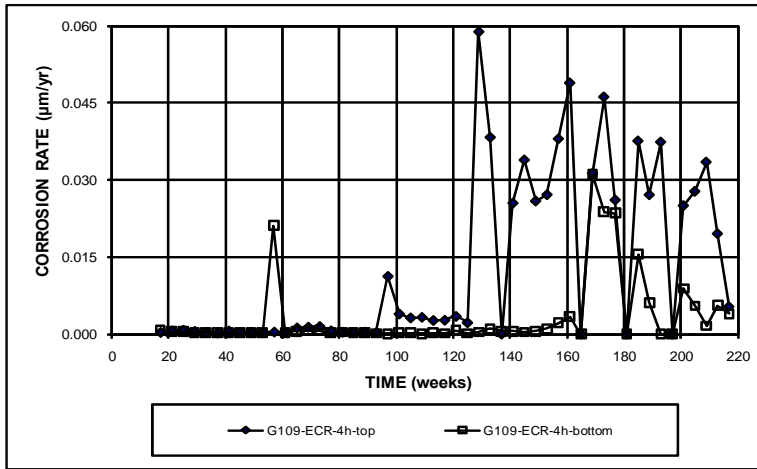


(c)

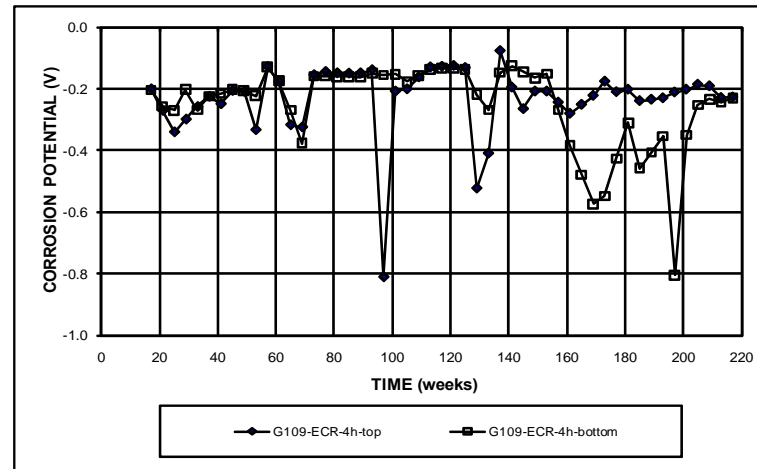


(b)

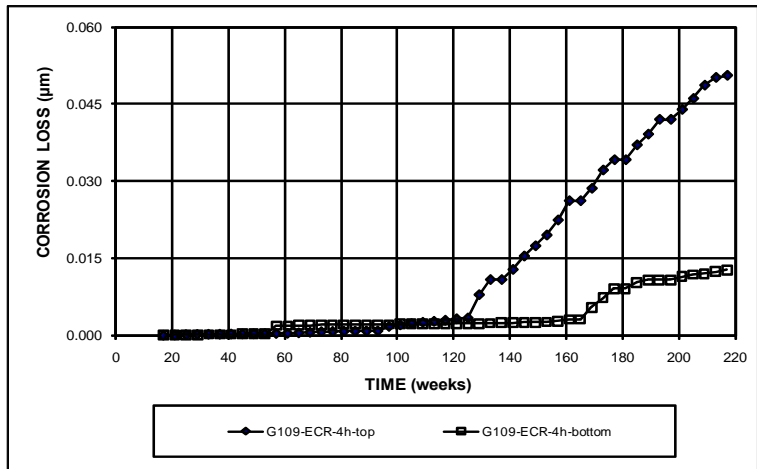
Figure D.11 – LPR Test. (a) Corrosion rates, (b) total corrosion losses, and (c) corrosion potentials with respect to a copper-copper sulfate electrode for ASTM G109 specimens with conventional steel.



(a)

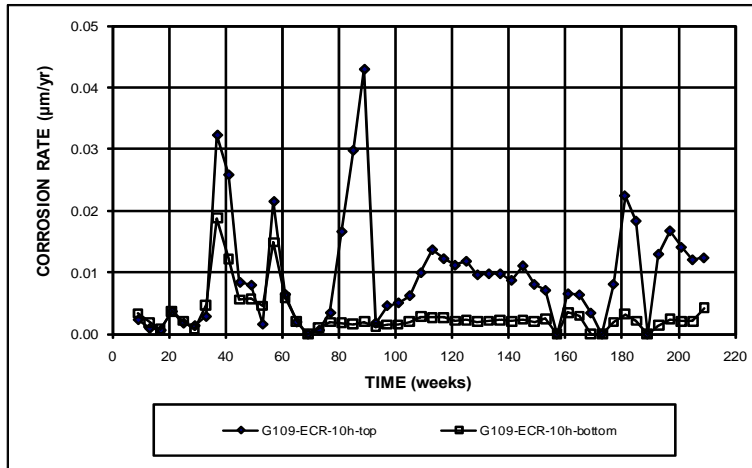


(c)

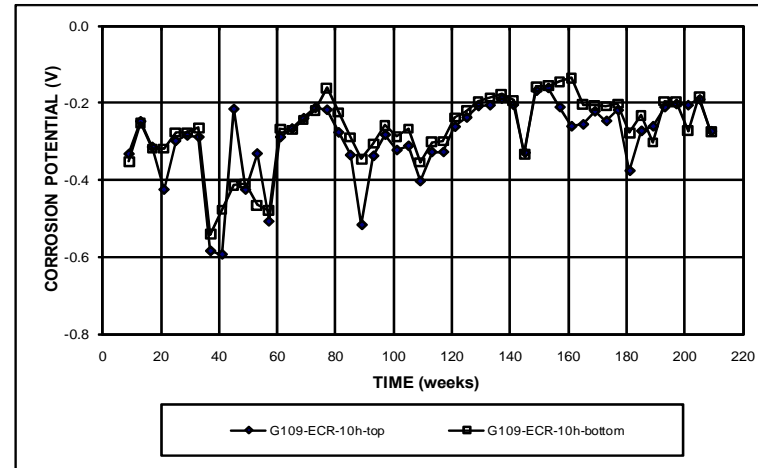


(b)

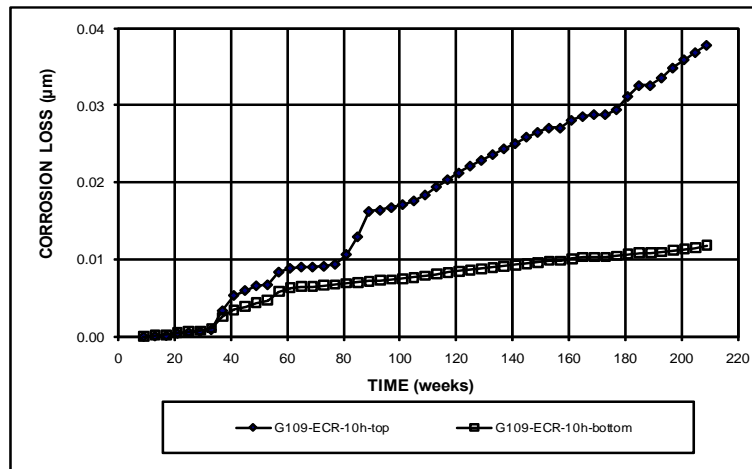
Figure D.12 – LPR Test. (a) Corrosion rates, (b) total corrosion losses, and (c) corrosion potentials with respect to a copper-copper sulfate electrode for ASTM G109 specimens with ECR (four holes).



(a)

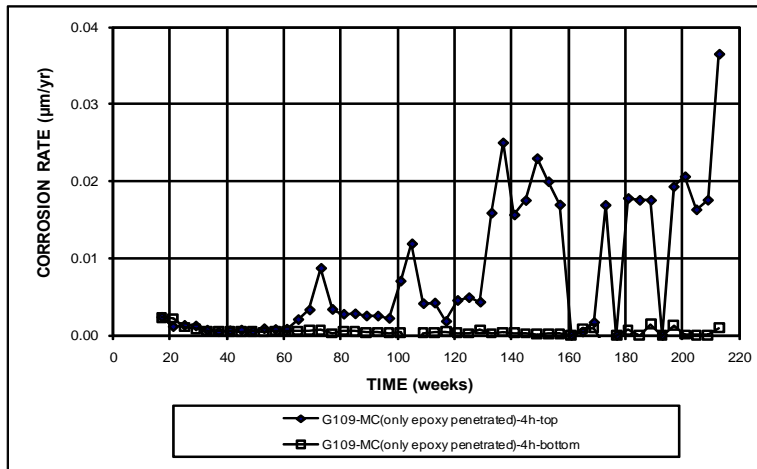


(c)

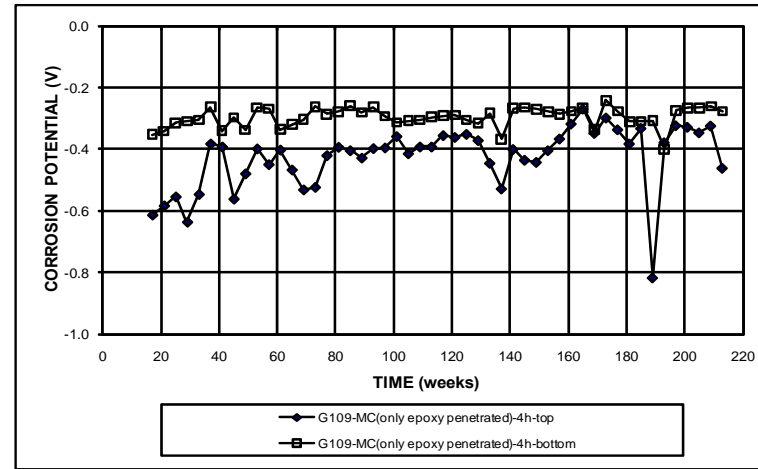


(b)

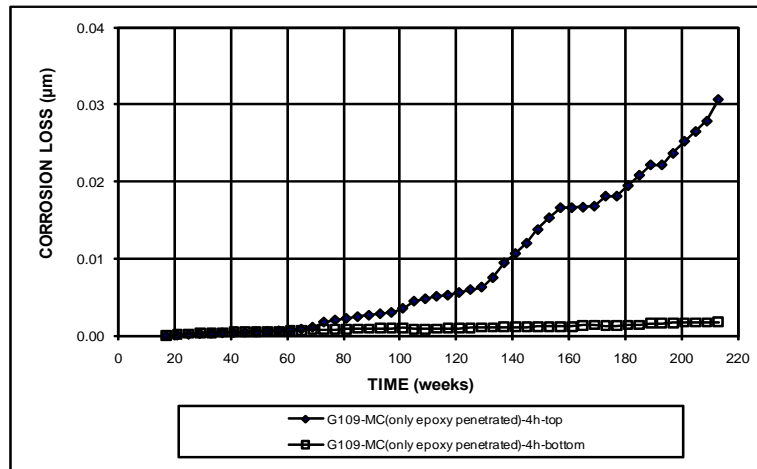
Figure D.13 – LPR Test. (a) Corrosion rates, (b) total corrosion losses, and (c) corrosion potentials with respect to a copper-copper sulfate electrode for ASTM G109 specimens with ECR (ten holes).



(a)

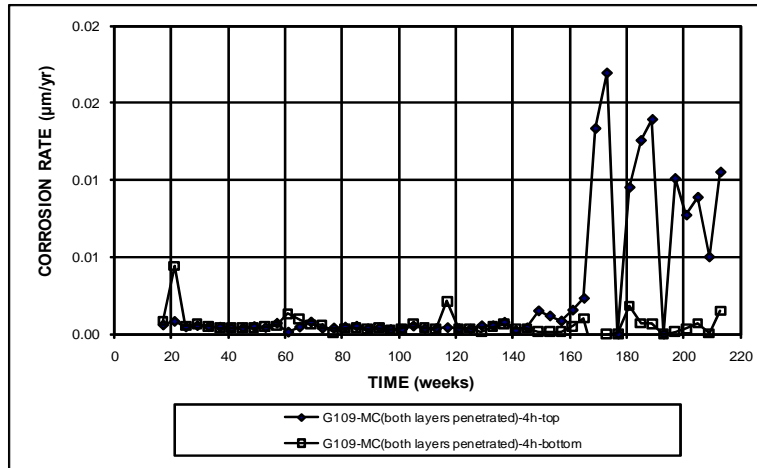


(c)

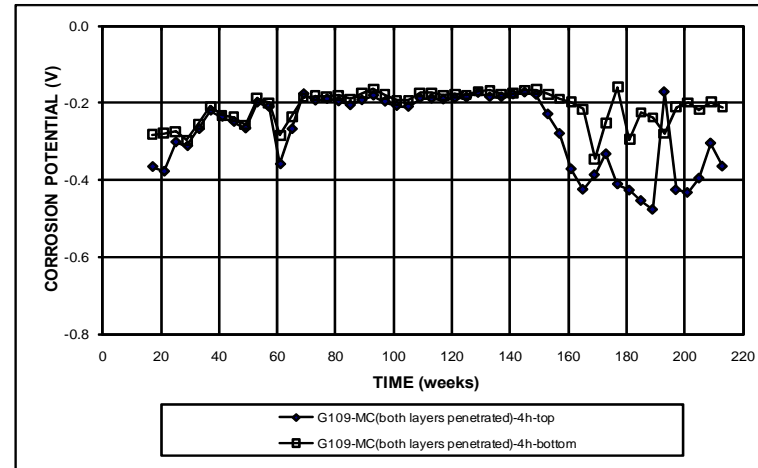


(b)

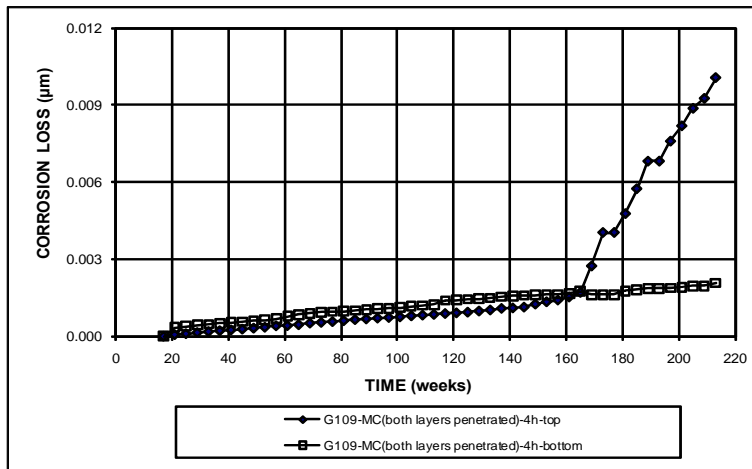
Figure D.14 – LPR Test. (a) Corrosion rates, (b) total corrosion losses, and (c) corrosion potentials with respect to a copper-copper sulfate electrode for ASTM G109 specimens with multiple-coated bars (four holes, only epoxy penetrated).



(a)

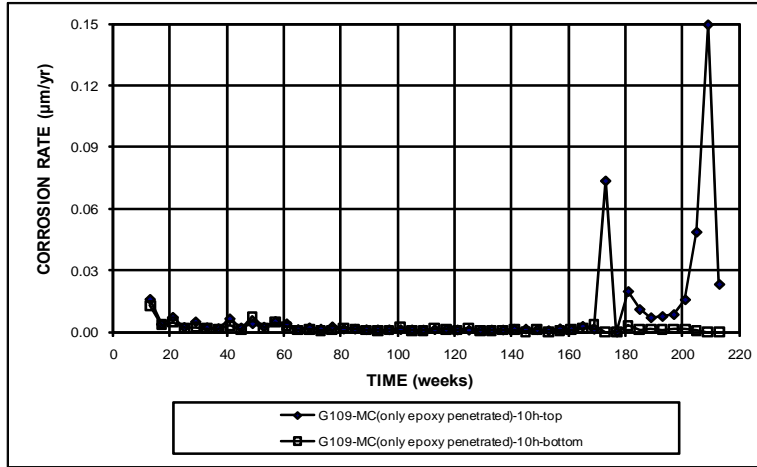


(c)

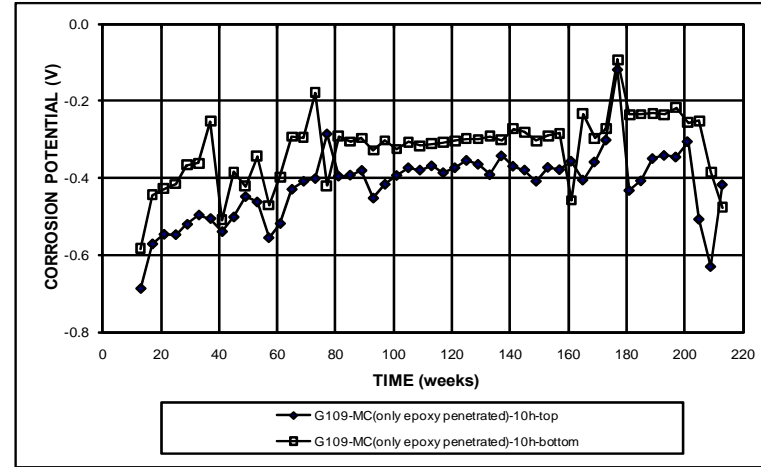


(b)

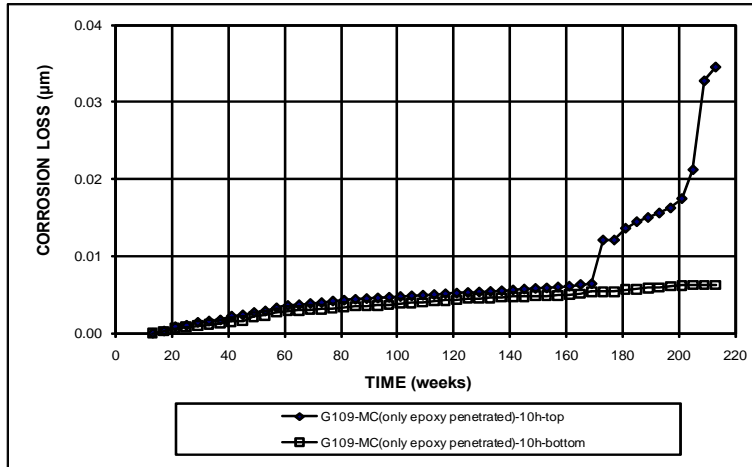
Figure D.15 – LPR Test. (a) Corrosion rates, (b) total corrosion losses, and (c) corrosion potentials with respect to a copper-copper sulfate electrode for ASTM G109 specimens with multiple-coated bars (four holes, both layers penetrated).



(a)

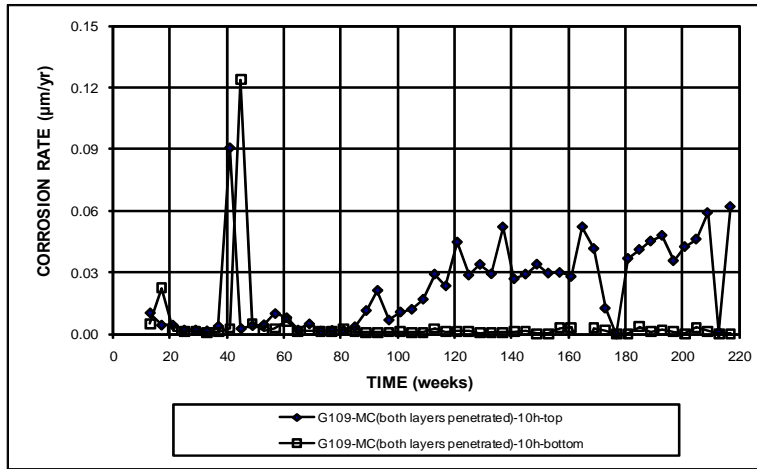


(c)

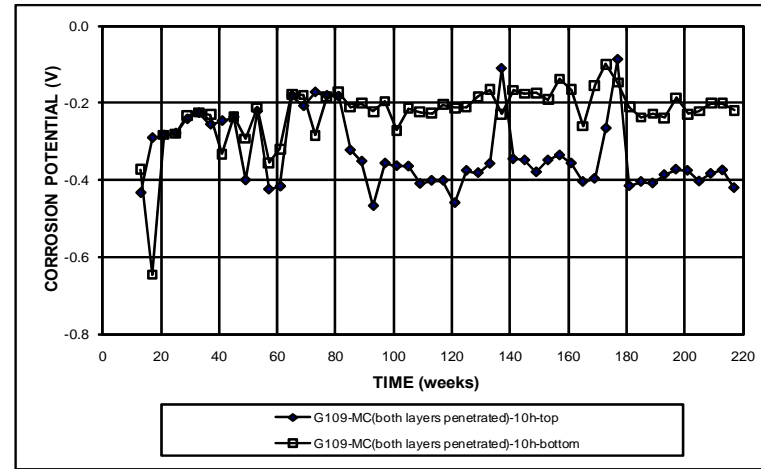


(b)

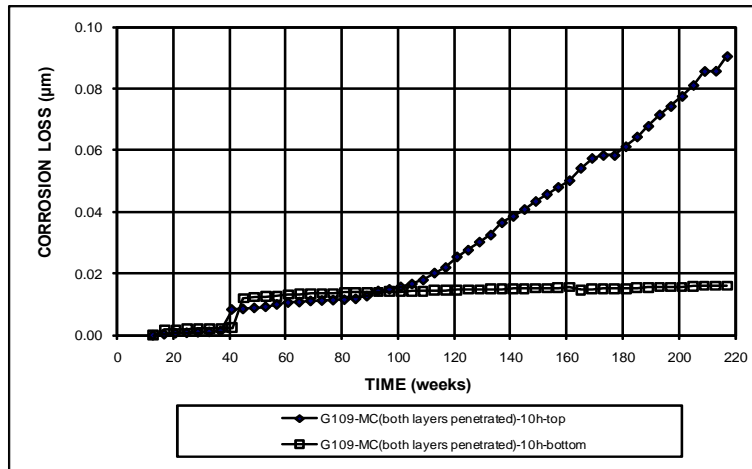
Figure D.16 – LPR Test. (a) Corrosion rates, (b) total corrosion losses, and (c) corrosion potentials with respect to a copper-copper sulfate electrode for ASTM G109 specimens with multiple-coated bars (ten holes, only epoxy penetrated).



(a)



(c)



(b)

Figure D.17 – LPR Test. (a) Corrosion rates, (b) total corrosion losses, and (c) corrosion potentials with respect to a copper-copper sulfate electrode for ASTM G109 specimens with multiple-coated bars (ten holes, both layers penetrated).